

Curtin Medical School

**Defining the Roles of Presenilin-1 and Presenilin-2
in A β Metabolism**

Melissa Kelly Eccles

0000-0003-0853-7833


**This thesis is presented for the Degree of
Doctor of Philosophy
of
Curtin University**

September 2023

This page intentionally left blank

DECLARATION

To the best of my knowledge and belief this thesis contains no material previously published by any other person except where due acknowledgment has been made. This thesis contains no material which has been accepted for the award of any other degree or diploma in any university.

Signature: 

Date: 28th September 2023

This page intentionally left blank

ABSTRACT

Presenilin is the catalytic component of the enzyme γ -secretase, an intramembrane protease that is most well-known for cleaving amyloid precursor protein (APP) to produce β -amyloid ($A\beta$) a toxic peptide associated with Alzheimer's disease (AD). There are two homologues of presenilin, presenilin-1 (PS1) and presenilin-2 (PS2), that form discrete γ -secretase complexes, along with the other critical components of the enzyme (nicastrin, anterior pharynx defective-1, and presenilin-enhancer-2) in a 1:1:1:1 stoichiometric ratio. The PS1 form of γ -secretase has received significantly more research focus in the AD field, since the discovery of both *PSENI* and *PSEN2*, for three main reasons: 1) The majority of identified clinical mutations that cause autosomal dominant AD occur in *PSENI*. 2) Loss of PS1 expression is embryonically lethal in mice. 3) PS1- γ -secretase is considered the more catalytically active form of the enzyme. Investigating the similarities and differences between PS1 and PS2 is needed to appreciate the roles that the proteins have in AD pathogenesis.

As essential catalytic components of γ -secretase, the presenilins are intimately involved in processing APP, to generate $A\beta$ peptides and the cleavage of over 149 other type I transmembrane protein substrates. This pleiotropic nature of γ -secretase has hampered its ability to be targeted therapeutically. Except for Notch-1, a protein that is associated with many cancers, many other substrates have been largely understudied. Underappreciated in the field is that many of these substrates regulate $A\beta$ metabolism either via APP trafficking, $A\beta$ clearance, $A\beta$ phagocytosis, or $A\beta$ degradation. The activity of γ -secretase on these substrates highlights avenues for targeting the presenilins beyond that of $A\beta$ production. This thesis begins to address this with the overall goal of assessing structural and functional differences between PS1- and PS2- γ -secretase, in both $A\beta$ generation and removal.

The first part of this thesis focusses on better understanding the specific contributions of PS1- and PS2- γ -secretase in $A\beta$ generation. To achieve this, several tools were developed to allow for the consideration of PS1 and PS2 protein expression in determining enzymatic activity, including a method for direct quantitation of endogenous presenilin levels (Chapter 2). The results show that in HEK-293 cells PS2- γ -secretase processes more APP and generates more of the neurotoxic, aggregative longer form $A\beta_{42}$, than PS1- γ -secretase, when differences in expression are accounted for. The mechanism by which PS2- γ -secretase generates more $A\beta_{42}$ was then explored using well-tempered metadynamics (WTMetaD) and binding free energy

calculations (Chapter 3). These data highlight differences in conformational dynamics of PS1- and PS2- γ -secretase binding to different APP-derived substrates and show that PS2- γ -secretase preferentially binds APP in a manner to initiate the A β 42 processing pathway rather than the A β 40 processing pathway.

In Chapter 4, the novel method for endogenous PS1 and PS2 quantitation was used to assess expression levels in human brain tissues from sporadic AD and other neurodegenerative conditions. A reduction of PS2 expression in AD hippocampal tissue was observed. Novel human neuroblastoma (M17) and microglia cells (HMC3) cells were generated in which either PS1 or PS2 were ablated using CRISPR technology to enable quantitative comparison of presenilin expression profiles, as well as examination of compensatory effects. PS1 and PS2 equally compensate for the loss of the alternate homologue in M17 cells. In HMC3 cells however, PS1 is significantly upregulated in response to the loss of PS2, suggesting a critical role for PS2 in human microglia. Additionally, the effect of neuronal-like differentiation in neuroblastoma cell lines (M17 and SH-SY5Y) led to higher PS2 expression levels than PS1.

The second part of this thesis focussed on elucidating the roles of PS1- and PS2- γ -secretase in A β metabolism more broadly. Firstly, the HMC3 human microglial cells in which PS1 or PS2 had been ablated were used to assess the functional roles of PS1 and PS2 in microglial A β removal (Chapter 5). This data shows that cells retaining PS2 have increased A β phagocytosis, and a specific cytokine response to lipopolysaccharide treatment. However, cells retaining PS1 have a specific cytokine response to A β treatment. Transcriptome analysis of these microglial cells revealed distinct transcription profiles between cells with either a PS1+/PS2+, PS1 only or PS2 only genotype, further indicating the functional distinction between PS1 and PS2. Secondly, the previously established simulation methods were utilised to investigate PS1- and PS2- γ -secretase specific binding preferences for substrates, other than APP, involved in A β metabolism (Chapter 6). The results indicate that PS1- and PS2- γ -secretase typically demonstrate specific substrate binding preferences, which may translate to specific substrate processing functions. Lastly, the effect of PS1 and PS2 clinical mutations on binding of APP and other substrates involved in A β metabolism were assessed using alchemical perturbation, with the aim of quantifying a relationship between a presenilin mutation's effect on substrate binding and disease severity (Chapter 6). The results of this analysis suggest that more aggressive PS1 mutations (associated with earlier age at onset) have a more pronounced effect

on A β generation, while less aggressive PS1 mutations (associated with later age at onset) may impact A β clearance mechanisms.

This thesis makes significant contributions to furthering our understanding of the complex roles of PS1 and PS2 in AD, shedding light on their diverse functions beyond the well-established involvement in A β generation. Notably, this thesis challenges conventional assumptions regarding the primary role of PS1- γ -secretase in A β production and underscores potentially critical functions of PS2- γ -secretase, not just in A β generation but also in A β removal processes. These findings warrant further investigation and carry important implications for future efforts aimed at selectively targeting presenilins/ γ -secretase in the context of AD.


ACKNOWLEDGEMENTS

The work presented in this thesis is dedicated to my grandmothers, June Zillman and Gwenyth Eccles, whose journey's with Alzheimer's disease started my journey in Alzheimer's disease research.

The completion of this thesis was made possible through the invaluable support and assistance of my supervisors, colleagues, friends, and family.

“A journey of a thousand miles begins with a single step” *Laozi*

My single step was a knock on the door of David Groth and a swift introduction to Giuseppe Verdile, a fortuitous event that began this eight-year journey. Beginning in my undergraduate studies, both Giuseppe and David have remained constant supervisors on this journey, through undergraduate projects, honours and this PhD. Giuseppe I am ever so grateful that you have allowed me the freedom I needed to make this PhD as fruitful as it has been. Your unwavering support and guidance have provided me with a remarkable foundation from which I can now confidently begin my scientific career. David, your consistent questioning of assumptions, and your sharp attention to detail have instilled in me the level of rigour demanded by a scientist. To Mark Agostino, a fantastic addition to my PhD supervisory team, your bringing of a different viewpoint and skill set has made all the difference to my PhD, it has elevated it significantly. Beyond your roles as supervisors, I consider you all good friends. I look forward to continuing our friendships and a collaboration or two.

I must acknowledge the generous financial support of Dementia Australia Research Foundation for my stipend scholarship, Curtin University for my completion scholarship, and the Australian Government Department of Education for my Fee Offset Scholarship. Additionally consumable funding was generously provided by Curtin Medical School, and the Verdile and Groth laboratories, with special thanks to the birds . All molecular modelling was supported by resources provided by the Pawsey Supercomputing Research Centre with funding from the Australian Government and the Government of Western Australia.

There is a long list of people from Curtin Medical School and Curtin Health Innovation Research Institute that have provided both technical and pastoral support throughout my PhD,

to whom I am very grateful. However, I must make special mention of the support and friendship I have received from Danielle Dye, Ben Dwyer, Rob Steuart, Kylie Munyard, Connie Jackaman and Pat Methoram.

I have been fortunate to have made amazing friendships during this journey, friendships that I know will last a while longer yet. In particular a very special mention goes to Sara Pasic, Zalitha Pieterse-Mulley, Tahlia Bastholm, Ayeisha Milligan Armstrong, Lelinh Duong and Nathan Main. Thank you for the welcome distractions, the coffee, the dinners, the constant support (particularly through this last push to the end), but most importantly thank you for the laughs, there have been a lot of laughs!! A special mention must also go to Tenielle Porter and Shane Fernandez, may we dine at many more fancy restaurants in the future.

To the Pryor's you have been a great support throughout, I always looked forward to our weekly dinner and quiz, they were always a welcome break from PhD life.

Finally, I must thank my family. Mum, Dad, Beccie, Lee and Charlee. This would not have been possible without your love and support, and while the end seemed like it may never come, on this rather long journey, it is here. Thank you!

CONTRIBUTIONS OF OTHERS

The results presented in this thesis “*Defining the Roles of Presenilin-1 and Presenilin-2 in A β Metabolism*” were all generated by Melissa Eccles, however the provision of certain materials and particular technical support must be acknowledged.

Chapter 2 – HEK 293 PS1^{-/-}PS2^{+/+} cells were provided as a polyclonal population generated in the laboratory of Professor Paul E Fraser, of the University of Toronto. All subcloning and subsequent experiments using these cells were completed by Melissa Eccles. Oxford Nanopore sequencing was completed under the guidance of Dr Rodrigo Carlessi.

Chapter 2 & 4 – Single cell sorting for monoclonal cell populations of CRISPR cells was completed by the technical staff at Curtin Innovation Health Research Institute.

Chapter 3 & 6 – Protocols for the molecular modelling methods used were developed by Dr Mark Agostino. The path between APP-bound and Notch1-bound PS1 γ used as a collective variable for the WTMetaD was prepared by Dr Mark Agostino.

Chapter 4 – The generation of the M17 and HMC3 (empty vector, PS1^{-/-}PS2^{+/+} and PS1^{+/+}PS2^{-/-}) CRISPR cell lines, was completed with assistance from Ayeisha Milligan Armstrong and Amy Woodfield, who assisted in subcloning and PCR screening.

PUBLICATIONS

Publications contributing to this thesis published on preprint server bioRxiv

Eccles MK, Main N, Carlessi R, et al. Quantitative comparison of presenilin protein expression reveals greater activity of PS2- γ -secretase. *The FASEB Journal*. 2023; 38:e23396. doi:[10.1096/fj.202300954RR](https://doi.org/10.1096/fj.202300954RR)

Eccles, M. K.; Groth, D.; Verdile, G.; Agostino, M., Presenilin homologues influence substrate binding and processing by γ -secretase: a molecular simulation study. bioRxiv 2023, 2023.05.17.541079.

Currently under consideration at ACS Chemical Neuroscience

Publications accepted through the course of the PhD but not contributing to the thesis

Moussavi Nik, S. H.; Porter, T.; Newman, M.; Bartlett, B.; Khan, I.; Sabale, M.; **Eccles, M.**; Woodfield, A.; Groth, D.; Dore, V.; Villemagne, V. L.; Masters, C. L.; Martins, R. N.; Laws, S. M.; Lardelli, M.; Verdile, G., Relevance of a Truncated PRESENILIN 2 Transcript to Alzheimer's Disease and Neurodegeneration. *Journal of Alzheimer's Disease* **2021**, 80 (4), 1479-1489.

Ioppolo, A.; **Eccles, M.**; Groth, D.; Verdile, G.; Agostino, M., Evaluation of Virtual Screening Strategies for the Identification of γ -Secretase Inhibitors and Modulators. *Molecules* **2021**, 27 (1).

Milligan Armstrong, A.; Woodfield, A.; **Eccles, M.**; Groth, D.; Verdile, G., The role of stress in mediating inflammation in the context of neurodegeneration. In. Fink, G., editor. STRESS: IMMUNOLOGY AND INFLAMMATION Handbook of Stress Volume 5. 1st ed. Academic Press; **2023**. p. 325-337

International conference proceedings

Eccles, M.; Groth, D.; Verdile, G.; Agostino, M., Metadynamics simulations of γ -secretases bound to β -amyloid peptides reveal the preference of Presenilin-2 for A β 42 production. *Poster presentation to the International Conference on Alzheimer's and Parkinson's Diseases and related neurological disorders, March 2022, Barcelona, Spain*

Eccles, M.; Woodfield, A.; Milligan Armstrong, A.; Fraser, P.E.; Groth, D.; Agostino, M.; Verdile, G., More than making amyloid-beta: Shedding light on the different roles of presenilin-1 and presenilin-2 in amyloid-beta removal. *On demand oral presentation to the International Conference on Alzheimer's and Parkinson's Diseases and related neurological disorders, March 2022, Barcelona, Spain*

Eccles, M.; Woodfield, A.; Milligan Armstrong, A.; Groth, D.; Agostino, M.; Verdile, G., Quantitating presenilin: Identifying the impact of presenilin expression on gamma-secretase activity and the functional implications. *Poster presentation to the International Conference on Alzheimer's and Parkinson's Diseases and related neurological disorders, March 2023, Gothenburg, Sweden*

Eccles, M.; Groth, D.; Verdile, G.; Agostino, M., Biophysical characterisation of wildtype and mutant gamma-secretase binding to substrates associated with β -amyloid removal. *Poster presentation to the International Conference on Alzheimer's and Parkinson's Diseases and related neurological disorders, March 2023, Gothenburg, Sweden*

Eccles, M.; Woodfield, A.; Milligan Armstrong, A.; Ash, J.; Fraser, P.E.; Groth, D.; Agostino, M.; Verdile, G., Defining the roles of presenilin-1 and presenilin-2 in microglial removal of β -amyloid. *In person oral presentation to the International Conference on Alzheimer's and Parkinson's Diseases and related neurological disorders, March 2023, Gothenburg, Sweden*

STATEMENT OF AUTHOR CONTRIBUTION FOR PUBLICATIONS INCLUDED IN THESIS

The thesis “*Defining the Roles of Presenilin-1 and Presenilin-2 in A β Metabolism*” includes publications. Below is a statement of Contribution of others for the publications included.

Publication Reference:

Chapter 1:

Eccles MK, Main N, Carlessi R, et al. Quantitative comparison of presenilin protein expression reveals greater activity of PS2- γ -secretase. *The FASEB Journal*. 2023; 38:e23396. doi:[10.1096/fj.202300954RR](https://doi.org/10.1096/fj.202300954RR)


- Contribution by Melissa Eccles is 60% (study design, data generation, data analysis, manuscript preparation)

Chapter 2:

Eccles, M. K.; Groth, D.; Verdile, G.; Agostino, M., Presenilin homologues influence substrate binding and processing by γ -secretase: a molecular simulation study. bioRxiv 2023, 2023.05.17.541079.

- Contribution by Melissa Eccles is 65% (study design, data generation, data analysis, manuscript preparation)

I, Melissa Eccles, contributed to the above listed publications at the stated level.


Signed: 

Date: 01/03/2024

I, as a co-author, endorse that this level of contribution by the candidate indicated above is appropriate.

Nathan Main:  04/03/24


Rodrigo Carlessi


Ayeisha Milligan Armstrong: 04/03/24


Miheer Sabale: 04/03/24


Brigid Roberts-Mok: 02/03/24


Janina E. E. Tirnitz-Parker: 06/03/24


Mark Agostino: 03/03/24


David Groth: 04/03/24


Paul E Fraser: 01/03/24


Giuseppe Verdile: 03/03/24

TABLE OF CONTENTS

DECLARATION	ii
ABSTRACT.....	iv
ACKNOWLEDGEMENTS.....	vii
CONTRIBUTIONS OF OTHERS.....	ix
PUBLICATIONS.....	x
STATEMENT OF AUTHOR CONTRIBUTION FOR PUBLICATIONS INCLUDED IN THESIS	xii
TABLE OF CONTENTS.....	xiv
LIST OF TABLES.....	xviii
LIST OF FIGURES	xix
LIST OF SUPPLEMENTAL TABLES.....	xxi
LIST OF SUPPLEMENTAL FIGURES	xxii
LIST OF ABBREVIATIONS.....	xxiii
1 INTRODUCTION	1
1.1 ALZHEIMER'S DISEASE.....	1
1.2 MECHANISMS OF AMYLOID- β METABOLISM.....	3
1.2.1 Amyloid- β generation.....	3
1.2.2 Amyloid- β clearance.....	6
1.3 THE γ -SECRETASE COMPLEX	8
1.3.1 The protein components of γ -secretase.....	8
1.3.2 γ -Secretase assembly, subunit function, and localisation	9
1.3.3 Structural determination of γ -secretase.....	14
1.3.4 Modelling γ -secretase	20
1.4 THE PRESENILINS: EXPRESSION AND FUNCTIONS.....	27
1.4.1 Expression profiles of PS1 and PS2.....	28
1.4.2 The differing roles of PS1 and PS2 in embryogenesis and neurodegeneration.....	30
1.4.3 γ -Secretase dependent functions of PS1 and PS2: Substrates galore	31
1.4.4 Non-proteolytic functions of PS1 and PS2	35
1.5 GENETICS OF INHERITED ALZHEIMER'S DISEASE.....	37
1.6 UNDERSTANDING γ -SECRETASE FOR IMPROVED THERAPEUTIC STRATEGIES.....	39
1.7 HYPOTHESIS AND AIMS.....	40
1.8 REFERENCES.....	41
1.9 SUPPLEMENTAL FIGURES	74
2 QUANTITATIVE COMPARISON OF PRESENILIN PROTEIN EXPRESSION REVEALS GREATER ACTIVITY OF PS2- γ -SECRETASE.....	77
2.1 INTRODUCTION.....	77
2.2 MATERIALS AND METHODS	80
2.2.1 Mammalian cell culture.....	80
2.2.2 CRISPR presenilin knockout in HEK-293	80
2.2.3 Plasmid construct generation	81
2.2.4 Whole genome sequencing and copy number variation analysis	81

2.2.5	Transient transfection.....	82
2.2.6	Quantitative PCR	83
2.2.7	Immunoblotting.....	84
2.2.8	PS1/2 fusion standard and absolute PS1 and PS2 quantitation.....	85
2.2.9	ELISA	86
2.2.10	Statistics	86
2.3	RESULTS.....	86
2.3.1	Presenilin knock-out cell line generation and characterisation.....	86
2.3.2	Exogenous PS expression highlights difference in PS levels and subsequently higher PS2 activity.....	89
2.3.3	PS1/2 fusion standard: A method for absolute quantitation of endogenous PS1 and PS2 93	
2.3.4	Endogenous PS2 demonstrates greater activity in cleaving APP and equivalent activity in cleaving Notch.	96
2.4	DISCUSSION	100
2.5	REFERENCES.....	104
2.6	SUPPLEMENTAL TABLES.....	110
2.7	SUPPLEMENTAL FIGURES	111
3	PRESENILIN HOMOLOGUES INFLUENCE SUBSTRATE BINDING AND PROCESSING BY γ -SECRETASE: A MOLECULAR SIMULATION STUDY.....	118
3.1	INTRODUCTION.....	118
3.2	MATERIALS AND METHODS	122
3.2.1	Structure preparation.....	122
3.2.2	Simulation box preparation.....	122
3.2.3	System Equilibration.....	123
3.2.4	Identification of a path between APP-bound and Notch-bound states	123
3.2.5	Metadynamics Simulations of γ -Secretase complexes	123
3.2.6	Identification of Low-Energy States of γ -Secretase complexes	124
3.2.7	Binding free energy calculations	124
3.3	RESULTS.....	125
3.3.1	Derivation of path between APP-bound and Notch1-bound PS1 γ	125
3.3.2	WTMetaD of PS1 γ and PS2 γ bound to APP substrates	125
3.3.3	Binding free energies of γ -secretase - APP bound complexes	129
3.3.4	Per residue decomposition of binding free energies for γ -secretase-APP bound complexes	130
3.3.5	WTMetaD and binding free energy calculations for PS1 γ and PS2 γ bound to Notch1 substrates.....	139
3.3.6	Per-residue decomposition of binding free energies for γ -secretase – Notch1 bound complexes.	141
3.4	DISCUSSION	146
3.5	REFERENCES.....	150
3.6	SUPPLEMENTAL FIGURES	156
4	ASSESSMENT OF PRESENILIN EXPRESSION IN HUMAN BRAIN TISSUE AND CNS RELATED CELL LINES	164
4.1	INTRODUCTION.....	164
4.2	MATERIALS AND METHODS	165

4.2.1	Human Brain Tissue Preparation.....	165
4.2.2	Cell Culture.....	166
4.2.3	CRISPR-Cas9 Presenilin Knock-Out	166
4.2.4	Neuroblastoma Differentiation	168
4.2.5	Sample Preparation	168
4.2.6	PAGE and Western Blotting.....	169
4.2.7	Endogenous Presenilin Quantitation.....	169
4.2.8	Quantitative PCR	170
4.2.9	Statistical Analysis.....	170
4.3	RESULTS.....	170
4.3.1	PS1 and PS2 protein expression in human brain tissue	171
4.3.2	Comparison of PS1 and PS2 expression profiles in neuronal and microglial cells 178	
4.3.3	PS1 and PS2 expression response to differentiation in neuroblastoma cell lines 182	
4.4	DISCUSSION	183
4.5	REFERENCES.....	187
4.6	SUPPLEMENTAL TABLES.....	194
4.7	SUPPLEMENTAL FIGURES	196
5	DIFFERENTIAL FUNCTIONS OF PRESENILIN-1 AND PRESENILIN-2 IN HUMAN MICROGLIA.....	199
5.1	INTRODUCTION.....	199
5.2	MATERIALS AND METHODS	201
5.2.1	Mammalian Cell Culture.....	201
5.2.2	DAPT treatments	201
5.2.3	LPS treatments	201
5.2.4	Cell Morphology	202
5.2.5	Bead Phagocytosis	202
5.2.6	A β Preparation and Phagocytosis	203
5.2.7	LPS Treatment and Cytokine and Chemokine Bead Array Assays.....	204
5.2.8	RNA and Protein Sample Preparation	204
5.2.9	Quantitative PCR	205
5.2.10	Immunoblotting.....	205
5.2.11	Bulk RNA Sequencing Analysis.....	208
5.2.12	Statistical Analysis.....	208
5.3	RESULTS.....	209
5.3.1	HMC3 cell response dampened in comparison with BV2.....	209
5.3.2	HMC3 PS2+ cells show altered morphology	210
5.3.3	HMC3 PS2+ cells show increased phagocytic capacity	212
5.3.4	PS1 and PS2 differentially regulate pro-inflammatory response to LPS and α A β 214	
5.3.5	Presenilin modulates A β degrading enzyme expression.....	216
5.3.6	γ -Secretase substrates associated with AD related microglial function are regulated by presenilin.....	218
5.3.7	Transcriptomic analysis identifies gene groups of interest in differential functional responses of PS1+ and PS2+ microglial cells.	220
5.4	DISCUSSION	228

5.5	REFERENCES.....	235
5.6	SUPPLEMENTARY TABLES.....	245
5.7	SUPPLEMENTARY FIGURES.....	254
6	BIOPHYSICAL CHARACTERISATION OF WILDTYPE AND MUTANT γ -SECRETASE BINDING TO SUBSTRATES ASSOCIATED WITH β -AMYLOID REMOVAL.....	258
6.1	INTRODUCTION.....	258
6.2	MATERIALS AND METHODS.....	261
6.2.1	Substrate selection.....	261
6.2.2	WTMetaD simulation of γ -secretase complexes.....	264
6.2.3	Mutation selection.....	265
6.2.4	Thermodynamic integration.....	267
6.2.5	Assessment of variant classification.....	268
6.2.6	Statistical analysis.....	268
6.3	RESULTS.....	268
6.3.1	WTMetaD and MM-GB/SA assessment of validation substrates.....	268
6.3.2	PS1 γ and PS2 γ form conformationally distinct complexes with A β metabolism related substrates.....	270
6.3.3	Evaluation of alchemical perturbation for classifying the disease association of variants in γ -secretase.....	274
6.3.4	Determination of pathogenicity by alchemical perturbation of PS variants on A β metabolism related substrates.....	276
6.3.5	PS1 mutation $\Delta\Delta G_{mut}$ for APP-CTF(A β 49) correlates with AAO.....	278
6.4	DISCUSSION.....	282
6.5	REFERENCES.....	289
6.6	SUPPLEMENTAL TABLES.....	299
6.7	SUPPLEMENTAL FIGURES.....	300
7	GENERAL DISCUSSION.....	313
7.1	GENERAL LIMITATIONS.....	319
7.2	FUTURE STUDIES.....	320
7.3	GENERAL CONCLUSION.....	321
7.4	REFERENCES.....	322

LIST OF TABLES

Table 1-1 Summary of molecular modelling studies of PS- γ -secretase complex	21
Table 2-1 qPCR primer sequences.....	84
Table 2-2 Antibody conditions for immunoblotting.....	85
Table 3-1 MM-GB/SA binding free energy of γ -secretase – APP bound complexes	130
Table 3-2 MM-GB/SA binding free energy of γ -secretase – Notch1 bound complexes.....	141
Table 4-1 CRISPR-Cas9 gRNA target sequences for PS1 and PS2 knockout	167
Table 5-1 Top 10 most significant genes for PS1+ vs PS2+ differential gene comparison ..	226
Table 5-2 Top 5 up and down regulated genes for PS1+ vs PS2+ differential gene comparison	227
Table 6-1 A β metabolism substrate function.....	263
Table 6-2 Energy minima parameters for validation substrates	272
Table 6-3 Energy minima parameters for A β metabolism related substrates in kcal/mol.....	272
Table 6-4 Effect of PS mutations on relative binding free energy (kcal/mol) for γ -secretase bound to APP-CTF	275

LIST OF FIGURES

Figure 1-1 Canonical APP cleavage pathways	4
Figure 1-2 The protein components of γ -secretase, and complex assembly.....	11
Figure 1-3 The evolution of the resolution of γ -secretase	17
Figure 1-4 PS1 and PS2 publication and expression patterns.....	29
Figure 1-5 γ -Secretase substrates perform a wide array of functions.....	32
Figure 1-6 A β metabolism related substrates of γ -secretase function via multiple mechanisms	35
Figure 2-1 Characterisation of HEK-293 PS1+PS2+, PS1+, PS2+ and PSnull cell lines.	88
Figure 2-2 APP processing by exogenous Myc-tagged PS1 and PS2 in PSnull cells.	90
Figure 2-3 Effect of exogenous PS normalisation on A β generation	91
Figure 2-4 Notch1 processing by exogenous Myc-tagged PS1 and PS2 in PSnull cells.....	92
Figure 2-5 Validation of novel method to directly compare endogenous PS1 and PS2 expression.	95
Figure 2-6 APP processing by endogenous PS1 and PS2 assessed in PS1+ and PS2+ cells. .	97
Figure 2-7 Effect of endogenous PS normalisation on A β generation	98
Figure 2-8 Notch1 processing by endogenous PS1 and PS2 assessed in PS1+ and PS2+ cells.	99
Figure 3-1 APP and Notch1 processing by γ -secretase.	119
Figure 3-2 Well-tempered metadynamics simulations of PS1 γ and PS2 γ in complex with A β 40 pathway substrates.	127
Figure 3-3 Well-tempered metadynamics simulations of PS1 γ and PS2 γ in complex with A β 42 pathway substrates.	128
Figure 3-4 A β 40 pathway complexes per residue heatmaps of $\Delta\Delta G_{PS Pref}$	133
Figure 3-5 Representative structures of substrate – enzyme molecular interactions contributing to $\Delta\Delta G_{PS Pref}$ in A β 40 pathway	134
Figure 3-6 A β 42 pathway complexes per residue heatmaps of $\Delta\Delta G_{PS Pref}$	137
Figure 3-7 Representative structures of substrate – enzyme molecular interactions contributing to $\Delta\Delta G_{PS Pref}$ in A β 42 pathway.	138
Figure 3-8 Well-tempered metadynamics simulations of PS1 γ and PS2 γ in complex with Notch1 substrates.....	140
Figure 3-9 Notch1 complexes per residue heatmaps of $\Delta\Delta G_{PS Pref}$	144
Figure 3-10 Representative structures of substrate – enzyme molecular interactions contributing to $\Delta\Delta G_{PS Pref}$ in Notch1 cleavage.....	145
Figure 4-1 PS1-NTF expression in human frontal cortex and hippocampus regions.....	173
Figure 4-2 PS1-NTF expression in human cerebellum.....	174
Figure 4-3 PS2-NTF expression in human hippocampus, frontal cortex, and cerebellum....	175
Figure 4-4 PS protein unit expression by brain region	177
Figure 4-5 PS1-NTF and PS2-NTF expression in HMC3, M17 and SHSY5Y cells	180
Figure 4-6 PS protein unit analysis in WT and PS deficient cell lines	181
Figure 4-7 Effect of differentiation on PS expression in neuroblastomas	183
Figure 5-1 Functional comparison of BV2 and HMC3 cells.....	210
Figure 5-2 Morphological assessment of HMC3 cells with altered PS genotypes.....	211
Figure 5-3 Bead and oA β phagocytosis in HMC3 cells with altered PS genotypes.....	214
Figure 5-4 Differential cytokine secretion by HMC3 cells with altered PS genotype in response to LPS and oA β treatment	216
Figure 5-5 Expression of A β degrading enzymes in HMC3 cells with altered PS genotype	217

Figure 5-6 Expression of γ -secretase substrates associated with A β removal and microglial phenotypes associated with AD.....	220
Figure 5-7 Transcript expression cluster analysis of HMC3 cells with altered PS genotype	223
Figure 5-8 Differential gene expression analysis of HMC3 cells with altered PS genotypes	223
Figure 5-9 Differential gene expression and pathway analysis of PS1+ and PS2+ HMC3 cells	225
Figure 6-1 Benign and pathogenic variant positions in PS1 and PS2.....	266
Figure 6-2 Validation substrate conformations.....	270
Figure 6-3 Representative complexes for conformational categories.....	273
Figure 6-4 Determination of pathogenic $\Delta\Delta G_{\text{path}}$ cut-off	276
Figure 6-5 Application of $\Delta\Delta G_{\text{path}}$ to assign pathogenicity related to substrate binding.....	277
Figure 6-6 $\Delta\Delta G_{\text{mut}}$ for PS1 γ and PS2 γ mutation complexes bound to APP-CTF substrates correlation with AAO and A β 42:A β 40	279
Figure 6-7 AAO correlation with $\Delta\Delta G_{\text{mut}}$ for PS1 γ mutation complexes bound to A β metabolism related substrates.....	281
Figure 6-8 AAO correlation with $\Delta\Delta G_{\text{mut}}$ for PS2 γ mutation complexes bound to A β metabolism related substrates	282
Figure 7-1 Summary of thesis key findings and outputs	314

LIST OF SUPPLEMENTAL TABLES

SI Table 2-1 List of commercial antibodies for potential use with PS-Std	110
SI Table 4-1 Australian Brain Bank Network donor demographic and pathology.....	194
SI Table 4-2 Wildtype allele specific PCR screening primers	195
SI Table 4-3 qPCR primer sequences	195
SI Table 5-1 qPCR primer sequences	245
SI Table 5-2 Antibody and sample treatment details for immunoblotting	246
SI Table 5-3 Top 10 most significant genes for PS2+ vs PS1+PS2+ and PS1+ vs PS1+PS2+ differential gene comparison	247
SI Table 5-4 Top 5 up and down regulated genes for for PS2+ vs PS1+PS2+ and PS1+ vs PS1+PS2+ differential gene comparison.....	248
SI Table 5-5 KEGG pathway genes specifically activated in PS2+ HMC3 cells.....	249
SI Table 5-6 KEGG pathway genes specifically activated/suppressed in PS1+ HMC3 cells	250
SI Table 5-7 RNASeq differential gene expression for A β degrading enzymes and A β removal related substrates investigated in Figure 5-5 and Figure 5-6.....	252
SI Table 5-8 E3 ligase and E3 ligase adaptor proteins with $\pm 1.5 \text{ Log}_2[\text{FC}]$	253
SI Table 6-1 Effect of pathogenic mutations on change in relative binding free energy (kcal/mol) for γ -secretase bound to A β metabolism related substrates.....	299

LIST OF SUPPLEMENTAL FIGURES

SI Figure 1-1 APP protein and mutation schematic.....	74
SI Figure 1-2 PS1 protein and mutation schematic	75
SI Figure 1-3 PS2 protein and mutation schematic	76
SI Figure 2-1 Characterisation of clonal populations of HEK-293 PS2+, PS1+, and PSnull cell lines.....	111
SI Figure 2-2 Sequence confirmation of CRISPR genetic ablation of PSEN1 and PSEN2..	112
SI Figure 2-3 Copy number variation analysis for HEK-293 PS1+PS2+, PS2+, PS1+ and PSnull cell lines	113
SI Figure 2-4 Exogenous Myc-PS1 and Myc-PS2 transfection titration.....	114
SI Figure 2-5 Validation of PS-Std detection by related and unrelated antibodies	115
SI Figure 2-6 Standard curves for quantitation of endogenous PS1 and PS2.....	116
SI Figure 2-7 High concentration of APP695 transfection causes cell death in PS1+ cells..	117
SI Figure 3-1 Sequence alignments used for homology modelling of substrates.....	156
SI Figure 3-2 Determination of σ for s and z.....	157
SI Figure 3-3 PS1 – APP substrate simulation convergence.....	157
SI Figure 3-4 PS2 – APP substrate simulation convergence.....	159
SI Figure 3-5 PS1 – Notch substrate simulation convergence.....	161
SI Figure 3-6 PS2 – Notch substrate simulation convergence.....	162
SI Figure 3-7 Path derivation between APP and Notch1 bound states.....	163
SI Figure 4-1 Wild type allele PCR screening of CRISPR knockouts	196
SI Figure 4-2 Characterisation of HMC3 PS1KO and PS2KO clones	197
SI Figure 4-3 Characterisation of M17 PS1KO and PS2KO clones.....	198
SI Figure 5-1 RNA sequencing read count and data transformation assessment	254
SI Figure 5-2 GO biological process network maps for clusters where PS2+ and PS1+ HMC3 cells have similar gene expression.....	255
SI Figure 5-3 Basal cytokine secretion by HMC3 cells with altered PS genotype.....	256
SI Figure 5-4 KEGG MAPK signalling pathway	257
SI Figure 6-1 Substrate alignments for homology modelling.....	300
SI Figure 6-2 PS1 γ complex simulation convergence	302
SI Figure 6-3 PS2 γ complex simulation convergence	305
SI Figure 6-4 PS1 γ and PS2 γ complexes are both conformationally 6IYC-like	308
SI Figure 6-5 PS1 γ and PS2 γ complexes are conformationally distinct.....	309
SI Figure 6-6 $\Delta\Delta G$ for PS1 γ and PS2 γ mutation complexes bound to APP-CTF substrates correlation with amount of A β 40 and A β 42.....	311
SI Figure 6-7 AAO correlations with the sum and absolute sum of $\Delta\Delta G$ for PS1 γ and PS2 γ mutation complexes.....	312

LIST OF ABBREVIATIONS

AAO	Age at Onset
AD	Alzheimer's Disease
ADAD	Autosomal Dominant Alzheimer's Disease
ADAM	A Disintegrin and Metalloproteinase
ADAM10	A Disintegrin and Metalloproteinase 10
ADAM17	A Disintegrin and Metalloproteinase 17
A β	Amyloid Beta
A β 38	A β 1-38 peptide
A β 40	A β 1-40 peptide
A β 42	A β 1-42 peptide
A β 43	A β 1-43 peptide
A β 45	A β 1-45 peptide
A β 46	A β 1-46 peptide
A β 48	A β 1-48 peptide
A β 49	A β 1-49 peptide
AICD	APP Intracellular Domain
AP-1	Adaptor Protein-1
AP-2	Adaptor Protein-2
AP-3	Adaptor Protein-3
APH1	Anterior-Pharynx Defective 1 protein
<i>APH1A</i>	Anterior-Pharynx Defective 1 isoform A gene
APH1a	Anterior-Pharynx Defective 1a protein
<i>APH1B</i>	Anterior-Pharynx Defective 1 isoform B gene
APH1b	Anterior-Pharynx Defective 1b protein
APLP2	Amyloid Beta Precursor Like Protein 2
APOE	Apolipoprotein E
<i>APP</i>	Amyloid Precursor Protein gene
APP	Amyloid Precursor Protein
APP-CTF	Amyloid Precursor Protein C-Terminal Fragment.
ARIA	Amyloid-Related Imaging Abnormalities
AUC	Area Under the Curve
AXL	Tyrosine-Protein Kinase Receptor UFO
<i>BACE1</i>	β -APP Cleaving Enzyme-1 gene
BACE1	β -APP Cleaving Enzyme-1 protein
<i>BACE2</i>	β -APP Cleaving Enzyme 2 gene
BACE2	β -APP Cleaving Enzyme 2 protein
BBB	Blood-Brain Barrier
BP	Biological Processes
BV2	Murine BV2 cell line
C3	Complement Component 3
CBA	Cytokine bead array
CBM	Cerebellum
<i>CD200</i>	Cluster of Differentiation 200 gene
<i>CD44</i>	CD44 Antigen gene
CD44	CD44 Antigen protein
CDH2	Cadherin-2
cDNA	Complementary DNA

CFH	Complement Factor H
Chr	Chromosome
CLU	Clusterin (also known as APOJ)
CMV	Cytomegalovirus promoter
CNS	Central nervous system
CNV	Copy Number Variation
CRISPR	Clustered Regularly Interspaced Short Palindromic Repeats
CSL	CBF1-suppressor of hairless-LAG1
CTF	C-terminal fragment.
CXCL	C-X-C Motif Chemokine Ligand
CYL	Cytoplasmic Loop
DAPT	Tert-Butyl(S)-{(2S)-2-[2-(3,5-difluorophenyl)acetamido]propanamido}phenylacetate or GSI-IX
DMEM	Dulbecco's Modified Eagle Medium
DMSO	Dimethyl sulfoxide
DNA	Deoxyribonucleic Acid
E3 ligase	Ubiquitin-Protein Ligase
<i>ECE1</i>	Endothelin-Converting Enzyme 1 gene
ECE1	Endothelin-Converting Enzyme 1 protein
ED	Extracellular Domain
ELISA	Enzyme-Linked Immunosorbent Assay
ENA-78	CXCL5
EV	Empty Vector
FBS	Fetal bovine serum
Fbw7	F-box/WD repeat-containing protein 7
FC	Frontal cortex
FDA	Food and Drug Administration
FDR	False Discovery Rate
FE65	Amyloid Precursor Protein-Binding Family A Member 1
FES	Free Energy Surface
FLIM-FRET Transfer	Fluorescence Lifetime Imaging Microscopy - Förster Resonance Energy Transfer
FTD	Frontotemporal dementia
GaMD	Gaussian Accelerated Molecular Dynamics
GAPDH	Glyceraldehyde-3-phosphate dehydrogenase gene
GAPDH	Glyceraldehyde-3-phosphate dehydrogenase protein
GO	Gene Ontology
GPCR	G Protein-Coupled Receptor
gRNA	Guide RNA
GRO α	CXCL1
GSAP	γ -Secretase Activating Protein
GSI	γ -Secretase Inhibitor
GSK3 β	Glycogen Synthase Kinase-3 Beta
GSM	γ -Secretase Modulator
HDR	Homology-Directed Repair
HEK-293	Human embryonic kidney 293 cells
WT	Wild type
HMC3	Human microglial clone 3 cells
HPC	Hippocampus
HRP	Horseradish peroxidase

HSPs	Heat Shock Proteins
ICD	Intracellular Domain
iCLiPs	Intramembrane Cleaving Proteases
<i>IDE</i>	Insulin Degrading Enzyme gene
IDE	Insulin Degrading Enzyme
IGFBP-4	Insulin-like growth factor binding protein 4
IL-6	Interleukin 6
IL-8	Interleukin 8
IL-18	Interleukin 18
IL-23	Interleukin 23
IL-1B	Interleukin 1 β
INSR	Insulin Receptor
iPSC	Induced Pluripotent Stem Cell
IP-10	CXCL10 or Interferon gamma-induced protein 10
KEGG	Kyoto Encyclopedia of Genes and Genomes
LBD	Lewy Body Dementia
LDLR	Low-Density Lipoprotein Receptor protein
LPS	Lipopolysaccharide
LRP1	Low-Density Lipoprotein Receptor-Related Protein 1 protein
LRP8	Low-Density Lipoprotein Receptor-Related Protein 8 protein
M17	BE(2)-M17 neuroblastoma cell line
MAM	Mastermind
MAPK	Mitogen-Activated Protein Kinase
<i>MAPT</i>	Microtubule Associated Protein Tau gene
MCC	Matthews Correlation Coefficient
MCP-1	Monocyte chemoattractant protein 1 or CCL2
MD	Molecular Dynamics.
MEM	Minimum Essential Medium
MER	Tyrosine-Protein Kinase Mer
MetaD	Metadynamics
MM/GB-SA	Molecular Mechanics/Generalized Born-Surface Area
<i>MME</i>	Membrane Metalloendopeptidase (Nepriylsin) gene
<i>MMP2</i>	Matrix Metalloproteinase 2 gene
MMP2	Matrix Metalloproteinase 2 protein
<i>MMP9</i>	Matrix Metalloproteinase 9 gene
MMP9	Matrix Metalloproteinase 9 protein
mRNA	Messenger RNA
MT5-MMP	Matrix Metalloproteinase MT5-MMPA β
mTOR	Mammalian Target of Rapamycin
MYD88	Myeloid Differentiation Primary Response 88
Na-pyruvate	Sodium pyruvate
<i>NCSTN</i>	Nicastrin gene
NCT	Nicastrin protein
NEP	Nepriylsin
NEXT	Notch1 Extracellular Truncation
NFDM	Non-fat dried milk
NICD	Notch Intracellular Domain.
NMR	Nuclear Magnetic Resonance.
NTF	N-Terminal Fragment
oA β	Oligomeric Amyloid-beta

P2RY12	Purinergic Receptor P2Y12 gene
PAGE	Polyacrylamide gel electrophoresis
PAL motif	Proline-Alanine-Leucine motif
PBS	Phosphate-buffered saline
PCA	Principal component analysis
PCR	Polymerase Chain Reaction
PDB	Protein Data Bank.
<i>PEN2</i>	Presenilin Enhancer-2 gene
PEN2	Presenilin Enhancer-2 protein
PKA	Protein Kinase A
PMEL	Premelanosome Protein
POPC	Palmitoyl-oleoyl-phosphatidylcholine
PPAR γ	Peroxisome Proliferator-Activated Receptor Gamma
PS	Presenilin
<i>PSENI</i>	Presenilin-1 gene
PS1	Presenilin-1 protein
PS1 γ	Presenilin-1 γ -secretase complex
<i>PSEN2</i>	Presenilin-2 gene
PS2	Presenilin 2 protein
PS2 γ	Presenilin-2 γ -secretase complex
PSH	Presenilin/signal peptide peptidase homologue
PS γ	Presenilin Gamma Secretase Complex (both PS1 γ and PS2 γ)
qPCR	Quantitative Polymerase Chain Reaction
RAGE	Receptor for Advanced Glycation Endproducts
Rer1	Retrieval to ER Protein 1
RICD	RAGE Intracellular Domain
RIP	Regulated Intramembrane Proteolysis
RIPA	Radioimmunoprecipitation assay buffer
RMSD	Root Mean Squared Deviation
RNA	Ribonucleic acid
RNAseq	RNA Sequencing
ROC	Receiver Operating Characteristic
ROS	Reactive Oxygen Species
RyR	Ryanodine Receptor
sAD	Sporadic Alzheimer's Disease
SCAM	Substituted Cysteine Accessibility Method
SD	Standard Deviation
SDS	Sodium dodecyl sulfate
SERCA2b	Sarco-/Endoplasmic Reticulum Ca ²⁺ ATPase
SH-SY5Y	SH-SY5Y neuroblastoma cell line subcloned from SK-N-SH
siRNA	Small interfering RNA
SORL1	Sortilin-Related Receptor
SORT1	Sortilin
SREBF1	Sterol Regulatory Element-Binding Protein 1
TBS	Tris-buffered saline
TLR2	Toll-Like Receptor 2
TLR3	Toll-Like Receptor 3
TM	Transmembrane Domain
TMEM119	Transmembrane Protein 119
TMP21	Transmembrane Protein 21

<i>TNFα</i>	Tumor Necrosis Factor α gene
TNF α	Tumor Necrosis Factor α protein
TNFRSR1B	Tumor Necrosis Factor Receptor Superfamily Member 1B
TREM2	Triggering Receptor Expressed on Myeloid Cells 2 gene
TREM2	Triggering Receptor Expressed on Myeloid Cells 2 protein
TSA	Transition State Analogue
TYRP1	Tyrosinase-Related Protein 1
VLDLR	Very Low-Density Lipoprotein Receptor gene
VLDLR	Very Low-Density Lipoprotein Receptor protein
WGS	Whole Genome Sequencing
WNT5A	Wingless-Type MMTV Integration Site Family Member 5A
WTMetaD	Well-Tempered Metadynamics
Δ EhNotch1	Human Notch1 with ectodomain removed
Δ G _{bind}	Binding free energy.
$\Delta\Delta$ G _{mut}	Difference in Binding Free Energy of Mutant Variants
$\Delta\Delta$ G _{PS Pref}	Relative change in binding energy per residue with respect to PS1 γ versus PS2 γ .

1 INTRODUCTION

1.1 ALZHEIMER'S DISEASE

Dementia, including the most common cause - Alzheimer's disease (accounting for 60-70% of cases) - is the seventh leading cause of death worldwide (2019).¹ In Australia, there are over 400,000 people living with dementia and it is the second leading cause of death (2020).² Alzheimer's disease (AD) is a progressive neurodegenerative disorder, with a complex aetiology involving a combination of genetic, environmental and lifestyle factors, that primarily lead to cognitive and memory impairments and changes in behaviour.³ The pathophysiological continuum of AD spans approximately 30 years. The initial prodromal phase, lasting 15 to 20 years, is typified initially by amyloid- β ($A\beta$) deposition in 'plaques' followed by associated neuroinflammation, tau protein accumulation and neurofibrillary 'tangle' formation, accompanied by synaptic dysfunction and neuronal loss, after which the symptomatic phase of cognitive dysfunction and brain volume loss then begins.^{Reviewed in 4, 5}

The protein components of the classical AD hallmarks – tau in neurofibrillary tangles and $A\beta$ in amyloid plaques – have key roles in the progression of the disease. Tau, encoded by microtubule associated protein tau gene (*MAPT*), is a critical component of neuronal axons, and to a lesser degree dendrites,⁶ where it promotes formation and stabilisation of microtubules by its interactions with tubulin.^{7, 8} Tau hyperphosphorylation reduces its affinity for tubulin, leading to reduced structural integrity of microtubules⁹ and increased propensity to accumulate and form neurofibrillary tangles.¹⁰ It is these tangles that correlate closely with the onset of cognitive impairment and disease progression.^{11, 12} However, preceding (and indeed inducing) tau pathology is $A\beta$ pathology, as shown in several *in vivo* and *in vitro* studies demonstrating that tau pathology progression is contingent on $A\beta$ pathology at baseline.¹³⁻¹⁸

$A\beta$ is found in multiple forms. While generated as a monomeric peptide, it aggregates into soluble oligomers, and subsequently into protofibrils and fibrils,^{19, 20} which then deposit, as a primary but not sole component, of senile plaques.^{21, 22} This deposited $A\beta$ is the central premise of the amyloid cascade hypothesis, posited by Hardy and Higgins in 1992.²³ The hypothesis proposes that $A\beta$ deposition is the genesis step, initiating subsequent tau deposition, synaptic and neuronal loss, and cognitive decline. In the decades following, as the field has matured, this hypothesis has been refined to acknowledge the nuanced and complex interrelationships

of diverse pathological mechanisms, and acknowledge the critical role of neuroinflammation.
24, 25

Significant evidence suggests that it is soluble A β oligomers that are the toxic species, inducing a plethora of molecular dysfunctions^{Reviewed in 26} including oxidative stress²⁷ and mitochondrial dysfunction,^{28, 29} disrupting synaptic plasticity and long term potentiation,³⁰⁻³² and directly triggering neuroinflammation.³³ This led to the notion that senile plaques may act as a ‘sink’ by which oligomers might be sequestered and hence render them inert, or alternatively, provide a reservoir for continued the release of toxic species, however a clear determination remains elusive.³⁴⁻³⁶ Furthermore, there is evidence that neuroinflammation is potentiated by senile plaques due to the significant spatial association and gliosis of plaque associated astrocytes and microglia.³⁷⁻³⁹

The pursuit of therapeutics to treat AD, by targeting A β , has recently been buoyed by the positive outcomes of immunotherapies that remove A β load from the brain, and the subsequent FDA approval of aducanumab in 2021^{40, 41} (although this has not been without controversy),⁴²⁻⁴⁵ and more recently, lecanemab.⁴⁶⁻⁴⁸ The trials have revealed that there is a significant but small clinical benefit in slowing cognitive decline. This together with the concern in the field regarding side effects of amyloid-related imaging abnormalities (ARIA) associated with neural oedema and microhaemorrhage,^{49, 50} puts into question the associated risk to benefit ratio of such therapies. The clinical outcomes of these immunotherapies on cognitive ability, however, do confirm A β as a therapeutic target for AD that has the potential to have meaningful impact on patient outcomes. While immunotherapies target removal of A β peptide protofibrils and fibrils from the brain,⁵¹ alternative therapeutic strategies have been aimed at regulating the generation of A β by targeting the secretase enzymes, β -secretase and γ -secretase, an approach that has been difficult to pursue due to their pleiotropic functions.^{52, 53} However, there is somewhat of a renaissance,⁵⁴⁻⁵⁶ with β -secretase inhibitors showing promise by inducing A β clearance by microglia,⁵⁷⁻⁵⁹ and γ -secretase modulators in preclinical studies showing potent reduction of toxic forms of A β .⁶⁰

This chapter will discuss the generation and removal of A β , highlighting the current understanding of underlying mechanisms. With a focus on key components of γ -secretase, the presenilins, this review not only discusses the widely explored A β generation role of γ -

secretase but also the relatively understudied role in A β clearance and degradation. Both these functions of γ -secretase are further explored in this thesis.

1.2 MECHANISMS OF AMYLOID- β METABOLISM

The homeostatic regulation of A β metabolism is a balance between A β generation and clearance mechanisms. Pathological accumulation of A β can occur as the result of either dysregulated A β generation or impaired A β clearance. The mechanistic cause of A β accumulation typically defines the type of AD. Autosomal dominant AD (ADAD) caused by rare mutations in **Amyloid Precursor Protein (APP)**, presenilin-1 (PS1), or presenilin-2 (PS2), is thought to be caused by the dysregulation of the amount and type of A β generated. In the more common sporadic form of AD (sAD) dysregulated A β clearance mechanisms play a crucial role in disease onset and progression.²⁵ Understanding the interplay between A β generation and clearance mechanisms is important for unravelling the complexities of AD, with implications for both sAD and ADAD.

1.2.1 Amyloid- β generation

The precursor to A β , APP is a type I transmembrane protein. While there are multiple isoforms, it is APP-695 that is most abundantly expressed in neural cells.⁶¹ As a type I transmembrane protein, APP can be divided into a large glycosylated N-terminal extracellular domain (ED), transmembrane domain (TM), and a short C-terminal intracellular domain (ICD). While APP is primarily recognised for its involvement in AD, several physiological functions are known, including synapse modulation and neural plasticity,^{62, 63} axonal growth and neural protection,^{64, 65} transcriptional regulation,⁶⁶⁻⁶⁸ and in microglia as an innate antiviral defence mechanism.⁶⁹ These functions are facilitated by either the secreted ED acting as a ligand, the full-length protein functioning as a receptor, interactions with multiple interacting proteins, or the release of the ICD by γ -secretase cleavage.^{Reviewed in 66, 70, 71}

APP is processed by a highly conserved mechanism termed **Regulated Intramembrane Proteolysis (RIP)**,⁷² where transmembrane spanning proteins are cleaved by iCLiPs, a family of **Intramembrane CLeaving Proteases** that includes γ -secretase, signal peptide peptidase family proteases, site-2 protease, and rhomboid proteases. With the exception of rhomboid proteases, RIP is a two-step process where the substrate protein ectodomain is first shed by another protease proximal to the membrane interface, after which the iCLiP cleaves within (or

close to) the membrane.⁷³ Canonical APP proteolytic processing occurs via two pathways: the non-amyloidogenic pathway and the amyloidogenic pathway (Figure 1-1A,B). These pathways are defined by enzymatic ectodomain shedding, with a disintegrin and metalloproteinase domain-containing protein 10 (ADAM10),⁷⁴ the primary α -secretase in the brain, initiating the non-amyloidogenic route, while β -APP cleaving enzyme 1 (BACE1),⁷⁵ the primary β -secretase, initiates the amyloidogenic pathway. Additional non-canonical pathways have been identified, where ectodomain shedding can occur by asparagine endopeptidase, matrix metalloproteinase MT5-MMP, and meprin- β cleavage. With the exception of meprin- β cleavage, the retained APP product is subsequently cleaved by either ADAM10 or BACE1, and so effectively then enters the non-amyloidogenic or amyloidogenic pathway, whereas meprin β cleaves one residues C-terminal of the BACE1 cleavage site generating an N-terminally truncated A β peptide.^{76, 77} and reviewed in 78

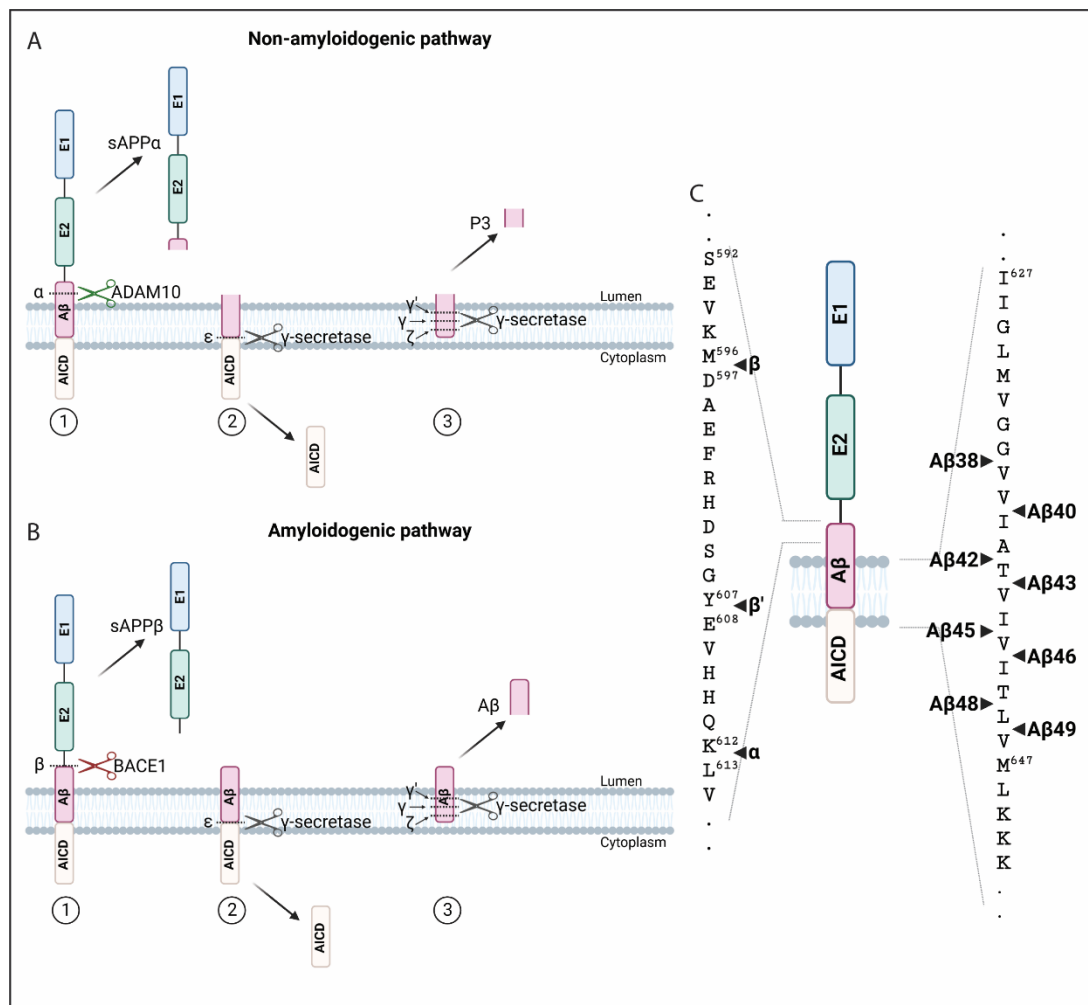


Figure 1-1 Canonical APP cleavage pathways

Non-amyloidogenic cleavage of APP is initiated by ADAM10 ectodomain shedding, at a cleavage position inside the A β peptide sequence, releasing the sAPP α product. The remaining

APP-CTF α product undergoes multiple cleavages by γ -secretase to release the AICD and the non-amyloidogenic P3 peptide (A). The amyloidogenic APP processing pathway is initiated by BACE1 cleavage at the N-terminus of the A β peptide sequence, releasing the sAPP β product. The membrane-retained APP-CTF β product is sequentially processed by γ -secretase; initial cleavage by γ -secretase releases the AICD product, and subsequent cleavages lead to the release of A β products with varying levels of amyloidogenicity (B). Cleavage sites for ADAM10 or BACE1 ectodomain shedding, and predominant cleavage sites for γ -secretase along the A β 40 and A β 42 pathways (C). (Created with BioRender.com)

The N-terminal sequence of A β ^{79, 80} aligns with the BACE1 cleavage site between APP695 residues Met596/Asp597, known as the β -site (Figure 1-1C). Cleavage at this site results in secretion of sAPP β and retention of the remaining β APP-C99 C-terminal fragment (CTF) in the membrane.⁸¹ An additional BACE1 cleavage site at Tyr681/Glu682, known as the β' -site, precludes amyloidogenic A β formation.^{75, 82} While under normal conditions the β' -site is favoured, genetic mutations in APP, hypoxic conditions and increased BACE1 expression shift cleavage to the amyloidogenic β -site.⁸²⁻⁸⁴ ADAM10 cleavage occurs at residues Lys612/Leu613 (known as the α -site) in APP695, yielding the sAPP α product and retention of α APP-C83 CTF in the membrane; this cleavage, 16 residues C-terminal of the β -site, also precludes amyloidogenic A β formation.⁷⁴ Notably, non-amyloidogenic processing typically occurs at the cell surface,^{85, 86} while amyloidogenic processing occurs intracellularly in the endosomal pathway.^{87, 88} Irrespective of the ectodomain shedding mechanism of APP, the retained APP C-terminal fragment (APP-CTF) is further cleaved by γ -secretase.

γ -Secretase is a large tetrameric intramembrane di-aspartyl protease that cleaves APP-CTF at multiple sites within the transmembrane domain.^{89, 90} Initial endopeptidase cleavage by γ -secretase occurs inside the inner leaflet of the membrane, after which 2-3 successive cleavages occur, spaced approximately every three residues (or one helical turn) apart. The initial cleavage, at the ϵ -site, releases the APP-intracellular domain (AICD). Subsequent cleavages at the ζ -site and γ -sites lead to release of tri- and tetra-peptides, and ultimately the release of A β peptides (amyloidogenic pathway) or P3 peptides (non-amyloidogenic pathway) of different lengths, from the luminal membrane leaflet.⁹¹⁻⁹³ This however is a complex processing mechanism, with multiple pathways (Figure 1-1C). γ -Secretase does not cleave a recognised motif, but rather, demonstrates a requirement for key structural features in its substrates.⁹⁴⁻⁹⁸ Initial γ -secretase cleavage typically occurs at one of two ϵ -sites, one residue apart at Leu49/Val50 and Thr48/Leu49 (residue number based on APP-CTF(C99)), which initiate the

two main pathways, resulting in release of the A β 1-40 (A β 40) and A β 1-42 (A β 42) peptides respectively.⁹⁹

Several other A β products of varying length can be produced. The ratios of these A β species are influenced by mutations in both APP and the presenilins (the catalytic components of γ -secretase), typically increasing the formation of longer species,¹⁰⁰⁻¹⁰² and can be modulated by small molecules to generate shorter species.^{60, 102-104} The length of the A β peptide dictates its toxicity and aggregative capacity, with longer peptides (\geq A β 42) being more hydrophobic, driving faster oligomerisation and subsequent aggregation, further acting as aggregation seeds for the predominant A β 40 species.¹⁰⁵⁻¹⁰⁷ Shorter A β species (\leq A β 40) have a reduced aggregative capability; indeed, A β 38 can prevent β -sheet aggregation induced by A β 42.^{106, 108} While initial ED cleavage by BACE1 at the β -site dictates the subsequent generation of A β peptides, γ -secretase processing determines the amyloidogenicity of these peptides.

In addition to APP, notch1, and indeed many other type I transmembrane proteins, also undergo similar RIP processing. Notch1 was confirmed as a substrate of γ -secretase shortly after APP,^{109, 110} and has been crucial to the field in understanding γ -secretase structure and mechanisms of action.

1.2.2 Amyloid- β clearance

Multiple clearance mechanisms have evolved to maintain A β equilibrium in the brain. These are critical, complex, processes that work in concert to prevent pathological A β accumulation. Enzymatic degradation plays a key role, with several enzymes identified as having A β degrading capacity,¹¹¹ primarily neprilysin (NEP)^{112, 113} and insulin degrading enzyme (IDE).^{114, 115} While both NEP and IDE have been shown to prevent amyloid plaque formation,¹¹⁶ a more recent study suggests that NEP is responsible for degrading insoluble parenchymal A β .¹¹⁷ IDE, however, was shown to target soluble, intracellular A β forms,¹¹⁷ which stands to reason given that IDE is a cytoplasmic protein that also rapidly degrades the AICD.¹¹⁸

A β is also degraded by more general cellular protein degradation mechanisms in particular lysosomal degradation, where, after endocytosis, generation in the endocytic pathway, or phagocytosis, the A β is trafficked to lysosomes containing acid proteases and hydrolases.^{111, 119} Phagocytosis is an A β clearance function undertaken by microglia and astrocytes. Specific A β -binding receptors, including triggering receptor expressed on myeloid cells 2 (TREM2) in

microglia,^{120, 121} and receptor for advanced glycation endproducts (RAGE) in astrocytes.¹²² Activation of these receptors induce engulfment and internalisation of A β in phagosomes that then fuse with lysosomes into phagolysosomes, to facilitate degradation.¹²³ Receptor mediated, clathrin and dynamin-dependent endocytosis of extracellular A β and subsequent degradation, has also been shown to occur, in neurons^{124, 125} and astrocytes.¹²⁶

A critical clearance mechanism is the removal of A β from the brain parenchyma for degradation in peripheral organs, including the liver and kidneys. Where it is suggested that up to 60% of brain-derived A β is cleared.^{Reviewed in 127} This occurs via transporter-mediated efflux across the blood-brain barrier (BBB) in a process termed efflux. Various lipoprotein receptor transporters are involved, the most significant being the low-density lipoprotein receptor-related protein 1 (LRP1). LRP1 on the abluminal (brain-facing) side of the endothelial cells in the BBB binds A β peptides. A β is then internalised in endosomes which may then fuse with lysosomes for degradation. A large portion of A β containing vesicles undergo transcytosis and are released into the circulatory system.¹²⁸⁻¹³¹ A counter mechanism also exists where peripheral A β is transported into the brain parenchyma via RAGE.^{129, 132} Additionally, cerebrospinal fluid (CSF) and perivascular glymphatic systems also clear A β from the parenchyma.^{133, 134} Although these mechanisms are still being explored, it is suggested that CSF clearance mechanisms relate to the rate of bulk fluid flow,¹³⁵ while glymphatic clearance is mediated by aquaporin-4 (AQP4).¹³⁶

Several chaperone proteins have also been identified that interact with A β , influencing aggregation and aiding in clearance. Most of these, however, can be considered ‘amateur’ chaperones, as their A β binding functions are secondary.¹³⁷ The primary function of apolipoprotein E (APOE), for example, is in lipid metabolism; however it can also bind A β , accelerating its aggregation into less toxic mature fibrils,^{19, 138} and facilitating clearance of APOE/A β complex by binding to lipoprotein receptors like LRP1.¹³⁹ It is noteworthy that the APOE ϵ 4 variant poses the highest risk for sAD.¹⁴⁰⁻¹⁴² Other examples of ‘amateur’ A β chaperones include clusterin, heparan sulfate proteoglycans, and complement factors, while the quintessential example of ‘professional’ A β chaperones are heat shock proteins (HSPs).¹³⁷ Multiple HSPs have been shown to bind A β , inhibiting aggregation and subsequent toxicity,¹⁴³ and activating microglia to induce phagocytosis.¹⁴⁴

Additional to the APOE $\epsilon 4$ variant, several other genetic risk variants for sAD have been identified in protein coding genes directly associated with A β clearance mechanisms. With variants occurring in *TREM2*, *SORL1* (sortilin-related receptor), *SORT1* (sortilin), *MME* (neprilysin), *CLU* (clusterin), and *ACE* (angiotensin-converting enzyme) they highlight the importance of A β clearance mechanisms and their relationship with sAD.¹⁴²

1.3 THE γ -SECRETASE COMPLEX

1.3.1 The protein components of γ -secretase

The identity of γ -secretase remained somewhat elusive until genetic linkage studies identified novel gene locations of mutations associated with an inherited, autosomal dominant, early onset form of AD (ADAD) in loci other than *APP*. Identified initially on chromosome 14,¹⁴⁵⁻¹⁴⁷ and subsequently on chromosome 1,¹⁴⁸⁻¹⁵⁰ the genes are respectively referred to as PRESENILIN-1 (*PSENI*) and PRESENILIN-2 (*PSEN2*). The protein products are presenilin-1 (PS1, a 467 amino acid protein with a mass of 52 kDa) and presenilin-2 (PS2, a 448 amino acid protein with a mass of 50 kDa), respectively. The genes share 67% sequence similarity,^{147, 148} likely arising from a gene duplication at the root of vertebrate evolution.¹⁵¹ PS1, was confirmed as a polytopic transmembrane protein¹⁵² that is endoproteolysed into two stable fragments, representing the N- and C-terminal fragments,¹⁵³ with two catalytic aspartates obligatory for both endoproteolysis and γ -secretase activity.¹⁵⁴ These same maturation mechanisms were similarly confirmed in PS2.^{155, 156}

The first evidence that γ -secretase was likely a protein complex and not just the singular presenilin proteins came from the recognition that PS1/PS2 endoproteolysis was rate-limited by other cellular components,^{157, 158} and that the fragments of PS1 were forming assemblies that were larger than the combined heterodimer fragments.^{159, 160} Furthermore, mutation of the catalytic aspartates prevented PS1/PS2 incorporation into these high molecular weight complexes, as well as preventing proteolytic processing of APP and Notch.¹⁵⁶ Nicastrin (NCT), a type I transmembrane protein with a large ectodomain decorated with multiple post translation modifications, was then identified in high molecular weight complexes with PS1/PS2. Findings that NCT co-immunoprecipitated with PS1/PS2 and APP-CTF, NCT mutation modulated A β generation, and knockdown of NCT expression impaired Notch

signalling, suggested that nicastrin was a bona fide functional component of a multi-protein complex involved in intramembrane protein cleaving.¹⁶¹

Signalling through Notch1, a critical mediator of developmental cell fate decisions, is contingent on γ -secretase cleavage of the ICD to enable transcriptional regulation. Indeed, presenilin deficiency in mice, *C. elegans*, and *Drosophila* result in an array of developmental phenotypes, that are ultimately embryonically lethal, and mimic Notch deficiency.¹⁶²⁻¹⁶⁹ Consequently, functional genetic deletion screens in *C. elegans* and *Drosophila*, identified anterior-pharynx defective 1 (*APH1*) and presenilin enhancer-2 (*PEN2*) deletions as causing similar phenotypes, suggesting that the protein products may be additional components of the γ -secretase complex.^{170, 171} Shortly thereafter, APH1 and PEN2 were then confirmed as obligatory components of γ -secretase.^{90, 172-176}

While PS1/PS2, NCT, APH1, and PEN2 are critical and sufficient for γ -secretase processing, discrepancies in observed mass (440 – 670 kDa) with the calculated stoichiometric mass of 220 kDa for γ -secretase (based on a component ratio of 1:1:1:1),¹⁷⁷ led to the notion that there were additional proteins interacting with γ -secretase.¹⁷⁸ This led to the identification of TMP21, a member of the p24 cargo protein family.¹⁷⁹ The TM of TMP21 was found to associate directly with PS to modulate the γ -site cleavage specifically,^{179, 180} while not affecting ϵ -site cleavage and subsequent AICD, or Notch ICD (NICD), generation.^{179, 181} Interestingly, another protein, γ -secretase activating protein (GSAP), was identified that specifically interacts with γ -secretase and APP-CTF to increase A β production, and does not interact with Notch-bound γ -secretase.¹⁸² Subsequently, several other proteins have been identified that interact transiently with the γ -secretase complex.¹⁸³⁻¹⁸⁷ These proteins have a variety of canonical functions, including subcellular trafficking, cytoskeletal structural proteins, mitochondrial transport proteins, heat shock chaperone proteins, and cell adhesion molecules,^{184, 186} and demonstrate distinct subcellular environmental signatures.^{184, 186, 187}

1.3.2 γ -Secretase assembly, subunit function, and localisation

The assembly of the γ -secretase subunits into the final tetrameric complex is a highly regulated process. Although still not entirely elucidated, there is evidence that assembly of all of the components occurs in the endoplasmic reticulum (ER), which are then trafficked within the cell as a complete complex.¹⁸⁸ This is also supported by several regulatory structures that retain individual components in the ER, including retrieval to ER protein 1 (Rer1) which has been

shown to regulate ER retention of both NCT¹⁸⁹ and PEN2¹⁹⁰, and the C-terminal residues of PS1 that regulate ER retention and PS1/NCT binding.¹⁹¹ The most likely process of assembly is an initial complex of APH1/NCT forms, followed by sequential binding of PS, and then PEN2 in the ER prior to trafficking and maturation (Figure 1-2).^{174, 188, 192} The stability of the individual components relies on complex formation, and the loss of any component leads to reduced levels of all of the other protein constituents.^{173, 192-194} These four critical components have distinct roles in the γ -secretase complex.

APH1, a seven TM multi-pass membrane protein,¹⁹⁵ is the scaffolding protein upon which γ -secretase is assembled (Figure 1-2A). It is critical for complex stability, binding directly with NCT and PS holoprotein. In addition it regulates NCT glycosylation, PS endoproteolysis and is required for an active γ -secretase.^{172, 173} Two key regions of APH1 regulate γ -secretase assembly and activity: the conserved GXXXG motif in TM4,¹⁹⁶ and the conserved polar residues His171 and His197 residues in TM5 and TM6.¹⁹⁷ The cryoelectron microscopy (cryoEM) atomic structure of γ -secretase has revealed that these regions of APH1 are in close proximity to the C-terminus of PS, where it binds with APH1.^{198, 199} These structures confirm that the C-terminus of PS does indeed penetrate into the membrane as speculated, binding directly with APH1 as opposed to NCT, and so implicates APH1 in the regulation of PS release from the ER, rather than NCT.¹⁹¹ In humans there are three APH1 isoforms that are denoted, APH1a [long (APH1a^L) and short (APH1a^S) splice variants]^{170, 172} and APH1b.^{170, 171} Mice have an additional APH1 homologue, APH1c.²⁰⁰

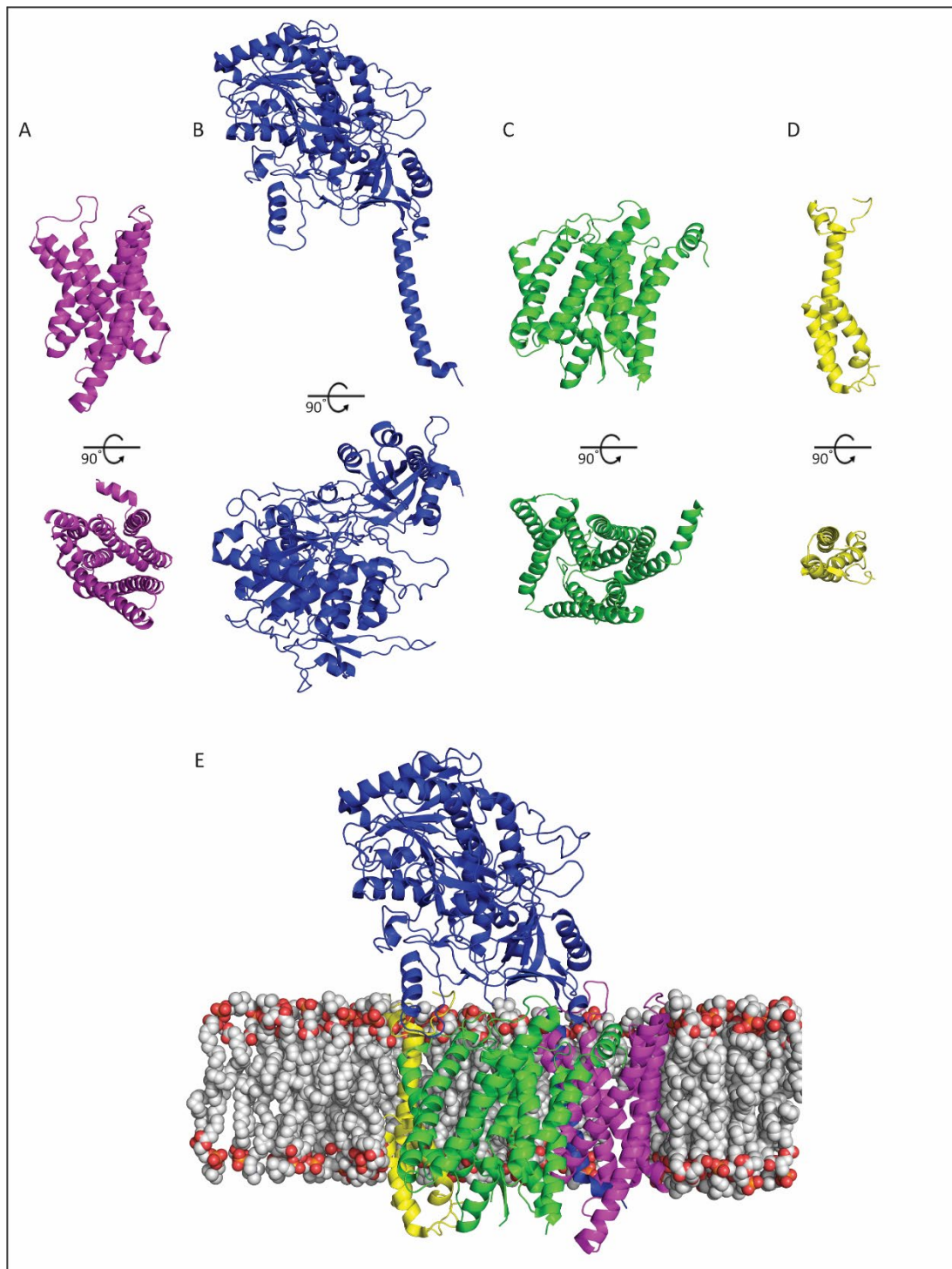


Figure 1-2 The protein components of γ -secretase, and complex assembly

γ -Secretase component structures from the γ -secretase complex with Notch1 (PDB:6IDF) shown individually, APH1 (A), NCT (B), PS (C), and PEN2 (D), and in complex (E) where APH1 = magenta, NCT = blue, PS = green, PEN2 = yellow. Note PDB:6IDF PS homologue is PS1, and APH1 is APH1a. The PS1 cytoplasmic N-terminal domain and large cytoplasmic loop were unable to be resolved. Notch1 substrate removed to show only γ -secretase. Images prepared using PyMOL.²⁰¹

NCT is a 709-residue type I transmembrane protein, with a large glycosylated ectodomain. It does not bind directly to PS; rather, the TM binds predominantly with the APH1 TM1, and in part TM7, while a portion of the ectodomain interfaces with the PEN2 C-terminus.^{198, 199} Trafficking-dependent maturation of NCT by N-glycosylation correlates with, and is necessary for, γ -secretase activity,²⁰² modulates PS binding,²⁰³ and is important for complex stability.¹⁹⁴ Although NCT has been suggested to be a substrate recognition receptor for γ -secretase,²⁰⁴ recent evidence suggests that it uses its large ectodomain to sterically hinder the binding of substrates that have not yet undergone ectodomain shedding.⁹⁴ Exosites involved in substrate recruitment have been identified on NCT; however, these sites are predominantly found in the TM regions of PEN2 and PS, implicating multiple components in the regulation of substrate binding.²⁰⁵ NCT also binds to APP-CTF but this process is likely stabilising the substrate within the binding channel, and indeed is important for modulating the γ -site cleavage events.²⁰⁵⁻²⁰⁷ Interestingly, although APH1/PS1/PEN2 complexes can occur in the absence of NCT, such complexes are unstable, with 50% less activity.²⁰⁸ However, an interesting observation from this study was that even in the absence of NCT, ectodomain shedding was still required for γ -secretase activity. This may suggest that although a substrate with a retained ectodomain should theoretically be able to bind in the absence of NCT, the large ectodomain of substrates likely impedes stable binding and turnover of the substrate. Proteolysis by γ -secretase is an 'unusually slow' process compared to other proteolytic enzymes.²⁰⁹ A potential reason may be due to NCT having evolved to ensure efficiency of substrate processing, by preventing substrates from binding unless the N-terminal domain is an appropriate length.

Compared to the other components, PEN2 is a smaller 101 residue protein which has three TMs. TM1 and TM2 are short and only traverse part way through the membrane at the inner leaflet, while TM3 spans the entire membrane. Here, the PEN2 C-terminus interfaces with NCT on the luminal juxtamembrane while the PEN2-PS interface is formed from hydrophobic interactions.^{198, 199} PEN2 regulates PS endoproteolysis, a process that is essential for γ -secretase activity. Assembly of PEN2 into γ -secretase is critical for the PS holoprotein to be cleaved into the PS-NTF and PS-CTF fragments, and subsequently stabilises the PS heterodimers in the γ -secretase complex.^{210, 211} The PEN2 TM1 region²¹² and C-terminal domain sequence^{213, 214} are binding sites for PS and NCT respectively, and are critical for stabilising γ -secretase and facilitating PS endoproteolysis.^{198, 199} Binding of PEN2 to PS is also critical for PEN2 stabilisation, as it is rapidly degraded by proteasomal degradation in the absence of PS,^{215, 216} and influences the ratio of PS1 versus PS2 γ -secretase complexes.²¹⁷

PS1 and PS2 are nine TM integral membrane proteins, with a large cytoplasmic N-terminal domain, large intervening hydrophilic loops between TM1 and TM2, and TM6 and TM7, and a luminal C-terminal tail that is embedded in the membrane and binds to APh1.^{198, 218, 219} Although PS1 and PS2 are topologically similar, the N-terminal domain and cytoplasmic loops vary in length. The N-terminal domain is six residues longer in PS2, which contains an endosomal localisation motif,²²⁰ while the large cytoplasmic loop is 25 residues longer in PS1. These are also the regions with the greatest sequence divergence between the two homologues.²²¹ The cytoplasmic loop is the site of auto-endoproteolysis, in the sequence encoded by exon 9, which contains a hydrophobic region suggested to act in a 'plug'-like manner, blocking the active site.^{93, 222} This notion was supported by the identification of the PS1- Δ E9 mutation, which lacks the exon 9 region and was not endoproteolysed¹⁵³ but still able to cleave substrates, albeit with reduced activity.²²³ Once the γ -secretase complex is assembled, this 'plug' is cleaved, in a processive manner comparable to the tri-peptide processing of APP-CTF, producing the NTF and CTF heterodimer fragments of PS, and ultimately activating the γ -secretase enzyme.⁹³ The catalytic aspartates are located in TM6 (PS1:Asp257, PS2:Asp263) and TM7 (PS1:Asp385, PS2:Asp366), such that one aspartate is retained in each fragment of the heterodimer, and are positioned in the inner leaflet proximal to the membrane boundary. Both aspartates are obligatory for auto-endoproteolysis and substrate cleavage.^{89, 154} The TM7 catalytic aspartate is part of a conserved GXGD motif, in which the glycine residues are also critical for γ -secretase activity, while residue X plays a role in substrate selectivity, where mutation of the wild-type human leucine residue does not affect APP-CTF cleavage, but impedes Notch cleavage.²²⁴⁻²²⁶ The PAL motif in TM9, evolutionarily conserved in presenilin homologues, has also been shown to be critical for γ -secretase activity,^{227, 228} suggested to influence the catalytic pore conformation,^{229, 230} a role which is now confirmed by atomic structures.^{198, 231, 232}

The two mammalian PS homologues form distinct γ -secretase complexes (herein referred to as PS1 γ and PS2 γ). However, with the presence of APh1 homologues and isoforms, a number of combinations can be generated. Each of the APh1 isoforms form distinct γ -secretase complexes, thus six discrete types of γ -secretase complex can form, all capable of generating A β .^{192, 233} While functional redundancy of both human PS1 and PS2 in rescuing the egg laying phenotype of *C. elegans* caused by loss of the PS homologue *sel-12*, a PS homologue, in *C. elegans*, has been shown,²³⁴ PS1 γ and PS2 γ specific differences have been demonstrated. This includes specific substrate cleavage preferences^{220, 235-237} and the existence of distinct protein

interactomes for PS1 γ and PS2 γ distinct protein interactomes.¹⁸⁴ APH1b has also been suggested to be redundant, as APH1b knockdown, unlike knockdown of APH1a, has no effect on the expression of the other γ -secretase components or processing of APP-CTF.¹⁹²

Recently, both the specific PS and APH1 components have been shown to be key factors in γ -secretase localisation.^{220, 238} Although γ -secretase subunits are synthesised and assembled in the endoplasmic reticulum, the complex is trafficked to other intracellular locations, where the mature γ -secretase is active.¹⁸⁴ PS1 γ complexes localise predominantly at the plasma membrane,^{220, 238} while PS2 γ complexes are localised to intracellular compartments in the trans-golgi network, recycling endosomes, late endosomes and lysosomes.^{220, 238} Interestingly, the intracellular compartmentalisation of PS2 γ is influenced by the specific APH1 component.²³⁸ The PS2 N-terminus contains an acidic-dileucine sorting motif – not present in PS1 – that is common in proteins that bind the AP-1 sorting complex, thereby promoting the trafficking of PS2 γ complexes to late endosome/lysosome compartments. The role of the N-terminal regions of the presenilins in γ -secretase sorting was confirmed when the PS1 and PS2 N-terminus sequences were swapped to the alternate homologue sequence, resulting in exchanged localisation;²²⁰ consequently, the internal localisation of PS2 γ contributed to the intracellular A β pool. Intracellular A β accumulations occur very early in AD pathogenesis, preceding plaque deposition,²³⁹ and are suggested to be the initiator of neuritic plaque formation.²⁴⁰⁻²⁴² Intracellular A β , however, is technically challenging to detect and quantify accurately; thus, its role in AD pathogenesis is likely underestimated.²⁴³

1.3.3 Structural determination of γ -secretase

As a large tetrameric integral membrane complex it has been challenging to solve the atomic structure of γ -secretase. The field's early understanding of the conformational complexity of γ -secretase was determined by multiple approaches. Fluorescence Lifetime Imaging Microscopy - Förster Resonance Energy Transfer (FLIM-FRET) methods were used to elucidate the global dynamics of PS1-NTF and -CTF proximity. This approach identified an “open” wild-type conformation and the effect of inherited mutations, which cause a tighter “closed” conformation of PS1.²⁴⁴⁻²⁴⁶ Photoaffinity labelling probes were used to identify the active site,^{247, 248} demonstrating that PS1 mutations affect the conformation of the active site binding pocket,²⁴⁹ and that loss of GSAP expression increased the distance between PS1-NTF and PS1-CTF, disrupting active site conformation.²⁵⁰ Substituted cysteine accessibility method (SCAM) was instrumental in elucidating the catalytic pore conformation, solvent accessibility,

and specific residues involved in inhibitor binding.^{230, 251} A series of complementary studies identified that the catalytic pore was composed of TM6 and TM7,²⁵¹ TM9,²³⁰ TM1,²⁵² and in part TM4 and TM5.²⁵³ The TM composition of the pore has largely been confirmed by subsequent cryoEM structures. Additionally, a key role for the intervening hydrophilic loop between TM1 and TM2 in substrate gating, and multiple substrate binding sites that differentially influence ϵ - and γ -cleavage of APP has were also identified by SCAM.²⁵⁴

The complete γ -secretase structure has eluded crystallisation, although some individual component orthologues have successfully been resolved by X-ray crystallography.²⁵⁵⁻²⁵⁷ The γ -secretase complex has however, been more amenable to electron microscopy methods (Figure 1-3).^{198, 199, 207, 231, 232, 258-266} The first cryoEM structure of γ -secretase was solved in 2006, revealing the general structure of the subunit assemble at low resolution.²⁵⁸ Over the next decade another eight low resolution structures were solved.^{259-262, 264} While these structures lacked the resolution to provide any detail regarding secondary structure, they provided insight into the global structure of the complex, and some consistent features began to emerge. The complex structure transitioned from a flat heart shape with a large internal cavity,^{258, 259} to a bi-lobed structure. One lobe was the membrane-embedded portion of the complex with a water accessible central pore and a lateral opening/cleft, while the second lobe was the extracellular ‘head’ structure of NCT.^{261, 262, 264} Large scale conformational changes were observed when the complex was bound to γ -secretase inhibitors; specifically, the NCT head structure hinged or rotated, altering the compactness of the complex.^{262, 264} Additionally, the lateral opening/cleft, which was suggested to be a likely substrate binding route, was closed.²⁶² These structures thus presented a relatively heterogenous set of conformations, which provided significant insight into the dynamic nature of γ -secretase.^{263, 264}

A substantial improvement in resolution was achieved by two studies. Lu et al., who improved resolution to 4.5 Å by replacing digitonin with amphipol, in an effort to minimise the effect of the disordered detergent molecules, and strict image selection (only 6% of particles were used for image reconstruction). All 19 α -helical TMs were able to be assigned, while β -strands structures in NCT and some side-chain densities were also resolved (EMDB: 2677).²⁶³ In their subsequent study, T4 lysozyme was fused to the N-terminus of PS1 in an effort to stabilise the TM regions. While this resulted in a marginal global improvement in resolution, there was a marked improvement in the resolution of the TMs, allowing an improved understanding of the specific associations between the individual protein subunits (PDB: 4UIS).²⁶⁵ Combined, these

two structures provided a significantly improved understanding of the complexity of the γ -secretase structure, identifying the seminal horseshoe structure of the transmembrane region of the complex. Furthermore, they confirmed close conformational similarity between the human PS1 structure and the presenilin/signal peptide peptidase homologue (PSH) from the archaeon *Methanoculleus marisnigri*.^{255, 265}

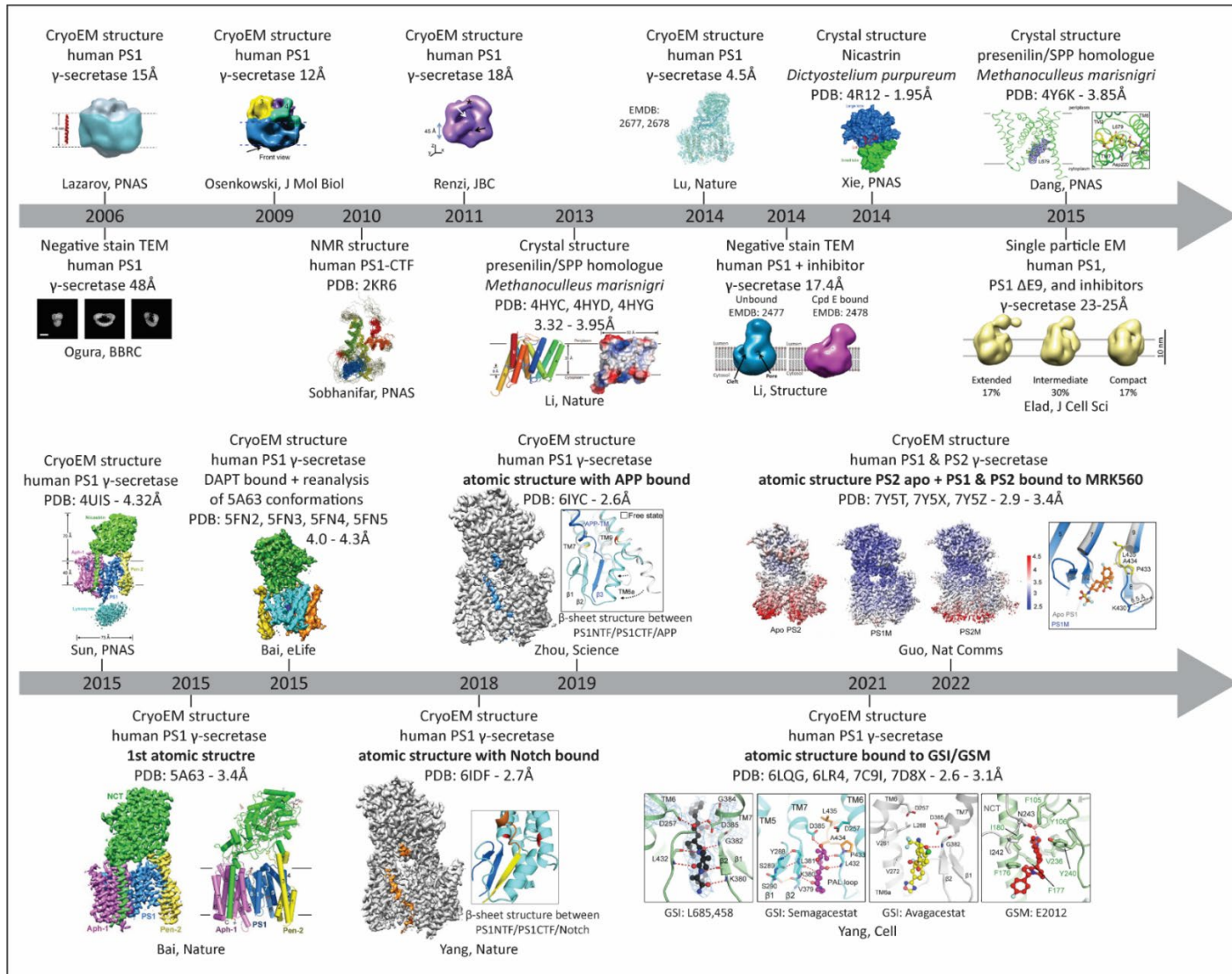


Figure 1-3 The evolution of the resolution of γ -secretase

Timeline representation of all solved structures of γ -secretase either as a whole complex or as individual components.

All high resolution γ -secretase structures have been published by the Shi group, with the first atomic structure released in 2015, a PS1 γ apo structure providing detailed insight into the specific intra- and inter-molecular interactions of the different components of γ -secretase.¹⁹⁸ Multiple PS1 γ structures have subsequently been published that continue to improve the fields understanding of this unique enzyme. Significant insight has been revealed regarding the enzymes interaction with substrates^{231, 232} and location of small molecule inhibitors and modulators.^{199, 207, 266} Most recently, PS2 γ structures have been determined enabling further structural insight into the differences between PS1 γ and PS2 γ .¹⁹⁹

The substrate-bound PS1 γ structures reveal several global conformational changes that are likely common to all substrates. In the apo state of PS1 γ , TM2 remained unresolved due to its dynamic nature, a characteristic that suggested its involvement in substrate binding. However, upon binding with either APP-C83 or notch-100, TM2 undergoes a conformational change, transitioning from a dynamic to a more stabilised state.^{198, 231, 232, 266} PS1 TM2, along with TM3, TM5, TM6, and TM7, forms the central pore with the substrate traversing the membrane. PS1 TM6, another dynamic feature in free PS1 γ , similarly stabilises when bound to substrate, but not before the inner membrane portion is unravelled and forms a rigid coil, followed C-terminally by a short α -helix (termed TM6a). Furthermore, within PS1, in the juxtamembrane region near the central substrate binding pore, additional residues (4 residues in NTF, 3 residues in CTF) of the formerly disordered cytoplasmic loop structure found in free γ -secretase, adopt an ordered conformation. This ordered state is characterised by the formation of two β -strands: one at the C-terminus of TM6 (β 1) and the other at the N-terminus of TM7 (β 2), both within the cytoplasmic loop structure.^{231, 232} Strikingly, the C-terminal portion of both APP-C83 and Notch-100 TM unwinds when bound to PS1 γ , forming a short β -strand (β 3). These β -strands form an antiparallel hybrid β -sheet, exposing the cleavage site, and stabilising the substrate C-terminus region.^{231, 232, 267} The N-terminus of the substrate binds to a hydrophobic pocket on the underside of the NCT head structure, stabilising the N-terminal coil while the intervening TM structure remains α -helical.^{231, 232} No substrate interactions or substantial conformational alterations were observed in PEN2 or APH1a as a consequence of substrate binding.

The large-scale global conformations observed, shared in both APP-C83 and notch-100 binding, are likely universal characteristics regardless of the substrate. However, structural rearrangements in the substrate binding region of PS1 were observed to differ between the binding of APP-C83 and notch-100.²³² There is a shift in positioning of structure from the C-

terminal half of TM2 to the N-terminal half of TM3, and the large hydrophilic loop between TM1 and TM2 exhibits a different conformation. These alterations in conformation are accounted for by distinctions between the APP-C83 and notch-100 sequence, particularly in the TM region, where notch-100 has four aromatic residues while APP-C83 has none, consequently the APP-C83 TM is narrower.²³² Additionally, the interaction between PS1 and each substrate is facilitated by a different set of residues. Leu85, Thr147, and Ile287 specifically bind with APP-C83, while Phe176 and Phe177 specifically interact with notch-100, while the residues that interact directly with both substrates are exemplified by Ser169 and Gly384. Notably, Gly384 is part of the GXGD motif critical for substrate cleavage²²⁴⁻²²⁶ and is adjacent to the catalytic aspartate Asp385, additionally there is an ADAD mutation Gly384Ala, that impedes cleavage of both APP and notch1.²⁶⁸ Furthermore, it's important to note that the Phe176 residue is not conserved between PS1 and PS2, with the analogous residue in PS2 being Leu182 (www.uniprot.org PS1: P49768, PS2: P49810). Although a structure of notch-100, or APP, bound to PS2 γ is yet to be published, the lack of conservation in residues may impact the binding of notch-100, as might other non-conserved residues, particularly those adjacent to residues directly involved in substrate binding.

The most recent structures published include PS1 γ bound to multiple small molecule inhibitors (L685,458, Avagacestat, and Semagacestat, MRK-560) and a modulator (E2012), and the first PS2 γ structures, an apo state and an inhibitor bound structures.^{199,207} These structures highlight the differential residue interactions between the multiple inhibitors, although significant spatial overlap occurs. The transition state analogue L685,458 engages both catalytic aspartates.²⁰⁷ Of the non-TSA inhibitors, only MRK-560 engages the active site¹⁹⁹ Binding of all inhibitors induced the formation of the β_1 and β_2 strands, binding in a position analogous to that of the substrate, forming the hybrid β -sheet, thus blocking substrate interaction.^{199, 207} The E2012 modulator binding was confirmed to bind at an allosteric site previously identified by SCAM, where it binds to Tyr106 in PS1.^{269,270} The phenyl and methylimidazole group of E2012 insert into a pocket formed by the hydrophilic loop between TM1 and TM2, TM3, TM5 and NCT loop that interfaces with PEN2.²⁰⁷ Binding of E2012 has been proposed to cause PS1 TM1 to move in a piston like function upwards in the membrane, increasing the substrate retention time and/or γ -secretase trimming to produce shorter, non-toxic A β peptides.²⁷⁰ Despite PS2 having 67% amino acid sequence similarity with PS1, the apo structures of PS1 γ and PS2 γ exhibit remarkable similarity, showing minor alterations in the positioning of TM6, TM7, and the PAL motif containing loop between TM8 and TM9.¹⁹⁹ It is probable that future substrate-bound

structures of PS2 γ will reveal noticeable distinctions, given the mentioned non-conserved residues and the relatively low residue conservation in TM3,²²¹ a key component of the substrate-containing pore. In support of this, the selective binding of MRK-560 to PS1 γ , which prompts substantial conformational shifts in PS1 γ akin to substrate binding effects, is determined by residues Thr281 and Leu282, which are not conserved in PS2 γ .¹⁹⁹

The availability of γ -secretase structures has significantly enhanced the field's understanding of γ -secretase complex assembly, substrate binding, and the mechanisms of small molecule targeting. However, despite the depth of detail these static snapshots offer, they only scratch the surface of the underlying complexity and subtleties, the details of which are critical for the advancement of therapeutics with greater substrate selectivity and minimal off target effects. Furthermore, it is essential to elucidate the disparities between PS1 γ and PS2 γ , including variations in substrate processing and drug targeting. This understanding is paramount in the quest for optimal drug development. The atomic structures serve as templates for molecular dynamics simulations, enabling exploration of broader conformational changes in γ -secretase, impacting substrate processing and facilitating structure-based drug design.

1.3.4 Modelling γ -secretase

The availability of atomic structures has opened new avenues for investigating the inter- and intramolecular interactions of γ -secretase and its substrates. Molecular modelling methods are powerful tools that provide the opportunity to understand dynamic molecular behaviour at the atomic level, offering insights that are difficult or impossible to currently obtain through experiments alone. Numerous molecular modelling studies have been undertaken since the publication of the first atomic structures of γ -secretase.^{198, 266} These studies have focused on understanding the mechanisms of γ -secretase dynamics, either in the apo state or, subsequently to the publication of APP and Notch bound structures,^{231, 232} in complex with the substrate. Furthermore, the use of molecular modelling has been instrumental in improving the field's understanding of the mechanisms by which the large number of ADAD mutations in PS1, PS2 and APP, may cause aberrant A β generation. The availability of γ -secretase structures has also provided an opportunity to understand the binding modes and mechanisms of action by which γ -secretase-inhibitors (GSI) and γ -secretase-modulators (GSM) exhibit activity, most recently complemented by the publication of PS1 γ bound to small molecules described in the preceding section.²⁰⁷ A summary of all of the computational studies of γ -secretase is presented in Table 1-1.

Table 1-1 Summary of molecular modelling studies of PS- γ -secretase complex

Study type¶	State	PS	Method§	Key Findings	Ref
PS γ dynamics	Apo	PS1	AA MD	CYL 'plugs' access to catalytic pocket. TM2 and TM6 act as a 'gate' controlling substrate access Mature PS1 with NTF & CTF 'plug' released and 'gate' opened.	271
	Apo	PS1	CG & AA MD	PS1 occupies two conformational states of active site. NCT ED two main movement Up/Down and Left/Right rotation. Three global states identified as compact, intermediate, and extended	272
	Apo	PS1	CG & AA MD	Charged lipids POPE and POPA impede TM1-TM2 loop and TM2 flexibility, likely inhibit activity. PS1 adapts conformation state in response to bilayer thickness. Increased lateral pressure associated with cholesterol favours active state	273
	Apo	PS1	AA MD	NCT ED movements are Up/Down and Left/Right. NCT ED has no effect on conformation or dynamics of membrane bound part of complex. Active/in-active states depend on distance of aspartates Active state is more rigid than in-active state	274
	Apo	PS1 & PS2	AA MD	PS1 γ vs PS2 γ large scale movements of NCT ED and PS-CYL are similar. Tilt angles of the TM2, TM6, TM7 and TM9 helices differ in PS1 γ vs PS2 γ . Suggest PS1 γ and PS2 γ have different substrate processing and substrate channels	275
PS γ dynamics + mutations	Apo	PS2	AA MD & stability tools	CYL between TM6 and TM7 acts as 'plug' impeding access to substrate channel. TM2, TM6, TM7 and TM9 flexibility controls substrate binding channel access and size. Examined all pathogenic PS2 mutations, they destabilise the complex	276
Enzyme-substrate complex dynamics	Apo & A β 40, A β 42, A β (15-55)	PS1	AA MD & substrate docking	Three states of PS1 - 'open', 'semi-open' and 'closed'. Position of TM2/TM3 directly controls access to active site. 'Semi-open' state most favourable for APP docking with increased retention time, 'open' state APP retention time decreased, 'closed' state access is occluded.	277
	Apo vs APP-C99 bound	PS1	AA MD	Two states of PS1 'open' and 'compact'. Binding cavity formed by TM2, TM3, TM5 with TM6 controlling precision and compactness of binding C99. 'Open' state accommodates more T48-L49 and L49-V50 cleavages, initiating both A β 42 and A β 40 pathways, 'Compact' state favours T48-L49 and thus A β 40	278
	APP-C99, A β 49, A β 46, A β 43 bound	PS1	AA MD	Substrates bind in TM2, TM3, TM5 cavity, & are in contact with the PS1 NTF & CTF. NCT ED important binding partner for A β n stabilising the E-S complex. Substrate kinks on entry at 'hinge' region to bypass small loop between TM2, TM3. Combination of unwinding and sliding of substrate required for repositioning scissile bonds.	279
	Apo & unbound APP-C99	PS1	AA MD	Both γ -secretase and APP-C99 cause localised membrane thinning in cholesterol rich membrane. Localised membrane thinning in proximity of TM6 and TM9. Cholesterol critical for association of substrate to PS1 TM6 TM9 exosite	280

Enzyme-substrate complex dynamics continued	A β 45 & A β 43 bound	PS1	AA MD	Cholesterol influences positioning of substrate between TM2/TM3. Higher cholesterol stabilises TM3 irrespective of substrate. Higher cholesterol increases probability of cleaving A β 45, compared to A β 43.	281
	Apo vs APP-C83 bound	PS1	pH-REMD	Apo state PS1 γ both D257 and D385 are unprotonated. APP-C83 bound state D385 is protonated aspartate	282
	Apo vs APP-C99, APP-C83, and Notch bound	PS1	AA MD	Substrate regulates global PS1 γ complex dynamics. Longer N-terminal domain substrates are more flexible and have more compact global complex. NCT has more influence on conformation in complexes with longer N-terminal domain substrates	283
	APP-C83 bound & APP-C99	PS1	CG & AA MD	PS1 γ can bind two substrates in parallel one at active site and one at exosite. C-term of substrate bound at exosite can interact with PS1 CYL inhibiting catalysis of active site bound substrate.	284
Enzyme-substrate complex dynamics +ADAD mutations	APP-C83 bound	PS1	GaMD	Activation of PS1 catalytic aspartates, water positioned for proteolysis at the ϵ cleavage site. ADAD mutations in APP I45F and T48P enhance initial ϵ cleavage between residues Leu49–Val50 (A β 40 pathway). APP M51F mutation shifted the ϵ cleavage site to the amide bond between Thr48–Leu49 (A β 42 pathway)	285
	APP-C83 & Notch bound	PS1	AA MD & stability tools	NCT ED Up/Down, Left/Right movement similar for APP-C83 and Notch bound complex. Variation in hybrid- β -sheet, Notch more variable than APP-C83. Asp-Asp distance APP-C83 > Notch, HL1 Notch > APP-C83, PAL motif Notch > APP-C83. TM tilt angles of TM2, TM5, TM6, TM6a different between APP-C83 and Notch. Examined all pathogenic PS1 mutations, they destabilise APP-C83 and Notch similarly	286
	APP-C83 & A β 49 bound	PS1	Pep-GaMD	Investigated the trimming mechanism of γ -secretase processing. C-term residues of A β unwind after cleavage for scissile amide bond access and position the catalytic aspartates. APP mutants, effect distance between aspartates and positioning of the scissile bond. Each mutation has own conformation set and activation pathway.	287
	Notch, C99(49), C99(48), A β 49, A β 46, A β 43, A β 40	PS1	AA MD	Internal binding site in PS1 TM3, TM5 in substrate channel identified at P6/P5 residue position in substrate stabilise substrate N-term of this site is helical, C-term of this site unwinds to position scissile bond. Internal substrate binding site opposes substrate dissociation due to hydrophobic mismatch	288
ADAD mutations	Apo	PS1	Stability tools	Examined all pathogenic PS1 mutations. Mutations effect on PS hydrophobicity, polarity, and stability correlate with A β 42/A β 40	289
	Apo	PS1	CG MD	Pathogenic mutations have allosteric effects on PS1-APH1 and PS1-PEN-2 interface, the catalytic site, substrate entry and docking site	290
	Apo vs APP-C83 bound	PS1	Stability tools	Examined all pathogenic PS1 mutations. PS1 mutations destabilise the Apo and APP bound complex, but do not affect APP binding affinity.	291

	Apo	PS1	Stability tools	Examined all pathogenic PS1 mutations. All tested methods failed to predict pathogenicity.	292
ADAD mutations continued	Apo vs APP-C83 bound	PS1	AA MD	Mutations allosteric to the substrate binding site effect 'open' vs 'closed' conformation equilibrium, by effecting geometry of aspartates, alter the interaction of TM6, TM7, TM9 keeping in 'closed' state, or disturbing TM6, TM7 hinge stability in 'open' state.	293
	APP-C83 bound	PS1	AA MD	Mutations increase complex flexibility. Mutations cause increased aspartate distance, increased distance between Asp and scissile bond, and less dynamic TM6a tilting. Mutants have more variable hydrogen bond networks; several mutations disrupt H-bonding with substrate.	294
	Apo	PS1	QM/MM	Mutations localised in catalytic pore cause structural alteration of active site, and shape of catalytic pore	295
	APP-C83 bound	PS1	GaMD	PS1 ADAD mutations alter positioning of APP-C99 L49 residue in the active site and/or distance between catalytic aspartates. Conformation of active sites vary and are not in same conformation as WT	296
GSI/GSM binding	Apo	PS1	AA MD	Characterised DAPT binding, enters through PS1 TM2, TM3 and interacts with PS1 TM2, TM6, and TM7 hydrophobic residues and with Asp257. Likely alters protonation state of catalytic aspartates, preventing γ -secretase being active. DAPT binding also decreases γ -secretase flexibility	297
	Apo	PS1	AA MD	L-658,458 mimics all substrate binding interactions at the active site forming transition state geometry with catalytic aspartates. Identified likely location of and residues forming the binding pockets S1', S2', S3', near active site which are occupied by chemical groups of L-658,458.	298
	APP-C83 bound	PS1	Docking	Binding site of pyridopyrazine-1,6-dione class GSMs identified between PS1 TM2, TM5, and APP-C83-TM	299
	APP-C83 bound	PS1	Docking & pharmacophore	Virtual screening strategy to identify GSI and GSM using pharmacophore and docking based screening	300
	Apo	PS1 & PS2	Docking & AA MD	Screened benzophenone integrated derivatives as potential GSI class, identified BID-16 as lead compound active against both PS1 and PS2	301

¶ Study type abbreviations are: ADAD = autosomal dominant Alzheimer's disease, GSI = γ -secretase inhibitor, GSM = γ -secretase modulator.

§ Method abbreviations are: AA MD = all atom molecular dynamics, CG MD = coarse grained molecular dynamics, stability tools = protein stability prediction tools (FoldX, I-mutant, POPMUSIC, mCSM), pH-REMD = pH - Replica Exchange Molecular Dynamics, GaMD = Gaussian accelerated molecular dynamics, Pep-GaMD = peptide - Gaussian accelerated molecular dynamics, QM/MM = quantum mechanics/molecular mechanics

Most computational studies of γ -secretase have used molecular dynamics (MD) simulations, and these have provided valuable insight into the structural dynamics of γ -secretase as outlined in Table 1-1. MD is a computational simulation method that enables the behaviour of atoms and molecules to be studied over time, enabling researchers to observe the motion and interaction of atoms and molecules at the atomistic level.³⁰² In general, MD simulations involve integrating Newton's equations of motion to generate atomic positions from velocities over time. Key parameters to be considered in MD include the force field (which describes the potential energy of the system), the conditions of the simulation box (including use of periodic boundary conditions, temperature, pressure, and presence of external fields), and treatment of solvation. Common force fields used in MD simulations of proteins include the AMBER force fields,³⁰³⁻³⁰⁵ CHARMM force fields,³⁰⁶ and GROMOS force fields³⁰⁷; these may be further complemented by force fields for lipids,³⁰⁸⁻³¹⁰ carbohydrates,³¹¹⁻³¹⁵ and small molecules^{316, 317} to simulate a wide variety of biomolecules and protein complexes with molecules of pharmacological interest. Solvation is another critical element in MD simulations, and is often treated explicitly in simulations,³¹⁸⁻³²¹ although may be treated implicitly where speed is of the essence (e.g., in simulations of protein folding).³²²⁻³²⁴

An objective of MD simulations is to broadly sample the free energy landscape of a given molecular system, thus providing insight into the most likely states that will be adopted by that system. The free energy landscape can be considered a representation of all the possible functions of a biological system. It defines the probability of states the system may be found in given a set of environmental conditions, and the possible paths between these states.³²⁵ Unbiased MD simulations are typically limited in their ability to broadly sample possible protein states, due to energy barriers that may be between states, and the simulation timescales that may be required overcome these.³²⁵ This is particularly likely in the case of γ -secretase, given that the complex is large and membrane-embedded.³²⁶ Coarse graining is a method that reduces resolution of the system, by collapsing individual atoms into larger beads, thus allowing longer timescales to be explored for a similar computational cost to all-atom MD.³²⁷ Indeed, coarse graining has been used to understand large scale motions of γ -secretase complexes,^{272, 273, 284, 290} however, this comes at a cost to the detail of the molecular interactions and has typically been coupled with all atom MD.^{272, 273, 284}

Enhanced sampling methods expand the utility of MD simulations by facilitating more extensive exploration of the configurational space of complex systems.³²⁸ γ -Secretase substrate

proteolysis is an extremely slow event with (k_{cat} in proteoliposomes ranges from 1.9 – 4.33 h⁻¹).^{94, 209} In the order to observe the activation of the catalytic site,²⁸⁵ the A β peptide trimming process,²⁸⁷ and the effect of mutations on PS1 γ activation,²⁹⁶ Miao and colleagues have employed Gaussian accelerated molecular dynamics (GaMD).³²⁸ GaMD uses a harmonic boost potential to smooth the energy landscape, accelerating biomolecular simulations significantly, so that slow reactions and events can be observed.³²⁹⁻³³² They found that ϵ -site cleavage requires specific positioning of a water atom in relation to the activated configuration of the catalytic aspartates, and that C-terminal residues of A β generating substrates unwind after cleavage to reposition the subsequent scissile bond for cleavage.^{285, 287} Furthermore, they observed that PS1 mutations affect the presentation of APP cleavage site and alter the configuration of the catalytic aspartates.²⁹⁶

As γ -Secretase is known to bind and cleave a multitude of substrates with diverse sequences³³³ (discussed in more detail below in 1.4.3) it is likely that many, if not all, of these substrates induce different conformations of γ -secretase upon binding. Certainly, the differences observed between the APP- and Notch- bound PS1 γ are evidence of such conformational variation.^{231, 232, 286} The availability of these structures enables the application of the enhanced sampling technique known as metadynamics (MetaD) to explore the conformational potential of substrate bound γ -secretase.^{328, 334} MetaD accelerates the sampling of rare-events by introducing a Gaussian bias potential that reduces the energy barriers between metastable states, and reconstructs the free-energy landscape to reveal energetically favourable states and transition pathways.³³⁵ An improvement on standard metadynamics is well tempered MetaD (WTMetaD) which adaptively reduces the height of the Gaussian bias potential, enabling more efficient convergence of the simulation.³³⁶ WTMetaD is valuable for studying infrequent and complex events, such as protein conformational changes and ligand binding. The success of WTMetaD relies on the selection of suitable collective variables to ensure the simulation is appropriately biased to effectively explore the conformational space.^{328, 334} This method has successfully been applied to G protein-coupled receptors (GPCRs), which similarly are multi-pass transmembrane proteins, to explore the conformational transitions between active and inactive states, and ligand binding.³³⁷⁻³⁴⁰

Molecular modelling studies of γ -secretase have predominantly focussed on PS1 γ in the context of APP binding and processing, with only three studies considering either PS2 γ ,^{275, 276, 301} or Notch substrate binding.^{283, 286, 288} Interestingly, the substrate binding pore TM

conformations were shown to be distinct in PS2 γ , suggesting variations in how PS1 γ and PS2 γ bind substrates, potentially leading to differential substrate processing.²⁷⁵ Furthermore substantial conformational differences were observed between APP and Notch1 substrate binding in PS1 γ .²⁸⁶ This highlights the need for more comprehensive studies focusing on PS2 γ conformations and molecular interactions, particularly with Notch and other substrates beyond APP. A deeper understanding of the conformational ensembles in both PS1 γ and PS2 γ , along with their distinct binding mechanisms, is essential for elucidating potential drug targeting opportunities specific to certain conformations.

Investigating the effects of mutations on a broader range of substrates, rather than just APP, will provide valuable insights into the functional diversity of γ -secretase and its implications for therapeutic interventions. PS mutations have been examined using a variety of methods, including stability tools, GaMD, and all atom MD.²⁸⁵⁻²⁹⁶ A common goal of the computational assessment of PS mutations is to predict the likely level and mechanism of dysfunction, including the effect on substrate-complex interactions. Experimental quantification of the strength of protein-protein binding is achieved by determining the absolute binding energy (ΔG) using biophysical techniques including surface plasmon resonance and isothermal titration calorimetry.³⁴¹ The application of these methods for a large multi-pass transmembrane complex like γ -secretase, however, is challenging and very time consuming, particularly given the number of PS mutations and substrate permutations. While computational approaches can be used to calculate ΔG , they range in accuracy and complexity, from empirical scoring functions (such as those used in molecular docking)³⁴²⁻³⁴⁴ to simulation-based approaches incorporating postprocessing by improved implicit solvation models (such as MM-GB/SA and MM-PB/SA)^{345, 346} or alchemical transformations.^{347, 348} Alchemical approaches represent the “gold standard” for accurate calculation of binding free energies, but have only become accessible in recent years with hardware (i.e., GPU computing capability) and software advances.³⁴⁹

They can be applied to determine both absolute binding free energies (e.g., as would be of interest in drug discovery) as well as relative binding free energies ($\Delta\Delta G$; as would be of interest in protein engineering and studying the effect of natural variations in proteins). Alchemical methods are generally more economical to implement computationally as they do not require direct simulation of ligand unbinding that would be required to replicate the experimental scenario. These methods generally utilise a gradual transformation from some initial state into some final state, reasonably continuously sampled along one or more MD

simulations.^{350, 351} This transformation is typically defined in terms of a coupling parameter, commonly denoted as λ , typically representing the fractional position along the transformation between the initial and final states. In apply alchemical approaches to determining absolute binding free energies for ligands binding to proteins, a common approach is to simulate the ligand in both protein-bound and unbound conformations, and to gradually decouple the ligand interactions from its environment (effectively moving it into a vacuum media). This approach, termed double decoupling,³⁵² is generally impractical for very large ligands, such as proteins, where substantial portions of the system are needed to be decoupled over the simulations. It is also relatively inefficient for exploring the effect of protein mutations on ligand binding, as it requires explicitly simulating all variants of interest; in this scenario, $\Delta\Delta G$ is often of greater interest than ΔG . To more directly facilitate $\Delta\Delta G$ calculations via alchemical approaches, specialised force fields are required that are capable of appropriately “transforming” functional groups within molecules³⁵³ or given protein residues between one another;³⁵⁴ nonetheless, where these are available, high performance in predicting both ligand binding free energies in congeneric series^{353, 355, 356} and classifying the functional impact of natural protein variants can be achieved.³⁵⁷

As yet, alchemical approaches have not been applied to γ -secretase, presenting an opportunity for assessing the impact of mutations, in both PS1 γ and PS2 γ , on the binding of multiple substrates relatively economically, as well as the potential for these approaches to enhance drug discovery at γ -secretase. These avenues of research are critical for advancing our knowledge of PS1 γ verse PS2 γ biology and developing targeted therapeutic strategies.

1.4 THE PRESENILINS: EXPRESSION AND FUNCTIONS

Since the discovery of the *PSEN1* and *PSEN2* genes¹⁴⁵⁻¹⁵⁰ there has been a greater focus on *PSEN1* and the protein PS1 (Figure 1-4A). This is attributable to three key reasons: loss of PS1, but not PS2, expression is embryonically lethal in mice;^{109, 163, 358} significantly more ADAD mutations are found in *PSEN1*;³⁵⁹ and PS1 γ is more active at processing APP and Notch1 than PS2 γ .^{238, 360, 361} Furthermore, the functions of PS1 and PS2 partially overlap,^{162, 166, 167, 362-364} and PS1 and PS2 are known to increase in expression to compensate for the loss of the alternate PS homologue *in vivo*³⁶⁵ and *in vitro*.^{364, 366-368} Understanding the biological functions of PS1

and PS2 is further complicated by their roles independent of their enzymatic functions within γ -secretase. This section outlines the multifaceted roles of PS1 and PS2.

1.4.1 Expression profiles of PS1 and PS2

PSEN1 and *PSEN2* transcripts exhibit low tissue specificity, with ubiquitous expression (Figure 1-4B,C). However, their expression levels differ across various tissues. Notably, *PSEN1* is typically expressed at higher levels than *PSEN2*, with this difference particularly pronounced in the brain and gastrointestinal tract (www.proteinatlas.org).³⁶⁹ Closer examination of the *PSEN1:PSEN2* expression ratio in different tissues reveals that the spinal cord has the highest ratio, indicating greater *PSEN1* expression, while the pancreas exhibits the lowest ratio, suggesting higher *PSEN2* expression (Figure 1-4D). At single cell resolution *PSEN1* is enriched in oligodendrocytes and monocytes, whereas *PSEN2* is enhanced in melanocytes, plasma cells, and gastric mucus-secreting cells (www.proteinatlas.org/ENSG00000080815-PSEN1/single+cell+type, www.proteinatlas.org/ENSG00000143801-PSEN2/single+cell+type retrieved on 13/09/2023).³⁷⁰ Additional complexity arises from temporal changes to *PSEN1* and *PSEN2* expression, and the accompanying effect on protein, that are observed. Both PS1 and PS2 undergo dynamic expression changes during development in human³⁷¹ and murine brains,³⁷¹⁻³⁷³ with PS1 peaking during embryonic development and decreasing postnatally.³⁷² Whereas aging mouse brains consistently show a decline in the PS1:PS2 expression ratio,³⁷³⁻³⁷⁷ which is associated with changes in sex hormone expression.^{375, 376} The spatial and temporal expression profiles in cells and tissues support the notion that PS1 and PS2 have overlapping and distinct functionalities.

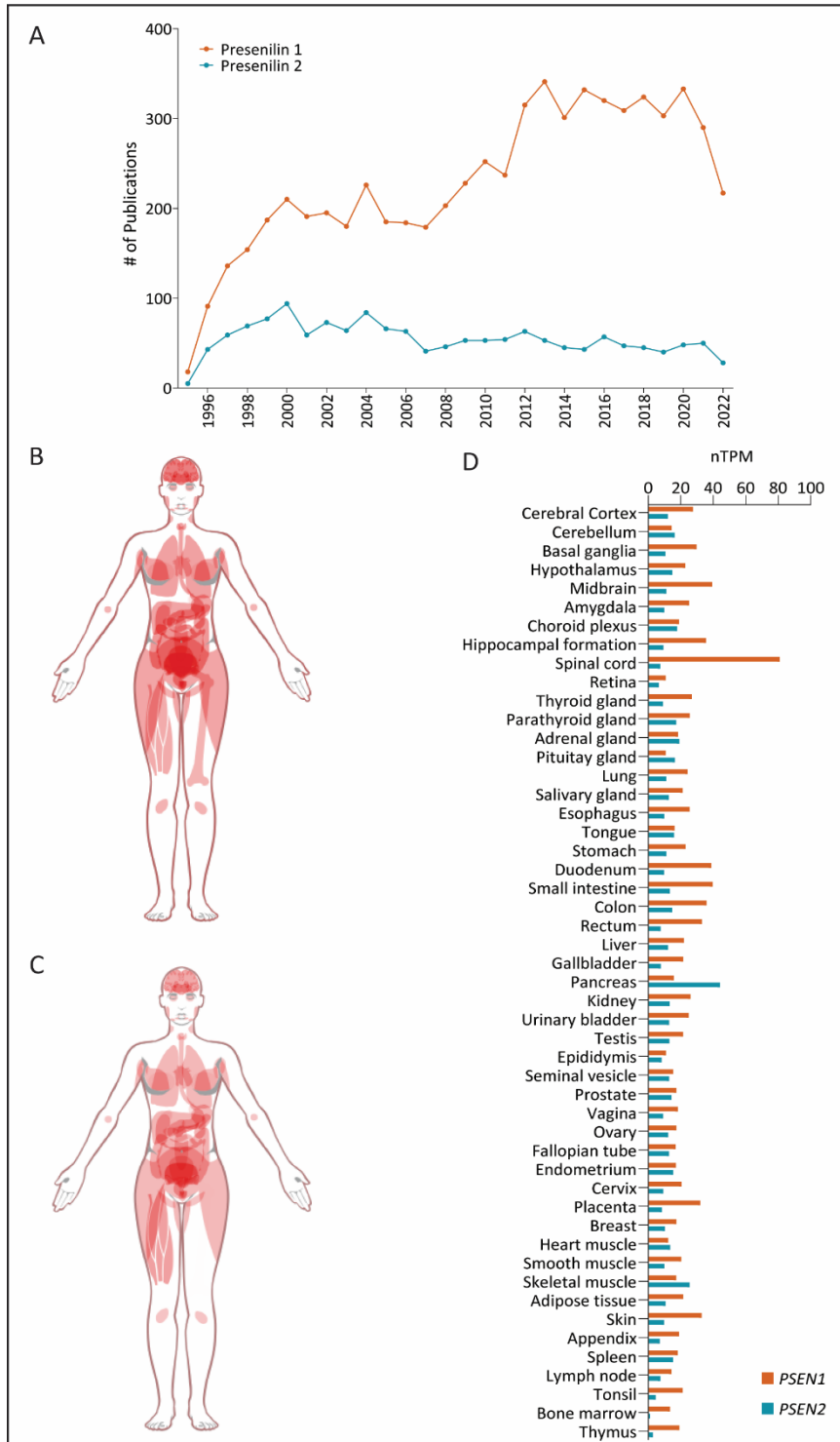


Figure 1-4 PS1 and PS2 publication and expression patterns

Number of publications for PS1 and PS2 in PubMed 1994-2022 (A). Organ distribution patterns of *PSEN1* (B) and *PSEN2* (C) and RNA expression levels in 55 tissues from The Human Protein Atlas consensus dataset (D). Data retrieved from PubMed database (www.ncbi.nlm.nih.gov/) using ‘Presenilin-1’ and ‘Presenilin-2’ MeSH terms on 12/09/2023 (A) and The Human Protein Atlas³⁶⁹ at www.proteinatlas.org/ENSG00000080815-PSEN1/tissue and www.proteinatlas.org/ENSG00000143801-PSEN2/tissue on 12/09/2023 (B-D).

1.4.2 The differing roles of PS1 and PS2 in embryogenesis and neurodegeneration

In murine studies, a vital role for PS1 in embryogenesis has been firmly established. The loss of PS1 expression results in late-stage embryonic/perinatal lethality characterised by impaired skeletal formation and somitogenesis. This outcome closely resembles the effects observed with Notch1 ablation, and is attributed to the absence of PS1 γ -mediated processing of Notch1.^{109, 358} In contrast, loss of PS2 does not have the same effect, resulting in viable pups with no obvious phenotype.^{163, 378} However, heterozygous ablation of PS2 exacerbates the phenotype, leading to more severe defects at the early somite stage and ultimately causing early embryonic lethality at around day 9.5 of development.¹⁶² The observed temporal changes to PS1 and PS2 expression throughout development suggest different functional roles in later life.³⁷¹⁻³⁷⁷

Numerous murine studies provide compelling evidence for the critical role of presenilins in neuronal maintenance and their influence on neurodegeneration. However, unlike embryogenesis this appears to require the loss of both PS1 and PS2 in neurons, as preservation of either homologue within neurons prevents the onset of neurodegenerative outcomes.^{365, 379-381} These findings indicate a greater potential for functional redundancy, and a more unrecognised significant role for PS2, in the context of neurodegeneration. Notably the murine models used for these studies are constitutive PS2 knockout and conditional PS1 knockout in excitatory^{365, 379-384} or inhibitory^{385, 386} neurons. The pathological phenotype associated with the loss of both neuronal PS1 and PS2 is characterised by increased cortical atrophy,^{365, 379, 385} neuronal apoptosis,^{365, 379, 383, 386} increased microgliosis^{365, 381, 382, 386} and astrogliosis^{365, 379, 381, 382, 384-386}, tau hyperphosphorylation and aggregation^{380, 381, 385}, and reduced synapse quantity and integrity.^{380, 385} Collectively, these detrimental phenotypes culminate to cause severe memory impairment,^{380, 381, 385} emphasising the crucial role of presenilins in maintaining neuronal integrity. Moreover, in mice without an altered PS genotype, memory impairment with age is associated with decreased PS1 expression and a concomitant increase in PS2,³⁷⁷ further highlighting the differential roles of PS1 and PS2 at different developmental stages.

1.4.3 γ -Secretase dependent functions of PS1 and PS2: Substrates galore

To date, over 149 substrates of γ -secretase have been identified, and while these are regularly reviewed,^{333, 387} new substrates continue to be identified.^{388, 389} Although γ -secretase typically processes type-I transmembrane proteins as substrates, it can also process proteins with a type-III topology. However, in the case of a type-III topology, an initial processing step is necessary to separate the type-I and type-II oriented TM domains before γ -secretase can effectively process the remaining type-I TM oriented protein.³⁹⁰ Additionally, prior ectodomain shedding, while most common, is not obligatory if the ectodomain is small enough to not sterically hinder substrate access.^{388, 391}

The determination of which substrates are cleaved γ -secretase has typically been determined by genetic or pharmacological inhibition,³⁸⁸ although the exact cleavage mechanisms have not been determined for many substrates. The field's understanding of γ -secretase substrate processing mechanisms is extrapolated from the more extensive knowledge of APP and Notch1 processing.^{92, 93, 231, 232, 392, 393} There is no substrate cleavage consensus sequence recognised by γ -secretase, although residue variation in the immediate vicinity of the cleavage site has been shown to affect substrate cleavage, due to steric clashes with the substrate binding pocket.⁹⁵ Additionally, a cluster of positively charged residues positioned at the cytoplasmic juxtamembrane is common to most substrates,^{333, 394, 395} which facilitates anchoring to the negatively charged lipid headgroups of the membrane.⁹⁸ Secondary and higher-order structural elements of substrates, such as helical destabilisation and substrate dimerisation also regulate cleavage.³⁹⁴ More recently, it has been observed that a hybrid- β sheet forms between the substrate, PS-NTF and PS-CTF, facilitating the unwinding of the substrate and positioning the scissile bonds,^{231, 232} and therefore is likely a critical structural element for γ -secretase cleavage.

How the structural differences between PS1 γ and PS2 γ ^{199, 275, 276} impact on substrate cleavage is poorly understood. The assertion that the majority of substrates are suggested to be cleaved by both PS1 γ and PS2 γ ,³³³ is certainly the case for some substrates,^{237, 367} but often this is an assumption as not all studies explicitly investigate PS2 γ cleavage.^{388, 389, 391} Both PS1 and PS2 γ -secretase specific substrates have been identified (Figure 1-5A).^{220, 235-237} While the exact mechanisms of substrate specificity remain unclear, sub-cellular localisation plays a role, as PS1 γ and PS2 γ localise differently.^{220, 237, 396, 397} Indeed in the absence of these spatial restrictions, cadherin-2 (CDH2) can be cleaved by PS2 γ , although the same experiments were

not completed for premelanosome (PMEL) and tyrosinase-related protein 1 (TYRP1), so it is not clear if factors other than cellular localisation are contributing.²²⁰

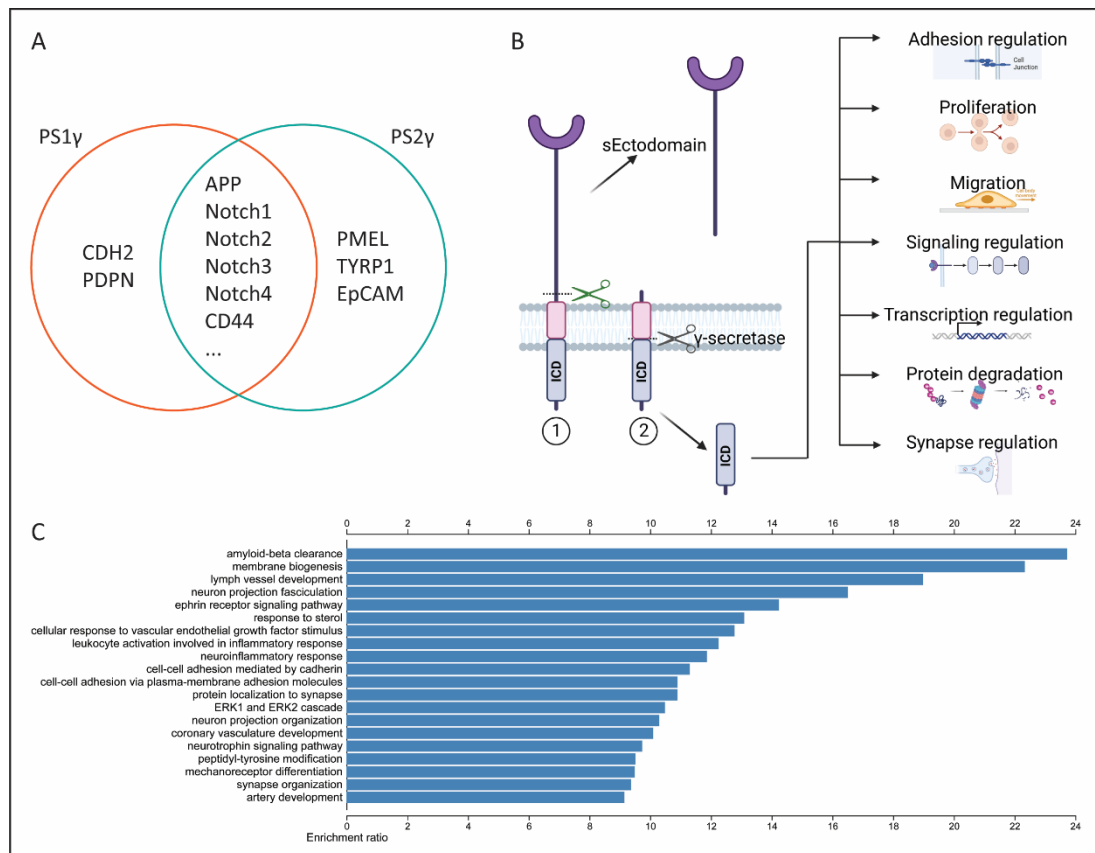


Figure 1-5 γ -Secretase substrates perform a wide array of functions

The majority of γ -secretase substrates can be cleaved by either PS1 γ or PS2 γ , while some substrates demonstrate PS specificity (A). Substrate cleavage by γ -secretase releases the intracellular domain (ICD) that can effect different functional outcomes, dependent on full length substrate protein function (B) (Created with BioRender.com). Gene over representation analysis completed using Webgestalt,³⁹⁸ complete set of substrates, using gene symbol, examined with gene ontology, biological processes database, FDR<0.05, restricted to top 20 highest enrichment ratio hits.(C)

It is the γ -secretase cleavage products of APP and Notch1 processing that have been most extensively studied. Notch signalling is initiated by ligand binding of mature cell surface Notch protein, which triggers ADAM cleavage and the RIP cascade, leading to Notch1 ICD (NICD1) release by γ -secretase cleavage.³⁹⁹ Canonical Notch signalling is a highly conserved pathway, critical for integrating extracellular microenvironments in multicellular organism development, through direct extracellular ligand binding.⁴⁰⁰ The released NICD1 has multiple domains and nuclear localisation signals, which facilitate formation of transcription complex with CSL (CBF1–suppressor of hairless–LAG1) and MAM (mastermind), and recruitment of co-

activator/co-repressor proteins.^{401, 402} This transcription complex causes large scale histone acetylation and chromatin remodelling stimulating (or modulating) target gene transcription.⁴⁰³ Multiple noncanonical Notch signalling pathways are also known that are regulated by crosstalk with other signalling pathways including reelin, integrin, TGF- β , WNT, and VEGF signalling.⁴⁰⁰ The NICD1 protein has an extensive interactome network (<https://reactome.org/PathwayBrowser/#/R-HSA-2122947>), and consequently a large array of biological functions, due to its critical role in cell fate determination, and organ development. Notch signalling plays a vital role in several essential organ systems, including somite-derived organs (i.e. vertebrae, skeletal muscle, dorsal root ganglia, dermal layer of skin), the cardiovascular system, the central nervous system, and the hematopoietic system.^{402, 404} Considering the importance of Notch signalling in various crucial organ systems, it follows that dysregulated Notch signalling can lead to multiple diseases, including various types of cancer.⁴⁰² As a result, γ -secretase inhibitors are being actively researched and developed as potential treatments for cancer.^{405, 406}

With respect to γ -secretase processing of APP, both the AICD and A β products have known functions. While the AICD has many potential outcomes and functions,^{Reviewed in 66, 407} its ultimate fate, whether it undergoes degradation or not, depends on where it is produced and what pathway generates it. If AICD is generated at the cell surface membrane through the amyloidogenic pathway,^{85, 86,} it is rapidly degraded by insulin-degrading enzyme.^{85, 86, 118} Alternatively, if AICD is generated by amyloidogenic processing in the endosomal pathway, degradation is avoided.^{87, 88 408} The AICD generated from β APP-C99 interacts with many protein partners, to modulate cell death, DNA repair, and gene expression; ultimately regulating neuronal migration, and neuronal and neuromuscular synaptic function.⁶⁶ Notably AICD plays a role in regulating the accumulation of A β . Acting as a transcription factor, AICD, in conjunction with FE65 and TIP60, forms the AFT complex. This complex regulates the expression of neprilysin, an A β degrading enzyme, thereby influencing A β levels.^{67, 68, 409}

A β has several physiological functions, but these typically require very low concentrations, in the picomolar range. A β ₁₋₄₀, particularly the A β ₄₀ isoform, is specifically required for neuronal cell viability.⁴¹⁰ The A β ₄₂ isoform has been shown to be important for long term potentiation, synaptic plasticity, and memory formation.^{411, 412} Additionally, A β can act as an antioxidant by chelating metal ions, is important for blood-brain barrier maintenance, and calcium homeostasis.⁴¹³ Furthermore, A β has been shown to have antimicrobial properties, albeit in

high concentrations or in AD models, indeed the mechanism of action is via ‘bioflocculation’, or the aggregation of microbes when bound to A β , and initiation of a reactive oxygen species response (ROS).⁴¹⁴ This is likely a coincidental benefit of a pathophysiological response given that increased A β levels can lead to ROS and lipid peroxidation.⁴¹⁵⁻⁴¹⁷ A β is also suggestive to be protective against cancer, in particular it has demonstrated anti-tumour proliferation⁴¹⁸ and angiogenesis effects,⁴¹⁹ although these are at pathological concentrations. Indeed, there is an inverse clinical relationship, where patients with AD have a lower risk of cancer,⁴²⁰ and so again this may be a coincidental benefit of the AD pathology. When the concentration of A β rises into the nano- to micromolar range, it can shift the balance from normal physiology to pathological conditions. Like flicking a switch many beneficial mechanisms, become neurotoxic in high A β concentrations, particularly when longer more aggregative forms of A β (i.e. \geq A β 42) are generated, increasing the ratios of oligomeric, protofibril and fibrillar A β . A β competes with canonical ligands for multiple membrane receptors and induces toxicity by enhancing oxidative stress and inflammation, disrupting normal synaptic maintenance, synaptic plasticity, and calcium homeostasis.^{24, 421, 422}

Given the plethora of γ -secretase substrates it is unsurprising that associated ICD protein products released have a range of functions; however these are typically related to the function of the full length substrate protein (Figure 1-5B).^{333, 387, 407} Interestingly, after completing gene over-representation analysis for Gene Ontology (GO) Biological Processes (BP), A β clearance was the most highly enriched GO BP (Figure 1-5C). Furthermore, several other BPs associated with neural homeostasis (thus having potential relevance to AD) are also highly enriched. These include BPs related to the projection of neurons, neuroinflammatory responses, and the regulation of synapses. In addition to APP, many γ -secretase substrates are involved in A β metabolism through a variety of mechanisms (Figure 1-6). In particular, several substrates influence A β generation through regulating APP trafficking and retention at the cell surface to promote ADAM cleavage and the non-amyloidogenic pathway.^{119, 423-427} While other substrates regulate A β clearance mechanisms, in particular expression of A β degrading enzymes,^{68, 428-430} flux of A β either into or from the periphery,^{128, 132, 431-434} and A β phagocytosis.^{120, 121, 435}

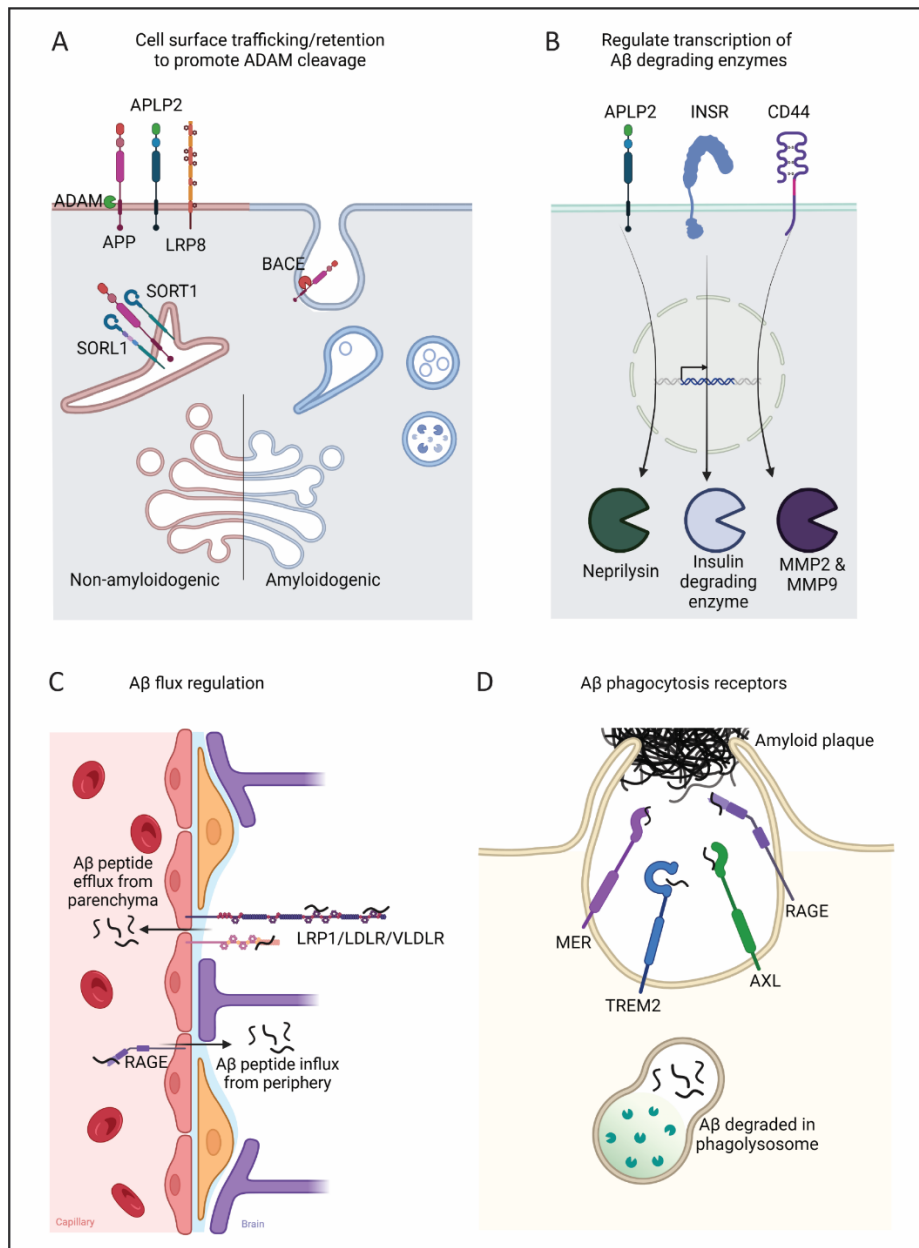


Figure 1-6 Aβ metabolism related substrates of γ -secretase function via multiple mechanisms

Substrates of γ -secretase involved in A β clearance function by regulating APP trafficking (A), A β degrading enzymes (B), A β flux (C), and A β phagocytosis (D). (Created with BioRender.com)

1.4.4 Non-proteolytic functions of PS1 and PS2

The first recognition of potential non-proteolytic functions came with the observation that mice lacking both PS1 and PS2 have no somites, while cervical somitogenesis proceeds with Notch1/Notch2 deficiency.⁴³⁶ Several studies in mosses (*Physcomitrella patens*)⁴³⁷ and Amoebazoa (*Dictyostelium discoideum*)^{438, 439} provide supporting evidence for this early developmental role. These studies are noteworthy because these organisms lack Notch

developmental pathways. They confirm development functions for both PS1 and PS2, and while some studies show this to be a non-proteolytic function,^{437, 439} other studies do not confirm if this is a proteolytic or non-proteolytic function.⁴³⁸ Several non-proteolytic functions of PS1 and PS2, have since been identified, with some of these been common and others likely being PS specific. Many studies, especially those focused on PS1, do not simultaneously investigate PS2, potentially leaving gaps in understanding the complete range of functions associated with both proteins. While several non-proteolytic functions of PS homologues have been suggested,^{Reviewed in 440-442} two well-established functions are discussed here.

In the earlier stages of research on presenilin biology, it was discovered that PS1 plays a role in regulating cell-cell adhesion by forming a complex with E-cadherin and β -catenin. This regulation occurs through the cleavage of E-cadherin in a γ -secretase-dependent manner by PS1.⁴⁴³ Consequently, it was observed that β -catenin directly interacts with the cytoplasmic loop domain of PS1.⁴⁴⁴ In a non-proteolytic capacity, PS1 acts as a scaffold, influencing the phosphorylation of β -catenin by glycogen synthase kinase-3 beta (GSK3 β) and protein kinase A (PKA).⁴⁴⁵ This leads to degradation of β -catenin, and so PS1 is a negative regulator of Wnt/ β -catenin signalling pathway.^{444, 446} While function has not been demonstrated in PS2, the PS1 binding region of β -catenin (PS1 aa 330-360) is largely not conserved between the PS homologues,²²¹ Furthermore, interactome studies confirm that β -catenin binds PS1 but not PS2.¹⁸⁴ Therefore, the regulation of β -catenin signalling can be regarded as a non-proteolytic function specific to PS1. In this capacity PS1 is associated with regulating tumourigenesis and tumour proliferation.⁴⁴⁵⁻⁴⁴⁷

Multiple presenilin related mechanisms of calcium (Ca^{2+}) regulation have been identified. Wildtype and mutant PS1 and PS2 have been shown to interact with inositol triphosphate receptors to regulate Ca^{2+} (IP₃R Ca^{2+}) signalling.⁴⁴⁸⁻⁴⁵⁰ Ryanodine receptor (RyR) binds to both PS1 and PS2 in the cytoplasmic N-terminal domain modulating RyR expression and recruitment to regulate IP₃R Ca^{2+} signalling.^{451, 452} Interestingly the RyR inhibitor, sorcin, binds specifically to PS2-CTF (and not the immature holo-protein) in the same non-conserved region that β -catenin binds PS1.^{453, 454} Consequently, PS2 is specifically involved in regulating RyR activity, and IP₃ Ca^{2+} mediated signalling. Additionally, PS1 and PS2 interact directly with SERCA2b a sarco-/endoplasmic reticulum Ca^{2+} ATPase to regulate IP₃ mediated Ca^{2+} release.⁴⁵⁵ It has also been suggested that the PS homologue may act as direct Ca^{2+} leak channels with TM7 and TM9 suggested to form a conductance pore.⁴⁵⁶⁻⁴⁵⁸ However, this has

been disputed,^{450, 459} and a recent molecular modelling study did not observe Ca²⁺ leakage, but rather identified persistent binding sites in the cytoplasmic loop domain, which are suggested to regulate IP₃ Ca²⁺ signalling.⁴⁶⁰ As a consequence of their involvement in Ca²⁺ signalling, the PS homologues are implicated in multiple Ca²⁺ associated functions, including dysregulated autophagy,^{461, 462} synaptic dysfunction,⁴⁶³ and dysregulated mitochondrial function.⁴⁶⁴

1.5 GENETICS OF INHERITED ALZHEIMER'S DISEASE

Several genetic risk factors for AD have been identified. While the majority of genes are associated with increased risk of developing late onset (i.e. age at onset > 65years) sporadic AD,¹⁴² mutations in *APP*, *PSEN1*, and *PSEN2* cause early-onset (i.e. age at onset <65 years) AD with autosomal dominant inheritance patterns.³⁵⁹ Located at chromosome 21q21.3, the observation that persons with Down syndrome, as a result of their trisomy 21, also developed cerebrovascular amyloidosis similar to persons with AD,⁴⁶⁵ led to the identification of the *APP* gene.⁶¹ Subsequently AD familial segregation in the absence of *APP* related mutations lead to the identification of *PSEN1* and *PSEN2* genes, at chromosome 14q24.2 and 1q42.13 respectively.¹⁴⁵⁻¹⁵⁰ To date 44 pathogenically associated variants have been identified *APP*, 200 in *PSEN1*, and 8 in *PSEN2* (SI Figure 1-1, 1-2, 1-3), while many other variants remain unclassified or of uncertain significance (www.alzforum.org/mutations accessed 18/09/2023). The majority of deleterious variants cause missense protein coding mutations, but triplication and duplication of *APP*,^{466, 467} exon 9 deletion in *PSEN1*⁴⁶⁸ and single nucleotide polymorphisms in the 3' untranslated regions of *APP*⁴⁶⁹ and *PSEN2*⁴⁷⁰ causal for AD pathogenesis have also been reported.

Increased amyloid plaque deposition, tau pathology, and cerebral amyloid angiopathy are consistent histopathological features in ADAD.⁴⁷¹ However variation in the age at onset (AAO) and symptom heterogeneity is evident among mutations originating from different genes, as well as among mutations occurring within the same gene. While the mean age at onset for ADAD is 46.2 years, there is a substantial range of <20 years to >70 years, with the AAO of *PSEN1* mutations been earliest, followed by *APP* mutations, and then *PSEN2* mutations.³⁵⁹ *APP* mutations can be classified into three groups based on the location in and mechanistic consequence: mutations affecting ectodomain cleavage; mutations in the A β sequence that cause rapid A β fibrilisation, and; mutations in the γ -secretase cleavage region

that increases the ratio of long ($\geq A\beta_{42}$) and short ($\leq A\beta_{40}$) peptides (typically measured as $A\beta_{42}:A\beta_{40}$), that ultimately influences the aggregation of $A\beta$.⁴⁷² While the effect of *APP* mutations are limited to *APP*-specific functions,⁴⁷³ the roles of PS1 and PS2, both proteolytic and non-proteolytic, means that mutations in *PSEN1* and *PSEN2* can have multiple biological effects. Furthermore, while *APP* mutations are localised within the cleavage regions or $A\beta$ peptide sequence,⁴⁷² *PSEN1* and *PSEN2* mutations are broadly distributed throughout the protein sequence. In the context of the γ -secretase structure mutations are positioned at APH1 and PEN2 subunit interfaces, within the substrate binding pore, and within the hydrophilic loop regions, thus affecting complex stability and substrate binding.^{276, 289-291, 294, 296, 474, 475} However, there is observable pathological differences in PS1 mutations, where those C-terminal of codon 200, generally present with more severe and distinct pathology, in particular the occurrence of cerebral amyloid angiopathy.^{471, 476, 477}

PS1 and PS2 mutations typically lead to an increase in the $A\beta_{42}:A\beta_{40}$ ratio,^{100, 220, 474} although this is often associated with a reduction in total $A\beta$ ($A\beta_{42} + A\beta_{40}$), and in some cases, almost a complete loss of processing.¹⁰⁰ This has led to the often-debated question of whether PS-related mutations are gain or loss of function? Further to this, there are mutations that either do not generate substantially different $A\beta_{42}:A\beta_{40}$ levels, or indeed, reduce the ratio compared to wild type but still are associated with ADAD.¹⁰⁰ While mutations in PS1 and PS2 lead to changes in $A\beta$ production, it is not surprising that detrimental impacts on the processing of other substrates have also been observed. Intriguingly, these effects also vary depending on the specific substrate in question, with identical mutations yielding differing outcomes for distinct substrates.^{220, 474} Beyond the effect on *APP* and other substrate processing, PS1 mutations have also been shown to affect lysosomal acidification⁴⁷⁸ and mitochondrial functions,^{464, 479, 480} linked to disrupted calcium signalling. Furthermore, PS2 mutations have been shown to alter microglial function.⁴⁸¹ Given the abundance of γ -secretase substrates, along with the non-proteolytic functions of PS1 and PS2, it is highly likely that the observed clinical heterogeneity results from the diverse effects of mutations on these multiple biological functions. The varying impacts of mutations on these multiple biological functions may act as compounding factors contributing to the clinical heterogeneity observed.

1.6 UNDERSTANDING γ -SECRETASE FOR IMPROVED THERAPEUTIC STRATEGIES

Given the role of γ -secretase in $A\beta$ generation the enzyme is a sought-after therapeutic target. While numerous GSIs have undergone clinical trials for treatment of AD,⁴⁸²⁻⁴⁸⁴ they have failed due to off target effects associated with the broad inhibition of substrates, in particular Notch.⁴⁸⁵ These GSIs caused increased risk of skin cancer and infections,⁴⁸⁵ and a worsening of cognition⁴⁸⁵ likely associated with increased brain atrophy.⁴⁸⁶ Consequently, allosteric modulators have been pursued,⁴⁸⁷ and show promise;^{60, 104} but have not yet made it into the clinic. GSMs function to decrease the amount of long $A\beta$ generated but do not alter the initial substrate cleavage of γ -secretase substrates,^{103, 207, 269, 488, 489} likely preventing the off-target effects observed with GSI use. One key learning from the clinical failures of GSIs was the identification of knowledge gaps regarding the biology of γ -secretase. This is further complicated by there being multiple γ -secretase enzymes. To date, all of the GSIs and GSMs developed bind, at least in part, to the PS component, so the presence of a PS1 γ and PS2 γ , which are distinct enzymes, adds complexity, which is highlighted by the variable specificity of several GSIs.^{199, 490} There is an evident bias in the AD and presenilin biology fields towards PS1 (Figure 1-4A), as a broad result PS2 tends to ‘come along for the ride’ with little consideration of the differences between the two PS homologues: Absence of evidence is not evidence of absence! An improved understanding of both the structural and functional differences between PS1 γ and PS2 γ in both $A\beta$ generation and clearance is critical for the development of targeted therapeutics and may highlight new treatment avenues previously not considered. This thesis intends to begin to change the rhetoric surrounding PS2 γ and elevate its place in the fields of γ -secretase and AD research.

1.7 HYPOTHESIS AND AIMS

The overarching hypothesis of this thesis is that *PS1 and PS2 exhibit distinct roles in A β metabolism*, and the specific contributions are dependent on differential functions of PS1 and PS2 related to both A β generation and A β removal. This will be addressed by the following aims.

Aim 1 (Chapter 2): To quantitatively evaluate and compare the individual enzymatic contributions of PS1 γ and PS2 γ in the process of A β generation.

Aim 2 (Chapter 3): To determine molecular mechanisms of differential A β generation by assessing A β substrate binding by PS1 γ and PS2 γ .

Aim 3 (Chapter 4): To quantitatively assess PS1 and PS2 levels in human brain tissue and neural cell lines.

Aim 4 (Chapter 5): To determine functional effects of the loss of PS1 or PS2 on human microglia.

Aim 5 (Chapter 6): To assess the differential effects of PS1 γ and PS2 γ and clinical mutations on A β clearance related substrate binding.

The research in this thesis has employed two distinct approaches: traditional in vitro cell biology techniques (Chapters 2, 4, and 5) and computational molecular modelling methods (Chapters 3 and 6). While the results chapters could have been arranged differently, I have opted to present them within a biological context. As such, I first discuss the findings related to A β generation (Chapters 2 and 3), followed by those pertaining to A β clearance (Chapters 5 and 6). Chapter 4, which is relevant to both A β generation and clearance, serves as a bridging chapter between these two aspects.

1.8 REFERENCES

1. Organization, W. H. (2021) Global status report on the public health response to dementia.
2. Welfare, A. I. o. H. a. (2022) Australia's health 2022: in brief. *catalogue number AUS 241. Australia's health series number 18, AIHW, Australian Government.*
3. Knopman, D. S., Amieva, H., Petersen, R. C., Chételat, G., Holtzman, D. M., Hyman, B. T., Nixon, R. A., and Jones, D. T. (2021) Alzheimer disease. *Nature Reviews Disease Primers* **7**, 33
4. DeTure, M. A., and Dickson, D. W. (2019) The neuropathological diagnosis of Alzheimer's disease. *Molecular neurodegeneration* **14**, 32
5. Long, J. M., and Holtzman, D. M. (2019) Alzheimer Disease: An Update on Pathobiology and Treatment Strategies. *Cell* **179**, 312-339
6. Ittner, L. M., Ke, Y. D., Delerue, F., Bi, M., Gladbach, A., van Eersel, J., Wölfing, H., Chieng, B. C., Christie, M. J., Napier, I. A., Eckert, A., Staufenbiel, M., Hardeman, E., and Götz, J. (2010) Dendritic Function of Tau Mediates Amyloid- β Toxicity in Alzheimer's Disease Mouse Models. *Cell* **142**, 387-397
7. Barbier, P., Zejneli, O., Martinho, M., Lasorsa, A., Belle, V., Smet-Nocca, C., Tsvetkov, P. O., Devred, F., and Landrieu, I. (2019) Role of Tau as a Microtubule-Associated Protein: Structural and Functional Aspects. *Front Aging Neurosci* **11**
8. Cleveland, D. W., Hwo, S.-Y., and Kirschner, M. W. (1977) Purification of tau, a microtubule-associated protein that induces assembly of microtubules from purified tubulin. *Journal of Molecular Biology* **116**, 207-225
9. Sengupta, A., Kabat, J., Novak, M., Wu, Q., Grundke-Iqbal, I., and Iqbal, K. (1998) Phosphorylation of Tau at Both Thr 231 and Ser 262 Is Required for Maximal Inhibition of Its Binding to Microtubules. *Archives of Biochemistry and Biophysics* **357**, 299-309
10. Bancher, C., Lassmann, H., Budka, H., Grundke-Iqbal, I., Iqbal, K., Wiche, G., Seitelberger, F., and Wisniewski, H. M. (1987) Neurofibrillary tangles in Alzheimer's disease and progressive supranuclear palsy: antigenic similarities and differences. *Acta neuropathologica* **74**, 39-46
11. Giannakopoulos, P., Herrmann, F. R., Bussière, T., Bouras, C., Kövari, E., Perl, D. P., Morrison, J. H., Gold, G., and Hof, P. R. (2003) Tangle and neuron numbers, but not amyloid load, predict cognitive status in Alzheimer's disease. *Neurology* **60**, 1495-1500
12. Nelson, P. T., Alafuzoff, I., Bigio, E. H., Bouras, C., Braak, H., et al. (2012) Correlation of Alzheimer disease neuropathologic changes with cognitive status: a review of the literature. *Journal of Neuropathology & Experimental Neurology* **71**, 362-381
13. Hanseeuw, B. J., Betensky, R. A., Jacobs, H. I. L., Schultz, A. P., Sepulcre, J., Becker, J. A., Cosio, D. M. O., Farrell, M., Quiroz, Y. T., Mormino, E. C., Buckley, R. F., Papp, K. V., Amariglio, R. A., Dewachter, I., Ivanoiu, A., Huijbers, W., Hedden, T., Marshall, G. A., Chhatwal, J. P., Rentz, D. M., Sperling, R. A., and Johnson, K. (2019) Association of Amyloid and Tau With Cognition in Preclinical Alzheimer Disease: A Longitudinal Study. *JAMA Neurology* **76**, 915-924
14. Sato, C., Barthélemy, N. R., Mawuenyega, K. G., Patterson, B. W., Gordon, B. A., Jockel-Balsarotti, J., Sullivan, M., Crisp, M. J., Kasten, T., Kirmess, K. M., Kanaan, N. M., Yarasheski, K. E., Baker-Nigh, A., Benzinger, T. L. S., Miller, T. M., Karch, C. M., and Bateman, R. J. (2018) Tau Kinetics in Neurons and the Human Central Nervous System. *Neuron* **97**, 1284-1298.e1287
15. Choi, S. H., Kim, Y. H., Hebisch, M., Sliwinski, C., Lee, S., D'Avanzo, C., Chen, H., Hooli, B., Asselin, C., Muffat, J., Klee, J. B., Zhang, C., Wainger, B. J., Peitz, M., Kovacs, D.

- M., Woolf, C. J., Wagner, S. L., Tanzi, R. E., and Kim, D. Y. (2014) A three-dimensional human neural cell culture model of Alzheimer's disease. *Nature* **515**, 274-278
16. He, Z., Guo, J. L., McBride, J. D., Narasimhan, S., Kim, H., Changolkar, L., Zhang, B., Gathagan, R. J., Yue, C., Dengler, C., Stieber, A., Nitla, M., Coulter, D. A., Abel, T., Brunden, K. R., Trojanowski, J. Q., and Lee, V. M. Y. (2018) Amyloid- β plaques enhance Alzheimer's brain tau-seeded pathologies by facilitating neuritic plaque tau aggregation. *Nature medicine* **24**, 29-38
 17. Pooler, A. M., Polydoro, M., Maury, E. A., Nicholls, S. B., Reddy, S. M., Wegmann, S., William, C., Saqran, L., Cagsal-Getkin, O., Pitstick, R., Beier, D. R., Carlson, G. A., Spires-Jones, T. L., and Hyman, B. T. (2015) Amyloid accelerates tau propagation and toxicity in a model of early Alzheimer's disease. *Acta neuropathologica communications* **3**, 14
 18. Ower, A. K., Hadjichrysanthou, C., Gras, L., Goudsmit, J., Anderson, R. M., and de Wolf, F. (2018) Temporal association patterns and dynamics of amyloid- β and tau in Alzheimer's disease. *European Journal of Epidemiology* **33**, 657-666
 19. Garai, K., Verghese, P. B., Baban, B., Holtzman, D. M., and Frieden, C. (2014) The Binding of Apolipoprotein E to Oligomers and Fibrils of Amyloid- β Alters the Kinetics of Amyloid Aggregation. *Biochemistry* **53**, 6323-6331
 20. Nirmalraj, P. N., List, J., Battacharya, S., Howe, G., Xu, L., Thompson, D., and Mayer, M. (2020) Complete aggregation pathway of amyloid β (1-40) and (1-42) resolved on an atomically clean interface. *Science Advances* **6**, eaaz6014
 21. Drummond, E., Kavanagh, T., Pires, G., Marta-Ariza, M., Kanshin, E., Nayak, S., Faustin, A., Berdah, V., Ueberheide, B., and Wisniewski, T. (2022) The amyloid plaque proteome in early onset Alzheimer's disease and Down syndrome. *Acta neuropathologica communications* **10**, 53
 22. Drummond, E., Nayak, S., Faustin, A., Pires, G., Hickman, R. A., Askenazi, M., Cohen, M., Haldiman, T., Kim, C., Han, X., Shao, Y., Safar, J. G., Ueberheide, B., and Wisniewski, T. (2017) Proteomic differences in amyloid plaques in rapidly progressive and sporadic Alzheimer's disease. *Acta neuropathologica* **133**, 933-954
 23. Hardy, J. A., and Higgins, G. A. (1992) Alzheimer's Disease: The Amyloid Cascade Hypothesis. *Science (New York, N.Y.)* **256**, 184-185
 24. De Strooper, B., and Karran, E. (2016) The Cellular Phase of Alzheimer's Disease. *Cell* **164**, 603-615
 25. Selkoe, D. J., and Hardy, J. (2016) The amyloid hypothesis of Alzheimer's disease at 25 years. *EMBO Molecular Medicine* **8**, 595-608
 26. Cline, E. N., Bicca, M. A., Viola, K. L., and Klein, W. L. (2018) The Amyloid- β Oligomer Hypothesis: Beginning of the Third Decade. *Journal of Alzheimer's Disease* **64**, S567-s610
 27. De Felice, F. G., Velasco, P. T., Lambert, M. P., Viola, K., Fernandez, S. J., Ferreira, S. T., and Klein, W. L. (2007) A β Oligomers Induce Neuronal Oxidative Stress through an N-Methyl-D-aspartate Receptor-dependent Mechanism That Is Blocked by the Alzheimer Drug Memantine. *The Journal of biological chemistry* **282**, 11590-11601
 28. Lustbader, J. W., Cirilli, M., Lin, C., Xu, H. W., Takuma, K., Wang, N., Caspersen, C., Chen, X., Pollak, S., Chaney, M., Trinchese, F., Liu, S., Gunn-Moore, F., Lue, L. F., Walker, D. G., Kuppusamy, P., Zewier, Z. L., Arancio, O., Stern, D., Yan, S. S., and Wu, H. (2004) ABAD directly links Abeta to mitochondrial toxicity in Alzheimer's disease. *Science (New York, N.Y.)* **304**, 448-452
 29. Reddy, P. H., Manczak, M., and Yin, X. (2017) Mitochondria-Division Inhibitor 1 Protects Against Amyloid- β induced Mitochondrial Fragmentation and Synaptic Damage in Alzheimer's Disease. *Journal of Alzheimer's Disease* **58**, 147-162

30. Huang, S., Tong, H., Lei, M., Zhou, M., Guo, W., Li, G., Tang, X., Li, Z., Mo, M., Zhang, X., Chen, X., Cen, L., Wei, L., Xiao, Y., Li, K., Huang, Q., Yang, X., Liu, W., Zhang, L., Qu, S., Li, S., and Xu, P. (2018) Astrocytic glutamatergic transporters are involved in A β -induced synaptic dysfunction. *Brain research* **1678**, 129-137
31. Walsh, D. M., Klyubin, I., Fadeeva, J. V., Cullen, W. K., Anwyl, R., Wolfe, M. S., Rowan, M. J., and Selkoe, D. J. (2002) Naturally secreted oligomers of amyloid beta protein potently inhibit hippocampal long-term potentiation in vivo. *Nature* **416**, 535-539
32. Smith, L. M., and Strittmatter, S. M. (2017) Binding Sites for Amyloid- β Oligomers and Synaptic Toxicity. *Cold Spring Harb Perspect Med* **7**
33. Liu, S., Liu, Y., Hao, W., Wolf, L., Kiliaan, A. J., Penke, B., Rube, C. E., Walter, J., Heneka, M. T., Hartmann, T., Menger, M. D., and Fassbender, K. (2012) TLR2 Is a Primary Receptor for Alzheimer's Amyloid β Peptide To Trigger Neuroinflammatory Activation. *The Journal of Immunology* **188**, 1098-1107
34. Esparza, T. J., Gangolli, M., Cairns, N. J., and Brody, D. L. (2018) Soluble amyloid-beta buffering by plaques in Alzheimer disease dementia versus high-pathology controls. *PLoS one* **13**, e0200251
35. Forloni, G., Lucca, E., Angeretti, N., Della Torre, P., and Salmona, M. (1997) Amidation of beta-amyloid peptide strongly reduced the amyloidogenic activity without alteration of the neurotoxicity. *Journal of neurochemistry* **69**, 2048-2054
36. Forloni, G., and Balducci, C. (2018) Alzheimer's Disease, Oligomers, and Inflammation. *Journal of Alzheimer's Disease* **62**, 1261-1276
37. El Hajj, H., Savage, J. C., Bisht, K., Parent, M., Vallières, L., Rivest, S., and Tremblay, M.-È. (2019) Ultrastructural evidence of microglial heterogeneity in Alzheimer's disease amyloid pathology. *J Neuroinflammation* **16**, 87-87
38. Serrano-Pozo, A., Mielke, M. L., Gómez-Isla, T., Betensky, R. A., Growdon, J. H., Frosch, M. P., and Hyman, B. T. (2011) Reactive glia not only associates with plaques but also parallels tangles in Alzheimer's disease. *The American journal of pathology* **179**, 1373-1384
39. Serrano-Pozo, A., Muzikansky, A., Gómez-Isla, T., Growdon, J. H., Betensky, R. A., Frosch, M. P., and Hyman, B. T. (2013) Differential Relationships of Reactive Astrocytes and Microglia to Fibrillar Amyloid Deposits in Alzheimer Disease. *Journal of Neuropathology & Experimental Neurology* **72**, 462-471
40. Administration, U. S. F. a. D. (2021) FDA's Decision to Approve New Treatment for Alzheimer's Disease.
41. Budd Haeberlein, S., Aisen, P. S., Barkhof, F., Chalkias, S., Chen, T., Cohen, S., Dent, G., Hansson, O., Harrison, K., von Hehn, C., Iwatsubo, T., Mallinckrodt, C., Mummery, C. J., Muralidharan, K. K., Nestorov, I., Nisenbaum, L., Rajagovindan, R., Skordos, L., Tian, Y., van Dyck, C. H., Vellas, B., Wu, S., Zhu, Y., and Sandrock, A. (2022) Two Randomized Phase 3 Studies of Aducanumab in Early Alzheimer's Disease. *The Journal of Prevention of Alzheimer's Disease* **9**, 197-210
42. Tampi, R. R., Forester, B. P., and Agronin, M. (2021) Aducanumab: evidence from clinical trial data and controversies. *Drugs Context* **10**
43. Mullard, A. (2021) FDA approval for Biogen's aducanumab sparks Alzheimer disease firestorm. *Nature Reviews Drug Discovery* **20**, 496
44. Fleck, L. M. (2021) Alzheimer's and Aducanumab: Unjust Profits and False Hopes. *Hastings Center Report* **51**, 9-11
45. Knopman, D. S., Jones, D. T., and Greicius, M. D. (2021) Failure to demonstrate efficacy of aducanumab: An analysis of the EMERGE and ENGAGE trials as reported by Biogen, December 2019. *Alzheimer's & Dementia* **17**, 696-701
46. van Dyck, C. H., Swanson, C. J., Aisen, P., Bateman, R. J., Chen, C., Gee, M., Kanekiyo, M., Li, D., Reyderman, L., Cohen, S., Froelich, L., Katayama, S., Sabbagh, M.,

- Vellas, B., Watson, D., Dhadda, S., Irizarry, M., Kramer, L. D., and Iwatsubo, T. (2023) Lecanemab in Early Alzheimer's Disease. *New England Journal of Medicine* **388**, 9-21
47. McDade, E., Cummings, J. L., Dhadda, S., Swanson, C. J., Reyderman, L., Kanekiyo, M., Koyama, A., Irizarry, M., Kramer, L. D., and Bateman, R. J. (2022) Lecanemab in patients with early Alzheimer's disease: detailed results on biomarker, cognitive, and clinical effects from the randomized and open-label extension of the phase 2 proof-of-concept study. *Alzheimer's research & therapy* **14**, 191
48. Administration, U. S. F. a. D. (2023) FDA Grants Accelerated Approval for Alzheimer's Disease Treatment.
49. Honig, L. S., Barakos, J., Dhadda, S., Kanekiyo, M., Reyderman, L., Irizarry, M., Kramer, L. D., Swanson, C. J., and Sabbagh, M. (2023) ARIA in patients treated with lecanemab (BAN2401) in a phase 2 study in early Alzheimer's disease. *Alzheimer's & Dementia: Translational Research & Clinical Interventions* **9**, e12377
50. Reish, N. J., Jamshidi, P., Stamm, B., Flanagan, M. E., Sugg, E., Tang, M., Donohue, K. L., McCord, M., Krumpelman, C., Mesulam, M. M., Castellani, R., and Chou, S. H. (2023) Multiple Cerebral Hemorrhages in a Patient Receiving Lecanemab and Treated with t-PA for Stroke. *New England Journal of Medicine* **388**, 478-479
51. Söderberg, L., Johannesson, M., Nygren, P., Laudon, H., Eriksson, F., Osswald, G., Möller, C., and Lannfelt, L. (2023) Lecanemab, Aducanumab, and Gantenerumab - Binding Profiles to Different Forms of Amyloid-Beta Might Explain Efficacy and Side Effects in Clinical Trials for Alzheimer's Disease. *Neurotherapeutics* **20**, 195-206
52. Selkoe, D. (2019) β -secretase inhibitors for Alzheimer's disease: heading in the wrong direction? *The Lancet Neurology* **18**, 624-626
53. De Strooper, B. (2014) Lessons from a failed γ -secretase Alzheimer trial. *Cell* **159**, 721-726
54. Dobrowolska Zakaria, J. A., and Vassar, R. J. (2021) A promising new γ -secretase modulator for Alzheimer's disease. *Journal of Experimental Medicine* **218**
55. Luo, J. E., and Li, Y.-M. (2022) Turning the tide on Alzheimer's disease: modulation of γ -secretase. *Cell & Bioscience* **12**, 2
56. Fagan, T. (2023) Give BACE Inhibitors a Second Chance? In *Alzforum*
57. Singh, N., Das, B., Zhou, J., Hu, X., and Yan, R. (2022) Targeted BACE-1 inhibition in microglia enhances amyloid clearance and improved cognitive performance. *Science Advances* **8**, eabo3610
58. Singh, N., Benoit, M. R., Zhou, J., Das, B., Davila-Velderrain, J., Kellis, M., Tsai, L. H., Hu, X., and Yan, R. (2022) BACE-1 inhibition facilitates the transition from homeostatic microglia to DAM-1. *Science Advances* **8**, eabo1286
59. Pratsch, K., Unemura, C., Ito, M., Lichtenthaler, S. F., Horiguchi, N., and Herms, J. (2023) New Highly Selective BACE1 Inhibitors and Their Effects on Dendritic Spine Density In Vivo. *International journal of molecular sciences* **24**
60. Rynearson, K. D., Ponnusamy, M., Prikhodko, O., Xie, Y., Zhang, C., Nguyen, P., Hug, B., Sawa, M., Becker, A., Spencer, B., Florio, J., Mante, M., Salehi, B., Arias, C., Galasko, D., Head, B. P., Johnson, G., Lin, J. H., Duddy, S. K., Rissman, R. A., Mobley, W. C., Thinakaran, G., Tanzi, R. E., and Wagner, S. L. (2021) Preclinical validation of a potent γ -secretase modulator for Alzheimer's disease prevention. *Journal of Experimental Medicine* **218**
61. Kang, J., Lemaire, H. G., Unterbeck, A., Salbaum, J. M., Masters, C. L., Grzeschik, K. H., Multhaup, G., Beyreuther, K., and Müller-Hill, B. (1987) The precursor of Alzheimer's disease amyloid A4 protein resembles a cell-surface receptor. *Nature* **325**, 733-736
62. Rice, H. C., de Malmazet, D., Schreurs, A., Frere, S., Van Molle, I., Volkov, A. N., Creemers, E., Vertkin, I., Nys, J., Ranaivoson, F. M., Comoletti, D., Savas, J. N., Remaut, H., Balschun, D., Wierda, K. D., Slutsky, I., Farrow, K., De Strooper, B., and de Wit, J. (2019)

Secreted amyloid- β precursor protein functions as a GABABR1a ligand to modulate synaptic transmission. *Science (New York, N.Y.)* **363**, eaao4827

63. Fanutza, T., Del Prete, D., Ford, M. J., Castillo, P. E., and D'Adamio, L. (2015) APP and APLP2 interact with the synaptic release machinery and facilitate transmitter release at hippocampal synapses. *eLife* **4**, e09743

64. Deyts, C., Clutter, M., Herrera, S., Jovanovic, N., Goddi, A., and Parent, A. T. (2016) Loss of presenilin function is associated with a selective gain of APP function. *eLife* **5**

65. Sosa, L. J., Cáceres, A., Dupraz, S., Oksdath, M., Quiroga, S., and Lorenzo, A. (2017) The physiological role of the amyloid precursor protein as an adhesion molecule in the developing nervous system. *Journal of neurochemistry* **143**, 11-29

66. Bukhari, H., Glotzbach, A., Kolbe, K., Leonhardt, G., Loosse, C., and Müller, T. (2017) Small things matter: Implications of APP intracellular domain AICD nuclear signaling in the progression and pathogenesis of Alzheimer's disease. *Progress in neurobiology* **156**, 189-213

67. Grimm, M. O. W., Mett, J., Stahlmann, C. P., Grösgen, S., Hauptenthal, V. J., Blümel, T., Hundsdörfer, B., Zimmer, V. C., Mylonas, N. T., Tanila, H., Müller, U., Grimm, H. S., and Hartmann, T. (2015) APP intracellular domain derived from amyloidogenic β - and γ -secretase cleavage regulates neprilysin expression. *Front Aging Neurosci* **7**, 77-77

68. Pardossi-Piquard, R., Petit, A., Kawarai, T., Sunyach, C., Da Costa, C. A., Vincent, B., Ring, S., D'Adamio, L., Shen, J., Müller, U., Hyslop, P. S. G., and Checler, F. (2005) Presenilin-dependent transcriptional control of the A β -degrading enzyme neprilysin by intracellular domains of β APP and APLP. *Neuron* **46**, 541-554

69. Chai, Q., Jovasevic, V., Malikov, V., Sabo, Y., Morham, S., Walsh, D., and Naghavi, M. H. (2017) HIV-1 counteracts an innate restriction by amyloid precursor protein resulting in neurodegeneration. *Nature Communications* **8**, 1522

70. Müller, U. C., Deller, T., and Korte, M. (2017) Not just amyloid: physiological functions of the amyloid precursor protein family. *Nature Reviews Neuroscience* **18**, 281-298

71. Gabriele, R. M. C., Abel, E., Fox, N. C., Wray, S., and Arber, C. (2022) Knockdown of Amyloid Precursor Protein: Biological Consequences and Clinical Opportunities. *Frontiers in neuroscience* **16**

72. Brown, M. S., Ye, J., Rawson, R. B., and Goldstein, J. L. (2000) Regulated Intramembrane Proteolysis: A Control Mechanism Conserved from Bacteria to Humans. *Cell* **100**, 391-398

73. Lal, M., and Caplan, M. (2011) Regulated Intramembrane Proteolysis: Signaling Pathways and Biological Functions. *Physiology* **26**, 34-44

74. Kuhn, P.-H., Wang, H., Dislich, B., Colombo, A., Zeitschel, U., Ellwart, J. W., Kremmer, E., Roßner, S., and Lichtenthaler, S. F. (2010) ADAM10 is the physiologically relevant, constitutive α -secretase of the amyloid precursor protein in primary neurons. *EMBO J* **29**, 3020-3032

75. Vassar, R., Bennett, B. D., Babu-Khan, S., Kahn, S., Mendiaz, E. A., Denis, P., Teplow, D. B., Ross, S., Amarante, P., Loeloff, R., Luo, Y., Fisher, S., Fuller, J., Edenson, S., Lile, J., Jarosinski, M. A., Biere, A. L., Curran, E., Burgess, T., Louis, J.-C., Collins, F., Treanor, J., Rogers, G., and Citron, M. (1999) β -Secretase Cleavage of Alzheimer's Amyloid Precursor Protein by the Transmembrane Aspartic Protease BACE. *Science (New York, N.Y.)* **286**, 735-741

76. Zhang, Z., Song, M., Liu, X., Su Kang, S., Duong, D. M., Seyfried, N. T., Cao, X., Cheng, L., Sun, Y. E., Ping Yu, S., Jia, J., Levey, A. I., and Ye, K. (2015) Delta-secretase cleaves amyloid precursor protein and regulates the pathogenesis in Alzheimer's disease. *Nature Communications* **6**, 8762

77. Bien, J., Jefferson, T., Causević, M., Jumpertz, T., Munter, L., Multhaup, G., Weggen, S., Becker-Pauly, C., and Pietrzik, C. U. (2012) The metalloprotease meprin β generates amino

terminal-truncated amyloid β peptide species. *The Journal of biological chemistry* **287**, 33304-33313

78. Andrew, R. J., Kellett, K. A., Thinakaran, G., and Hooper, N. M. (2016) A Greek Tragedy: The Growing Complexity of Alzheimer Amyloid Precursor Protein Proteolysis. *The Journal of biological chemistry* **291**, 19235-19244

79. Masters, C. L., Simms, G., Weinman, N. A., Multhaup, G., McDonald, B. L., and Beyreuther, K. (1985) Amyloid plaque core protein in Alzheimer disease and Down syndrome. *Proceedings of the National Academy of Sciences of the United States of America* **82**, 4245-4249

80. Glenner, G. G., and Wong, C. W. (1984) Alzheimer's disease: Initial report of the purification and characterization of a novel cerebrovascular amyloid protein. *Biochemical and biophysical research communications* **120**, 885-890

81. Haass, C., Schlossmacher, M. G., Hung, A. Y., Vigo-Pelfrey, C., Mellon, A., Ostaszewski, B. L., Lieberburg, I., Koo, E. H., Schenk, D., Teplow, D. B., and et al. (1992) Amyloid beta-peptide is produced by cultured cells during normal metabolism. *Nature* **359**, 322-325

82. Deng, Y., Wang, Z., Wang, R., Zhang, X., Zhang, S., Wu, Y., Staufenbiel, M., Cai, F., and Song, W. (2013) Amyloid- β protein (A β) Glu11 is the major β -secretase site of β -site amyloid- β precursor protein-cleaving enzyme 1(BACE1), and shifting the cleavage site to A β Asp1 contributes to Alzheimer pathogenesis. *European Journal of Neuroscience* **37**, 1962-1969

83. Li, Y., Zhou, W., Tong, Y., He, G., and Song, W. (2006) Control of APP processing and Abeta generation level by BACE1 enzymatic activity and transcription. *The FASEB Journal* **20**, 285-292

84. Zhang, S., Wang, Z., Cai, F., Zhang, M., Wu, Y., Zhang, J., and Song, W. (2017) BACE1 Cleavage Site Selection Critical for Amyloidogenesis and Alzheimer's Pathogenesis. *The Journal of Neuroscience* **37**, 6915-6925

85. Sisodia, S. S. (1992) Beta-amyloid precursor protein cleavage by a membrane-bound protease. *Proceedings of the National Academy of Sciences of the United States of America* **89**, 6075-6079

86. Carey, R. M., Balcz, B. A., Lopez-Coviella, I., and Slack, B. E. (2005) Inhibition of dynamin-dependent endocytosis increases shedding of the amyloid precursor protein ectodomain and reduces generation of amyloid β protein. *BMC Cell Biology* **6**, 30

87. Goodger, Z. V., Rajendran, L., Trutzel, A., Kohli, B. M., Nitsch, R. M., and Konietzko, U. (2009) Nuclear signaling by the APP intracellular domain occurs predominantly through the amyloidogenic processing pathway. *Journal of cell science* **122**, 3703-3714

88. Rajendran, L., Honscho, M., Zahn, T. R., Keller, P., Geiger, K. D., Verkade, P., and Simons, K. (2006) Alzheimer's disease beta-amyloid peptides are released in association with exosomes. *Proceedings of the National Academy of Sciences of the United States of America* **103**, 11172-11177

89. Kimberly, W. T., Xia, W., Rahmati, T., Wolfe, M. S., and Selkoe, D. J. (2000) The transmembrane aspartates in presenilin 1 and 2 are obligatory for γ -secretase activity and amyloid β -protein generation. *The Journal of biological chemistry* **275**, 3173-3178

90. Kimberly, W. T., LaVoie, M. J., Ostaszewski, B. L., Ye, W., Wolfe, M. S., and Selkoe, D. J. (2003) γ -Secretase is a membrane protein complex comprised of presenilin, nicastrin, aph-1, and pen-2. *Proceedings of the National Academy of Sciences of the United States of America* **100**, 6382-6387

91. Matsumura, N., Takami, M., Okochi, M., Wada-Kakuda, S., Fujiwara, H., Tagami, S., Funamoto, S., Ihara, Y., and Morishima-Kawashima, M. (2014) γ -Secretase associated with

lipid rafts: multiple interactive pathways in the stepwise processing of β -carboxyl-terminal fragment. *The Journal of biological chemistry* **289**, 5109-5121

92. Takami, M., Nagashima, Y., Sano, Y., Ishihara, S., Morishima-Kawashima, M., Funamoto, S., and Ihara, Y. (2009) γ -Secretase: Successive tripeptide and tetrapeptide release from the transmembrane domain of β -carboxyl terminal fragment. *The Journal of Neuroscience* **29**, 13042-13052

93. Fukumori, A., Fluhner, R., Steiner, H., and Haass, C. (2010) Three-Amino Acid Spacing of Presenilin Endoproteolysis Suggests a General Stepwise Cleavage of γ -Secretase-Mediated Intramembrane Proteolysis. *The Journal of Neuroscience* **30**, 7853-7862

94. Bolduc, D. M., Montagna, D. R., Gu, Y., Selkoe, D. J., and Wolfe, M. S. (2016) Nicastrin functions to sterically hinder γ -secretase-substrate interactions driven by substrate transmembrane domain. *Proceedings of the National Academy of Sciences of the United States of America* **113**, E509-E518

95. Bolduc, D. M., Montagna, D. R., Seghers, M. C., Wolfe, M. S., and Selkoe, D. J. (2016) The amyloid-beta forming tripeptide cleavage mechanism of γ -secretase. *eLife* **5**, e17578

96. Fernandez, M. A., Biette, K. M., Dolios, G., Seth, D., Wang, R., and Wolfe, M. S. (2016) Transmembrane Substrate Determinants for γ -Secretase Processing of APP CTF β . *Biochemistry* **55**, 5675-5688

97. Solenne, O., Arman, S., Aurelie, B., Christophe, L., Stephane, G., Francis, V., Bruno, P., Ishrut, H., and Dirk, B. (2013) Substrate determinants in the C99 juxtamembrane domains differentially affect γ -secretase cleavage specificity and modulator pharmacology. *Journal of neurochemistry* **125**, 610-619

98. Yan, Y., Xu, T.-H., Melcher, K., and Xu, H. E. (2017) Defining the minimum substrate and charge recognition model of gamma-secretase. *Acta Pharmacologica Sinica*

99. Fukumori, A., Okochi, M., Tagami, S., Jiang, J., Itoh, N., Nakayama, T., Yanagida, K., Ishizuka-Katsura, Y., Morihara, T., Kamino, K., Tanaka, T., Kudo, T., Tanii, H., Ikuta, A., Haass, C., and Takeda, M. (2006) Presenilin-Dependent γ -Secretase on Plasma Membrane and Endosomes Is Functionally Distinct. *Biochemistry* **45**, 4907-4914

100. Sun, L., Zhou, R., Yang, G., and Shi, Y. (2017) Analysis of 138 pathogenic mutations in presenilin-1 on the in vitro production of A β 42 and A β 40 peptides by γ -secretase. *Proceedings of the National Academy of Sciences of the United States of America* **114**, E476-E485

101. Petit, D., Fernández, S. G., Zoltowska, K. M., Enzlein, T., Ryan, N. S., O'Connor, A., Szaruga, M., Hill, E., Vandenberghe, R., Fox, N. C., and Chávez-Gutiérrez, L. (2022) A β profiles generated by Alzheimer's disease causing PSEN1 variants determine the pathogenicity of the mutation and predict age at disease onset. *Molecular Psychiatry* **27**, 2821-2832

102. Page, R. M., Baumann, K., Tomioka, M., Pérez-Revuelta, B. I., Fukumori, A., Jacobsen, H., Flohr, A., Luebbbers, T., Ozmen, L., Steiner, H., and Haass, C. (2008) Generation of A β 38 and A β 42 is independently and differentially affected by familial Alzheimer disease-associated presenilin mutations and gamma-secretase modulation. *The Journal of biological chemistry* **283**, 677-683

103. Ran, Y., Cruz, P. E., Ladd, T. B., Fauq, A. H., Jung, J. I., Matthews, J., Felsenstein, K. M., and Golde, T. E. (2014) γ -Secretase Processing and Effects of γ -Secretase Inhibitors and Modulators on Long A β Peptides in Cells. *The Journal of biological chemistry* **289**, 3276-3287

104. Kounnas, M. Z., Lane-Donovan, C., Nowakowski, D. W., Herz, J., and Comer, W. T. (2017) NGP 555, a γ -secretase modulator, lowers the amyloid biomarker, A β 42, in cerebrospinal fluid while preventing Alzheimer's disease cognitive decline in rodents. *Alzheimer's & Dementia: Translational Research & Clinical Interventions* **3**, 65-73

105. Burnouf, S., Gorsky, M. K., Dols, J., Grönke, S., and Partridge, L. (2015) A β 43 is neurotoxic and primes aggregation of A β 40 in vivo. *Acta neuropathologica* **130**, 35-47

106. Fu, L., Sun, Y., Guo, Y., Chen, Y., Yu, B., Zhang, H., Wu, J., Yu, X., Kong, W., and Wu, H. (2017) Comparison of neurotoxicity of different aggregated forms of A β 40, A β 42 and A β 43 in cell cultures. *Journal of Peptide Science* **23**, 245-251
107. Saito, T., Suemoto, T., Brouwers, N., Slegers, K., Funamoto, S., Mihira, N., Matsuba, Y., Yamada, K., Nilsson, P., Takano, J., Nishimura, M., Iwata, N., Van Broeckhoven, C., Ihara, Y., and Saido, T. C. (2011) Potent amyloidogenicity and pathogenicity of A β 43. *Nature neuroscience* **14**, 1023-1032
108. Quartey, M. O., Nyarko, J. N. K., Maley, J. M., Barnes, J. R., Bolanos, M. A. C., Heistad, R. M., Knudsen, K. J., Pennington, P. R., Buttigieg, J., De Carvalho, C. E., Leary, S. C., Parsons, M. P., and Mousseau, D. D. (2021) The A β (1–38) peptide is a negative regulator of the A β (1–42) peptide implicated in Alzheimer disease progression. *Scientific Reports* **11**, 431
109. Wong, P. C., Zheng, H., Chen, H., Becher, M. W., Sirinathsingji, D. J. S., Trumbauer, M. E., Chen, H. Y., Price, D. L., Van Der Ploeg, L. H. T., and Sisodia, S. S. (1997) Presenilin 1 is required for Notch 1 and DII 1 expression in the paraxial mesoderm. *Nature* **387**, 288-292
110. De Strooper, B., Annaert, W., Cupers, P., Saftig, P., Craessaerts, K., Mumm, J. S., Schroeter, E. H., Schrijvers, V., Wolfe, M. S., Ray, W. J., Goate, A., and Kopan, R. (1999) A presenilin-1-dependent [γ]-secretase-like protease mediates release of Notch intracellular domain. *Nature* **398**, 518-522
111. Baranello, R. J., Bharani, K. L., Padmaraju, V., Chopra, N., Lahiri, D. K., Greig, N. H., Pappolla, M. A., and Sambamurti, K. (2015) Amyloid-Beta Protein Clearance and Degradation (ABCD) Pathways and their Role in Alzheimer's Disease. *Current Alzheimer research* **12**, 32-46
112. Iwata, N., Tsubuki, S., Takaki, Y., Watanabe, K., Sekiguchi, M., Hosoki, E., Kawashima-Morishima, M., Lee, H. J., Hama, E., Sekine-Aizawa, Y., and Saido, T. C. (2000) Identification of the major Abeta1-42-degrading catabolic pathway in brain parenchyma: suppression leads to biochemical and pathological deposition. *Nature medicine* **6**, 143-150
113. Iwata, N., Tsubuki, S., Takaki, Y., Shirotani, K., Lu, B., Gerard, N. P., Gerard, C., Hama, E., Lee, H. J., and Saido, T. C. (2001) Metabolic regulation of brain Abeta by neprilysin. *Science (New York, N.Y.)* **292**, 1550-1552
114. Qiu, W. Q., Walsh, D. M., Ye, Z., Vekrellis, K., Zhang, J., Podlisny, M. B., Rosner, M. R., Safavi, A., Hersh, L. B., and Selkoe, D. J. (1998) Insulin-degrading enzyme regulates extracellular levels of amyloid beta-protein by degradation. *The Journal of biological chemistry* **273**, 32730-32738
115. Farris, W., Mansourian, S., Chang, Y., Lindsley, L., Eckman, E. A., Frosch, M. P., Eckman, C. B., Tanzi, R. E., Selkoe, D. J., and Guenette, S. (2003) Insulin-degrading enzyme regulates the levels of insulin, amyloid beta-protein, and the beta-amyloid precursor protein intracellular domain in vivo. *Proceedings of the National Academy of Sciences of the United States of America* **100**, 4162-4167
116. Leissring, M. A., Farris, W., Chang, A. Y., Walsh, D. M., Wu, X., Sun, X., Frosch, M. P., and Selkoe, D. J. (2003) Enhanced proteolysis of beta-amyloid in APP transgenic mice prevents plaque formation, secondary pathology, and premature death. *Neuron* **40**, 1087-1093
117. Sasaguri, H., Takamura, R., Watamura, N., Kakiya, N., Ohshima, T., Fujioka, R., Yamazaki, N., Sekiguchi, M., Iwata, K., Matsuba, Y., Hashimoto, S., Tsubuki, S., Saito, T., Iwata, N., and Saido, T. C. (2021) Neprilysin-sensitive amyloidogenic A β versus IDE-sensitive soluble A β : a probable mechanistic cause for sporadic Alzheimer's disease. *bioRxiv*, 2021.2008.2022.457281
118. Edbauer, D., Willem, M., Lammich, S., Steiner, H., and Haass, C. (2002) Insulin-degrading Enzyme Rapidly Removes the β -Amyloid Precursor Protein Intracellular Domain (AICD). *The Journal of biological chemistry* **277**, 13389-13393

119. Barthelson, K., Newman, M., and Lardelli, M. (2020) Sorting Out the Role of the Sortilin-Related Receptor 1 in Alzheimer's Disease. *Journal of Alzheimer's Disease Reports* **4**, 123-140
120. Zhao, Y., Wu, X., Li, X., Jiang, L.-L., Gui, X., Liu, Y., Sun, Y., Zhu, B., Piña-Crespo, J. C., Zhang, M., Zhang, N., Chen, X., Bu, G., An, Z., Huang, T. Y., and Xu, H. (2018) TREM2 Is a Receptor for β -Amyloid that Mediates Microglial Function. *Neuron* **97**, 1023-1031.e1027
121. Lessard, C. B., Malnik, S. L., Zhou, Y., Ladd, T. B., Cruz, P. E., Ran, Y., Mahan, T. E., Chakrabaty, P., Holtzman, D. M., Ulrich, J. D., Colonna, M., and Golde, T. E. (2018) High-affinity interactions and signal transduction between A β oligomers and TREM2. *EMBO Molecular Medicine* **10**, e9027
122. Jones, R. S., Minogue, A. M., Connor, T. J., and Lynch, M. A. (2013) Amyloid- β -induced astrocytic phagocytosis is mediated by CD36, CD47 and RAGE. *Journal of Neuroimmune Pharmacology* **8**, 301-311
123. Nguyen, J. A., and Yates, R. M. (2021) Better Together: Current Insights Into Phagosome-Lysosome Fusion. *Frontiers in Immunology* **12**
124. Shi, J.-M., Zhu, L., Lan, X., Zhao, D.-W., He, Y.-J., Sun, Z.-Q., Wu, D., and Li, H.-Y. (2020) Endocytosis Is a Key Mode of Interaction between Extracellular β -Amyloid and the Cell Membrane. *Biophysical Journal* **119**, 1078-1090
125. Wesén, E., Jeffries, G. D. M., Matson Dzebo, M., and Esbjörner, E. K. (2017) Endocytic uptake of monomeric amyloid- β peptides is clathrin- and dynamin-independent and results in selective accumulation of A β (1-42) compared to A β (1-40). *Scientific Reports* **7**, 2021
126. Domínguez-Prieto, M., Velasco, A., Tabernero, A., and Medina, J. M. (2018) Endocytosis and Transcytosis of Amyloid- β Peptides by Astrocytes: A Possible Mechanism for Amyloid- β Clearance in Alzheimer's Disease. *Journal of Alzheimer's Disease* **65**, 1109-1124
127. Cheng, Y., Tian, D.-Y., and Wang, Y.-J. (2020) Peripheral clearance of brain-derived A β in Alzheimer's disease: pathophysiology and therapeutic perspectives. *Translational neurodegeneration* **9**, 16
128. Deane, R., Wu, Z., Sagare, A., Davis, J., Du Yan, S., Hamm, K., Xu, F., Parisi, M., LaRue, B., Hu, H. W., Spijkers, P., Guo, H., Song, X., Lenting, P. J., Van Nostrand, W. E., and Zlokovic, B. V. (2004) LRP/Amyloid β -Peptide Interaction Mediates Differential Brain Efflux of A β Isoforms. *Neuron* **43**, 333-344
129. Deane, R., Wu, Z., and Zlokovic, B. V. (2004) RAGE (yin) versus LRP (yang) balance regulates alzheimer amyloid beta-peptide clearance through transport across the blood-brain barrier. *Stroke* **35**, 2628-2631
130. Ramanathan, A., Nelson, A., Sagare, A., and Zlokovic, B. (2015) Impaired vascular-mediated clearance of brain amyloid beta in Alzheimer's disease: The role, regulation and restoration of LRP1. *Front Aging Neurosci* **7**
131. Storck, S. E., Hartz, A. M. S., Bernard, J., Wolf, A., Kachlmeier, A., Mahringer, A., Weggen, S., Pahnke, J., and Pietrzik, C. U. (2018) The concerted amyloid-beta clearance of LRP1 and ABCB1/P-gp across the blood-brain barrier is linked by PICALM. *Brain, behavior, and immunity* **73**, 21-33
132. Deane, R., Du Yan, S., Subramanian, R. K., LaRue, B., Jovanovic, S., Hogg, E., Welch, D., Manness, L., Lin, C., Yu, J., Zhu, H., Ghiso, J., Frangione, B., Stern, A., Schmidt, A. M., Armstrong, D. L., Arnold, B., Liliensiek, B., Nawroth, P., Hofman, F., Kindy, M., Stern, D., and Zlokovic, B. (2003) RAGE mediates amyloid- β peptide transport across the blood-brain barrier and accumulation in brain. *Nature medicine* **9**, 907-913

133. Benveniste, H., Liu, X., Koundal, S., Sanggaard, S., Lee, H., and Wardlaw, J. (2018) The Glymphatic System and Waste Clearance with Brain Aging: A Review. *Gerontology* **65**, 106-119
134. Li, Y., Rusinek, H., Butler, T., Glodzik, L., Pirraglia, E., Babich, J., Mozley, P. D., Nehmeh, S., Pahlajani, S., Wang, X., Tanzi, E. B., Zhou, L., Strauss, S., Carare, R. O., Theise, N., Okamura, N., and de Leon, M. J. (2022) Decreased CSF clearance and increased brain amyloid in Alzheimer's disease. *Fluids and Barriers of the CNS* **19**, 21
135. de Leon, M. J., Li, Y., Okamura, N., Tsui, W. H., Saint-Louis, L. A., Glodzik, L., Osorio, R. S., Fortea, J., Butler, T., Pirraglia, E., Fossati, S., Kim, H. J., Carare, R. O., Nedergaard, M., Benveniste, H., and Rusinek, H. (2017) Cerebrospinal Fluid Clearance in Alzheimer Disease Measured with Dynamic PET. *Journal of Nuclear Medicine* **58**, 1471-1476
136. Silva, I., Silva, J., Ferreira, R., and Trigo, D. (2021) Glymphatic system, AQP4, and their implications in Alzheimer's disease. *Neurological Research and Practice* **3**, 5
137. Wilhelmus, M. M., de Waal, R. M., and Verbeek, M. M. (2007) Heat shock proteins and amateur chaperones in amyloid-Beta accumulation and clearance in Alzheimer's disease. *Molecular Neurobiology* **35**, 203-216
138. Endo, Y., Hasegawa, K., Nomura, R., Arishima, H., Kikuta, K.-i., Yamashita, T., Inoue, Y., Ueda, M., Ando, Y., Wilson, M. R., Hamano, T., Nakamoto, Y., and Naiki, H. (2019) Apolipoprotein E and clusterin inhibit the early phase of amyloid- β aggregation in an in vitro model of cerebral amyloid angiopathy. *Acta neuropathologica communications* **7**, 12
139. Bilousova, T., Melnik, M., Miyoshi, E., Gonzalez, B. L., Poon, W. W., Vinters, H. V., Miller, C. A., Corrada, M. M., Kawas, C., Hatami, A., Albay, R., Glabe, C., and Gylys, K. H. (2019) Apolipoprotein E/Amyloid- β Complex Accumulates in Alzheimer Disease Cortical Synapses via Apolipoprotein E Receptors and Is Enhanced by APOE4. *The American journal of pathology* **189**, 1621-1636
140. Strittmatter, W. J., Saunders, A. M., Schmechel, D., Pericak-Vance, M., Enghild, J., Salvesen, G. S., and Roses, A. D. (1993) Apolipoprotein E: high-avidity binding to beta-amyloid and increased frequency of type 4 allele in late-onset familial Alzheimer disease. *Proceedings of the National Academy of Sciences of the United States of America* **90**, 1977-1981
141. Saunders, A. M., Hulette, C., Welsh-Bohmer, K. A., Schmechel, D. E., Crain, B., Burke, J. R., Alberts, M. J., Strittmatter, W. J., Breitner, J. C. S., Rosenberg, C., Scott, S. V., Gaskell, P. C., Jr., Pericak-Vance, M. A., and Roses, A. D. (1996) Specificity, sensitivity, and predictive value of apolipoprotein-E genotyping for sporadic Alzheimer's disease. *The Lancet* **348**, 90-93
142. Bellenguez, C., Küçükali, F., Jansen, I. E., Kleindam, L., Moreno-Grau, S., et al. (2022) New insights into the genetic etiology of Alzheimer's disease and related dementias. *Nature Genetics* **54**, 412-436
143. Wilhelmus, M. M., Boelens, W. C., Otte-Höller, I., Kamps, B., de Waal, R. M., and Verbeek, M. M. (2006) Small heat shock proteins inhibit amyloid-beta protein aggregation and cerebrovascular amyloid-beta protein toxicity. *Brain research* **1089**, 67-78
144. Kakimura, J.-I., Kitamura, Y., Takata, K., Umeki, M., Suzuki, S., Shibagaki, K., Taniguchi, T., Nomura, Y., Gebicke-Haerter, P. J., Smith, M. A., Perry, G., and Shimohama, S. (2002) Microglial activation and amyloid- β clearance induced by exogenous heat-shock proteins. *The FASEB Journal* **16**, 601-603
145. Mullan, M., Houlden, H., Windelspecht, M., Fidani, L., Lombardi, C., Diaz, P., Rossor, M., Crook, R., Hardy, J., Duff, K., and Crawford, F. (1992) A locus for familial early-onset Alzheimer's disease on the long arm of chromosome 14, proximal to the [alpha]1-antichymotrypsin gene. *Nature Genetics* **2**, 340-342

146. Haltia, M., Viitanen, M., Sulkava, R., Ala-Hurula, V., Poyhonen, M., Goldfarb, L., Brown, P., Levy, E., Houlde, H., Crook, R., Goate, A., Clark, R., Korenblat, K., Pandit, S., Keller, H. D., Llius, L., Liu, L., Axelman, K., Forsell, L., Winblad, B., Lannfelt, L., and Hardy, J. (1994) Chromosome 14-encoded Alzheimer's disease: Genetic and clinicopathological description. *Annals of neurology* **36**, 362-367
147. Sherrington, R., Rogaev, E. I., Liang, Y., Rogaeva, E. A., and et al. (1995) Cloning of a gene bearing missense mutations in early-onset familial Alzheimer's disease. *Nature* **375**, 754-760
148. Levy-Lahad, E., Wasco, W., Poorkaj, P., Romano, D. M., Oshima, J., Pettingell, W. H., Yu, C.-e., Jondro, P. D., Schmidt, S. D., Wang, K., Crowley, A. C., Fu, Y.-H., Guenette, S. Y., Galas, D., Nemens, E., Wijsman, E. M., Bird, T. D., Schellenberg, G. D., and Tanzi, R. E. (1995) Candidate Gene for the Chromosome 1 Familial Alzheimer's Disease Locus. *Science (New York, N.Y.)* **269**, 973-977
149. Levy-Lahad, E., Wijsman, E., Nemens, E., Anderson, L., Goddard, K., Weber, J., Bird, T., and Schellenberg, G. (1995) A familial Alzheimer's disease locus on chromosome 1. *Science (New York, N.Y.)* **269**, 970-973
150. Rogaev, E. I., Sherrington, R., Rogaeva, E. A., Levesque, G., Ikeda, M., Liang, Y., Chi, H., Lin, C., Holman, K., Tsuda, T., Mar, L., Sorbi, S., Nacmias, B., Piacentini, S., Amaducci, L., Chumakov, I., Cohen, D., Lannfelt, L., Fraser, P. E., Rommens, J. M., and George-Hyslop, P. H. S. (1995) Familial Alzheimer's disease in kindreds with missense mutations in a gene on chromosome 1 related to the Alzheimer's disease type 3 gene. *Nature* **376**, 775-778
151. Khan, A. A., Ali, R. H., and Mirza, B. (2020) Evolutionary History of Alzheimer Disease-Causing Protein Family Presenilins with Pathological Implications. *Journal of molecular evolution* **88**, 674-688
152. Doan, A., Thinakaran, G., Borchelt, D. R., Slunt, H. H., Ratovitsky, T., Podlisny, M., Selkoe, D. J., Seeger, M., Gandy, S. E., Price, D. L., and Sisodia, S. S. (1996) Protein Topology of Presenilin 1. *Neuron* **17**, 1023-1030
153. Thinakaran, G., Borchelt, D. R., Lee, M. K., Slunt, H. H., Spitzer, L., Kim, G., Ratovitsky, T., Davenport, F., Nordstedt, C., Seeger, M., Hardy, J., Levey, A. I., Gandy, S. E., Jenkins, N. A., Copeland, N. G., Price, D. L., and Sisodia, S. S. (1996) Endoproteolysis of presenilin 1 and accumulation of processed derivatives in vivo. *Neuron* **17**, 181-190
154. Wolfe, M. S., Xia, W., Ostaszewski, B. L., Diehl, T. S., Kimberly, W. T., and Selkoe, D. J. (1999) Two transmembrane aspartates in presenilin-1 required for presenilin endoproteolysis and γ -secretase activity. *Nature* **398**, 513-517
155. Shirotani, K., Takahashi, K., Ozawa, K., Kunishita, T., and Tabira, T. (1997) Determination of a cleavage site of presenilin 2 protein in stably transfected SH-SY5Y human neuroblastoma cell lines. *Biochemical and biophysical research communications* **240**, 728-731
156. Yu, G., Chen, F., Nishimura, M., Steiner, H., Tandon, A., Kawarai, T., Arawaka, S., Supala, A., Song, Y.-Q., Rogaeva, E., Holmes, E., Zhang, D. M., Milman, P., Fraser, P., Haass, C., and St George-Hyslop, P. (2000) Mutation of conserved aspartates affect maturation of presenilin 1 and presenilin 2 complexes. *Acta Neurologica Scandinavica* **102**, 6-11
157. Thinakaran, G., Harris, C. L., Ratovitski, T., Davenport, F., Slunt, H. H., Price, D. L., Borchelt, D. R., and Sisodia, S. S. (1997) Evidence that levels of presenilins (PS1 and PS2) are coordinately regulated by competition for limiting cellular factors. *The Journal of biological chemistry* **272**, 28415-28422
158. Ratovitski, T., Slunt, H. H., Thinakaran, G., Price, D. L., Sisodia, S. S., and Borchelt, D. R. (1997) Endoproteolytic Processing and Stabilization of Wild-type and Mutant Presenilin *The Journal of biological chemistry* **272**, 24536-24541
159. Seeger, M., Nordstedt, C., Petanceska, S., Kovacs, D. M., Gouras, G. K., Hahne, S., Fraser, P., Levesque, L., Czernik, A. J., George-Hyslop, P. S., Sisodia, S. S., Thinakaran, G.,

- Tanzi, R. E., Greengard, P., and Gandy, S. (1997) Evidence for phosphorylation and oligomeric assembly of presenilin 1. *Proceedings of the National Academy of Sciences of the United States of America* **94**, 5090-5094
160. Capell, A., Grünberg, J., Pesold, B., Diehlmann, A., Citron, M., Nixon, R., Beyreuther, K., Selkoe, D. J., and Haass, C. (1998) The proteolytic fragments of the Alzheimer's disease-associated presenilin-1 form heterodimers and occur as a 100-150-kDa molecular mass complex. *The Journal of biological chemistry* **273**, 3205-3211
161. Yu, G., Nishimura, M., Arawaka, S., Levitan, D., Zhang, L., Tandon, A., Song, Y. Q., Rogaeva, E., Chen, F., Kawarai, T., Supala, A., Levesque, L., Yu, H., Yang, D. S., Holmes, E., Milman, P., Liang, Y., Zhang, D. M., Xu, D. H., Sato, C., Rogaeve, E., Smith, M., Janus, C., Zhang, Y., Aebbersold, R., Farrer, L., Sorbl, S., Bruni, A., Fraser, P., and George-Hyslop, P. S. (2000) Nicastrin modulates presenilin-mediated notch/glp-1 signal transduction and β APP processing. *Nature* **407**, 48-54
162. Donoviel, D. B., Hadjantonakis, A.-K., Ikeda, M., Zheng, H., Hyslop, P. S. G., and Bernstein, A. (1999) Mice lacking both presenilin genes exhibit early embryonic patterning defects. *Genes & development* **13**, 2801-2810
163. Herreman, A., Hartmann, D., Annaert, W., Saftig, P., Craessaerts, K., Serneels, L., Umans, L., Schrijvers, V., Checler, F., Vanderstichele, H., Baekelandt, V., Dressel, R., Cupers, P., Huylebroeck, D., Zwijsen, A., Van Leuven, F., and De Strooper, B. (1999) Presenilin 2 Deficiency Causes a Mild Pulmonary Phenotype and no Changes in Amyloid Precursor Protein Processing but Enhances the Embryonic Lethal Phenotype of Presenilin 1 Deficiency. *Proceedings of the National Academy of Sciences of the United States of America* **96**, 11872-11877
164. Struhl, G., and Greenwald, I. (1999) Presenilin is required for activity and nuclear access of Notch in Drosophila. *Nature* **398**, 522-525
165. Struhl, G., and Greenwald, I. (2001) Presenilin-Mediated Transmembrane Cleavage is Required for Notch Signal Transduction in Drosophila. *Proceedings of the National Academy of Sciences of the United States of America* **98**, 229-234
166. Li, X., and Greenwald, I. (1997) HOP-1, a Caenorhabditis elegans presenilin, appears to be functionally redundant with SEL-12 presenilin and to facilitate LIN-12 and GLP-1 signaling. *Proceedings of the National Academy of Sciences of the United States of America* **94**, 12204-12209
167. Westlund, B., Parry, D., Clover, R., Basson, M., and Johnson, C. D. (1999) Reverse genetic analysis of Caenorhabditis elegans presenilins reveals redundant but unequal roles for sel-12 and hop-1 in Notch-pathway signaling. *Proceedings of the National Academy of Sciences of the United States of America* **96**, 2497-2502
168. Swiatek, P. J., Lindsell, C. E., del Amo, F. F., Weinmaster, G., and Gridley, T. (1994) Notch1 is essential for postimplantation development in mice. *Genes & development* **8**, 707-719
169. Conlon, R. A., Reaume, A. G., and Rossant, J. (1995) Notch1 is required for the coordinate segmentation of somites. *Development (Cambridge, England)* **121**, 1533-1545
170. Francis, R., McGrath, G., Zhang, J., Ruddy, D. A., Sym, M., Apfeld, J., Nicoll, M., Maxwell, M., Hai, B., Ellis, M. C., Parks, A. L., Xu, W., Li, J., Gurney, M., Myers, R. L., Himes, C. S., Hiebsch, R., Ruble, C., Nye, J. S., and Curtis, D. (2002) Aph-1 and Pen-2 Are Required for Notch Pathway Signaling, γ -Secretase Cleavage of β APP, and Presenilin Protein Accumulation. *Developmental Cell* **3**, 85-97
171. Goutte, C., Tsunozaki, M., Hale, V. A., and Priess, J. R. (2002) APH-1 is a Multipass Membrane Protein Essential for the Notch Signaling Pathway in Caenorhabditis elegans Embryos. *Proceedings of the National Academy of Sciences of the United States of America* **99**, 775-779

172. Lee, S. F., Shah, S., Li, H., Yu, C., Han, W., and Yu, G. (2002) Mammalian APH-1 interacts with presenilin and nicastrin and is required for intramembrane proteolysis of amyloid-beta precursor protein and Notch. *The Journal of biological chemistry* **277**, 45013-45019
173. Gu, Y., Chen, F., Sanjo, N., Kawarai, T., Hasegawa, H., Duthie, M., Li, W., Ruan, X., Luthra, A., Mount, H. T., Tandon, A., Fraser, P. E., and St George-Hyslop, P. (2003) APH-1 interacts with mature and immature forms of presenilins and nicastrin and may play a role in maturation of presenilin.nicastrin complexes. *The Journal of biological chemistry* **278**, 7374-7380
174. LaVoie, M. J., Fraering, P. C., Ostaszewski, B. L., Ye, W., Kimberly, W. T., Wolfe, M. S., and Selkoe, D. J. (2003) Assembly of the γ -Secretase Complex Involves Early Formation of an Intermediate Subcomplex of Aph-1 and Nicastrin. *The Journal of biological chemistry* **278**, 37213-37222
175. Marlow, L., Canet, R. M., Haugabook, S. J., Hardy, J. A., Lahiri, D. K., and Sambamurti, K. (2003) APH1, PEN2, and Nicastrin increase A β levels and γ -secretase activity. *Biochemical and biophysical research communications* **305**, 502-509
176. Steiner, H., Winkler, E., Edbauer, D., Prokop, S., Basset, G., Yamasaki, A., Kostka, M., and Haass, C. (2002) PEN-2 is an integral component of the γ -secretase complex required for coordinated expression of presenilin and nicastrin. *The Journal of biological chemistry* **277**, 39062-39065
177. Sato, T., Diehl, T. S., Narayanan, S., Funamoto, S., Ihara, Y., De Strooper, B., Steiner, H., Haass, C., and Wolfe, M. S. (2007) Active γ -secretase complexes contain only one of each component. *The Journal of biological chemistry* **282**, 33985-33993
178. Gu, Y., Sanjo, N., Chen, F., Hasegawa, H., Petit, A., Ruan, X., Li, W., Shier, C., Kawarai, T., Schmitt-Ulms, G., Westaway, D., St George-Hyslop, P., and Fraser, P. E. (2004) The presenilin proteins are components of multiple membrane-bound complexes that have different biological activities. *The Journal of biological chemistry* **279**, 31329-31336
179. Chen, F., Hasegawa, H., Schmitt-Ulms, G., Kawarai, T., Böhm, C., Katayama, T., Gu, Y., Sanjo, N., Glista, M., Rogaeve, E., Wakutani, Y., Pardossi-Piquard, R., Ruan, X., Tandon, A., Checler, F., Marambaud, P., Hansen, K., Westaway, D., St George-Hyslop, P., and Fraser, P. (2006) TMP21 is a presenilin complex component that modulates [γ]-secretase but not [ϵ]-secretase activity. *Nature* **440**, 1208-1212
180. Pardossi-Piquard, R., Böhm, C., Chen, F., Kanemoto, S., Checler, F., Schmitt-Ulms, G., St. George-Hyslop, P., and Fraser, P. E. (2009) TMP21 Transmembrane Domain Regulates γ -Secretase Cleavage. *The Journal of biological chemistry* **284**, 28634-28641
181. Dolcini, V., Dunys, J., Sevalle, J., Chen, F., Guillot-Sestier, M.-V., St. George-Hyslop, P., Fraser, P. E., and Checler, F. (2008) TMP21 regulates A β production but does not affect caspase-3, p53, and neprilysin. *Biochemical and biophysical research communications* **371**, 69-74
182. He, G., Luo, W., Li, P., Remmers, C., Netzer, W. J., Hendrick, J., Bettayeb, K., Flajolet, M., Gorelick, F., Wennogle, L. P., and Greengard, P. (2010) Gamma-secretase activating protein is a therapeutic target for Alzheimer's disease. *Nature* **467**, 95-98
183. Wakabayashi, T., Craessaerts, K., Bammens, L., Bentahir, M., Borgions, F., Herdewijn, P., Staes, A., Timmerman, E., Vandekerckhove, J., Rubinstein, E., Boucheix, C., Gevaert, K., and De Strooper, B. (2009) Analysis of the [γ]-secretase interactome and validation of its association with tetraspanin-enriched microdomains. *Nature cell biology* **11**, 1340-1346
184. Jeon, A. H. W., Böhm, C., Chen, F., Huo, H., Ruan, X., Ren, C. H., Ho, K., Qamar, S., Mathews, P. M., Fraser, P. E., Mount, H. T. J., St George-Hyslop, P., and Schmitt-Ulms, G. (2013) Interactome Analyses of Mature γ -Secretase Complexes Reveal Distinct Molecular

Environments of Presenilin (PS) Paralogs and Preferential Binding of Signal Peptide Peptidase to PS2. *The Journal of biological chemistry* **288**, 15352-15366

185. Teranishi, Y., Hur, J.-Y., Welander, H., Frånberg, J., Aoki, M., Winblad, B., Frykman, S., and Tjernberg, L. O. (2010) Affinity pulldown of γ -secretase and associated proteins from human and rat brain. *Journal of cellular and molecular medicine* **14**, 2675-2686

186. Hur, J.-Y., Teranishi, Y., Kihara, T., Yamamoto, N. G., Inoue, M., Hosia, W., Hashimoto, M., Winblad, B., Frykman, S., and Tjernberg, L. O. (2012) Identification of novel γ -secretase-associated proteins in detergent-resistant membranes from brain. *The Journal of biological chemistry* **287**, 11991-12005

187. Frykman, S., Teranishi, Y., Hur, J.-Y., Sandebring, A., Goto Yamamoto, N., Ancarcrona, M., Nishimura, T., Winblad, B., Bogdanovic, N., Schedin-Weiss, S., Kihara, T., and Tjernberg, L. O. (2012) Identification of two novel synaptic γ -secretase associated proteins that affect amyloid β -peptide levels without altering Notch processing. *Neurochemistry International* **61**, 108-118

188. Capell, A., Behr, D., Prokop, S., Steiner, H., Kaether, C., Shearman, M. S., and Haass, C. (2005) γ -Secretase Complex Assembly within the Early Secretory Pathway. *The Journal of biological chemistry* **280**, 6471-6478

189. Spasic, D., Raemaekers, T., Dillen, K., Declerck, I., Baert, V., Serneels, L., Füllekrug, J., and Annaert, W. (2007) Rer1p competes with APH-1 for binding to nicastrin and regulates gamma-secretase complex assembly in the early secretory pathway. *The Journal of cell biology* **176**, 629-640

190. Kaether, C., Scheuermann, J., Fassler, M., Zilow, S., Shirotani, K., Valkova, C., Novak, B., Kacmar, S., Steiner, H., and Haass, C. (2007) Endoplasmic reticulum retention of the gamma-secretase complex component Pen2 by Rer1. *EMBO Reports* **8**, 743-748

191. Kaether, C., Capell, A., Edbauer, D., Winkler, E., Novak, B., Steiner, H., and Haass, C. (2004) The presenilin C-terminus is required for ER-retention, nicastrin-binding and γ -secretase activity. *EMBO J* **23**, 4738-4748

192. Shirotani, K., Edbauer, D., Prokop, S., Haass, C., and Steiner, H. (2004) Identification of Distinct γ -Secretase Complexes with Different APH-1 Variants. *The Journal of biological chemistry* **279**, 41340-41345

193. Herreman, A., Van Gassen, G., Bentahir, M., Nyabi, O., Craessaerts, K., Mueller, U., Annaert, W., and De Strooper, B. (2003) γ -Secretase activity requires the presenilin-dependent trafficking of nicastrin through the Golgi apparatus but not its complex glycosylation. *Journal of cell science* **116**, 1127-1136

194. Zhang, Y. W., Luo, W. J., Wang, H., Lin, P., Vetrivel, K. S., Liao, F., Li, F., Wong, P. C., Farquhar, M. G., Thinakaran, G., and Xu, H. (2005) Nicastrin is critical for stability and trafficking but not association of other presenilin/gamma-secretase components. *The Journal of biological chemistry* **280**, 17020-17026

195. Fortna, R. R., Crystal, A. S., Morais, V. A., Pijak, D. S., Lee, V. M. Y., and Doms, R. W. (2004) Membrane Topology and Nicastrin-enhanced Endoproteolysis of APH-1, a Component of the γ -Secretase Complex. *The Journal of biological chemistry* **279**, 3685-3693

196. Lee, S. F., Shah, S., Yu, C., Wigley, W. C., Li, H., Lim, M., Pedersen, K., Han, W., Thomas, P., Lundkvist, J., Hao, Y. H., and Yu, G. (2004) A conserved GXXXG motif in APH-1 is critical for assembly and activity of the gamma-secretase complex. *The Journal of biological chemistry* **279**, 4144-4152

197. Pardossi-Piquard, R., Yang, S. P., Kanemoto, S., Gu, Y., Chen, F., Böhm, C., Sevalle, J., Li, T., Wong, P. C., Checler, F., Schmitt-Ulms, G., St. George-Hyslop, P., and Fraser, P. E. (2009) APH1 polar transmembrane residues regulate the assembly and activity of presenilin complexes. *The Journal of biological chemistry* **284**, 16298-16307

198. Bai, X.-c., Yan, C., Yang, G., Lu, P., Ma, D., Sun, L., Zhou, R., Scheres, S. H. W., and Shi, Y. (2015) An atomic structure of human γ -secretase. *Nature* **525**, 212-217
199. Guo, X., Wang, Y., Zhou, J., Jin, C., Wang, J., Jia, B., Jing, D., Yan, C., Lei, J., Zhou, R., and Shi, Y. (2022) Molecular basis for isoform-selective inhibition of presenilin-1 by MRK-560. *Nature Communications* **13**, 6299
200. Hébert, S. S., Serneels, L., Dejaegere, T., Horr , K., Dabrowski, M., Baert, V., Annaert, W., Hartmann, D., and De Strooper, B. (2004) Coordinated and widespread expression of γ -secretase in vivo: evidence for size and molecular heterogeneity. *Neurobiology of disease* **17**, 260-272
201. Schrodinger, LLC. The PyMOL Molecular Graphics System, Version 2.1.0.
202. Arawaka, S., Hasegawa, H., Tandon, A., Janus, C., Chen, F., Yu, G., Kikuchi, K., Koyama, S., Kato, T., Fraser, P. E., and St George-Hyslop, P. (2002) The levels of mature glycosylated nicastrin are regulated and correlate with γ -secretase processing of amyloid β -precursor protein. *Journal of neurochemistry* **83**, 1065-1071
203. Yang, D.-S., Tandon, A., Chen, F., Yu, G., Yu, H., Arawaka, S., Hasegawa, H., Duthie, M., Schmidt, S. D., Ramabhadran, T. V., Nixon, R. A., Mathews, P. M., Gandy, S. E., Mount, H. T. J., St George-Hyslop, P., and Fraser, P. E. (2002) Mature glycosylation and trafficking of nicastrin modulate its binding to presenilins. *The Journal of biological chemistry* **277**, 28135-28142
204. Shah, S., Lee, S.-F., Tabuchi, K., Hao, Y.-H., Yu, C., LaPlant, Q., Ball, H., Dann Iii, C. E., S dhof, T., and Yu, G. (2005) Nicastrin Functions as a γ -Secretase-Substrate Receptor. *Cell* **122**, 435-447
205. Fukumori, A., and Steiner, H. (2016) Substrate recruitment of γ -secretase and mechanism of clinical presenilin mutations revealed by photoaffinity mapping. *EMBO J* **35**, 1628-1643
206. Petit, D., Hitzenberger, M., Lismont, S., Zoltowska, K. M., Ryan, N. S., Mercken, M., Bischoff, F., Zacharias, M., and Ch vez-Guti rrez, L. (2019) Extracellular interface between APP and Nicastrin regulates A β length and response to γ -secretase modulators. *EMBO J* **38**, e101494
207. Yang, G., Zhou, R., Guo, X., Yan, C., Lei, J., and Shi, Y. (2021) Structural basis of γ -secretase inhibition and modulation by small molecule drugs. *Cell* **184**, 521-533.e514
208. Zhao, G., Liu, Z., Ilagan, M. X. G., and Kopan, R. (2010) γ -Secretase Composed of PS1/Pen2/Aph1a Can Cleave Notch and Amyloid Precursor Protein in the Absence of Nicastrin. *The Journal of Neuroscience* **30**, 1648-1656
209. Kamp, F., Winkler, E., Trambauer, J., Ebke, A., Fluhrer, R., and Steiner, H. (2015) Intramembrane Proteolysis of β -Amyloid Precursor Protein by γ -Secretase Is an Unusually Slow Process. *Biophysical Journal* **108**, 1229-1237
210. Luo, W. J., Wang, H., Li, H., Kim, B. S., Shah, S., Lee, H. J., Thinakaran, G., Kim, T. W., Yu, G., and Xu, H. (2003) PEN-2 and APH-1 coordinately regulate proteolytic processing of presenilin 1. *The Journal of biological chemistry* **278**, 7850-7854
211. Prokop, S., Shirotani, K., Edbauer, D., Haass, C., and Steiner, H. (2004) Requirement of PEN-2 for stabilization of the presenilin N-/C-terminal fragment heterodimer within the gamma-secretase complex. *The Journal of biological chemistry* **279**, 23255-23261
212. Kim, S.-H., and Sisodia, S. S. (2005) A Sequence within the First Transmembrane Domain of PEN-2 Is Critical for PEN-2-mediated Endoproteolysis of Presenilin 1. *The Journal of biological chemistry* **280**, 1992-2001
213. Hasegawa, H., Sanjo, N., Chen, F., Gu, Y. J., Shier, C., Petit, A., Kawarai, T., Katayama, T., Schmidt, S. D., Mathews, P. M., Schmitt-Ulms, G., Fraser, P. E., and St George-Hyslop, P. (2004) Both the sequence and length of the C terminus of PEN-2 are critical for

intermolecular interactions and function of presenilin complexes. *The Journal of biological chemistry* **279**, 46455-46463

214. Prokop, S., Haass, C., and Steiner, H. (2005) Length and overall sequence of the PEN-2 C-terminal domain determines its function in the stabilization of presenilin fragments. *Journal of neurochemistry* **94**, 57-62

215. Bergman, A., Hansson, E. M., Pursglove, S. E., Farmery, M. R., Lannfelt, L., Lendahl, U., Lundkvist, J., and Näslund, J. (2004) Pen-2 Is Sequestered in the Endoplasmic Reticulum and Subjected to Ubiquitylation and Proteasome-mediated Degradation in the Absence of Presenilin. *The Journal of biological chemistry* **279**, 16744-16753

216. Crystal, A. S., Morais, V. A., Fortna, R. R., Carlin, D., Pierson, T. C., Wilson, C. A., Lee, V. M. Y., and Doms, R. W. (2004) Presenilin Modulates Pen-2 Levels Posttranslationally by Protecting It from Proteasomal Degradation. *Biochemistry* **43**, 3555-3563

217. Placanica, L., Tarassishin, L., Yang, G., Peethumnongsin, E., Kim, S.-H., Zheng, H., Sisodia, S. S., and Li, Y.-M. (2009) Pen2 and presenilin-1 modulate the dynamic equilibrium of presenilin-1 and presenilin-2 γ -secretase complexes. *The Journal of biological chemistry* **284**, 2967-2977

218. Laudon, H., Hansson, E. M., Melén, K., Bergman, A., Farmery, M. R., Winblad, B., Lendahl, U., von Heijne, G., and Näslund, J. (2005) A Nine-transmembrane Domain Topology for Presenilin 1. *The Journal of biological chemistry* **280**, 35352-35360

219. Spasic, D., Tolia, A., Dillen, K., Baert, V., De Strooper, B., Vrijens, S., and Annaert, W. (2006) Presenilin-1 Maintains a Nine-Transmembrane Topology throughout the Secretory Pathway. *The Journal of biological chemistry* **281**, 26569-26577

220. Sannerud, R., Esselens, C., Ejsmont, P., Mattera, R., Rochin, L., et al. (2016) Restricted location of PSEN2/ γ -secretase determines substrate specificity and generates an intracellular A β pool. *Cell* **166**, 193-208

221. Schmidt, F. C., Fitz, K., Feilen, L. P., Okochi, M., Steiner, H., and Langosch, D. (2023) Different transmembrane domains determine the specificity and efficiency of the cleavage activity of the γ -secretase subunit presenilin. *The Journal of biological chemistry* **299**, 104626

222. Knappenberger, K. S., Tian, G., Ye, X., Sobotka-Briner, C., Ghanekar, S. V., Greenberg, B. D., and Scott, C. W. (2004) Mechanism of γ -Secretase Cleavage Activation: Is γ -Secretase Regulated through Autoinhibition Involving the Presenilin-1 Exon 9 Loop? *Biochemistry* **43**, 6208-6218

223. Woodruff, G., Young, J. E., Martinez, F. J., Buen, F., Gore, A., Kinaga, J., Li, Z., Yuan, S. H., Zhang, K., and Goldstein, L. S. B. (2013) The Presenilin-1 Δ E9 mutation results in reduced γ -secretase activity, but not total loss of PS1 function, in isogenic human stem cells. *Cell Reports* **5**, 10.1016/j.celrep.2013.1010.1018

224. Yamasaki, A., Eimer, S., Okochi, M., Smialowska, A., Kaether, C., Baumeister, R., Haass, C., and Steiner, H. (2006) The GxGD Motif of Presenilin Contributes to Catalytic Function and Substrate Identification of γ -Secretase. *The Journal of Neuroscience* **26**, 3821-3828

225. Pérez-Revuelta, B. I., Fukumori, A., Lammich, S., Yamasaki, A., Haass, C., and Steiner, H. (2010) Requirement for small side chain residues within the GxGD-motif of presenilin for γ -secretase substrate cleavage. *Journal of neurochemistry* **112**, 940-950

226. Kretner, B., Fukumori, A., Kuhn, P.-H., Pérez-Revuelta, B. I., Lichtenthaler, S. F., Haass, C., and Steiner, H. (2013) Important functional role of residue x of the presenilin GxGD protease active site motif for APP substrate cleavage specificity and substrate selectivity of γ -secretase. *Journal of neurochemistry* **125**, 144-156

227. Tomita, T., Watabiki, T., Takikawa, R., Morohashi, Y., Takasugi, N., Kopan, R., De Strooper, B., and Iwatsubo, T. (2001) The First Proline of PALP Motif at the C Terminus of

- Presenilins Is Obligatory for Stabilization, Complex Formation, and γ -Secretase Activities of Presenilins. *The Journal of biological chemistry* **276**, 33273-33281
228. Wang, J., Brunkan, A. L., Hecimovic, S., Walker, E., and Goate, A. (2004) Conserved "PAL" sequence in presenilins is essential for γ -secretase activity, but not required for formation or stabilization of γ -secretase complexes. *Neurobiology of disease* **15**, 654-666
229. Wang, J., Beher, D., Nyborg, A. C., Shearman, M. S., Golde, T. E., and Goate, A. (2006) C-terminal PAL motif of presenilin and presenilin homologues required for normal active site conformation. *Journal of neurochemistry* **96**, 218-227
230. Sato, C., Takagi, S., Tomita, T., and Iwatsubo, T. (2008) The C-Terminal PAL Motif and Transmembrane Domain 9 of Presenilin 1 Are Involved in the Formation of the Catalytic Pore of the γ -Secretase. *The Journal of Neuroscience* **28**, 6264-6271
231. Yang, G., Zhou, R., Zhou, Q., Guo, X., Yan, C., Ke, M., Lei, J., and Shi, Y. (2018) Structural basis of Notch recognition by human γ -secretase. *Nature*
232. Zhou, R., Yang, G., Guo, X., Zhou, Q., Lei, J., and Shi, Y. (2019) Recognition of the amyloid precursor protein by human γ -secretase. *Science (New York, N.Y.)*, eaaw0930
233. Shirotani, K., Tomioka, M., Kremmer, E., Haass, C., and Steiner, H. (2007) Pathological activity of familial Alzheimer's disease-associated mutant presenilin can be executed by six different γ -secretase complexes. *Neurobiology of disease* **27**, 102-107
234. Levitan, D., Doyle, T. G., Brousseau, D., Lee, M. K., Thinakaran, G., Slunt, H. H., Sisodia, S. S., and Greenwald, I. (1996) Assessment of normal and mutant human presenilin function in *Caenorhabditis elegans*. *Proceedings of the National Academy of Sciences of the United States of America* **93**, 14940-14944
235. Yurrita, M. M., Fernández-Muñoz, B., Del Castillo, G., Martín-Villar, E., Renart, J., and Quintanilla, M. (2014) Podoplanin is a substrate of presenilin-1/ γ -secretase. *The international journal of biochemistry & cell biology* **46**, 68-75
236. Maetzel, D., Denzel, S., Mack, B., Canis, M., Went, P., Benk, M., Kieu, C., Papior, P., Baeuerle, P. A., Munz, M., and Gires, O. (2009) Nuclear signalling by tumour-associated antigen EpCAM. *Nature cell biology* **11**, 162-171
237. Watanabe, H., Imaizumi, K., Cai, T., Zhou, Z., Tomita, T., and Okano, H. (2021) Flexible and accurate substrate processing with distinct presenilin/ γ -secretases in human cortical neurons. *eNeuro* **8**, ENEURO.0500-0520.2021
238. Meckler, X., and Checler, F. (2016) Presenilin 1 and presenilin 2 target γ -secretase complexes to distinct cellular compartments. *The Journal of biological chemistry* **291**, 12821-12837
239. Gouras, G. K., Tsai, J., Naslund, J., Vincent, B., Edgar, M., Checler, F., Greenfield, J. P., Haroutunian, V., Buxbaum, J. D., Xu, H., Greengard, P., and Relkin, N. R. (2000) Intraneuronal A β 42 accumulation in human brain. *The American journal of pathology* **156**, 15-20
240. Bayer, Thomas A., and Wirths, O. (2011) Intraneuronal A β as a trigger for neuron loss: can this be translated into human pathology? *Biochemical Society Transactions* **39**, 857-861
241. Pensalfini, A., Albay Iii, R., Rasool, S., Wu, J. W., Hatami, A., Arai, H., Margol, L., Milton, S., Poon, W. W., Corrada, M. M., Kawas, C. H., and Glabe, C. G. (2014) Intracellular amyloid and the neuronal origin of Alzheimer neuritic plaques. *Neurobiology of disease* **71**, 53-61
242. Gouras, G. K., Willén, K., and Faideau, M. (2014) The Inside-Out Amyloid Hypothesis and Synapse Pathology in Alzheimer's Disease. *Neuro - Degenerative Diseases* **13**, 142-146
243. Gouras, G. K., Willén, K., and Tampellini, D. (2012) Critical role of intraneuronal A β in Alzheimer's disease: Technical challenges in studying intracellular A β . *Life Sciences* **91**, 1153-1158

244. Berezovska, O., Lleo, A., Herl, L. D., Frosch, M. P., Stern, E. A., Bacskai, B. J., and Hyman, B. T. (2005) Familial Alzheimer's Disease Presenilin 1 Mutations Cause Alterations in the Conformation of Presenilin and Interactions with Amyloid Precursor Protein. *The Journal of Neuroscience* **25**, 3009-3017
245. Wahlster, L., Arimon, M., Nasser-Ghodsi, N., Post, K. L., Serrano-Pozo, A., Uemura, K., and Berezovska, O. (2013) Presenilin-1 adopts pathogenic conformation in normal aging and in sporadic Alzheimer's disease. *Acta neuropathologica* **125**, 187-199
246. Wang, X., Cui, J., Li, W., Zeng, X., Zhao, J., and Pei, G. (2015) γ -Secretase Modulators and Inhibitors Induce Different Conformational Changes of Presenilin 1 Revealed by FLIM and FRET. *Journal of Alzheimer's Disease* **47**, 927-937
247. Li, Y.-M., Xu, M., Lai, M.-T., Huang, Q., Castro, J. L., DiMuzio-Mower, J., Harrison, T., Lellis, C., Nadin, A., Neduelil, J. G., Register, R. B., Sardana, M. K., Shearman, M. S., Smith, A. L., Shi, X.-P., Yin, K.-C., Shafer, J. A., and Gardell, S. J. (2000) Photoactivated γ -secretase inhibitors directed to the active site covalently label presenilin 1. *Nature* **405**, 689-694
248. Xu, M., Lai, M.-T., Huang, Q., DiMuzio-Mower, J., Castro, J. L., Harrison, T., Nadin, A., Neduelil, J. G., Shearman, M. S., Shafer, J. A., Gardell, S. J., and Li, Y.-M. (2002) γ -Secretase: characterization and implication for Alzheimer disease therapy. *Neurobiology of aging* **23**, 1023-1030
249. Chau, D.-M., Crump, C. J., Villa, J. C., Scheinberg, D. A., and Li, Y.-M. (2012) Familial Alzheimer Disease Presenilin-1 Mutations Alter the Active Site Conformation of γ -secretase. *The Journal of biological chemistry* **287**, 17288-17296
250. Wong, E., Liao, G. P., Chang, J. C., Xu, P., Li, Y.-M., and Greengard, P. (2019) GSAP modulates γ -secretase specificity by inducing conformational change in PS1. *Proceedings of the National Academy of Sciences of the United States of America* **116**, 6385-6390
251. Sato, C., Morohashi, Y., Tomita, T., and Iwatsubo, T. (2006) Structure of the Catalytic Pore of γ -Secretase Probed by the Accessibility of Substituted Cysteines. *The Journal of Neuroscience* **26**, 12081-12088
252. Takagi, S., Tominaga, A., Sato, C., Tomita, T., and Iwatsubo, T. (2010) Participation of Transmembrane Domain 1 of Presenilin 1 in the Catalytic Pore Structure of the γ -Secretase. *The Journal of Neuroscience* **30**, 15943-15950
253. Tominaga, A., Cai, T., Takagi-Niidome, S., Iwatsubo, T., and Tomita, T. (2016) Conformational Changes in Transmembrane Domain 4 of Presenilin 1 Are Associated with Altered Amyloid- β 42 Production. *The Journal of Neuroscience* **36**, 1362-1372
254. Takagi-Niidome, S., Sasaki, T., Osawa, S., Sato, T., Morishima, K., Cai, T., Iwatsubo, T., and Tomita, T. (2015) Cooperative Roles of Hydrophilic Loop 1 and the C-Terminus of Presenilin 1 in the Substrate-Gating Mechanism of γ -Secretase. *The Journal of Neuroscience* **35**, 2646-2656
255. Li, X., Dang, S., Yan, C., Gong, X., Wang, J., and Shi, Y. (2013) Structure of a presenilin family intramembrane aspartate protease. *Nature* **493**, 56-61
256. Xie, T., Yan, C., Zhou, R., Zhao, Y., Sun, L., Yang, G., Lu, P., Ma, D., and Shi, Y. (2014) Crystal structure of the γ -secretase component nicastrin. *Proceedings of the National Academy of Sciences of the United States of America* **111**, 13349-13354
257. Dang, S., Wu, S., Wang, J., Li, H., Huang, M., He, W., Li, Y.-M., Wong, C. C. L., and Shi, Y. (2015) Cleavage of amyloid precursor protein by an archaeal presenilin homologue PSH. *Proceedings of the National Academy of Sciences of the United States of America* **112**, 3344-3349
258. Lazarov, V. K., Fraering, P. C., Ye, W., Wolfe, M. S., Selkoe, D. J., and Li, H. (2006) Electron microscopic structure of purified, active γ -secretase reveals an aqueous

intramembrane chamber and two pores. *Proceedings of the National Academy of Sciences of the United States of America* **103**, 6889-6894

259. Ogura, T., Mio, K., Hayashi, I., Miyashita, H., Fukuda, R., Kopan, R., Kodama, T., Hamakubo, T., Iwatsubo, T., Tomita, T., and Sato, C. (2006) Three-dimensional structure of the gamma-secretase complex. *Biochemical and biophysical research communications* **343**, 525-534

260. Osenkowski, P., Li, H., Ye, W., Li, D., Aeschbach, L., Fraering, P. C., Wolfe, M. S., Selkoe, D. J., and Li, H. (2009) Cryoelectron Microscopy Structure of Purified γ -Secretase at 12 Å Resolution. *Journal of Molecular Biology* **385**, 642-652

261. Renzi, F., Zhang, X., Rice, W. J., Torres-Arancivia, C., Gomez-Llorente, Y., Diaz, R., Ahn, K., Yu, C., Li, Y. M., Sisodia, S. S., and Ubarretxena-Belandia, I. (2011) Structure of gamma-secretase and its trimeric pre-activation intermediate by single-particle electron microscopy. *The Journal of biological chemistry* **286**, 21440-21449

262. Li, Y., Lu, Stephen H.-J., Tsai, C.-J., Bohm, C., Qamar, S., Dodd, Roger B., Meadows, W., Jeon, A., McLeod, A., Chen, F., Arimon, M., Berezovska, O., Hyman, Bradley T., Tomita, T., Iwatsubo, T., Johnson, Christopher M., Farrer, Lindsay A., Schmitt-Ulms, G., Fraser, Paul E., and St George-Hyslop, Peter H. (2014) Structural Interactions between Inhibitor and Substrate Docking Sites Give Insight into Mechanisms of Human PS1 Complexes. *Structure* **22**, 125-135

263. Lu, P., Bai, X.-c., Ma, D., Xie, T., Yan, C., Sun, L., Yang, G., Zhao, Y., Zhou, R., Scheres, S. H. W., and Shi, Y. (2014) Three-dimensional structure of human γ -secretase. *Nature* **512**, 166-170

264. Elad, N., De Strooper, B., Lismont, S., Hagen, W., Veugelen, S., Arimon, M., Horr , K., Berezovska, O., Sachse, C., and Ch vez-Guti rrez, L. (2015) The dynamic conformational landscape of γ -secretase. *Journal of cell science* **128**, 589-598

265. Sun, L., Zhao, L., Yang, G., Yan, C., Zhou, R., Zhou, X., Xie, T., Zhao, Y., Wu, S., Li, X., and Shi, Y. (2015) Structural basis of human γ -secretase assembly. *Proceedings of the National Academy of Sciences of the United States of America* **112**, 6003-6008

266. Bai, X. C., Rajendra, E., Yang, G., Shi, Y., and Scheres, S. H. (2015) Sampling the conformational space of the catalytic subunit of human gamma-secretase. *eLife* **4**

267. Deatherage, C. L., Lu, Z., Kroncke, B. M., Ma, S., Smith, J. A., Voehler, M. W., McFeeters, R. L., and Sanders, C. R. (2017) Structural and biochemical differences between the Notch and the amyloid precursor protein transmembrane domains. *Science Advances* **3**, e1602794

268. Futai, E., Osawa, S., Cai, T., Fujisawa, T., Ishiura, S., and Tomita, T. (2016) Suppressor Mutations for Presenilin 1 Familial Alzheimer Disease Mutants Modulate γ -Secretase Activities. *The Journal of biological chemistry* **291**, 435-446

269. Takeo, K., Tanimura, S., Shinoda, T., Osawa, S., Zahariev, I. K., Takegami, N., Ishizuka-Katsura, Y., Shinya, N., Takagi-Niidome, S., Tominaga, A., Ohsawa, N., Kimura-Someya, T., Shirouzu, M., Yokoshima, S., Yokoyama, S., Fukuyama, T., Tomita, T., and Iwatsubo, T. (2014) Allosteric regulation of γ -secretase activity by a phenylimidazole-type γ -secretase modulator. *Proceedings of the National Academy of Sciences of the United States of America* **111**, 10544-10549

270. Cai, T., Yonaga, M., and Tomita, T. (2017) Activation of γ -Secretase Trimming Activity by Topological Changes of Transmembrane Domain 1 of Presenilin 1. *The Journal of Neuroscience* **37**, 12272-12280

271. Somavarapu, A. K., and Kepp, K. P. (2016) The dynamic mechanism of presenilin-1 function: Sensitive gate dynamics and loop unplugging control protein access. *Neurobiology of disease* **89**, 147-156

272. Aguayo-Ortiz, R., Chavez-Garcia, C., Straub, J. E., and Dominguez, L. (2017) Characterizing the structural ensemble of γ -secretase using a multiscale molecular dynamics approach. *Chemical Science* **8**, 5576-5584
273. Aguayo-Ortiz, R., Straub, J. E., and Dominguez, L. (2018) Influence of membrane lipid composition on the structure and activity of γ -secretase. *Physical Chemistry Chemical Physics* **20**, 27294-27304
274. Hitzenberger, M., and Zacharias, M. (2018) γ -Secretase Studied by Atomistic Molecular Dynamics Simulations: Global Dynamics, Enzyme Activation, Water Distribution and Lipid Binding. *Frontiers in Chemistry* **6**, 640
275. Dehury, B., Tang, N., Blundell, T. L., and Kepp, K. P. (2019) Structure and dynamics of γ -secretase with presenilin 2 compared to presenilin 1. *RSC Advances* **9**, 20901-20916
276. Dehury, B., Tang, N., and Kepp, K. P. (2020) Insights into membrane-bound presenilin 2 from all-atom molecular dynamics simulations. *Journal of Biomolecular Structure and Dynamics* **38**, 3196-3210
277. Somavarapu, A. K., and Kepp, K. P. (2017) Membrane Dynamics of γ -Secretase Provides a Molecular Basis for β -Amyloid Binding and Processing. *ACS Chemical Neuroscience*
278. Dehury, B., Tang, N., and Kepp, K. P. (2019) Molecular dynamics of C99-bound γ -secretase reveal two binding modes with distinct compactness, stability, and active-site retention: implications for A β production. *Biochemical Journal* **476**, 1173-1189
279. Hitzenberger, M., and Zacharias, M. (2019) Structural Modeling of γ -Secretase A β n Complex Formation and Substrate Processing. *ACS Chemical Neuroscience* **10**, 1826-1840
280. Nierzwicki, Ł., Olewniczak, M., Chodnicki, P., and Czub, J. (2021) Role of cholesterol in substrate recognition by [Formula: see text]-secretase. *Scientific Reports* **11**, 15213
281. Orzeł, U., Jakowiecki, J., Młynarczyk, K., and Filipek, S. (2021) The Role of Cholesterol in Amyloidogenic Substrate Binding to the γ -Secretase Complex. *Biomolecules* **11**
282. Guzmán-Ocampo, D. C., Aguayo-Ortiz, R., Velasco-Bolom, J.-L., Gupta, P. L., Roitberg, A. E., and Dominguez, L. (2022) Elucidating the Protonation State of the γ -Secretase Catalytic Dyad. *ACS Chemical Neuroscience*
283. Velasco-Bolom, J. L., and Domínguez, L. (2022) Mechanistic regulation of γ -secretase by their substrates. *Physical Chemistry Chemical Physics* **24**, 19223-19232
284. Svedružić Ž, M., Šendula Jengiđ, V., and Ostojić, L. (2023) The Binding of Different Substrate Molecules at the Docking Site and the Active Site of γ -Secretase Can Trigger Toxic Events in Sporadic and Familial Alzheimer's Disease. *International journal of molecular sciences* **24**
285. Bhattarai, A., Devkota, S., Bhattarai, S., Wolfe, M. S., and Miao, Y. (2020) Mechanisms of γ -Secretase Activation and Substrate Processing. *ACS Central Science* **6**, 969-983
286. Dehury, B., Tang, N., Mehra, R., Blundell, T. L., and Kepp, K. P. (2020) Side-by-side comparison of Notch- and C83 binding to γ -secretase in a complete membrane model at physiological temperature. *RSC Advances* **10**, 31215-31232
287. Bhattarai, A., Devkota, S., Do, H. N., Wang, J., Bhattarai, S., Wolfe, M. S., and Miao, Y. (2022) Mechanism of Tripeptide Trimming of Amyloid β -Peptide 49 by γ -Secretase. *Journal of the American Chemical Society* **144**, 6215-6226
288. Chen, S. Y., and Zacharias, M. (2022) An internal docking site stabilizes substrate binding to γ -secretase: Analysis by molecular dynamics simulations. *Biophysical Journal* **121**, 2330-2344
289. Somavarapu, A. K., and Kepp, K. P. (2016) Loss of stability and hydrophobicity of presenilin 1 mutations causing Alzheimer's disease. *Journal of neurochemistry* **137**, 101-111

290. Chávez-García, C., Aguayo-Ortiz, R., and Dominguez, L. (2019) Quantifying correlations between mutational sites in the catalytic subunit of γ -secretase. *Journal of Molecular Graphics and Modelling* **88**, 221-227
291. Mehra, R., and Kepp, K. P. (2019) Computational analysis of Alzheimer-causing mutations in amyloid precursor protein and presenilin 1. *Archives of Biochemistry and Biophysics* **678**, 108168
292. Tang, N., Dehury, B., and Kepp, K. P. (2019) Computing the Pathogenicity of Alzheimer's Disease Presenilin 1 Mutations. *Journal of Chemical Information and Modeling* **59**, 858-870
293. Chen, S.-Y., and Zacharias, M. (2020) How Mutations Perturb γ -Secretase Active Site Studied by Free Energy Simulations. *ACS Chemical Neuroscience* **11**, 3321-3332
294. Dehury, B., Somavarapu, A. K., and Kepp, K. P. (2020) A computer-simulated mechanism of familial Alzheimer's disease: Mutations enhance thermal dynamics and favor looser substrate-binding to γ -secretase. *Journal of Structural Biology* **212**, 107648
295. Soto-Ospina, A., Araque Marín, P., Bedoya, G., Sepulveda-Falla, D., and Villegas Lanau, A. (2021) Protein Predictive Modeling and Simulation of Mutations of Presenilin-1 Familial Alzheimer's Disease on the Orthosteric Site. *Frontiers in Molecular Biosciences* **8**, 649990
296. Do, H. N., Devkota, S., Bhattarai, A., Wolfe, M. S., and Miao, Y. (2023) Effects of presenilin-1 familial Alzheimer's disease mutations on γ -secretase activation for cleavage of amyloid precursor protein. *Communications Biology* **6**, 174
297. Aguayo-Ortiz, R., Guzmán-Ocampo, D. C., and Dominguez, L. (2019) Toward the Characterization of DAPT Interactions with γ -Secretase. *ChemMedChem* **14**, 1005-1010
298. Hitzenberger, M., and Zacharias, M. (2019) Uncovering the Binding Mode of γ - Secretase Inhibitors. *ACS Chemical Neuroscience* **10**, 3398-3403
299. Mehra, R., and Kepp, K. P. (2021) Computational prediction and molecular mechanism of γ -secretase modulators. *European Journal of Pharmaceutical Sciences* **157**, 105626
300. Ioppolo, A., Eccles, M., Groth, D., Verdile, G., and Agostino, M. (2021) Evaluation of Virtual Screening Strategies for the Identification of γ -Secretase Inhibitors and Modulators. *Molecules* **27**
301. Martiz, R. M., Patil, S. M., Ramu, R., M, K. J., P, A., Ranganatha, L. V., Khanum, S. A., Silina, E., Stupin, V., and Achar, R. R. (2022) Discovery of novel benzophenone integrated derivatives as anti-Alzheimer's agents targeting presenilin-1 and presenilin-2 inhibition: A computational approach. *PloS one* **17**, e0265022
302. Hollingsworth, S. A., and Dror, R. O. (2018) Molecular Dynamics Simulation for All. *Neuron* **99**, 1129-1143
303. Hornak, V., Abel, R., Okur, A., Strockbine, B., Roitberg, A., and Simmerling, C. (2006) Comparison of multiple Amber force fields and development of improved protein backbone parameters. *Proteins* **65**, 712-725
304. Lindorff-Larsen, K., Piana, S., Palmo, K., Maragakis, P., Klepeis, J. L., Dror, R. O., and Shaw, D. E. (2010) Improved side-chain torsion potentials for the Amber ff99SB protein force field. *Proteins* **78**, 1950-1958
305. Maier, J. A., Martinez, C., Kasavajhala, K., Wickstrom, L., Hauser, K. E., and Simmerling, C. (2015) ff14SB: Improving the Accuracy of Protein Side Chain and Backbone Parameters from ff99SB. *J Chem Theory Comput* **11**, 3696-3713
306. MacKerell, A. D., Bashford, D., Bellott, M., Dunbrack, R. L., Evanseck, J. D., et al. (1998) All-atom empirical potential for molecular modeling and dynamics studies of proteins. *The journal of physical chemistry. B* **102**, 3586-3616
307. Scott, W. R. P., Hünenberger, P. H., Tironi, I. G., Mark, A. E., Billeter, S. R., Fennen, J., Torda, A. E., Huber, T., Krüger, P., and Gunsteren, W. F. v. (1999) The GROMOS

- Biomolecular Simulation Program Package. *The Journal of Physical Chemistry A* **103**, 3596-3607
308. Feller, S. E., and MacKerell, A. D. (2000) An Improved Empirical Potential Energy Function for Molecular Simulations of Phospholipids. *The Journal of Physical Chemistry B* **104**, 7510-7515
309. Dickson, C. J., Madej, B. D., Skjevik, A. A., Betz, R. M., Teigen, K., Gould, I. R., and Walker, R. C. (2014) Lipid14: The Amber Lipid Force Field. *J Chem Theory Comput* **10**, 865-879
310. Skjevik Å, A., Madej, B. D., Walker, R. C., and Teigen, K. (2012) LIPID11: a modular framework for lipid simulations using amber. *The journal of physical chemistry. B* **116**, 11124-11136
311. Kirschner, K. N., Yongye, A. B., Tschampel, S. M., González-Outeiriño, J., Daniels, C. R., Foley, B. L., and Woods, R. J. (2008) GLYCAM06: a generalizable biomolecular force field. Carbohydrates. *J Comput Chem* **29**, 622-655
312. Hatcher, E., Guvench, O., and Mackerell, A. D. (2009) CHARMM additive all-atom force field for aldopentofuranoses, methyl-aldopentofuranosides, and fructofuranose. *The journal of physical chemistry. B* **113**, 12466-12476
313. Guvench, O., Hatcher, E. R., Venable, R. M., Pastor, R. W., and Mackerell, A. D. (2009) CHARMM Additive All-Atom Force Field for Glycosidic Linkages between Hexopyranoses. *J Chem Theory Comput* **5**, 2353-2370
314. Hatcher, E., Guvench, O., and Mackerell, A. D., Jr. (2009) CHARMM Additive All-Atom Force Field for Acyclic Polyalcohols, Acyclic Carbohydrates and Inositol. *J Chem Theory Comput* **5**, 1315-1327
315. Guvench, O., Greene, S. N., Kamath, G., Brady, J. W., Venable, R. M., Pastor, R. W., and Mackerell, A. D., Jr. (2008) Additive empirical force field for hexopyranose monosaccharides. *J Comput Chem* **29**, 2543-2564
316. Malde, A. K., Zuo, L., Breeze, M., Stroet, M., Poger, D., Nair, P. C., Oostenbrink, C., and Mark, A. E. (2011) An Automated Force Field Topology Builder (ATB) and Repository: Version 1.0. *J Chem Theory Comput* **7**, 4026-4037
317. Wang, J., Wolf, R. M., Caldwell, J. W., Kollman, P. A., and Case, D. A. (2004) Development and testing of a general amber force field. *J Comput Chem* **25**, 1157-1174
318. Berendsen, H. J. C., Postma, J. P. M., Gunsteren, W. F. v., and Hermans, J. (1981) Interaction Models for Water in Relation to Protein Hydration.
319. Jorgensen, W. L., Chandrasekhar, J., Madura, J. D., Impey, R. W., and Klein, M. L. (1983) Comparison of simple potential functions for simulating liquid water. *The Journal of Chemical Physics* **79**, 926-935
320. Berendsen, H. J. C., Grigera, J. R., and Straatsma, T. P. (1987) The missing term in effective pair potentials. *The Journal of Physical Chemistry A* **91**, 6269-6271
321. Mahoney, M. W., and Jorgensen, W. L. (2000) A five-site model for liquid water and the reproduction of the density anomaly by rigid, nonpolarizable potential functions. *The Journal of Chemical Physics* **112**, 8910-8922
322. Im, W., Feig, M., and Brooks, C. L., 3rd. (2003) An implicit membrane generalized born theory for the study of structure, stability, and interactions of membrane proteins. *Biophys J* **85**, 2900-2918
323. Onufriev, A., Case, D. A., and Bashford, D. (2002) Effective Born radii in the generalized Born approximation: the importance of being perfect. *J Comput Chem* **23**, 1297-1304
324. Zhou, R. (2003) Free energy landscape of protein folding in water: explicit vs. implicit solvent. *Proteins* **53**, 148-161

325. Bergh, C. (2023) From Static Structures to Free Energy Landscapes: Characterizing Conformational Transitions in Biological Macromolecules. In *Biophysics* Vol. PhD, KTH Royal Institute of Technology, Stockholm, Sweden
326. Almeida, J. G., Preto, A. J., Koukos, P. I., Bonvin, A. M. J. J., and Moreira, I. S. (2017) Membrane proteins structures: A review on computational modeling tools. *Biochimica et Biophysica Acta (BBA) - Biomembranes* **1859**, 2021-2039
327. Ingólfsson, H. I., Lopez, C. A., Uusitalo, J. J., de Jong, D. H., Gopal, S. M., Periole, X., and Marrink, S. J. (2014) The power of coarse graining in biomolecular simulations. *WIREs Computational Molecular Science* **4**, 225-248
328. Hénin, J., Lelièvre, T., Shirts, M. R., Valsson, O., and Delemotte, L. (2022) Enhanced Sampling Methods for Molecular Dynamics Simulations [Article v1.0]. *Living Journal of Computational Molecular Science* **4**, 1583
329. Miao, Y., Feher, V. A., and McCammon, J. A. (2015) Gaussian Accelerated Molecular Dynamics: Unconstrained Enhanced Sampling and Free Energy Calculation. *Journal of Chemical Theory and Computation* **11**, 3584-3595
330. Miao, Y. (2018) Acceleration of biomolecular kinetics in Gaussian accelerated molecular dynamics. *The Journal of Chemical Physics* **149**, 072308
331. Miao, Y., and McCammon, J. A. (2016) Unconstrained Enhanced Sampling for Free Energy Calculations of Biomolecules: A Review. *Molecular Simulation* **42**, 1046-1055
332. Wang, J., and Miao, Y. (2020) Peptide Gaussian accelerated molecular dynamics (Pep-GaMD): Enhanced sampling and free energy and kinetics calculations of peptide binding. *The Journal of Chemical Physics* **153**, 154109
333. Güner, G., and Lichtenthaler, S. F. (2020) The substrate repertoire of γ -secretase/presenilin. *Seminars in cell & developmental biology* **105**, 27-42
334. Bussi, G., and Laio, A. (2020) Using metadynamics to explore complex free-energy landscapes. *Nature Reviews Physics* **2**, 200-212
335. Laio, A., and Parrinello, M. (2002) Escaping free-energy minima. *Proceedings of the National Academy of Sciences of the United States of America* **99**, 12562-12566
336. Barducci, A., Bussi, G., and Parrinello, M. (2008) Well-Tempered Metadynamics: A Smoothly Converging and Tunable Free-Energy Method. *Physical Review Letters* **100**, 020603
337. Ibrahim, P., and Clark, T. (2019) Metadynamics simulations of ligand binding to GPCRs. *Current Opinion in Structural Biology* **55**, 129-137
338. Meral, D., Provasi, D., and Filizola, M. (2018) An efficient strategy to estimate thermodynamics and kinetics of G protein-coupled receptor activation using metadynamics and maximum caliber. *The Journal of Chemical Physics* **149**, 224101
339. Peters, B. L., Deng, J., and Ferguson, A. L. (2020) Free energy calculations of the functional selectivity of 5-HT_{2B} G protein-coupled receptor. *PloS one* **15**, e0243313
340. Saleh, N., Ibrahim, P., Saladino, G., Gervasio, F. L., and Clark, T. (2017) An Efficient Metadynamics-Based Protocol To Model the Binding Affinity and the Transition State Ensemble of G-Protein-Coupled Receptor Ligands. *Journal of Chemical Information and Modeling* **57**, 1210-1217
341. Du, X., Li, Y., Xia, Y.-L., Ai, S.-M., Liang, J., Sang, P., Ji, X.-L., and Liu, S.-Q. (2016) Insights into Protein–Ligand Interactions: Mechanisms, Models, and Methods. *International journal of molecular sciences* **17**, 144
342. Friesner, R. A., Banks, J. L., Murphy, R. B., Halgren, T. A., Klicic, J. J., Mainz, D. T., Repasky, M. P., Knoll, E. H., Shelley, M., Perry, J. K., Shaw, D. E., Francis, P., and Shenkin, P. S. (2004) Glide: a new approach for rapid, accurate docking and scoring. 1. Method and assessment of docking accuracy. *J Med Chem* **47**, 1739-1749

343. Trott, O., and Olson, A. J. (2010) AutoDock Vina: improving the speed and accuracy of docking with a new scoring function, efficient optimization, and multithreading. *J Comput Chem* **31**, 455-461
344. Gray, J. J., Moughon, S. E., Kortemme, T., Schueler-Furman, O., Misura, K. M., Morozov, A. V., and Baker, D. (2003) Protein-protein docking predictions for the CAPRI experiment. *Proteins* **52**, 118-122
345. Woo, H.-J., and Roux, B. (2005) Calculation of absolute protein–ligand binding free energy from computer simulations. *Proceedings of the National Academy of Sciences* **102**, 6825-6830
346. Genheden, S., and Ryde, U. (2015) The MM/PBSA and MM/GBSA methods to estimate ligand-binding affinities. *Expert Opinion on Drug Discovery* **10**, 449-461
347. Abel, R., Wang, L., Mobley, D. L., and Friesner, R. A. (2017) A Critical Review of Validation, Blind Testing, and Real- World Use of Alchemical Protein-Ligand Binding Free Energy Calculations. *Curr Top Med Chem* **17**, 2577-2585
348. de Ruiter, A., and Oostenbrink, C. (2011) Free energy calculations of protein-ligand interactions. *Curr Opin Chem Biol* **15**, 547-552
349. Gapsys, V., Michielssens, S., Seeliger, D., and Groot, B. L. d. (2014) pmx: Automated protein structure and topology generation for alchemical perturbations. *J Comput Chem* **36**, 348-354
350. Bhati, A. P., Wan, S., Wright, D. W., and Coveney, P. V. (2017) Rapid, Accurate, Precise, and Reliable Relative Free Energy Prediction Using Ensemble Based Thermodynamic Integration. *Journal of Chemical Theory and Computation* **13**, 210-222
351. de Ruiter, A., Petrov, D., and Oostenbrink, C. (2021) Optimization of Alchemical Pathways Using Extended Thermodynamic Integration. *Journal of Chemical Theory and Computation* **17**, 56-65
352. Gilson, M. K., Given, J. A., Bush, B. L., and McCammon, J. A. (1997) The statistical-thermodynamic basis for computation of binding affinities: a critical review. *Biophys J* **72**, 1047-1069
353. Ross, G. A., Lu, C., Scarabelli, G., Albanese, S. K., Houang, E., Abel, R., Harder, E. D., and Wang, L. (2023) The maximal and current accuracy of rigorous protein-ligand binding free energy calculations. *Commun Chem* **6**, 222
354. Hayes, R. L., and Brooks, C. L., 3rd. (2021) A strategy for proline and glycine mutations to proteins with alchemical free energy calculations. *J Comput Chem* **42**, 1088-1094
355. Hahn, D. F., Bayly, C. I., Macdonald, H. E. B., Chodera, J. D., Mey, A., Mobley, D. L., Benito, L. P., Schindler, C. E. M., Tresadern, G., and Warren, G. L. (2022) Best practices for constructing, preparing, and evaluating protein-ligand binding affinity benchmarks [Article v0.1]. *Living J Comput Mol Sci* **4**
356. Lu, C., Wu, C., Ghoreishi, D., Chen, W., Wang, L., Damm, W., Ross, G. A., Dahlgren, M. K., Russell, E., Von Bargen, C. D., Abel, R., Friesner, R. A., and Harder, E. D. (2021) OPLS4: Improving Force Field Accuracy on Challenging Regimes of Chemical Space. *J Chem Theory Comput* **17**, 4291-4300
357. Blake, S., Hemming, I., Heng, J. I.-T., and Agostino, M. (2021) Structure-Based Approaches to Classify the Functional Impact of ZBTB18 Missense Variants in Health and Disease. *ACS Chemical Neuroscience* **12**, 979-989
358. Shen, J., Bronson, R. T., Chen, D. F., Xia, W., Selkoe, D. J., and Tonegawa, S. (1997) Skeletal and CNS Defects in Presenilin-1-Deficient Mice. *Cell* **89**, 629-639
359. Ryman, D. C., Acosta-Baena, N., Aisen, P. S., Bird, T., Danek, A., Fox, N. C., Goate, A., Frommelt, P., Ghetti, B., Langbaum, J. B. S., Lopera, F., Martins, R., Masters, C. L., Mayeux, R. P., McDade, E., Moreno, S., Reiman, E. M., Ringman, J. M., Salloway, S., Schofield, P. R., Sperling, R., Tariot, P. N., Xiong, C., Morris, J. C., Bateman, R. J., and And

- the Dominantly Inherited Alzheimer, N. (2014) Symptom onset in autosomal dominant Alzheimer disease: A systematic review and meta-analysis. *Neurology* **83**, 253-260
360. Acx, H., Chávez-Gutiérrez, L., Serneels, L., Lismont, S., Benurwar, M., Elad, N., and De Strooper, B. (2014) Signature amyloid β profiles are produced by different γ -secretase complexes. *The Journal of biological chemistry* **289**, 4346-4355
361. Yonemura, Y., Futai, E., Yagishita, S., Kaether, C., and Ishiura, S. (2016) Specific combinations of presenilins and Aph1s affect the substrate specificity and activity of γ -secretase. *Biochemical and biophysical research communications* **478**, 1751-1757
362. Hashimoto-Gotoh, T., Tsujimura, A., Watanabe, Y., Iwabe, N., Miyata, T., and Tabira, T. (2003) A unifying model for functional difference and redundancy of presenilin-1 and -2 in cell apoptosis and differentiation. *Gene* **323**, 115-123
363. Madsen, L. B., Thomsen, B., Larsen, K., Bendixen, C., Holm, I. E., Fredholm, M., Jørgensen, A. L., and Nielsen, A. L. (2007) Molecular characterization and temporal expression profiling of presenilins in the developing porcine brain. *BMC neuroscience* **8**, 72-72
364. Lai, M.-T., Chen, E., Crouthamel, M.-C., DiMuzio-Mower, J., Xu, M., Huang, Q., Price, E., Register, R. B., Shi, X.-P., Donoviel, D. B., Bernstein, A., Hazuda, D., Gardell, S. J., and Li, Y.-M. (2003) Presenilin-1 and presenilin-2 exhibit distinct yet overlapping γ -secretase activities. *The Journal of biological chemistry* **278**, 22475-22481
365. Watanabe, H., Iqbal, M., Zheng, J., Wines-Samuels, M., and Shen, J. (2014) Partial Loss of Presenilin Impairs Age-Dependent Neuronal Survival in the Cerebral Cortex. *The Journal of Neuroscience* **34**, 15912-15922
366. Pimenova, A. A., and Goate, A. M. (2020) Novel presenilin 1 and 2 double knock-out cell line for in vitro validation of PSEN1 and PSEN2 mutations. *Neurobiology of disease*, 104785
367. Lessard, C. B., Rodriguez, E., Ladd, T. B., Minter, L. M., Osborne, B. A., Miele, L., Golde, T. E., and Ran, Y. (2019) Individual and combined presenilin 1 and 2 knockouts reveal that both have highly overlapping functions in HEK293T cells. *The Journal of biological chemistry* **294**, 11276-11285
368. Jayadev, S., Case, A., Eastman, A. J., Nguyen, H., Pollak, J., Wiley, J. C., Möller, T., Morrison, R. S., and Garden, G. A. (2010) Presenilin 2 Is the Predominant γ -Secretase in Microglia and Modulates Cytokine Release. *PloS one* **5**
369. Uhlén, M., Fagerberg, L., Hallström, B. M., Lindskog, C., Oksvold, P., et al. (2015) Tissue-based map of the human proteome. *Science (New York, N.Y.)* **347**, 1260419
370. Karlsson, M., Zhang, C., Méar, L., Zhong, W., Digre, A., Katona, B., Sjöstedt, E., Butler, L., Odeberg, J., Dusart, P., Edfors, F., Oksvold, P., von Feilitzen, K., Zwahlen, M., Arif, M., Altay, O., Li, X., Ozcan, M., Mardinoglu, A., Fagerberg, L., Mulder, J., Luo, Y., Ponten, F., Uhlén, M., and Lindskog, C. (2021) A single-cell type transcriptomics map of human tissues. *Science Advances* **7**, eabh2169
371. Lee, M. K., Slunt, H. H., Martin, L. J., Thinakaran, G., Kim, G., Gandy, S. E., Seeger, M., Koo, E., Price, D. L., and Sisodia, S. S. (1996) Expression of presenilin 1 and 2 (PS1 and PS2) in human and murine tissues. *The Journal of Neuroscience* **16**, 7513-7525
372. Kumar, A., and Thakur, M. K. (2012) Presenilin 1 and 2 are expressed differentially in the cerebral cortex of mice during development. *Neurochemistry International* **61**, 778-782
373. Thakur, M. K., and Ghosh, S. (2007) Age and sex dependent alteration in presenilin expression in mouse cerebral cortex. *Cellular and molecular neurobiology* **27**, 1059-1067
374. Placanica, L., Zhu, L., and Li, Y.-M. (2009) Gender- and age-dependent gamma-secretase activity in mouse brain and its implication in sporadic Alzheimer disease. *PloS one* **4**, e5088-e5088
375. Ghosh, S., and Thakur, M. K. (2008) PS1 Expression is Downregulated by Gonadal Steroids in Adult Mouse Brain. *Neurochemical research* **33**, 365-369

376. Ghosh, S., and Thakur, M. K. (2008) PS2 protein expression is upregulated by sex steroids in the cerebral cortex of aging mice. *Neurochemistry International* **52**, 363-367
377. Kaja, S., Sumien, N., Shah, V. V., Puthawala, I., Maynard, A. N., Khullar, N., Payne, A. J., Forster, M. J., and Koulen, P. (2015) Loss of spatial memory, learning and motor coordination during normal aging is accompanied by changes in brain presenilin 1 and 2 expression levels. *Molecular Neurobiology* **52**, 545-554
378. Steiner, H., Duff, K., Capell, A., Romig, H., Grim, M. G., Lincoln, S., Hardy, J., Yu, X., Picciano, M., Fichtler, K., Citron, M., Kopan, R., Pesold, B., Keck, S., Baader, M., Tomita, T., Iwatsubo, T., Baumeister, R., and Haass, C. (1999) A Loss of Function Mutation of Presenilin-2 Interferes with Amyloid β -Peptide Production and Notch Signaling. *The Journal of biological chemistry* **274**, 28669-28673
379. Feng, R., Wang, H., Wang, J., Shrom, D., Zeng, X., and Tsien, J. Z. (2004) Forebrain degeneration and ventricle enlargement caused by double knockout of Alzheimer's presenilin-1 and presenilin-2. *Proceedings of the National Academy of Sciences of the United States of America* **101**, 8162-8167
380. Saura, C. A., Choi, S.-Y., Beglopoulos, V., Malkani, S., Zhang, D., Rao, B. S. S., Chattarji, S., Kelleher Iii, R. J., Kandel, E. R., Duff, K., Kirkwood, A., and Shen, J. (2004) Loss of Presenilin Function Causes Impairments of Memory and Synaptic Plasticity Followed by Age-Dependent Neurodegeneration. *Neuron* **42**, 23-36
381. Soto-Faguás, C. M., Sanchez-Molina, P., and Saura, C. A. (2021) Loss of presenilin function enhances tau phosphorylation and aggregation in mice. *Acta neuropathologica communications* **9**, 162
382. Peng, W., Xie, Y., Liao, C., Bai, Y., Wang, H., and Li, C. (2022) Spatiotemporal patterns of gliosis and neuroinflammation in presenilin 1/2 conditional double knockout mice. *Front Aging Neurosci* **14**
383. Wines-Samuels, M., Schulte, E. C., Smith, M. J., Aoki, C., Liu, X., Kelleher, R. J., III, and Shen, J. (2010) Characterization of Age-Dependent and Progressive Cortical Neuronal Degeneration in Presenilin Conditional Mutant Mice. *PloS one* **5**, e10195
384. Zhu, M., Gu, F., Shi, J., Hu, J., Hu, Y., and Zhao, Z. (2008) Increased oxidative stress and astrogliosis responses in conditional double-knockout mice of Alzheimer-like presenilin-1 and presenilin-2. *Free Radical Biology and Medicine* **45**, 1493-1499
385. Cao, T., Zhou, X., Zheng, X., Cui, Y., Tsien, J. Z., Li, C., and Wang, H. (2018) Histone Deacetylase Inhibitor Alleviates the Neurodegenerative Phenotypes and Histone Dysregulation in Presenilins-Deficient Mice. *Front Aging Neurosci* **10**
386. Kang, J., and Shen, J. (2020) Cell-autonomous role of Presenilin in age-dependent survival of cortical interneurons. *Molecular neurodegeneration* **15**, 72
387. Haapasalo, A., and Kovacs, D. M. (2011) The Many Substrates of Presenilin/ γ -Secretase. *Journal of Alzheimer's Disease* **25**, 3-28
388. Güner, G., Abfal, M., Zhao, K., Dreyer, T., Lahiri, S., Lo, Y., Slivinski, B. I., Imhof, A., Jocher, G., Strohm, L., Behrends, C., Langosch, D., Bronger, H., Nimsky, C., Bartsch, J. W., Riddell, S. R., Steiner, H., and Lichtenthaler, S. F. (2022) Proteolytically generated soluble Tweak Receptor Fn14 is a blood biomarker for γ -secretase activity. *EMBO Molecular Medicine* **14**, e16084
389. Stalin, J., Harhour, K., Hubert, L., Garrigue, P., Nollet, M., Essaadi, A., Muller, A., Foucault-Bertaud, A., Bachelier, R., Sabatier, F., Pisano, P., Peiretti, F., Leroyer, A. S., Guillet, B., Bardin, N., Dignat-George, F., and Blot-Chaubaud, M. (2016) Soluble CD146 boosts therapeutic effect of endothelial progenitors through proteolytic processing of short CD146 isoform. *Cardiovascular Research* **111**, 240-251
390. Fleck, D., Voss, M., Brankatschk, B., Giudici, C., Hampel, H., Schwenk, B., Edbauer, D., Fukumori, A., Steiner, H., Kremmer, E., Haug-Kröper, M., Rossner, M. J., Flührer, R.,

- Willem, M., and Haass, C. (2016) Proteolytic Processing of Neuregulin 1 Type III by Three Intramembrane-cleaving Proteases. *The Journal of biological chemistry* **291**, 318-333
391. Laurent, S. A., Hoffmann, F. S., Kuhn, P. H., Cheng, Q., Chu, Y., Schmidt-Supprian, M., Hauck, S. M., Schuh, E., Krumbholz, M., Rübsamen, H., Wanngren, J., Khademi, M., Olsson, T., Alexander, T., Hiepe, F., Pfister, H. W., Weber, F., Jenne, D., Wekerle, H., Hohlfeld, R., Lichtenthaler, S. F., and Meinel, E. (2015) γ -Secretase directly sheds the survival receptor BCMA from plasma cells. *Nature Communications* **6**, 7333
392. Okochi, M., Steiner, H., Fukumori, A., Tani, H., Tomita, T., Tanaka, T., Iwatsubo, T., Kudo, T., Takeda, M., and Haass, C. (2002) Presenilins mediate a dual intramembraneous gamma-secretase cleavage of Notch-1. *EMBO J* **21**, 5408-5416
393. Tagami, S., Okochi, M., Yanagida, K., Ikuta, A., Fukumori, A., Matsumoto, N., Ishizuka-Katsura, Y., Nakayama, T., Itoh, N., Jiang, J., Nishitomi, K., Kamino, K., Morihara, T., Hashimoto, R., Tanaka, T., Kudo, T., Chiba, S., and Takeda, M. (2008) Regulation of Notch signaling by dynamic changes in the precision of S3 cleavage of Notch-1. *Mol Cell Biol* **28**, 165-176
394. Beel, A. J., and Sanders, C. R. (2008) Substrate specificity of γ -secretase and other intramembrane proteases. *Cellular and Molecular Life Sciences* **65**, 1311-1334
395. Hemming, M. L., Elias, J. E., Gygi, S. P., and Selkoe, D. J. (2008) Proteomic Profiling of γ -Secretase Substrates and Mapping of Substrate Requirements. *PLoS Biology* **6**, e257
396. Tarassishin, L., Yin, Y. I., Bassit, B., and Li, Y. M. (2004) Processing of Notch and amyloid precursor protein by γ -secretase is spatially distinct. *Proceedings of the National Academy of Sciences of the United States of America* **101**, 17050-17055
397. Vetrivel, K. S., Cheng, H., Kim, S.-H., Chen, Y., Barnes, N. Y., Parent, A. T., Sisodia, S. S., and Thinakaran, G. (2005) Spatial Segregation of γ -Secretase and Substrates in Distinct Membrane Domains. *The Journal of biological chemistry* **280**, 25892-25900
398. Liao, Y., Wang, J., Jaehnig, E. J., Shi, Z., and Zhang, B. (2019) WebGestalt 2019: gene set analysis toolkit with revamped UIs and APIs. *Nucleic Acids Res* **47**, W199-W205
399. Schroeter, E. H., Kisslinger, J. A., and Kopan, R. (1998) Notch-1 signalling requires ligand-induced proteolytic release of intracellular domain. *Nature* **393**, 382-386
400. LaFoya, B., Munroe, J. A., Mia, M. M., Detweiler, M. A., Crow, J. J., Wood, T., Roth, S., Sharma, B., and Albig, A. R. (2016) Notch: A multi-functional integrating system of microenvironmental signals. *Developmental Biology* **418**, 227-241
401. Andersson, E. R., Sandberg, R., and Lendahl, U. (2011) Notch signaling: simplicity in design, versatility in function. *Development (Cambridge, England)* **138**, 3593-3612
402. Siebel, C., and Lendahl, U. (2017) Notch Signaling in Development, Tissue Homeostasis, and Disease. *Physiological Reviews* **97**, 1235-1294
403. Bray, S. J. (2016) Notch signalling in context. *Nature Reviews: Molecular Cell Biology* **17**, 722-735
404. Meier-Stiegen, F., Schwanbeck, R., Bernoth, K., Martini, S., Hieronymus, T., Ruau, D., Zenke, M., and Just, U. (2010) Activated Notch1 Target Genes during Embryonic Cell Differentiation Depend on the Cellular Context and Include Lineage Determinants and Inhibitors. *PloS one* **5**
405. Olsauskas-Kuprys, R., Zlobin, A., and Osipo, C. (2013) Gamma secretase inhibitors of Notch signaling. *OncoTargets and therapy* **6**, 943-955
406. Ran, Y., Hossain, F., Pannuti, A., Lessard, C. B., Ladd, G. Z., Jung, J. I., Minter, L. M., Osborne, B. A., Miele, L., and Golde, T. E. (2017) γ -Secretase inhibitors in cancer clinical trials are pharmacologically and functionally distinct. *EMBO Molecular Medicine* **9**, 950-966
407. Pardossi-Piquard, R., and Checler, F. (2012) The physiology of the β -amyloid precursor protein intracellular domain AICD. *Journal of neurochemistry* **120 Suppl 1**, 109-124

408. Flammang, B., Pardossi-Piquard, R., Sevalle, J., Debayle, D., Dabert-Gay, A. S., Thévenet, A., Lauritzen, I., and Checler, F. (2012) Evidence that the amyloid- β protein precursor intracellular domain, AICD, derives from β -secretase-generated C-terminal fragment. *Journal of Alzheimer's Disease* **30**, 145-153
409. Pardossi-Piquard, R., Dunys, J., Kawarai, T., Sunyach, C., Alves da Costa, C., Vincent, B., Sévalle, J., Pimplikar, S., St George-Hyslop, P., and Checler, F. (2007) Response to Correspondence: Pardossi-Piquard et al., "Presenilin-Dependent Transcriptional Control of the A β -Degrading Enzyme Neprilysin by Intracellular Domains of β APP and APLP." *Neuron* **46**, 541–554. *Neuron* **53**, 483-486
410. Plant, L. D., Boyle, J. P., Smith, I. F., Peers, C., and Pearson, H. A. (2003) The production of amyloid beta peptide is a critical requirement for the viability of central neurons. *The Journal of Neuroscience* **23**, 5531-5535
411. Puzzo, D., Privitera, L., Leznik, E., Fà, M., Staniszewski, A., Palmeri, A., and Arancio, O. (2008) Picomolar amyloid-beta positively modulates synaptic plasticity and memory in hippocampus. *The Journal of Neuroscience* **28**, 14537-14545
412. Puzzo, D., Privitera, L., Fa, M., Staniszewski, A., Hashimoto, G., Aziz, F., Sakurai, M., Ribe, E. M., Troy, C. M., Mercken, M., Jung, S. S., Palmeri, A., and Arancio, O. (2011) Endogenous amyloid- β is necessary for hippocampal synaptic plasticity and memory. *Annals of neurology* **69**, 819-830
413. Cárdenas-Aguayo, M. d. C., Silva-Lucero, M. d. C., Cortes-Ortiz, M., Jiménez-Ramos, B., Gómez-Virgilio, L., Ramírez-Rodríguez, G., Arroyo, E. V.-., Fiorentino-Pérez, R., García, U., Luna-Muñoz, J., and Meraz-Ríos, M. A. (2014) Physiological Role of Amyloid Beta in Neural Cells: The Cellular Trophic Activity. In *Neurochemistry* (Thomas, H., ed) p. Ch. 9, IntechOpen, Rijeka
414. Gosztyla, M. L., Brothers, H. M., and Robinson, S. R. (2018) Alzheimer's Amyloid- β is an Antimicrobial Peptide: A Review of the Evidence. *Journal of Alzheimer's Disease* **62**, 1495-1506
415. Curtain, C. C., Ali, F., Volitakis, I., Cherny, R. A., Norton, R. S., Beyreuther, K., Barrow, C. J., Masters, C. L., Bush, A. I., and Barnham, K. J. (2001) Alzheimer's disease amyloid-beta binds copper and zinc to generate an allosterically ordered membrane-penetrating structure containing superoxide dismutase-like subunits. *The Journal of biological chemistry* **276**, 20466-20473
416. Huang, X., Atwood, C. S., Hartshorn, M. A., Multhaup, G., Goldstein, L. E., Scarpa, R. C., Cuajungco, M. P., Gray, D. N., Lim, J., Moir, R. D., Tanzi, R. E., and Bush, A. I. (1999) The A beta peptide of Alzheimer's disease directly produces hydrogen peroxide through metal ion reduction. *Biochemistry* **38**, 7609-7616
417. Huang, X., Cuajungco, M. P., Atwood, C. S., Hartshorn, M. A., Tyndall, J. D., Hanson, G. R., Stokes, K. C., Leopold, M., Multhaup, G., Goldstein, L. E., Scarpa, R. C., Saunders, A. J., Lim, J., Moir, R. D., Glabe, C., Bowden, E. F., Masters, C. L., Fairlie, D. P., Tanzi, R. E., and Bush, A. I. (1999) Cu(II) potentiation of alzheimer abeta neurotoxicity. Correlation with cell-free hydrogen peroxide production and metal reduction. *The Journal of biological chemistry* **274**, 37111-37116
418. Zhao, H., Zhu, J., Cui, K., Xu, X., O'Brien, M., Wong, K. K., Kesari, S., Xia, W., and Wong, S. T. (2009) Bioluminescence imaging reveals inhibition of tumor cell proliferation by Alzheimer's amyloid beta protein. *Cancer Cell International* **9**, 15
419. Paris, D., Townsend, K., Quadros, A., Humphrey, J., Sun, J., Brem, S., Wotoczek-Obadia, M., DelleDonne, A., Patel, N., Obregon, D. F., Crescentini, R., Abdullah, L., Coppola, D., Rojiani, A. M., Crawford, F., Sebt, S. M., and Mullan, M. (2004) Inhibition of angiogenesis by Abeta peptides. *Angiogenesis* **7**, 75-85

420. Shi, H. B., Tang, B., Liu, Y. W., Wang, X. F., and Chen, G. J. (2015) Alzheimer disease and cancer risk: a meta-analysis. *Journal of Cancer Research and Clinical Oncology* **141**, 485-494
421. Benilova, I., Karran, E., and De Strooper, B. (2012) The toxic A β oligomer and Alzheimer's disease: an emperor in need of clothes. *Nature neuroscience* **15**, 349-357
422. Deane, R., Singh, I., Sagare, A. P., Bell, R. D., Ross, N. T., LaRue, B., Love, R., Perry, S., Paquette, N., Deane, R. J., Thiyagarajan, M., Zarcone, T., Fritz, G., Friedman, A. E., Miller, B. L., and Zlokovic, B. V. (2012) A multimodal RAGE-specific inhibitor reduces amyloid β -mediated brain disorder in a mouse model of Alzheimer disease. *The Journal of clinical investigation* **122**, 1377-1392
423. Kaden, D., Voigt, P., Munter, L.-M., Bobowski, K. D., Schaefer, M., and Multhaup, G. (2009) Subcellular localization and dimerization of APLP1 are strikingly different from APP and APLP2. *Journal of cell science* **122**, 368-377
424. Eggert, S., Midthune, B., Cottrell, B., and Koo, E. H. (2009) Induced Dimerization of the Amyloid Precursor Protein Leads to Decreased Amyloid- β Protein Production *The Journal of biological chemistry* **284**, 28943-28952
425. Hoe, H. S., Wessner, D., Beffert, U., Becker, A. G., Matsuoka, Y., and Rebeck, G. W. (2005) F-spondin interaction with the apolipoprotein E receptor ApoEr2 affects processing of amyloid precursor protein. *Mol Cell Biol* **25**, 9259-9268
426. He, X., Cooley, K., Chung, C. H., Dashti, N., and Tang, J. (2007) Apolipoprotein receptor 2 and X11 alpha/beta mediate apolipoprotein E-induced endocytosis of amyloid-beta precursor protein and beta-secretase, leading to amyloid-beta production. *The Journal of Neuroscience* **27**, 4052-4060
427. Gustafsen, C., Glerup, S., Pallesen, L. T., Olsen, D., Andersen, O. M., Nykjær, A., Madsen, P., and Petersen, C. M. (2013) Sortilin and SorLA display distinct roles in processing and trafficking of amyloid precursor protein. *The Journal of Neuroscience* **33**, 64-71
428. Takahashi, K., Eto, H., and Tanabe, K. K. (1999) Involvement of CD44 in matrix metalloproteinase-2 regulation in human melanoma cells. *International journal of cancer* **80**, 387-395
429. Dorandish, S., Williams, A., Atali, S., Sendo, S., Price, D., Thompson, C., Guthrie, J., Heyl, D., and Evans, H. G. (2021) Regulation of amyloid- β levels by matrix metalloproteinase-2/9 (MMP2/9) in the media of lung cancer cells. *Scientific Reports* **11**, 9708
430. Zhao, L., Teter, B., Morihara, T., Lim, G. P., Ambegaokar, S. S., Ubeda, O. J., Frautschy, S. A., and Cole, G. M. (2004) Insulin-degrading enzyme as a downstream target of insulin receptor signaling cascade: implications for Alzheimer's disease intervention. *The Journal of Neuroscience* **24**, 11120-11126
431. Deane, R., Sagare, A., Hamm, K., Parisi, M., Lane, S., Finn, M. B., Holtzman, D. M., and Zlokovic, B. V. (2008) apoE isoform-specific disruption of amyloid beta peptide clearance from mouse brain. *The Journal of clinical investigation* **118**, 4002-4013
432. Castellano, J. M., Deane, R., Gottesdiener, A. J., Verghese, P. B., Stewart, F. R., West, T., Paoletti, A. C., Kasper, T. R., DeMattos, R. B., Zlokovic, B. V., and Holtzman, D. M. (2012) Low-density lipoprotein receptor overexpression enhances the rate of brain-to-blood A β clearance in a mouse model of β -amyloidosis. *Proceedings of the National Academy of Sciences of the United States of America* **109**, 15502-15507
433. Castellano, J. M., Kim, J., Stewart, F. R., Jiang, H., DeMattos, R. B., Patterson, B. W., Fagan, A. M., Morris, J. C., Mawuenyega, K. G., Cruchaga, C., Goate, A. M., Bales, K. R., Paul, S. M., Bateman, R. J., and Holtzman, D. M. (2011) Human apoE isoforms differentially regulate brain amyloid- β peptide clearance. *Science Translational Medicine* **3**, 89ra57
434. Kim, J., Castellano, J. M., Jiang, H., Basak, J. M., Parsadanian, M., Pham, V., Mason, S. M., Paul, S. M., and Holtzman, D. M. (2009) Overexpression of low-density lipoprotein

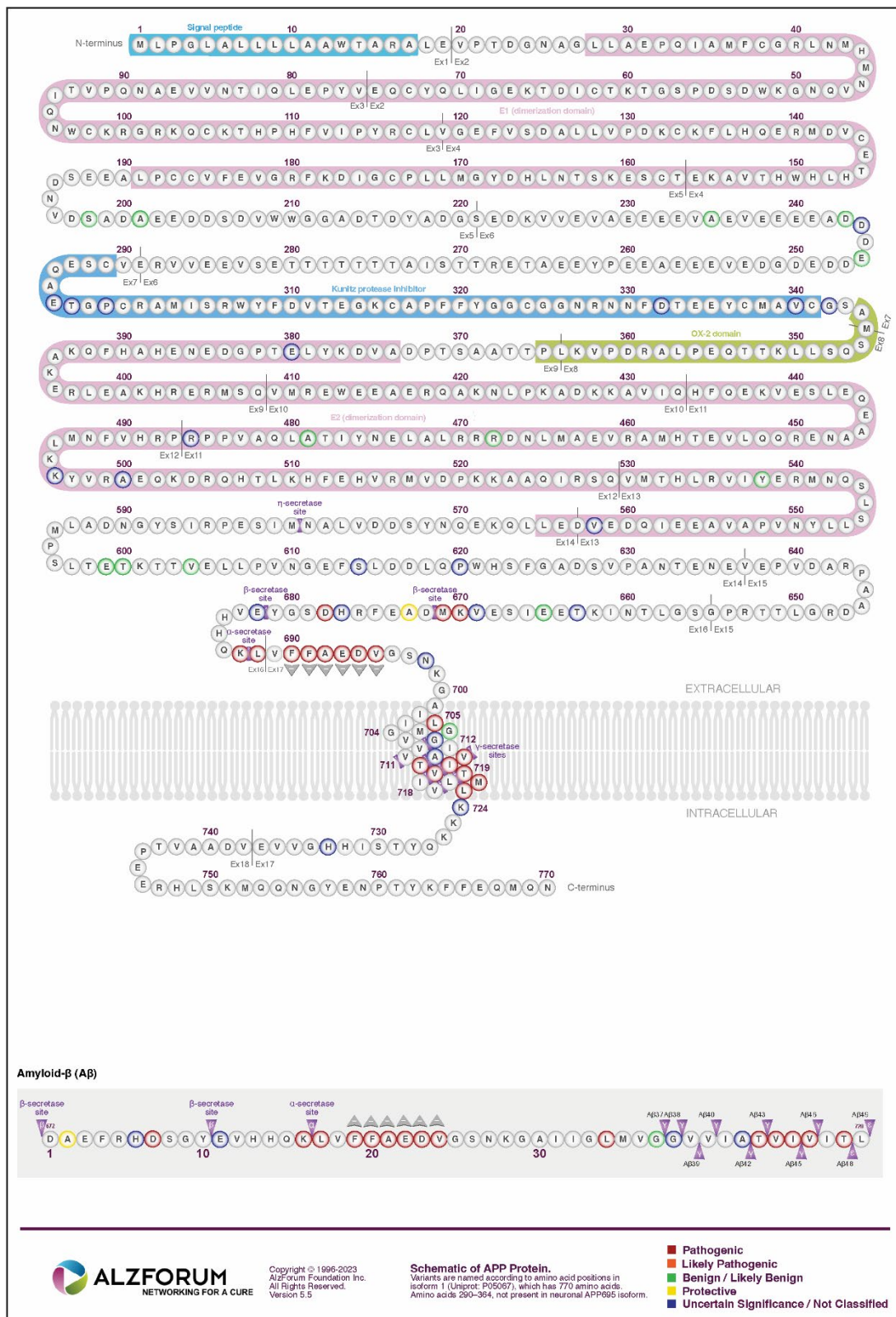
- receptor in the brain markedly inhibits amyloid deposition and increases extracellular A beta clearance. *Neuron* **64**, 632-644
435. Huang, Y., Happonen, K. E., Burrola, P. G., O'Connor, C., Hah, N., Huang, L., Nimmerjahn, A., and Lemke, G. (2021) Microglia use TAM receptors to detect and engulf amyloid β plaques. *Nature Immunology* **22**, 586-594
436. Huppert, S. S., Ilagan, M. X., De Strooper, B., and Kopan, R. (2005) Analysis of Notch function in presomitic mesoderm suggests a gamma-secretase-independent role for presenilins in somite differentiation. *Developmental Cell* **8**, 677-688
437. Khandelwal, A., Chandu, D., Roe, C. M., Kopan, R., and Quatrano, R. S. (2007) Moonlighting activity of presenilin in plants is independent of gamma-secretase and evolutionarily conserved. *Proceedings of the National Academy of Sciences of the United States of America* **104**, 13337-13342
438. McMains, V. C., Myre, M., Kreppel, L., and Kimmel, A. R. (2010) Dictyostelium possesses highly diverged presenilin/gamma-secretase that regulates growth and cell-fate specification and can accurately process human APP: a system for functional studies of the presenilin/gamma-secretase complex. *Disease models & mechanisms* **3**, 581-594
439. Ludtmann, M. H., Otto, G. P., Schilde, C., Chen, Z. H., Allan, C. Y., Brace, S., Beesley, P. W., Kimmel, A. R., Fisher, P., Killick, R., and Williams, R. S. (2014) An ancestral non-proteolytic role for presenilin proteins in multicellular development of the social amoeba *Dictyostelium discoideum*. *Journal of cell science* **127**, 1576-1584
440. Zhang, S., Zhang, M., Cai, F., and Song, W. (2013) Biological function of Presenilin and its role in AD pathogenesis. *Translational neurodegeneration* **2**, 15-15
441. Oikawa, N., and Walter, J. (2019) Presenilins and γ -Secretase in Membrane Proteostasis. *Cells* **8**, 209
442. Makarov, M., Kushnireva, L., Papa, M., and Korkotian, E. (2023) Presenilins and mitochondria-an intriguing link: mini-review. *Frontiers in neuroscience* **17**, 1249815
443. Baki, L., Marambaud, P., Efthimiopoulos, S., Georgakopoulos, A., Wen, P., Cui, W., Shioi, J., Koo, E., Ozawa, M., Friedrich, V. L., and Robakis, N. K. (2001) Presenilin-1 binds cytoplasmic epithelial cadherin, inhibits cadherin/p120 association, and regulates stability and function of the cadherin/catenin adhesion complex. *Proceedings of the National Academy of Sciences of the United States of America* **98**, 2381-2386
444. Soriano, S., Kang, D. E., Fu, M., Pestell, R., Chevallier, N., Zheng, H., and Koo, E. H. (2001) Presenilin 1 Negatively Regulates β -Catenin/T Cell Factor/Lymphoid Enhancer Factor-1 Signaling Independently of β -Amyloid Precursor Protein and Notch Processing. *The Journal of cell biology* **152**, 785-794
445. Kang, D. E., Soriano, S., Xia, X., Eberhart, C. G., De Strooper, B., Zheng, H., and Koo, E. H. (2002) Presenilin couples the paired phosphorylation of beta-catenin independent of axin: implications for beta-catenin activation in tumorigenesis. *Cell* **110**, 751-762
446. Yang, W., Wu, P.-f., Ma, J.-x., Liao, M.-j., Xu, L.-s., Xu, M.-h., and Yi, L. (2020) Presenilin1 exerts antiproliferative effects by repressing the Wnt/ β -catenin pathway in glioblastoma. *Cell Communication and Signaling* **18**, 22
447. Xia, X., Qian, S., Soriano, S., Wu, Y., Fletcher, A. M., Wang, X.-J., Koo, E. H., Wu, X., and Zheng, H. (2001) Loss of presenilin 1 is associated with enhanced β -catenin signaling and skin tumorigenesis. *Proceedings of the National Academy of Sciences of the United States of America* **98**, 10863-10868
448. Leissring, M. A., Parker, I., and LaFerla, F. M. (1999) Presenilin-2 mutations modulate amplitude and kinetics of inositol 1, 4,5-trisphosphate-mediated calcium signals. *The Journal of biological chemistry* **274**, 32535-32538

449. Leissring, M. A., Paul, B. A., Parker, I., Cotman, C. W., and LaFerla, F. M. (1999) Alzheimer's presenilin-1 mutation potentiates inositol 1,4,5-trisphosphate-mediated calcium signaling in *Xenopus* oocytes. *Journal of neurochemistry* **72**, 1061-1068
450. Cheung, K. H., Shineman, D., Müller, M., Cárdenas, C., Mei, L., Yang, J., Tomita, T., Iwatsubo, T., Lee, V. M., and Foskett, J. K. (2008) Mechanism of Ca²⁺ disruption in Alzheimer's disease by presenilin regulation of InsP₃ receptor channel gating. *Neuron* **58**, 871-883
451. Rybalchenko, V., Hwang, S. Y., Rybalchenko, N., and Koulen, P. (2008) The cytosolic N-terminus of presenilin-1 potentiates mouse ryanodine receptor single channel activity. *The international journal of biochemistry & cell biology* **40**, 84-97
452. Hayrapetyan, V., Rybalchenko, V., Rybalchenko, N., and Koulen, P. (2008) The N-terminus of presenilin-2 increases single channel activity of brain ryanodine receptors through direct protein-protein interaction. *Cell calcium* **44**, 507-518
453. Pack-Chung, E., Meyers, M. B., Pettingell, W. P., Moir, R. D., Brownawell, A. M., Cheng, I., Tanzi, R. E., and Kim, T.-W. (2000) Presenilin 2 Interacts with Sorcin, a Modulator of the Ryanodine Receptor *. *The Journal of biological chemistry* **275**, 14440-14445
454. Lokuta, A. J., Meyers, M. B., Sander, P. R., Fishman, G. I., and Valdivia, H. H. (1997) Modulation of cardiac ryanodine receptors by sorcin. *The Journal of biological chemistry* **272**, 25333-25338
455. Green, K. N., Demuro, A., Akbari, Y., Hitt, B. D., Smith, I. F., Parker, I., and LaFerla, F. M. (2008) SERCA pump activity is physiologically regulated by presenilin and regulates amyloid beta production. *The Journal of cell biology* **181**, 1107-1116
456. Tu, H., Nelson, O., Bezprozvanny, A., Wang, Z., Lee, S.-F., Hao, Y.-H., Serneels, L., De Strooper, B., Yu, G., and Bezprozvanny, I. (2006) Presenilins Form ER Ca²⁺ Leak Channels, a Function Disrupted by Familial Alzheimer's Disease-Linked Mutations. *Cell* **126**, 981-993
457. Nelson, O., Tu, H., Lei, T., Bentahir, M., de Strooper, B., and Bezprozvanny, I. (2007) Familial Alzheimer disease-linked mutations specifically disrupt Ca²⁺ leak function of presenilin 1. *The Journal of clinical investigation* **117**, 1230-1239
458. Nelson, O., Supnet, C., Tolia, A., Horr , K., De Strooper, B., and Bezprozvanny, I. (2011) Mutagenesis mapping of the presenilin 1 calcium leak conductance pore. *The Journal of biological chemistry* **286**, 22339-22347
459. Cheung, K. H., Mei, L., Mak, D. O., Hayashi, I., Iwatsubo, T., Kang, D. E., and Foskett, J. K. (2010) Gain-of-function enhancement of IP₃ receptor modal gating by familial Alzheimer's disease-linked presenilin mutants in human cells and mouse neurons. *Science Signaling* **3**, ra22
460. Mehra, R., and Kepp, K. P. (2020) Identification of Structural Calcium Binding Sites in Membrane-Bound Presenilin 1 and 2. *The Journal of Physical Chemistry B* **124**, 4697-4711
461. Neely, K. M., Green, K. N., and LaFerla, F. M. (2011) Presenilin is necessary for efficient proteolysis through the autophagy-lysosome system in a γ -secretase-independent manner. *The Journal of Neuroscience* **31**, 2781-2791
462. Coen, K., Flannagan, R. S., Baron, S., Carraro-Lacroix, L. R., Wang, D., Vermeire, W., Michiels, C., Munck, S., Baert, V., Sugita, S., Wuytack, F., Hiesinger, P. R., Grinstein, S., and Annaert, W. (2012) Lysosomal calcium homeostasis defects, not proton pump defects, cause endo-lysosomal dysfunction in PSEN-deficient cells. *The Journal of cell biology* **198**, 23-35
463. Wu, B., Yamaguchi, H., Lai, F. A., and Shen, J. (2013) Presenilins regulate calcium homeostasis and presynaptic function via ryanodine receptors in hippocampal neurons. *Proceedings of the National Academy of Sciences of the United States of America* **110**, 15091-15096

464. Korkotian, E., Meshcheriakova, A., and Segal, M. (2019) Presenilin 1 Regulates [Ca(2+)]i and Mitochondria/ER Interaction in Cultured Rat Hippocampal Neurons. *Oxidative Medicine and Cellular Longevity* **2019**, 7284967
465. Glenner, G. G., and Wong, C. W. (1984) Alzheimer's disease and Down's syndrome: Sharing of a unique cerebrovascular amyloid fibril protein. *Biochemical and biophysical research communications* **122**, 1131-1135
466. Grangeon, L., Charbonnier, C., Zarea, A., Rousseau, S., Rovelet-Lecrux, et al. (2023) Phenotype and imaging features associated with APP duplications. *Alzheimer's research & therapy* **15**, 93
467. Sleegers, K., Brouwers, N., Gijselinck, I., Theuns, J., Goossens, D., Wauters, J., Del-Favero, J., Cruts, M., van Duijn, C. M., and Van Broeckhoven, C. (2006) APP duplication is sufficient to cause early onset Alzheimer's dementia with cerebral amyloid angiopathy. *Brain : a journal of neurology* **129**, 2977-2983
468. Perez-Tur, J., Froelich, S., Prihar, G., Crook, R., Baker, M., Duff, K., Wragg, M., Busfield, F., Lendon, C., Clark, R. F., and et al. (1995) A mutation in Alzheimer's disease destroying a splice acceptor site in the presenilin-1 gene. *Neuroreport* **7**, 297-301
469. Nicolas, G., Wallon, D., Goupil, C., Richard, A. C., Pottier, C., Dorval, V., Sarov-Rivière, M., Riant, F., Hervé, D., Amouyel, P., Guerchet, M., Ndamba-Bandzouzi, B., Mbelesso, P., Dartigues, J. F., Lambert, J. C., Preux, P. M., Frebourg, T., Campion, D., Hannequin, D., Tournier-Lasserre, E., Hébert, S. S., and Rovelet-Lecrux, A. (2016) Mutation in the 3'untranslated region of APP as a genetic determinant of cerebral amyloid angiopathy. *European Journal of Human Genetics* **24**, 92-98
470. Pang, Y., Li, T., Wang, Q., Qin, W., Li, Y., Wei, Y., and Jia, L. (2021) A rare variation in the 3' untranslated region of the presenilin 2 gene is linked to Alzheimer's disease. *Molecular Neurobiology* **58**, 4337-4347
471. Ringman, J. M., Monsell, S., Ng, D. W., Zhou, Y., Nguyen, A., Coppola, G., Van Berlo, V., Mendez, M. F., Tung, S., Weintraub, S., Mesulam, M.-M., Bigio, E. H., Gitelman, D. R., Fisher-Hubbard, A. O., Albin, R. L., and Vinters, H. V. (2016) Neuropathology of Autosomal Dominant Alzheimer Disease in the National Alzheimer Coordinating Center Database. *Journal of Neuropathology & Experimental Neurology* **75**, 284-290
472. Tcw, J., and Goate, A. M. (2017) Genetics of β -Amyloid Precursor Protein in Alzheimer's Disease. *Cold Spring Harb Perspect Med* **7**
473. Schilling, S., Pradhan, A., Heesch, A., Helbig, A., Blennow, K., Koch, C., Bertgen, L., Koo, E. H., Brinkmalm, G., Zetterberg, H., Kins, S., and Eggert, S. (2023) Differential effects of familial Alzheimer's disease-causing mutations on amyloid precursor protein (APP) trafficking, proteolytic conversion, and synaptogenic activity. *Acta neuropathologica communications* **11**, 87
474. Chávez-Gutiérrez, L., Bammens, L., Benilova, I., Vandersteen, A., Benurwar, M., Borgers, M., Lismont, S., Zhou, L., Van Cleynenbreugel, S., Esselmann, H., Wiltfang, J., Serneels, L., Karran, E., Gijsen, H., Schymkowitz, J., Rousseau, F., Broersen, K., and De Strooper, B. (2012) The mechanism of γ -Secretase dysfunction in familial Alzheimer disease. *EMBO J* **31**, 2261-2274
475. Szaruga, M., Munteanu, B., Lismont, S., Veugelen, S., Horr , K., Mercken, M., Saido, T. C., Ryan, N. S., De Vos, T., Savvides, S. N., Gallardo, R., Schymkowitz, J., Rousseau, F., Fox, N. C., Hopf, C., De Strooper, B., and Ch vez-Guti rrez, L. (2017) Alzheimer's-Causing Mutations Shift A β Length by Destabilizing γ -Secretase-A β n Interactions. *Cell* **170**, 443-456.e414
476. Ryan, N. S., and Rossor, M. N. (2010) Correlating familial Alzheimer's disease gene mutations with clinical phenotype. *Biomarkers in medicine* **4**, 99-112

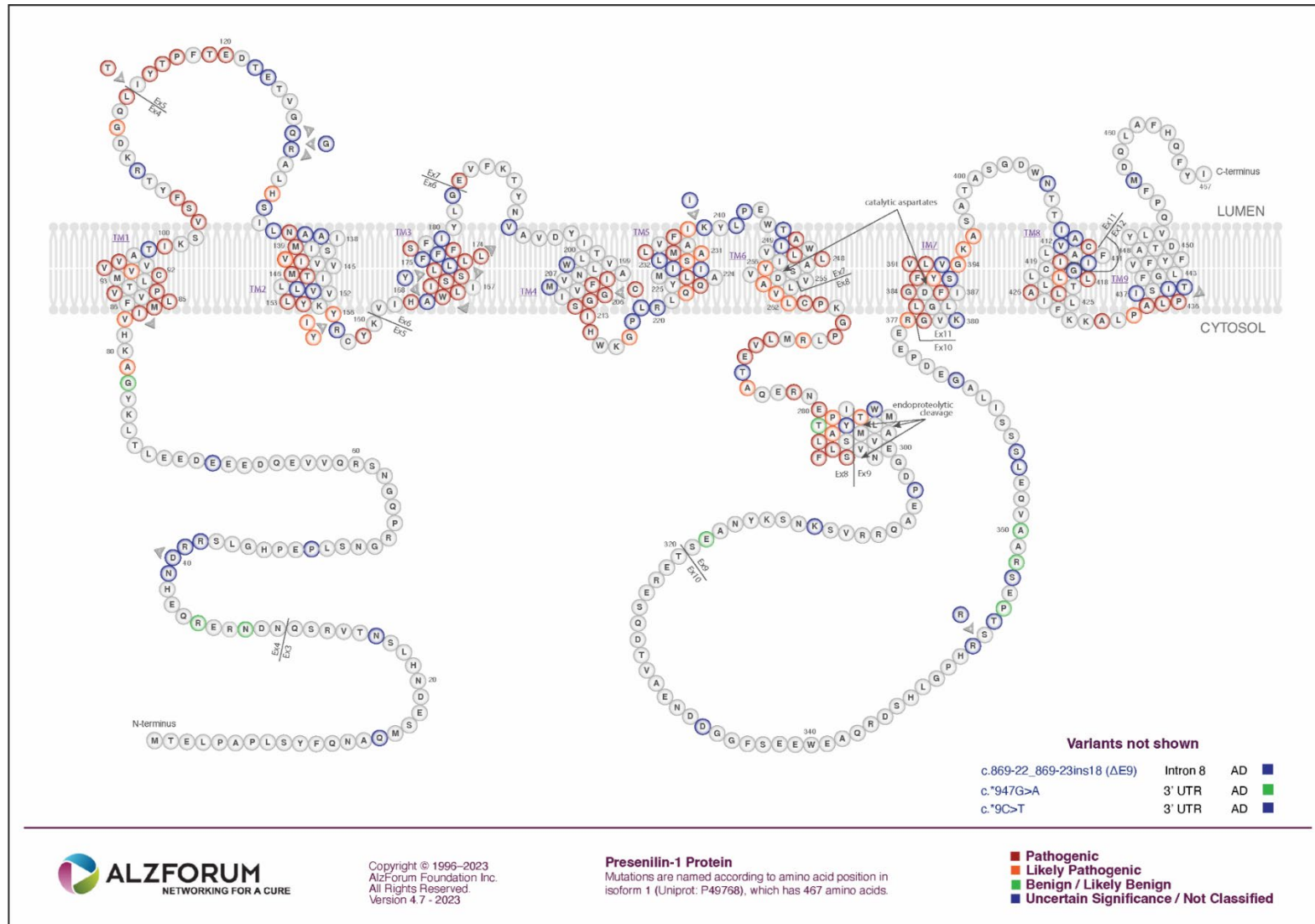
477. Mann, D. M., Pickering-Brown, S. M., Takeuchi, A., and Iwatsubo, T. (2001) Amyloid angiopathy and variability in amyloid beta deposition is determined by mutation position in presenilin-1-linked Alzheimer's disease. *The American journal of pathology* **158**, 2165-2175
478. Lee, J. H., McBrayer, M. K., Wolfe, D. M., Haslett, L. J., Kumar, A., Sato, Y., Lie, P. P., Mohan, P., Coffey, E. E., Kompella, U., Mitchell, C. H., Lloyd-Evans, E., and Nixon, R. A. (2015) Presenilin 1 Maintains Lysosomal Ca(2+) Homeostasis via TRPML1 by Regulating vATPase-Mediated Lysosome Acidification. *Cell Rep* **12**, 1430-1444
479. Han, J., Park, H., Maharana, C., Gwon, A. R., Park, J., Baek, S. H., Bae, H. G., Cho, Y., Kim, H. K., Sul, J. H., Lee, J., Kim, E., Kim, J., Cho, Y., Park, S., Palomera, L. F., Arumugam, T. V., Mattson, M. P., and Jo, D. G. (2021) Alzheimer's disease-causing presenilin-1 mutations have deleterious effects on mitochondrial function. *Theranostics* **11**, 8855-8873
480. Sarasija, S., Laboy, J. T., Ashkavand, Z., Bonner, J., Tang, Y., and Norman, K. R. (2018) Presenilin mutations deregulate mitochondrial Ca(2+) homeostasis and metabolic activity causing neurodegeneration in *Caenorhabditis elegans*. *eLife* **7**
481. Fung, S., Smith, C. L., Prater, K. E., Case, A., Green, K., Osnis, L., Winston, C., Kinoshita, Y., Sopher, B., Morrison, R. S., Garden, G. A., and Jayadev, S. (2020) Early-Onset Familial Alzheimer Disease Variant PSEN2 N141I Heterozygosity is Associated with Altered Microglia Phenotype. *Journal of Alzheimer's Disease* **77**, 675-688
482. Coric, V., van Dyck, C. H., Salloway, S., and et al. (2012) Safety and tolerability of the γ -secretase inhibitor avagacestat in a phase 2 study of mild to moderate Alzheimer disease. *Archives of Neurology* **69**, 1430-1440
483. Tong, G., Wang, J.-S., Sverdllov, O., Huang, S.-P., Slemmon, R., Croop, R., Castaneda, L., Gu, H., Wong, O., Li, H., Berman, R. M., Smith, C., Albright, C. F., and Dockens, R. (2013) A contrast in safety, pharmacokinetics and pharmacodynamics across age groups after a single 50 mg oral dose of the γ -secretase inhibitor avagacestat. *British Journal of Clinical Pharmacology* **75**, 136-145
484. Wyeth, and Pfizer. (2011) Study Evaluating The Coadministration of Begacestat And Donepezil. In *ClinicalTrials.gov* Vol. 2017, National Library of Medicine (US), Bethesda (MD)
485. Penninkilampi, R., Brothers, H. M., and Eslick, G. D. (2016) Pharmacological Agents Targeting gamma-Secretase Increase Risk of Cancer and Cognitive Decline in Alzheimer's Disease Patients: A Systematic Review and Meta-Analysis. *Journal of Alzheimer's Disease* **53**, 1395-1404
486. Alves, F., Kalinowski, P., and Ayton, S. (2023) Accelerated Brain Volume Loss Caused by Anti- β -Amyloid Drugs: A Systematic Review and Meta-analysis. *Neurology* **100**, e2114-e2124
487. Crump, C. J., Johnson, D. S., and Li, Y.-M. (2013) Development and Mechanism of γ -Secretase Modulators for Alzheimer's Disease. *Biochemistry* **52**, 3197-3216
488. Lessard, C. B., Cottrell, B. A., Maruyama, H., Suresh, S., Golde, T. E., and Koo, E. H. (2015) γ -Secretase Modulators and A β 1 Isoforms Modulate γ -Secretase Cleavage but Not Position of ϵ -Cleavage of the Amyloid Precursor Protein (APP). *PloS one* **10**, e0144758
489. Lessard, C. B., Rodriguez, E., Ladd, T. B., Minter, L. M., Osborne, B. A., Miele, L., Golde, T. E., and Ran, Y. (2020) γ -Secretase modulators exhibit selectivity for modulation of APP cleavage but inverse γ -secretase modulators do not. *Alzheimer's research & therapy* **12**, 61
490. Lee, J., Song, L., Terracina, G., Bara, T., Josien, H., Asberom, T., Sasikumar, T. K., Burnett, D. A., Clader, J., Parker, E. M., and Zhang, L. (2011) Identification of presenilin 1-selective γ -secretase inhibitors with reconstituted γ -secretase complexes. *Biochemistry* **50**, 4973-4980

1.9 SUPPLEMENTAL FIGURES



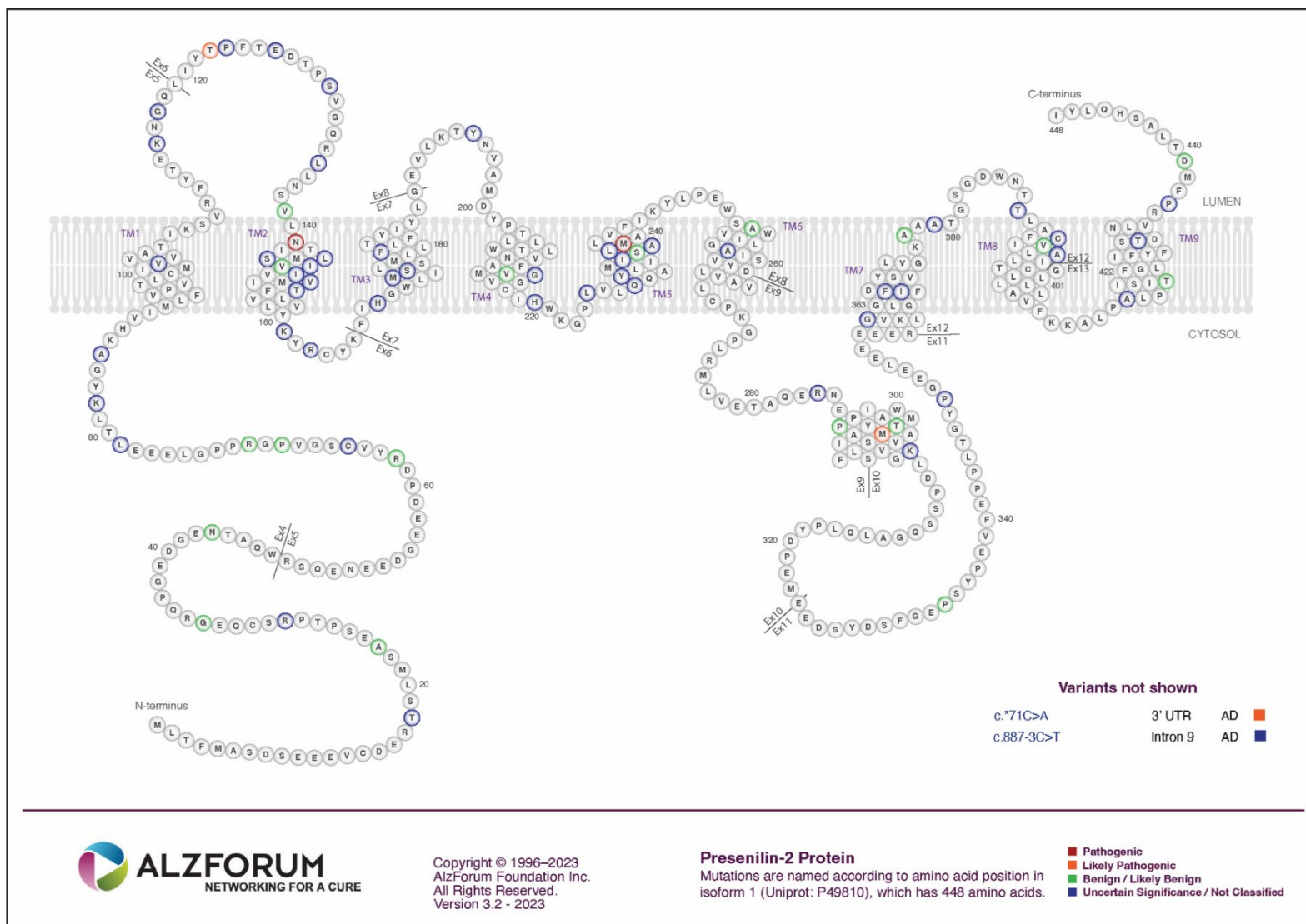
SI Figure 1-1 APP protein and mutation schematic

Retrieved from www.alzforum.org/mutations/app on 18/09/2023



SI Figure 1-2 PS1 protein and mutation schematic

Retrieved from www.alzforum.org/mutations/psen-1 on 18/09/2023



SI Figure 1-3 PS2 protein and mutation schematic

Retrieved from www.alzforum.org/mutations/psen-2 on 18/09/2023

2 QUANTITATIVE COMPARISON OF PRESENILIN PROTEIN EXPRESSION REVEALS GREATER ACTIVITY OF PS2- γ -SECRETASE

2.1 INTRODUCTION

Presenilin (PS) is the catalytic component of γ -secretase, a tetrameric enzyme that cleaves type I transmembrane proteins. The two PS homologues, PS1 and PS2, share approximately 67% amino acid sequence similarity, and form active γ -secretase complexes when incorporated with nicastrin (Nct), anterior pharynx defective-1 (Aph1), and presenilin enhancer-2 (Pen-2).¹ The γ -secretase enzyme has been shown to cleave a large repertoire of substrates,² the most well investigated of which are amyloid precursor protein (APP)³ and Notch1.⁴ The cleavage of APP has received the most attention as it ultimately results in the generation of amyloid- β (A β) peptides, accumulation of which contributes to Alzheimer's disease (AD) pathogenesis.⁵ Consequently, γ -secretase has been proposed as a therapeutic target, with the development of inhibitors of PS-related γ -secretase activity.⁶⁻¹⁰ However, these molecules have failed in clinical trials due to off-target effects, which are thought to be caused by the inhibition of substrates other than APP, particularly Notch1,^{7, 11, 12} and may be influenced by differences in affinity for PS1- and PS2- γ -secretase.¹³⁻¹⁵ More recently, the focus has shifted to the development of γ -secretase modulators (GSMs), small molecules that modulate the type of A β peptides released, while still maintaining cleavage of the intracellular domain of substrates.¹⁶⁻¹⁸ However, there is still a need for improved understanding of γ -secretase activity and insight into the differing roles of PS1- and PS2- γ -secretase enzymes.

γ -Secretase cleaves its substrates via a process termed regulated intramembrane proteolysis (RIP), where type I transmembrane proteins undergo multiple cleavages as part of the signalling or degradation processes. The first step in RIP is the shedding of the substrate ectodomain by proteases, in particular ADAM (a disintegrin and metalloproteinase) family enzymes and the aspartyl proteases BACE1 (β -APP cleaving enzyme) and BACE2.^{19, 20} The second step is performed by γ -secretase, where multiple intramembrane cleavages of the substrate transmembrane domain lead to release of the intracellular domain (ICD) and secreted peptides.^{3, 21} APP processing can be initiated by either ADAM or BACE cleavage,^{22, 23} however, it is BACE1 cleavage that initiates the amyloidogenic pathway, leading to the generation of A β peptides. γ -Secretase is known to successively 'trim' APP after the initial

cleavage by tri- and tetrapeptide cleavages until the A β peptide is released from the luminal membrane.^{24, 25} It must be acknowledged that much of how APP is cleaved has been determined via investigations of PS1- γ -secretase, with little understanding of whether this process differs for PS2- γ -secretase.

The focus on PS1 appears to be largely a result of the significantly greater number of familial AD causing missense mutations in *PSEN1* (200+) compared to *PSEN2* (20+) (retrieved from www.alzforum.org/mutations September 2022).²⁶ While both *PSEN1* and *PSEN2* mutations generally cause increased A β 42:A β 40 ratios, *PSEN1* mutations have an earlier average age of onset and are typically more aggressive.²⁷ However, the recent identification of a *PSEN2* variant in the 3' UTR that mutates a miRNA-binding region suggests PS2 protein expression may influence AD pathology.^{28, 29} This mutation has been shown to cause upregulated PS2 protein expression and subsequently increased A β 42:A β 40 ratio.²⁹

While there is considerable functional overlap between PS1- and PS2- γ -secretase, there are several key differences. Subcellular localisation has been shown to differ, with PS2- γ -secretase localised to late endosomal and lysosomal compartments,³⁰⁻³² while the localisation of PS1- γ -secretase predominately resides within the plasma membrane.^{30, 31} As ectodomain shedding by BACE1 is a prerequisite for A β formation, its localisation in intracellular organelles, including endosomal compartments,³³ links the PS2- γ -secretase complex to A β generation. PS2 has been shown to generate significantly more intracellular A β ^{31, 34} and produce a higher A β 42:A β 40 ratio,^{32, 35-37} supporting its greater activity within the endosomal-lysosomal cellular compartment.

One aspect of PS1- and PS2- γ -secretase activity, which is not often considered, is expression within cells and tissues. Evidence derived from post-mortem tissues and in vivo studies suggest that PS expression levels vary with age and other AD-associated changes. Lee et al.³⁸ show that transcript expression of PS1 is significantly higher than PS2 in human fetal cortex, and that following birth and with age, a concomitant decrease in PS1 and increase in PS2 leads to approximately equal PS1 and PS2 expression. A similar PS expression profile has been observed during terminal differentiation of iPSC-derived neurons, where PS1 expression decreases and PS2 expression increases.³² Interestingly, PS1 protein expression is decreased in human AD cortex and hippocampus,³⁹ and in aged murine cortex, there is a concomitant decrease in PS1 and increase in PS2 protein expression.⁴⁰ These observations are suggestive

of a PS2 role in neuronal maturation and, considered together with the role of PS2- γ -secretase in generating intracellular A β and increased A β 42 product, may indicate that PS2 contributes more to AD pathology than previously credited.

In vitro studies comparing PS1- and PS2- γ -secretase activity have typically shown PS1-complexes to be more active at processing APP and Notch. However, a major limitation of this work, is the assumption that PS1 and PS2 expression levels are equal. A comparable assessment of PS1 and PS2 expression is difficult, as there are no common PS antibodies that detect both PS1 and PS2. To address the inability to assess PS1 and PS2 endogenous expression directly, activity is often determined in cells, where both PS1 and PS2 have been ablated and the PS is exogenously re-introduced to the cell. This presents an opportunity to tag the exogenous PS enabling equi-detection. However, to our knowledge, this approach has only been presented twice; firstly for determining the cellular localisation of PS1 vs. PS2,³¹ and secondly for use in PS quantitation, after which it was determined that, when PS expression was considered, there was no significant difference in γ -secretase activity.⁴¹ Other studies using the relative levels of mature Nct to normalise for exogenous PS expression have shown discordant results; no difference in APP and Notch ICD generation,⁴² or reduced A β generation by PS2- γ -secretase.⁴³ Lastly, the only evidence we are aware of, where endogenous PS expression has been compared, utilised radioactive methionine labelling to correlate PS1 and PS2 antibody detection and showed that in murine blastocyte-derived membranes and cells, PS1- γ -secretase generated more A β than PS2- γ -secretase.⁴⁴

Given the observed differences in tissues/cells, it is crucial to resolve the limitations of directly comparing cellular expression of PS1 and PS2 protein units and understand how this relates to γ -secretase activity. In this study, we investigated the activity of PS1 and PS2 in relation to the expression levels of these proteins, with an overarching hypothesis that PS1 does not have greater activity than PS2. We address this hypothesis using two approaches: 1) Myc-tagging of the PS N-terminus to allow for detection of exogenous PS1 and PS2 via the same antibody, and 2) development of a novel PS1/2 fusion standard to enable, for the first-time, absolute quantitative assessment of endogenous PS1 and PS2 protein using specific antibodies. Our results demonstrate that in both the exogenous and endogenous PS expression systems, PS1 and PS2 are not equally expressed, and when PS expression is accounted for, PS2 is at least as active as PS1 at processing APP and Notch in HEK cells.

2.2 MATERIALS AND METHODS

2.2.1 Mammalian cell culture.

All cell lines were cultured in Dulbecco's Modified Eagle Medium (Sigma D5671) supplemented with 1 mM sodium pyruvate (Sigma S8636), 1 mM L-glutamine (Sigma G7513), 100 units/ml penicillin 0.1 mg/ml streptomycin (Sigma P4333), and 10% v/v fetal bovine serum (Serana FBS-Au-015). Cells were incubated at 37 °C with 5% v/v atmospheric carbon dioxide.

2.2.2 CRISPR presenilin knockout in HEK-293

To generate HEK PS2+ cells, PS1 was knocked out of HEK-293 cells using presenilin 1 CRISPR/Cas9 KO plasmid in conjunction with presenilin 1 HDR Plasmid from Santa Cruz Biotechnology (sc-401227 and sc-401227-HDR), as per the supplier protocol. Briefly HEK-293 cells were plated in 6-well plates (1.0×10^6 cells/well), 24 hrs prior to transfection. When cells were approximately 80% confluent, 1.25 µg each of the CRISPR/Cas9 KO and HDR plasmids were transfected into cells, using Lipofectamine 3000 (Invitrogen L3000015) as per the manufacturer's instructions. Cells were then incubated overnight, after which the medium was changed. At 48 hrs post transfection, cells were sorted for GFP-positive and RFP-positive cells and cultured in puromycin selection medium (0.25 µg/ml). Cells were selected for 8 days with medium replacement every 48 hrs.

PS2 knockout was completed using the pSp-Cas9-(BB)-2A-GFP vector and methodology previously described by Ran et al.⁴⁵ Guide RNA sequences were designed using ChopChop.com.au, two guide sets were used in combination to generate the PS2KO in the cells. The guide sequences used were 5'GCTCCCCTACGACCCGGAGA3' and 5'ACGATCATGCACAGAGTGAC3'. 10 µM each of sense and antisense synthesised oligonucleotides with appropriate flanking sequences,⁴⁵ were phosphorylated using T4 PNK (NEB M0201) in a 10 µl reaction, as per the manufacturer's protocol. The reaction was incubated at 37 °C for 30 min, before heating to 95 °C for 5 min followed by a temperature ramp of 1 °C per min until reaching 25 °C to anneal the oligonucleotides. Oligonucleotides were ligated into pSp-Cas9-(BB)-2A-GFP plasmid that had been linearised by digestion with BbsI-HF (NEB R3539) and gel purified (Bioline BIO-52060), as per the supplier protocols. Briefly, 2 µmol of dsDNA guide was ligated into 10 ng of pSp-Cas9-(BB)-2A-GFP using 400 units T4 DNA ligase (NEB M0202) and incubated for 16 hrs at 16 °C. 5 µl of ligation product

was transformed into chemically competent *E.coli* XL10 cells and grown overnight on agar plates supplemented with 100 µg/ml ampicillin. Individual colonies were selected and cultured overnight in 5 ml Luria Broth supplemented with 100 µg/ml ampicillin. Plasmids were extracted (Bioline BIO-52057) and correct insertion of the guide RNA sequence was confirmed by sequencing.

To generate HEK-293 PS1+ and HEK-293 PSnull cells, we seeded HEK-293 PS1+PS2+ and HEK-293 PS2+ cells in 6-well plates at 1.0×10^6 cells per well, 24 hrs prior to transfection. 1.25 µg each of the two guide plasmids were prepared using Lipofectamine 3000 and cells transfected as per the manufacturer's instructions. Cells were incubated for 24 hrs, after which they were sorted using a BD FACSJazz cell sorter at 1 cell per well into 96-well plates, gated for medium GFP intensity and no/minimal propidium iodide intensity. Monoclonal populations were expanded and screened for PS1 and PS2 protein expression, and selected clones were further screened for substrate processing (SI Figure 2-1). One representative clone was selected for subsequent experiments.

2.2.3 Plasmid construct generation

All plasmid constructs used for transient transfection of PS and substrate proteins were generated in the backbone vector pIRES2-AcGFP1 (Takarabio). Human PS1 and PS2 cDNA sequence with Myc N-terminal tags, human APP695Swe and human Notch1 (lacking the extracellular domain (21-1713bp) termed Δ EhNotch1) sequences were cloned into pIRES2-AcGFP1 vector linearised via digestion by restriction enzymes at sites EcoRI and BamHI (PS1, PS2 and Δ EhNotch1) and Sall and XmaI (hAPP695Swe). After sequence confirmation, 50 ml cultures were grown in Luria Broth and plasmids extracted (BioRad 7326120).

2.2.4 Whole genome sequencing and copy number variation analysis

Genomic DNA was extracted from HEK 293 PS1+PS2+, HEK 293 PS1+, HEK 293 PS2+ and HEK 293 PSnull cells using the Monarch Genomic DNA Purification Kit (NEB T3010S) as per manufacturer instructions and eluted in nuclease free H₂O. DNA was assessed for quality and concentration using Nanodrop ND-1000 spectrophotometer and Qubit 4 Fluorometer respectively. 4 µg of genomic DNA from each cell line was sheared to a target size of 8 kb, using g-TUBEs (Covaris 520079) as per manufacturer instructions. Sample concentrations were again measured, and libraries subsequently prepared for Oxford Nanopore Technologies

(ONT) sequencing using Native Barcoding Kit 24 V14 (SQK-NBD114.24) as per manufacturer instructions. Briefly, 1 µg of DNA from each cell line was individually end repaired and dA-tailed using NEBNext Ultra II End Repair/dA-Tailing Module (NEB E7546), then, ligated to unique ONT barcodes. Barcoded samples were pooled and purified using AMPure XP beads. Native adapters were ligated, after which DNA was enriched for fragments > 3 kb using the long fragment buffer and purified again with AMPure XP beads. The concentration of the resultant library was measured and 20 fmol library prepared in elution buffer. The multiplexed DNA library was loaded onto a PromethION R10.4.1 flow cell (FLO-PRO114M) and run on P2 Solo sequencing device. During the 72-hour sequencing run, the flow cell was twice washed and reloaded with the same library to maximize output.

Raw Pod5 files were basecalled and aligned to the GRCh38 reference using Dorado v0.3.1 with the high-accuracy model “dna_r10.4.1_e8.2_400bps_hac@v4.1.0” into a single aligned BAM. Demultiplexing was performed using guppy_barcode with default parameters. The wf-human-variation workflow (<https://github.com/epi2me-labs/wf-human-variation>) was implemented with genomic bins size set to 10 kb to obtain a copy number variation (CNV) output for each individual barcode. Gene edits were confirmed at target loci by viewing of sequence data using Integrative Genomics Viewer (IGV_2.16.2).⁴⁶

2.2.5 Transient transfection

Transient transfection experiments were performed in 6-well plates, with cells seeded at 4.0×10^5 per well. Prior to plating cells, plates were coated overnight with 50 µg/ml poly-L-lysine (Sigma P9155) to improve adherence of PS knockout cell lines. The medium was replaced with antibiotic-free medium 24 hours after plating and cells transiently transfected. Lipofectamine 3000 was used for co-transfection of PSnull cells (Figure 2-2, Figure 2-4, Figure 2-2 APP processing by exogenous Myc-tagged PS1 and PS2 in PSnull cells.). PEI Max (Polysciences 24765), using 3 µg PEI per 1 µg DNA, was used for substrate only transfections for investigation of endogenous PS (Figure 2-6, Figure 2-8). Where substrate (pIRES2-hAPP695Swe-AcGFP1 or pIRES2-ΔEhNotch1-AcGFP1) and presenilin (pIRES2-Myc-PS1-AcGFP1 or pIRES2-Myc-PS2-AcGFP1) co-transfection was undertaken in PSnull cells, the vectors were used in a PS:Substrate per unit ratio of 1:3, such that the total amount of DNA transfected was 500 ng. For transfection of substrate only, to investigate endogenous PS activity, the same amount of substrate vector was transfected as per the co-transfection assays. Cells were incubated for 24 hrs, after which conditioned media and whole cell lysates were

collected. Conditioned media were collected, for all hAPP695Swe transfections, in microfuge tubes, centrifuged at 17,000 g for 5 min, the supernatant transferred into a clean tube and snap frozen in liquid nitrogen and stored at -80 °C. For lysate collection, the medium was aspirated, and plates washed with cold PBS and aspirated. Cells were scrapped into 100 µl of RIPA lysis buffer (Astral Scientific 786-490) supplemented with protease inhibitor cocktail (Roche 11697498001) and transferred to microfuge tubes. Lysate samples were incubated for 1 hr at 4 °C with rotation, centrifuged at 14,000 g for 10 min at 4 °C, and the supernatant collected and stored at -20 °C.

2.2.6 Quantitative PCR

Cells were grown to confluency in 6-well plates and harvested for mRNA extraction. Briefly, plates were washed twice with cold PBS and cells scrapped and collected. Cells were centrifuged at 300 g for 5 min, after which supernatant was aspirated. RNA was extracted using ISOLATE II RNA Mini kit as per the manufacturer's instructions (Bioline BIO-52072) and RNA concentration and quality determined by Nanodrop (Thermo Fisher). To generate cDNA using Tetro cDNA synthesis kit (Bioline BIO-65043), 0.5 µg of RNA was used in a 10 µl reaction with a 1:1 ratio of random hexamer and oligo (dT)₁₈ primer mix, as per the manufacturer's instructions. Resultant cDNA samples were diluted to a final volume of 100 µl for use in qPCR. GoTaq qPCR master mix (Promega A6001) was used in a final reaction volume of 20 µl. For all genes, diluted cDNA solution (2 µl) was used in 20 µl reactions. Primer details are listed in Table 2-1, and were designed using NCBI Primer-BLAST,⁴⁷ except *GAPDH* primers.⁴⁸ Each biological replicate was run in technical triplicate using the Applied Biosystems Viia7 real-time PCR system, and average Ct values determined for each gene. Human *UBC* and *GAPDH* reference genes were used for normalisation. Gene expression levels were calculated using the Pfaffl method,⁴⁹ and expression relative to PS1+PS2+ cells determined.

Table 2-1 qPCR primer sequences

Gene Target	Forward Primer	Reverse Primer
PSEN1	5'CCAGAGGAAAGGGGAGTAAACTT3'	5'ACAGGCTATGGTGTGTTC3'
PSEN2	5'TCATCTGCCATGGTGTGGAC3'	5'GTCTTCTCCATCTCCGGGT3'
APH1a	5'GGTGTTTTTTCGGCTGCACTT3'	5'CAGAAAAATGCCCCTGCGAC3'
APH1b	5'CTGCGCCTTCATTGCCTTC3'	5'GAAGAAAGCTCCGGCGATGA3'
NCSTN	5'ACTAGCAGGTTTGTGCAGGG3'	5'TCTGATGAGTGGCGTTGAGC3'
PEN2	5'TGCCTTTTCTCTGGTTGGTCA3'	5'CGCCAGACATAGCCTTTGAT3'
UBC	5'CCGGGATTTGGGTCGCAG3'	5'TCACGAAGATCTGCATTGTCAAG3'
GAPDH47	5'CTGCTTTTAACTCTGGTAAAGT3'	5'GCGCCAGCATCGCCCA3'

2.2.7 Immunoblotting

Total protein concentration of cell lysates was determined using micro-BCA kit (Thermo Fisher 23235). Presenilin and APP proteins were separated with 12% v/v acrylamide, tris-tricine gel chemistry. Notch, Pen-2, Aph1a, and Nct proteins were separated with 8-10% v/v acrylamide, bis-tris gel chemistry (Invitrogen Surecast system). Samples were prepared using either 4x tris-tricine sample buffer (16% w/v SDS, 200 mM tris, 48% v/v glycerol, 0.5% w/v Coomassie G-250) or 4x LDS sample buffer (Thermo Fisher B0007) as appropriate, reducing agent and treatment conditions vary dependent on the protein of interest (see Table 2-2). Samples were vortexed for 30 seconds, heated for 10 min (as per temperature in Table 2-2), centrifuged at 17,000 g for 5 minutes, then electrophoresed at 100 V for 1 hour 45 minutes. Proteins were transferred to 0.2 µm nitrocellulose membrane (BioRad 1620112), via wet transfer method using tris-glycine buffer (19.2 mM glycine, 2.5 mM tris, 20% v/v methanol) at 150 mA for 16 hrs at 4°C. Membranes were stained with Ponceau S (1% w/v Ponceau S, 5% v/v acetic acid) for 5 minutes to assess transfer quality before destaining with boiled TBS (2 mM tris, 1.5 mM NaCl). Membranes were subsequently incubated in blocking buffer, as appropriate for the primary antibody used, for 1 hour at room temperature with agitation. Membranes were incubated in primary antibody (all antibody conditions and details are available in Table 2-2) overnight at 4 °C. Membranes were subsequently washed three times in TBS-tween (0.05% v/v tween) for 10 minutes with agitation. Membranes were then incubated with appropriate secondary antibody, anti-mouse or anti-rabbit IgG HRP-conjugated secondary antibody (Thermo Fisher 31430, 31460), diluted at 1:20,000 in 0.5% w/v non-fat dry milk in TBS-tween, for 1 hour at room temperature with agitation. Membranes were then washed again three times in TBS-tween, followed by a 5-minute wash with TBS. Membranes

were incubated in either Clarity ECL (BioRad 1705061) or Prime ECL (Cytiva GERPN2232) (see Table 2-2) for 5 minutes as per the manufacturer's instructions, then imaged on a BioRad ChemiDoc MP system.

Table 2-2 Antibody conditions for immunoblotting

Protein Target	Antibody	Reducing agent	Treatment temp	Blocking/Antibody diluent #	Antibody dilution	ECL
Myc-tag	Myc-Tag 9B11 CST 2276S	None	37°C	3%BSA/3%BSA	1/1000	Clarity
PS1 NTF	PS1 NT1 Biologend 823401	None	37°C	5%NFDM/0.5%NFDM	1/2000	Clarity
PS1 CTF	PS1 D39D1 CST 5643S	None	37°C	5%NFDM/0.5%NFDM	1/1000	Clarity
PS2 NTF	PS2 Biologend 814204	DTT	37°C	5%NFDM/0.5%NFDM	1/2000	Prime
PS2 CTF	PS2 EP1515Y Abcam ab51249	DTT	No Heat	5%NFDM/0.5%NFDM	1/20000	Clarity
Aph1a	In-house provided by PE Fraser	DTT	No Heat	5%NFDM/0.5%NFDM	1/500	Prime
Nicastrin	Nicastrin Sigma-Aldrich N1660	BME	70°C	5%NFDM/0.5%NFDM	1/1000	Clarity
Pen-2	Pen-2 Sigma-Aldrich P5622	BME	55°C	5%NFDM/0.5%NFDM	1/500	Clarity
APP-FL & CTF	APP C1/6.1 Biologend	DTT	75°C	5%NFDM/0.5%NFDM	1/2000	Clarity
ΔEhNotch1	Notch1 Origene TA500078	DTT	75°C	5%NFDM/0.5%NFDM	1/1000	Clarity
NICD	Notch Val1744 CST 4147	DTT	75°C	3%BSA/3%BSA	1/1000	Clarity
GAPDH	GAPDH CST 5174	As per initial sample, blots stripped and reprobod		3%BSA/3%BSA	1/5000	Clarity
GAPDH	GAPDH Abclonal A19056			5%NFDM/0.5%NFDM	1/10000	Clarity

All blocking and antibody diluent concentrations provided are % w/v

Note: DTT = Dithiothreitol [50 mM], BME = β-Mercaptoethanol [10% v/v], BSA = bovine serum albumin, NFDM = non-fat dried milk powder. Clarity ECL (Biorad; #1705061), Prime ECL (Aversham; #RPN2232)

2.2.8 PS1/2 fusion standard and absolute PS1 and PS2 quantitation

The presenilin fusion standard (PS-Std) (see results section, Figure 2-5A) was recombinantly generated in *E. coli* and purified by GenScript. The final size of the protein including tags is 30.7 kDa, which equates to 5.10×10^{-11} ng per protein unit. In order to use the standard to quantify the number of endogenous PS protein units, a 5- to 6-point standard curve was generated on every PS immunoblot. The actual range used was determined empirically and is dependent on the total protein of sample used, the protein fragment being detected i.e., PS1 or PS2, NTF or CTF, and the specific antibody used. The ng of PS-Std is converted to protein units of PS-Std as follows; protein units PS-Std = [(ng PS-Std) x 90%]/ 5.10×10^{-11} – note the PS-Std purity was determined to be 90% in quality control report from supplier. This value was then plotted against the corresponding densitometry units quantitated from the immunoblot for

the corresponding PS-Std band, to generate a standard curve, using multiple replicates. The standard curve line of best fits equation was used to determine the PS1 or PS2 protein units in the sample. Therefore, the total PS protein units in PS1+PS2+ cells will be the sum of PS1 and PS2 protein units.

2.2.9 ELISA

ELISA kits were used to detect A β 40 (Invitrogen KHB3482) and A β 42 (Invitrogen KHB3442) in conditioned media as per the manufacturer's instructions. For detection of A β 40 from conditioned media, endogenous PS activity samples were diluted 1/6, while exogenous PS activity samples were diluted 1/3. No dilution was necessary for detection of A β 42 in conditioned media.

2.2.10 Statistics

All statistical analyses were completed using GraphPad Prism 9.5.0. Three to six experimental replicates were completed for all assays. Statistical significance was determined via unpaired T-test, where only two groups were examined. For comparisons of more than two groups, one-way ANOVA or two-way ANOVA analysis, with Holm-Šidák's multiple comparison tests were used, as appropriate.

2.3 RESULTS

2.3.1 Presenilin knock-out cell line generation and characterisation.

To evaluate and compare the influence of exogenous and endogenous PS1 or PS2 on γ -secretase, presenilin knockout cell lines derived from HEK-293WT (PS1+PS2+) were generated. The cell lines included those lacking PS1 but retaining PS2 expression, lacking PS2 but retaining PS1 expression, or lacking both PS1 and PS2 protein expression. These cell lines were referred to as PS2+, PS1+, and PSnull, respectively. Six to eight monoclonal populations of each cell line were assessed for PS1 and PS2 expression as well as γ -secretase processing of APP and Notch1 substrates (SI Figure 2-1SI Figure 2-1 Characterisation of clonal populations of HEK-293 PS2+, PS1+, and PSnull cell lines). The clone representative of average substrate processing was selected for use in subsequent assays. As genomic copy number variations (CNV) have been observed in genetically altered HEK-293 cells,⁵⁰ and as PS1 and PS2 were ablated using different CRISPR vectors, we used low coverage long-read whole genome

sequencing to assess the structural landscape of each of the monoclonal cell lines to be used for subsequent experiments (see methods in supplementary material). These sequencing data were also leveraged to confirm that successful gene edits of *PSEN1* or *PSEN2* in the appropriate cell lines occurred at the CRISPR gRNA targeted sites (SI Figure 2-2). We found similar CNV architecture between the CRISPR cell lines and their HEK-293WT counterpart (SI Figure 2-3), indicating that any observed expression changes were likely the result of the loss of PS1 or PS2 protein expression.

The expression of the components of γ -secretase is regulated by the formation of the enzyme complex.^{1, 51-53} Therefore, to assess the effect of the absence or presence of PS on the expression of γ -secretase components and to further characterise the cell lines, expression of PS1, PS2, Aph1, Pen-2 and Nct were assessed at transcript (Figure 2-1A) and protein levels (Figure 2-1B-F). As expected, compared to the wildtype, *PSEN1* and *PSEN2* mRNA expression is absent or markedly reduced in cells, where the specific PS has been ablated. In the single PS knockout cell lines, an increase in mRNA expression was observed for the alternate homologue, indicating that loss of one PS homologue is causing a compensatory increase in transcript expression of the alternate homologue. For all other components of γ -secretase, mRNA expression was significantly reduced in the PS2+ and PSnull cell lines, while no significant changes were observed in the PS1+ cell line.

PS1 and PS2 protein expression (Figure 2-1B, C, E) is commensurate with observed mRNA expression. No PS1 or PS2 protein was detected in cells, where the respective PS had been knocked out. Increases in PS1 and PS2 protein were observed in the PS1+ and PS2+ cell lines respectively, in line with the observed mRNA results. Aph1a protein levels similarly aligned with the mRNA results (Figure 2-1D, E). However, Pen-2 protein levels differed from the mRNA expression profile, with significant reduction in protein levels evident in both the PS1+ and PS2+ cell lines, and no protein detected in PSnull cells (Figure 2-1D, E).

In all cell lines except for PSnull, Nct was detected as two protein bands, representing immature and mature protein (Figure 2-1D, F). In the PSnull cells, Nct was detected as immature protein only, as has been previously reported in double knockout cells^{36, 42} and consistent with the requirement of presenilin for maturation of Nct.⁵³ Notably, mature vs. immature Nct levels vary in a PS-dependent manner, consistent with previous reports.^{31, 36} Where PS1+PS2+ cells have approximately 4-times more mature Nct, PS2+ cells have approximately equal levels of

immature and immature Nct, and PS1+ cells have approximately 4-times more immature Nct levels.

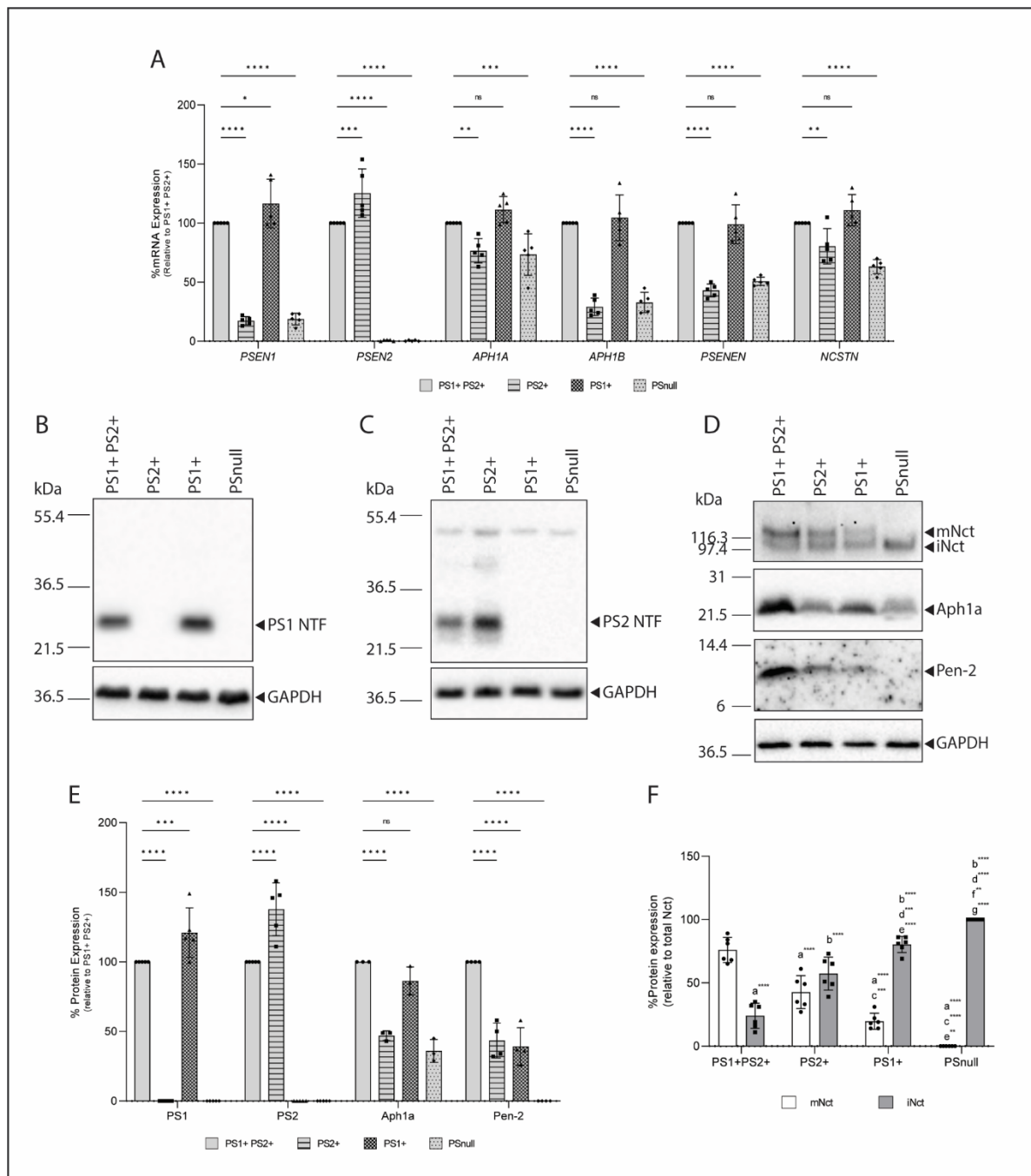


Figure 2-1 Characterisation of HEK-293 PS1+PS2+, PS1+, PS2+ and PSnull cell lines.

Cell lines were generated by CRISPR-Cas9 knockout of PSEN1 and/or PSEN2 from HEK-293 cell lines. Representative clone of each cell line selected for further analysis by mRNA expression of γ -secretase subunits PS1, PS2, Aph1a, Aph1b, Pen-2 and Nct and presented relative to PS1+PS2+ cell line expression (A). Whole cell lysates were analysed by immunoblot for detection of PS1 protein (B) PS2 protein (C) and Aph1a, Pen-2 and Nct proteins (D). Protein expression levels were quantitated by densitometry analysis and are presented relative to PS1+PS2+ cell line expression for PS1, PS2, Aph1a and Pen-2 (E). Both mature Nct (mNct)

and immature Nct (iNct) were quantitated and the percentage of each relative to total Nct calculated (F). Values shown are mean \pm SD of $n = 3-6$ independent experiments. Two-way ANOVA with Holm-Šidák's multiple comparison was completed for (A, E, F). For (F) a = significantly different to mNct PS1+PS2+, b = significantly different to iNct PS1+PS2+, c = significantly different to mNct PS2+, d = significantly different to iNct PS2+, e = significantly different to mNct PS1+, f = significantly different to iNct PS1+, g = significantly different to mNct PSnull. For all quantitated data; ns = $P > 0.05$, * = $P < 0.05$, ** = $P < 0.01$, *** = $P < 0.001$, **** = $P < 0.0001$.

2.3.2 Exogenous PS expression highlights difference in PS levels and subsequently higher PS2 activity

To directly compare exogenously expressed PS1- and PS2- γ -secretase processing of hAPP695Swe and hNotch1, PS1 and PS2 constructs N-terminally tagged with Myc were transfected into PSnull cells. N-terminal tagging has been previously used for exogenous PS expression,^{31,41} while C-terminal tagging would be unsuitable, as this region interacts with the Aph1 component of γ -secretase.⁵⁴ Exogenous, Myc-tagged, PS1 (exPS1) or PS2 (exPS2) was co-transfected with either hAPP695Swe or Δ EhNotch1 at a ratio of 1:3 (PS:Substrate). The amount of exPS used in the transfections was titrated to reduce the amount of unincorporated full-length protein, while retaining maximum PS-NTF levels (SI Figure 2-4).

APP processing was assessed via immunoblotting (Figure 2-2A) of whole cell lysates APP full length (APP-FL) and APP C-terminal fragment (APP-CTF) levels were quantitated and expressed as the ratio of APP-CTF/APP-FL as an initial indicator of γ -secretase activity. APP-CTF protein accumulation was significantly reduced with the co-expression of either exPS1 or exPS2 compared to control; notably, APP-CTF accumulation was 2.0-fold lower with exPS2 compared to exPS1 (Figure 2-2B). In contrast, the A β 40 and A β 42 levels in conditioned media detected by ELISA, were significantly higher when hAPP695Swe was co-expressed with exPS1 (Figure 2-2C, D).

It was observed that Myc-PS2 NTF expression levels were dramatically lower than Myc-PS1 NTF expression, consequently the total protein loaded had to be adjusted for appropriate detection of Myc-PS NTF, and 3-times more protein was loaded for exPS2 cell lysates (Figure 2-2E). Normalised quantitation of the Myc-PS-NTF showed that in the absence of hAPP695Swe expression, exPS1-NTF expression was 5.5-fold higher than exPS2-NTF. In the presence of hAPP695Swe, exPS1-NTF expression significantly increased, and exPS2-NTF expression trended toward an increase (Figure 2-2F). Having directly quantitated exPS1- and

exPS2-NTF expression levels by detecting the Myc-tag, we normalised the hAPP695Swe substrate processing products to determine the specific contributions of exPS1- and exPS2- γ -secretase. Consequently, the normalised results showed that exPS1- γ -secretase accumulated 8.1-fold more APP-CTF than exPS2- γ -secretase (Figure 2-2G). Additionally, after normalisation for the levels of exPS1-NTF and exPS2-NTF there were no significant differences in A β 40 or A β 42 levels observed between exPS1- and exPS2- γ -secretase (Figure 2-2H, I), schematic representation of these results is presented in Figure 2-3. Furthermore, no significant difference in the A β 42:A β 40 ratios between exPS1 and exPS2 co-expression systems was evident (Figure 2-2J).

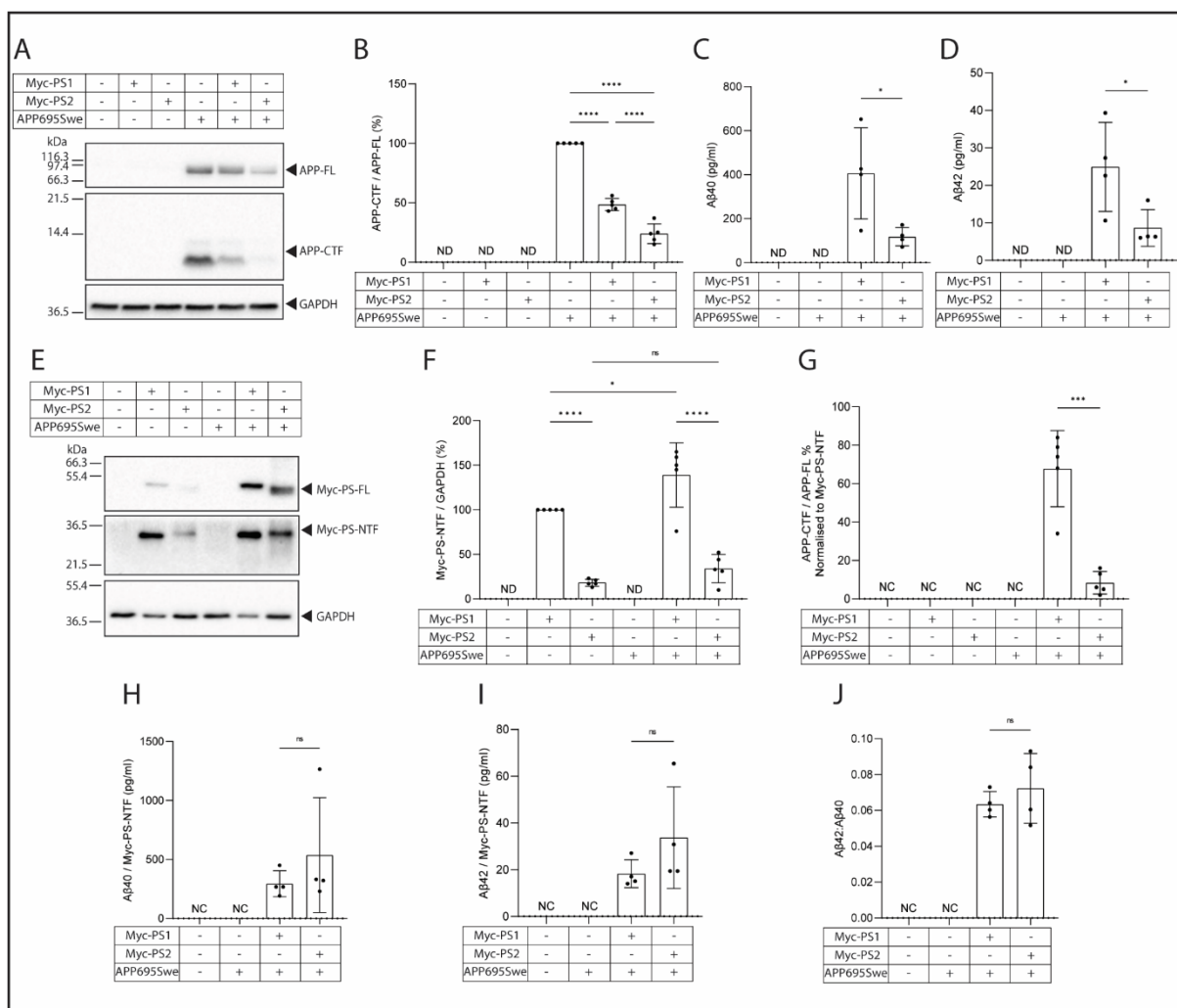


Figure 2-2 APP processing by exogenous Myc-tagged PS1 and PS2 in PSnull cells.

Both hAPP695Swe and Myc-tagged PS were transiently co-expressed in PSnull cells to assess APP processing and directly compare PS1 and PS2 expression to enable the effect of variable expression to be considered. Whole cell lysates were assessed via immunoblotting to determine APP-FL and APP-CTF protein levels (A) and the accumulation of APP-CTF/APP-FL quantitatively determined by densitometry assessment and presented relative to PSnull cells transfected with hAPP695Swe only (B). Conditioned media was collected concurrently with

whole cell lysates for analysis of A β 40 (C) and A β 42 (D) levels (pg/ml) by ELISA. Exogenous PS1 and PS2 expression was directly compared by immunoblotting using antibody directed against the Myc-tagged N-terminus of exPS1 and exPS2 (E). Note that to enable simultaneous detection of exPS1 and exPS2 the total protein loaded was adjusted, for exPS1 transfected lysates 10 μ g total protein was loaded, while for exPS2 transfected lysates 30 μ g of protein was loaded. Myc-PS-NTF levels were quantitated by densitometry analysis and normalised for GAPDH to account for the different amounts of total protein loaded between exPS1 and exPS2 samples (F). APP-CTF, A β 40 and A β 42 were subsequently normalised for Myc-PS-NTF levels to account for variable PS1 and PS2 expression (G-I). A β 42:A β 40 ratio was calculated (J). Values shown are mean \pm SD of n = 4-5 independent experiments. Statistical tests applied were unpaired t- test for (C, D, G-J) and ordinary one-way ANOVA with Holm-Šidák's multiple comparison for (B, F) where ns = P > 0.05, * = P < 0.05, ** = P < 0.01, *** = P < 0.001, **** = P < 0.0001.

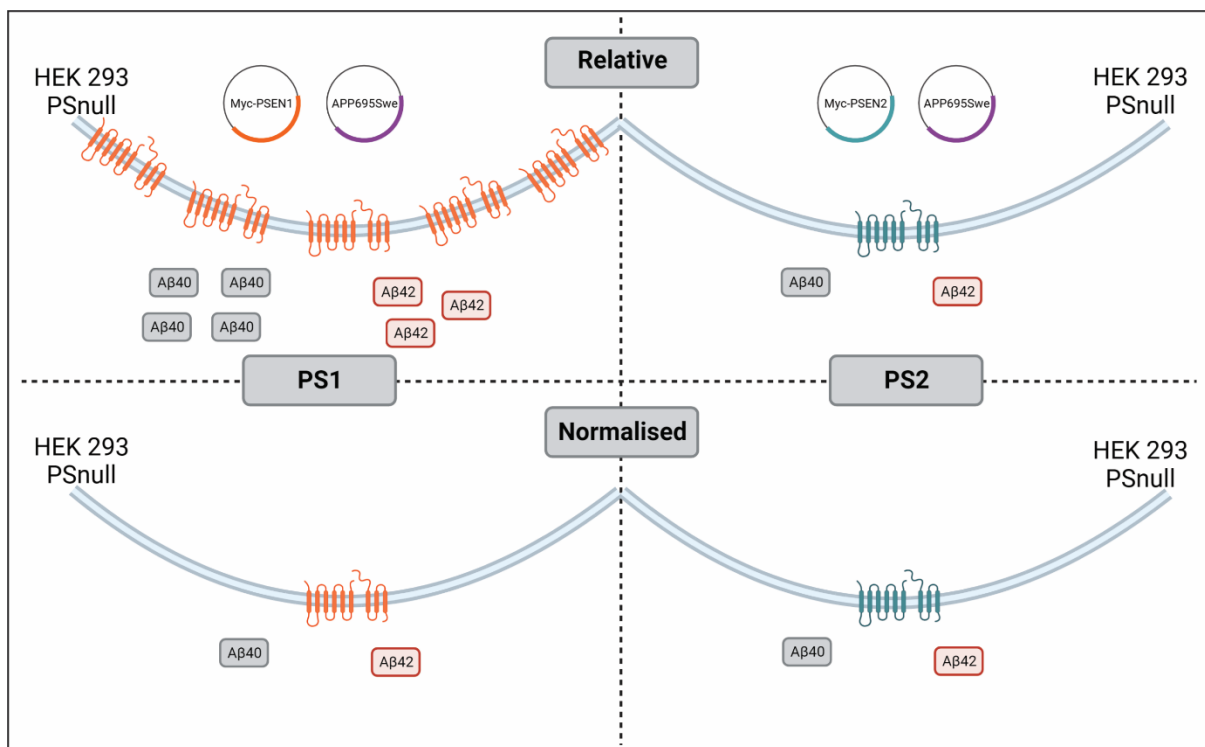


Figure 2-3 Effect of exogenous PS normalisation on A β generation

Exogenous expression of PS1-NTF and PS2-NTF was directly compared using the Myc-tag and the relative exPS1:exPS2 expression ratio was calculated to be 5.5:1. Subsequently the A β 40 and A β 42 levels were normalised to determine the amount of A β generated by a single PS1- or PS2- γ -secretase enzyme. Consequently, the levels of A β generated by an individual exPS1- γ -secretase or exPS2- γ -secretase enzyme were not significantly different. Note A β 40 and A β 42 changes are represented relatively, and are not a direct comparison, for absolute A β 40 and A β 42 levels refer to Figure 2-2. Created with BioRender.com

The effect of presenilin expression on Notch1 cleavage was similarly examined. The Notch1 ICD (NICD), which directly reflects γ -secretase activity, and Δ EhNotch1 proteins were detected via immunoblotting of whole cell lysates, from exPS1 or exPS2 co-transfection with

Δ EhNotch1. The NICD/ Δ EhNotch1 ratio was assessed, initially without consideration of exPS-NTF expression. As expected, no NICD product was detected in the absence of PS expression, and exPS1 co-transfection led to a 2.7-fold higher NICD generation than exPS2 co-transfection (Figure 2-4A,B). Myc-PS-NTF levels in the absence or presence of Δ EhNotch1 expression were quantitated and used to normalise the NICD levels (Figure 2-4). In the absence of substrate overexpression, 4.5-fold more exPS1-NTF was expressed than exPS2-NTF (Figure 2-4C, D). Δ EhNotch1 co-expression with exPS1 increased Myc-PS1-NTF levels, while no change was observed in Myc-PS2-NTF levels with co-expression (Figure 2-4C, D). These results indicate that exPS1 but not exPS2 is upregulated when Notch substrate is expressed. Subsequent normalisation of Δ EhNotch1 processing with the Myc-PS expression data, to account for the different expression levels, showed that exPS2- γ -secretase generated 2.8-fold more NICD exPS1- γ -secretase (Figure 2-4E).

Overall, the findings indicate that exogenous expression of PS1 and PS2 does not lead to comparable expression of the γ -secretase incorporated Myc-PS-NTF proteins. Interestingly, when the difference in expression was accounted for, exogenously expressed PS2 was more active than PS1 at cleaving hAPP695Swe and Δ EhNotch1.

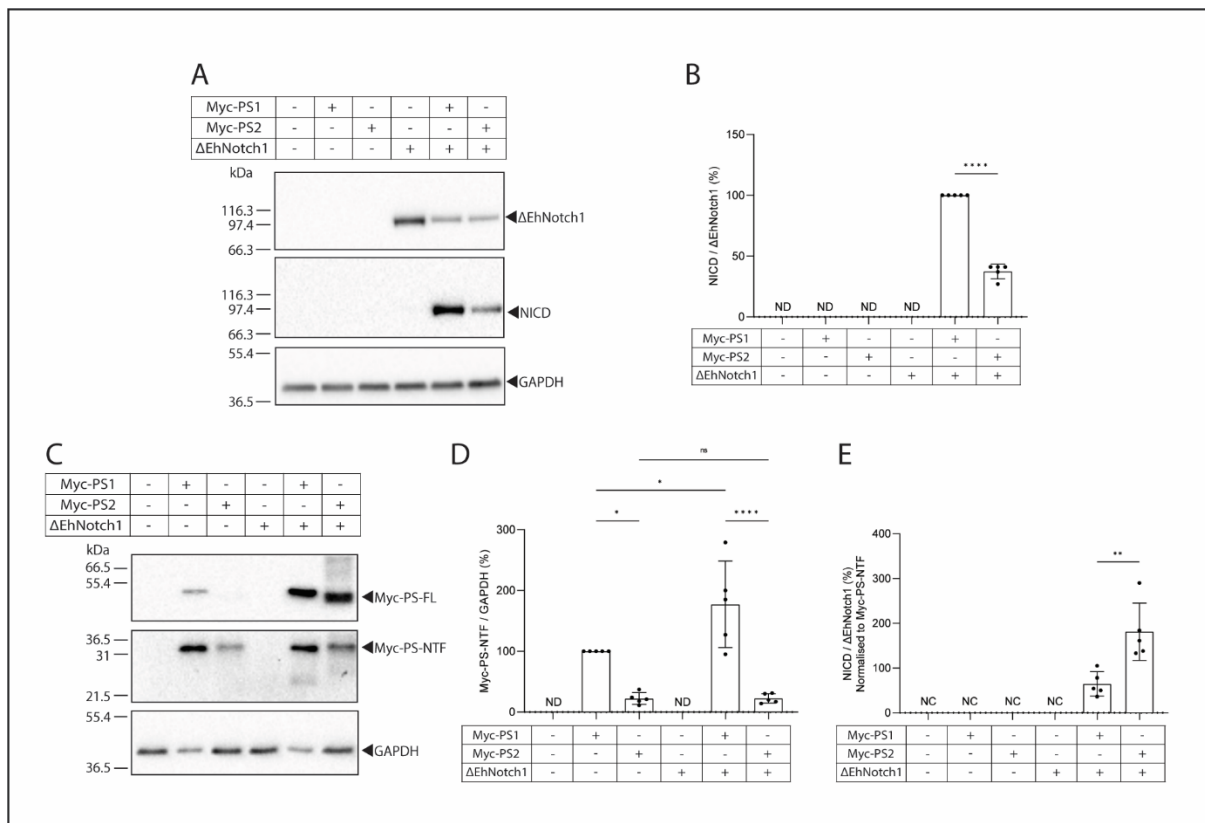


Figure 2-4 Notch1 processing by exogenous Myc-tagged PS1 and PS2 in PSnull cells.

Both Δ EhNotch1 and Myc-tagged PS were transiently co-expressed in PSnull cells to assess Notch1 processing and directly compare PS1 and PS2 expression to enable the effect of variable expression to be considered. Whole cell lysates were assessed via immunoblotting to determine Δ EhNotch1 and NICD protein levels (A) and the level of NICD/ Δ EhNotch1 quantitatively determined by densitometry assessment and presented relative to exPS1 transfection with Δ EhNotch1 (B). Exogenous PS1 and PS2 expression was directly compared by immunoblotting using an antibody directed against the Myc-tagged N-terminus of exPS1 and exPS2 (C). Note that to enable simultaneous detection of exPS1 and exPS2 the total protein loaded was adjusted, for exPS1 transfected lysates 10 μ g total protein was loaded, while for exPS2 transfected lysates 30 μ g of protein was loaded. Myc-PS-NTF levels were quantitated by densitometry analysis and normalised for GAPDH to account for the different amounts of total protein loaded between exPS1 and exPS2 samples (D). NICD was subsequently normalised for Myc-PS-NTF levels to account for variable PS1 and PS2 expression (E). Values shown are mean \pm SD of n = 5 independent experiments. Statistical tests applied were unpaired t- test for (B, E) and ordinary one-way ANOVA with Holm-Šidák's multiple comparison for (D) where ns = P > 0.05, * = P < 0.05, ** = P < 0.01, *** = P < 0.001, **** = P < 0.0001.

2.3.3 PS1/2 fusion standard: A method for absolute quantitation of endogenous PS1 and PS2

Recognising that significantly more PS1 was expressed than PS2 in an exogenous system, we sought to understand whether this PS expression profile (and effects on γ -secretase activity) was an artifact or recapitulated the endogenous expression profile. The ability to quantitatively compare endogenous PS1 (enPS1) and PS2 (enPS2) expression levels remains a challenge, as PS1 and PS2 are detected by different antibodies, with no commercially available antibody able to detect both homologues. To facilitate this, we designed a presenilin fusion standard (PS-Std). The PS-Std incorporates residues from the N-terminal sequence and the cytoplasmic loop of human PS1 and PS2. These regions are hydrophilic, non-transmembrane regions that contain the epitopes for several commercially available antibodies (Figure 2-5A, SI Table 2-1).

PS1 and PS2 antibodies that detect either the N-terminal fragment (NTF) or C-terminal fragment (CTF) were used to probe for the PS-Std via immunoblot (Figure 2-5). All antibodies detected a single band on a tris-tricine gel under denatured conditions across the mass range of PS-Std used. The theoretical size of the PS-Std is 30.7kDa, however, the standard migrates at approximately 37 kDa, likely due to it being relatively acidic (pI=4.15).^{55,56} When probed with unrelated antibodies, anti-GAPDH and anti-GSK3 β , no bands were detected in the PS-std samples (SI Figure 2-5), confirming that the PS-std contains PS epitopes specific to PS1 and PS2 antibodies. Having validated antibody detection of the standard, we set out to quantitate endogenous PS expression levels in the HEK presenilin knockout cell lines generated.

To quantitatively assess expression, varying amounts of the PS-Std underwent SDS-PAGE along with whole cell lysate samples from the cell lines and were subsequently detected via immunoblotting using PS1-NTF, PS1-CTF, PS2-NTF and PS2-CTF antibodies (Figure 2-5B-E). The densitometry results for the PS-Std were used to generate standard curves for each antibody and set of immunoblot replicates. Due to protein size differences between the PS-Std, and the NTF and CTF of PS1 and PS2, we did not simply determine the equivalent mass of standard, but rather, determined the number of PS protein units. This was achieved by calculating the number of PS-Std units of protein per ng of PS-Std (given one PS-Std unit is 5.10×10^{-11} ng) and plotting against the corresponding densitometry values (SI Figure 2-6). The equations from the resultant standard curves were used to convert the densitometry results to the number of PS1 or PS2 protein units. This value was subsequently normalised for total protein loaded on the PAGE, to determine the PS protein units per μg total protein.

Importantly, no significant differences were observed in any of the cell lines between the expression levels of the NTF and CTF proteins for either PS1 or PS2 (Figure 2-5F). This result further supports the use of the PS-Std for quantitation, as γ -secretase is known to contain components in a stoichiometric ratio of 1:1:1:1,⁵⁷ and PS NTF and CTF fragments are tightly regulated at a 1:1 ratio.⁵⁸ We calculated the difference in PS1 and PS2 expression, and determined that in the wild-type (PS1+PS2+ cells), PS1 expression was 5.2-fold higher than PS2 expression, which closely aligns with the exogenous expression profile determined above (see results section *Exogenous PS expression highlights difference in PS levels and subsequently higher PS2 activity*), reflecting that PS expression is tightly regulated at a homologue-specific level.

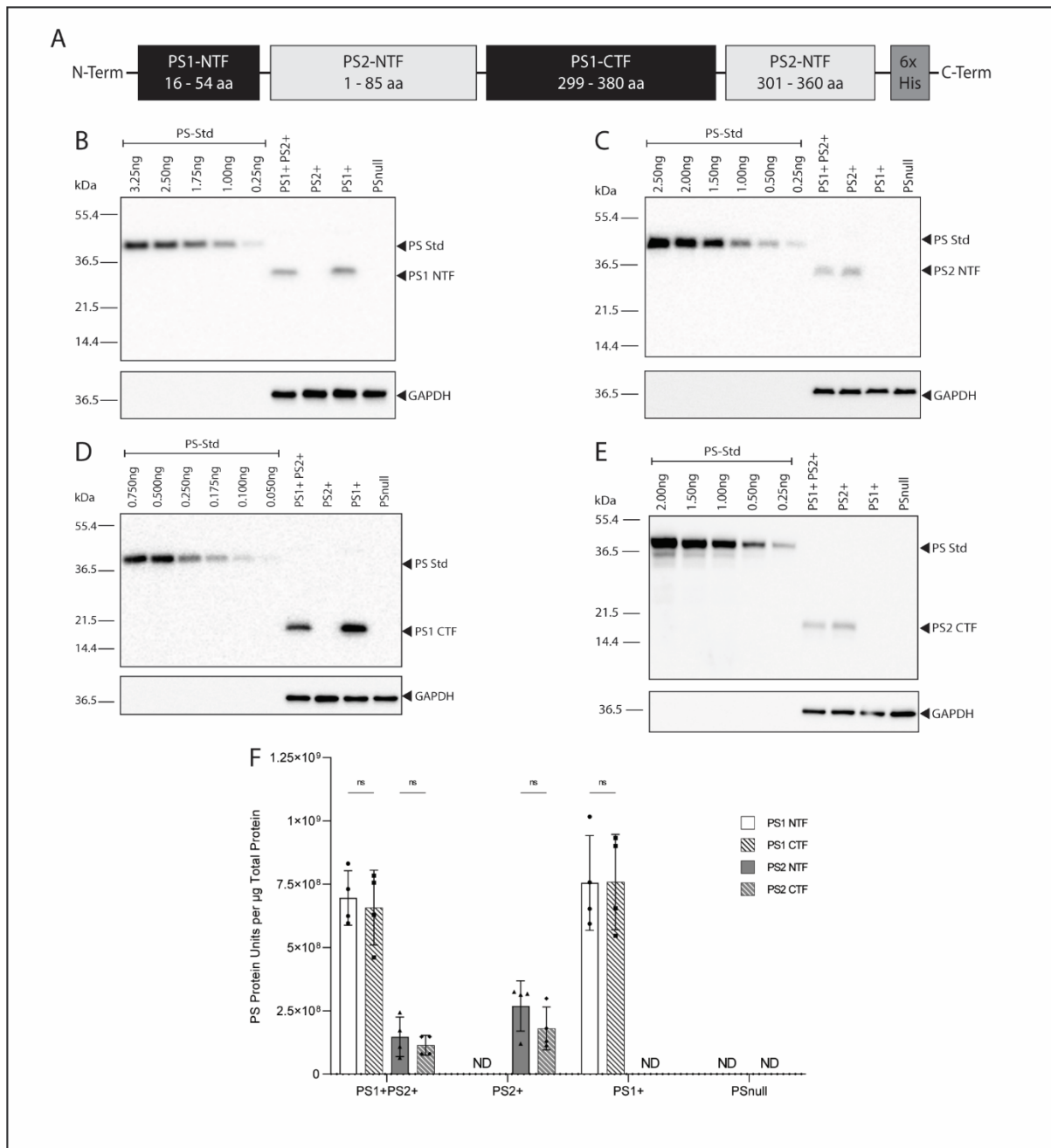


Figure 2-5 Validation of novel method to directly compare endogenous PS1 and PS2 expression.

No commercially available antibody detects both PS1 and PS2. Thus, to enable direct quantitation of endogenous PS1 and PS2 expression, we developed a synthetic PS1/2 fusion protein (PS-Std) containing multiple epitope regions for several commercially available antibodies for use as a standard to enable comparative quantitation. The PS-Std contains protein sequences for the N-terminus and the cytoplasmic loop regions of PS1 and PS2 as shown schematically (A). A range of amounts of the PS-Std were immunoblotted alongside whole cell lysates from the PS1+PS2+, PS1+, PS2+ and PSnull cells to generate a standard curve using the same experimental conditions and probed with antibodies directed against the PS1 NTF (B), PS2 NTF (C), PS1 CTF (D) and PS2 CTF (E). Immunoblot bands underwent densitometry assessment for quantitation and the PS-Std densitometry results were used to generate a standard curve for each replicate set of immunoblots relative to the number of PS-Std protein units $[(\text{ng PS-STD}) \times 90\%] / 5.10 \times 10^{-11}$ (Figure 2-6). The resultant standard curve was used to

calculate the amount of PS protein units detected in the whole cell lysate samples for each cell line (F). Values shown are mean \pm SD of $n = 4$ independent experiments and analysed using two-way ANOVA with Holm-Šidák's multiple comparison, where $ns = P > 0.05$.

2.3.4 Endogenous PS2 demonstrates greater activity in cleaving APP and equivalent activity in cleaving Notch.

Having validated the method for quantitating endogenous PS protein levels, we next sought to investigate γ -secretase substrate processing by endogenous PS1- and PS2- γ -secretase in the HEK presenilin knockout cell lines. hAPP695Swe was transiently transfected into the cell lines, and whole cell lysates were harvested for immunoblotting 24 hrs after transfection; additionally, conditioned media was collected for the determination of A β generation.

APP-FL and APP-CTF levels were detected via immunoblotting and quantitated (Figure 2-6A, B). Levels of overexpressed APP-FL were noticeably variable between the cell lines (particularly in the absence of PS1), despite equal levels of GAPDH loading control. Consequently, APP-CTF accumulation was represented as a ratio of APP-FL, to measure PS-specific γ -secretase activity. In the PSnull cells, considerable APP-CTF accumulated as a result of lack of γ -secretase activity, due to the absence of PS. Comparatively, less than 2% APP-CTF was detected in PS1+PS2+ cells. While the accumulation of APP-CTF protein in both the PS2+ and PS1+ cells was significantly less than the PSnull cells, significantly higher APP-CTF levels were detected in PS2+ cells compared with the PS1+PS2+ cells. Conditioned medium samples collected from hAPP695Swe transfections were analysed via ELISA. A β 40 levels are significantly higher in the PS1+ cells compared to both the PS1+PS2+ and PS2+ cells, whereas both PS1+ and PS2+ cells generate increased A β 42 compared to PS1+PS2+ cells (Figure 2-6C, D). These results are indicative of PS2- γ -secretase preferentially initiating the A β 42 generation pathway, consequently leading to a higher A β 42:A β 40 ratio (Figure 2-6K).

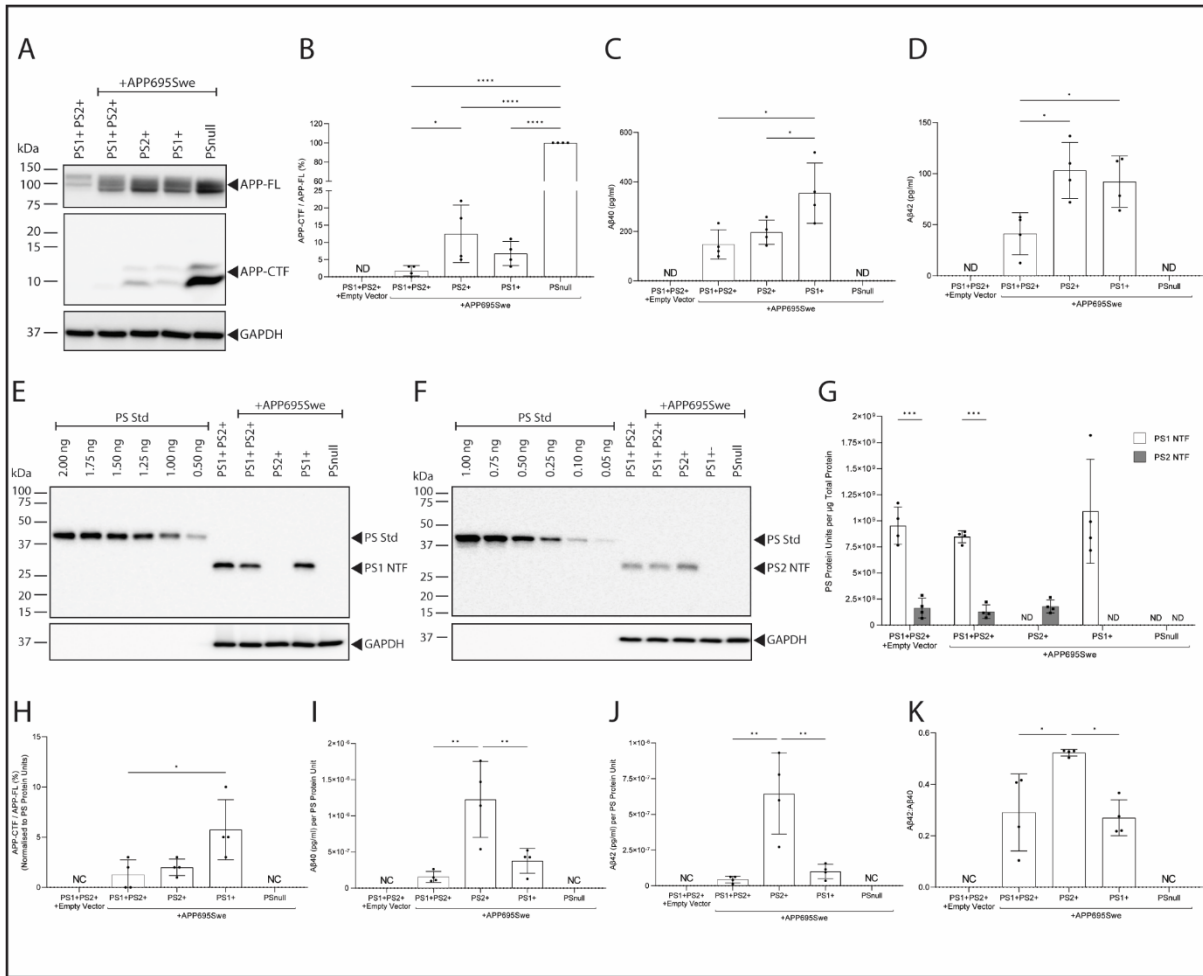


Figure 2-6 APP processing by endogenous PS1 and PS2 assessed in PS1+ and PS2+ cells.

hAPP695Swe was transiently expressed in PS1+PS2+, PS1+, PS2+ and PSnull cells to assess APP processing by endogenous PS1 and PS2 and our novel PS-Std used to quantitatively determine PS1 and PS2 expression to enable the effect of variable expression to be considered. Whole cell lysates were assessed via immunoblot to determine APP-FL and APP-CTF protein levels (A) and the accumulation of APP-CTF/APP-FL quantitatively determined by densitometry assessment and presented relative to PSnull cells (B). Conditioned media was collected concurrently with whole cell lysates for analysis of A β 40 (C) and A β 42 (D) levels (pg/ml) by ELISA. Endogenous PS1 and PS2 expression was determined by immunoblotting using antibodies directed against the PS1 NTF and PS2 NTF (E, F). PS1 NTF and PS2 NTF levels were quantitated by densitometry analysis and the PS protein units determined using standard curves generated alongside the whole cell lysates (G). APP-CTF, A β 40 and A β 42 were subsequently normalised for PS protein units to account for variable PS1 and PS2 expression (H-J). A β 42:A β 40 ratio was calculated (K). Values shown are mean \pm SD of n = 4 independent experiments. Statistical tests applied were ordinary one-way ANOVA with Holm-Šidák's multiple comparison (B-D, H-K) and two-way ANOVA with Holm-Šidák's multiple comparison for (G) where ns = P > 0.05, * = P < 0.05, ** = P < 0.01, *** = P < 0.001, **** = P < 0.0001.

Endogenous PS1 and PS2 levels were detected via immunoblotting and quantitated against the PS-Std to determine PS protein units (Figure 2-6E-G). The expression level of enPS1 was greater than enPS2 in PS1+PS2+ cells (5.9-fold higher). When hAPP695swe was over-expressed in the PS1+PS2+ cells, enPS1 was 6.5-fold higher than enPS2. No significant difference was observed in the level of either enPS1 or enPS2 in the absence of the alternate PS homologue. We next assessed substrate processing at a per PS unit level to allow for a more accurate assessment of γ -secretase activity. Prior to normalisation, it was observed that more APP-CTF accumulated in PS2+ cells, compared to PS1+ cells, which is indicative of less processing (Figure 2-6B). Normalising for PS units reveals that, when the lower levels of PS2 were considered, PS2+ cells show less APP-CTF compared to PS1+ cells, indicative of increased processing (Figure 2-6H). Taken together with the results of A β 40 and A β 42 (Figure 2-6I, J), these findings suggest that PS2 γ -secretase is more active at processing hAPP695swe (Figure 2-6I, J), and is schematically presented in Figure 2-7.

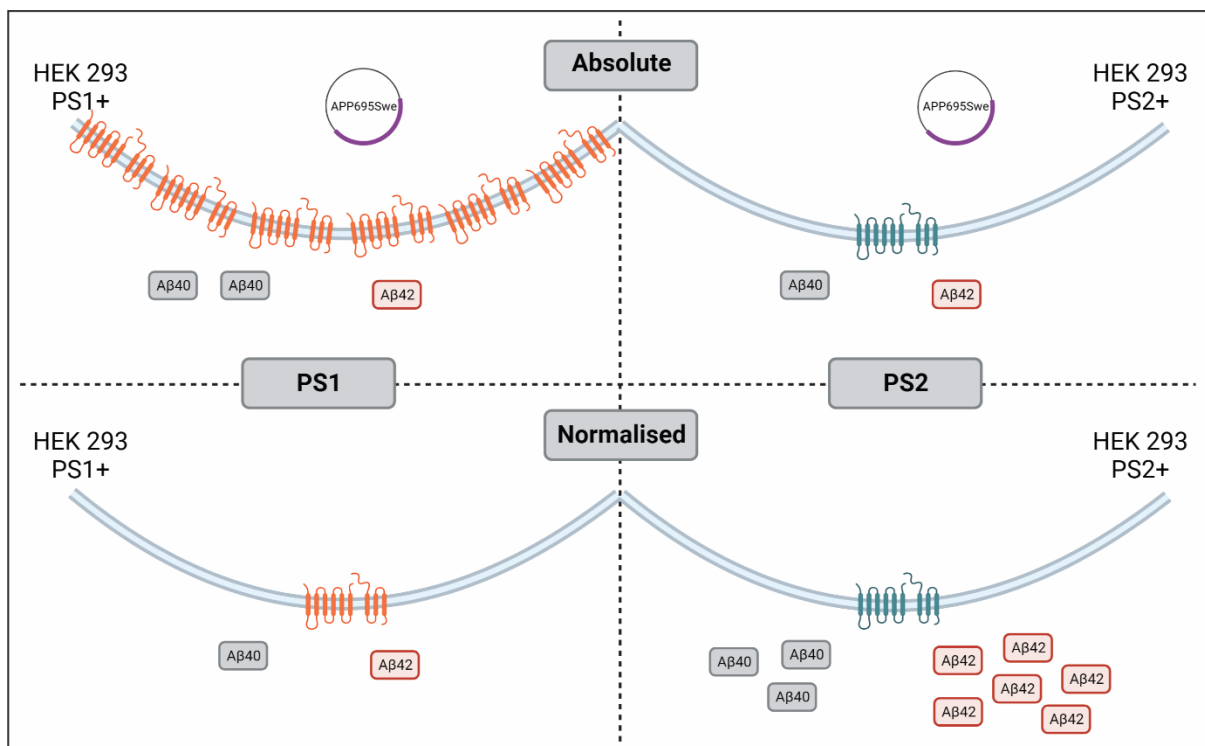


Figure 2-7 Effect of endogenous PS normalisation on A β generation

Absolute levels of endogenous PS1-NTF and PS2-NTF were determined using the PS-Std, enabling direct comparison of enPS1 and enPS2 levels. This facilitated normalisation of the A β 40 and A β 42 levels produced from enPS1- γ -secretase or enPS2- γ -secretase. Consequently, the levels of A β generated by an individual enPS2- γ -secretase enzyme are significantly higher than that generated by an enPS1- γ -secretase enzyme. Notably this result does not align with the exogenous PS system, demonstrating that exPS does not recapitulate the endogenous system. Note A β 40 and A β 42 changes are represented relatively, and are not a direct

comparison, for absolute A β 40 and A β 42 levels refer to Figure 2-6. Created with BioRender.com

Furthermore, endogenous PS processing of Notch1 was investigated by transiently transfecting cell lines with the Δ EhNotch1 vector and collecting whole cell lysates after 24 hrs. NICD levels and Δ EhNotch1 levels were detected via immunoblotting, and the NICD/ Δ EhNotch1 levels determined (Figure 2-8A,B). As expected, no NICD was detected in either the PS1+PS2+ cells transfected with the vector control or in the PSnull cells. Prior to any consideration of PS expression levels, there was no significant difference observed between the levels of NICD generated by PS1+PS2+ and PS1+ cells. The PS2+ cells, however, generated 3.0-fold less NICD than either the PS1+PS2+ or PS1+ cells. On quantitating PS expression levels, significantly higher expression of enPS1 than enPS2 expression (4.8-fold higher enPS1) was observed in PS1+PS2+ cells (Figure 2-8C-E). No significant differences between enPS1 or enPS2 levels were observed in either PS1+ or PS2+ cells, compared with PS1+PS2+ cells. Subsequently, after normalising NICD generation for the PS protein units expressed, no difference was observed between any cell lines (Figure 2-8F).

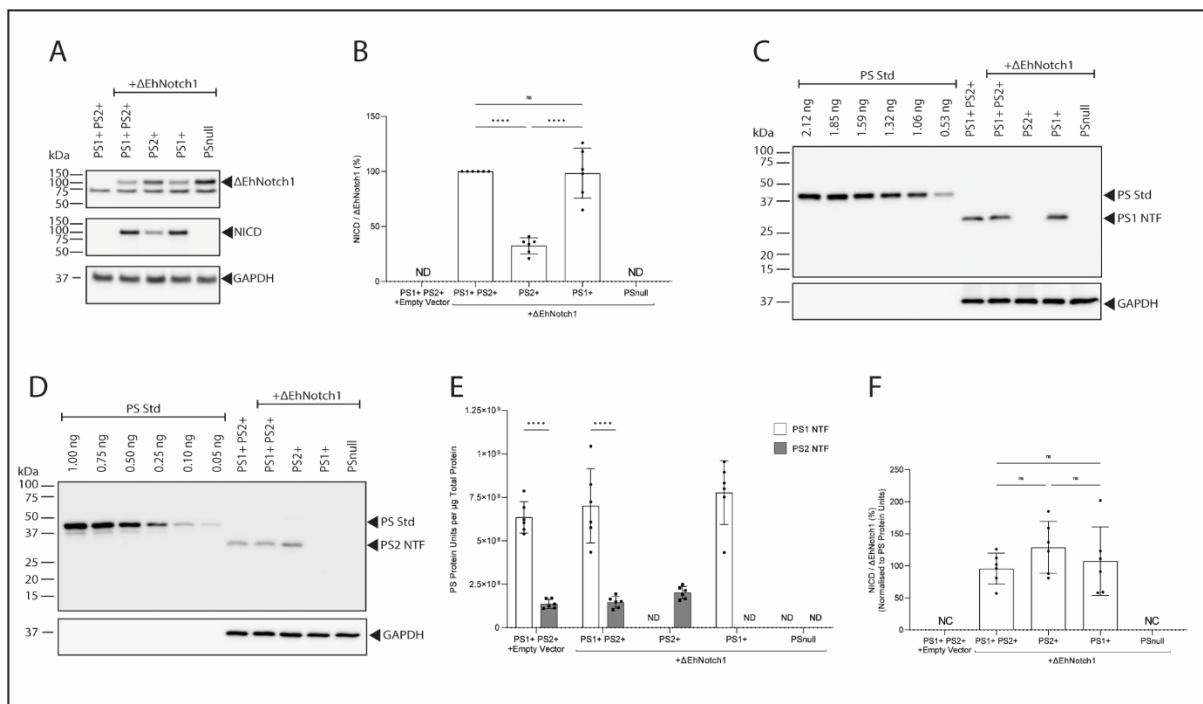


Figure 2-8 Notch1 processing by endogenous PS1 and PS2 assessed in PS1+ and PS2+ cells.

Δ EhNotch1 was transiently expressed in PS1+PS2+, PS1+, PS2+ and PSnull cells to assess Notch1 processing by endogenous PS1 and PS2 and our novel PS-Std used to quantitatively determine PS1 and PS2 expression to enable the effect of variable expression to be considered. Whole cell lysates were assessed via immunoblot to determine Δ EhNotch1 and NICD protein

levels (A) and the generation of NICD/ Δ EhNotch1 quantitatively determined by densitometry assessment and presented relative to PS1+PS2+ cells (B). Endogenous PS1 and PS2 expression was determined by immunoblotting using antibodies directed against the PS1 NTF and PS2 NTF (C, D). PS1 NTF and PS2 NTF levels were quantitated by densitometry analysis and the PS protein units determined using standard curves generated alongside the whole cell lysates (E). NICD was subsequently normalised for PS protein units to account for variable PS1 and PS2 expression (F). Values shown are mean \pm SD of $n = 6$ independent experiments. Statistical tests applied were ordinary one-way ANOVA with Holm-Šidák's multiple comparison (B, F) and two-way ANOVA with Holm-Šidák's multiple comparison for (E) where ns = $P > 0.05$, * = $P < 0.05$, ** = $P < 0.01$, *** = $P < 0.001$, **** = $P < 0.0001$.

2.4 DISCUSSION

The study of the specific contributions of PS1 and PS2 proteins to γ -secretase substrate processing, be it using endogenous PS or exogenous overexpression of PS, typically does not consider PS1 vs. PS2 expression levels. While only a handful of studies have directly compared presenilin expression, showing higher PS1 expression than PS2,^{41,44} there is evidence that PS2 expression increases with age,^{38,40} is associated with ADAD²⁹ and increases in response to mutant PS1 expression,³⁷ suggesting the importance of PS2 in AD pathogenesis. The current study has developed and applied the use of new methods for the direct quantitation of both exogenous and endogenous PS expression. Our findings highlight the importance of considering PS expression when interpreting γ -secretase activity. We show that in HEK-293WT (PS1+PS2+) cells, there is 5.2-times more PS1 than PS2 expression, possibly as a result of the embryonic origin of this cell line.³⁸ Importantly, we identify that this expression profile is retained when exogenous PS1 and PS2 are expressed after PS ablation. Finally, we have demonstrated that when PS expression is considered, PS2- γ -secretase processes at least equal amounts, if not more, APP and Notch1 than PS1- γ -secretase, depending upon the experimental system in use.

Our novel method for quantitating endogenous PS demonstrates that in HEK-293 cells, PS1 expression is significantly higher than PS2. Interestingly, the endogenous PS1:PS2 profile is maintained when PS is exogenously expressed. This contrasts with the generally accepted rationale that ectopic gene expression using a constitutive promoter, such as CMV used in this study, will result in comparable protein levels of homologous proteins in the same cell lines. The differential PS1 and PS2 expression is likely the effect of post-translational protein regulation influenced by PS specific-localisation^{30,31,59} and the requisite involvement of other proteins for stable protein retention, namely Nct, Aph1 and Pen-2.^{1,51-53,60-62} The transfection

of exogenous PS into cells has shown that PS holoprotein is quickly degraded, while the endoproteolysed PS heterodimer fragments, by virtue of being incorporated into γ -secretase, are more stable.⁶³ γ -Secretase incorporation of exogenously expressed PS is limited by the normal cellular regulation of the other complex components, and it appears from our data that the innate cellular regulation of PS1 and PS2 is likely driven by the specific PS homologues. Equal ectopic expression of PS1- and PS2- γ -secretase could presumably be achieved by simultaneous overexpression of all γ -secretase components, such as that employed by Meckler and Checler.³⁰ However, the extent to which PS expression is regulated by subcellular localisation, and organelle compartment size, remains unclear, and may be potentiated by the use of a variety of cell models.

Despite similar PS1:PS2 ratios, we show that there is variation in APP processing between the exogenous (ex) and endogenous (en) PS expression systems, used in this study, prior to normalising for PS expression. A notable example is the difference in APP-CTF levels observed between expression systems (Figure 2-2, Figure 2-6). Similarly, differences in the A β 40 and A β 42 levels generated between exogenous and endogenous systems results in different A β 42:A β 40 ratios between PS1 and PS2. Specifically, we observed that enPS2 generated a higher A β 42:A β 40 ratio, driven by lower A β 40 production, compared with enPS1, while no difference was observed between exogenous PS. Our results for Notch1 processing, however, are recapitulated between the exogenous and endogenous system prior to normalisation of PS expression. There is no consensus in the literature regarding the A β 42:A β 40 ratio^{30-32, 34, 36, 37} or NICD^{21, 31, 34, 64} generation by PS1- vs PS2- γ -secretase, which is likely the result of the variety of expression systems, cell types and activity assays used. However, the differences observed between enPS and exPS processing of APP in this study may be the result of exogenous PS overexpression leading to alterations in the normal subcellular distribution,³¹ causing an increase in cell surface PS2 expression. Interestingly PS1 and PS2 localisation does not affect NICD production but does influence A β generation.³¹ Thus the differences observed in APP processing in this study, may be a function of altered PS localisation, although further experiments are required to confirm this. An additional difference we observed between experimental systems, was that exPS1-NTF levels significantly increase in response to co-expression with either APP or Notch1, while exPS2-NTF levels do not differ. This is not observed in the endogenous PS system, and is further evidence that exogenous PS is not a faithful mimic of endogenous PS. The use of endogenous PS systems reduces the

potential introduction of experimental artifacts and should be the preferred system, particularly given the current availability of CRISPR-Cas9 technology for cell line development.

Similar to other recent studies, we used CRISPR-Cas9 technology to develop HEK-293 cell lines that retain enPS1 or enPS2, allowing us to study PS-specific γ -secretase function. While these recent studies use a variety of cell lines,^{31, 32, 36} the most comparable cell line to those used in this study are the HEK-293T cells developed by Lessard et al.³⁴ These authors present both intracellular and extracellular levels of total A β , A β 40 and A β 42 using the HEK-293T cell line, and show that PS2-expressing cells generate significantly more intracellular total A β , A β 40 and A β 42.³⁴ While we successfully measured extracellular A β , several attempts to detect intracellular A β were unsuccessful. We found that the amount of exogenous hAPP695Swe required for detection of intracellular A β by the ELISA assay used caused considerable cell death in the enPS1+ cells (SI Figure 2-7). This may be due to the use of the HEK-293 cell line in this study rather than HEK-293T used by Lessard et al. While we similarly show no significant difference in the absolute amount of secreted A β 40 and A β 42 between the PS1+ and PS2+ cell lines, we did show a significant increase in the A β 42:A β 40 ratio associated with enPS2 expression, due to accompanying reduction in A β 40 generation. These findings are consistent with results reported in murine N2a cells lacking PS1³⁶ and iPSC cells, where PS1 and/or PS2 were conditionally knocked out and differentiated into neurons.³² Watanabe et al.³² further showed that during extended neuronal maturation of iPSCs, there is a concomitant decrease in PS1 expression and increase in PS2 expression. Combined with our findings, these studies highlight the importance of PS2 in AD pathogenesis and the need to directly compare PS1 and PS2 expression to enable appropriate interpretation of PS-specific γ -secretase contributions across multiple experimental systems.

There have only been a handful of studies that consider PS expression, or mature Nct as a measure of γ -secretase expression. Yonemura and colleagues⁴¹ used Myc-tagged exogenous PS in a yeast system, and demonstrated that PS1-NTF levels are approximately 28-times higher than PS2, concluding that, after normalising for expression, there was no difference in overall activity. Lai et al.⁴⁴ used radioactive labelling to determine PS1- and PS2-specific antibody sensitivity in order to calculate endogenous PS expression levels; in doing so, they identified that PS1 expression is approximately 1.4-times higher than PS2 in a murine blastocyte model. While Lai et al. ultimately concluded that PS1 generates more A β than PS2, they interestingly observed that while PS1 is similarly active in both membrane-enriched cell-free γ -secretase

assays and in-cell assays, PS2 is significantly less active in the membrane-based assay compared with the in-cell assay – an additional confounding feature to consider when interpreting the many γ -secretase activity studies. The use of mature Nct as a measure of active γ -secretase has also been used to normalise for activity between PS1 and PS2.^{42, 43} These studies conclude that PS1- γ -secretase generates more A β ,^{42, 43} and similar levels of AICD and NICD;⁴² however, the use of cell-free membrane-based assays,⁴³ and poor evidence of Nct maturation,⁴² potentially confound interpretation. To our knowledge, our findings provide the first reported absolute quantitative measure of endogenous presenilin expression and demonstrate that PS2- γ -secretase processes equal amounts of Notch1 and more APP, compared to PS1- γ -secretase, when considered at an enzymatic unit level.

It should be acknowledged that our findings in HEK-293 cells cannot be generalised to other cell types, which may show different presenilin expression profiles related to their developmental origin and function. Additionally, it must be noted that substrate-specific localisation will likely affect the accessibility of PS1- and PS2- γ -secretase to certain substrate pools, influencing overall substrate processing capability.^{31, 32} Nonetheless, we have developed useful tools that allow us to address this in future studies. Another potential limitation of this study is the use of incorporated PS expression as a measure of γ -secretase levels, which does not consider evidence suggesting that there is a pool of in-active γ -secretase. This evidence is from pulldown studies using modified γ -secretase inhibitors to capture ‘active’ γ -secretase complexes.^{37, 65, 66} The L685,458 inhibitor used as the basis for these studies does not, however, have equal affinity for PS1 and PS2.^{13, 15} Additionally, these experiments were performed using membrane extractions, which reduce PS2 - but not PS1 activity,⁴⁴ potentially resulting in biased capture of PS1-complexes. Future experiments should consider the use of the BMS708163-derived γ -secretase capture tools,^{67, 68} which has comparable affinity for both PS1 and PS2.⁶ Additionally, these experiments should be developed in cell-based systems for accurate reflection of the active γ -secretase pool and can be used in conjunction with the PS quantitation method developed in this study for a more robust understanding of PS1 and PS2 specific γ -secretase expression and activity.

With the recognition that both PS1 and PS2 expression are important in the context of AD pathogenesis,^{29, 39} that PS1 and PS2 are differentially expressed throughout development,^{38, 40} and varies between cell types,^{31, 41, 44} the field must look to methods that enable direct comparison of PS1 and PS2 expression when interpreting data. We acknowledge investigating

individual endogenous PS in the absence of the homologous counterpart is not reflective of the physiological environment, and may belie the realities of the dynamic interplay between PS1 and PS2 for the other components of γ -secretase.^{37,69,70} However, we believe that coupling the use of an endogenous PS model, with a method to quantitate PS expression, presents a suitably representative experimental system to assess γ -secretase activity and the specific contributions of PS1 and PS2. To achieve this, we have developed and validated a PS1/2 fusion standard that, when used in conjunction with appropriate standard curves, calculates the number of PS protein units. This represents a novel approach to the absolute quantitation of presenilin levels in a cellular system that can be extended to tissues. Furthermore, we have demonstrated that endogenous PS expression is recapitulated in an exogenous expression system. While the resultant substrate processing is not in complete agreement, we have shown that PS2- γ -secretase is at least as active, if not more, than PS1- γ -secretase at processing both APP and Notch substrates.

There is a growing body of evidence that suggests that PS2 has greater implications for A β -related pathogenesis in AD than previously considered. In particular PS2- γ -secretase generates higher A β 42:A β 40 ratios shown in this study and others,^{32,36,37} and more intracellular A β .^{31,34} Furthermore PS2 expression increases with neuronal maturation,^{32,71} age,^{38,40} in response to PS1 mutations,³⁷ and a rare autosomal dominant AD mutation.^{28,29} We have presented tools here that enable accurate, direct comparison between PS1 and PS2 expression, and demonstrate how these can be used to improve our understanding and interpretation of the effect of PS expression on γ -secretase activity.

2.5 REFERENCES

1. Kimberly, W. T., LaVoie, M. J., Ostaszewski, B. L., Ye, W., Wolfe, M. S., and Selkoe, D. J. (2003) γ -Secretase is a membrane protein complex comprised of presenilin, nicastrin, aph-1, and pen-2. *Proceedings of the National Academy of Sciences of the United States of America* **100**, 6382-6387
2. Güner, G., and Lichtenthaler, S. F. (2020) The substrate repertoire of γ -secretase/presenilin. *Seminars in cell & developmental biology* **105**, 27-42
3. Kimberly, W. T., Xia, W., Rahmati, T., Wolfe, M. S., and Selkoe, D. J. (2000) The transmembrane aspartates in presenilin 1 and 2 are obligatory for γ -secretase activity and amyloid β -protein generation. *The Journal of biological chemistry* **275**, 3173-3178
4. De Strooper, B., Annaert, W., Cupers, P., Saftig, P., Craessaerts, K., Mumm, J. S., Schroeter, E. H., Schrijvers, V., Wolfe, M. S., Ray, W. J., Goate, A., and Kopan, R. (1999) A presenilin-1-dependent [γ]-secretase-like protease mediates release of Notch intracellular domain. *Nature* **398**, 518-522

5. DeTure, M. A., and Dickson, D. W. (2019) The neuropathological diagnosis of Alzheimer's disease. *Molecular neurodegeneration* **14**, 32
6. Borgegård, T., Gustavsson, S., Nilsson, C., Parpal, S., Klintonberg, R., Berg, A.-L., Rosqvist, S., Serneels, L., Svensson, S., Olsson, F., Jin, S., Yan, H., Wanngren, J., Jureus, A., Ridderstad-Wollberg, A., Wollberg, P., Stockling, K., Karlström, H., Malmberg, Å., Lund, J., Arvidsson, P. I., De Strooper, B., Lendahl, U., and Lundkvist, J. (2012) Alzheimer's disease: Presenilin-2 sparing γ -secretase inhibition is a tolerable A β peptide-lowering strategy. *The Journal of Neuroscience* **32**, 17297-17305
7. Doody, R. S., Raman, R., Farlow, M., Iwatsubo, T., Vellas, B., Joffe, S., Kieburtz, K., He, F., Sun, X., Thomas, R. G., Aisen, P. S., Siemers, E., Sethuraman, G., and Mohs, R. (2013) A phase 3 trial of semagacestat for treatment of Alzheimer's disease. *New England Journal of Medicine* **369**, 341-350
8. Gillman, K. W., Starrett, J. E., Parker, M. F., Xie, K., Bronson, J. J., Marcin, L. R., McElhone, K. E., Bergstrom, C. P., Mate, R. A., Williams, R., Meredith, J. E., Burton, C. R., Barten, D. M., Toyn, J. H., Roberts, S. B., Lentz, K. A., Houston, J. G., Zaczek, R., Albright, C. F., Decicco, C. P., Macor, J. E., and Olson, R. E. (2010) Discovery and evaluation of BMS-708163, a potent, selective and orally bioavailable γ -secretase inhibitor. *ACS Medicinal Chemistry Letters* **1**, 120-124
9. Golde, T. E., Koo, E. H., Felsenstein, K. M., Osborne, B. A., and Miele, L. (2013) γ -Secretase inhibitors and modulators. *Biochimica et Biophysica Acta (BBA) - Biomembranes* **1828**, 2898-2907
10. Shearman, M. S., Beher, D., Clarke, E. E., Lewis, H. D., Harrison, T., Hunt, P., Nadin, A., Smith, A. L., Stevenson, G., and Castro, J. L. (2000) L-685,458, an aspartyl protease transition state mimic, is a potent inhibitor of amyloid beta-protein precursor gamma-secretase activity. *Biochemistry* **39**, 8698-8704
11. Coric, V., van Dyck, C. H., Salloway, S., and et al. (2012) Safety and tolerability of the γ -secretase inhibitor avagacestat in a phase 2 study of mild to moderate Alzheimer disease. *Archives of Neurology* **69**, 1430-1440
12. Yang, Z. Y., Li, J. M., Xiao, L., Mou, L., Cai, Y., Huang, H., Luo, X. G., and Yan, X. X. (2014) [(3) H]-L685,458 binding sites are abundant in multiple peripheral organs in rats: implications for safety assessment of putative γ -secretase targeting drugs. *Basic & Clinical Pharmacology & Toxicology* **115**, 518-526
13. Ebke, A., Luebbers, T., Fukumori, A., Shirotani, K., Haass, C., Baumann, K., and Steiner, H. (2011) Novel γ -secretase enzyme modulators directly target presenilin protein. *The Journal of biological chemistry* **286**, 37181-37186
14. Guo, X., Wang, Y., Zhou, J., Jin, C., Wang, J., Jia, B., Jing, D., Yan, C., Lei, J., Zhou, R., and Shi, Y. (2022) Molecular basis for isoform-selective inhibition of presenilin-1 by MRK-560. *Nature Communications* **13**, 6299
15. Lee, J., Song, L., Terracina, G., Bara, T., Josien, H., Asberom, T., Sasikumar, T. K., Burnett, D. A., Clader, J., Parker, E. M., and Zhang, L. (2011) Identification of presenilin 1-selective γ -secretase inhibitors with reconstituted γ -secretase complexes. *Biochemistry* **50**, 4973-4980
16. Bursavich, M. G., Harrison, B. A., and Blain, J.-F. (2016) Gamma secretase modulators: New Alzheimer's drugs on the horizon? *Journal of Medicinal Chemistry* **59**, 7389-7409
17. Kounnas, M. Z., Lane-Donovan, C., Nowakowski, D. W., Herz, J., and Comer, W. T. (2017) NGP 555, a γ -secretase modulator, lowers the amyloid biomarker, A β 42, in cerebrospinal fluid while preventing Alzheimer's disease cognitive decline in rodents. *Alzheimer's & Dementia: Translational Research & Clinical Interventions* **3**, 65-73

18. Oehlrich, D., Berthelot, D. J., and Gijssen, H. J. (2011) γ -Secretase modulators as potential disease modifying anti-Alzheimer's drugs. *Journal of Medicinal Chemistry* **54**, 669-698
19. Buxbaum, J. D., Liu, K. N., Luo, Y., Slack, J. L., Stocking, K. L., Peschon, J. J., Johnson, R. S., Castner, B. J., Cerretti, D. P., and Black, R. A. (1998) Evidence that tumor necrosis factor alpha converting enzyme is involved in regulated alpha-secretase cleavage of the Alzheimer amyloid protein precursor. *The Journal of biological chemistry* **273**, 27765-27767
20. Mumm, J. S., Schroeter, E. H., Saxena, M. T., Griesemer, A., Tian, X., Pan, D. J., Ray, W. J., and Kopan, R. (2000) A ligand-induced extracellular cleavage regulates γ -secretase-like proteolytic activation of notch1. *Molecular Cell* **5**, 197-206
21. Zhang, Z., Nadeau, P., Song, W., Donoviel, D., Yuan, M., Bernstein, A., and Yankner, B. A. (2000) Presenilins are required for [gamma]-secretase cleavage of [beta]-APP and transmembrane cleavage of Notch-1. *Nature cell biology* **2**, 463-465
22. Lammich, S., Kojro, E., Postina, R., Gilbert, S., Pfeiffer, R., Jasionowski, M., Haass, C., and Fahrenholz, F. (1999) Constitutive and regulated alpha-secretase cleavage of Alzheimer's amyloid precursor protein by a disintegrin metalloprotease. *Proceedings of the National Academy of Sciences of the United States of America* **96**, 3922-3927
23. Vassar, R., Bennett, B. D., Babu-Khan, S., Kahn, S., Mendiaz, E. A., Denis, P., Teplow, D. B., Ross, S., Amarante, P., Loeloff, R., Luo, Y., Fisher, S., Fuller, J., Edenson, S., Lile, J., Jarosinski, M. A., Biere, A. L., Curran, E., Burgess, T., Louis, J.-C., Collins, F., Treanor, J., Rogers, G., and Citron, M. (1999) β -Secretase Cleavage of Alzheimer's Amyloid Precursor Protein by the Transmembrane Aspartic Protease BACE. *Science (New York, N.Y.)* **286**, 735-741
24. Matsumura, N., Takami, M., Okochi, M., Wada-Kakuda, S., Fujiwara, H., Tagami, S., Funamoto, S., Ihara, Y., and Morishima-Kawashima, M. (2014) γ -Secretase associated with lipid rafts: multiple interactive pathways in the stepwise processing of β -carboxyl-terminal fragment. *The Journal of biological chemistry* **289**, 5109-5121
25. Takami, M., Nagashima, Y., Sano, Y., Ishihara, S., Morishima-Kawashima, M., Funamoto, S., and Ihara, Y. (2009) γ -Secretase: Successive tripeptide and tetrapeptide release from the transmembrane domain of β -carboxyl terminal fragment. *The Journal of Neuroscience* **29**, 13042-13052
26. Alzforum. Mutation Database. In *Alzforum* Vol. 2018, Alzforum, Cambridge (USA)
27. Ryman, D. C., Acosta-Baena, N., Aisen, P. S., Bird, T., Danek, A., Fox, N. C., Goate, A., Frommelt, P., Ghetti, B., Langbaum, J. B. S., Lopera, F., Martins, R., Masters, C. L., Mayeux, R. P., McDade, E., Moreno, S., Reiman, E. M., Ringman, J. M., Salloway, S., Schofield, P. R., Sperling, R., Tariot, P. N., Xiong, C., Morris, J. C., Bateman, R. J., and And the Dominantly Inherited Alzheimer, N. (2014) Symptom onset in autosomal dominant Alzheimer disease: A systematic review and meta-analysis. *Neurology* **83**, 253-260
28. Jia, L., Fu, Y., Shen, L., Zhang, H., Zhu, M., Qiu, Q., Wang, Q., Yan, X., Kong, C., Hao, J., Wei, C., Tang, Y., Qin, W., Li, Y., Wang, F., Guo, D., Zhou, A., Zuo, X., Yu, Y., Li, D., Zhao, L., Jin, H., and Jia, J. (2020) PSEN1, PSEN2, and APP mutations in 404 Chinese pedigrees with familial Alzheimer's disease. *Alzheimer's & Dementia* **16**, 178-191
29. Pang, Y., Li, T., Wang, Q., Qin, W., Li, Y., Wei, Y., and Jia, L. (2021) A rare variation in the 3' untranslated region of the presenilin 2 gene is linked to Alzheimer's disease. *Molecular Neurobiology* **58**, 4337-4347
30. Meckler, X., and Checler, F. (2016) Presenilin 1 and presenilin 2 target γ -secretase complexes to distinct cellular compartments. *The Journal of biological chemistry* **291**, 12821-12837

31. Sannerud, R., Esselens, C., Ejsmont, P., Mattera, R., Rochin, L., Tharkeshwar, Arun K., De Baets, G., De Wever, V., Habets, R., Baert, V., Vermeire, W., Michiels, C., Groot, Arjan J., Wouters, R., Dillen, K., Vints, K., Baatsen, P., Munck, S., Derua, R., Waelkens, E., Basi, Guriqbal S., Mercken, M., Vooijs, M., Bollen, M., Schymkowitz, J., Rousseau, F., Bonifacino, Juan S., Van Niel, G., De Strooper, B., and Annaert, W. (2016) Restricted location of PSEN2/ γ -secretase determines substrate specificity and generates an intracellular A β pool. *Cell* **166**, 193-208
32. Watanabe, H., Imaizumi, K., Cai, T., Zhou, Z., Tomita, T., and Okano, H. (2021) Flexible and accurate substrate processing with distinct presenilin/ γ -secretases in human cortical neurons. *eNeuro* **8**, ENEURO.0500-0520.2021
33. Zhu, L., Su, M., Lucast, L., Liu, L., Netzer, W. J., Gandy, S. E., and Cai, D. (2012) Dynamin 1 regulates amyloid generation through modulation of BACE-1. *PLoS one* **7**, e45033
34. Lessard, C. B., Rodriguez, E., Ladd, T. B., Minter, L. M., Osborne, B. A., Miele, L., Golde, T. E., and Ran, Y. (2019) Individual and combined presenilin 1 and 2 knockouts reveal that both have highly overlapping functions in HEK293T cells. *The Journal of biological chemistry* **294**, 11276-11285
35. Acx, H., Chávez-Gutiérrez, L., Serneels, L., Lismont, S., Benurwar, M., Elad, N., and De Strooper, B. (2014) Signature amyloid β profiles are produced by different γ -secretase complexes. *The Journal of biological chemistry* **289**, 4346-4355
36. Pimenova, A. A., and Goate, A. M. (2020) Novel presenilin 1 and 2 double knock-out cell line for in vitro validation of PSEN1 and PSEN2 mutations. *Neurobiology of disease*, 104785
37. Placanica, L., Tarassishin, L., Yang, G., Peethumnongsin, E., Kim, S.-H., Zheng, H., Sisodia, S. S., and Li, Y.-M. (2009) Pen2 and presenilin-1 modulate the dynamic equilibrium of presenilin-1 and presenilin-2 γ -secretase complexes. *The Journal of biological chemistry* **284**, 2967-2977
38. Lee, M. K., Slunt, H. H., Martin, L. J., Thinakaran, G., Kim, G., Gandy, S. E., Seeger, M., Koo, E., Price, D. L., and Sisodia, S. S. (1996) Expression of presenilin 1 and 2 (PS1 and PS2) in human and murine tissues. *The Journal of Neuroscience* **16**, 7513-7525
39. Davidsson, P., Bogdanovic, N., Lannfelt, L., and Blennow, K. (2001) Reduced expression of amyloid precursor protein, presenilin-1 and rab3a in cortical brain regions in Alzheimer's disease. *Dementia and Geriatric Cognitive Disorders* **12**, 243-250
40. Thakur, M. K., and Ghosh, S. (2007) Age and sex dependent alteration in presenilin expression in mouse cerebral cortex. *Cellular and molecular neurobiology* **27**, 1059-1067
41. Yonemura, Y., Futai, E., Yagishita, S., Suo, S., Tomita, T., Iwatsubo, T., and Ishiura, S. (2011) Comparison of presenilin 1 and presenilin 2 γ -secretase activities using a yeast reconstitution system. *The Journal of biological chemistry* **286**, 44569-44575
42. Pintchovski, S. A., Schenk, D. B., and Basi, G. S. (2013) Evidence that enzyme processivity mediates differential A β production by PS1 and PS2. *Current Alzheimer research* **10**, 4-10
43. Shirovani, K., Tomioka, M., Kremmer, E., Haass, C., and Steiner, H. (2007) Pathological activity of familial Alzheimer's disease-associated mutant presenilin can be executed by six different γ -secretase complexes. *Neurobiology of disease* **27**, 102-107
44. Lai, M.-T., Chen, E., Crouthamel, M.-C., DiMuzio-Mower, J., Xu, M., Huang, Q., Price, E., Register, R. B., Shi, X.-P., Donoviel, D. B., Bernstein, A., Hazuda, D., Gardell, S. J., and Li, Y.-M. (2003) Presenilin-1 and presenilin-2 exhibit distinct yet overlapping γ -secretase activities. *The Journal of biological chemistry* **278**, 22475-22481
45. Ran, F. A., Hsu, P. D., Wright, J., Agarwala, V., Scott, D. A., and Zhang, F. (2013) Genome engineering using the CRISPR-Cas9 system. *Nature Protocols* **8**, 2281

46. Robinson, J. T., Thorvaldsdóttir, H., Winckler, W., Guttman, M., Lander, E. S., Getz, G., and Mesirov, J. P. (2011) Integrative genomics viewer. *Nature Biotechnology* **29**, 24-26
47. Ye, J., Coulouris, G., Zaretskaya, I., Cutcutache, I., Rozen, S., and Madden, T. L. (2012) Primer-BLAST: a tool to design target-specific primers for polymerase chain reaction. *BMC bioinformatics* **13**, 134
48. Koch, P., Tamboli, I. Y., Mertens, J., Wunderlich, P., Ladewig, J., Stüber, K., Esselmann, H., Wiltfang, J., Brüstle, O., and Walter, J. (2012) Presenilin-1 L166P mutant human pluripotent stem cell-derived neurons exhibit partial loss of γ -secretase activity in endogenous amyloid- β generation. *The American journal of pathology* **180**, 2404-2416
49. Pfaffl, M. W. (2001) A new mathematical model for relative quantification in real-time RT-PCR. *Nucleic Acids Res* **29**, e45-e45
50. Lin, Y.-C., Boone, M., Meuris, L., Lemmens, I., Van Roy, N., Soete, A., Reumers, J., Moisse, M., Plaisance, S., Drmanac, R., Chen, J., Speleman, F., Lambrechts, D., Van de Peer, Y., Tavernier, J., and Callewaert, N. (2014) Genome dynamics of the human embryonic kidney 293 lineage in response to cell biology manipulations. *Nature Communications* **5**, 4767
51. Luo, W. J., Wang, H., Li, H., Kim, B. S., Shah, S., Lee, H. J., Thinakaran, G., Kim, T. W., Yu, G., and Xu, H. (2003) PEN-2 and APH-1 coordinately regulate proteolytic processing of presenilin 1. *The Journal of biological chemistry* **278**, 7850-7854
52. Steiner, H., Winkler, E., Edbauer, D., Prokop, S., Basset, G., Yamasaki, A., Kostka, M., and Haass, C. (2002) PEN-2 is an integral component of the γ -secretase complex required for coordinated expression of presenilin and nicastrin. *The Journal of biological chemistry* **277**, 39062-39065
53. Yang, D.-S., Tandon, A., Chen, F., Yu, G., Yu, H., Arawaka, S., Hasegawa, H., Duthie, M., Schmidt, S. D., Ramabhadran, T. V., Nixon, R. A., Mathews, P. M., Gandy, S. E., Mount, H. T. J., St George-Hyslop, P., and Fraser, P. E. (2002) Mature glycosylation and trafficking of nicastrin modulate its binding to presenilins. *The Journal of biological chemistry* **277**, 28135-28142
54. Bai, X.-c., Yan, C., Yang, G., Lu, P., Ma, D., Sun, L., Zhou, R., Scheres, S. H. W., and Shi, Y. (2015) An atomic structure of human γ -secretase. *Nature* **525**, 212-217
55. Guan, Y., Zhu, Q., Huang, D., Zhao, S., Jan Lo, L., and Peng, J. (2015) An equation to estimate the difference between theoretically predicted and SDS PAGE-displayed molecular weights for an acidic peptide. *Scientific Reports* **5**, 13370
56. Tiwari, P., Kaila, P., and Guptasarma, P. (2019) Understanding anomalous mobility of proteins on SDS-PAGE with special reference to the highly acidic extracellular domains of human E- and N-cadherins. *Electrophoresis* **40**, 1273-1281
57. Sato, T., Diehl, T. S., Narayanan, S., Funamoto, S., Ihara, Y., De Strooper, B., Steiner, H., Haass, C., and Wolfe, M. S. (2007) Active γ -secretase complexes contain only one of each component. *The Journal of biological chemistry* **282**, 33985-33993
58. Thinakaran, G., Borchelt, D. R., Lee, M. K., Slunt, H. H., Spitzer, L., Kim, G., Ratovitsky, T., Davenport, F., Nordstedt, C., Seeger, M., Hardy, J., Levey, A. I., Gandy, S. E., Jenkins, N. A., Copeland, N. G., Price, D. L., and Sisodia, S. S. (1996) Endoproteolysis of presenilin 1 and accumulation of processed derivatives in vivo. *Neuron* **17**, 181-190
59. Yousefi, R., Jevdokimenko, K., Kluever, V., Pacheu-Grau, D., and Fornasiero, E. F. (2021) Influence of subcellular localization and functional state on protein turnover. *Cells* **10**
60. Edbauer, D., Winkler, E., Haass, C., and Steiner, H. (2002) Presenilin and nicastrin regulate each other and determine amyloid β -peptide production via complex formation. *Proceedings of the National Academy of Sciences of the United States of America* **99**, 8666-8671

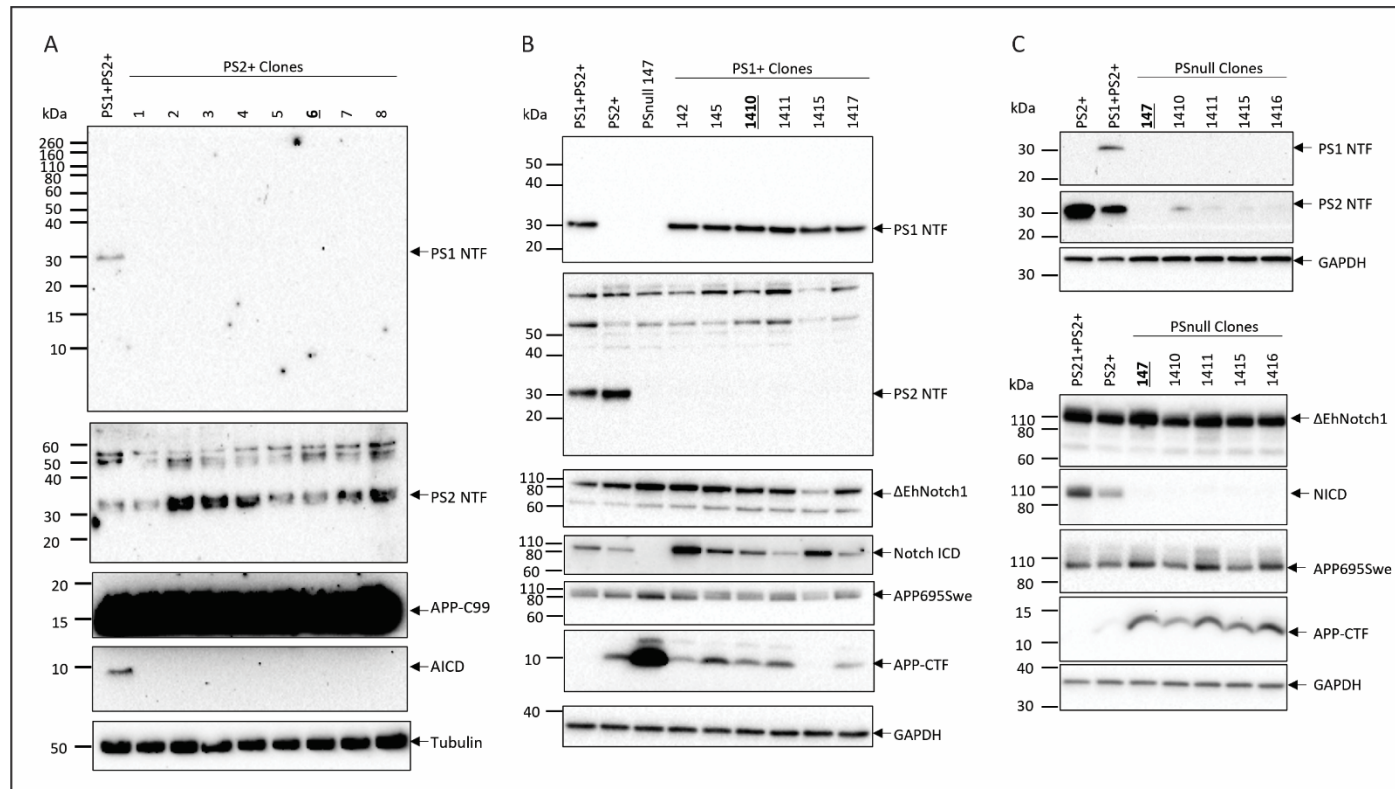
61. Fraser, P. E., Levesque, G., Yu, G., Mills, L. R., Thirlwell, J., Frantseva, M., Gandy, S. E., Seeger, M., Carlen, P. L., and St George-Hyslop, P. (1998) Presenilin 1 is actively degraded by the 26S proteasome. *Neurobiology of aging* **19**, S19-S21
62. Thinakaran, G., Harris, C. L., Ratovitski, T., Davenport, F., Slunt, H. H., Price, D. L., Borchelt, D. R., and Sisodia, S. S. (1997) Evidence that levels of presenilins (PS1 and PS2) are coordinately regulated by competition for limiting cellular factors. *The Journal of biological chemistry* **272**, 28415-28422
63. Zhang, Z., Hartmann, H., Do, V. M., Abramowski, D., Sturchler-Pierrat, C., Staufenbiel, M., Sommer, B., van de Wetering, M., Clevers, H., Saftig, P., De Strooper, B., He, X., and Yankner, B. A. (1998) Destabilization of beta-catenin by mutations in presenilin-1 potentiates neuronal apoptosis. *Nature* **395**, 698-702
64. Yonemura, Y., Futai, E., Yagishita, S., Kaether, C., and Ishiura, S. (2016) Specific combinations of presenilins and Aph1s affect the substrate specificity and activity of γ -secretase. *Biochemical and biophysical research communications* **478**, 1751-1757
65. Frånberg, J., Svensson, A. I., Winblad, B., Karlström, H., and Frykman, S. (2011) Minor contribution of presenilin 2 for γ -secretase activity in mouse embryonic fibroblasts and adult mouse brain. *Biochemical and biophysical research communications* **404**, 564-568
66. Teranishi, Y., Hur, J.-Y., Welander, H., Frånberg, J., Aoki, M., Winblad, B., Frykman, S., and Tjernberg, L. O. (2010) Affinity pulldown of γ -secretase and associated proteins from human and rat brain. *Journal of cellular and molecular medicine* **14**, 2675-2686
67. Crump, C. J., Murrey, H. E., Ballard, T. E., Am Ende, C. W., Wu, X., Gertsik, N., Johnson, D. S., and Li, Y. M. (2016) Development of sulfonamide photoaffinity inhibitors for probing cellular γ -secretase. *ACS Chemical Neuroscience* **7**, 1166-1173
68. Gertsik, N., am Ende, C. W., Geoghegan, K. F., Nguyen, C., Mukherjee, P., Mente, S., Seneviratne, U., Johnson, D. S., and Li, Y.-M. (2017) Mapping the binding site of BMS-708163 on γ -secretase with cleavable photoprobes. *Cell Chemical Biology* **24**, 3-8
69. Chen, F., Tandon, A., Sanjo, N., Gu, Y.-J., Hasegawa, H., Arawaka, S., Lee, F. J. S., Ruan, X., Mastrangelo, P., Erdebil, S., Wang, L., Westaway, D., Mount, H. T. J., Yankner, B., Fraser, P. E., and George-Hyslop, P. S. (2003) Presenilin 1 and presenilin 2 have differential effects on the stability and maturation of nicastrin in mammalian brain. *The Journal of biological chemistry* **278**, 19974-19979
70. Pardossi-Piquard, R., Yang, S. P., Kanemoto, S., Gu, Y., Chen, F., Böhm, C., Sevalle, J., Li, T., Wong, P. C., Checler, F., Schmitt-Ulms, G., St. George-Hyslop, P., and Fraser, P. E. (2009) APH1 polar transmembrane residues regulate the assembly and activity of presenilin complexes. *The Journal of biological chemistry* **284**, 16298-16307
71. Culvenor, J. G., Evin, G., Cooney, M. A., Wardan, H., Sharples, R. A., Maher, F., Reed, G., Diehlmann, A., Weidemann, A., Beyreuther, K., and Masters, C. L. (2000) Presenilin 2 expression in neuronal cells: induction during differentiation of embryonic carcinoma cells. *Experimental cell research* **255**, 192-206

2.6 SUPPLEMENTAL TABLES

SI Table 2-1 List of commercial antibodies for potential use with PS-Std

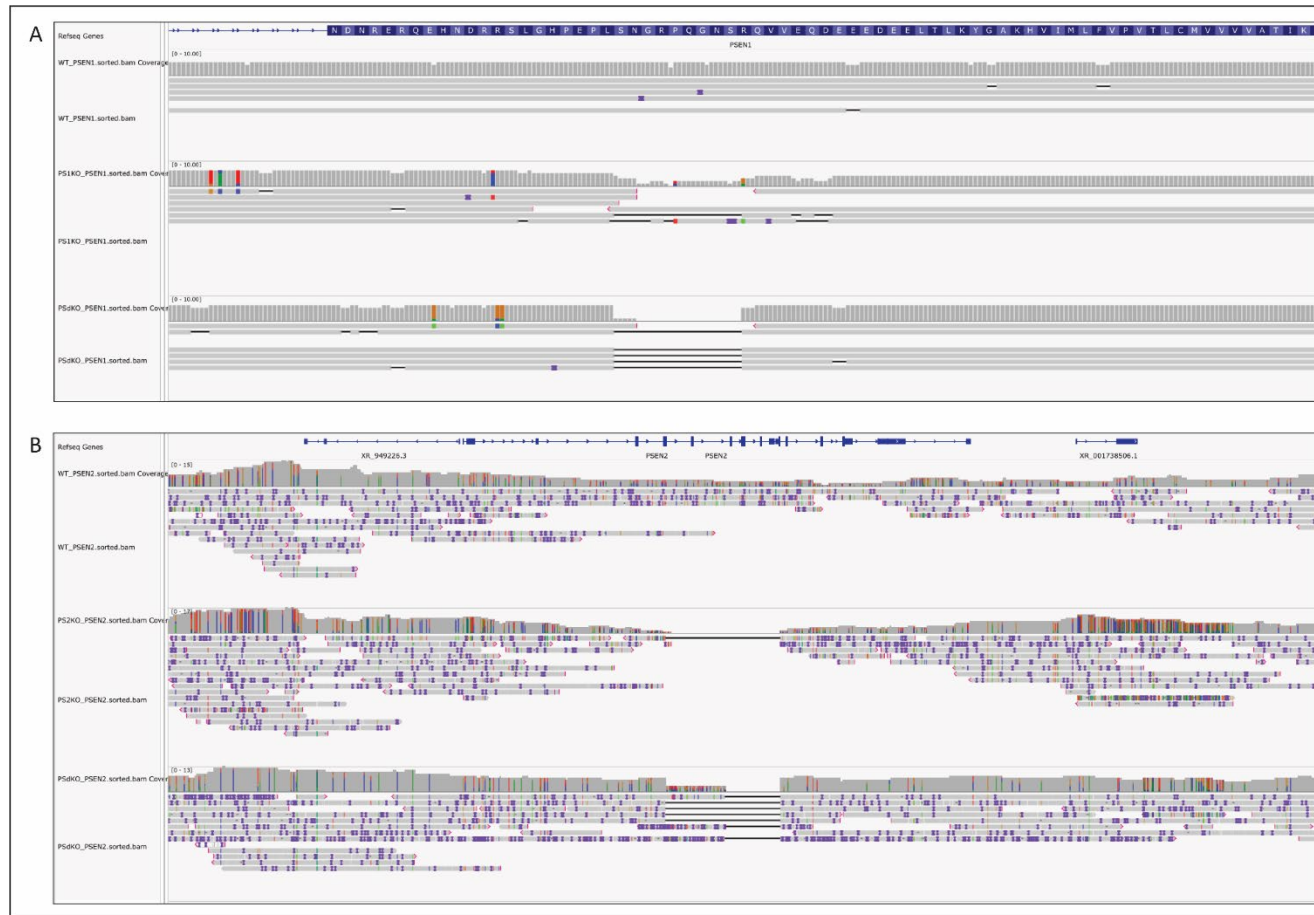
Protein target		Antibody Clone	Supplier & Catalogue#		Epitope region (aa)	In PS-Std	Tested with PS-Std
PS1	NTF	NT1	Biolegend	823401	41-49	YES	YES
PS1	NTF		Abcam	ab252856	propriety	Unknown	No
PS1	NTF		Abcam	ab216400	1-100	Partial	No
PS1	NTF		Abcam	ab255850	propriety	Unknown	No
PS1	NTF	APS11	Multiple		21-34	YES	No
PS1	NTF		ThermoFisher	PA5-98093	1-160	Partial	No
PS1	NTF	ARC0440	ThermoFisher	MA5-35263	1-100	Partial	No
PS1	NTF		ThermoFisher	PA5-119872	330-380	YES	No
PS1	NTF		ThermoFisher	PA5-98092	4-218	Partial	No
PS1	NTF		ThermoFisher/Fabgennix	PSEN-101AP	1-50	Partial	No
PS1	NTF		Sigma-Aldrich	MAB1563	21-80	Partial	No
PS1	NTF		ABclonal	A19103	1-100	Partial	No
PS1	CTF	D39D1	Cell Signalling	5643S	300-380	YES	YES
PS1	CTF		Cell Signalling	3622	around V293	YES	No
PS1	CTF	APS18	Multiple		313-334	Partial	YES
PS1	CTF		Abcam	EP2000Y	propriety	Unknown	No
PS1	CTF		ThermoFisher	BS-0025M	299-350	YES	No
PS1	CTF		ThermoFisher	PA5-96088	290-380	Partial	No
PS1	CTF		ThermoFisher	PA5-30585	257-352	Partial	No
PS1	CTF		Sigma-Aldrich	AB5308	275-367	Partial	No
PS1	CTF		Sigma-Aldrich	MAB5232	263-378	Partial	No
PS1	CTF		ABclonal	A2187	290-380	YES	No
PS2	NTF		Biolegend	814204	1-87	YES	YES
PS2	NTF	APS21	Multiple		31-45	YES	YES
PS2	NTF		ThermoFisher	PA5-112675	7-77	YES	No
PS2	NTF		ThermoFisher	PA5-94969	39-51	YES	No
PS2	NTF		ThermoFisher/Bioss	BS-3815R	51-150	Partial	No
PS2	NTF		Santa-Cruz	sc-393758	1-76	YES	No
PS2	NTF		ABclonal	A7719	1-75	YES	No
PS2	CTF	EP1515Y	Abcam	ab51249	300-400	Partial	YES
PS2	CTF		ThermoFisher/Bethyl Laboratories	A304-342A	275-325	Partial	No
PS2	CTF		ThermoFisher	PA5-96774	300-400	Partial	No
PS2	CTF		ThermoFisher	PA5-115793	316-344	YES	No

2.7 SUPPLEMENTAL FIGURES



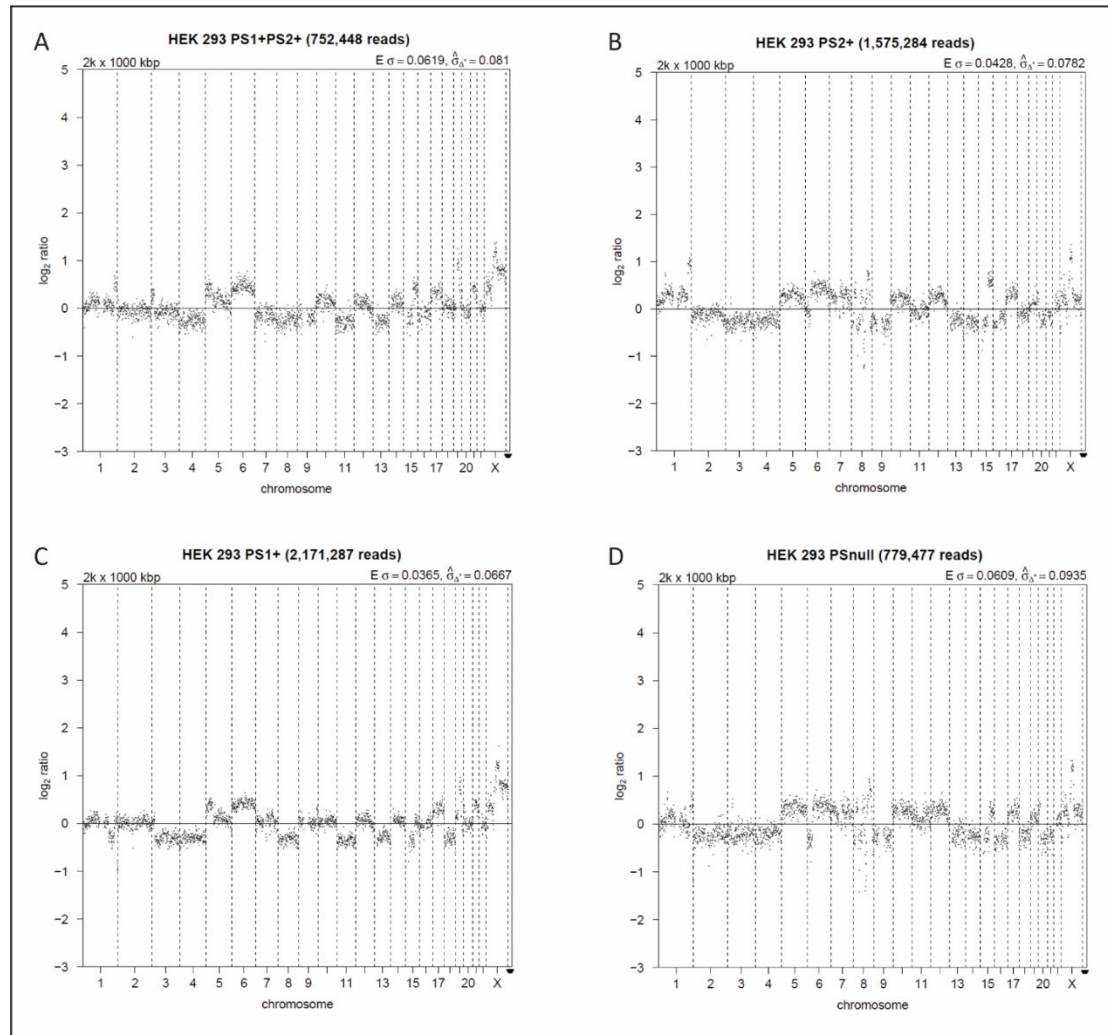
SI Figure 2-1 Characterisation of clonal populations of HEK-293 PS2+, PS1+, and PSnull cell lines

Multiple clones of presenilin knockout cell lines were assessed for PS1 and PS2 expression and either AICD generation via cell-free assay using crude CHAPSO cell membrane lysates, or APP-CTF accumulation and NICD generation with hAPP695Swe or ΔEhNotch1 transient transfection. Clones were selected on the bases of complete loss of appropriate PS homologues and average expression or processing compared to other clones. Immunoblot results for PS2+ clones assessed for PS1 and PS2 NTF expression and AICD generation (A). PS1+ clones assessed for PS1 and PS2 NTF expression, APP-CTF accumulation and NICD generation (B). PSnull clones assessed for PS1 and PS2 NTF expression, APP-CTF accumulation and NICD generation. Selected clone numbers are bolded and underlined (C).



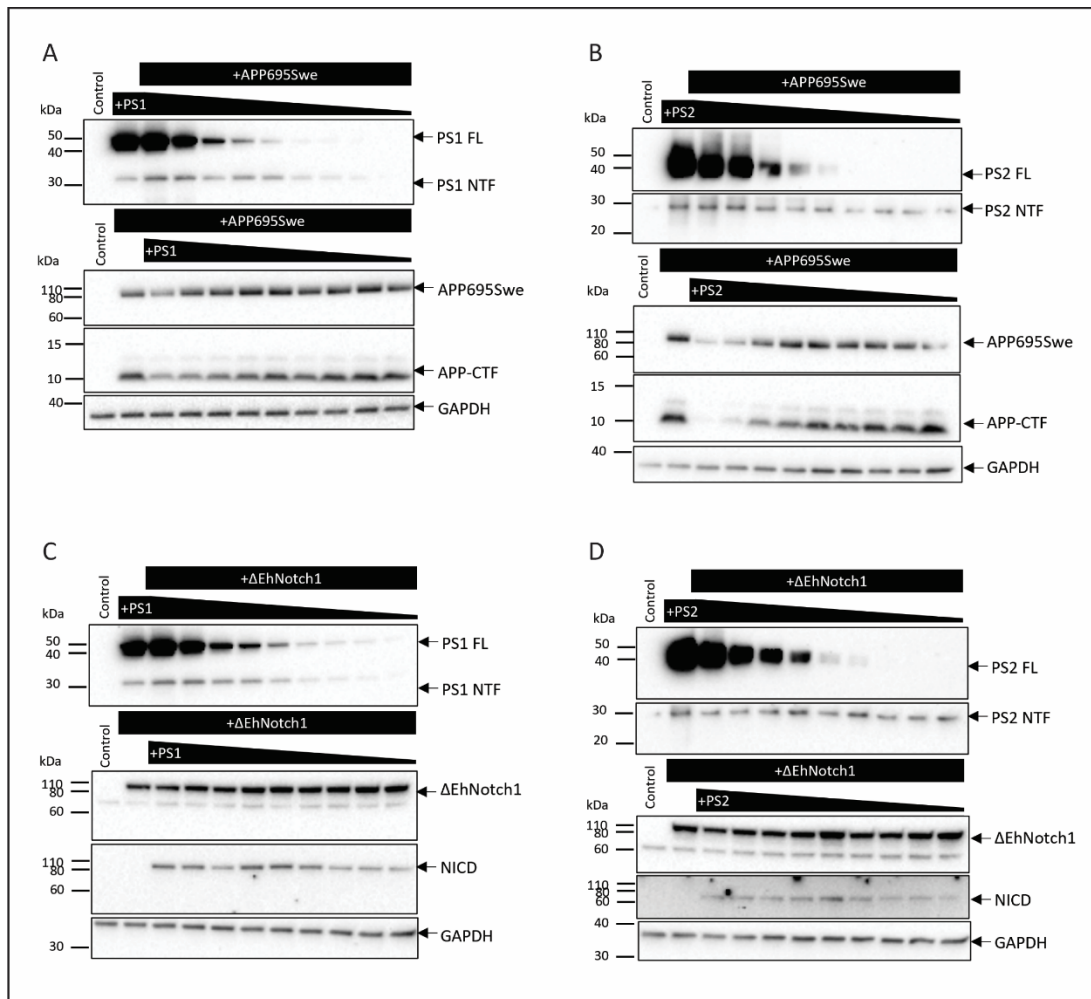
SI Figure 2-2 Sequence confirmation of CRISPR genetic ablation of *PSEN1* and *PSEN2*

Oxford Nanopore sequencing results viewed in Integrative Genome Viewer showing gene disruption in *PSEN1* for HEK PS2+ (PS1KO) and HEK PSnull (PSdKO) (A) and *PSEN2* for HEK PS1+ (PS2KO) and HEK PSnull (PSdKO) (B).



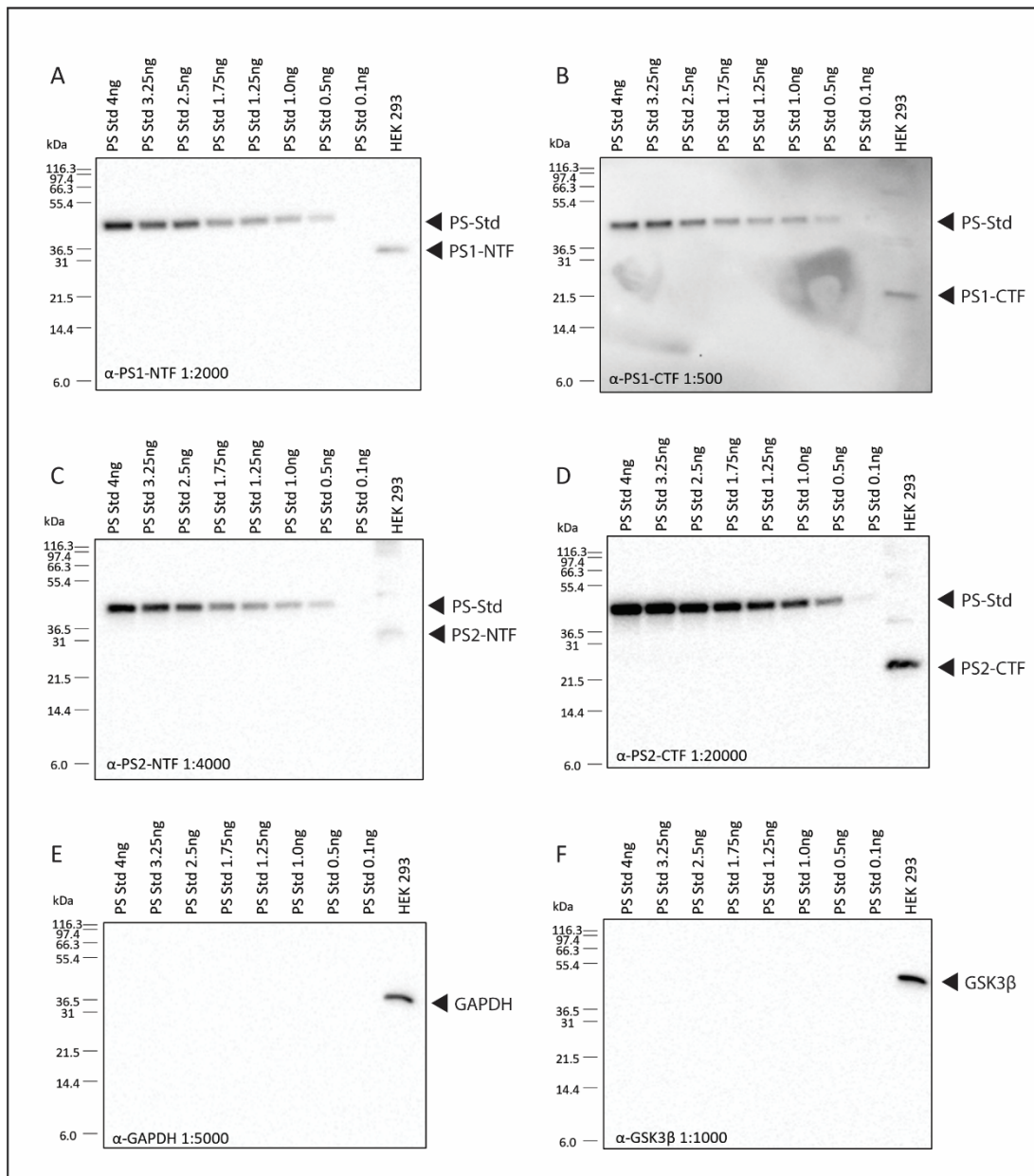
SI Figure 2-3 Copy number variation analysis for HEK-293 PS1+PS2+, PS2+, PS1+ and PSnull cell lines

Copy number variation for HEK PS1+PS2+ (A), HEK PS2+ (B), HEK PS1+ (C), and HEK PSnull (D) cell lines. Determined by analysis of multiplexed whole genome sequencing completed using Oxford Nanopore sequencing.



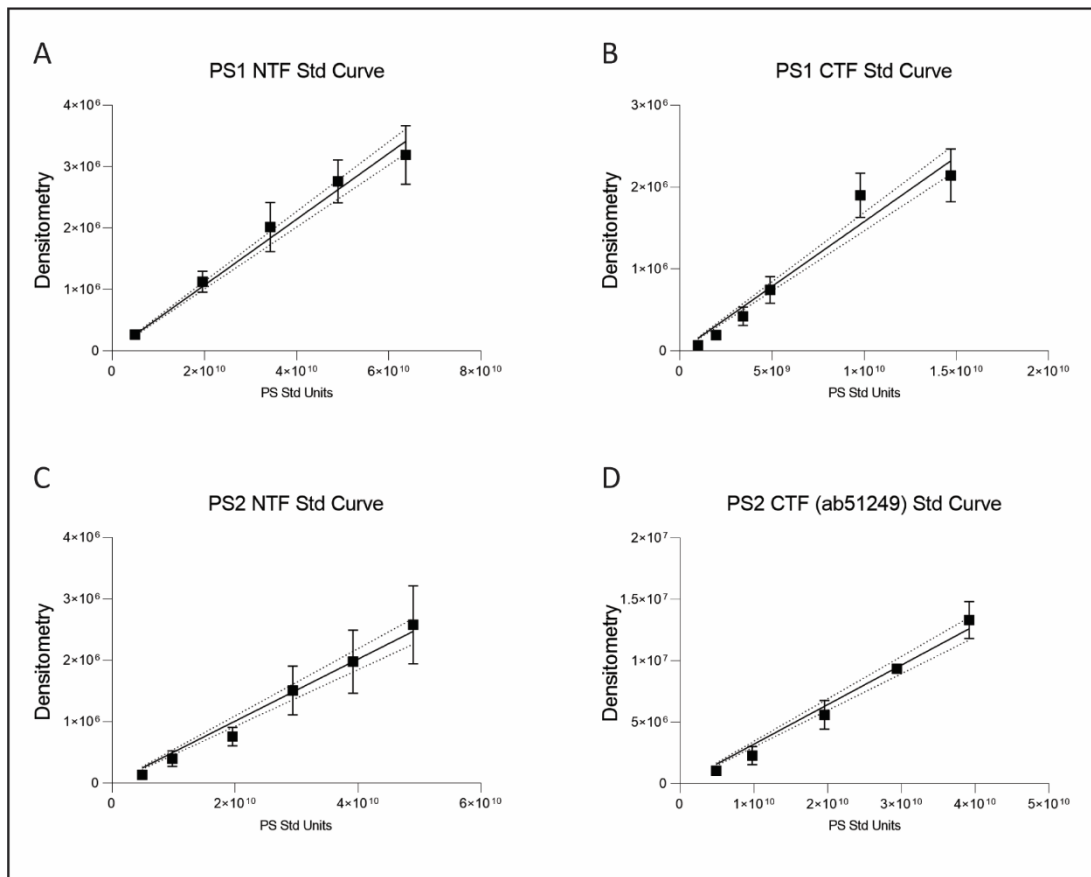
SI Figure 2-4 Exogenous Myc-PS1 and Myc-PS2 transfection titration

Titration of exogenous PS1 and PS2 transfections to determine amount of PS that maximises PS-NTF incorporation and minimises the amount of PS-FL overexpression. The selected amount of PS used for experiments was 116ng for transfection with APP695Swe and 111ng for transfection with ΔEhNotch1 (Note: Substrate was transfected at 3:1 Substrate-vector:PS-vector ratio, all ng amounts were calculated based on specific vector base pair sizes) PS1 co-transfected with APP695Swe (A). PS2 co-transfected with APP695Swe (B). PS1 co-transfected with ΔEhNotch1 (C). PS2 co-transfected with ΔEhNotch1 (D).



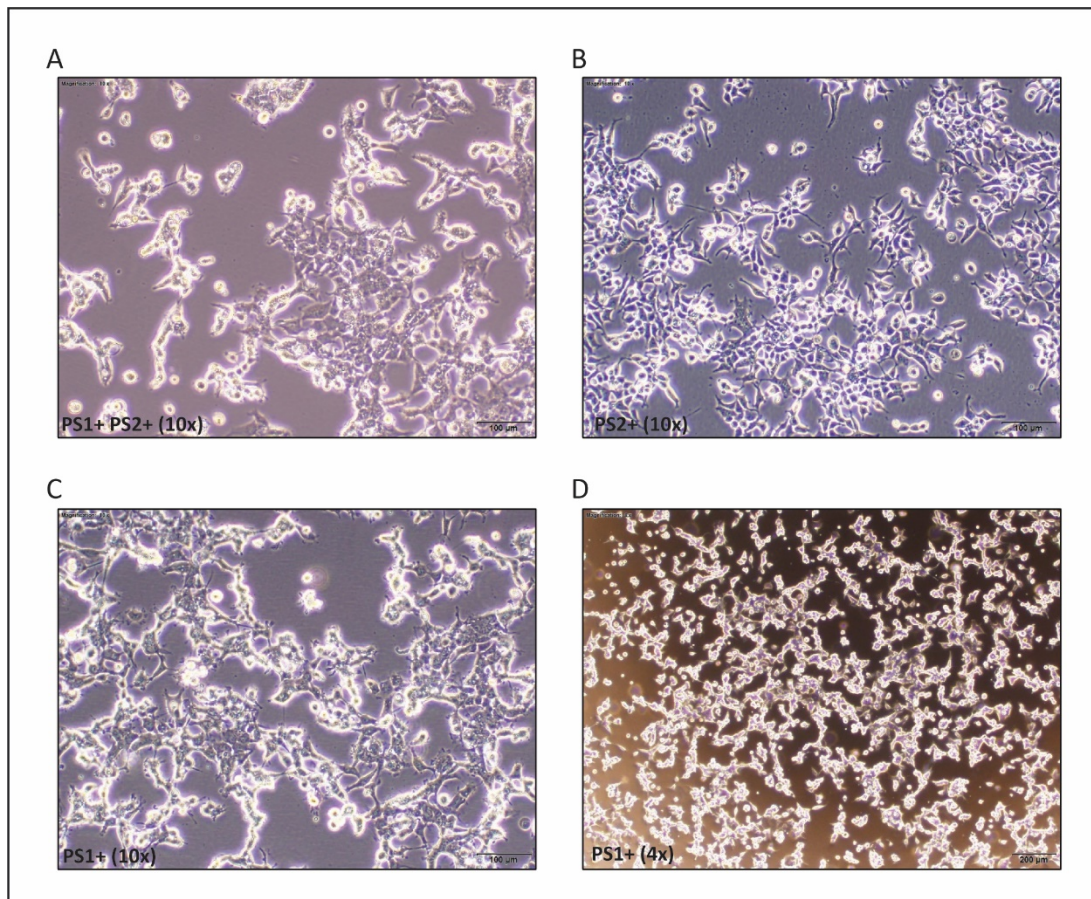
SI Figure 2-5 Validation of PS-Std detection by related and unrelated antibodies

PS-std incorporates N-terminal and cytoplasmic loop antibody epitope regions of human PS1 and PS2 and is detected by multiple commercial PS antibodies, but not by antibodies targeting unrelated proteins. PS1 NTF – Biologend (823401) (A), PS1 CTF – Abcam (ab15458) (B), PS2 NTF in house antibody courtesy P.E. Fraser (C), PS2 CTF – Abcam (ab51249) (D), GAPDH – Cell Signalling (5174) (E), GSK3 β (D5C5Z) – Cell Signalling (12456) (F).



SI Figure 2-6 Standard curves for quantitation of endogenous PS1 and PS2

Endogenous PS quantitation standard curves generated by plotting the number of PS-Std Units loaded against the quantitated band densitometry to determine equation then applied to the band densitometry for the endogenous PS detected in whole cell lysates. Standard curves shown here for quantitation shown in Figure 2-5. Standard curves are specific to the antibody used and the replicate set of immunoblots. PS1 NTF – Biologend (823401) (A), PS2 NTF – Biologend (814204) (B), PS1 CTF – Cell Signalling (5643S) (C), PS2 CTF – Abcam (ab51249) (D).



SI Figure 2-7 High concentration of APP695 transfection causes cell death in PS1+ cells

Cell line transfection of hAPP695Swe for intracellular A β detection caused cell death in PS1+ cells. The amount of hAPP695Swe construct required to detect intracellular A β using either human A β 40 ELISA (Thermofisher KHB3482) or human A β 42 Ultrasensitive ELISA (Thermofisher KHB3544) had to be increased to 2500 ng per 6 well dish compared with 384 ng used for detection in conditioned media. Significant cell death was observed, particularly in the PS1+ cells, making the experiment untenable. Bright field microscopy images of cells approximately 20hrs post transfection PS1+PS2+ cells at 10x magnification (A), PS2+ cells at 10x magnification (B), PS1+ cells at 10x and 4x magnification respectively (C-D).

3 PRESENILIN HOMOLOGUES INFLUENCE SUBSTRATE BINDING AND PROCESSING BY γ -SECRETASE: A MOLECULAR SIMULATION STUDY.

3.1 INTRODUCTION

Alzheimer's disease (AD) is the most common form of dementia, affecting approximately 35 million people worldwide. With no effective drug interventions that prevent or markedly slow down disease progression, a greater understanding of disease pathogenesis is required.¹ A key pathological hallmark of AD is the formation of cerebral amyloid plaques, which contain Amyloid- β (A β) peptides.² The A β peptides are of multiple lengths and are categorized into long (≥ 42 amino acids) and short (≤ 40 amino acids) forms, with the long forms being the pathogenic peptides with increased aggregative capacity.³⁻⁵ The most common A β forms generated are A β 40, accounting for the majority of peptides produced, and A β 42, accounting for a substantial minority of peptides produced, with the homeostatic A β 42:A β 40 ratio being approximately 1:9.⁶ However, these product ratios often shift in AD, such that increased production of longer forms - particularly A β 42 and A β 43 - occurs,^{3, 7, 8} leading to increased A β aggregation.^{4, 5} Thus, modulation of the production of A β peptides represents a potential therapeutic strategy for the treatment of AD.^{9, 10}

A β peptides are generated via the regulated intramembrane proteolysis (RIP) of Amyloid Precursor Protein (APP), a Type I single-pass transmembrane protein. Initial cleavage by β -APP cleaving enzyme-1 (BACE1) results in ectodomain shedding of APP, allowing the membrane-embedded C-terminal fragment to be cleaved by the integral membrane enzyme γ -secretase, ultimately releasing the APP IntraCellular Domain of APP (AICD) and A β peptides.¹¹ The γ -secretase enzyme (Figure 3-1A) is a heteromeric multi-subunit integral membrane protein consisting of: Presenilin - the catalytic subunit; Nicastrin (NCT) – involved in substrate gating; Anterior Pharynx Defective 1 (APH1) – a scaffolding and stabilization protein; and Presenilin Enhancer 2 (PEN2) – important for stabilization and enzyme activation.¹²⁻¹⁶ There are two homologues of Presenilin (PS) – Presenilin-1 (PS1) and Presenilin-2 (PS2) – and three isoforms of APH1 – APH1A^S, APH1A^L, APH1B – giving rise to six discrete forms of the γ -secretase enzyme.¹⁷ As the catalytic subunit, the PS homologue has considerable influence over enzymatic activity and genetic mutations in both PS1 and PS2 are causally associated with Autosomal Dominant AD (ADAD).¹⁸⁻²¹

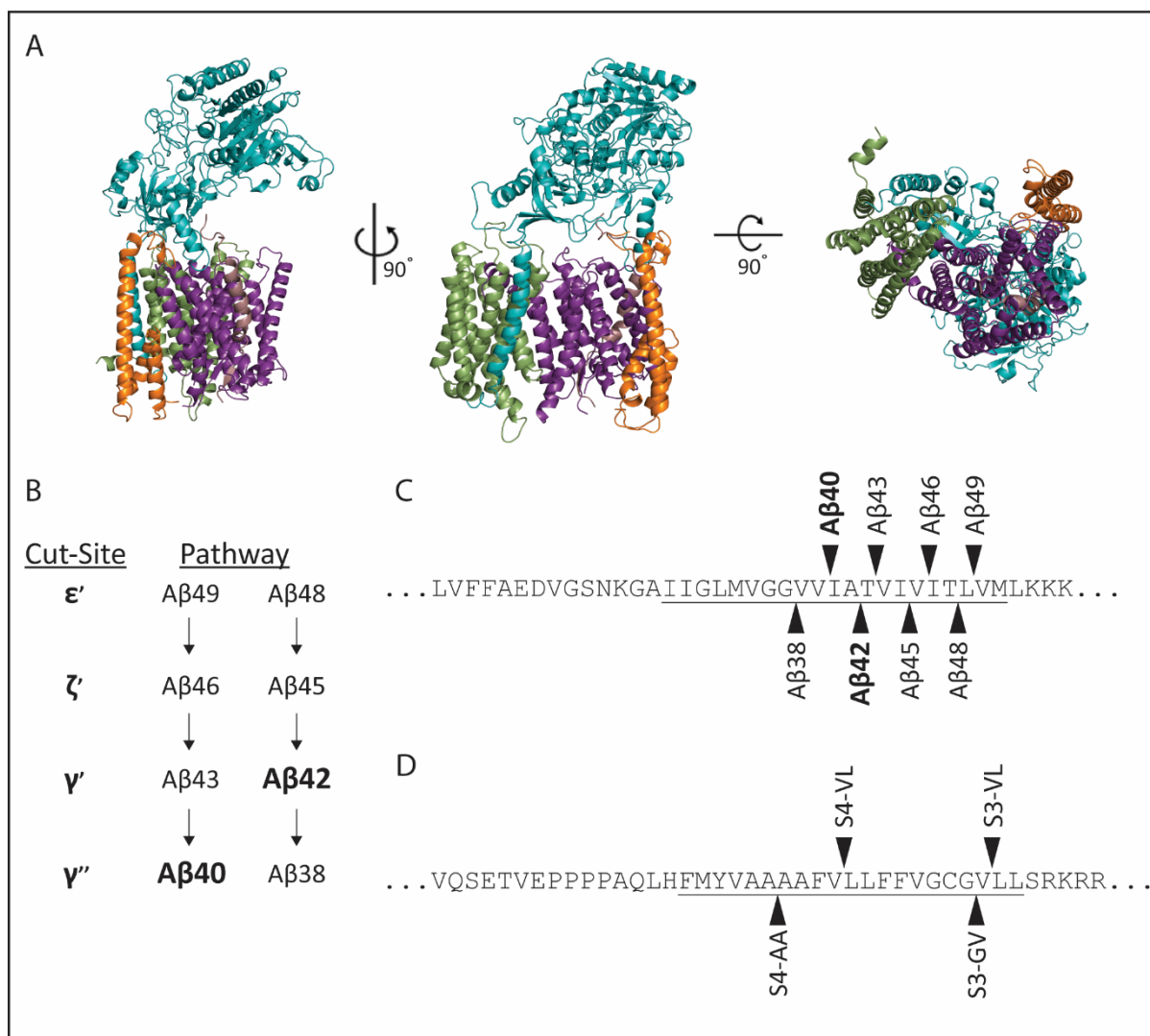


Figure 3-1 APP and Notch1 processing by γ -secretase.

Representative structures of γ -secretase components (A) colored as APH1A = green, Nicastrin = blue, PEN2 = orange, Presenilin = purple, APP substrate = light pink. A β 40 and A β 42 sequential processing pathways and cut-site terminology (B)²² Position of γ -secretase cleavage sites in APP sequence denoted by arrowhead (▲), TM region of APP-C99 substrate underlined (C). Position of γ -secretase cleavage sites in Notch1 sequence denoted by arrowhead (▲), TM region of Notch1 substrate underlined (D).

γ -Secretase generates A β peptides via a series of sequential cleavages of the transmembrane domain of APP. These cleavages occur within the lipid bilayer and involve an initial cleavage, releasing the AICD, followed by 2-3 further cleavages spaced at approximately three amino acids between each cleavage (approximately one helical turn). ultimately resulting in the A β peptide to be released from the membrane.^{22, 23} The APP processing pathway is well defined, and although there are multiple product lines, two primary pathways have been determined (Figure 3-1B, C).²³ These pathways produce A β 40 and A β 42 as their major products. The initial substrate, APP-C99, is the same for both product lines, and is cleaved to release the AICD.^{22,}

²³ However, the cleavage position varies by one residue between the two pathways, with this initial cleavage site being the primary determinant of the product pathway. Cleavage between residues Leu49 and Val50 typically leads to the production of the A β 40 product, whereas cleavage between Thr48 and Leu49 leads to A β 42 product generation (Figure 3-1B, C).^{22, 23}

Initial efforts to target γ -secretase involved the development of inhibitors; however, this has been hampered as a therapeutic strategy by side-effects believed to be associated with concurrent inhibition of the processing of other substrates, including Notch-1, which has a diverse array of cell type dependent signaling functions.²⁴ Notch-1 is processed similarly to APP, where, prior to γ -secretase processing, ectodomain shedding by ADAM10 occurs,^{25, 26} and the membrane retained product, referred to as the **Notch1 Extracellular Truncation (NEXT)**, is the γ -secretase substrate. NEXT is initially cleaved by γ -secretase at the S3 site to release the **Notch1 Intra Cellular Domain (NICD1)**.^{27, 28} Subsequent cleavage leads to the release of an A β -equivalent product, and the final cleavage site is the S4 site (Figure 3-1D).^{28, 29} Multiple S3 and S4 sites are known, and it is likely that there are similar intermediate processing pathways to those identified for APP processing; however, this has not been definitively determined for Notch.

A key advance in improving the functional understanding of γ -secretase has been the determination of its three-dimensional atomic structure via cryo-electron microscopy (cryoEM). The first structure by Bai et al.,³⁰ was a 3.4 Å resolution structure (PDB 5A63), followed closely by an additional four structures³¹ ranging from 4.0 – 4.3 Å resolution. These structures included an *apo*-state structure (PDB 5FN5), a DAPT-bound state (a γ -secretase inhibitor; although the structure of the inhibitor could not be resolved) (PDB 5FN2), and two structures containing a volume believed to represent a substrate helix (PDB 5FN3 and 5FN4). Subsequently, higher resolution, substrate-bound cryoEM structures have been published of PS1- γ -secretase (herein referred to as PS1 γ) bound to APP (2.6 Å) (PDB 6IYC)³² and Notch-1 (2.7 Å) (PDB 6IDF)³³. While these cryoEM structures provide static snapshots, they can be utilized to inform our understanding of the structure and dynamics of γ -secretase. Considerable molecular dynamics work has been completed using these structures, in particular, those prior to the most recent substrate bound structures, investigating the dynamics of substrate docking and entry pathways³⁴⁻³⁸ and the effect of lipids on γ -secretase conformation.^{37, 39} More recently, the effect of presenilin mutations on γ -secretase conformation and substrate binding have been investigated.^{40, 41} Prediction of the binding site of γ -secretase modulators and inhibitors^{42, 43} has

been complemented by the most recent atomic structures of PS1 γ with inhibitory and modulatory small molecules bound.⁴⁴

PS1 is typically considered the more important PS in the context of AD, as the vast majority of pathogenic mutations in the presenilin protein associated with AD occur in PS1 compared with PS2.⁴⁵ However, PS2 expression has been shown to increase over time with *in vitro* neuronal differentiation^{46, 47} and in the human and murine brain with age,^{48, 49} while in cell culture, PS2- γ -secretase (herein referred to as PS2 γ) has been shown to generate more intracellular A β ^{50, 51} and increased A β 42:A β 40 ratio.^{17, 47, 52, 53} These observations collectively suggest a role for PS2 γ in disease presentation and progression. Understanding the specific mechanisms and contributions of PS1 γ and PS2 γ to substrate binding and processing is therefore important to ensure that effective therapeutics are developed that target PS1 and PS2 complexes effectively.

This study used enhanced sampling approaches, specifically, targeted molecular dynamics and well-tempered metadynamics (WTMetaD), to explore the conformational landscape of PS1 γ and PS2 γ in the context of APP and Notch1 processing to examine the similarities and differences and enable improved structural understanding for the future development of A β modulating therapies. These approaches were further complemented by binding energy calculations to suggest specific preferences for substrate binding to the different forms of γ -secretase. Traditional experimental methods are limited in their ability to readily provide conformational information about the various states of γ -secretase bound to the multiple A β peptides. Similarly, traditional simulation approaches may overly sample specific protein conformations and lead to an incomplete understanding of the potential states that may be adopted by a given protein or protein complex. Homology modelling and metadynamics provide a tool kit that can allow the investigation of multiple γ -secretase and substrate combinations. The aim of this chapter is to determine the molecular mechanisms of differential A β generation by assessing A β substrate binding by PS1 γ and PS2 γ .

3.2 MATERIALS AND METHODS

3.2.1 Structure preparation

The structures of PS1 γ bound to APP (PDB 6IYC) and Notch1 (PDB 6IDF) were obtained from the Protein Data Bank and used for the PS1:CTF(A β 49) and PS1:NEXT(VL) models. The subsequent PS1 γ models with either the APP or Notch substrate in different positions commensurate with the intermediate substrate and positioned for the expected product (SI Figure 3-1), and all PS2 γ models were generated using Advanced Homology Modelling within Schrodinger 2018-3. ProPKA⁵⁴ was used to assign protonation states within prepared structures, typically predicting the catalytic aspartate Asp385/Asp366 to be protonated/neutral in charge and the catalytic aspartate Asp257/Asp263 to be deprotonated/charged. Once built, the structure was aligned to its coordinates as deposited in the Orientations of Protein in Membranes (OPM) database,⁵⁵ to facilitate the subsequent system setup for molecular dynamics simulations. Acetyl caps at the N-terminus and N-methylamine caps at the C-terminus were added to the PS-NTF chain, while the PS-CTF chain was only capped at its N-terminus, and APH1A, NCT and the APP-CTF and NEXT substrates were only capped at the C-terminus. The PEN2 chain and subsequent substrates were not capped.

3.2.2 Simulation box preparation.

Built complexes were set up for simulation adapting procedures from the Amber lipid force field tutorial.⁵⁶ Briefly, built complexes were submitted to the CHARMM-GUI web server,⁵⁷ where they were embedded in POPC bilayers (120 x 120 lipids in size) and solvated (to create a box with a minimum distance of 15 Å between the edge of the protein and the box edge), with salt added for charge neutralization of the system and for simulating relevant physiological ionic strength (150mM NaCl). Aguayo-Ortiz et al.³⁹ have shown that γ -secretase in- silico conformational behavior is similar in different homogenous membrane environments, hence γ -secretase was simulated 100% POPC. Relevant caps were chosen during CHARMM-GUI preparation to preserve the caps used during structure preparation.

Conversion of the prepared system from CHARMM to AMBER format, as well as system parameterization, was performed using AmberTools.⁵⁸ The protein was parameterized using the AMBER *ff14SB* force field.⁵⁹ Lipids were parameterized using Lipid14.⁶⁰ TIP3P water was

used throughout.⁶¹ The Joung-Cheatham ion parameters were used for sodium and chloride.⁶² The resulting topology was then ported to GROMACS format using *acpype*.⁶³

3.2.3 System Equilibration

Simulations were performed using GROMACS 2018.3⁶⁴ patched with PLUMED 2.5.⁶⁵ Equilibrations of the system in the NVT and NPT ensembles were adapted from previously described procedures for equilibration of membrane proteins.⁶⁶ Briefly, heavy atoms in the protein and lipids were position-restrained with harmonic restraints at 240 kJ/(mol nm²), and the system gradually heated in the NVT ensemble from 0K to 100K over 0.1ns, followed by heating in the NPT ensemble from 100K to 300K for a further 0.1ns. Following this, further NPT simulations (0.1ns in duration each) were conducted with only the protein heavy atoms position-restrained, utilizing gradually decreasing force constants (120 kJ/(mol nm²), 96 kJ/(mol nm²), 72 kJ/(mol nm²), 48 kJ/(mol nm²), 24 kJ/(mol nm²)), with a further 0.1ns simulation performed without position restraints.

3.2.4 Identification of a path between APP-bound and Notch-bound states

Targeted molecular dynamics was used to derive a path between the APP-bound and Notch1-bound states of PS1 γ . 10 simulations of 5ns duration were conducted, each starting from the APP-bound state of γ -secretase biasing towards the Notch1-bound states. During these simulations, a restraint of 50 kcal/mol was employed on the root mean squared deviation (RMSD) of all heavy atoms to the Notch1-bound state, as well as a concurrent added restraint of 100 kcal/mol on the RMSD of heavy atoms of presenilin transmembrane regions 2, 3 and 4, which are key interactors with the substrate. Frames from each simulation were clustered to 0.1nm, with the simulation giving rise to the largest number of clusters used to give the frames of the path. A vehicle routing solver⁶⁷ on the RMSD matrix of the clusters was used to identify the order of clusters giving rise to the smallest distance between adjacent frames. With the exclusion of the nicastrin ectodomain, all heavy atoms were used in the final determined path.

The frames comprising the PS2 γ path were generated by homology modelling against each corresponding frame of the PS1 γ path determined by targeted molecular dynamics.

3.2.5 Metadynamics Simulations of γ -Secretase complexes

After equilibration, the systems underwent well-tempered metadynamics (WTMetaD) to explore the conformational ensembles of PS1 γ and PS2 γ enzymes bound to APP and Notch derived substrates, similarly to that previously reported.⁶⁸ Briefly, the collective variables for the WTMetaD bias were the position along the targeted MD-generated path (s) and the distance from this path (z). σ for s and z were set as 0.5 and 0.001 respectively, as determined by approximately half of the standard deviation in these variables at the conclusion of a 5ns unbiased simulation of PS1 γ bound to APP (SI Figure 3-2). Simulations were performed at 310 K for 500 ns, with Gaussian hills 1 kJ/mol in size added every 1 ps and employing a bias factor of 40. Calculation of the metadynamics reweighting factor⁶⁹ was enabled and the bias was stored on a grid for computational efficiency (updated every 10 ps using grid bin widths of 0.2 in s and 0.0005 in z). Atomic coordinates, velocities and energies were saved every 10 ps. To limit the exploration of deviations from the defined path, an upper wall in z at 0.1 was used, with a force constant of 100 and a rescaling factor of 0.001.

3.2.6 Identification of Low-Energy States of γ -Secretase complexes

Free energy surfaces (FESs) in terms of s and z were calculated from the WTMetaD simulations and reported relative to the lowest energy value in the determined FES. Convergence of FESs was assessed by monitoring the difference between free energy surfaces at 1ns intervals, as well as the Gaussian hill height and the collective variable space sampled over the duration of the simulations (SI Figure 3-3, SI Figure 3-4, SI Figure 3-5, SI Figure 3-6). Structural ensembles for each minimum in the FES within 2.5 kJ/mol of the global minimum were extracted from the WTMetaD simulations and clustered using the GROMACS *gmx cluster* utility, employing the GROMOS algorithm⁷⁰ and a 0.2nm threshold.

3.2.7 Binding free energy calculations

The structural ensembles extracted for each energetic minimum were used to calculate the substrate-enzyme binding energies, which were determined using the molecular mechanics generalized Born/surface area (MM-GB/SA) approach, facilitated by the *MMPBSA.py* tool of AmberTools.⁷¹ The single-trajectory protocol was utilized,⁷² with the following equation:

$$\begin{aligned}\Delta G_{bind} &= G_{complex} - G_{protein} - G_{ligand} = \Delta H + \Delta G_{solvation} - T\Delta S \\ &= \Delta G_{vdw} + \Delta G_{ele} + \Delta G_{GB} + \Delta G_{SA} - T\Delta S\end{aligned}$$

Where ΔG_{vdw} is the molecular mechanics van der Waals interaction energy, ΔG_{ele} is the molecular mechanics electrostatic interaction energy, ΔG_{GB} is the change in polar desolvation energy upon complex formation and ΔG_{SA} is the change in nonpolar desolvation energy upon complex formation. The entropic term ($-T\Delta S$) was not calculated, due to high computational cost and poor accuracy. The GBneck2 model ($igb = 5$) was used to calculate the polar desolvation energy.⁷³ The non-polar component of the desolvation energy was calculated via solvent accessible surface areas calculated with the LCPO method.⁷⁴ MM-GB/SA energies were also decomposed per-residue ($idecomp = 1$).

To determine the preference between PS1 γ and PS2 γ complexes bound to the same substrate the following was calculated:

$$\Delta\Delta G_{PS Pref} = \Delta G_{bind PS2} - \Delta G_{bind PS1}$$

Where positive values indicate preference for PS1 γ , while negative values indicate preference for PS2 γ .

3.3 RESULTS

3.3.1 Derivation of path between APP-bound and Notch1-bound PS1 γ

Targeted molecular dynamics and analysis of the derived trajectories was initially performed to identify a potential path linking the APP-bound and Notch1-bound states of PS1 γ . The path ultimately identified was 20 frames in length. Key regions of dynamic movement in the frames comprising the path, representing key regions of structural variation between the two complex structures, are the region between the second and third transmembrane helices of presenilin, the region between the sixth and seventh transmembrane helices of presenilin, and the region between the third and fourth transmembrane helices of APH1A (SI Figure 3-7A). All of these regions are located on the luminal side of the complex. The corresponding PS2 γ path was derived via homology modelling to the component frames of the PS1 γ path, on the assumption that PS2 γ is likely to display similar dynamics to PS1 γ .

3.3.2 WTMetaD of PS1 γ and PS2 γ bound to APP substrates

Using the cryoEM structure of PS1 γ bound to APP-CTF in position for the initial cleavage of the A β 40 pathway (PDB:6IYC)³², homology models of PS1 and PS2 γ bound to APP-CTF (and

intermediate fragments) in position for cleaving A β 49, A β 48, A β 46, A β 45, A β 43, A β 42, A β 40, and A β 38 were prepared. Using the path derived from targeted MD simulation, WTMetaD in the position along (denoted as s , where $s = 1$ represents γ -secretase bound to APP as per PDB 6IYC, herein referred to as the 6IYC-like conformation of γ -secretase, and $s = 20$ represents γ -secretase bound to Notch1 as per PDB 6IDF, herein referred to as the 6IDF-like conformation of γ -secretase) and deviation from (denoted as z , with $z = 0$ being along the path, and $z > 0$ being a deviation from the path) the path was performed. WTMetaD of both PS1 γ and PS2 γ bound to the initial APP-CTF substrate in the cleavage position for initiating the A β 40 pathway (i.e. to generate the intermediate A β 49 product) revealed only one major energetic minimum for both complexes, with similar 6IYC-like conformations (Figure 3-2A: PS1:CTF(A β 49) $s \approx 4$, $z \approx 0.04$; Figure 3-2B: PS2:CTF(A β 49) $s \approx 3$, $z \approx 0.035$).

Energetic minima derived from WTMetaD of PS1 γ and PS2 γ bound to APP-CTF in the cleavage position to initiate the A β 42 pathway (i.e., to generate the intermediate A β 48 product) revealed two energetic minima for the PS1:CTF(A β 48) complex, both of which are 6IYC-like (Figure 3-3A: PS1:CTF(A β 48) $s \approx 3$, $z \approx 0.035$ and $s \approx 1.5$, $z \approx 0.08$). The lowest energy minimum of the PS1:CTF(A β 48) complex ($s \approx 3$, $z \approx 0.035$) is comparable to the PS1:CTF(A β 49) complex minimum in contour breadth, suggesting a similar conformational flexibility in PS1 γ when binding either substrate. However, the PS2 complex has only one 6IYC-like energetic minimum (Figure 3-3E: PS2:CTF(A β 48) $s \approx 1.5$, $z \approx 0.04$), and while similarly positioned with respect to the path compared to the PS2:CTF(A β 49) complex, this minimum has broader contours, suggesting that this complex is likely more flexible than the equivalent complex with PS1.

WTMetaD of PS1 γ and PS2 γ in complex with all intermediate substrates of the A β 40 and A β 42 processing pathways was then performed (Figure 3-2, Figure 3-3). All subsequent γ -secretase–substrate complexes, after the initial cleavage to release AICD, have one energetic minimum, with the exception of the PS1:A β 48(A β 45) complex, which has two energetic minima (Figure 3-3B). All minima are 6IYC-like ($s < 5$ in all cases). The contour breadth in the PS1 γ complexes with A β 40 pathway substrates is considerably tighter in the shorter substrates further along the pathway, in comparison to the initial CTF(A β 49) substrate (Figure 3-2B-D), compared to the broader contours in the equivalent complexes with PS2 γ (Figure 3-2F-H). In contrast, PS2 γ displays a restricted conformational ensemble when binding to the initial CTF(A β 48) substrate in the A β 42 pathway (Figure 3-3E), while subsequent enzyme-substrate complexes in the

pathway (with the exception of the PS2:A β 42(A β 38) complex) display relatively broader free energy surface contouring, suggesting increased conformational flexibility (Figure 3-3F-H).

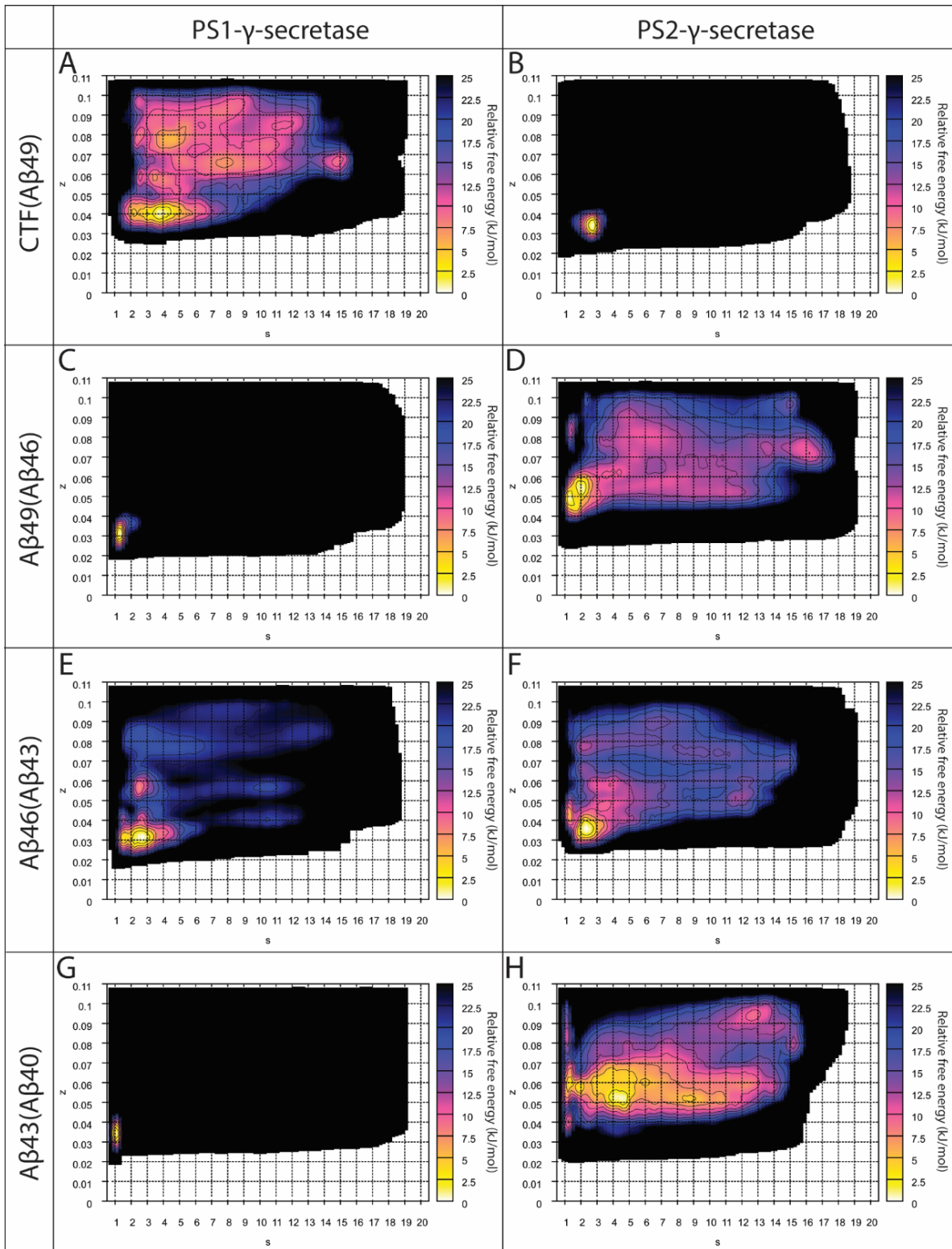


Figure 3-2 Well-tempered metadynamics simulations of PS1 γ and PS2 γ in complex with A β 40 pathway substrates.

Relative free energy surfaces for PS1 γ (A, C, E, G) and PS2 γ (B, D, F, H) in complex with substrates [denoted as substrate(cleavage position)] CTF(A β 49) (A, B), A β 49(A β 46) (C, D), A β 46(A β 43) (E, F), A β 43(A β 40) (G, H).

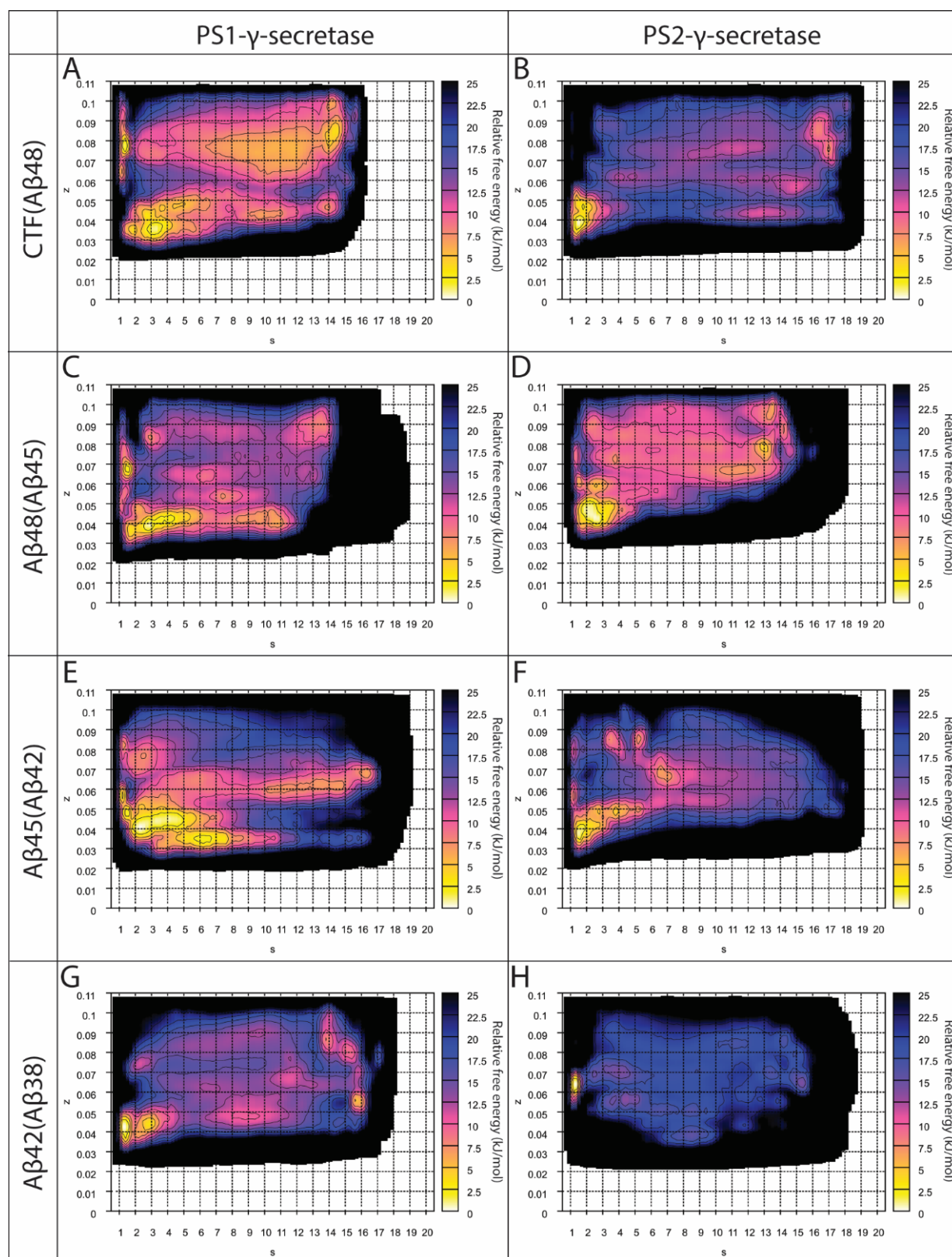


Figure 3-3 Well-tempered metadynamics simulations of PS1 γ and PS2 γ in complex with A β 2 pathway substrates.

Relative free energy surfaces for PS1 γ (A, C, E, G) and PS2 γ (B, D, F, H) in complex with substrates [denoted as substrate(cleavage position)] CTF(A β 48) (A, B), A β 48(A β 45) (C, D), A β 45(A β 42) (E, F), A β 42(A β 38) (G, H).

3.3.3 Binding free energies of γ -secretase - APP bound complexes

Molecular mechanics-generalized Born/surface area calculations (MM-GB/SA) were performed for all enzyme-substrate complexes to estimate the binding energies (ΔG_{bind}) for γ -secretase with each of the substrates (Table 3-1). Structures corresponding to low energy regions of the free energy surfaces derived from the WTMetaD simulations were used for the MM-GB/SA calculations. The PS1:CTF(A β 49) complex, in the position to initiate the A β 40 pathway, has a more favorable binding energy compared to the PS2:CTF(A β 49) complex. However, the opposite preference is observed for CTF(A β 48), where PS2:CTF(A β 48) has a marginally lower binding energy than PS1:CTF(A β 48). While there are two minima evident from the metadynamics simulation for the PS1:CTF(A β 48) complex, MM-GB/SA calculations at both minima afford a higher binding energy compared to the PS2:CTF(A β 48) complex. Thus, CTF(A β 48) is predicted to have a preference for binding PS2 γ over PS1 γ . Considering the binding energy results for all four complexes bound to the APP-CTF, there is a preference for both PS1 γ and PS2 γ to bind the APP-CTF in the A β 48 position over the A β 49 position.

The binding energies for the subsequent complexes in the A β 40 pathway suggest that while PS2 γ has a preference for binding to the A β 49(A β 46) substrate over PS1 γ , the PS2 γ enzyme binds A β 46(A β 43) significantly less favorably than the PS1 γ enzyme. Both PS1 γ and PS2 γ enzymes have approximately equal preference for binding the A β 43(A β 40) substrate. In the A β 42 pathway, however, the subsequent PS1 complexes - PS1:A β 48(A β 45), PS1:A β 45(A β 42) and PS1:A β 42(A β 38) – have consistently more favorable binding energy than the equivalent PS2 complexes.

Table 3-1 MM-GB/SA binding free energy of γ -secretase – APP bound complexes

A β 40 Pathway				A β 42 Pathway			
Substrate	Product	PS1 [§]	PS2 [§]	Substrate	Product	PS1 [§]	PS2 [§]
APP-CTF	A β 49	-189.7 \pm 1.5	-178.4 \pm 2.7	APP-CTF	A β 48	-205.6 \pm 1.8*	-208.9 \pm 2.6
A β 49	A β 46	-142.2 \pm 3.1	-158.3 \pm 1.1	A β 48	A β 45	-181.1 \pm 0.8 [#]	-164.7 \pm 1.8
A β 46	A β 43	-165.0 \pm 3.4	-148.6 \pm 1.3	A β 45	A β 42	-145.6 \pm 0.5	-122.4 \pm 1.5
A β 43	A β 40	-123.2 \pm 1.9	-124.4 \pm 1.3	A β 42	A β 38	-153.1 \pm 1.1	-132.3 \pm 1.0

*The PS1 γ complex bound to APP-CTF in position to generate the A β 48 product has a second minima located at $s = 0$ to $s = 2$ and $z = 0.07$ to $z = 0.09$, this complex conformation has a MMGBSA binding free energy of -194.7 ± 3.0 kcal/mol

#The PS1 γ complex bound to A β 48 to generate the A β 45 product has a second minima located at $s = 0$ to $s = 3$ and $z = 0.06$ to $z = 0.08$, this complex conformation has a MMGBSA binding free energy of -181.1 ± 3.8 kcal/mol

§Values shown are in kcal/mol +/- standard error

3.3.4 Per residue decomposition of binding free energies for γ -secretase-APP bound complexes

Per-residue decompositions of the MM-GB/SA binding energies were performed to determine the individual contributions of residues from the enzyme and the substrate to the overall binding energy. The relative change in binding energy per-residue with respect to PS1 γ versus PS2 γ was also calculated ($\Delta\Delta G_{PS Pref}$, calculation described in Methods) to determine the precise contributors to selectivity (Figure 3-4, Figure 3-6).

The APP-CTF substrate bound in position to produce the A β 49 product, thus initiating the A β 40 pathway, shows preference for binding to PS1 γ over PS2 γ . This preference is driven by a series of contributions clustered at the N-terminus of the substrate, specifically, nicastrin residues Ile246 ($\Delta\Delta G_{PS Pref} = +2.49$ kcal/mol) and Arg652 ($\Delta\Delta G_{PS Pref} = +6.07$ kcal/mol), which form hydrogen bonds (mediated by the Ile246 backbone amide) and a salt bridge respectively with Glu22 ($\Delta G_{bind PS1} = +0.87$ kcal/mol) in the substrate. Substrate residue Leu17 ($\Delta\Delta G_{PS Pref} = +4.26$ kcal/mol), which forms a hydrogen bond between its backbone carbonyl with the backbone amide of Trp653 ($\Delta G_{bind PS1} = -8.64$ kcal/mol) in nicastrin, and the PS1 residue Arg108 ($\Delta\Delta G_{PS Pref} = +4.29$ kcal/mol), which is likely forming cation- π interactions with the substrate residues Phe19 ($\Delta G_{bind PS1} = -4.60$ kcal/mol) and Phe20 ($\Delta G_{bind PS1} = -2.17$ kcal/mol), also contribute to this preference. Arg108 also forms a salt bridge with Nct Glu245. Arg108 is not conserved in PS2 and is replaced by a glutamate at the analogous position (PS2 Glu114),

with this residue unable to make the same interactions (Figure 3-4, Figure 3-5A). Further contributions more favorable in the PS1 γ complex occur at the C-terminal region of the substrate, specifically involving Val50 ($\Delta\Delta G_{PS \text{ Pref}} = +1.94$ kcal/mol), which forms multiple hydrophobic interactions with Val272 ($\Delta G_{\text{bind PS1}} = -1.22$ kcal/mol) and Ile287 ($\Delta\Delta G_{PS \text{ Pref}} = -1.47$ kcal/mol) in PS1, and Lys54 ($\Delta\Delta G_{PS \text{ Pref}} = +1.86$ kcal/mol), which forms hydrogen bonds and a salt bridge between PS1 residues Thr291 ($\Delta\Delta G_{PS \text{ Pref}} = +0.56$ kcal/mol) and Glu376 ($\Delta\Delta G_{PS \text{ Pref}} = +0.99$ kcal/mol), respectively (Figure 3-4, Figure 3-5B). Additionally, PS1 residue Gly384 ($\Delta\Delta G_{PS \text{ Pref}} = +2.16$ kcal/mol) forms hydrogen bonds with the backbone of Val46 ($\Delta\Delta G_{PS \text{ Pref}} = +0.13$ kcal/mol) and PS1 Leu425 ($\Delta\Delta G_{PS \text{ Pref}} = +2.18$ kcal/mol) hydrophobically interacts with substrate residue Met51 ($\Delta\Delta G_{PS \text{ Pref}} = +0.77$ kcal/mol). These interactions likely contribute to the stabilization of the β -sheet structure between PS1 and the substrate that is a key feature of the γ -secretase bound substrate,^{32, 33} and do not readily occur in the PS2 complex.

The subsequent complex in the A β 40 pathway, the A β 49 substrate positioned to produce the A β 46 product, demonstrates a preference for binding to PS2 γ over PS1 γ . This preference is a result of two key regions of interactions. PS2 Gln118 ($\Delta\Delta G_{PS \text{ Pref}} = -3.97$ kcal/mol) forms a hydrogen bond with substrate residue Val24 ($\Delta\Delta G_{PS \text{ Pref}} = -2.19$ kcal/mol) in the luminal juxtamembrane region, which does not occur in the PS1 γ complex (Figure 3-4, Figure 3-5C). The PS2 residues Arg358 ($\Delta\Delta G_{PS \text{ Pref}} = -1.64$ kcal/mol) and Lys361 ($\Delta\Delta G_{PS \text{ Pref}} = -2.08$ kcal/mol) coordinate a network of hydrogen bonds with the substrate C-terminal residues Thr48 ($\Delta\Delta G_{PS \text{ Pref}} = -0.26$ kcal/mol) and Leu49 ($\Delta\Delta G_{PS \text{ Pref}} = -0.76$ kcal/mol), likely stabilizing the C-terminus of the substrate; the majority of these interactions do not occur in the PS1 γ complex (Figure 3-4, Figure 3-5D).

The A β 46 substrate, processing of which leads to the generation of the A β 43 product in the A β 40 pathway, shows a preference for binding to PS1 γ over PS2 γ . Key contributors to the binding preference are the nicastrin residue Arg652 ($\Delta\Delta G_{PS \text{ Pref}} = +4.27$ kcal/mol), and the PS1 residue Arg108 ($\Delta\Delta G_{PS \text{ Pref}} = +4.24$ kcal/mol), which forms electrostatic interactions with Glu22 ($\Delta G_{\text{bind PS1}} = -0.85$ kcal/mol) in the substrate. As previously noted, the PS1 Arg108 residue is not conserved in PS2, with the analogous residue in PS2 being Glu14; consequently, these interactions cannot occur in the PS2 γ complex. Substrate residues at the N-terminal juxtamembrane region, Ser26 ($\Delta\Delta G_{PS \text{ Pref}} = +2.45$ kcal/mol) and Asn27 ($\Delta\Delta G_{PS \text{ Pref}} = +2.28$ kcal/mol), further contribute to the substrate preference for PS1 by forming a greater network

of hydrogen bonds with residues in the loop between TM-1 and TM-2 (Ile114: $\Delta\Delta G_{\text{PS Pref}} = +0.81$ kcal/mol; Thr116: $\Delta\Delta G_{\text{PS Pref}} = +0.58$ kcal/mol), which does not occur in the PS2 γ complex (Figure 3-4, Figure 3-5E). Additionally, a series of interactions between PS1 and substrate residues in the inner-leaflet transmembrane domain (TM) region and the C-terminal juxta-membrane region form, that do not occur in the PS2 γ complex (Figure 3-4, Figure 3-5F). PS1 residue Ser169 ($\Delta\Delta G_{\text{PS Pref}} = +2.28$ kcal/mol) forms hydrogen bonds between its backbone amine group and the backbone carbonyl group of Met35 ($\Delta G_{\text{bind PS1}} = -1.51$ kcal/mol), as well as utilizing its sidechain hydroxyl group to form a hydrogen bond with the amide of Gly38 ($\Delta\Delta G_{\text{PS Pref}} = +0.54$ kcal/mol). Leu286 ($\Delta\Delta G_{\text{PS Pref}} = +3.17$ kcal/mol) forms a network of hydrophobic interactions with Ile41 ($\Delta\Delta G_{\text{PS Pref}} = +0.80$ kcal/mol) and Ala42 ($\Delta\Delta G_{\text{PS Pref}} = +0.71$ kcal/mol); notably, these appear to stabilize the β -sheet structure between the substrate C-terminus and PS1 previously noted.^{32,33} These interactions occur in tandem with the Trp165 ($\Delta G_{\text{bind PS1}} = -4.28$ kcal/mol) sidechain forming a CH- π bond with Gly38 ($\Delta\Delta G_{\text{PS Pref}} = 0.54$ kcal/mol) in the substrate. The analogous tryptophan in PS2, Trp171 ($\Delta G_{\text{bind PS2}} = -4.29$ kcal/mol), is positioned such that it interacts with Val39 ($\Delta G_{\text{bind PS2}} = -4.61$ kcal/mol), forming a CH- π bond. The residue adjacent to Trp165/Trp171 is not conserved between PS1 and PS2, being an alanine in PS1 (Ala164) and a glycine in PS2 (Gly170); this likely influences the presentation of the tryptophan sidechain, as the backbone in this region is expected to exhibit greater flexibility in PS2- vs PS1 γ .

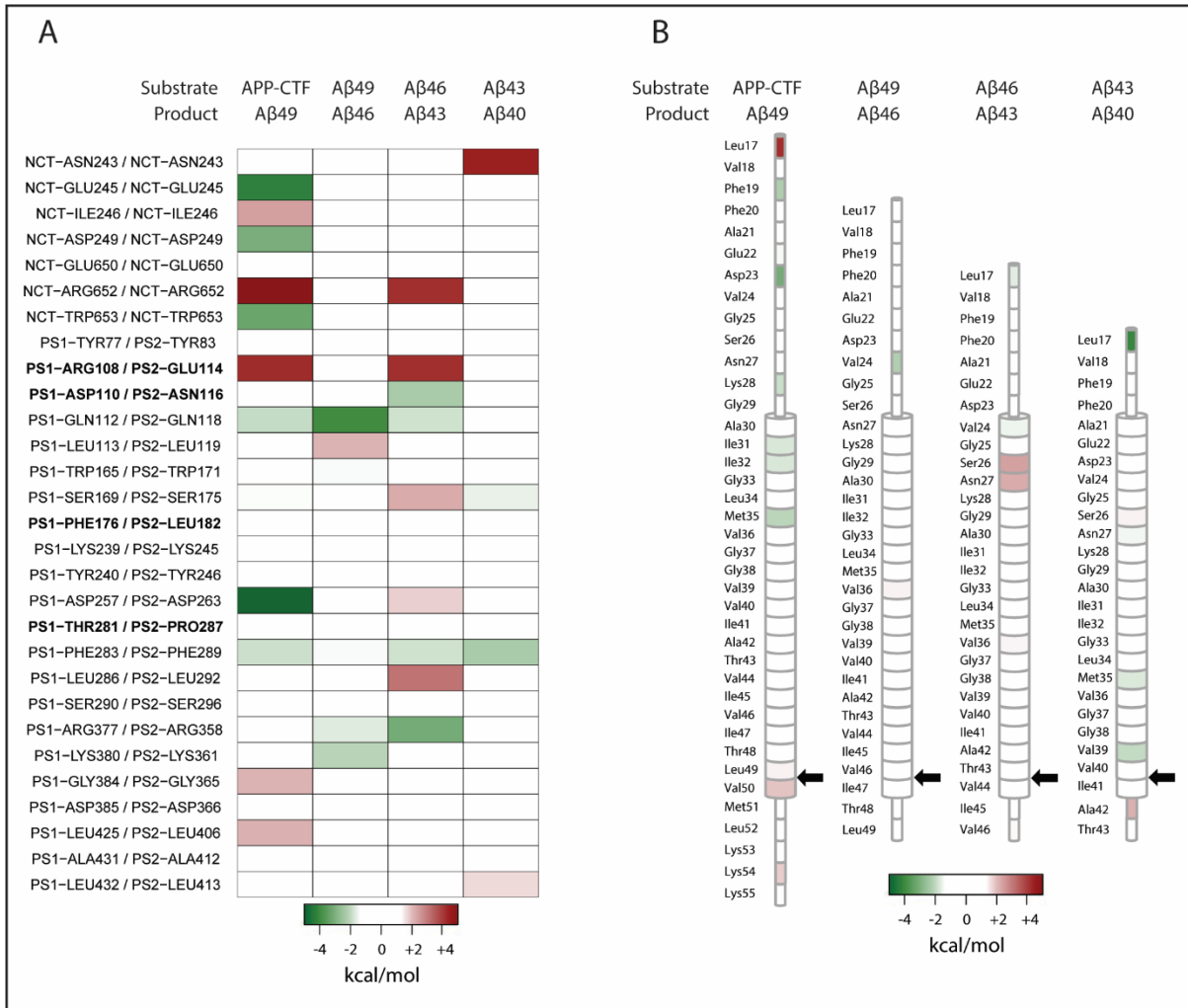


Figure 3-4 A β 40 pathway complexes per residue heatmaps of $\Delta\Delta G_{PS Pref}$.

Enzyme $\Delta\Delta G_{PS Pref}$ values (A). Only residues where the $\Delta\Delta G_{PS Pref}$ magnitude is greater than 1.5 kcal/mol in any complex are shown. Substrate $\Delta\Delta G_{PS Pref}$ values (B). Cleavage position denoted by arrow. Positive (red) $\Delta\Delta G_{PS Pref}$ values indicate preference for PS1, negative (green) $\Delta\Delta G_{PS Pref}$ values indicate preference for PS2.

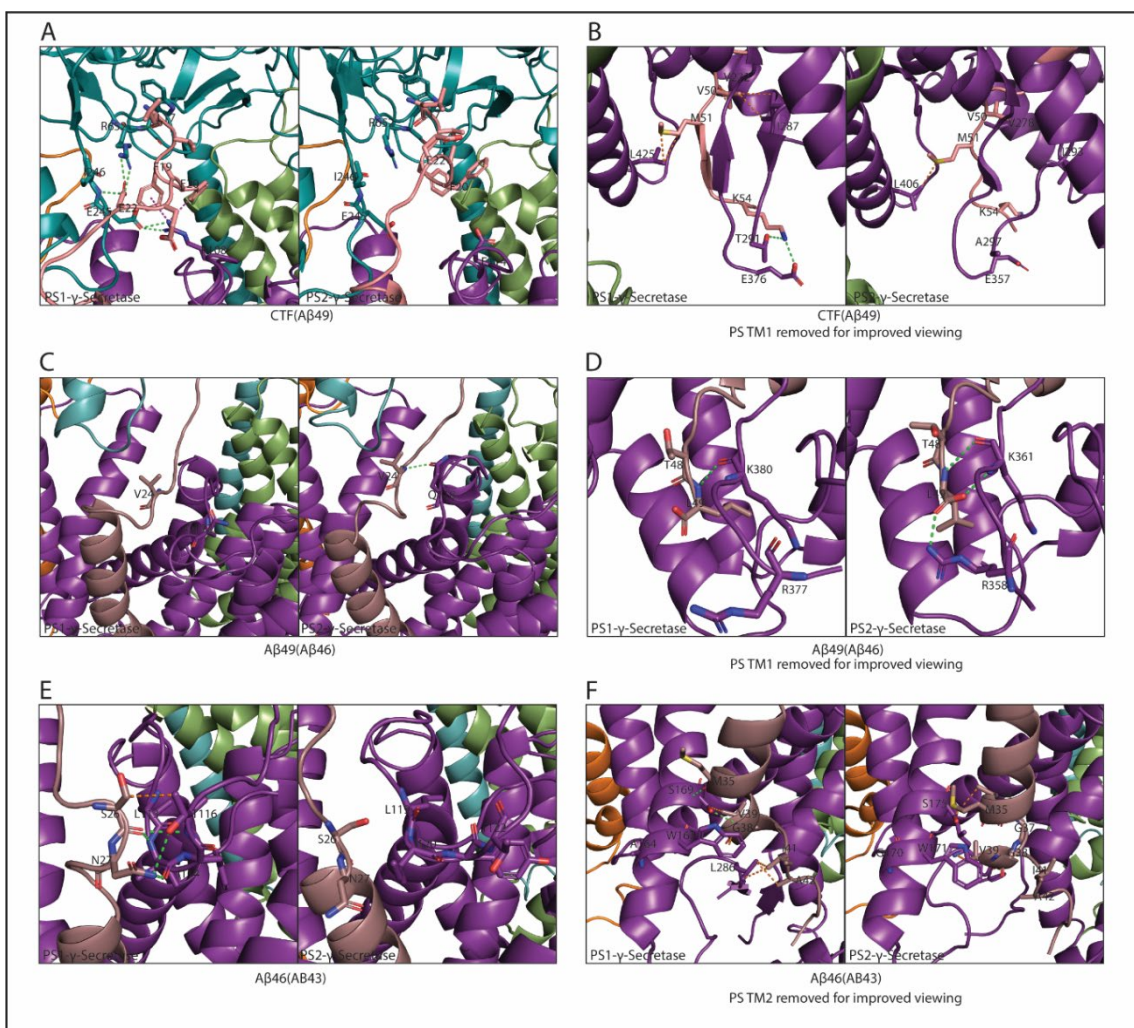


Figure 3-5 Representative structures of substrate – enzyme molecular interactions contributing to $\Delta\Delta G_{PS Pref}$ in $A\beta_{40}$ pathway

APP-CTF(A β 49) substrate N-terminal residues Leu17 to Glu22 (A), APP-CTF(A β 49) substrate C-terminal residues Val50 to Lys54 (B), A β 49(A β 46) substrate N-terminal juxta-membrane residues Val24 (C), A β 49(A β 46) substrate N-terminal residues Thr48 – Leu49 (D), A β 46(A β 43) substrate N-terminal juxta-membrane Ser26 – Asn27 (E), A β 46(A β 43) substrate C-terminal inner leaflet – juxta-membrane residues Met35 – Ala42 (F). Complex components represented in cartoon coloured as nicastrin = teal, presenilin1/presenilin2 = purple, APH1 = green, PEN2 = orange, substrate = light pink, with specific residues involved in interactions depicted in stick format. Hydrogen bonds represented in green dashed lines, π interactions represented by purple dashed lines, hydrophobic interactions represented in orange dashed lines.

APP-CTF bound in the position to generate the A β 48 product, representing the initial substrate in the A β 42 pathway, has a slight preference for binding to PS2 γ over PS1 γ . The primary residue contributing to this preference is the PS2 residue Asp263 ($\Delta\Delta G_{PS Pref} = -9.28$ kcal/mol), which is the catalytic aspartate in the N-terminal fragment of PS2 (Figure 3-6). Asp366, protonated in the models in this study, is presented in PS2 in a manner that allows for multiple hydrogen bonds between its side chain with substrate residue Thr48 and the backbone amine

of Leu49 (Figure 3-6, Figure 3-7A), unlike the equivalent residue in PS1, where these interactions are absent. Additionally, the N-terminal residues of APP-CTF (Val18 ($\Delta\Delta G_{PS \text{ Pref}} = -1.75$ kcal/mol) and Phe20 ($\Delta\Delta G_{PS \text{ Pref}} = -0.24$ kcal/mol) interact with a cluster of nicastrin residues (Asp249 ($\Delta\Delta G_{PS \text{ Pref}} = -3.80$ kcal/mol), Glu650 ($\Delta\Delta G_{PS \text{ Pref}} = -2.98$ kcal/mol), and Trp653 ($\Delta\Delta G_{PS \text{ Pref}} = -3.18$ kcal/mol)) and residues in the TM1 to TM2 loop region of PS2 (Asn116 ($\Delta\Delta G_{PS \text{ Pref}} = -1.94$ kcal/mol)), forming hydrogen bonds and hydrophobic interactions that are not evident in the PS1 γ complex (Figure 3-6, Figure 3-7B). Notably, Asn116 in PS2 is not conserved in PS1, the analogous residue being Asp110; the negatively charged aspartate residue in PS1 forms a salt-bridge with the positively charged Arg108 in PS1, preventing interactions with the substrate.

The subsequent substrates in the A β 42 pathway all demonstrate preference for binding to PS1 γ (Table 3-1). The primary contributors to this preference in the γ -secretase complexes bound to the A β 48 substrate in position to generate the A β 45 product are the nicastrin residue Asn243 ($\Delta\Delta G_{PS \text{ Pref}} = +1.68$ kcal/mol), and the PS1 residues Arg108 ($\Delta\Delta G_{PS \text{ Pref}} = +2.41$ kcal/mol) and Lys239 ($\Delta\Delta G_{PS \text{ Pref}} = +3.15$ kcal/mol). These enzyme residues are positioned around a cluster of residues in the N-terminal juxtamembrane region of the substrate, including Ala21 ($\Delta\Delta G_{PS \text{ Pref}} = +1.62$ kcal/mol), Glu22 ($\Delta\Delta G_{PS \text{ Pref}} = +2.39$ kcal/mol), Asp23 ($\Delta\Delta G_{PS \text{ Pref}} = +5.13$ kcal/mol), and Val24 ($\Delta\Delta G_{PS \text{ Pref}} = +1.76$ kcal/mol), forming a salt bridge and hydrogen bonds (Figure 3-6, Figure 3-7C). This cluster of interactions is facilitated by PS1 Arg108, which interacts with the main chain carbonyl groups of the substrate residues Ala21 and Glu22, forming hydrogen bonds and stabilizing the substrate N-terminus. These interactions are not formed in the PS2 complex, as Arg108 is replaced with Glu114 in PS2 (Figure 3-6, Figure 3-7C). Additionally, a network of hydrophobic interactions forms between substrate residue Ile32 ($\Delta\Delta G_{PS \text{ Pref}} = +2.53$ kcal/mol), with PS1 Ile114 and Tyr240, and Met35 ($\Delta\Delta G_{PS \text{ Pref}} = +1.81$ kcal/mol), with PS1 Leu172, Phe177 and Val236 (Figure 3-6, Figure 3-7D). These interactions do not form in the PS2 γ complex; notably, PS1 residue Leu172 is not conserved (analogous PS2 residue is Met178), nor is the residue immediately adjacent to Phe177 (PS1 Phe176 analogous PS2 residue is Leu182), likely influencing the observed interactions between the PS1 γ and PS2 γ complex. The substrate helix itself in the PS2 γ complex is observably disrupted at its di-glycine motif, which has been identified as a point of flexibility in APP,⁷⁵ and also likely contributes to the reduced interactions with PS2 residues in the substrate binding pocket. Lastly, interactions involving Ile47 ($\Delta\Delta G_{PS \text{ Pref}} = +1.91$ kcal/mol), at the C-terminal end of the substrate, which interacts via hydrogen bonds to the backbone and hydrophobic

interactions to the sidechain of Leu432 ($\Delta\Delta G_{\text{PS Pref}} = +1.63$ kcal/mol), are not replicated in the PS2 γ complex.

The A β 45 substrate, which is cleaved to the A β 42 product, similarly shows a preference for binding to PS1 γ over PS2 γ . Key residues contributing to this preference include the nicastrin residue Glu245 ($\Delta\Delta G_{\text{PS Pref}} = +1.84$ kcal/mol), which is positioned proximally to a cluster of residues in the N-terminal juxta-membrane region that contribute to the preference for PS1 γ , specifically, Val18 ($\Delta\Delta G_{\text{PS Pref}} = +1.72$ kcal/mol), Phe20 ($\Delta\Delta G_{\text{PS Pref}} = +3.54$ kcal/mol), Ala21 ($\Delta\Delta G_{\text{PS Pref}} = +1.56$ kcal/mol) (Figure 3-6, Figure 3-7E). The N-terminal region of the substrate appears to be stabilized by cation- π interactions between PS1 Arg108 and substrate residue Phe20; equivalent interactions do not occur in the PS2 γ complex as the analogous residue to Arg108 in PS2 is the negatively charged Glu114. The primary PS1 residues that contribute to this preference are Ala431 ($\Delta\Delta G_{\text{PS Pref}} = +2.23$ kcal/mol), which forms hydrophobic interactions with Ile45, and the adjacent Leu432 ($\Delta\Delta G_{\text{PS Pref}} = +4.36$ kcal/mol), which forms hydrogen bonds between the backbone amide group and the carbonyl of Val44 ($\Delta\Delta G_{\text{PS Pref}} = +3.45$ kcal/mol) in the substrate. Additionally, the substrate residue Thr43 ($\Delta\Delta G_{\text{PS Pref}} = +2.55$ kcal/mol) contributes to the PS1 γ complex preference via hydrophobic interactions between its side chain carbon and the sidechains of PS1 Val261 and Val272. The β -strand of the substrate contributing to the hybrid β -sheet with presenilin is disrupted in the PS2 γ complex, which appears to preclude the majority of these interactions from occurring (Figure 3-6, Figure 3-7F).

The final complexes modelled in the A β 42 pathway feature A β 42 itself as the substrate, positioned for the generation of A β 38 as the final product in the pathway. From the binding free energies determined by MM-GB/SA, this substrate exhibits a preference for PS1 γ over PS2 γ . The preference is driven by the PS1 residue Phe176 ($\Delta\Delta G_{\text{PS Pref}} = +2.44$ kcal/mol), which can form NH- π interactions⁷⁶ with the substrate residue Asn27. An equivalent interaction is unable to form in the PS2 γ complex, as Phe176 is replaced by Leu182 (Figure 3-7G). Substrate residues Val24 ($\Delta\Delta G_{\text{PS Pref}} = +2.33$ kcal/mol) and Lys28 ($\Delta\Delta G_{\text{PS Pref}} = +2.37$ kcal/mol) (specifically, carbons along the sidechain) interact with Tyr240 ($\Delta G_{\text{bind PS1}} = -1.51$ kcal/mol) and Ile114 ($\Delta\Delta G_{\text{PS Pref}} = +0.98$ kcal/mol) in PS1, respectively, via hydrophobic interactions (Figure 3-6, Figure 3-7G). Additionally, the substrate residues Ile41 ($\Delta\Delta G_{\text{PS Pref}} = +1.76$ kcal/mol) and Ala42 ($\Delta\Delta G_{\text{PS Pref}} = +2.73$ kcal/mol) form a spatial cluster of residues at the C-terminus of the substrate that contribute to the PS1 complex preference. This cluster of interactions is predominated by salt-bridge interactions between PS1 Lys380 ($\Delta\Delta G_{\text{PS Pref}} =$

+2.26 kcal/mol) and Lys429 ($\Delta\Delta G_{PS Pref} = +1.45$ kcal/mol) with the carboxyl group on the C-terminus of the substrate, interactions that do not occur in the modelling of the PS2 complex (Figure 3-6, Figure 3-7H).

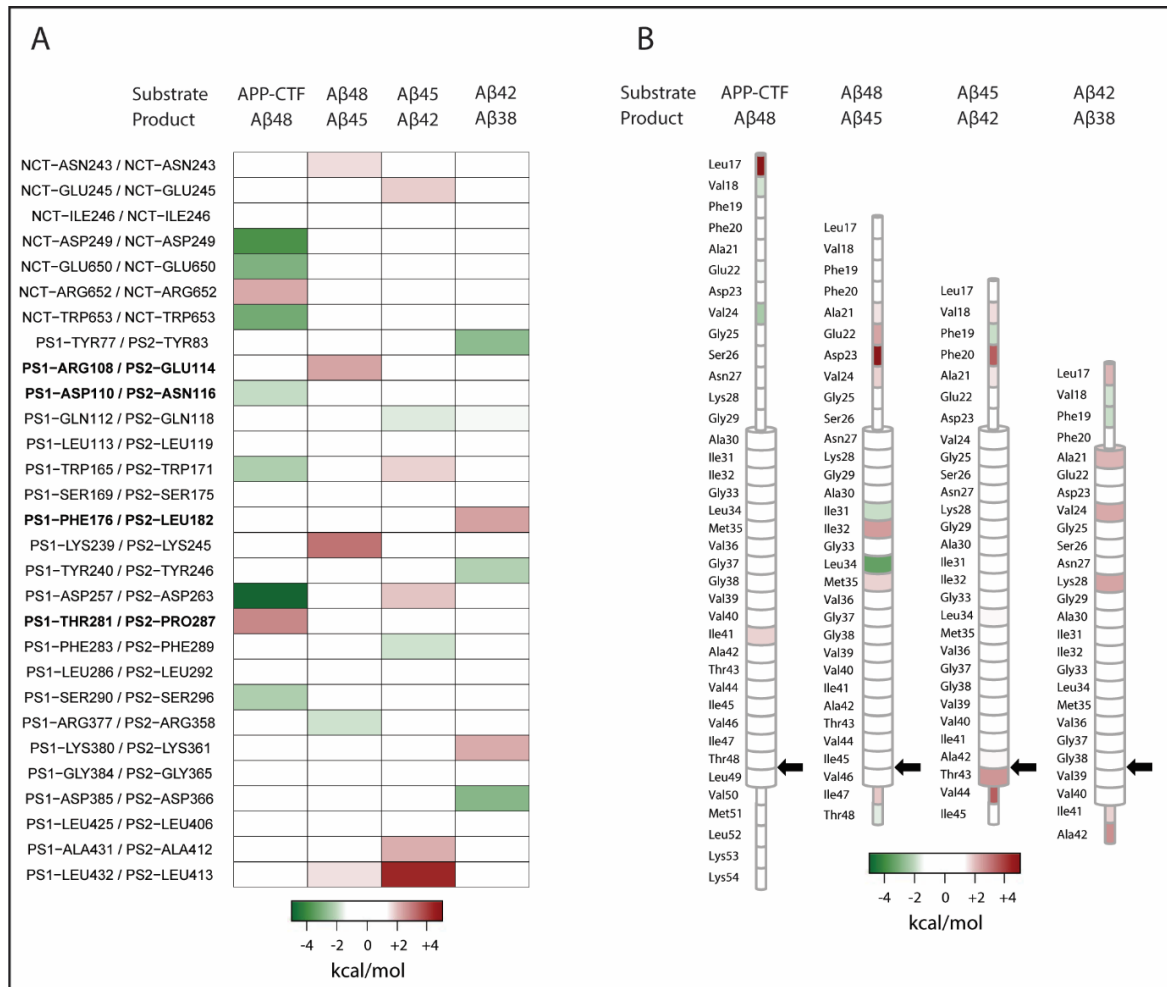


Figure 3-6 Aβ42 pathway complexes per residue heatmaps of $\Delta\Delta G_{PS Pref}$

Enzyme $\Delta\Delta G_{PS Pref}$ values (A). Only residues where the $\Delta\Delta G_{PS Pref}$ magnitude is greater than 1.5 kcal/mol in any complex are shown. Substrate $\Delta\Delta G_{PS Pref}$ values (B). Cleavage position denoted by arrow. Positive (red) $\Delta\Delta G_{PS Pref}$ values indicate preference for PS1, negative (green) $\Delta\Delta G_{PS Pref}$ values indicate preference for PS2.

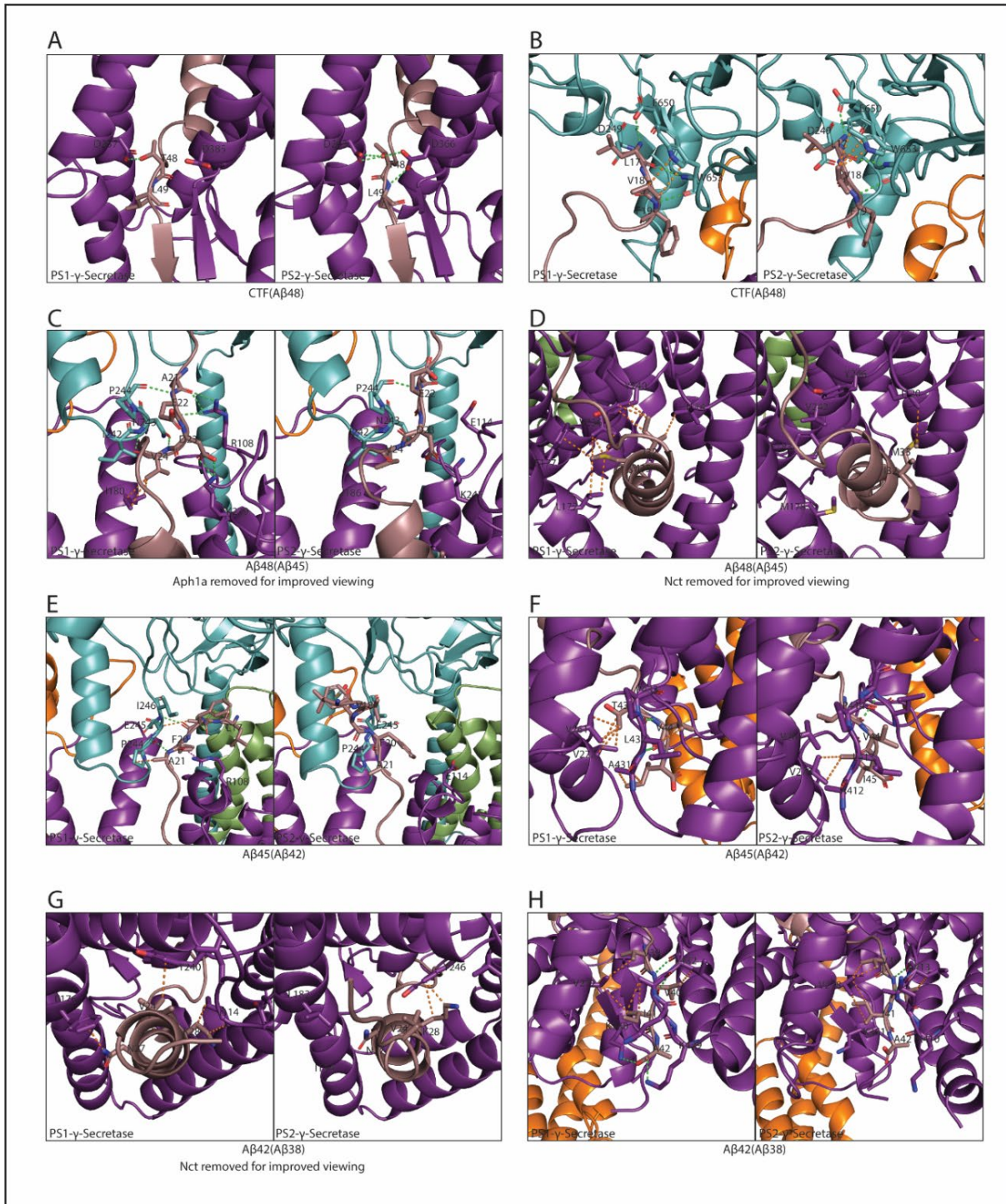


Figure 3-7 Representative structures of substrate – enzyme molecular interactions contributing to $\Delta\Delta G_{PS Pref}$ in $A\beta_{42}$ pathway.

APP-CTF($A\beta_{48}$) substrate cleavage site residues Thr48 – Leu49 (A), APP-CTF($A\beta_{48}$) substrate N-terminal residues Leu17 – phe19 (B), $A\beta_{48}(A\beta_{45})$ substrate N-terminal juxta-membrane residues Ala21 – Val24 (C), $A\beta_{48}(A\beta_{45})$ substrate TM residues Ile32 – Met35 (D), $A\beta_{45}(A\beta_{42})$ substrate N-terminal residues Leu17 – Ala21 (E), $A\beta_{45}(A\beta_{42})$ substrate C-terminal residues Thr43 – Ile45 (F), $A\beta_{42}(A\beta_{38})$ N-terminal juxta-membrane residues Val24 – Lys28 (G), $A\beta_{42}(A\beta_{38})$ C-terminal residues Val39 – Ala42 (H). Complex components represented in cartoon coloured as nicastrin = teal, presenilin1/presenilin2 = purple, APH1 = green, PEN2 = orange, substrate = light pink, with specific residues involved in interactions

depicted in stick format. Hydrogen bonds represented in green dashed lines, π interactions represented by purple dashed lines, hydrophobic interactions represented in orange dashed lines.

3.3.5 WTMetaD and binding free energy calculations for PS1 γ and PS2 γ bound to Notch1 substrates

Given the functional implications of Notch1 inhibition, it is imperative that Notch1 processing by γ -secretase is considered in future therapeutic targeting of the enzyme. Consequently, Notch1 was examined, bound to PS1 γ and PS2 γ enzymes positioned for processing at the two primary S3 sites - Val1754/Leu1755 and Gly1753/Val1754 - and the two primary S4 sites - Val1745/Leu1746 and Ala1741/Ala1742. The cryoEM structure of PS1 γ bound to Notch1 in the Val1754/Leu1755 (PDB: 6IDF)³³ was used to generate homology models of PS1 γ and PS2 γ enzymes bound to substrates in the S3 and S4 positions.

WTMetaD in the position along and deviation from the path was performed, using the path derived from targeted MD. WTMetaD of all four substrate/cleavage positions in complex with the PS1 γ or PS2 γ enzyme revealed only one energetic minimum for each complex, except for PS1 γ bound to the S3 substrate in position to cleave at the Ala1741/Ala1742 S4 site, where two minima are evident (Figure 3-8). The energetic minima derived from the PS2 γ bound to NEXT in the two S3 cleavage positions are both in a more 6IDF-like position (PS2:NEXT(VL) $s \approx 14$, $z \approx 0.04$; PS2:NEXT(GV) $s \approx 15$, $z \approx 0.04$) compared with the PS1 γ complexes (PS1:NEXT(VL) $s \approx 12$, $z \approx 0.04$; PS2:NEXT(GV) $s \approx 11$, $z \approx 0.04$). The resultant S3 product, after the cleavage and release of the NICD1, was then examined. The energetic minima for the substrate positioned for either of the S4 cleavages are similar (PS1:S3(VL) $s \approx 14$, $z \approx 0.04$; PS2:S3(VL) $s \approx 13$, $z \approx 0.04$, PS1:S3(AA) $s \approx 12$, $z \approx 0.05$ and $s \approx 14$, $z \approx 0.05$; PS2:S3(AA) $s \approx 14$, $z \approx 0.04$).

The binding energies for the Notch complexes were determined by MM-GB/SA using the structures corresponding to the energetic minima derived from WTMetaD (Table 3-2). The data indicates that the NEXT substrate demonstrates a considerable preference for binding PS2 γ in both the Val1754/Leu1755 and Gly1753/Val1754 positions compared to PS1 γ . Similarly, the S3 substrate positioned to cleave at the Val1745/Leu1746 S4 site exhibits a preference for binding to PS2 γ . The S3 substrate positioned to cleave at the Ala1741/Ala1742 S4 site, however, preferentially binds PS1 γ .

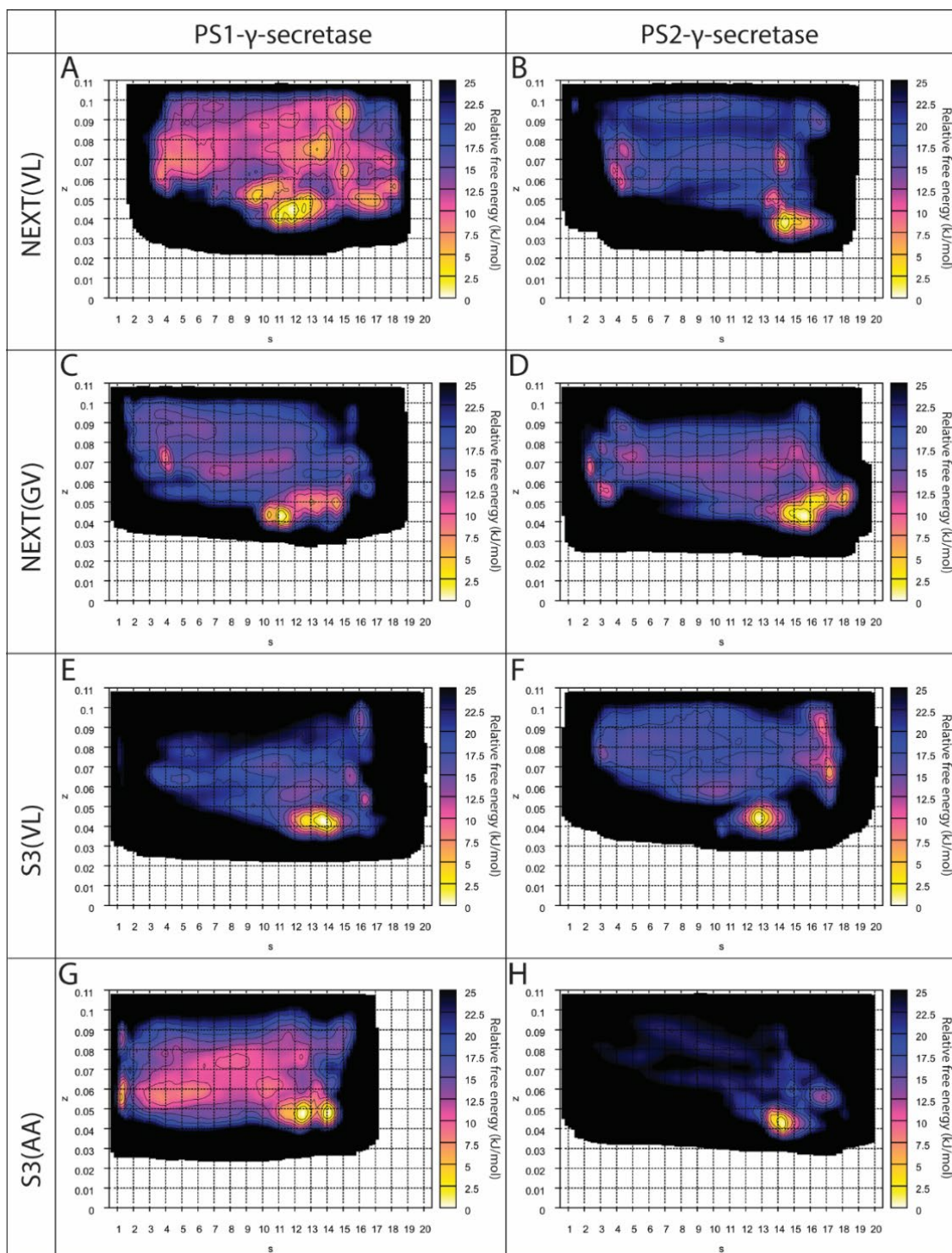


Figure 3-8 Well-tempered metadynamics simulations of PS1 γ and PS2 γ in complex with Notch1 substrates.

Relative free energy surfaces for PS1 γ (A, C, E, G) and PS2 γ (B, D, F, H) in complex with substrates [denoted as substrate(cleavage position)] NEXT(VL) (A, B), NEXT(GV) (C, D), S3(VL) (E, F), S3(AA) (G, H).

Table 3-2 MM-GB/SA binding free energy of γ -secretase – Notch1 bound complexes

Substrate	Cleavage position	PS1 [§]	PS2 [§]
Next	V1754/L1755	-193.1 ± 5.5	-220.1 ± 2.1
Next	G1753/V1754	-175.6 ± 4.2	-214.1 ± 1.6
Notch-S3	V1745/L1746	-166.4 ± 1.1	-199.3 ± 1.9
Notch-S3	A1741/A1742	-181.5 ± 1.1*	-154.0 ± 2.7

*The PS1 γ complex bound to Notch-S3 in the cleavage position A1741/A1742 has a second minima located at $s = 13$ to $s = 14$ and $z = 0.04$ to $z = 0.055$, this complex conformation has a MMGBSA binding free energy of -180.4 ± 1.3 kcal/mol

§Values shown are in kcal/mol +/- standard error

3.3.6 Per-residue decomposition of binding free energies for γ -secretase – Notch1 bound complexes.

The preference of the NEXT substrate bound in position to cleave at the S3 site (Val1754/Leu1755) for binding to PS2 γ over PS1 γ is determined by a cluster of residues at the substrate N-terminus – Val1721 ($\Delta\Delta G_{PS \text{ Pref}} = -10.29$ kcal/mol), Gln1722 ($\Delta\Delta G_{PS \text{ Pref}} = -2.20$ kcal/mol), Ser1723 ($\Delta\Delta G_{PS \text{ Pref}} = -2.91$ kcal/mol) and Glu1724 ($\Delta\Delta G_{PS \text{ Pref}} = -2.21$ kcal/mol) – that form several hydrogen bonds and electrostatic interactions with nicastrin residue Asp655 ($\Delta\Delta G_{PS \text{ Pref}} = -7.85$ kcal/mol), none of which occur in the PS1 γ complex (Figure 3-9, Figure 3-10A). Further to this, the substrate residue Val1745 ($\Delta\Delta G_{PS \text{ Pref}} = -2.62$ kcal/mol) forms hydrophobic interactions with carbon atoms in the sidechains of PS2 Met174 ($\Delta\Delta G_{PS \text{ Pref}} = -0.77$ kcal/mol) and Ser175 ($\Delta\Delta G_{PS \text{ Pref}} = -0.97$ kcal/mol) (Figure 3-9, Figure 3-10B). Met174 is not conserved between PS homologues, with the analogous residue in PS1 being Ile168. The PS1 Ile168 faces outward to interact with the lipid bilayer rather than the substrate, while the PS2 Met174 interacts with the substrate. Additionally, Phe1748 ($\Delta\Delta G_{PS \text{ Pref}} = -2.28$ kcal/mol) in the substrate interacts with PS2 Trp171 ($\Delta\Delta G_{PS \text{ Pref}} = -1.83$ kcal/mol) via a π - π interaction, while PS2 Leu292 ($\Delta\Delta G_{PS \text{ Pref}} = -2.27$ kcal/mol) forms a CH- π bond with the substrate residue Phe1749 ($\Delta\Delta G_{PS \text{ Pref}} = -1.03$ kcal/mol). The protonated catalytic aspartate, PS2 Asp366 ($\Delta\Delta G_{PS \text{ Pref}} = -2.76$ kcal/mol), forms a hydrogen bond with the carbonyl group on the backbone of the substrate cleavage site residue, Val1754 ($\Delta\Delta G_{PS \text{ Pref}} = -0.72$ kcal/mol).

Similarly, the NEXT substrate bound to be cleaved at the S3 site (Gly1753/Val1754) demonstrates a preference for PS2 γ over PS1 γ . This preference is predominantly driven by interactions with the N- and C-terminus of the substrate. At the substrate N-terminus, nicastrin residue Asp655 ($\Delta\Delta G_{PS \text{ Pref}} = -2.49$ kcal/mol) and the substrate residue Val1721 ($\Delta\Delta G_{PS \text{ Pref}} = -4.80$ kcal/mol) form a salt-bridge between the N-terminal amino group of the substrate and

the aspartate side chain carboxyl group; additional hydrophobic interactions between the valine side chain and the mainchain α -carbon also occur. The adjacent substrate residue, Gln1722 ($\Delta\Delta G_{\text{PS Pref}} = -5.40$ kcal/mol), forms hydrogen bonds with nicastrin residues Glu245 ($\Delta\Delta G_{\text{PS Pref}} = -0.35$ kcal/mol) and Arg652 ($\Delta\Delta G_{\text{PS Pref}} = -0.67$ kcal/mol) (Figure 3-9, Figure 3-10C). Reorganization of the substrate N-terminal loop in the PS1 γ complex relative to that in the PS2 γ complex precludes these interactions from occurring. At the substrate C-terminus, a network of hydrogen bonds and electrostatic interactions occurs between Gln282 ($\Delta\Delta G_{\text{PS Pref}} = -2.54$ kcal/mol) and Glu283 ($\Delta\Delta G_{\text{PS Pref}} = -2.57$ kcal/mol) with the substrate residues Arg1758 ($\Delta\Delta G_{\text{PS Pref}} = -1.27$ kcal/mol), Arg1760 ($\Delta\Delta G_{\text{PS Pref}} = -6.87$ kcal/mol) and Arg1761 ($\Delta\Delta G_{\text{PS Pref}} = -2.36$ kcal/mol). Repositioning of the TM6a helix in the PS1 γ complex prevents these interactions from occurring (Figure 3-9, Figure 3-10D). Additional residues throughout the substrate further contribute to the preference for the PS2 γ complex, including: Leu1747 ($\Delta\Delta G_{\text{PS Pref}} = -2.73$ kcal/mol), which forms CH- π interactions with PS2 Trp171 ($\Delta\Delta G_{\text{PS Pref}} = -0.83$ kcal/mol); Gly1751 ($\Delta\Delta G_{\text{PS Pref}} = -2.08$ kcal/mol), where the carbonyl group forms a hydrogen bond with the main chain amide group of PS2 Leu364 ($\Delta\Delta G_{\text{PS Pref}} = -2.05$ kcal/mol); and Val1754 ($\Delta\Delta G_{\text{PS Pref}} = -2.35$ kcal/mol) (the C-terminal-most residue of the substrate cleavage site), where a hydrogen bond occurs between the main chain carbonyl group and the main chain amine group of PS2 Ala415 ($\Delta\Delta G_{\text{PS Pref}} = -0.90$ kcal/mol), which occurs in the PAL motif of PS2. None of these interactions are evident in the equivalent PS1 γ substrate complex.

The binding energies for the enzyme bound to the S3 substrate in position for the final γ -secretase cleavage at S4 site Val1745/Leu1746 suggest a substrate binding preference for PS2 γ (Table 2). This preference is supported by three key interacting regions. At the luminal juxtamembrane region, the substrate residue Val1726 ($\Delta\Delta G_{\text{PS Pref}} = -2.21$ kcal/mol) forms hydrophobic interactions with nicastrin residues Phe240 and Ile242 ($\Delta\Delta G_{\text{PS Pref}} = -2.08$ kcal/mol), which do not occur in the PS1 γ complex. Two PS2 residues, Met152 ($\Delta\Delta G_{\text{PS Pref}} = -2.25$ kcal/mol) and Phe183 ($\Delta\Delta G_{\text{PS Pref}} = -2.29$ kcal/mol), co-ordinate CH- π interactions with substrate residues Tyr1738 and Met1737 respectively, that do not occur in the PS1 γ complex (Figure 3-9, Figure 3-10E). Lastly, a cluster of substrate residues around the cleavage site and PS2 residues in spatial proximity to these substrate residues contribute to the PS2 γ complex preference. Several polar interactions, a CH- π interaction and hydrophobic interactions are evident between substrate residues Phe1744 ($\Delta\Delta G_{\text{PS Pref}} = -1.80$ kcal/mol), Leu1746 ($\Delta\Delta G_{\text{PS Pref}} = -2.86$ kcal/mol), Leu1747 ($\Delta\Delta G_{\text{PS Pref}} = -3.65$ kcal/mol), and Phe1748 ($\Delta\Delta G_{\text{PS Pref}} = -2.68$ kcal/mol) with PS2 residues Leu292 ($\Delta\Delta G_{\text{PS Pref}} = -3.55$ kcal/mol), Lys361, Gly363, Gly365

and Leu413 ($\Delta\Delta G_{\text{PS Pref}} = -3.35$ kcal/mol), the majority of which do not occur in the PS1 γ complex (Figure 3-9, Figure 3-10F).

The S3 substrate in position to cleave at the Ala1741/Ala1742 S4 site for peptide release shows a preference for binding to PS1 γ over PS2 γ , unlike the other Notch complexes. This preference for binding to PS1 γ is predominantly driven by the interactions of the substrate C-terminal residues. Phe1748 ($\Delta\Delta G_{\text{PS Pref}} = +5.23$ kcal/mol) and Leu1747 ($\Delta\Delta G_{\text{PS Pref}} = +6.14$ kcal/mol) utilize the C-terminal carboxyl group and main chain carbonyl group, respectively, to form a salt bridge and hydrogen bonds with PS1 Lys380 ($\Delta\Delta G_{\text{PS Pref}} = +1.40$ kcal/mol). Leu1747 ($\Delta\Delta G_{\text{PS Pref}} = +6.14$ kcal/mol) forms hydrophobic interactions with the carbons along the length of the sidechain of Thr281 ($\Delta\Delta G_{\text{PS Pref}} = +2.03$ kcal/mol) and Arg377 ($\Delta\Delta G_{\text{PS Pref}} = +1.45$ kcal/mol) (Figure 3-9, Figure 3-10G). None of these interactions occur in the PS2 complex, and notably, the PS1 residue Thr281 is not conserved in PS2, with the analogous residue being Pro287. Further contributions to the PS1 γ complex preference occur within the substrate transmembrane domain, facilitated by Ala1732 ($\Delta\Delta G_{\text{PS Pref}} = +1.58$ kcal/mol), which forms hydrophobic interactions with the side chains of PS1 residues Trp165 ($\Delta\Delta G_{\text{PS Pref}} = +0.67$ kcal/mol), and Ile168 ($\Delta\Delta G_{\text{PS Pref}} = +0.29$ kcal/mol), and Tyr1738 ($\Delta\Delta G_{\text{PS Pref}} = +2.56$ kcal/mol), where the main chain carbonyl forms a hydrogen bond with the amide of PS1 Gly384 ($\Delta\Delta G_{\text{PS Pref}} = +0.29$ kcal/mol). Neither interaction occurs in the PS2 γ complex (Figure 3-9, Figure 3-10H).

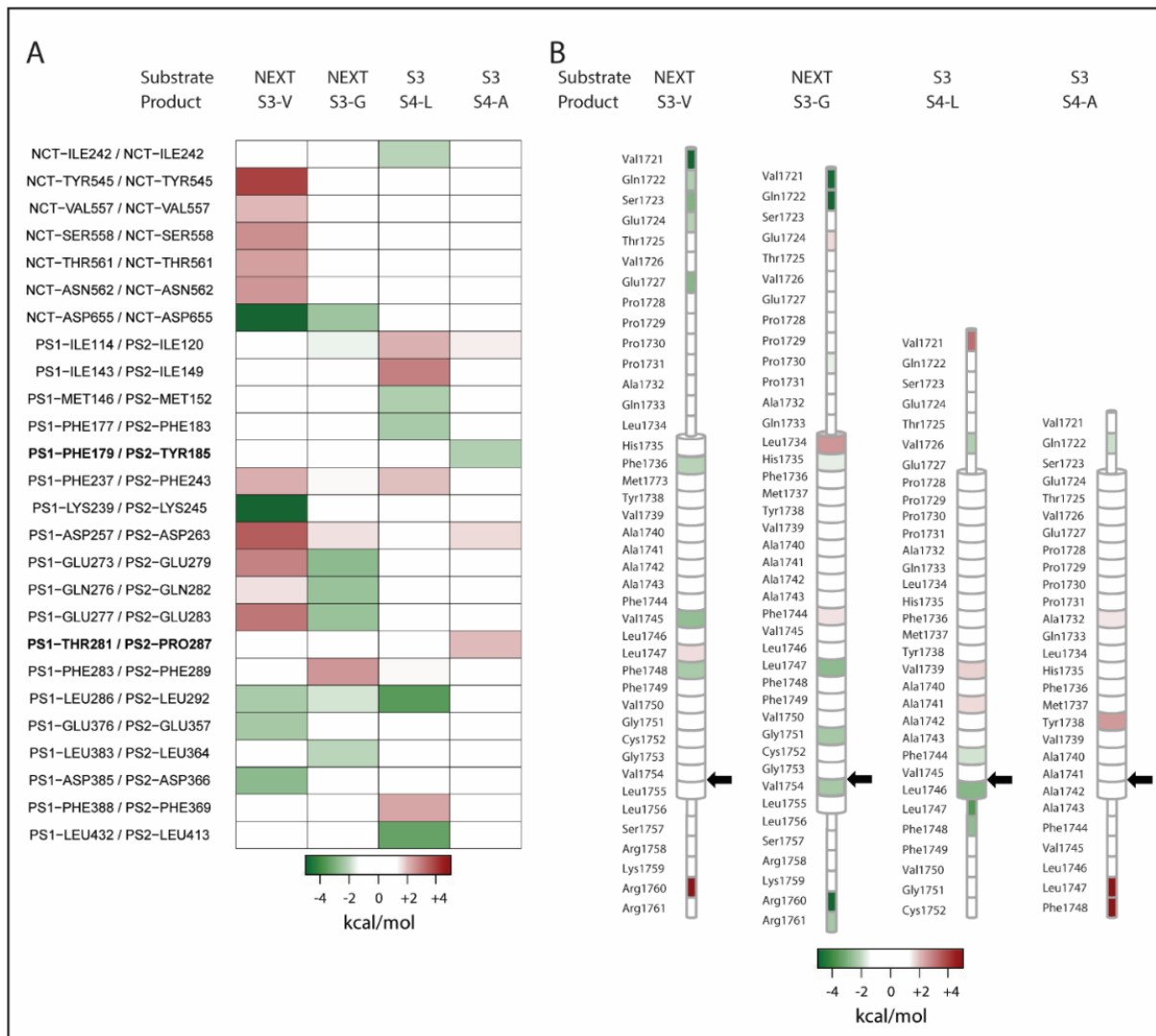


Figure 3-9 Notch1 complexes per residue heatmaps of $\Delta\Delta G_{PS Pref}$.

Enzyme $\Delta\Delta G_{PS Pref}$ values (A). Only residues where the $\Delta\Delta G_{PS Pref}$ magnitude is greater than 1.5 kcal/mol in any complex are shown. Substrate $\Delta\Delta G_{PS Pref}$ values (B). Cleavage position denoted by arrow. Positive (red) $\Delta\Delta G_{PS Pref}$ values indicate preference for PS1, negative (green) $\Delta\Delta G_{PS Pref}$ values indicate preference for PS2.

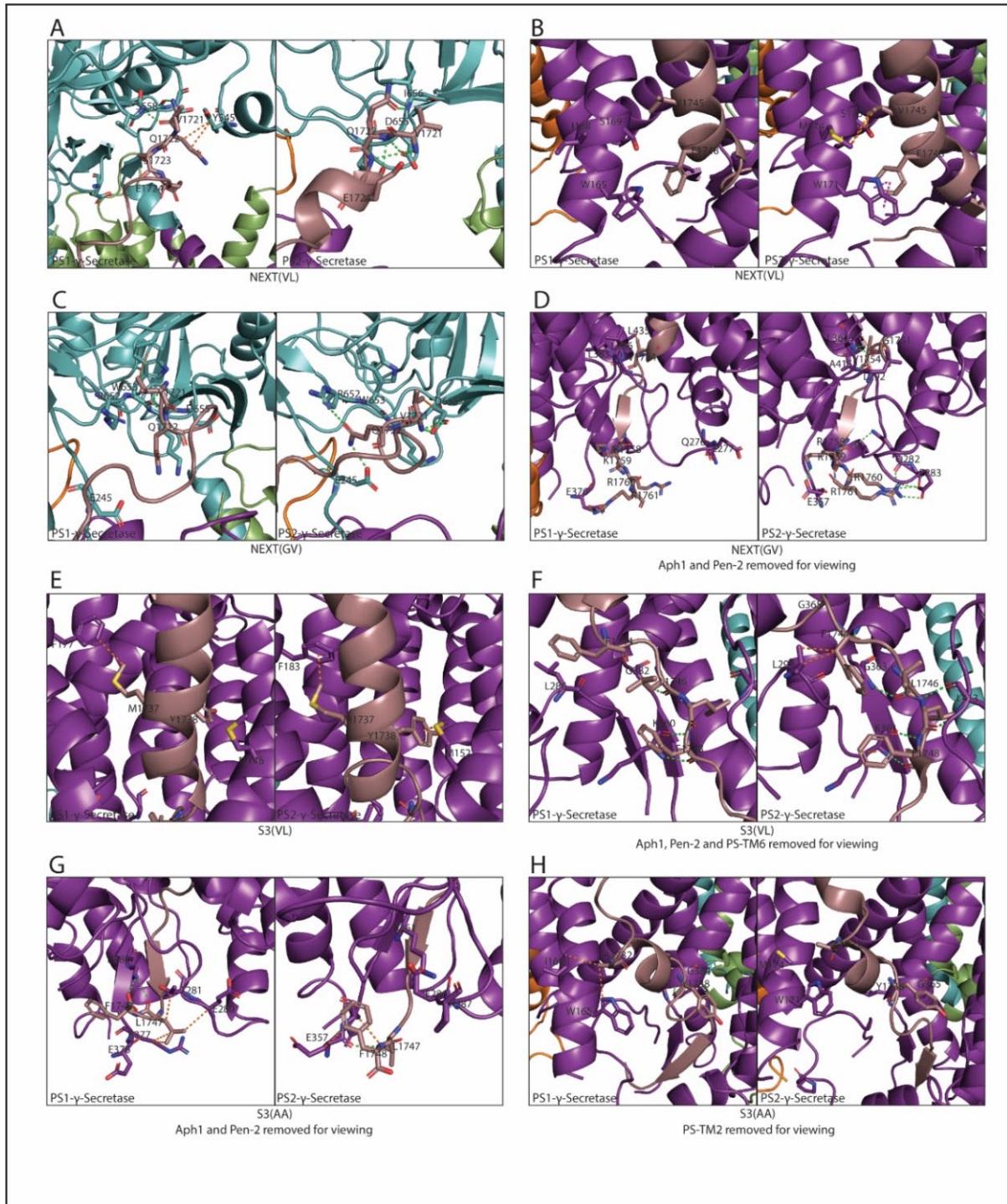


Figure 3-10 Representative structures of substrate – enzyme molecular interactions contributing to $\Delta\Delta G_{PS Pref}$ in Notch1 cleavage

NEXT(VL) substrate N-terminus residues Val1721 – Glu1724 (A) NEXT(VL) substrate TM residues Val1745 – Phe1748 (B) NEXT(GV) substrate N-terminal residues Val1721 – Gln1722 (C) NEXT(GV) substrate C-terminal inner leaflet – juxta-membrane residues Gly1751 – Arg1761 (D) S3(VL) substrate TM residues Met1737 – Tyr1738 (E) S3(VL) substrate C-terminal juxta-membrane residues Phe1744 – Phe1748 (F) S3(AA) substrate C-terminal residues Leu1747 – Phe1748 (G) S3(AA) substrate TM residues Ala1732 – Tyr1738 (H). Complex components represented in cartoon coloured as nicastrin = teal, presenilin1/presenilin2 = purple, APH1 = green, PEN2 = orange, substrate = light pink, with specific residues involved in interactions depicted in stick format. Hydrogen bonds represented

in green dashed lines, π interactions represented by purple dashed lines, hydrophobic interactions represented in orange dashed lines.

3.4 DISCUSSION

The propensity for either PS1 γ or PS2 γ to generate a specific profile of A β species is a function of both the initial cleavage site and the subsequent likelihood of the successive tri/tetra-peptide cleavage events occurring. In this study, well-tempered metadynamics simulations were undertaken for PS1 γ and PS2 γ enzymes complexes with the initial and intermediate APP substrates of the two major A β species, as well as Notch1-derived substrates. These simulations were analysed to determine the likely low energy states for γ -secretase-substrate complexes and the binding free energy for each substrate bound to γ -secretase. All data was generated and compared for both PS1 γ and PS2 γ enzymes in order to assess enzyme preference for given substrates.

The metadynamics results presented here suggest a comparable ability for PS1 γ complexes to initiate either the A β 40 or A β 42 pathway (Figure 3-2A, Figure 3-3A), while binding of subsequent substrates in the A β 40 pathway (Figure 3-2B-D) involves a restricted conformational ensemble and may be less favorable. PS1 γ binding free energy results indicate a preference for binding APP in the position to initiate the A β 42 pathway. Interestingly, subsequent substrates in both pathways are generally more efficiently bound, suggesting that PS1 γ processing of APP likely leads to the release of shorter A β peptides (Table 3-1). The metadynamics results for PS2 γ suggest a preference for PS2 γ to initiate the A β 42 pathway over the A β 40 pathway, marked by a less restricted versus a more restricted conformational ensemble for binding the respective substrates (Figure 3-2B, Figure 3-3B). The subsequent substrates in each pathway, however, elicit broad conformational flexibility in PS2 γ , with the exception of the A β 42(A β 38) substrate, which yields a restricted conformational ensemble and may suggest reduced propensity for PS2 γ to generate A β 38 products (Figure 3-3H). Binding free energy results for PS2 γ complexes support a considerable preference for binding APP-CTF to initiate the A β 42 pathway. Interestingly, PS2 γ generally binds subsequent substrates in both pathways with lower binding energy (Table 3-1), suggesting that PS2 γ may generate longer A β products.

While it is likely that Notch undergoes similar tri- and tetra-peptide successive cleavage, this detail has not been elucidated; however, multiple initial cleavage (S3 sites) and final cleavage (S4 sites) γ -secretase sites have been identified.^{28,29,77} Here, PS1 γ and PS2 γ binding to Notch1 substrates aligned with the primary S3 and S4 sites were examined. While PS1 γ and PS2 γ complexes bound to the NEXT substrates in the S3 cleavage site positions elicit similar conformational flexibility in γ -secretase, the conformation of γ -secretase suggested by metadynamics simulations in the PS2 complexes is more akin to the cryoEM PS1 γ Notch complex (PDB 6IDF) than the PS1 complexes (Figure 3-8A-D). Furthermore, the PS2:NEXT(VL) and PS2:NEXT(GV) complexes have considerably more favorable binding energies over the equivalent complexes with PS1 (Table 3-2). The data presented here suggests that PS2 γ would preferentially process Notch1 substrates to generate the NICD1 over PS1 γ .

Generation of AICD and NICD1 products is indicative of the propensity for the initial cleavage by PS1 γ and PS2 γ , however, experimental data identifying PS1 γ or PS2 γ ICD generation levels is discordant. Some studies show that PS1 γ generates more AICD (or APP-CTF accumulation) or NICD1,⁷⁸⁻⁸² while others show that PS1 γ and PS2 γ produce similar levels of ICD products.^{17, 50} Notably, these studies are undertaken in different experimental conditions, use different cell lines, and importantly, do not account for differences in PS1 and PS2 expression that will likely influence total γ -secretase activity levels. In Chapter 2 it was shown that PS1 expression is approximately 5-times that of PS2 expression and that this expression profile is retained in an exogenous expression system in HEK293 cells. Subsequently when PS expression was accounted for, PS2 γ processed more APP and Notch substrate than PS1 γ in an exogenous system.⁵³ In this study, both PS1 γ and PS2 γ have comparable conformational flexibility when bound to NEXT substrates (Figure 3-8A-D). However, the substantial preference for PS2 γ binding of NEXT substrates (Table 3-2) shown in this study supports the notion that PS2 γ would generate more NICD1 product at an individual enzymatic level.

With respect to APP processing, it is the initial cleavage position and the different propensities for PS1 γ vs PS2 γ to cleave these, that is important in the context of AD and A β generation. However, any preference for the initial cleavage site between PS1 γ and PS2 γ remains contentious; one study⁸³, using PS1+/+ PS2+/+ genotype HEK293 and HeLa cells, shows that the AICD products aligning with A β 42 pathway initiation predominates in endosomal fractions, where PS2 localises,^{50, 81} whereas AICD products aligning with A β 40 pathway initiation predominate in plasma membrane fractions, where PS1 primarily localises.^{50, 81}

Another study shows that both PS1 γ and PS2 γ generate similar ratios of the AICD product of both A β 40 and A β 42 pathways.⁸⁴ While studies investigating the gamut of A β products by both PS1 γ and PS2 γ are not plentiful, PS2 γ has been shown to generate a higher A β 42:A β 40 ratio than PS1 γ .^{47, 52, 53, 85} Additionally, PS1 γ generates higher levels of A β 38 than A β 42, while the opposite is true of PS2 γ .^{78, 80, 84, 86} The final A β profile generated by γ -secretase is affected not only by the initial cleavage site, but also by the likelihood of continued processing. The data presented in this study shows that PS2 γ not only has a preference for binding to CTF(A β 48), but also a broader conformational ensemble when binding this substrate, compared with CTF(A β 49) (Table 3-1, Figure 3-2A-B, Figure 3-3A-B), supporting the view that PS2 γ is likely the predominant A β 42-generating enzyme. This is further supported by comparably unfavorable free binding energies of the PS2 γ bound to subsequent substrates of the A β 42 pathway (Table 3-1), and the restricted conformational ensembles observed for the PS2:A β 42(A β 38) complex (Figure 3-3H). Combined, these data indicate that PS2 γ will preferentially initiate A β 42 pathway and will likely release the substrate prior to A β 38 product generation.

Although this study presents, to our knowledge the first WTMetaD application for investigating the γ -secretase, the collective variable space available is due to the availability of only two substrate-bound structures.^{32, 33} This extends to the templates available for homology modelling, where using PS1 γ substrate-bound structures as templates for PS2 γ homology models may introduce inaccuracies. While PS2 γ apo and inhibitor bound structures were recently published,⁸⁷ no substrate bound structures are available. The PS2 γ apo state structure is remarkably similar to the PS1 γ apo structure, with only minor differences in the positioning of TM6, TM7 and the loop containing the PAL motif between TM8 and TM9. Additionally, as the MRK-560 inhibitor is selective for PS1, it is not resolved in the PS2 γ MRK-560 bound structure, and the conformational alterations that occur with inhibitor binding, that mimic the effects of substrate binding, do not occur. Consequently, these PS2 γ structures are not representative of the substrate bound state and do not currently offer a superior template for use in homology modelling. Lastly, we must acknowledge that the PS1 γ APP bound structure (PDB: 6IYC) is bound to the APP-C83 substrate, and not APP-C99 which gives rise to the aggregative A β products. APP-C83 substrate interaction with γ -secretase is stronger than the APP-C99 substrate, as shorter ectodomain substrates are preferred.⁸⁸ This improved substrate interaction is more amenable for purification and subsequent successful cryoEM, with the

authors commenting that the interactions observed between PS1 γ and APP-C83 are likely to be identical for APP-C99.³²

Improved understanding of PS1 γ and PS2 γ specific substrate processivity and the repertoire of enzyme-substrate conformations is critical for the future development of novel γ -secretase targeting therapeutics. Following the failures of γ -secretase inhibitors to gain traction, attention has turned to the development of molecules that selectively inhibit the processing of APP – γ -secretase modulators (GSM). These molecules functionally lead to increased production of shorter A β products, in particular A β 38 and A β 37, with concomitant reductions in the A β 42 and A β 40 products, and leave the processing of Notch and other substrate unaffected.^{44, 84, 86, 89-91} The atomic structure of PS1 γ bound to the GSM E2012 was recently solved, however this structure was also bound with the GSI L685,458 making it difficult to identify the specific GSM mechanism of action.⁴⁴ However an earlier study, that identified the same binding site for E2012 by substituted cysteine accessibility method proposed that it facilitated an upward shift of TM1 in the membrane increasing the retention time of APP and/or improving the processivity of γ -secretase to produce shorter A β peptides.⁹² This study identifies conformational bottlenecks between PS1 γ and PS2 γ , in particular, with APP processing, presenting opportunities to stabilize or destabilize specific states. Additionally, providing insight into γ -secretase targeting more broadly, i.e. APP vs Notch vs other substrates, as different types of substrates are shown to affect γ -secretase conformation differently; which may be harnessed for future structure based drug design.⁹³ Notably, different conformations between PS1 γ and PS2 γ bound to NEXT substrates are observed, implying that PS1 γ and PS2 γ complexes could be targeted differently. This is supported by PS1 vs PS2 selectivity that is already evident in γ -secretase-targeting small molecules that have been developed through traditional medicinal chemistry pipelines.^{51, 80, 86, 87} This study provides insight into the conformational repertoire of γ -secretase bound to the various substrates within a cleavage pathway, improving the understanding of substrate processivity and highlights the importance of due consideration for both PS1 γ and PS2 γ in structure-based drug design.

3.5 REFERENCES

1. World Health Organisation. (2021) Towards a dementia-inclusive society: WHO toolkit for dementia-friendly initiatives (DFIs). World Health Organisation, Geneva
2. Serrano-Pozo, A., Frosch, M. P., Masliah, E., and Hyman, B. T. (2011) Neuropathological alterations in Alzheimer disease. *Cold Spring Harbor Perspectives in Medicine* **1**, a006189
3. Gravina, S. A., Ho, L., Eckman, C. B., Long, K. E., Otvos, L., et al. (1995) Amyloid β Protein ($A\beta$) in Alzheimer's Disease Brain: Biochemical and immunocytochemical analysis with antibodies specific for forms ending at $A\beta$ 40 or $A\beta$ 42(43). *The Journal of Biological Chemistry* **270**, 7013-7016
4. Kuperstein, I., Broersen, K., Benilova, I., Rozenski, J., Jonckheere, W., et al. (2010) Neurotoxicity of Alzheimer's disease $A\beta$ peptides is induced by small changes in the $A\beta$ (42) to $A\beta$ (40) ratio. *The EMBO Journal* **29**, 3408-3420
5. Pauwels, K., Williams, T. L., Morris, K. L., Jonckheere, W., Vandersteen, A., et al. (2012) Structural Basis for Increased Toxicity of Pathological $A\beta$ 42: $A\beta$ 40 Ratios in Alzheimer Disease. *The Journal of Biological Chemistry* **287**, 5650-5660
6. Scheuner, D., Eckman, C., Jensen, M., Song, X., Citron, M., et al. (1996) Secreted amyloid beta-protein similar to that in the senile plaques of Alzheimer's disease is increased in vivo by the presenilin 1 and 2 and APP mutations linked to familial Alzheimer's disease. *Nature Medicine* **2**, 864-870
7. Suzuki, N., Cheung, T. T., Cai, X. D., Odaka, A., Otvos, L., Jr., et al. (1994) An increased percentage of long amyloid beta protein secreted by familial amyloid beta protein precursor (beta APP717) mutants. *Science* **264**, 1336-1340
8. Duff, K., Eckman, C., Zehr, C., Yu, X., Prada, C. M., et al. (1996) Increased amyloid-beta42(43) in brains of mice expressing mutant presenilin 1. *Nature* **383**, 710-713
9. Luo, J. E., and Li, Y.-M. (2022) Turning the tide on Alzheimer's disease: modulation of γ -secretase. *Cell & Bioscience* **12**, 2
10. Song, C., Shi, J., Zhang, P., Zhang, Y., Xu, J., et al. (2022) Immunotherapy for Alzheimer's disease: targeting β -amyloid and beyond. *Translational Neurodegeneration* **11**, 18
11. Lichtenthaler, S. F., Haass, C., and Steiner, H. (2011) Regulated intramembrane proteolysis – lessons from amyloid precursor protein processing. *Journal of Neurochemistry* **117**, 779-796
12. Bolduc, D. M., Montagna, D. R., Gu, Y., Selkoe, D. J., and Wolfe, M. S. (2016) Nicastrin functions to sterically hinder γ -secretase–substrate interactions driven by substrate transmembrane domain. *Proceedings of the National Academy of Sciences of the United States of America* **113**, E509-E518
13. Sato, T., Diehl, T. S., Narayanan, S., Funamoto, S., Ihara, Y., et al. (2007) Active γ -secretase complexes contain only one of each component. *The Journal of Biological Chemistry* **282**, 33985-33993
14. Shah, S., Lee, S.-F., Tabuchi, K., Hao, Y.-H., Yu, C., et al. (2005) Nicastrin Functions as a γ -Secretase-Substrate Receptor. *Cell* **122**, 435-447
15. Wolfe, M. S., Xia, W., Ostaszewski, B. L., Diehl, T. S., Kimberly, W. T., et al. (1999) Two transmembrane aspartates in presenilin-1 required for presenilin endoproteolysis and γ -secretase activity. *Nature* **398**, 513-517
16. Ahn, K., Shelton, C. C., Tian, Y., Zhang, X., Gilchrist, M. L., et al. (2010) Activation and intrinsic γ -secretase activity of presenilin 1. *Proceedings of the National Academy of Sciences of the United States of America* **107**, 21435-21440

17. Yonemura, Y., Futai, E., Yagishita, S., Kaether, C., and Ishiura, S. (2016) Specific combinations of presenilins and Aph1s affect the substrate specificity and activity of γ -secretase. *Biochemical and Biophysical Research Communications* **478**, 1751-1757
18. Levy-Lahad, E., Wasco, W., Poorkaj, P., Romano, D. M., Oshima, J., et al. (1995) Candidate Gene for the Chromosome 1 Familial Alzheimer's Disease Locus. *Science* **269**, 973-977
19. Sherrington, R., Rogaev, E. I., Liang, Y., Rogaeva, E. A., and et al. (1995) Cloning of a gene bearing missense mutations in early-onset familial Alzheimer's disease. *Nature* **375**, 754-760
20. Tanzi, R. E., Kovacs, D. M., Kim, T. W., Moir, R. D., Guenette, S. Y., et al. (1996) The gene defects responsible for familial Alzheimer's disease. *Neurobiology of disease* **3**, 159-168
21. Wu, L., Rosa-Neto, P., Hsiung, G.-Y. R., Sadovnick, A. D., Masellis, M., et al. (2012) Early-Onset Familial Alzheimer's Disease (EOFAD). *Canadian Journal of Neurological Sciences* **39**, 436-445
22. Takami, M., Nagashima, Y., Sano, Y., Ishihara, S., Morishima-Kawashima, M., et al. (2009) γ -Secretase: Successive tripeptide and tetrapeptide release from the transmembrane domain of β -carboxyl terminal fragment. *The Journal of Neuroscience* **29**, 13042-13052
23. Matsumura, N., Takami, M., Okochi, M., Wada-Kakuda, S., Fujiwara, H., et al. (2014) γ -Secretase associated with lipid rafts: multiple interactive pathways in the stepwise processing of β -carboxyl-terminal fragment. *The Journal of Biological Chemistry* **289**, 5109-5121
24. Siebel, C., and Lendahl, U. (2017) Notch Signaling in Development, Tissue Homeostasis, and Disease. *Physiological Reviews* **97**, 1235-1294
25. Mumm, J. S., Schroeter, E. H., Saxena, M. T., Griesemer, A., Tian, X., et al. (2000) A ligand-induced extracellular cleavage regulates γ -secretase-like proteolytic activation of notch1. *Molecular Cell* **5**, 197-206
26. van Tetering, G., van Diest, P., Verlaan, I., van der Wall, E., Kopan, R., et al. (2009) Metalloprotease ADAM10 is required for Notch1 site 2 cleavage. *The Journal of Biological Chemistry* **284**, 31018-31027
27. Schroeter, E. H., Kisslinger, J. A., and Kopan, R. (1998) Notch-1 signalling requires ligand-induced proteolytic release of intracellular domain. *Nature* **393**, 382-386
28. Tagami, S., Okochi, M., Yanagida, K., Ikuta, A., Fukumori, A., et al. (2008) Regulation of Notch signaling by dynamic changes in the precision of S3 cleavage of Notch-1. *Molecular and Cellular Biology* **28**, 165-176
29. Okochi, M., Steiner, H., Fukumori, A., Tanii, H., Tomita, T., et al. (2002) Presenilins mediate a dual intramembranous gamma-secretase cleavage of Notch-1. *The EMBO Journal* **21**, 5408-5416
30. Bai, X.-c., Yan, C., Yang, G., Lu, P., Ma, D., et al. (2015) An atomic structure of human γ -secretase. *Nature* **525**, 212-217
31. Bai, X.-c., Rajendra, E., Yang, G., Shi, Y., and Scheres, S. H. W. (2015) Sampling the conformational space of the catalytic subunit of human γ -secretase. *eLife* **4**, e11182
32. Zhou, R., Yang, G., Guo, X., Zhou, Q., Lei, J., et al. (2019) Recognition of the amyloid precursor protein by human γ -secretase. *Science*, eaaw0930
33. Yang, G., Zhou, R., Zhou, Q., Guo, X., Yan, C., et al. (2018) Structural basis of Notch recognition by human γ -secretase. *Nature*
34. Hitzenberger, M., and Zacharias, M. (2019) Structural Modeling of γ -Secretase A β n Complex Formation and Substrate Processing. *ACS Chemical Neuroscience* **10**, 1826-1840
35. Somavarapu, A. K., and Kepp, K. P. (2017) Membrane Dynamics of γ -Secretase Provides a Molecular Basis for β -Amyloid Binding and Processing. *ACS Chemical Neuroscience*

36. Aguayo-Ortiz, R., Chavez-Garcia, C., Straub, J. E., and Dominguez, L. (2017) Characterizing the structural ensemble of γ -secretase using a multiscale molecular dynamics approach. *Chemical Science* **8**, 5576-5584
37. Hitzenberger, M., and Zacharias, M. (2018) γ -Secretase Studied by Atomistic Molecular Dynamics Simulations: Global Dynamics, Enzyme Activation, Water Distribution and Lipid Binding. *Frontiers in Chemistry* **6**, 640
38. Dehury, B., Tang, N., and Kepp, K. P. (2019) Molecular dynamics of C99-bound γ -secretase reveal two binding modes with distinct compactness, stability, and active-site retention: implications for A β production. *Biochemical Journal* **476**, 1173-1189
39. Aguayo-Ortiz, R., Straub, J. E., and Dominguez, L. (2018) Influence of membrane lipid composition on the structure and activity of γ -secretase. *Physical Chemistry Chemical Physics* **20**, 27294-27304
40. Chen, S.-Y., and Zacharias, M. (2020) How Mutations Perturb γ -Secretase Active Site Studied by Free Energy Simulations. *ACS Chemical Neuroscience* **11**, 3321-3332
41. Dehury, B., Somavarapu, A. K., and Kepp, K. P. (2020) A computer-simulated mechanism of familial Alzheimer's disease: Mutations enhance thermal dynamics and favor looser substrate-binding to γ -secretase. *Journal of Structural Biology* **212**, 107648
42. Mehra, R., and Kepp, K. P. (2021) Computational prediction and molecular mechanism of γ -secretase modulators. *European Journal of Pharmaceutical Sciences* **157**, 105626
43. Hitzenberger, M., and Zacharias, M. (2019) Uncovering the Binding Mode of γ - Secretase Inhibitors. *ACS Chemical Neuroscience* **10**, 3398-3403
44. Yang, G., Zhou, R., Guo, X., Yan, C., Lei, J., et al. (2021) Structural basis of γ -secretase inhibition and modulation by small molecule drugs. *Cell* **184**, 521-533.e514
45. Landrum, M. J., Lee, J. M., Benson, M., Brown, G. R., Chao, C., et al. (2018) ClinVar: improving access to variant interpretations and supporting evidence. *Nucleic Acids Research* **46**, D1062-d1067
46. Culvenor, J. G., Evin, G., Cooney, M. A., Wardan, H., Sharples, R. A., et al. (2000) Presenilin 2 expression in neuronal cells: induction during differentiation of embryonic carcinoma cells. *Experimental Cell Research* **255**, 192-206
47. Watanabe, H., Imaizumi, K., Cai, T., Zhou, Z., Tomita, T., et al. (2021) Flexible and accurate substrate processing with distinct presenilin/ γ -secretases in human cortical neurons. *eNeuro* **8**, ENEURO.0500-0520.2021
48. Lee, M. K., Slunt, H. H., Martin, L. J., Thinakaran, G., Kim, G., et al. (1996) Expression of presenilin 1 and 2 (PS1 and PS2) in human and murine tissues. *The Journal of Neuroscience* **16**, 7513-7525
49. Kumar, A., and Thakur, M. K. (2012) Presenilin 1 and 2 are expressed differentially in the cerebral cortex of mice during development. *Neurochemistry International* **61**, 778-782
50. Sannerud, R., Esselens, C., Ejsmont, P., Mattera, R., Rochin, L., et al. (2016) Restricted location of PSEN2/ γ -secretase determines substrate specificity and generates an intracellular A β pool. *Cell* **166**, 193-208
51. Lessard, C. B., Rodriguez, E., Ladd, T. B., Minter, L. M., Osborne, B. A., et al. (2019) Individual and combined presenilin 1 and 2 knockouts reveal that both have highly overlapping functions in HEK293T cells. *The Journal of Biological Chemistry* **294**, 11276-11285
52. Pimenova, A. A., and Goate, A. M. (2020) Novel presenilin 1 and 2 double knock-out cell line for in vitro validation of PSEN1 and PSEN2 mutations. *Neurobiology of Disease*, 104785
53. Eccles, M. K., Main, N., Sabale, M., Roberts-Mok, B., Agostino, M., et al. (2023) Quantitative Comparison of Presenilin Protein Expression Reveals Greater Activity of PS2- γ -Secretase. *bioRxiv*, 2023.2005.2009.540102

54. Madhavi Sastry, G., Adzhigirey, M., Day, T., Annabhimoju, R., and Sherman, W. (2013) Protein and ligand preparation: parameters, protocols, and influence on virtual screening enrichments. *Journal of Computer-Aided Molecular Design* **27**, 221-234
55. Lomize, M. A., Pogozheva, I. D., Joo, H., Mosberg, H. I., and Lomize, A. L. (2012) OPM database and PPM web server: resources for positioning of proteins in membranes. *Nucleic Acids Research* **40**, D370-D376
56. Madej, B. D., and Walker, R. C. (2014) An Amber Lipid Force Field Tutorial: Lipid14 Edition.
57. Jo, S., Cheng, X., Lee, J., Kim, S., Park, S.-J., et al. (2017) CHARMM-GUI 10 Years for Biomolecular Modeling and Simulation. *Journal of Computational Chemistry* **38**, 1114-1124
58. Salomon-Ferrer, R., Case, D. A., and Walker, R. C. (2013) An overview of the Amber biomolecular simulation package. *Wiley Interdisciplinary Reviews: Computational Molecular Science* **3**, 198-210
59. Maier, J. A., Martinez, C., Kasavajhala, K., Wickstrom, L., Hauser, K. E., et al. (2015) ff14SB: Improving the Accuracy of Protein Side Chain and Backbone Parameters from ff99SB. *Journal of Chemical Theory and Computation* **11**, 3696-3713
60. Dickson, C. J., Madej, B. D., Skjevik, Å. A., Betz, R. M., Teigen, K., et al. (2014) Lipid14: The Amber Lipid Force Field. *Journal of Chemical Theory and Computation* **10**, 865-879
61. Jorgensen, W. L., Chandrasekhar, J., and Madura, J. D. (1983) Comparison of simple potential functions for simulating liquid water. *The Journal of Chemical Physics* **79**, 926-935
62. Joung, I. S., and Cheatham, T. E. (2008) Determination of Alkali and Halide Monovalent Ion Parameters for Use in Explicitly Solvated Biomolecular Simulations. *The Journal of Physical Chemistry B* **112**, 9020-9041
63. Sousa da Silva, A. W., and Vranken, W. F. (2012) ACPYPE - AnteChamber PYthon Parser interface. *BMC Research Notes* **5**, 367
64. Abraham, M. J., Murtola, T., Schulz, R., Páll, S., Smith, J. C., et al. (2015) GROMACS: High performance molecular simulations through multi-level parallelism from laptops to supercomputers. *SoftwareX* **1-2**, 19-25
65. Tribello, G. A., Bonomi, M., Branduardi, D., Camilloni, C., and Bussi, G. (2014) PLUMED 2: New feathers for an old bird. *Computer Physics Communications* **185**, 604-613
66. Huang, W., Manglik, A., Venkatakrisnan, A. J., Laeremans, T., Feinberg, E. N., et al. (2015) Structural insights into μ -opioid receptor activation. *Nature* **524**, 315-321
67. Perron, L., and Furnon, V. OR-Tools v7.2. *Google*
68. Agostino, M., McKenzie, F., Buck, C., Woodward, K. J., Atkinson, V. J., et al. (2022) Studying Disease-Associated UBE3A Missense Variants Using Enhanced Sampling Molecular Simulations. *ACS Omega* **7**, 25039-25045
69. Tiwary, P., and Parrinello, M. (2015) A time-independent free energy estimator for metadynamics. *The Journal of Physical Chemistry B* **119**, 736-742
70. Daura, X., Gademann, K., Jaun, B., Seebach, D., Van Gunsteren, W. F., et al. (1999) Peptide folding: when simulation meets experiment. *Angewandte Chemie International Edition* **38**, 236-240
71. Miller, B. R., McGee, T. D., Swails, J. M., Homeyer, N., Gohlke, H., et al. (2012) MMPBSA.py: An Efficient Program for End-State Free Energy Calculations. *Journal of Chemical Theory and Computation* **8**, 3314-3321
72. Gohlke, H., Kiel, C., and Case, D. A. (2003) Insights into Protein-Protein Binding by Binding Free Energy Calculation and Free Energy Decomposition for the Ras-Raf and Ras-RalGDS Complexes. *Journal of Molecular Biology* **330**, 891-913

73. Nguyen, H., Roe, D. R., and Simmerling, C. (2013) Improved Generalized Born Solvent Model Parameters for Protein Simulations. *Journal of Chemical Theory and Computation* **9**, 2020-2034
74. Jörg, W., S., S. P., and Clark, S. W. (1999) Approximate atomic surfaces from linear combinations of pairwise overlaps (LCPO). *Journal of Computational Chemistry* **20**, 217-230
75. Barrett, P. J., Song, Y., Van Horn, W. D., Hustedt, E. J., Schafer, J. M., et al. (2012) The Amyloid Precursor Protein has a Flexible Transmembrane Domain and Binds Cholesterol. *Science* **336**, 1168-1171
76. Tsuzuki, S., Honda, K., Uchamaru, T., Mikami, M., and Tanabe, K. (2000) Origin of the Attraction and Directionality of the NH/ π Interaction: Comparison with OH/ π and CH/ π Interactions. *Journal of the American Chemical Society* **122**, 11450-11458
77. Okochi, M., Fukumori, A., Jiang, J., Itoh, N., Kimura, R., et al. (2006) Secretion of the Notch-1 A β -like peptide during Notch signaling. *The Journal of Biological Chemistry* **281**, 7890-7898
78. Acx, H., Chávez-Gutiérrez, L., Serneels, L., Lismont, S., Benurwar, M., et al. (2014) Signature amyloid β profiles are produced by different γ -secretase complexes. *The Journal of Biological Chemistry* **289**, 4346-4355
79. Frånberg, J., Svensson, A. I., Winblad, B., Karlström, H., and Frykman, S. (2011) Minor contribution of presenilin 2 for γ -secretase activity in mouse embryonic fibroblasts and adult mouse brain. *Biochemical and Biophysical Research Communications* **404**, 564-568
80. Lee, J., Song, L., Terracina, G., Bara, T., Josien, H., et al. (2011) Identification of presenilin 1-selective γ -secretase inhibitors with reconstituted γ -secretase complexes. *Biochemistry* **50**, 4973-4980
81. Meckler, X., and Checler, F. (2016) Presenilin 1 and presenilin 2 target γ -secretase complexes to distinct cellular compartments. *The Journal of Biological Chemistry* **291**, 12821-12837
82. Zhang, Z., Nadeau, P., Song, W., Donoviel, D., Yuan, M., et al. (2000) Presenilins are required for [γ]-secretase cleavage of [β]-APP and transmembrane cleavage of Notch-1. *Nature Cell Biology* **2**, 463-465
83. Fukumori, A., Okochi, M., Tagami, S., Jiang, J., Itoh, N., et al. (2006) Presenilin-Dependent γ -Secretase on Plasma Membrane and Endosomes Is Functionally Distinct. *Biochemistry* **45**, 4907-4914
84. Lessard, C. B., Rodriguez, E., Ladd, T. B., Minter, L. M., Osborne, B. A., et al. (2020) γ -Secretase modulators exhibit selectivity for modulation of APP cleavage but inverse γ -secretase modulators do not. *Alzheimer's Research & Therapy* **12**, 61
85. Placanica, L., Tarassishin, L., Yang, G., Peethumnongsin, E., Kim, S.-H., et al. (2009) Pen2 and presenilin-1 modulate the dynamic equilibrium of presenilin-1 and presenilin-2 γ -secretase complexes. *The Journal of Biological Chemistry* **284**, 2967-2977
86. Ebke, A., Luebbers, T., Fukumori, A., Shirotani, K., Haass, C., et al. (2011) Novel γ -secretase enzyme modulators directly target presenilin protein. *The Journal of Biological Chemistry* **286**, 37181-37186
87. Guo, X., Wang, Y., Zhou, J., Jin, C., Wang, J., et al. (2022) Molecular basis for isoform-selective inhibition of presenilin-1 by MRK-560. *Nature Communications* **13**, 6299
88. Funamoto, S., Sasaki, T., Ishihara, S., Nobuhara, M., Nakano, M., et al. (2013) Substrate ectodomain is critical for substrate preference and inhibition of γ -secretase. *Nature Communications* **4**, 2529
89. Kounnas, M. Z., Danks, A. M., Cheng, S., Tyree, C., Ackerman, E., et al. (2010) Modulation of γ -Secretase Reduces β -Amyloid Deposition in a Transgenic Mouse Model of Alzheimer's Disease. *Neuron* **67**, 769-780

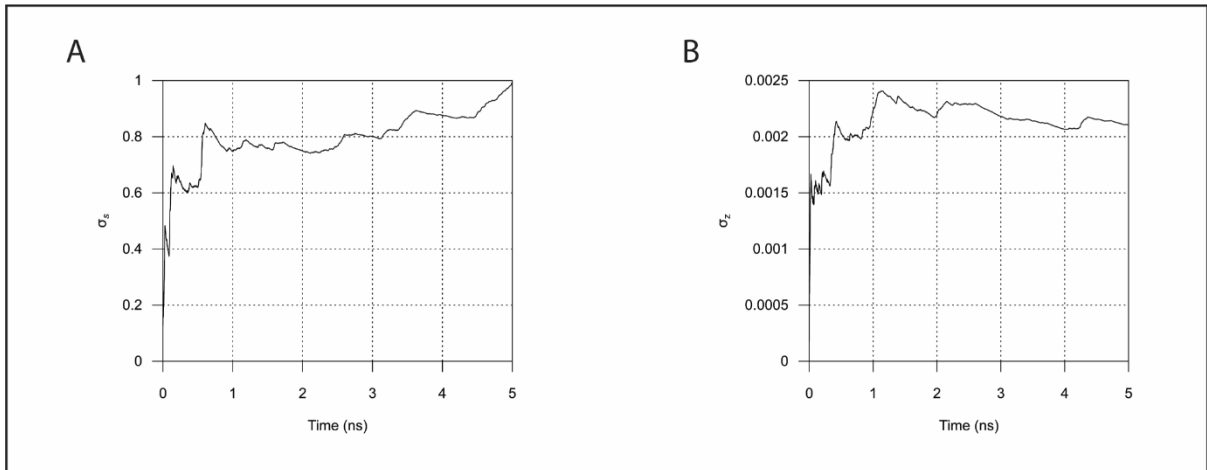
90. Pozdnyakov, N., Murrey, H. E., Crump, C. J., Pettersson, M., Ballard, T. E., et al. (2013) γ -Secretase Modulator (GSM) Photoaffinity Probes Reveal Distinct Allosteric Binding Sites on Presenilin. *The Journal of Biological Chemistry* **288**, 9710-9720
91. Kounnas, M. Z., Lane-Donovan, C., Nowakowski, D. W., Herz, J., and Comer, W. T. (2017) NGP 555, a γ -secretase modulator, lowers the amyloid biomarker, A β 42, in cerebrospinal fluid while preventing Alzheimer's disease cognitive decline in rodents. *Alzheimer's & Dementia: Translational Research & Clinical Interventions* **3**, 65-73
92. Cai, T., Yonaga, M., and Tomita, T. (2017) Activation of γ -Secretase Trimming Activity by Topological Changes of Transmembrane Domain 1 of Presenilin 1. *The Journal of Neuroscience* **37**, 12272-12280
93. Ioppolo, A., Eccles, M., Groth, D., Verdile, G., and Agostino, M. (2021) Evaluation of Virtual Screening Strategies for the Identification of γ -Secretase Inhibitors and Modulators. *Molecules* **27**

3.6 SUPPLEMENTAL FIGURES

A	
6IYC APP-CTF - A β 49	LVFFAEDVGSNKGAI IGLMVGGVVIATVIVIT <u>LV</u> MLKKK LVFFAEDVGSNKGAI IGLMVGGVVIATVIVIT <u>LV</u> MLKKK
6IYC A β 49 - A β 46	LVFFAEDVGSNKGAI IGLMVGGVVIATVIVIT <u>LV</u> MLKKK LVFFAEDV---GSNKGAI IGLMVGGVVIATVIVIT <u>VI</u> TL
6IYC A β 46 - A β 43	LVFFAEDVGSNKGAI IGLMVGGVVIATVIVIT <u>LV</u> MLKKK LVFFAE-----DVGSNKGAI IGLMVGGVVIATVIVIT <u>TV</u> IV
6IYC A β 43 - A β 40	LVFFAEDVGSNKGAI IGLMVGGVVIATVIVIT <u>LV</u> MLKKK ---LV-----FFAEDVGSNKGAI IGLMVGGVVIATVIVIT <u>VI</u> AT
B	
6IYC APP-CTF - A β 48	LVFFAEDVGSNKGAI IGLMVGGVVIATVIVIT <u>LV</u> MLKKK LVFFAEDV-GSNKGAI IGLMVGGVVIATVIVIT <u>TL</u> VMLKKK
6IYC A β 48 - A β 45	LVFFAEDVGSNKGAI IGLMVGGVVIATVIVIT <u>LV</u> MLKKK LVFFAE----DVGSNKGAI IGLMVGGVVIATVIVIT <u>IV</u> IT
6IYC A β 45 - A β 42	LVFFAEDVGSNKGAI IGLMVGGVVIATVIVIT <u>LV</u> MLKKK -LVFFA-----EDVGSNKGAI IGLMVGGVVIATVIVIT <u>AT</u> VI
6IYC A β 42 - A β 38	LVFFAEDVGSNKGAI IGLMVGGVVIATVIVIT <u>LV</u> MLKKK -----LVFFAEDVGSNKGAI IGLMVGGVVIATVIVIT <u>GV</u> VIA
C	
6IDF NEXT - S3VL	VQSETVEPPPPAQLHFMYVAAAFAVLLFFVGC <u>GV</u> LRSRKR VQSETVEPPPPAQLHFMYVAAAFAVLLFFVGC <u>GV</u> LRSRKR
6IDF NEXT - S3GV	VQSETVEP-PPPAQLHFMYVAAAFAVLLFFVGC <u>GV</u> LRSRKR -VQSETVEPPPPA-QLHFMYVAAAFAVLLFFVGC <u>GV</u> LRSRKR
6IDF S3GV - S4VL	VQSETVEPPPPAQLHFMYVAAAFAVLLFFVGC <u>GV</u> LRSRKR -----VQSETVEPPPPAQLHFMYVAAAFAVLLFFVGC
6IDF S3GV - S4AA	VQSETVEPPPPAQLHFMYVAAAFAVLLFFVGC <u>GV</u> LRSRKR -----VQSETVEPPPPAQLHFMYVAAAFAVLLFF

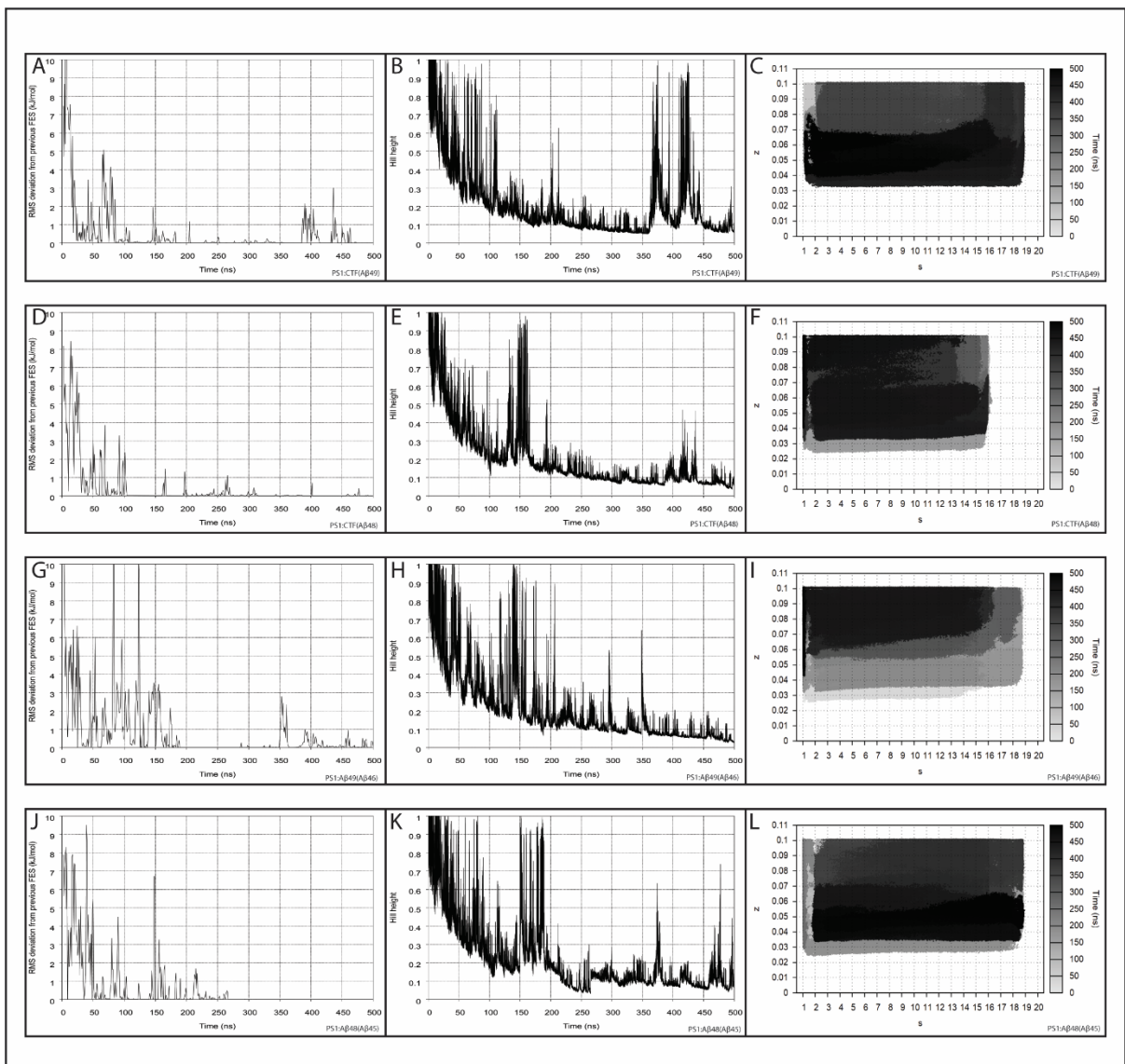
SI Figure 3-1 Sequence alignments used for homology modelling of substrates.

Substrate alignments for A β 40 pathway (A), A β 42 pathway (B) and Notch1 cleavage (C).

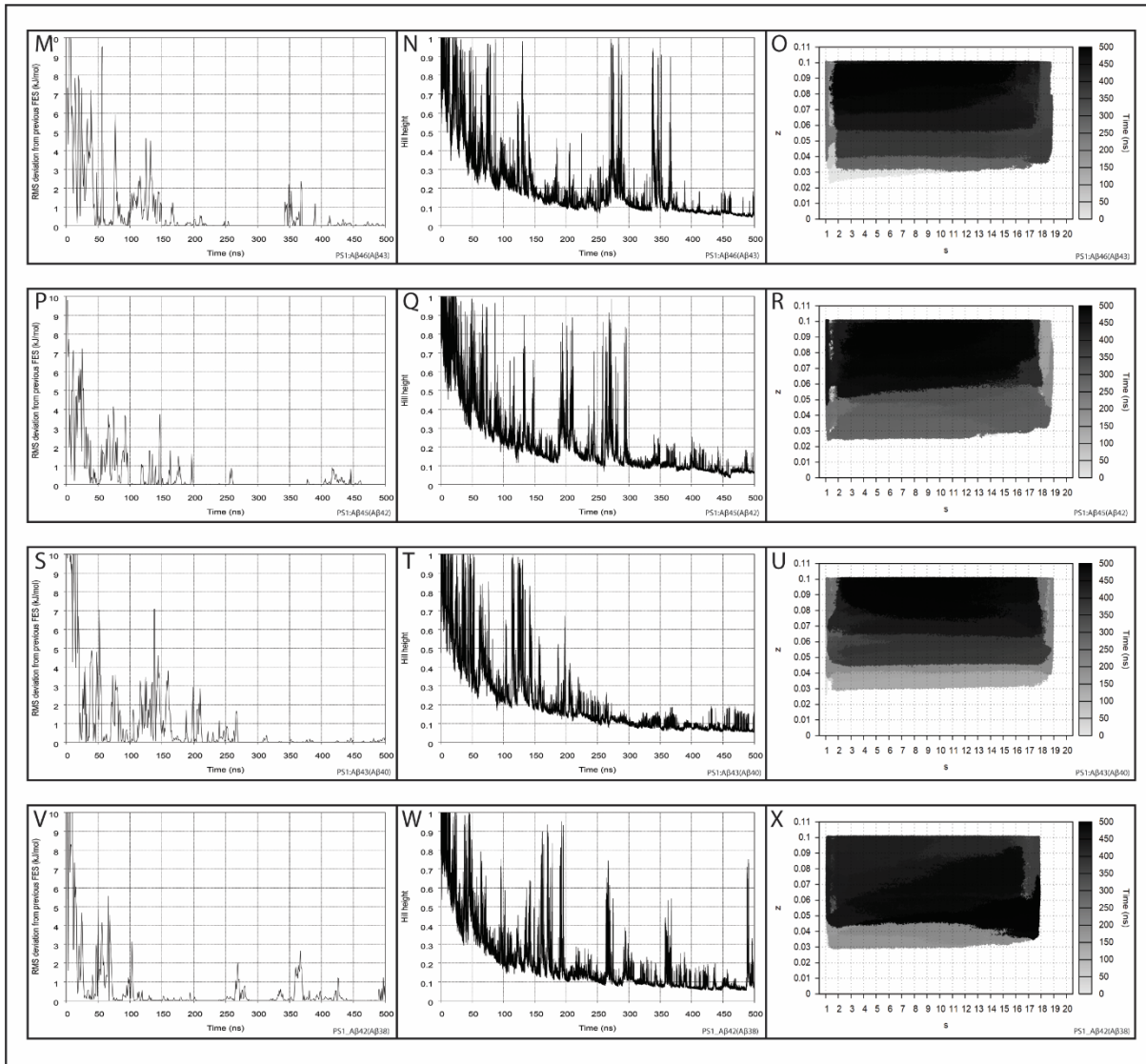


SI Figure 3-2 Determination of σ for s and z .

σ_s (A) and σ_z (B) from 5ns unbiased simulation of PS1 γ bound to APP

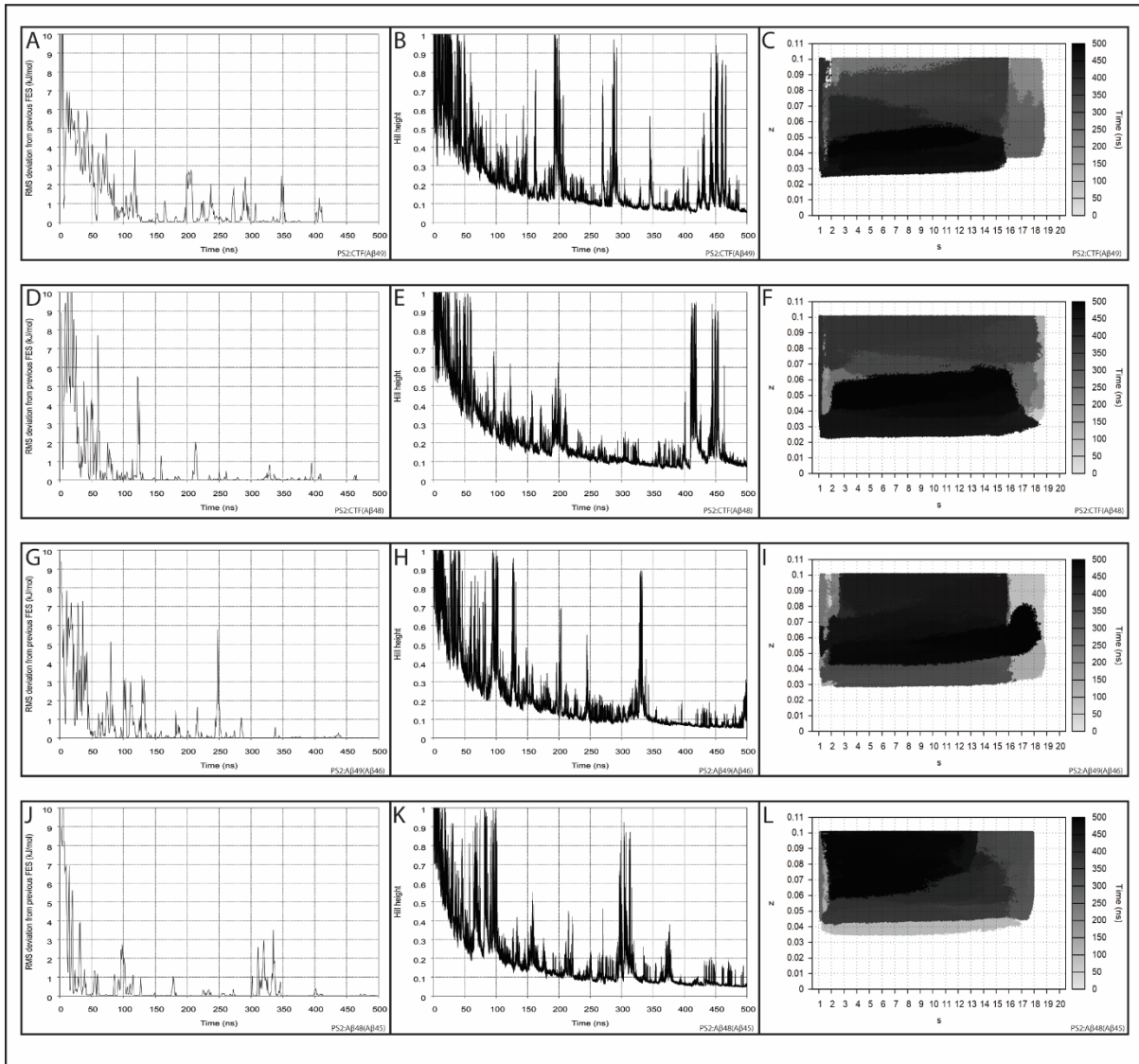


SI Figure 3-3 PS1 – APP substrate simulation convergence.

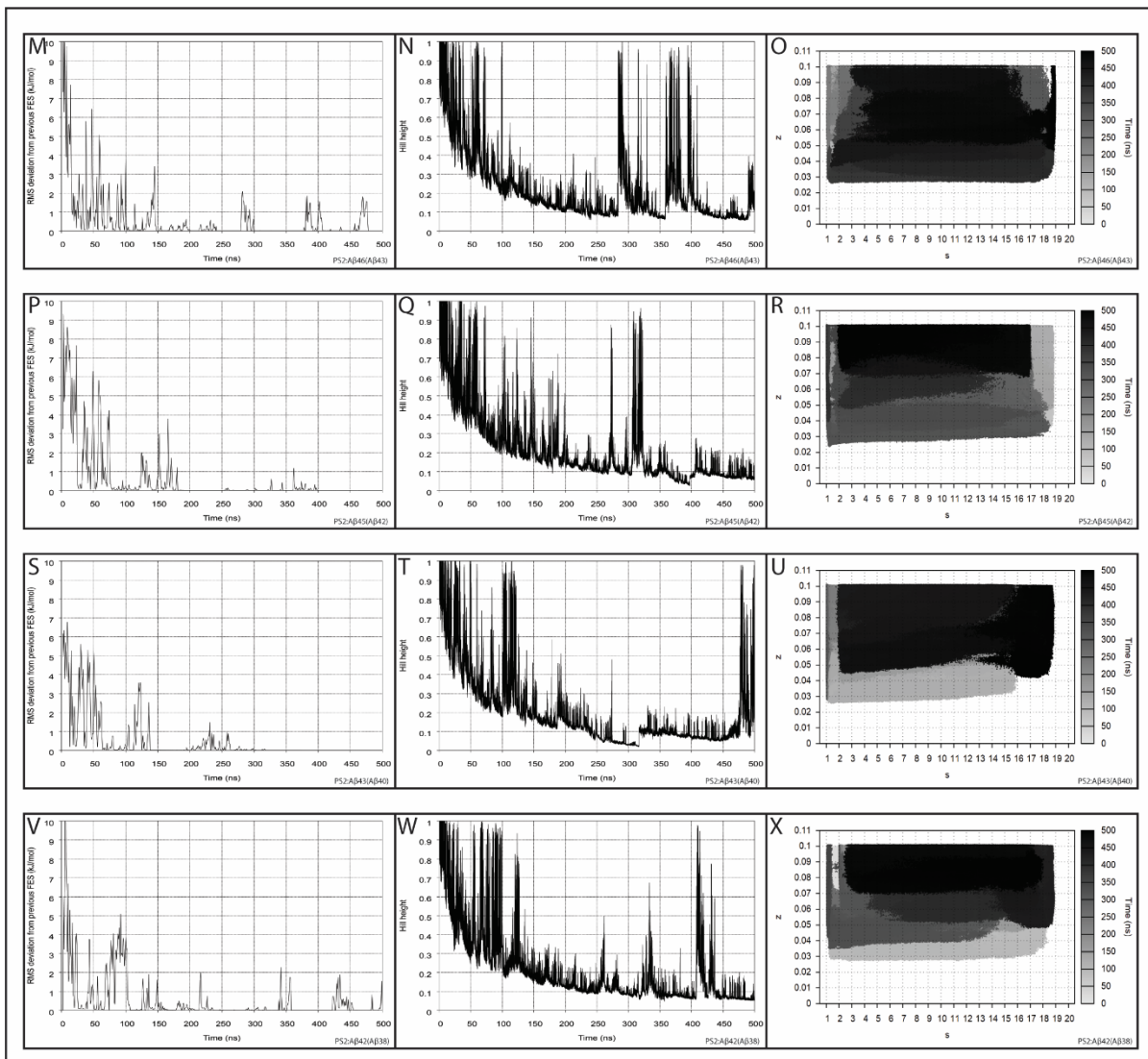


SI Figure 3-3 (continued) PS1 – APP substrate simulation convergence.

Simulation convergence for PS1-APP models assessed via monitoring RMSD from previous FES at 1ns intervals (A, D, G, J, M, P, S, V), Gaussian hill height (B, E, H, K, N, Q, T, W), and the collective variable space over duration of simulation (C, F, I, L, O, R, U, X).

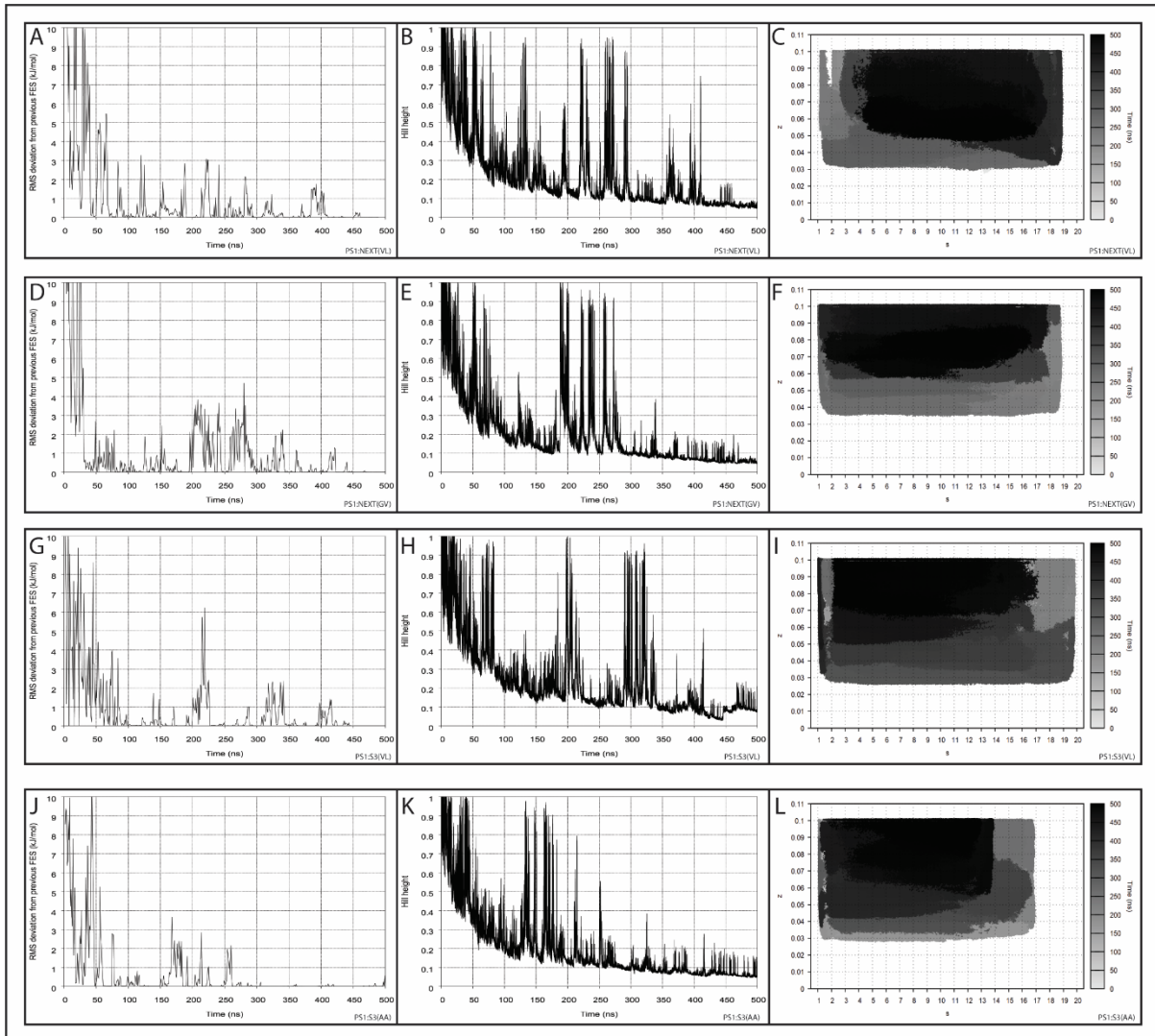


SI Figure 3-4 PS2 – APP substrate simulation convergence.



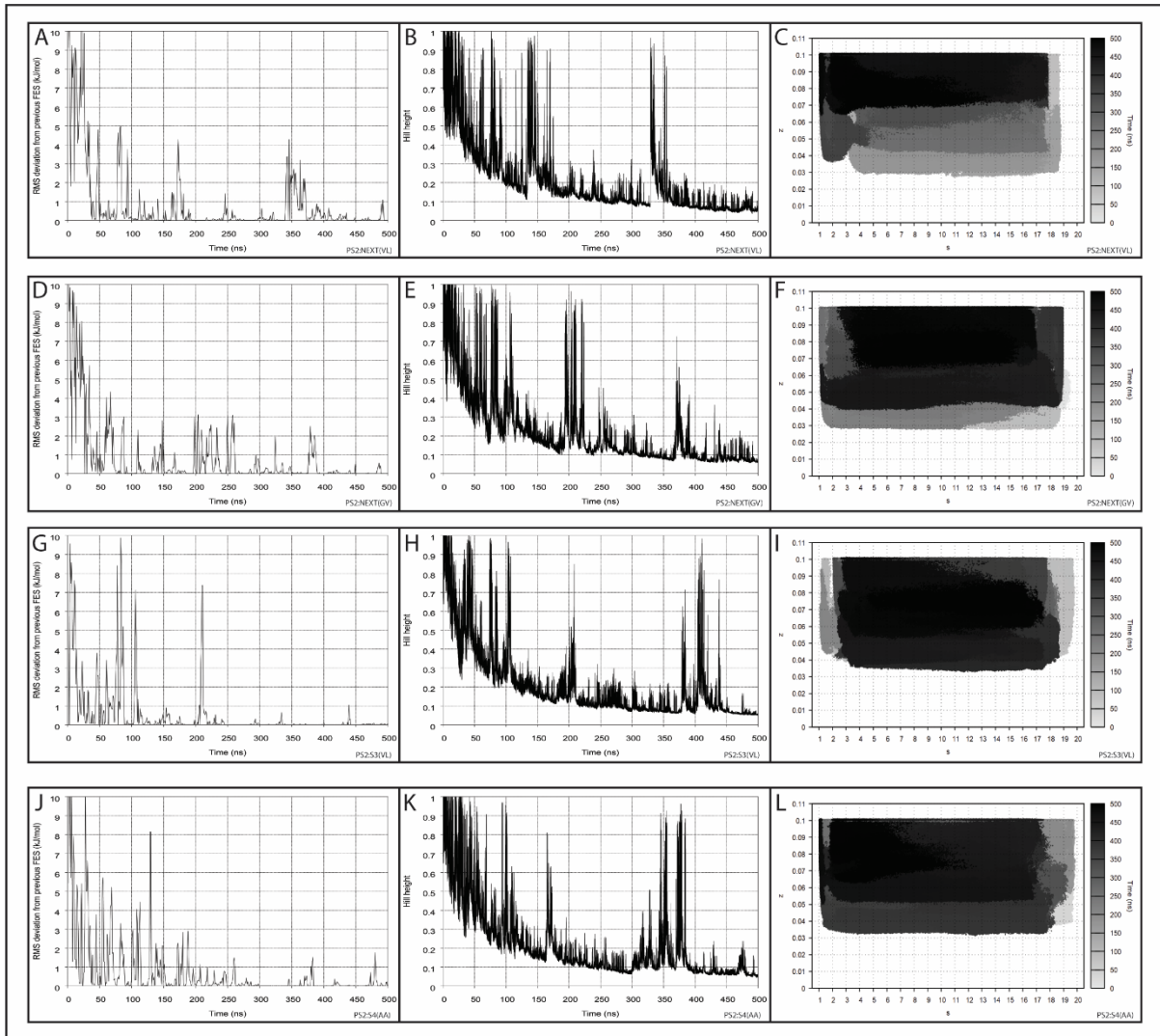
SI Figure 3-4 (continued) PS2 – APP substrate simulation convergence.

Simulation convergence for PS2-APP models assessed via monitoring RMSD from previous FES at 1ns intervals (A, D, G, J, M, P, S, V), Gaussian hill height (B, E, H, K, N, Q, T, W), and the collective variable space over duration of simulation (C, F, I, L, O, R, U, X).



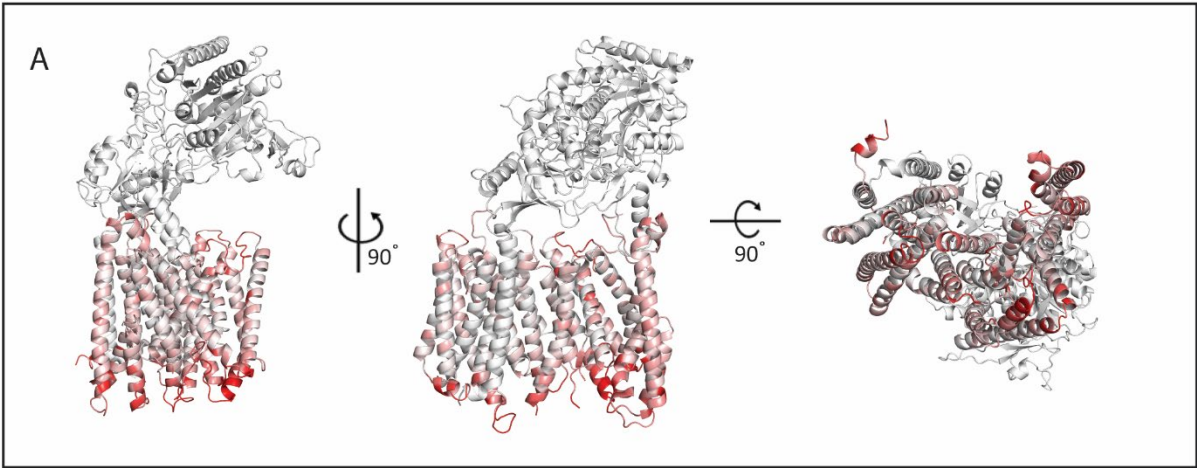
SI Figure 3-5 PS1 – Notch substrate simulation convergence.

Simulation convergence for PS1-Notch models assessed via monitoring RMSD from previous FES at 1ns intervals (A, D, G, J), Gaussian hill height (B, E, H, K), and the collective variable space over duration of simulation (C, F, I, L).



SI Figure 3-6 PS2 – Notch substrate simulation convergence.

Simulation convergence for PS2-Notch models assessed via monitoring RMSD from previous FES at 1ns intervals (A, D, G, J), Gaussian hill height (B, E, H, K), and the collective variable space over duration of simulation (C, F, I, L).



SI Figure 3-7 Path derivation between APP and Notch1 bound states.

Path derivation illustrated as Root Mean Squared Fluctuation (RMSF) range of 0.00nm (white) to 0.20nm (red) of PS1, Aph1a, and Pen-2 components used for path derivation (A).

4 ASSESSMENT OF PRESENILIN EXPRESSION IN HUMAN BRAIN TISSUE AND CNS RELATED CELL LINES

4.1 INTRODUCTION

The Presenilin protein is the catalytic component of γ -secretase.¹ In this capacity it is intimately linked with Alzheimer's disease (AD), as this enzyme cleaves the amyloid precursor protein (APP) to generate amyloid- β (A β) peptides¹ (after ectodomain shedding by BACE-1), and mutations in presenilin cause autosomal dominant forms of AD.² While it is typically referred to as 'presenilin' there are two actual proteins, Presenilin-1 (PS1) and Presenilin-2 (PS2), located on Chr14^{3, 4} and Chr1^{5, 6} respectively. They are homologs sharing ~67% sequence identity, and both are capable of forming discrete, active, γ -secretase enzymes,⁷ herein referred to as PS1 γ and PS2 γ . PS1 γ has garnered the vast majority of the fields attention for three key reasons: 1) PS1 harbours significantly more pathogenic mutations associated with an earlier age of onset than PS2.² 2) PS1 ablation in murine models is lethal in late-stage embryogenesis, while PS2 ablation leads to viable pups that only display a negative pulmonary associated phenotype at approximately 90 days.⁸⁻¹⁰ 3) PS1 γ is generally considered the more active enzyme, processing more APP and Notch1 substrate than PS2 γ .^{7, 11, 12}

A critical role for PS1 in embryogenesis has been well established in murine studies,^{8-10, 13, 14} but the consideration of PS1 as the more critical protein should not be directly assigned to a later life stage phenotype like AD without appropriate consideration of PS2. PS1 and PS2 expression levels vary throughout development, in both human¹⁵ and mice brains.¹⁵⁻¹⁷ Both PS1 and PS2 protein expression fluctuates throughout murine brain development. PS1 protein expression, highest during embryonic development, reduces significantly postnatally and is lowest in adulthood, while PS2 protein expression is lowest during postnatal development and rises during adolescence and into adulthood.¹⁶ However, in an aged mouse brain, the ratio of PS1:PS2 expression is consistently decreased compared to younger mice.¹⁷⁻²⁰ These findings are in line with human transcript data suggesting that in the adult cortex, *PSENI* expression is lower than *PSEN2*;¹⁵ this study did not report on the respective protein levels.

Several murine studies show that neuronal loss of both presenilins, leads to significant, accelerated neurodegeneration.²¹⁻²⁹ This is exemplified by increased cortical atrophy,^{21, 22, 27} neuronal apoptosis,^{22, 23, 27, 28} gliosis,^{21-24, 26, 27, 29} and tau hyperphosphorylation,^{21, 26} along with

reduced synapse quantity²¹ and synaptic plasticity²⁵, ultimately leading to severe memory impairment.^{21, 25} However, the retention of either PS1 or PS2 expression prevents these outcomes.^{22, 25-27} The loss of PS2 expression in mice reportedly does not affect PS1 expression in the murine brain.³⁰ The effect of the loss of PS1 expression on PS2 expression however is conflicting. Where conditional knockout of PS1 has been shown in one study to have no effect on PS2 expression,³¹ another study reports a 30% increase in PS2 expression.²⁷ Although it has been suggested that compensatory regulation of the alternate PS homologue may be protective in this context²⁷, it remains to be confirmed.

While it is known that PS1 and PS2 expression levels change in the brain throughout development,¹⁵⁻²⁰ the effect in specific central nervous system (CNS) related cells has not been determined. We have recently shown that when PS expression is considered, PS2 γ is more active at processing APP and processes Notch1 equally, compared to PS1 γ , as an individual enzyme unit.³² Consequently, alterations in PS expression will likely impact on γ -secretase related processing and subsequent downstream functions. As a first step in understanding this effect, endogenous PS1 and PS2 expression were quantitated using our PS-Std³² and levels directly compared across different CNS related cell lines and human brain from AD and other dementias. Thus, it is the aim of this chapter to quantitatively assess PS1 and PS2 levels in human brain tissue and neural cell lines.

4.2 MATERIALS AND METHODS

4.2.1 Human Brain Tissue Preparation

Human brain tissue from the Australian Brain Bank Network (ABBN) was homogenised for use in a previous study.³³ These studies were performed according to ethics applications approved by Curtin University (#SOBS-O2-14), Hollywood Private Hospital (HPH264) and Edith Cowan University (ECUMartins3325) respective human ethics committees. Homogenates were stored at -80 °C. Details of brain tissue are outlined in our previous study³³ and available in SI Table 4-1. Briefly, approximately 150 mg of brain tissue was excised from the provided sample and placed in a 2 ml cryotube with 3-5 ceramic beads. Excised samples were kept on ice at all times unless otherwise stated. 3 μ l per mg of tissue of ice-cold tris buffered saline (TBS: 2 mM tris, 1.5 mM NaCl) supplemented with 2 \times protease inhibitor cocktail (Roche 11697498001) was added to the tissue sample and the sample homogenised

using a Bead Beater FastPrep-24 5G at 6.0 m/s for 40 seconds. After homogenisation, 3 μ l per mg of tissue of 2x RIPA lysis buffer (Astral Scientific 786-490) was added, such that the final concentration of RIPA was 1x. Samples were then incubated with rotation for 2 hr at 4 °C, then clarified by centrifugation at 14,000 g for 10 min at 4 °C, the supernatant was collected, aliquoted and stored at -80 °C, the remaining pellet was discarded.

4.2.2 Cell Culture

SK-N-BE(2)-M17 (RRID:CVCL_0167),³⁴ herein referred to as M17, and SH-SY5Y (RRID:CVCL_0019)³⁵ neuroblastoma cell lines were cultured in DMEM:F12 (Sigma D8437) and the human microglial clone 3 (HMC3) (RRID:CVCL_II76)³⁶ cell lines (gifted from Dr Ryan Anderton) were cultured in MEM (Sigma M5650). All media was supplemented with 1 mM L-glutamine (Sigma G7513), 1 mM Na-pyruvate (Sigma S8636), 100 units/ml Penicillin 0.1 mg/ml Streptomycin (Sigma P4333), and 10% v/v foetal bovine serum (Serana FBS-Au-015). Cultures were incubated at 37 °C with 5% v/v atmospheric CO₂.

4.2.3 CRISPR-Cas9 Presenilin Knock-Out

PS1 and PS2 knockout cell lines were generated in M17 and HMC3 cells using pSp-Cas9-(BB)-2A-GFP vector.³⁷ gRNA sequences were designed and selected using CHOP-CHOP^{38,39} and Broad Institute.^{40,41} 5' phosphorylation of synthesised oligonucleotides was completed by the addition of 10 units of T4 polynucleotide kinase (NEB M0201S) to 10 μ M of forward and reverse oligonucleotide, with 1 \times T4 ligase buffer (NEB B0202S) and made to a final volume of 10 μ l with UltraPureTM H₂O (Invitrogen 10977015). The reaction was incubated at 37 °C for 30 min, the polynucleotide kinase reaction was then inactivated by heating the reaction to 95 °C for 5 min, after which the forward and reverse oligonucleotide sequences were annealed by cooling by 2 °C per minute to 25 °C, to generate dsDNA. pSp-Cas9-(BB)-2A-GFP plasmid was prepared by digestion with restriction enzyme Bsb1 and subsequent gel purification using PCR and gel purification kit (Bioline BIO-52060). 2 μ M of the dsDNA guide RNA sequence was ligated into 10 ng of linearised pSp-Cas9-(BB)-2A-GFP vector, in a 10 μ l reaction, with 1 \times T4 DNA ligase buffer and 400 units of T4 DNA ligase (NEB M0202S). The reaction was incubated at 16 °C for 16 hrs, after which chemically competent XL10 *E. coli* cells (gifted from Dr Carl Mousley, CHIRI, Curtin University) were transformed with 5 μ l of the ligation reaction. Briefly, the ligation reaction was incubated with 25 μ l of XL10 *E. coli* cells for 30 min on ice, followed by 42 °C for 45 sec, after which cells were incubated for 5 min on ice.

The transformed *E. coli* were allowed to recover for 1 hr, by addition of 175 µl of SOC buffer (0.5% w/v yeast extract, 2% w/v tryptone, 10 mM NaCl, 2.5 mM KCl, 20 mM MgSO₄, 0.4% v/v glucose) and incubation at 37 °C with agitation, after which the transformed *E. coli* was plated on Luria Broth agar plates (1% w/v tryptone, 1% w/v NaCl, 0.5% w/v yeast extract, 1.5% w/v agar) supplemented with 100 µg/ml ampicillin and incubated overnight at 37 °C. The following day 5 ml of Luria Broth (1% w/v tryptone, 1% w/v NaCl, 0.5% w/v yeast extract) supplemented with 100 µg/ml ampicillin, was inoculated with individual colonies, cultured overnight at 37 °C with agitation. Cells were collected by centrifugation at 3,150 g, subsequently lysed and the plasmid purified using a plasmid extraction kit (Bioline BIO-52057). The plasmids were sequenced to confirm gRNA sequence was correctly inserted.

M17 (4x10⁵ per well) and HMC3 (7.5x10⁴ per well) cells were plated in 6-well plates, and incubated for 24 hours, after which cells were transfected with pSp-Cas9-(BB)-2A-GFP vectors with gRNA sequence targeting either *PSEN1*, *PSEN2*, or empty vector for control cell lines. Two sites per gene were targeted simultaneously by using a 1:1 ratio of the vectors (Table 4-1), transfected using Lipofectamine 3000 (Invitrogen L3000015) as per manufactures instructions, note that 7.5 µl of Lipofectamine 3000 was used for M17 cells while 3.75 µl was used for HMC3 cells, per well in 6-well plate. 24 hours post transfection cells were trypsinised, prepared in single cell suspension and single cell sorted using a BD FACSJazz, gating for mid-level GFP expression as marker for pSp-Cas9-(BB)-2A-GFP transfection, and propidium iodide for live/dead cell differentiation.

Table 4-1 CRISPR-Cas9 gRNA target sequences for PS1 and PS2 knockout

Cell Line	Target Gene	gRNA site 1	gRNA site 2
HMC3	PSEN1	5'GTTTCAACCAGCATACGAA G ^{3'}	5'TAAAACCTATAACGTTGCT G ^{3'}
	PSEN2	5'GCTCCCCTACGACCCGGAG A ^{3'}	5'ACGATCATGCACAGAGTGA C ^{3'}
M17	PSEN1	5'TTATCTAATGGACGACCCC A ^{3'}	5'GAGCAATACTGTACGTAGC C ^{3'}
	PSEN2	5'GCTCCCCTACGACCCGGAG A ^{3'}	5'ACGATCATGCACAGAGTGA C ^{3'}

Cells were then incubated at 37 °C with 5% v/v CO₂ and colonies expanded and screened via two methods. Initial screening was completed by wild-type allele PCR of both CRISPR target

sites, primer annealing conditions were optimised for high stringency, primers and annealing temperature are available in SI Table 4-2. If DNA demonstrated any disturbance to the wild-type sequence (i.e. did not amplify at either CRISPR target site) the colony was maintained for further screening (SI Figure 4-1). Confirmatory screening was via PAGE and western blotting to determine protein knock out. Three clones of each cell line were selected for further characterisation.

4.2.4 Neuroblastoma Differentiation

Cells were differentiated as described previously.^{42,43} Briefly M17 cells were plated at 2187.5 cells/cm², in 100mm dishes. 24 hrs after plating, 10 mM Retinoic Acid differentiation media was added. Media was replaced every 24 hrs. SH-SY5Y cells were plated at 2187.5 cells/cm², in 100mm dishes. 24 hrs after plating, 10 nM staurosporine differentiation media was added. Media was replaced every 48hrs. Control cells were treated with DMSO as appropriate to mimic the differentiation vehicle, and cells were harvested for lysates after 7 days of differentiation.

Cell lysates were prepared as follows, media was aspirated and discarded, cells were washed in approximately 5 ml of ice-cold PBS, then scraped in 1 ml of ice cold PBS and collected into a 1.5 ml microfuge tube and centrifuged at 300 g for 5 min. PBS was aspirated and the cell pellet resuspended in RIPA buffer with protease inhibitor cocktail, vortexed and rotated for 1 hr at 4 °C, then centrifuged at 14,000 g for 10 min at 4 °C and the supernatant collected and stored at -20 °C.

4.2.5 Sample Preparation

All protein concentrations ($\mu\text{g}/\mu\text{l}$) of homogenates and lysates were determined by BCA (Pierce Micro BCA kit Thermo Fisher 23235). 15-30 μg of total protein for tissue homogenates and cell lysates, or appropriate ng amount of PS Std were prepared in tris tricine sample buffer to a final concentration of 4% w/v SDS, 50 mM tris, 12% v/v glycerol, 0.125% w/v Coomassie G-250. For the detection of PS1 no reducing agent was added, for the detection of PS2 proteins DTT was added to a final concentration of 50 mM. All samples were normalised to equal volume by addition of milliQ water. Samples were vigorously vortexed for 30 sec, then heat treated for 10 min at 37 °C, centrifuged at 17,000 g for 5 min, and immediately loaded onto PAGE.

4.2.6 PAGE and Western Blotting

12% w/v Tris-tricine poly acrylamide gels were prepared using the Invitrogen SureCast system. Samples were electrophoresed at 100 V for approximately 1 hr 45 min, in tris-tricine cathode buffer (100 mM tris, 100 mM tricine, pH8.3) and tris anode buffer (200 mM tris, pH8.8). Gels were transferred to 0.2 μ m nitrocellulose membrane (BioRad) via wet transfer in 19.2 mM tris, 2.5 mM glycine, 20 % v/v methanol buffer, at 150 mAmps overnight at 4 °C. Membranes were stained in ponceau (1% w/v ponceau S, 5% v/v acetic acid) for 5 min and visualised to confirm transfer quality, membranes were destained by incubation in boiled TBS with agitation until no evidence of ponceau remained. Membranes were blocked with 5% w/v non-fat dried milk powder (NFDM) in TBS for 1 hr at room temperature with agitation. Then incubated overnight at 4 °C with either a-PS1 NTF antibody (1:2000; Biolegend PS1 NT1 823401) or a-PS2 NTF antibody (1:1000, Biolegend PS2 814204) prepared in 0.5% skim milk in TBST (TBS with addition of 0.05% v/v tween-20). Membranes were subsequently washed 3-times in TBST for 10 min with agitation, followed by incubation with α -mouse IgG HRP conjugated secondary antibody (1:20,000; Thermo Fisher 31430) prepared in 0.5% w/v skim milk in TBST, for 1 hr at room temperature. Membranes were again washed 3-times in TBST as above, then once in TBS for 5 min. Membranes were prepared for imaging by incubating them with either Clarity ECL (BioRad 1705061), for PS1 NTF detection, or Prime ECL (Cytiva GERPN2232), for PS2 NTF detection. Western blots were imaged on BioRad ChemiDoc MP system and band densitometry quantitated using ImageLab (BioRad, version 6.1.0 build 7).

4.2.7 Endogenous Presenilin Quantitation

Endogenous presenilin expression was quantitated as previously described.³² Briefly using the PS-Std an appropriate range was determined via western blotting of representative samples such that the samples would fall within the range of the standard curve. A minimum of four quantitation standards were used to generate the standard curve (the nanogram range of PS Std used are shown in table S1), and a minimum of 3 replicates of the standard curve were generated concurrently via PAGE and western blot for each experiment. After western blotting with appropriate PS antibody the standard curve was quantitated using ImageLab to determine the densitometry for the standard curve. The densitometry (arbitrary units) was plotted against the number of PS-Std units, determined by $\text{PS-Std ng} / 5.10 \times 10^{-11} \text{ ng}$, where $5.10 \times 10^{-11} \text{ ng}$ is the mass of 1 unit of PS-Std. The equation for the standard curve was then used to calculate

the number of PS1 or PS2 protein units from the western blot band densitometry, and subsequently normalised per μg of total protein and by loading control.

4.2.8 Quantitative PCR

RNA was extracted from cultures at approximately 90% confluence, using ISOLATE II RNA extraction kit as per instructions (Bioline BIO-52072). cDNA was generated using Tetro cDNA kit (Bioline BIO-65043), with the following adaptations: 1) Random hexamers and oligo dTs were used in 1:1 ratio such that final volume of primers was as per recommended amount for reaction volume. 2) Reaction was incubated at room temperature for 10 min at room temperature followed by 45 °C for 1 hour.

cDNA generated from wild type cell RNA extracts was used to generate standard curves for all qPCR targets to determine appropriate amount of RNA $\mu\text{g}/\mu\text{l}$ to be used for specific targets, and primer efficiencies for use in relative quantitation calculations.⁴⁴ Primer sequences were designed at NCBI PrimerBlast, unless otherwise stated, and are presented in SI Table 4-3. Quantitative PCR reactions with final primer concentration of 500 nM were prepared using GoTaq qPCR master mix (Promega A6001) in 20 μl reactions and run on a Viia 7 (Invitrogen).

4.2.9 Statistical Analysis

All statistical analysis was completed using GraphPad Prism 9.5.0. Three to four biological replicates were completed for all *in-vitro* experiments. Shapiro-Wilk normality test was completed to determine if data was normally distributed. Statistical significance for normally distributed data was determined via unpaired T-test where only two groups were examined. Where more than two groups are examined, one-way ANOVA or two-way ANOVA analysis with Holm-Šidák's multiple comparison tests are used as appropriate. Where data was not normally distributed, the Mann-Whitney test was used for testing between two groups, while the Kruskal-Wallis test was used for multiple group analysis and posthoc analysis completed using Dunn's multiple comparison test.

4.3 RESULTS

4.3.1 PS1 and PS2 protein expression in human brain tissue

A quantitative comparison of PS1 and PS2 protein expression in human brain across regions and neurodegenerative diseases has not been previously reported. To address this gap in knowledge, available brain tissue homogenates were assessed for PS1-NTF and PS2-NTF protein levels using our previously described quantitative immunoblotting method.³² Expression of PS1 and PS2 was quantitatively assessed and compared in human brain regions including the cerebellum (CBM), frontal cortex (FC), and hippocampus (HPC) from control, Alzheimer's disease (AD), frontotemporal dementia (FTD) and Lewy body disease (LBD) (Figure 4-1 and Figure 4-2 for PS1, and Figure 4-3 for PS2). Notably, two AD (FC) samples and one FTD (HPC) sample (indicated by *) showed none to very low detection of PS1 or GAPDH (possibly due to loss of sample integrity) and were unable to be quantitated. A prominent protein band detected at ~28KDa, corresponding to PS1-NTF, was present in all samples (Figure 4-1, Figure 4-2). In the majority of HPC and FC samples and in two CBM samples (AD and LBD), an additional, ~12 kDa band was detected, which may represent a proteasomal degradation product.⁴⁵ PS2-NTF was detected as a doublet ~30 kDa protein band in all homogenates. To our knowledge, PS2-NTF has not been detected as a doublet previously and was evident only in the brain homogenates in this study. In neuronal and microglial cell lines only a single PS2-NTF protein band is observed (see below) and thus its presence is not likely an artefact of the antibody or method used.

The upper and lower bands were quantitated and the ratio of PS2-NTF Upper:Lower determined, to establish if any variation in expression levels of the two bands was evident. Initial assessment by brain region showed that upper to lower band ratio in the HPC is significantly lower compared to the CBM, and trends towards being lower than the FC ($p=0.1016$) (Figure 4-3N). Analysis of this ratio by pathology (Figure 4-3**Error! Reference source not found.**O), however, reveals no significant differences, indicating the reduced ratio in the HPC may be a regional effect and not a result of pathology.

PS1 and PS2 expression levels, quantitated as protein units calculated from the respective standard curves, are presented in Figure 4-4 (PS2-NTF upper and lower bands were summed for presentation of total PS2). Firstly, to determine any changes across regions, PS expression was assessed without any consideration of the underlying pathology (Figure 4-4A). PS1 is significantly higher (at least an order of magnitude higher) in all brain regions compared with PS2. PS1 expression is significantly lower in the HPC (3.65×10^8 PS1 units) compared to both

FC (5.39×10^8 PS1 units) and CBM (5.04×10^8 PS1 units) regions. No significant difference in PS2 is evident, with average expression in the FC, HPC and CBM of 1.88×10^7 , 2.05×10^7 , and 1.79×10^7 PS2 units respectively. Calculation of the PS1:PS2 ratio (Figure 4-4B), showed that this ratio in the HPC (32.3) was significantly lower than that in the FC (49.2), driven by the lower expression of PS1 in the HPC.

To determine if expression was altered by pathology, PS expression was assessed within brain regions and grouped by clinical classification. Significantly higher PS1 expression was observed in the CBM region of LBD samples (7.31×10^8 PS1 units) compared to AD samples (4.17×10^8 PS1 units) (Figure 4-4C). Of particular note, changes in PS2 expression across clinical groups were observed in the HPC, where lower levels were seen in AD samples (1.35×10^7 PS2 units) compared to both control (3.15×10^7 PS2 units) and FTD samples (3.05×10^7 PS2 units) (Figure 4-4D). This appears to drive the significant increase in PS1:PS2 ratio observed in the HPC region of AD samples (Figure 4-4E), compared to the other groups.

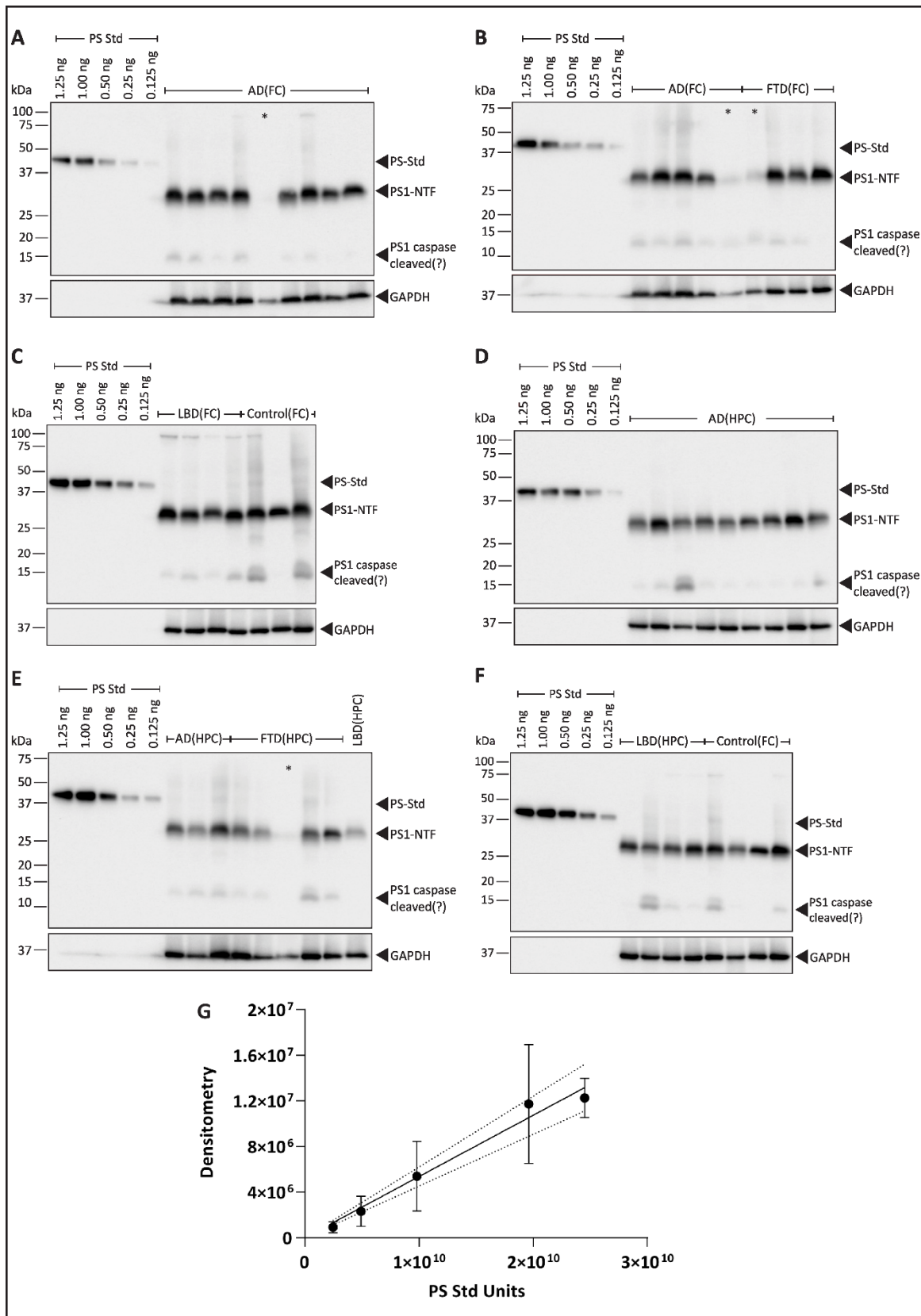


Figure 4-1 PS1-NTF expression in human frontal cortex and hippocampus regions

Immunoblot results for PS1-NTF for FC samples (A-C) and HPC samples (D-E) and resultant PS-Std standard curve for PS1-NTF FC and HPC quantitation (G), dashed line represents 95%

confidence interval. Note asterisk (*) in (A,B,E) identifies samples in which sample integrity is poor and little to no PS1-NTF or GAPDH is detectable.

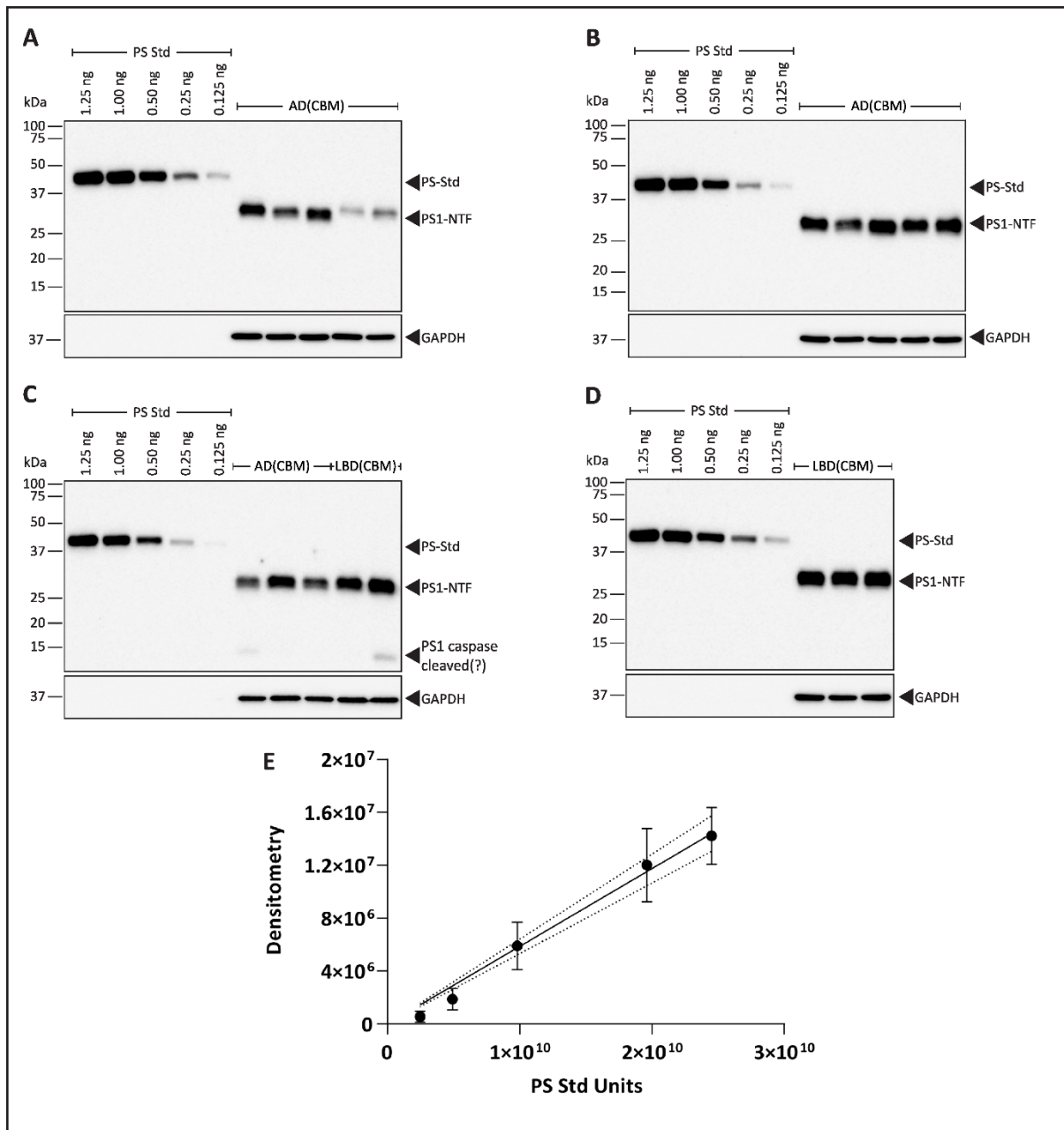


Figure 4-2 PS1-NTF expression in human cerebellum

Immunoblot results for PS1-NTF for CBM samples (A-D) and resultant PS-Std standard curve for PS1-NTF CBM quantitation (E), dashed line represents 95% confidence interval.

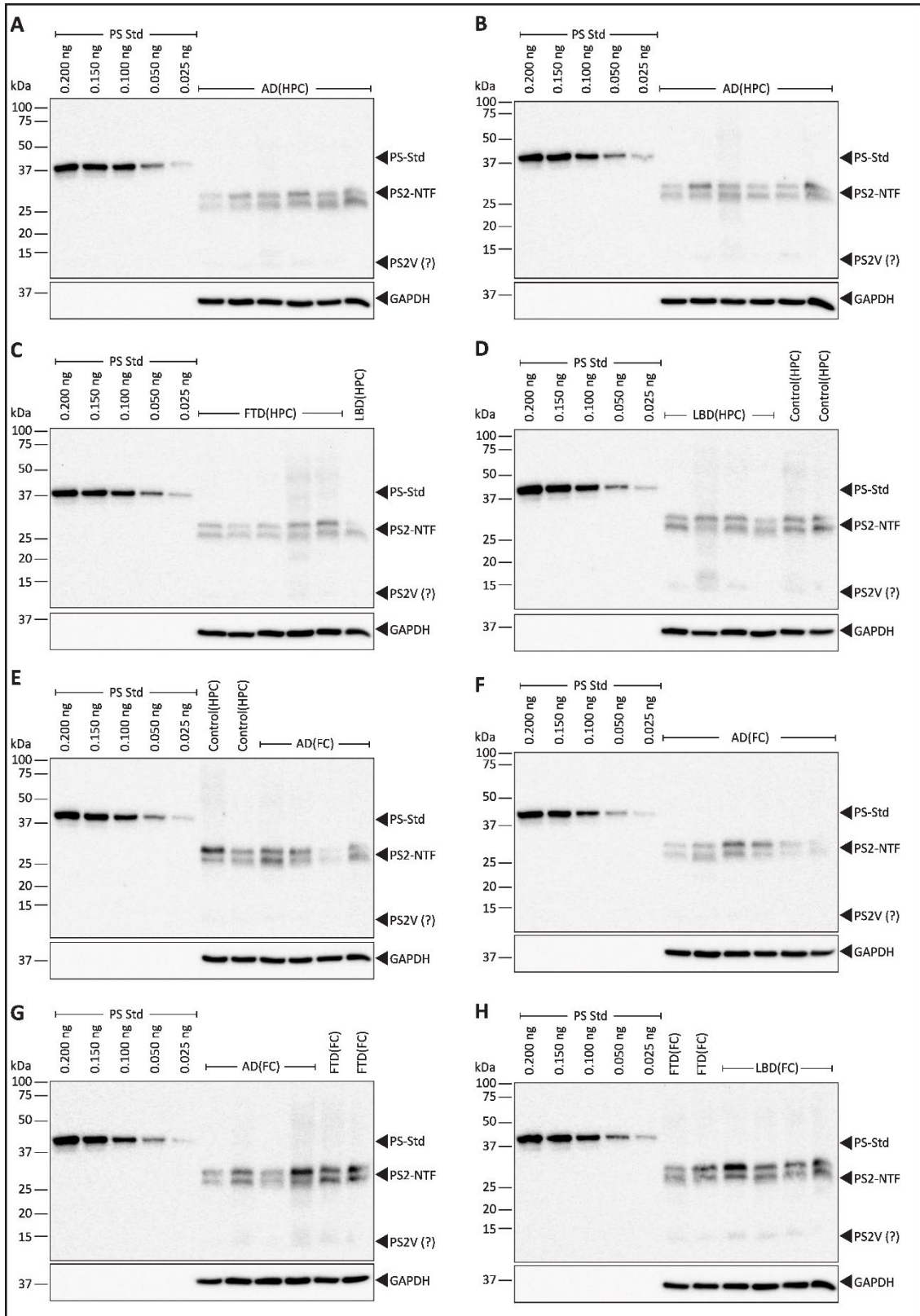


Figure 4-3 PS2-NTF expression in human hippocampus, frontal cortex, and cerebellum

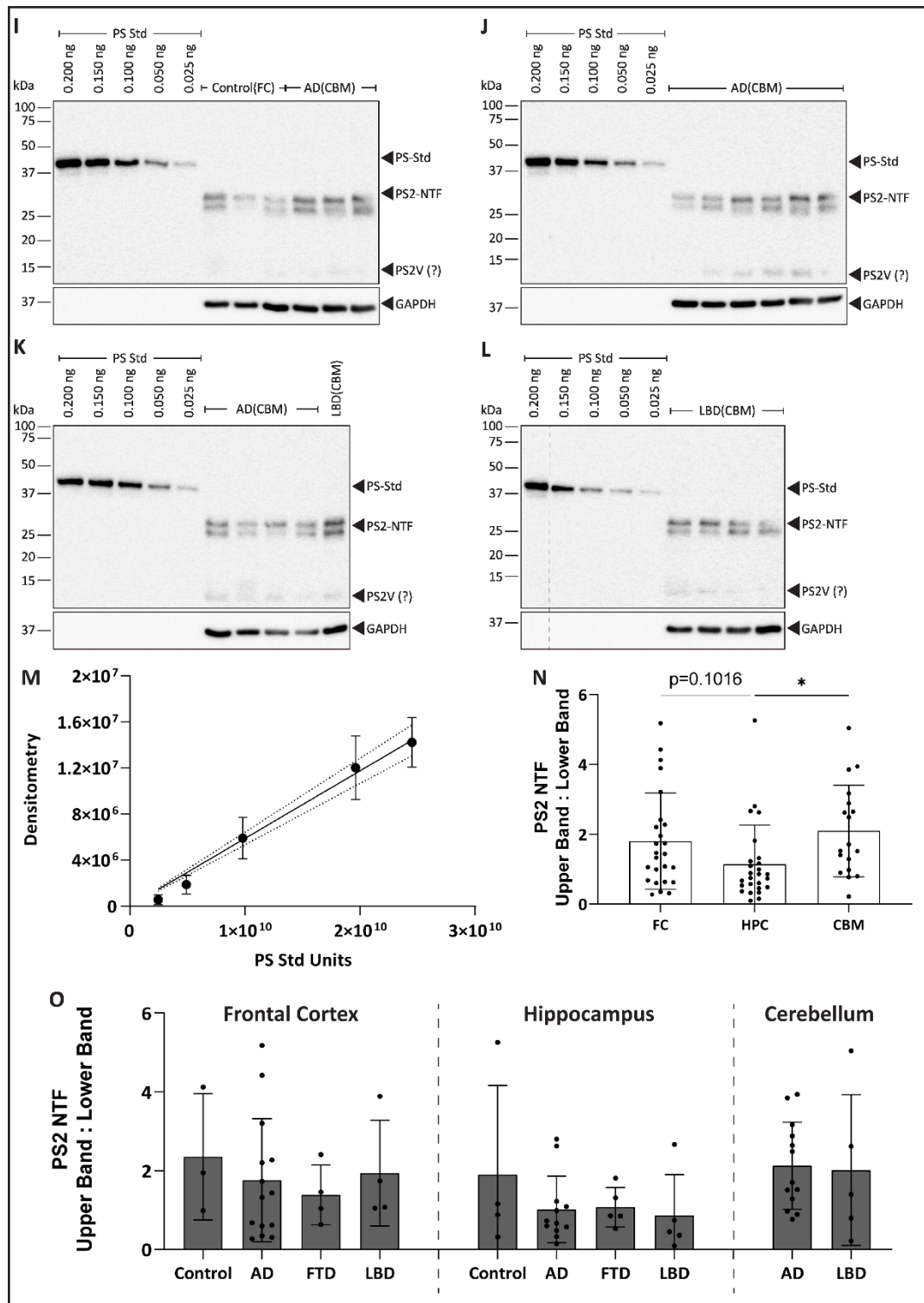


Figure 4-3 (continued) PS2-NTF expression in human hippocampus, frontal cortex, and cerebellum

Immunoblot results for PS2-NTF for HPC, FC and CBM samples (A-L), resultant PS-Std standard curve for PS2-NTF quantitation (M), dashed line represents 95% confidence interval. PS2-NTF upper:lower band ratio between brain region (N) and by pathology in different brain regions (O). Note: dashed line in (L) denotes where two empty lanes were cropped out of the immunoblot image, lanes left empty due to damaged well. Values shown are mean \pm SD,

statistical tests applied were Kruskal-Wallis test with Dunn's multiple comparison test (N, O) where * = $P < 0.05$.

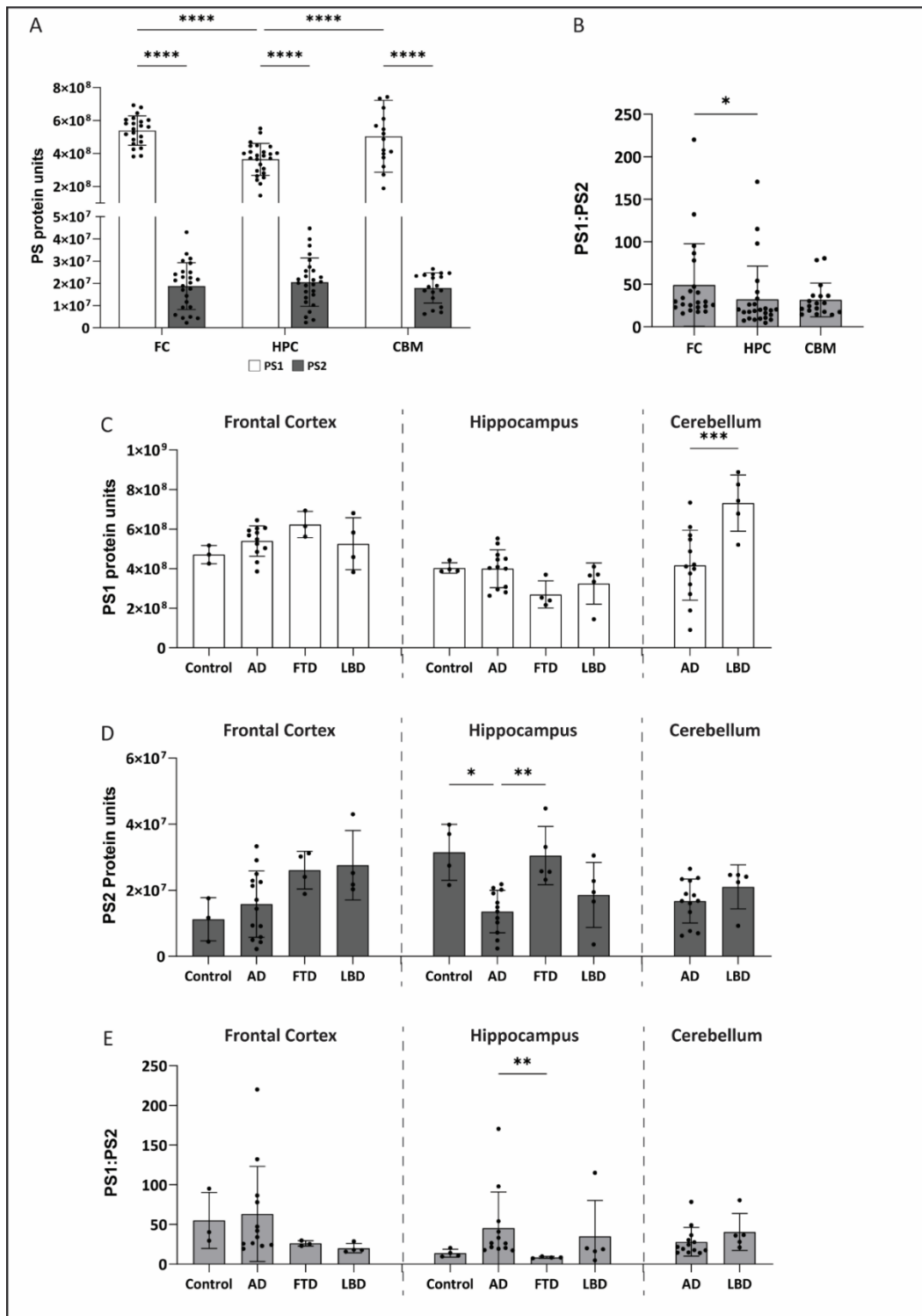


Figure 4-4 PS protein unit expression by brain region

Quantitation of PS protein units by brain region (A) and PS1:PS2 ratio by brain region (B). PS1 protein units by pathology in the frontal cortex, hippocampus and cerebellum (C). PS2 protein units by pathology in the FC, HPC, and CBM (D). PS1:PS2 ratio by pathology in the frontal cortex, hippocampus and cerebellum (E). Note: PS2-NTF upper and lower bands were

summed for presentation of total PS2. Values shown are mean \pm SD. Statistical tests applied were Two-way ANOVA with Holm-Šidák's multiple comparison test (A), Kruskal-Wallis test with Dunn's multiple comparison test (B, E), one-way ANOVA with Holm-Šidák's multiple comparison (C, D), where * = $P < 0.05$, ** = $P < 0.01$, *** = $P < 0.001$, **** = $P < 0.0001$.

4.3.2 Comparison of PS1 and PS2 expression profiles in neuronal and microglial cells

The findings described above show that there are changes in PS expression across brain regions and clinical groups. It is possible that cell-specific changes in presenilin expression occur, where neurons may for example show changes in expression of one type of presenilin compared to another cell such as microglia. Indeed, alterations in PS expression are observed with neuronal differentiation⁴⁶⁻⁴⁸ and PS2 is suggested to be the predominant functional presenilin in microglia.⁴⁹ We sought to investigate PS expression in human derived CNS-related cell lines that are commonly used for AD-related research. PS1 and PS2 were quantitatively assessed, via immunoblot (Figure 4-5), in immortalised human neuroblastoma M17 and SH-SY5Y cells and microglial HMC3 cells. Additionally, SH-SY5Y cells genetically modified to overexpress APP695 or APP695Swe are also commonly used, and so were also included.

Quantitation and comparison of the PS1 and PS2 expression levels in cells with the PS1+/+PS2+/+ genotype show that PS1 expression is significantly higher than PS2 expression in all cell lines except within the M17 cell line, where PS2 expression trends ($p=0.0508$) toward being higher than PS1 expression (Figure 4-6A). The PS expression profile was determined as the PS1:PS2 ratio for all cell lines and compared to all other cell lines to generate a PS1:PS2 matrix (Figure 4-6B). From this matrix, it can be seen that, with the exception of the SH-SY5Y-derived cell lines, the PS expression profiles of all cell lines are significantly different.

The loss of PS1 has previously been shown to result in a compensatory relative upregulation of PS2 expression, and vice-versa in HEK293T cells⁵⁰ and HEK293 cells.³² As such we sought to investigate this response in the HMC3 and M17 cells lines, in order to determine the effect of the loss of either PS1 or PS2 on expression of the corresponding alternate PS homologue and the sum of total PS units expressed. To achieve this, PS1 or PS2 were ablated from HMC3 and M17 cells using CRISPR-Cas9. Attempts to generate SH-SY5Y cells with ablated PS1 or PS2 were unsuccessful. Three clones each of PS1-/-PS2+/+ (PS1KO) and PS1+/+PS2-/- (PS2KO) genotype cell line for both HMC3 and M17, as well as empty vector controls, were

generated. The three clones of PS1KO and PS2KO, from both HMC3 and M17 cell lines, were assessed via immunoblotting and qPCR to identify a representative clone for use in subsequent experiments. Firstly, all cell lines were screened to ensure that PS1 or PS2 protein expression was appropriately ablated and relative expression levels were comparable (HMC3 - SI Figure 4-2 A, B; M17 - SI Figure 4-3A, B). Further assessment of mRNA expression of all components of γ -secretase, cell type specific markers, and reference genes was completed (HMC3 - SI Figure 4-2 C-K; M17 - SI Figure 4-3C-K). The following clones were selected as 'representative' and used for subsequent experiments; HMC3 PS1KO(345), HMC3 PS2KO(141), M17 PS1KO(2920), and M17 PS2KO(1418), and will be referred to herein without the clone reference.

To demonstrate the magnitude of these changes in total PS and the absolute PS1/PS2 expression levels, PS1 and PS2 protein units have been presented as a stacked graph in Figure 4-6C. While the loss of PS1 protein in HMC3 cells does not lead to an increase in PS2 expression, the loss of PS2 protein results in a significant upregulation of PS1. Consequently, compared to HMC3 cells containing both presenilins, the loss of PS1 results in a trend ($p=0.089$) towards less total PS protein, whereas the loss of PS2 leads to significantly more total PS protein. These data indicate that PS2 could be more critical in microglial cells. Similarly, in M17 cells, the loss of PS2 leads to an increase in PS1 expression, while no effect on PS2 expression was observed as a result of the loss of PS1. Consequently, as the level of PS2 is higher than PS1 in the PS1+/+PS2+/+ cells, there are no differences between the total PS units expressed with the loss of either PS1 or PS2. This suggests that, in the M17 neuroblastoma cells, PS1 and PS2 may have considerable functional overlap as compensation for the loss of either homologue results in overall equal total PS expression.

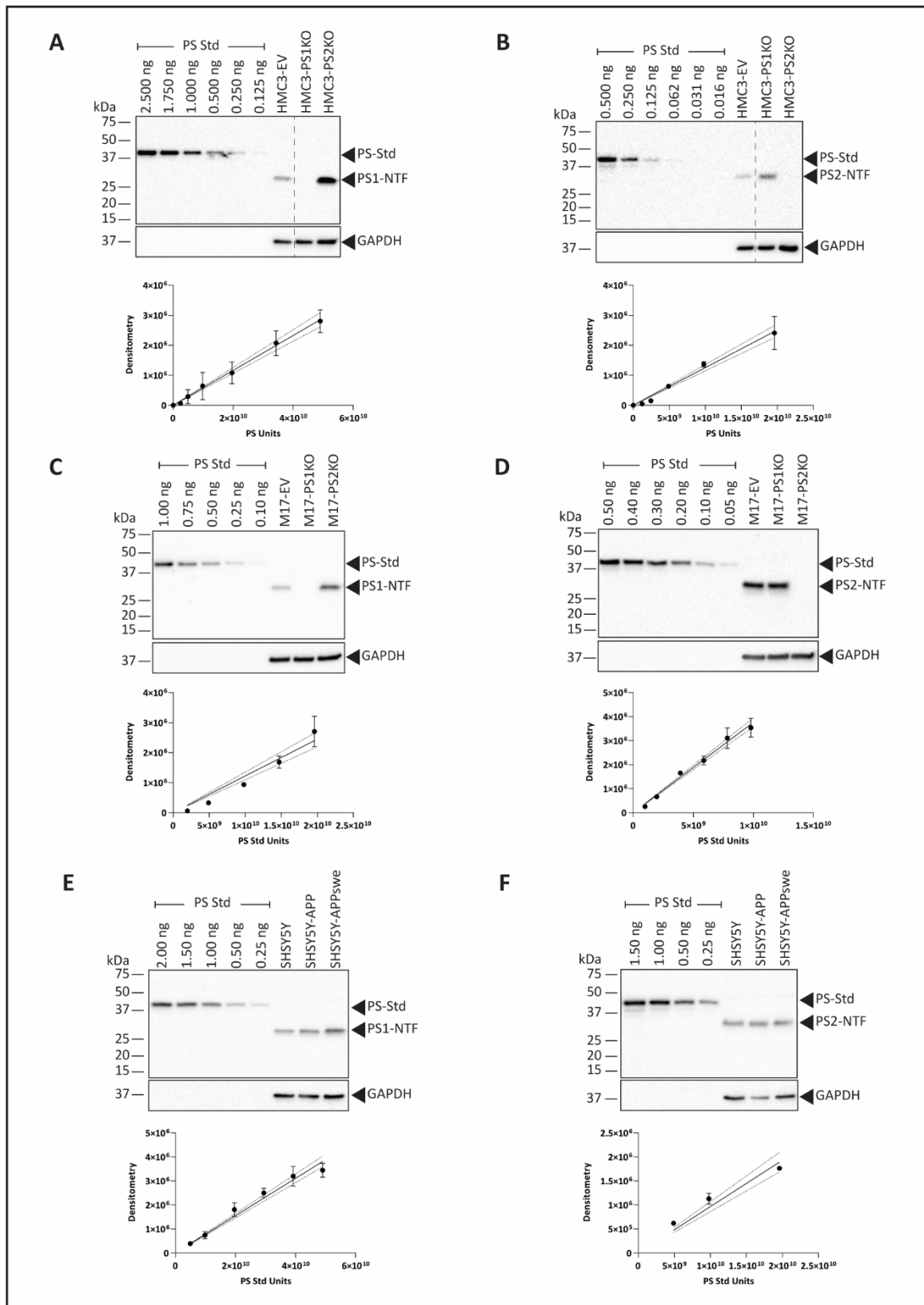


Figure 4-5 PS1-NTF and PS2-NTF expression in HMC3, M17 and SHSY5Y cells

Immunoblot results and PS-Std standard curves for PS1-NTF (A, C, E) and PS2-NTF (B, D, F) for HMC3-EV, -EV+DAPT, -PS1KO and -PS2KO cell lines (A-B), M17-EV, -PS1KO, and -PS2KO cell lines (C-D), and SH-SY5Y, SH-SY5Y-APP, and SH-SY5Y-APPswe cell lines (E-F). Representative blot of 3 to 4 biological replicates presented.

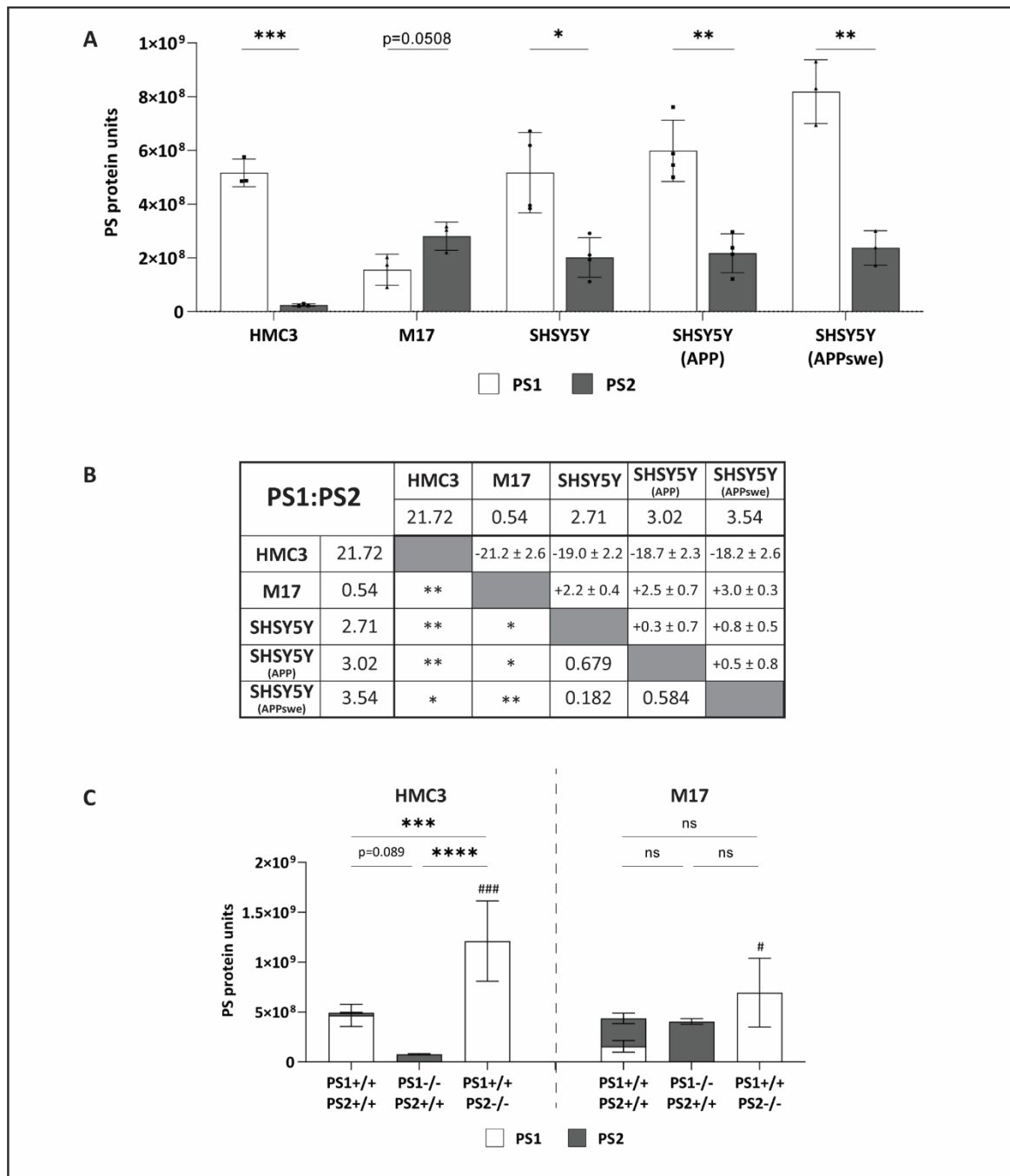


Figure 4-6 PS protein unit analysis in WT and PS deficient cell lines

Quantitation of PS protein units in cell lines with PS1^{+/+} PS2^{+/+} genotype (A). PS1:PS2 ratio comparison matrix between cell lines where data above the diagonal is the difference in the PS1:PS2 ratio between the two cell lines as determined by unpaired t-test, below the diagonal is the statistical significance of the unpaired t-test after FDR correction for multiple testing (B). PS protein units in HMC3 and M17 cells with altered PS genotypes, significant statistical differences in PS1 expression represented by #, no differences in PS2 expression reach statistical significance, results of statistical assessment of the sum of PS1 and PS2 represented by * or ns (C). Values shown are mean ± SD. Statistical tests applied were unpaired t-test, with FDR correction for multiple testing (A, B), two-way ANOVA with Holm-Šidák's multiple comparison test (within cell lines) (C) where */# = P < 0.05, **/### = P < 0.01, ***/#### = P < 0.001, ****/##### = P < 0.0001.

4.3.3 PS1 and PS2 expression response to differentiation in neuroblastoma cell lines

It has previously been reported that PS expression increases in cells with neuronal differentiation.⁴⁶⁻⁴⁸ In this study, PS1 and PS2 expression levels were quantitated in differentiated M17 and SH-SY5Y cells to directly compare PS expression in response to neuronal differentiation. Cells were differentiated for 7 days with either 10 mM retinoic acid (M17 cells) or 10 nM staurosporine (SH-SY5Y cells), as these methods have been reported to result in improved differentiation for the specific cell lines.^{42, 43} Whole cell lysates were subsequently immunoblotted for detection of PS1 and PS2 (Figure 4-7A-B), alongside the PS-Std, to quantitate and compare the PS1 and PS2 protein response.

In undifferentiated cells, the level of PS1 expression was observed to be significantly lower than PS2 expression in the M17 cells, while the PS1 expression levels were significantly higher than PS2 levels of expression in the SH-SY5Y cells. This is also reflected in the markedly increased PS1:PS2 ratio observed in SH-SY5Y cells compared to M17 cells (Figure 4-7D). These findings correspond with those shown in Figure 4-6A above. The expression of PS2 significantly increased in differentiated M17 and SH-SY5Y cells, compared to undifferentiated cells (Figure 4-7C). However, differences were observed with PS1 expression upon differentiation; while increases were observed in M17 cells, no change occurred in SH-SY5Y cells (Figure 4-7C). As a consequence of the altered PS1 and PS2 expression, the PS1:PS2 ratio is the same in both differentiated cell lines (M17 = 0.76; SH-SY5Y = 0.70) (Figure 4-7D). Overall, these findings indicate that although both M17 and SH-SY5Y are both neuroblastoma cells, they have vastly different PS expression profiles in an undifferentiated state, but differentiation to a more “neuronal like state”, alters the profiles such that the PS1:PS2 ratio is similar. Furthermore, in the differentiated state, these neuroblastoma cell lines exhibit higher PS2 expression than PS1 expression.

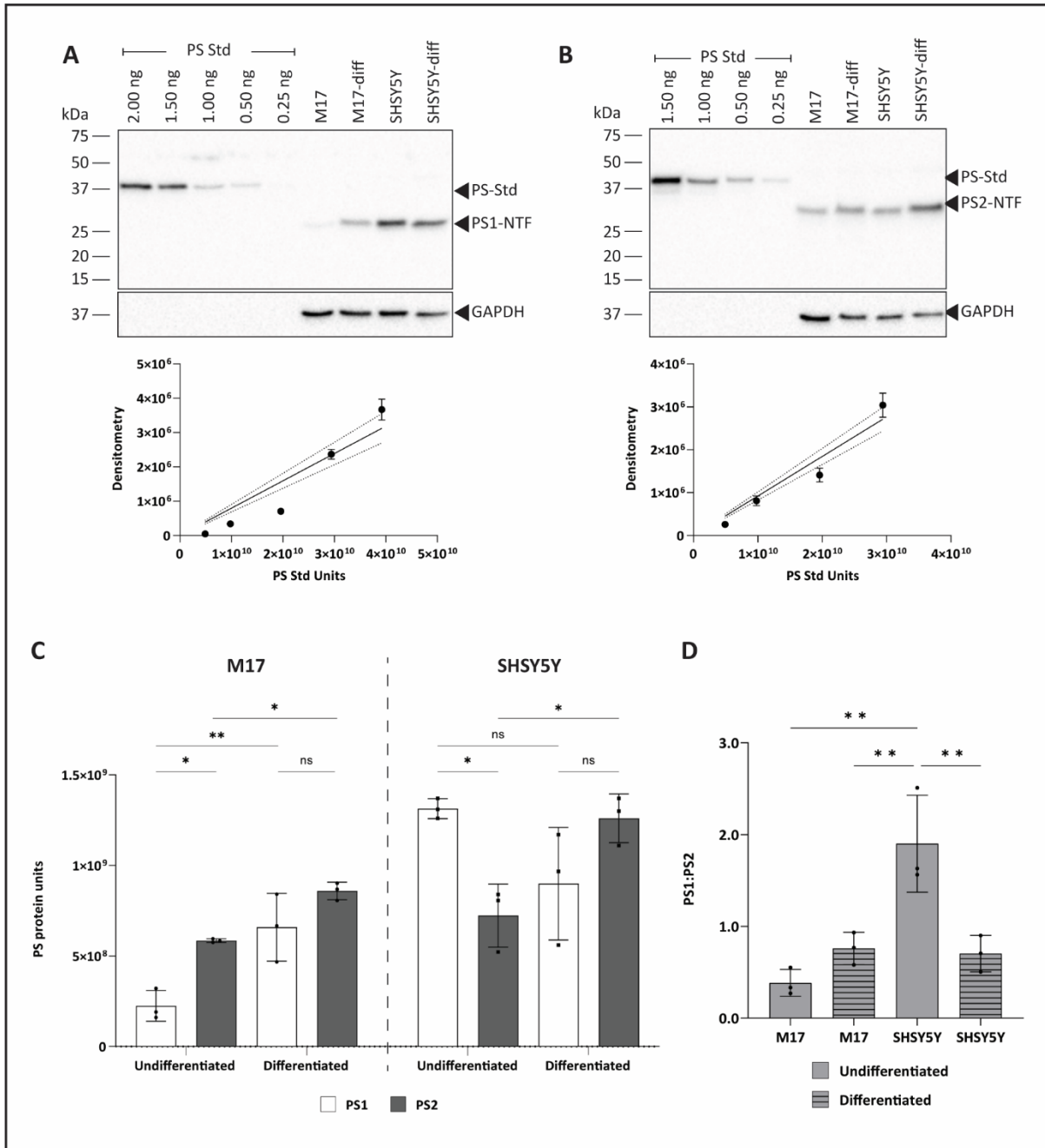


Figure 4-7 Effect of differentiation on PS expression in neuroblastomas

Immunoblot results and PS-Std curves of PS1-NTF (A) and PS2-NTF (B) in M17 and SHSY5Y neuroblastoma cell lines with and without differentiation, representative blots of 3 biological replicates. Quantiated PS protein units in differentiated and undifferentiated M17 and SH-SY5Y cells (C). Ratio of PS1:PS2 protein levels in differentiated and undifferentiated M17 and SH-SY5Y cells (D). Values shown are mean \pm SD. Statistical tests applied were two-way ANOVA (C) and one-way ANOVA (D) with Holm-Šidák's multiple comparison test where ns = not significant, * = $P < 0.05$, ** = $P < 0.01$, *** = $P < 0.001$, **** = $P < 0.0001$

4.4 DISCUSSION

Our understanding of the functional roles of presenilin, like many other proteins, has been shaped by the use of knockout mice models, cell lines, and the subsequent rescue in *in-vitro* cell lines. However, the presence of two homologous presenilins, with structural and functional overlap, complicates the interpretation of results. A large portion of studies fail to acknowledge the presence of two presenilins, often knocking out PS1 and assigning the observed outcome to PS1 with no consideration of PS2. Is the loss/gain of function observed a result of the loss of the ablated homologue or the possible upregulation of the alternate homologue? *In-vitro* studies utilising the expression of ectopic PS1 or PS2 on a PSnull background rarely tag PS proteins, with only two studies, to our knowledge, that have tagged the exogenous PS and compared corresponding expression levels.^{51,52} This is likely because it is assumed that ectopic expression, using constitutive promoters, generates similar expression levels of closely homologous proteins.⁵³ We have shown that this assumption is incorrect for overexpressed PS1 and PS2 incorporation into γ -secretase,³² which is likely due to regulation of complex formation by the other critical components of the enzyme.⁵⁴⁻⁵⁹ In this study I demonstrate the utility of our recently developed novel tool that allows absolute quantitation of endogenous PS1 and PS2, highlighting the importance of understanding PS expression when interpreting functional consequences.

This study presents, to the best of our knowledge, the first direct comparison of quantitated PS1 and PS2 protein expression in human brain tissue homogenates from FC, HPC and CBM regions, with different neurodegenerative pathologies. While direct comparison of the expression of *PSEN1* and *PSEN2* transcripts has previously been reported,¹⁵ relative assessments of mRNA or protein expression are typically presented.^{17-20, 60-64} The results presented in this chapter show that overall the PS1 expression is 30-50 times higher (dependent on the brain region) than PS2. There were also regional differences observed, where the hippocampus showed the lowest levels of PS1. However, it must be acknowledged, that in this study, whole region homogenates were used, and therefore include glial cells and neurons, which may display cell type specific PS1/PS2 expression profiles (indeed findings presented in Figures 5-7 and discussed further below support this notion). In all regions assessed, two PS2-NTF bands were detected. Multiple sized NTF proteins have previously been reported for both PS1 and PS2, associated with neuronal maturation where expression of the larger NTF protein increases with maturation, and is likely indicative of alternative proteolytic cleavage of the PS-holoprotein.⁶⁵ In the current study, only observed multiple NTF cleavage products for the PS2 protein were detected, quantitation of which showed the ratio of upper and lower bands

to decrease in the HPC. Whether these protein bands represent different forms of PS2, or post-translational modification, was not confirmed, but the changes within the hippocampus could reflect the loss of mature neurons. Furthermore, unlike a study by Mathews et al.,⁶⁶ full length PS2 protein was not detected in any human brain samples used in the current study. However, similarly to Mathews et al., full length PS1 was not detected. The data presented in the current study used the same PS1-NTF antibody clone (NT1) as Mathews et al., thereby reflecting similar findings.⁶⁶ The PS2-NTF antibody, however, is not the same and thus could reflect the differences between the two studies observed for PS2. Notably in this study a monoclonal antibody was used, whereas in Mathews et al, a polyclonal antibody was used. Additionally, it must be acknowledged that the conditions for sample preparation and PAGE chemistries used were different in this study compared with Mathews et al. Interestingly the conditions used in Mathews et al, could be considered harsher, and more likely to lead to potential protein degradation, the main difference being higher sample treatment temperature and the addition of urea. The effect of these differing conditions should be considered in future studies.

A comparison of presenilin expression between control, AD and the other neurodegenerative diseases revealed changes in the hippocampus of the AD brain. Previous reports of PS1 and PS2 expression changes in human brain with sporadic AD pathology are not consistent. While one study reports that *PSEN1* expression increases in the temporal lobe,⁶⁷ others report decreases in *PSEN1* in both the temporal and frontal cortices⁶⁸ and *PSEN2* in all hippocampal regions.⁶⁹ Protein expression reports are similarly discordant; where one study found no difference in PS1 or PS2 levels in the FC,⁶⁶ yet another reports that PS1 expression decreased in the frontal and temporal cortices, and the hippocampus.⁷⁰ In this study, we observe no changes to PS1 expression compared with control in either the FC or HPC. In the CBM region PS1 expression in AD samples is significantly lower than LBD samples, however the lack of control samples precludes any opportunity to comment on the pathological significance of this observation. Interestingly PS2 expression is decreased in AD samples compared to both control and FTD, specifically in the HPC. The reduction in PS2 is consistent with decreases in *PSEN2* transcript that we have previously observed in the same samples and may reflect a reduction in PS2 associated with AD pathology or pathogenesis³³. However, it must be acknowledged that the number of control samples available in this (and the previous study³³) are low, suggesting that some caution on the interpretation of the results is required. The ability to quantitate PS levels in brain homogenates demonstrated in this chapter can be used to expand the study to a larger number of samples to validate our preliminary findings in future work.

In-vitro studies of human PS have commonly been undertaken using exogenous re-expression of either *PSEN1* or *PSEN2* in mouse embryonic fibroblast in which the endogenous murine *Psen1* and *Psen2* have been ablated. More recently, the advancement of CRISPR technology has enabled the development of new cell lines and several cell lines of PS1^{-/-}, PS2^{-/-} and/or double knockout (PS1^{-/-}PS2^{-/-}) genotype to be generated.^{32, 48, 50, 71, 72} The relative ratios of PS1 and PS2 in various human cell lines have been reported as both similar⁵⁰ and variable.⁵¹ The current study investigated human immortalised cell lines commonly used for *in-vitro* AD studies, and observed significantly different PS1 and PS2 expression levels in all cell lines (except M17 which trended towards significance). Furthermore, the PS1:PS2 ratios ranged from 21.72 to 0.54, and were significantly different between cells of different origin, highlighting the importance of understanding comparative PS expression levels in cellular models of AD.

Cognisance of PS expression is particularly important for ascertaining the specific contributions of PS1 γ versus PS2 γ . It has been observed that the A β 42:A β 40 ratio increases, while the PS1:PS2 expression ratio decreases, with age in murine models.¹⁸ Similarly in mice, where PS1 is conditionally ablated, but PS2 expression is retained, the A β 42:A β 40 ratio is increased.³¹ The observed increase in A β 42:A β 40 ratio may be a consequence of decreased PS1:PS2 expression ratio, particularly with age, as several studies have shown that PS2 γ generates higher A β 42:A β 40 ratio than PS1 γ .^{32, 48, 71, 73} Interestingly advances in single cell RNA sequencing technologies are providing new insights into *PSEN1* and *PSEN2* expression in neurons and glial cells, where *PSEN2* is more highly expressed in neurons, compared with *PSEN1* which is mostly highly expressed in oligodendrocytes.^{74, 75} The current study presents two key results that suggest PS2 may play a more important role in neurons. Firstly, the loss of either PS1 or PS2 in M17 cells results in compensatory upregulation of the alternate PS homologue, such that there is no significant difference in total PS expression. Secondly, PS2 upregulation occurs in both M17 and SH-SY5Y cells that have been differentiated, to be more neuronally representative, such that the PS1:PS2 ratios are <1.0. These results suggest important roles for both PS1 and PS2 in mature neurons, and support previous results in iPSCs showing an increase of PS2 expression with differentiation, concomitant with no change in PS1 expression.⁴⁸

Further to the AD-associated functional roles of PS1 and PS2 in neurons,^{21-29, 48, 72} important roles for presenilin in microglial cytokine response^{49, 76} and A β clearance^{77, 78} have also been

reported. Furthermore, several substrates important for the microglia response to A β are actually substrates of γ -secretase,⁷⁸⁻⁸⁶ and PS2 is suggested to be critical for microglial cytokine responses.^{49, 76} In contrast to the suggested importance of PS2 in microglial function, it has been observed in this study, that of all the cells examined, PS2 expression is lowest in HMC3 cells – at least an order of magnitude lower compared to the next lowest SH-SY5Y cells. Interestingly, while the loss of either PS1 or PS2 is significantly compensated by the alternative homologue, total PS units expressed are significantly higher in cells lacking PS2, while those that retain PS2 have significantly lower total PS expression. This observation aligns with previous reports of significantly increased PS1 expression with loss of PS2 in murine microglia.⁴⁹ Although not conclusive evidence, the level of increase of PS1 expression in response to the loss of PS2 is certainly suggestive of a critical role for PS2 in microglial function and is further support for the higher efficiency of PS2 γ as an enzyme as presented in Chapter 2 (Quantitative comparison of presenilin protein expression reveals greater activity of PS2- γ -secretase). The functional effect of the loss of PS1 or PS2 in microglia is further investigated in Chapter 5 (Differential functions of presenilin-1 and presenilin-2 in human microglia).

In conclusion, the utility of the PS-Std tool for direct quantitative assessment of endogenous PS1 and PS2 expression has been demonstrated, highlighting the potential applications and novel insights that can be achieved by quantitatively comparing PS protein expression. Recognising that PS1 and PS2 expression is highly variable in different cell types emphasises the need for due consideration of expression to ensure accurate interpretation of the functional roles of PS1 and PS2 in different settings. Furthermore, the comparative assessment of PS1 and PS2 expression will provide valuable information that enables improved development of γ -secretase targeting therapeutics.

4.5 REFERENCES

1. Kimberly, W. T., Xia, W., Rahmati, T., Wolfe, M. S., and Selkoe, D. J. (2000) The transmembrane aspartates in presenilin 1 and 2 are obligatory for γ -secretase activity and amyloid β -protein generation. *The Journal of biological chemistry* **275**, 3173-3178
2. Ryman, D. C., Acosta-Baena, N., Aisen, P. S., Bird, T., Danek, A., Fox, N. C., Goate, A., Frommelt, P., Ghetti, B., Langbaum, J. B. S., Lopera, F., Martins, R., Masters, C. L., Mayeux, R. P., McDade, E., Moreno, S., Reiman, E. M., Ringman, J. M., Salloway, S., Schofield, P. R., Sperling, R., Tariot, P. N., Xiong, C., Morris, J. C., Bateman, R. J., and And

- the Dominantly Inherited Alzheimer, N. (2014) Symptom onset in autosomal dominant Alzheimer disease: A systematic review and meta-analysis. *Neurology* **83**, 253-260
3. Mullan, M., Houlden, H., Windelspecht, M., Fidani, L., Lombardi, C., Diaz, P., Rossor, M., Crook, R., Hardy, J., Duff, K., and Crawford, F. (1992) A locus for familial early-onset Alzheimer's disease on the long arm of chromosome 14, proximal to the [alpha]1-antichymotrypsin gene. *Nature Genetics* **2**, 340-342
 4. Sherrington, R., Rogaev, E. I., Liang, Y., Rogaeva, E. A., and et al. (1995) Cloning of a gene bearing missense mutations in early-onset familial Alzheimer's disease. *Nature* **375**, 754-760
 5. Levy-Lahad, E., Wasco, W., Poorkaj, P., Romano, D. M., Oshima, J., Pettingell, W. H., Yu, C.-e., Jondro, P. D., Schmidt, S. D., Wang, K., Crowley, A. C., Fu, Y.-H., Guenette, S. Y., Galas, D., Nemens, E., Wijsman, E. M., Bird, T. D., Schellenberg, G. D., and Tanzi, R. E. (1995) Candidate Gene for the Chromosome 1 Familial Alzheimer's Disease Locus. *Science (New York, N.Y.)* **269**, 973-977
 6. Rogaev, E. I., Sherrington, R., Rogaeva, E. A., Levesque, G., Ikeda, M., Liang, Y., Chi, H., Lin, C., Holman, K., Tsuda, T., Mar, L., Sorbi, S., Nacmias, B., Piacentini, S., Amaducci, L., Chumakov, I., Cohen, D., Lannfelt, L., Fraser, P. E., Rommens, J. M., and George-Hyslop, P. H. S. (1995) Familial Alzheimer's disease in kindreds with missense mutations in a gene on chromosome 1 related to the Alzheimer's disease type 3 gene. *Nature* **376**, 775-778
 7. Yonemura, Y., Futai, E., Yagishita, S., Kaether, C., and Ishiura, S. (2016) Specific combinations of presenilins and Aph1s affect the substrate specificity and activity of γ -secretase. *Biochemical and biophysical research communications* **478**, 1751-1757
 8. Herreman, A., Hartmann, D., Annaert, W., Saftig, P., Craessaerts, K., Serneels, L., Umans, L., Schrijvers, V., Checler, F., Vanderstichele, H., Baekelandt, V., Dressel, R., Cupers, P., Huylebroeck, D., Zwijsen, A., Van Leuven, F., and De Strooper, B. (1999) Presenilin 2 Deficiency Causes a Mild Pulmonary Phenotype and no Changes in Amyloid Precursor Protein Processing but Enhances the Embryonic Lethal Phenotype of Presenilin 1 Deficiency. *Proceedings of the National Academy of Sciences of the United States of America* **96**, 11872-11877
 9. Shen, J., Bronson, R. T., Chen, D. F., Xia, W., Selkoe, D. J., and Tonegawa, S. (1997) Skeletal and CNS Defects in Presenilin-1-Deficient Mice. *Cell* **89**, 629-639
 10. Wong, P. C., Zheng, H., Chen, H., Becher, M. W., Sirinathsinghji, D. J. S., Trumbauer, M. E., Chen, H. Y., Price, D. L., Van Der Ploeg, L. H. T., and Sisodia, S. S. (1997) Presenilin 1 is required for Notch 1 and DII 1 expression in the paraxial mesoderm. *Nature* **387**, 288-292
 11. Acx, H., Chávez-Gutiérrez, L., Serneels, L., Lismont, S., Benurwar, M., Elad, N., and De Strooper, B. (2014) Signature amyloid β profiles are produced by different γ -secretase complexes. *The Journal of biological chemistry* **289**, 4346-4355
 12. Meckler, X., and Checler, F. (2016) Presenilin 1 and presenilin 2 target γ -secretase complexes to distinct cellular compartments. *The Journal of biological chemistry* **291**, 12821-12837
 13. Mastrangelo, P., Mathews, P. M., Chishti, M. A., Schmidt, S. D., Gu, Y., Yang, J., Mazzella, M. J., Coomaraswamy, J., Horne, P., Strome, B., Pelly, H., Levesque, G., Ebeling, C., Jiang, Y., Nixon, R. A., Rozmahel, R., Fraser, P. E., St George-Hyslop, P., Carlson, G. A., Westaway, D., and Prusiner, S. B. (2005) Dissociated Phenotypes in Presenilin Transgenic Mice Define Functionally Distinct γ -Secretases. *Proceedings of the National Academy of Sciences of the United States of America* **102**, 8972-8977
 14. Donoviel, D. B., Hadjantonakis, A.-K., Ikeda, M., Zheng, H., Hyslop, P. S. G., and Bernstein, A. (1999) Mice lacking both presenilin genes exhibit early embryonic patterning defects. *Genes & development* **13**, 2801-2810

15. Lee, M. K., Slunt, H. H., Martin, L. J., Thinakaran, G., Kim, G., Gandy, S. E., Seeger, M., Koo, E., Price, D. L., and Sisodia, S. S. (1996) Expression of presenilin 1 and 2 (PS1 and PS2) in human and murine tissues. *The Journal of Neuroscience* **16**, 7513-7525
16. Kumar, A., and Thakur, M. K. (2012) Presenilin 1 and 2 are expressed differentially in the cerebral cortex of mice during development. *Neurochemistry International* **61**, 778-782
17. Thakur, M. K., and Ghosh, S. (2007) Age and sex dependent alteration in presenilin expression in mouse cerebral cortex. *Cellular and molecular neurobiology* **27**, 1059-1067
18. Placanica, L., Zhu, L., and Li, Y.-M. (2009) Gender- and age-dependent gamma-secretase activity in mouse brain and its implication in sporadic Alzheimer disease. *PloS one* **4**, e5088-e5088
19. Ghosh, S., and Thakur, M. K. (2008) PS2 protein expression is upregulated by sex steroids in the cerebral cortex of aging mice. *Neurochemistry International* **52**, 363-367
20. Kaja, S., Sumien, N., Shah, V. V., Puthawala, I., Maynard, A. N., Khullar, N., Payne, A. J., Forster, M. J., and Koulen, P. (2015) Loss of spatial memory, learning and motor coordination during normal aging is accompanied by changes in brain presenilin 1 and 2 expression levels. *Molecular Neurobiology* **52**, 545-554
21. Cao, T., Zhou, X., Zheng, X., Cui, Y., Tsien, J. Z., Li, C., and Wang, H. (2018) Histone Deacetylase Inhibitor Alleviates the Neurodegenerative Phenotypes and Histone Dysregulation in Presenilins-Deficient Mice. *Front Aging Neurosci* **10**
22. Feng, R., Wang, H., Wang, J., Shrom, D., Zeng, X., and Tsien, J. Z. (2004) Forebrain degeneration and ventricle enlargement caused by double knockout of Alzheimer's presenilin-1 and presenilin-2. *Proceedings of the National Academy of Sciences of the United States of America* **101**, 8162-8167
23. Kang, J., and Shen, J. (2020) Cell-autonomous role of Presenilin in age-dependent survival of cortical interneurons. *Molecular neurodegeneration* **15**, 72
24. Peng, W., Xie, Y., Liao, C., Bai, Y., Wang, H., and Li, C. (2022) Spatiotemporal patterns of gliosis and neuroinflammation in presenilin 1/2 conditional double knockout mice. *Front Aging Neurosci* **14**
25. Saura, C. A., Choi, S.-Y., Beglopoulos, V., Malkani, S., Zhang, D., Rao, B. S. S., Chattarji, S., Kelleher Iii, R. J., Kandel, E. R., Duff, K., Kirkwood, A., and Shen, J. (2004) Loss of Presenilin Function Causes Impairments of Memory and Synaptic Plasticity Followed by Age-Dependent Neurodegeneration. *Neuron* **42**, 23-36
26. Soto-Faguás, C. M., Sanchez-Molina, P., and Saura, C. A. (2021) Loss of presenilin function enhances tau phosphorylation and aggregation in mice. *Acta neuropathologica communications* **9**, 162
27. Watanabe, H., Iqbal, M., Zheng, J., Wines-Samuelson, M., and Shen, J. (2014) Partial Loss of Presenilin Impairs Age-Dependent Neuronal Survival in the Cerebral Cortex. *The Journal of Neuroscience* **34**, 15912-15922
28. Wines-Samuelson, M., Schulte, E. C., Smith, M. J., Aoki, C., Liu, X., Kelleher, R. J., III, and Shen, J. (2010) Characterization of Age-Dependent and Progressive Cortical Neuronal Degeneration in Presenilin Conditional Mutant Mice. *PloS one* **5**, e10195
29. Zhu, M., Gu, F., Shi, J., Hu, J., Hu, Y., and Zhao, Z. (2008) Increased oxidative stress and astrogliosis responses in conditional double-knockout mice of Alzheimer-like presenilin-1 and presenilin-2. *Free Radical Biology and Medicine* **45**, 1493-1499
30. Steiner, H., Duff, K., Capell, A., Romig, H., Grim, M. G., Lincoln, S., Hardy, J., Yu, X., Picciano, M., Fichtler, K., Citron, M., Kopan, R., Pesold, B., Keck, S., Baader, M., Tomita, T., Iwatsubo, T., Baumeister, R., and Haass, C. (1999) A Loss of Function Mutation of Presenilin-2 Interferes with Amyloid β -Peptide Production and Notch Signaling. *The Journal of biological chemistry* **274**, 28669-28673

31. Yu, H., Saura, C. A., Choi, S.-Y., Sun, L. D., Yang, X., Handler, M., Kawarabayashi, T., Younkin, L., Fedeles, B., Wilson, M. A., Younkin, S., Kandel, E. R., Kirkwood, A., and Shen, J. (2001) APP Processing and Synaptic Plasticity in Presenilin-1 Conditional Knockout Mice. *Neuron* **31**, 713-726
32. Eccles, M. K., Main, N., Sabale, M., Roberts-Mok, B., Agostino, M., Groth, D., Fraser, P. E., and Verdile, G. (2023) Quantitative Comparison of Presenilin Protein Expression Reveals Greater Activity of PS2- γ -Secretase. *bioRxiv*, 2023.2005.2009.540102
33. Moussavi Nik, S. H., Porter, T., Newman, M., Bartlett, B., Khan, I., Sabale, M., Eccles, M., Woodfield, A., Groth, D., Dore, V., Villemagne, V. L., Masters, C. L., Martins, R. N., Laws, S. M., Lardelli, M., and Verdile, G. (2021) Relevance of a Truncated PRESENILIN 2 Transcript to Alzheimer's Disease and Neurodegeneration. *Journal of Alzheimer's Disease* **80**, 1479-1489
34. Ciccarone, V., Spengler, B. A., Meyers, M. B., Biedler, J. L., and Ross, R. A. (1989) Phenotypic diversification in human neuroblastoma cells: expression of distinct neural crest lineages. *Cancer Research* **49**, 219-225
35. Biedler, J. L., Helson, L., and Spengler, B. A. (1973) Morphology and growth, tumorigenicity, and cytogenetics of human neuroblastoma cells in continuous culture. *Cancer Research* **33**, 2643-2652
36. Janabi, N., Peudenier, S., Héron, B., Ng, K. H., and Tardieu, M. (1995) Establishment of human microglial cell lines after transfection of primary cultures of embryonic microglial cells with the SV40 large T antigen. *Neuroscience letters* **195**, 105-108
37. Ran, F. A., Hsu, P. D., Wright, J., Agarwala, V., Scott, D. A., and Zhang, F. (2013) Genome engineering using the CRISPR-Cas9 system. *Nature Protocols* **8**, 2281
38. Montague, T. G., Cruz, J. M., Gagnon, J. A., Church, G. M., and Valen, E. (2014) CHOPCHOP: a CRISPR/Cas9 and TALEN web tool for genome editing. *Nucleic Acids Res* **42**, W401-W407
39. Labun, K., Montague, T. G., Gagnon, J. A., Thyme, S. B., and Valen, E. (2016) CHOPCHOP v2: a web tool for the next generation of CRISPR genome engineering. *Nucleic Acids Res* **44**, W272-W276
40. Doench, J. G., Fusi, N., Sullender, M., Hegde, M., Vaimberg, E. W., Donovan, K. F., Smith, I., Tothova, Z., Wilen, C., Orchard, R., Virgin, H. W., Listgarten, J., and Root, D. E. (2016) Optimized sgRNA design to maximize activity and minimize off-target effects of CRISPR-Cas9. *Nature Biotechnology* **34**, 184-191
41. Sanson, K. R., Hanna, R. E., Hegde, M., Donovan, K. F., Strand, C., Sullender, M. E., Vaimberg, E. W., Goodale, A., Root, D. E., Piccioni, F., and Doench, J. G. (2018) Optimized libraries for CRISPR-Cas9 genetic screens with multiple modalities. *Nature Communications* **9**, 5416
42. Andres, D., Keyser, B. M., Petrali, J., Benton, B., Hubbard, K. S., McNutt, P. M., and Ray, R. (2013) Morphological and functional differentiation in BE(2)-M17 human neuroblastoma cells by treatment with Trans-retinoic acid. *BMC neuroscience* **14**, 49
43. Filograna, R., Civiero, L., Ferrari, V., Codolo, G., Greggio, E., Bubacco, L., Beltramini, M., and Bisaglia, M. (2015) Analysis of the Catecholaminergic Phenotype in Human SH-SY5Y and BE(2)-M17 Neuroblastoma Cell Lines upon Differentiation. *PloS one* **10**, e0136769- e0136769
44. Pfaffl, M. W. (2001) A new mathematical model for relative quantification in real-time RT-PCR. *Nucleic Acids Res* **29**, e45-e45
45. Fraser, P. E., Levesque, G., Yu, G., Mills, L. R., Thirlwell, J., Frantseva, M., Gandy, S. E., Seeger, M., Carlen, P. L., and St George-Hyslop, P. (1998) Presenilin 1 is actively degraded by the 26S proteasome. *Neurobiology of aging* **19**, S19-S21

46. Culvenor, J. G., Evin, G., Cooney, M. A., Wardan, H., Sharples, R. A., Maher, F., Reed, G., Diehlmann, A., Weidemann, A., Beyreuther, K., and Masters, C. L. (2000) Presenilin 2 expression in neuronal cells: induction during differentiation of embryonic carcinoma cells. *Experimental cell research* **255**, 192-206
47. Flood, F., Sundström, E., Samuelsson, E.-B., Wiehager, B., Seiger, Å., Johnston, J. A., and Cowburn, R. F. (2004) Presenilin expression during induced differentiation of the human neuroblastoma SH-SY5Y cell line. *Neurochemistry International* **44**, 487-496
48. Watanabe, H., Imaizumi, K., Cai, T., Zhou, Z., Tomita, T., and Okano, H. (2021) Flexible and accurate substrate processing with distinct presenilin/ γ -secretases in human cortical neurons. *eNeuro* **8**, ENEURO.0500-0520.2021
49. Jayadev, S., Case, A., Eastman, A. J., Nguyen, H., Pollak, J., Wiley, J. C., Möller, T., Morrison, R. S., and Garden, G. A. (2010) Presenilin 2 Is the Predominant γ -Secretase in Microglia and Modulates Cytokine Release. *PLoS one* **5**
50. Lessard, C. B., Rodriguez, E., Ladd, T. B., Minter, L. M., Osborne, B. A., Miele, L., Golde, T. E., and Ran, Y. (2019) Individual and combined presenilin 1 and 2 knockouts reveal that both have highly overlapping functions in HEK293T cells. *The Journal of biological chemistry* **294**, 11276-11285
51. Sannerud, R., Esselens, C., Ejsmont, P., Mattera, R., Rochin, L., Tharkeshwar, Arun K., De Baets, G., De Wever, V., Habets, R., Baert, V., Vermeire, W., Michiels, C., Groot, Arjan J., Wouters, R., Dillen, K., Vints, K., Baatsen, P., Munck, S., Derua, R., Waelkens, E., Basi, Guriqbal S., Mercken, M., Vooijs, M., Bollen, M., Schymkowitz, J., Rousseau, F., Bonifacino, Juan S., Van Niel, G., De Strooper, B., and Annaert, W. (2016) Restricted location of PSEN2/ γ -secretase determines substrate specificity and generates an intracellular A β pool. *Cell* **166**, 193-208
52. Yonemura, Y., Futai, E., Yagishita, S., Suo, S., Tomita, T., Iwatsubo, T., and Ishiura, S. (2011) Comparison of presenilin 1 and presenilin 2 γ -secretase activities using a yeast reconstitution system. *The Journal of biological chemistry* **286**, 44569-44575
53. Xia, W., Bringmann, P., McClary, J., Jones, P. P., Manzana, W., Zhu, Y., Wang, S., Liu, Y., Harvey, S., Madlansacay, M. R., McLean, K., Rosser, M. P., MacRobbie, J., Olsen, C. L., and Cobb, R. R. (2006) High levels of protein expression using different mammalian CMV promoters in several cell lines. *Protein Expression and Purification* **45**, 115-124
54. Edbauer, D., Winkler, E., Haass, C., and Steiner, H. (2002) Presenilin and nicastrin regulate each other and determine amyloid β -peptide production via complex formation. *Proceedings of the National Academy of Sciences of the United States of America* **99**, 8666-8671
55. Luo, W. J., Wang, H., Li, H., Kim, B. S., Shah, S., Lee, H. J., Thinakaran, G., Kim, T. W., Yu, G., and Xu, H. (2003) PEN-2 and APH-1 coordinately regulate proteolytic processing of presenilin 1. *The Journal of biological chemistry* **278**, 7850-7854
56. Steiner, H., Winkler, E., Edbauer, D., Prokop, S., Basset, G., Yamasaki, A., Kostka, M., and Haass, C. (2002) PEN-2 is an integral component of the γ -secretase complex required for coordinated expression of presenilin and nicastrin. *The Journal of biological chemistry* **277**, 39062-39065
57. Thinakaran, G., Harris, C. L., Ratovitski, T., Davenport, F., Slunt, H. H., Price, D. L., Borchelt, D. R., and Sisodia, S. S. (1997) Evidence that levels of presenilins (PS1 and PS2) are coordinately regulated by competition for limiting cellular factors. *The Journal of biological chemistry* **272**, 28415-28422
58. Kimberly, W. T., LaVoie, M. J., Ostaszewski, B. L., Ye, W., Wolfe, M. S., and Selkoe, D. J. (2003) γ -Secretase is a membrane protein complex comprised of presenilin, nicastrin, aph-1, and pen-2. *Proceedings of the National Academy of Sciences of the United States of America* **100**, 6382-6387

59. Yang, D.-S., Tandon, A., Chen, F., Yu, G., Yu, H., Arawaka, S., Hasegawa, H., Duthie, M., Schmidt, S. D., Ramabhadran, T. V., Nixon, R. A., Mathews, P. M., Gandy, S. E., Mount, H. T. J., St George-Hyslop, P., and Fraser, P. E. (2002) Mature glycosylation and trafficking of nicastrin modulate its binding to presenilins. *The Journal of biological chemistry* **277**, 28135-28142
60. Deng, G., Su, J. H., and Cotman, C. W. (1996) Gene expression of Alzheimer-associated presenilin-2 in the frontal cortex of Alzheimer and aged control brain. *FEBS Letters* **394**, 17-20
61. Suzuki, T., Nishiyama, K., Murayama, S., Yamamoto, A., Sato, S., Kanazawa, I., and Sakaki, Y. (1996) Regional and Cellular Presenilin 1 Gene Expression in Human and Rat Tissues. *Biochemical and biophysical research communications* **219**, 708-713
62. Benkovic, S. A., McGowan, E. M., Rothwell, N. J., Hutton, M., Morgan, D. G., and Gordon, M. N. (1997) Regional and Cellular Localization of Presenilin-2 RNA in Rat and Human Brain. *Experimental Neurology* **145**, 555-564
63. Takami, K., Terai, K., Matsuo, A., Walker, D. G., and McGeer, P. L. (1997) Expression of presenilin-1 and -2 mRNAs in rat and Alzheimer's disease brains. *Brain research* **748**, 122-130
64. Kovacs, D. M., Fausett, H. J., Page, K. J., Kim, T.-W., Moir, R. D., Merriam, D. E., Hollister, R. D., Hallmark, O. G., Mancini, R., Felsenstein, K. M., Hyman, B. T., Tanzi, R. E., and Wasco, W. (1996) Alzheimer-associated presenilins 1 and 2 : Neuronal expression in brain and localization to intracellular membranes in mammalian cells. *Nature medicine* **2**, 224-229
65. Capell, A., Saffrich, R., Olivo, J.-C., Meyn, L., Walter, J., Grünberg, J., Mathews, P., Nixon, R., Dotti, C., and Haass, C. (1997) Cellular Expression and Proteolytic Processing of Presenilin Proteins Is Developmentally Regulated During Neuronal Differentiation. *Journal of neurochemistry* **69**, 2432-2440
66. Mathews, P. M., Cataldo, A. M., Kao, B. H., Rudnicki, A. G., Qin, X., Yang, J. L., Jiang, Y., Picciano, M., Hulette, C., Lippa, C. F., Bird, T. D., Nochlin, D., Walter, J., Haass, C., Lévesque, L., Fraser, P. E., Andreadis, A., and Nixon, R. A. (2000) Brain Expression of Presenilins in Sporadic and Early-onset, Familial Alzheimer's Disease. *Molecular Medicine* **6**, 878-891
67. Ikeda, K., Urakami, K., Arai, H., Wada, K., and et al. (2000) The expression of presenilin 1 mRNA in skin fibroblasts and brains from sporadic Alzheimer's disease. *Dementia and Geriatric Cognitive Disorders* **11**, 245-250
68. Johnston, J. A., Froelich, S., Lannfelt, L., and Cowburn, R. F. (1996) Quantification of presenilin-1 mRNA in Alzheimer's disease brains. *FEBS Letters* **394**, 279-284
69. McMillan, P. J., Leverenz, J. B., and Dorsa, D. M. (2000) Specific downregulation of presenilin 2 gene expression is prominent during early stages of sporadic late-onset Alzheimer's disease. *Molecular Brain Research* **78**, 138-145
70. Davidsson, P., Bogdanovic, N., Lannfelt, L., and Blennow, K. (2001) Reduced expression of amyloid precursor protein, presenilin-1 and rab3a in cortical brain regions in Alzheimer's disease. *Dementia and Geriatric Cognitive Disorders* **12**, 243-250
71. Pimenova, A. A., and Goate, A. M. (2020) Novel presenilin 1 and 2 double knock-out cell line for in vitro validation of PSEN1 and PSEN2 mutations. *Neurobiology of disease*, 104785
72. Lauer, A. A., Mett, J., Janitschke, D., Thiel, A., Stahlmann, C. P., Bachmann, C. M., Ritzmann, F., Schrul, B., Müller, U. C., Stein, R., Riemenschneider, M., Grimm, H. S., Hartmann, T., and Grimm, M. O. W. (2020) Regulatory feedback cycle of the insulin-degrading enzyme and the amyloid precursor protein intracellular domain: Implications for Alzheimer's disease. *Aging cell* **19**, e13264

73. Placanica, L., Tarassishin, L., Yang, G., Peethumnongsin, E., Kim, S.-H., Zheng, H., Sisodia, S. S., and Li, Y.-M. (2009) Pen2 and presenilin-1 modulate the dynamic equilibrium of presenilin-1 and presenilin-2 γ -secretase complexes. *The Journal of biological chemistry* **284**, 2967-2977
74. Kelley, K. W., Nakao-Inoue, H., Molofsky, A. V., and Oldham, M. C. (2018) Variation among intact tissue samples reveals the core transcriptional features of human CNS cell classes. *Nature neuroscience* **21**, 1171-1184
75. Herring, C. A., Simmons, R. K., Freytag, S., Poppe, D., Moffet, J. J. D., Pflueger, J., Buckberry, S., Vargas-Landin, D. B., Clément, O., Echeverría, E. G., Sutton, G. J., Alvarez-Franco, A., Hou, R., Pflueger, C., McDonald, K., Polo, J. M., Forrest, A. R. R., Nowak, A. K., Voineagu, I., Martelotto, L., and Lister, R. (2022) Human prefrontal cortex gene regulatory dynamics from gestation to adulthood at single-cell resolution. *Cell* **185**, 4428-4447.e4428
76. Jayadev, S., Case, A., Alajajian, B., Eastman, A. J., Möller, T., and Garden, G. A. (2013) Presenilin 2 influences miR146 level and activity in microglia. *Journal of neurochemistry* **127**, 592-599
77. Farfara, D., Trudler, D., Segev-Amzaleg, N., Galron, R., Stein, R., and Frenkel, D. (2011) γ -Secretase component presenilin is important for microglia β -amyloid clearance. *Annals of neurology* **69**, 170-180
78. Wunderlich, P., Glebov, K., Kemmerling, N., Tien, N. T., Neumann, H., and Walter, J. (2013) Sequential proteolytic processing of the triggering receptor expressed on myeloid cells-2 (TREM2) protein by ectodomain shedding and γ -secretase-dependent intramembranous cleavage. *The Journal of biological chemistry* **288**, 33027-33036
79. Fourgeaud, L., Través, P. G., Tufail, Y., Leal-Bailey, H., Lew, E. D., Burrola, P. G., Callaway, P., Zagórska, A., Rothlin, C. V., Nimmerjahn, A., and Lemke, G. (2016) TAM receptors regulate multiple features of microglial physiology. *Nature* **532**, 240-244
80. Manocha, G. D., Floden, A. M., Rausch, K., Kulas, J. A., McGregor, B. A., Rojanathammanee, L., Puig, K. R., Puig, K. L., Karki, S., Nichols, M. R., Darland, D. C., Porter, J. E., and Combs, C. K. (2016) APP Regulates Microglial Phenotype in a Mouse Model of Alzheimer's Disease. *The Journal of Neuroscience* **36**, 8471-8486
81. Kemmerling, N., Wunderlich, P., Theil, S., Linnartz-Gerlach, B., Hersch, N., Hoffmann, B., Heneka, M. T., Strooper, B. d., Neumann, H., and Walter, J. (2017) Intramembranous processing by γ -secretase regulates reverse signaling of ephrin-B2 in migration of microglia. *Glia* **65**, 1103-1118
82. Huang, Y., Happonen, K. E., Burrola, P. G., O'Connor, C., Hah, N., Huang, L., Nimmerjahn, A., and Lemke, G. (2021) Microglia use TAM receptors to detect and engulf amyloid β plaques. *Nat Immunol* **22**, 586-594
83. Güner, G., and Lichtenthaler, S. F. (2020) The substrate repertoire of γ -secretase/presenilin. *Seminars in cell & developmental biology* **105**, 27-42
84. Zhao, Y., Zeng, C. Y., Li, X. H., Yang, T. T., Kuang, X., and Du, J. R. (2020) Klotho overexpression improves amyloid- β clearance and cognition in the APP/PS1 mouse model of Alzheimer's disease. *Aging cell* **19**, e13239
85. Rangaraju, S., Dammer, E. B., Raza, S. A., Rathakrishnan, P., Xiao, H., Gao, T., Duong, D. M., Pennington, M. W., Lah, J. J., Seyfried, N. T., and Levey, A. I. (2018) Identification and therapeutic modulation of a pro-inflammatory subset of disease-associated-microglia in Alzheimer's disease. *Molecular neurodegeneration* **13**, 24
86. Kim, S., Cho, S. H., Kim, K. Y., Shin, K. Y., Kim, H. S., Park, C. H., Chang, K. A., Lee, S. H., Cho, D., and Suh, Y. H. (2009) Alpha-synuclein induces migration of BV-2 microglial cells by up-regulation of CD44 and MT1-MMP. *Journal of neurochemistry* **109**, 1483-1496

4.6 SUPPLEMENTAL TABLES

SI Table 4-1 Australian Brain Bank Network donor demographic and pathology.

Identifier	Age	Gender¶	Region§	Pathology†
R09A 13L	57	M	C/F/H	AD
R07A 32R	64	M	C/F/H	AD
R07A 29L	60	F	C/F/H	AD
R07A 21T	91	F	C/F/H	AD
R07A 09T	92	F	C/F	AD
R07A 06A	76	F	C/F/H	AD
R06A 20F	100	F	C/F/H	AD
R06A 16K	93	F	C/F/H	AD
R06A 06B	58	F	F/H	AD
R05A 22L	76	M	C/F/H	AD
R05A 20H	80	F	C/F/H	AD
R05A 02T	83	M	C/F/H	AD
R04A 36F	84	F	C/F	AD
R04A 29P	73	M	C/F/H	AD
R10A 11F	78	F	F/H	FTD
R09A 19A	58	M	F/H	FTD
R08A 19B	63	M	F/H	FTD
R07A 38F	60	M	F/H	FTD
R06A 18N	63	F	F/H	FTD
R09A 35J	79	F	C/H	LBD
R09A 32N	82	M	C/F/H	LBD
R09A 02M	88	F	C/F/H	LBD
R08A 15R	78	M	C/F/H	LBD
R07A 28X	77	M	C/F/H	LBD
R09A 11H	47	M	F/H	Control
R07A 34X	67	M	H	Control
R07A 33H	66	M	F/H	Control
R06A 21W	70	M	F/H	Control

¶ Gender abbreviations; F = Female, M = Male

§ Brain region abbreviations; C = Cerebellum, F = Frontal Cortex, H = Hippocampus

† Pathology abbreviations; AD = Alzheimer's disease, FTD = Frontotemporal dementia, LBD = Lewy body disease, Control = no dementia related pathology

SI Table 4-2 Wildtype allele specific PCR screening primers

Cell Line	Target Gene	gRNA Site	Forward Primer	Reverse Primer	Annealing Temp °C
HMC3	PSEN1	1	5'CCTGTTTCTGCTCACTGTAGGT ^{3'}	5'GCTGTTTCAACCAGCATACGA ^{3'}	63
	PSEN1	2	5'TGTTTAAAACCTATAACGTTGC ^{3'}	5'GGGATGTACACGTTACCATT ^{3'}	61
	PSEN2	1	5'CTCCCCTACGACCCGGA ^{3'}	5'CTCCTCTTCCTCCAGCTCCT ^{3'}	65
	PSEN2	2	5'TGACCTCCTGAGTCCCTGTA ^{3'}	5'CCACGATCATGCACAGAGTG ^{3'}	65
M17	PSEN1	1	5'GCCATTATCTAATGGACGACCC ^{3'}	5'TCCAGCTAAGTCATGCCCT ^{3'}	66
	PSEN1	2	5'ACCTGAGCAATACTGTACGTAG ^{3'}	5'CATGAACTATGAGGCGCTGC ^{3'}	63
	PSEN2	1	5'CTCCCCTACGACCCGGA ^{3'}	5'CTCCTCTTCCTCCAGCTCCT ^{3'}	65
	PSEN2	2	5'TGACCTCCTGAGTCCCTGTA ^{3'}	5'CCACGATCATGCACAGAGTG ^{3'}	65

SI Table 4-3 qPCR primer sequences

Gene Target	Forward Primer	Reverse Primer
PSEN1	5'CCAGAGGAAAGGGGAGTAAACTT ^{3'}	5'ACAGGCTATGGTTGTGTTCCA ^{3'}
PSEN2	5'TCATCTGCCATGGTGTGGAC ^{3'}	5'GTCTTCTTCCATCTCCGGGT ^{3'}
APH1a	5'GGTGTTTTTTCGGCTGCACTT ^{3'}	5'CAGAAAAATGCCCTGCGAC ^{3'}
APH1b	5'CTGCGCCTTCATTGCCTTC ^{3'}	5'GAAGAAAGCTCCGGCGATGA ^{3'}
NCSTN	5'ACTAGCAGGTTTGTGCAGGG ^{3'}	5'TCTGATGAGTGGCGTTGAGC ^{3'}
PSENE1	5'TGCCTTTTCTCTGGTTGGTCA ^{3'}	5'CGCCAGACATAGCCTTTGAT ^{3'}
TMEM119¶	5'CTTCTGATGGGATAGTGGAC ^{3'}	5'GCACAGACGATGAACATCAGC ^{3'}
P2RY12	5'CCACTCTGCAGGTTGCAATAAC ^{3'}	5'TTGCATTCTTGTGGTTACCTGA ^{3'}
RPLP0¶	5'GAAACTCTGCATTCTCGCTTCC ^{3'}	5'GAAACTCTGCATTCTCGCTTCC ^{3'}
CDC73	5'CCTGGCGTCGTGATTAGTGAT ^{3'}	5'TCGAGCAAGACGTTTCAGTCC ^{3'}
CD200	5'GTGCACAGCACAAGTGCAAG ^{3'}	5'TGGGCATTTTGCAGAGAGCA ^{3'}
CX3CL1	5'CCACGGTGTGACGAAATGC ^{3'}	5'GTCTCGTCTCCAAGATGATTGC ^{3'}
POLR2A	5'TCCTCGCATGATTGTCACCC ^{3'}	5'GTTTCATCACTTCACCCCGCT ^{3'}
GAPDH§	5'CTGCTTTTAACTCTGGTAAAGT ^{3'}	5'GCGCCAGCATCGCCCCA ^{3'}

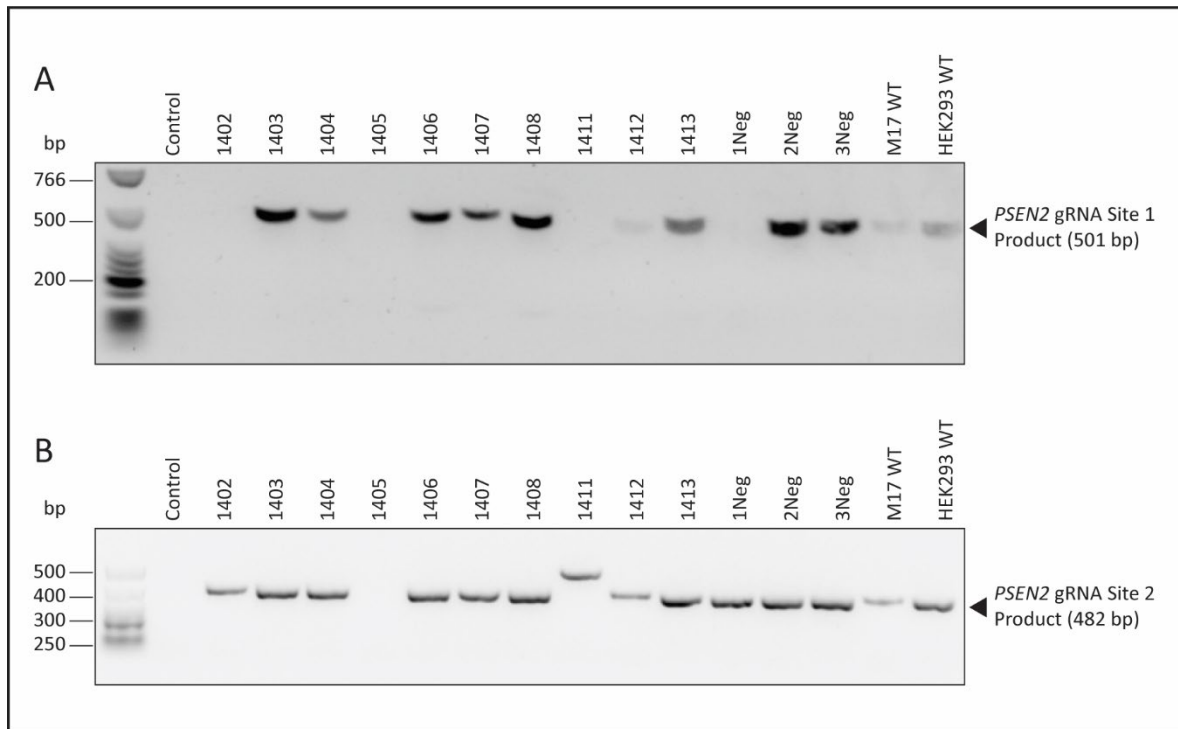
¶ TMEM119 and RPLP0 primers are from Bennet et al. (2016)

§ GAPDH primers are from Koch et al. (2012)

Bennett, M. L., Bennett, F. C., Liddel, S. A., Ajami, B., Zamanian, J. L., Fernhoff, N. B., Mulinyawe, S. B., Bohlen, C. J., Adil, A., Tucker, A., Weissman, I. L., Chang, E. F., Li, G., Grant, G. A., Hayden Gephart, M. G., and Barres, B. A. (2016) New tools for studying microglia in the mouse and human CNS. *Proceedings of the National Academy of Sciences* 113, E1738-E1746

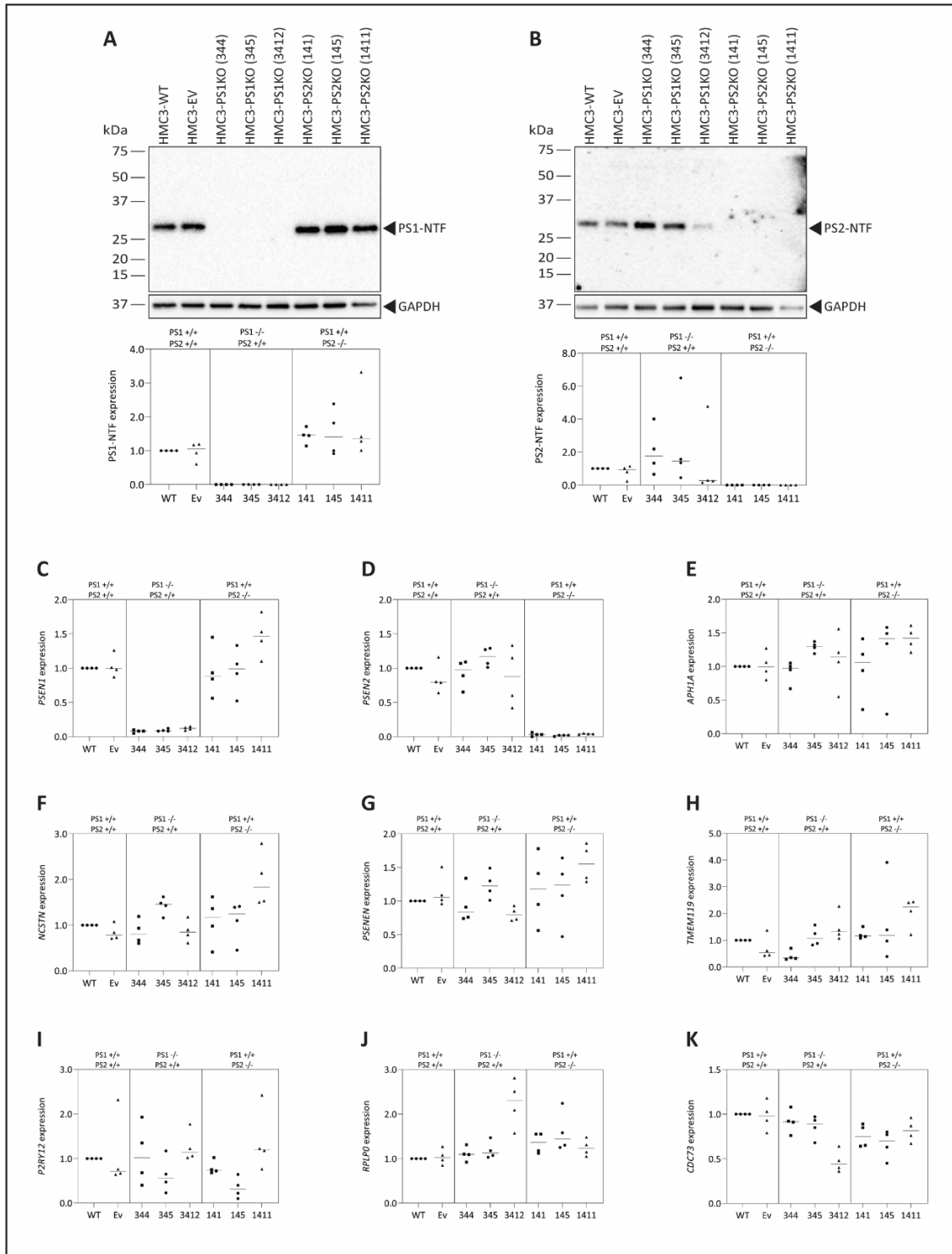
Koch, P., Tamboli, I. Y., Mertens, J., Wunderlich, P., Ladewig, J., Stüber, K., Esselmann, H., Wiltfang, J., Brüstle, O., and Walter, J. (2012) Presenilin-1 L166P mutant human pluripotent stem cell-derived neurons exhibit partial loss of γ -secretase activity in endogenous amyloid- β generation. *The American Journal of Pathology* 180, 2404-2416

4.7 SUPPLEMENTAL FIGURES



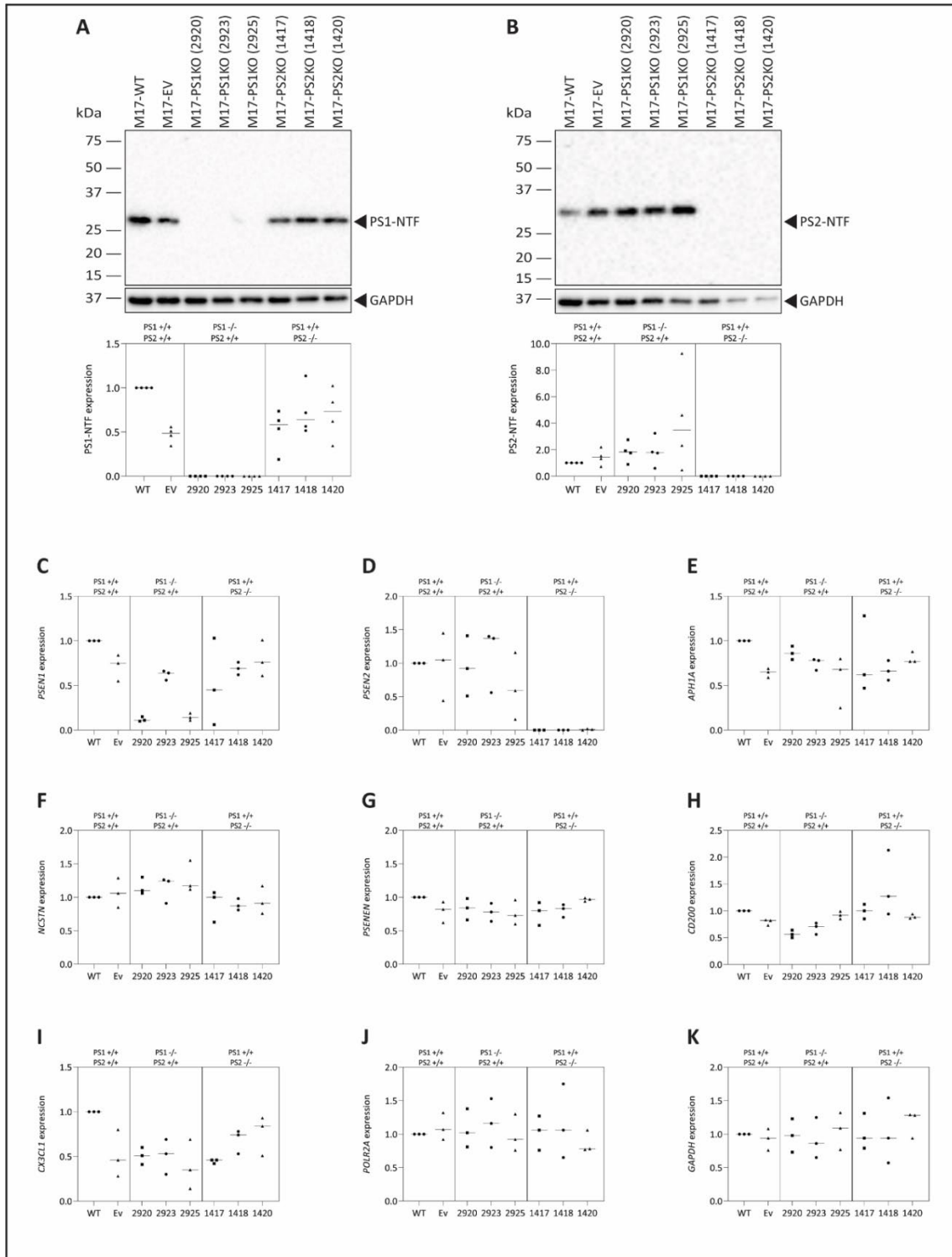
SI Figure 4-1 Wild type allele PCR screening of CRISPR knockouts

CRISPR-Cas9 PCR screening example for PSEN2 target site 1 (A) and PSEN2 target site 2 (B) for M17 PS2KO cell generation. No band present in end-point PCR suggests DNA disruption these clones were retained for further screening, clones with bands present in both target site screens were discarded. In this example clones 1402, 1405, 1411 and 1412 were retained for further screening. Control = no template control.



SI Figure 4-2 Characterisation of HMC3 PS1KO and PS2KO clones

Assessment of HMC3 PS1KO and PS2KO clones via immunblotting of PS1-NTF (A), PS2-NTF (B) and qPCR of PSEN1 (C), PSEN2 (D), APOA (E), NCSTN (F), PSENEN (G), TMEM119 (H), P2RY12 (I), RPLP0 (J), CDC73 (K).



SI Figure 4-3 Characterisation of M17 PS1KO and PS2KO clones

Assessment of M17 PS1KO and PS2KO clones via immunoblotting of PS1-NTF (A), PS2-NTF (B) and qPCR of PSEN1 (C), PSEN2 (D), APOE4 (E), NCSTN (F), PSENEN (G), CD200 (H), CX3CL1 (I), POLR2A (J), GAPDH (K).

5 DIFFERENTIAL FUNCTIONS OF PRESENILIN-1 AND PRESENILIN-2 IN HUMAN MICROGLIA

5.1 INTRODUCTION

Microglia are the primary immune cell of the brain. They surveil their surrounding parenchyma detecting and responding to external insults, phagocytosing cell debris, A β and other deposited proteins, secreting neurotrophins and cytokines to regulate myelination and support neurogenesis.¹⁻⁷ To achieve this they are highly dynamic, with specific, stimuli dependent responses.⁸ Publications on neuroinflammation and its role in the pathogenesis of Alzheimer's disease (AD) have risen substantially in the last decade, and along with it our understanding of role of microglial and its subtypes in promoting AD.⁹ Microgliosis and astrogliosis are considered pathophysiological events in AD that occur concurrently with A β deposition.¹⁰ This is supported by numerous genetic variants identified in immune-related genes associated with microglial functions being identified as risk factors for AD.^(Reviewed in 11, 12) Furthermore, of the currently identified AD risk genes,¹⁴ over 60% are highly expressed in microglia.¹³ These include triggering receptor expressed on myeloid cells 2 (*TREM2* – A β phagocytic receptor),¹⁴ sortilin-related receptor (*SORL1* – binds and traffics A β to lysosome),¹⁶ and sortilin (*SORT1* - facilitates endocytosis of APOE bound A β),¹⁷ all of which are substrates of γ -secretase.¹⁸ In addition to these, several other proteins involved in microglial functions related to A β clearance are substrates of γ -secretase, including CD44, LDLR, LRP1, LRP8, VLDLR, MER, AXL and RAGE.¹⁹⁻²⁴

Mutations in the catalytic components of γ -secretase – presenilin-1 (PS1) and presenilin-2 (PS2) – cause autosomal dominant AD (ADAD), by dysregulating amyloid precursor protein cleavage, resulting in an increased A β 42:A β 40 ratio.²⁵ ADAD mutations in both *PSENI*²⁶ and *PSEN2*^{27, 28} cause altered murine microglial function including enhanced microglial activation,²⁶ inflammatory cytokine release²⁶⁻²⁸ and increased A β phagocytosis.²⁷ The specific mechanisms by which these mutations cause microglial dysfunction have not been determined, although it may be postulated that they cause dysregulated processing of substrates associated with A β clearance.

Significant^{29, 30} and specific³⁰ roles for PS2 in microglia have been identified. PS2 ablation caused reduced cytokine response to LPS treatment,^{29, 30} A β -degrading enzyme and microglial

activation marker expression,²⁹ cell migration,²⁹ and A β phagocytosis.²⁹ However, these studies have been undertaken in murine models. Confirmation of the roles of PS1 and PS2 in human microglia is prudent, given the known divergence between human and murine microglia, particularly in relation to the response to AD pathology.^{31, 32} The findings in chapter 4 provided support for a critical role for PS2, in human microglial cells (HMC3), where a significant compensatory increase of PS1 protein was observed in response to the loss of PS2. How this impacts function and gene transcription will be further explored in the current chapter.

Proteolytic degradation of A β is an additional clearance mechanism facilitated by microglia, in addition to other neuronal cells.^{29, 33} Several enzyme classes degrade different A β species, including metallo-endopeptidases (neprilysin (NEP, encoded by *MME*), insulin degrading enzyme (IDE), and endothelial converting enzymes-1 (ECE1)) and matrix-metalloproteinases-2 and 9 (MMP2, MMP9).^{33, 34} BACE1, which is critical for the generation of A β , also has A β degrading capabilities.³⁵⁻³⁷ A β -degrading enzymes may be secreted into the parenchyma or retained intracellularly, thus functioning both on secreted A β and on intracellular A β .^{38, 39} Presenilin expression and γ -secretase activity have been shown to regulate the expression of NEP,^{40, 41} IDE and MMP9,²⁹ and BACE1³⁵⁻³⁷. However, this has not been investigated in the context of human microglia.

In this chapter PS knockout HMC3 cells, that were generated in Chapter 4, are used to investigate the role of PS1 and PS2 in human microglial A β removal functions, including A β phagocytosis, cytokine responses, degrading enzyme expression, and A β clearance related substrates. These cells are used to address the hypothesis that PS1 and PS2 have differential functions in human microglia, and that loss of PS2 will cause significant microglial dysfunction. Using HMC3 cells with genotypes of PS1^{+/+}PS2^{+/+}, PS1^{-/-}PS2^{+/+}, PS1^{+/+}PS2^{-/-} (herein referred to as PS1⁺PS2⁺, PS2⁺, and PS1⁺ respectively), the functional roles of PS1 and PS2 with respect A β -related microglial functions were investigated. Additionally, whether microglia function is related to γ -secretase activity was assessed by inhibition using DAPT. Specific pro-inflammatory responses of PS2⁺ and PS1⁺ microglia to LPS and oligomeric A β respectively, and an increase in phagocytosis in PS2⁺ cells were observed. Finally, transcriptomic analysis was performed to identify potential genes and pathways with altered regulation specific to either the PS2⁺ or PS1⁺ genotype that may contribute to the functional outcomes observed.

5.2 MATERIALS AND METHODS

5.2.1 Mammalian Cell Culture

Immortalised BV2 murine microglia (RRID:CVCL_0182)⁴² (gifted by Dr Anna Baron) and human microglial clone 3 cells (HMC3) (RRID:CVCL_II76)⁴³ (gifted by Dr Ryan Anderton) were maintained and expanded in DMEM (Sigma D5671) and MEM (Sigma M5650) base media respectively. Base media was supplemented with 1 mM L-glutamine (Sigma G7513), 1 mM Na-pyruvate (Sigma S8636), 100 units/ml penicillin 0.1 mg/ml streptomycin (Sigma P4333), and 10% v/v foetal bovine serum (FBS) (Serana FBS-Au-015), referred to as complete media. Where serum starvation occurred in an experiment, the media used was as above, excluding FBS, referred to as serum free media. Media used for phagocytosis experiments was as above, excluding penicillin-streptomycin, referred to as antibiotic free media. Cells were incubated at 37 °C with 5% v/v atmospheric CO₂. PS1 knockout, PS2 knockout and empty vector control human microglial clone 3 (HMC3) cell generation and characterisation were presented in Chapter 4 (Assessment of presenilin expression in human brain and CNS related cell lines).

5.2.2 DAPT treatments

BV2 and HMC3 wild type cells were plated in 6 well plates at a seeding density of 20,500 cells/cm² and 7,815 cells/cm² and incubated for 24 hours. Media was replaced with fresh MEM media containing tert-Butyl (S)-{(2S)-2-[2-(3,5-difluorophenyl)acetamido]propanamido}phenylacetate (DAPT, GSI-IX, Selleckchem S2215) at final concentrations of 0.1 µM, 1.0 µM or 10 µM DAPT or 0.5% v/v dimethyl sulfoxide (DMSO, Sigma 276855) as vehicle control, and incubated for a further 24 hours. Cells were then harvested to generate whole cell protein lysates. Briefly cells were washed with cold PBS and scraped in 40 µl of 1x RIPA buffer (Astral Scientific 786-490) prepared in milliQ water supplemented with protease inhibitor cocktail (Roche 11697498001). Lysates were incubated at 4 °C for 1 hour on rotation, clarified by centrifugation at 14,000 g for 10 minutes at 4 °C and the supernatant collected.

5.2.3 LPS treatments

BV2 and HMC3 wild type cells were plated in 100mm dishes at seeding density outlined above and incubated for 24 hours, after which media was replaced with fresh media containing

100ng/ml of LPS or 2% v/v PBS as vehicle control. Four hours post treatment cells were harvested and processed for RNA.

5.2.4 Cell Morphology

HMC3 cells were seeded at a density of 5,750 cells/cm² in PhenoPlate 96-well microplates (PerkinElmer 6055300) in complete media and incubated for 24 hours. After which the plate was imaged on a Perkin Elmer Operetta CLS, bright field images were taken at 10x magnification, and analysed using Harmony High-Content Imaging and Analysis Software (version 4.9, PerkinElmer HH17000010).

5.2.5 Bead Phagocytosis

For BV2 and HMC3 bead phagocytosis presented in Figure 5-1 cells were plated in 12 well plates at a seeding density of 15,000 cells/cm² and 5,750 cells/cm² and incubated for 24 hours. After which media was aspirated and replaced with antibiotic free media containing 0.4% v/v IgG-FITC beads (Cayman Chemical 500290) at staggered incubation start points such that bead incubation intervals of 3, 6, 9, and 12 hours were achieved. All cells were processed for flow concurrently.

Media was removed and cells washed in phosphate buffered saline (PBS), followed by incubation for 1 minute with 0.04% v/v trypan blue in PBS to quench any fluorescent signal from beads that had not been ingested. Cells were then washed three times with PBS, followed by 37 °C incubation in 750 µl 0.25% v/v trypsin-EDTA (Sigma T4049) for approximately 3 minutes. Trypsin was deactivated with 750 µl of complete media, cells collected in microfuge tubes and pelleted by centrifugation at 300 g for 5 minutes. Supernatant was aspirated and the cells resuspended in 400 µl of chilled 1% w/v bovine serum albumin (BSA) in PBS (flow buffer) and centrifuged at 300 g for 5 minutes, this was repeated twice. After a total of three washes, the cell pellet was resuspended in 400 µl of flow buffer. Immediately prior to analysis by flow cytometry, 0.25% v/v propidium iodide was added (Invitrogen P3566). Bead phagocytosis was analysed using a BD LSRFortessa flow cytometer. Data was analysed using FlowJo (v10.7.1) and the median fluorescence of the cell population after phagocytosis determined.

Please note due to supply issues the beads used for experiments presented in Figure 5-3 were changed to 0.03 µm, carboxylate modified, yellow green-fluorescent polystyrene beads (Sigma

L5155). HMC3 cells were plated in 6 well plates at a seeding density of 5,750 cells/cm² and incubated for 24 hours. 16 hours prior to addition of beads media was changed to serum free media, additionally a set of HMC3-EV cells were treated with 10 µM DAPT, to simulate γ -secretase inhibition, and HMC3-EV, PS1KO and PS2KO cells were treated with 0.5% DMSO vehicle control. Cells were incubated with 0.03 µm, carboxylate modified, yellow green-fluorescent polystyrene beads (Sigma L5155) at a concentration of 0.1% v/v in antibiotic free media, with 10 µM DAPT or 0.05% v/v DMSO vehicle control, for 60 min, after which cells were processed for flow cytometry as above.

5.2.6 A β Preparation and Phagocytosis

HiLyte Fluor 555 labelled A β (1-42) (Anaspec AS-60480-01), referred to as A β -555, was prepared as described.⁴⁴ 0.1 mg Lyophilised A β -555 was solubilised in 100 µl of 1,1,1,3,3,3-Hexafluoro-2-propanol (Sigma 105228), and aliquoted into Protein LoBind tubes (Eppendorf EP0030108116), with 0.025 mg A β -555 per tube. A β -555 films were dried overnight, followed by 10 minutes of additional drying with nitrogen gas, prior to storage protected from light at -20 °C. 24 hours prior to use oligomeric A β -555 (oA β) was prepared, 0.025 mg A β -555 was solubilised in anhydrous-DMSO to a final concentration of 2.5 mM, this was vortexed vigorously for 30 seconds, briefly centrifuged, then bath sonicated for 10 minutes at 25 °C. Phenol free Ham's F12 nutrient mix (US Biological Life Science N8543-06) was added such that a final concentration of 50 µM oA β was prepared, this was vortexed for 15 seconds, and incubated at 4 °C, protected from light.

Cells were seeded at a density of 5,750 cells/cm² in PhenoPlate 96-well microplates (PerkinElmer 6055300) in complete media and incubated for 24 hours. 16 hours prior to addition of oA β cells media was changed to serum free media, with either 10 µM DAPT or 0.5% DMSO. Serum free media was replaced with complete media containing 100 nM lysotracker deep red (Invitrogen L12492), and DAPT or DMSO as appropriate, and incubated for 30 minutes, after which cells were washed twice with PBS. Antibiotic free media with 10 µM Hoechst (Invitrogen 33342), and 2% v/v PBS (vehicle control for LPS treatment, see below) was prepared with 1 µM final concentration of oA β , or vehicle control, with DAPT or DMSO as appropriate. After aspiration of final PBS wash, oA β media or control media was added to cells, and incubated for 1 hour, after which the plate was imaged using a Perkin Elmer Operetta CLS, with images taken hourly. Images were analysed using CellProfiler (version 4.2.4).⁴⁵ Media was collected after 24 hours for use in cytokine bead array (CBA).

5.2.7 LPS Treatment and Cytokine and Chemokine Bead Array Assays

Cells were concurrently plated as per the oA β phagocytosis assay, in a 96 well plate (ThermoFisher 167008), and serum starved. After 16 hours of serum starvation, media was changed to antibiotic free media, with 2% v/v DMSO+F12 (oA β vehicle control) and 2% v/v PBS (LPS vehicle control) and cells incubated for a further 20 hours, such that cells were treated with the same conditions as per the oA β experiment. Cells were then incubated in antibiotic free media containing 100 ng/ml lipopolysaccharide (LPS), and appropriate vehicle controls as above, for 4 hours after which media was collected for CBA. Cells were either DAPT or DMSO treated as appropriate, beginning at serum starvation and maintained till collection of samples.

Cytokine and chemokine expression in conditioned media was analysed using LEGENDplex assays for human macrophage and microglial (13-plex) panel (BioLegend 740502), human vascular inflammation (12-plex) panel (BioLegend 740589) and human proinflammatory chemokine panel (13-plex) (BioLegend 740003). Assays were completed as per manufacturer protocol, with the minor changes. Standards for each kit were prepared as directed, 10 μ l each of assay buffer, standard or sample (vehicle control samples for oA β and LPS treatments were pooled), and bead mix were prepared in 96 well U-bottom plates, sealed and incubated for 2 hours on plate shaker at approximately 800 rpm. Plates were then centrifuged at 250 g for 5 minutes, and supernatant discarded. Plates were washed by addition of 200 μ l of prepared wash buffer, incubated for 1 minute followed by centrifugation and the wash buffer discarded. The plate was washed twice, after which 10 μ l of detection antibody was added to the plate sealed and covered for light protection and incubated on a plate shaker for 1 hour. 10 μ l of SA-PE solution was added to the plate, which was then incubated for a further 30 minutes with shaking. The plates were then centrifuged and washed twice. The beads were resuspended in 150 μ l of wash buffer and analysed on a BD LSRFortessa flow cytometer. Data was analysed using LEGENDplex Data Analysis Software online platform (www.legendplex.qognit.com).

5.2.8 RNA and Protein Sample Preparation

Cell were plated in 100mm dishes at a seeding density of 7500 cells/cm² and incubated for 24 hours. Media was replaced with 10 μ M DAPT or vehicle control treatment in complete media and cells incubated for a further 24 hours. RNA was extracted using Isolate II RNA extraction

kit (Bioline BIO-52073) as per kit protocol. Resulting RNA concentrations were determined using Nanodrop 1000 (ThermoFisher) and samples stored at -80 °C.

Whole cell protein lysates were prepared by washing plates with cold PBS and scraping the cells in 1ml of cold PBS, the cell suspension was collected in a microfuge tube and centrifuged at 300 g for 5 minutes, the supernatant was aspirated and the cell pellet resuspended in 100 µl of 1x RIPA buffer (Astral Scientific 786-490) prepared in milliQ water supplemented with protease inhibitor cocktail (Roche 11697498001). Lysates were incubated at 4 °C for 1 hour on rotation, clarified by centrifugation at 14,000 g for 10 minutes at 4 °C and the supernatant collected. Protein concentration of cell lysates was determined by BCA (Pierce Micro BCA kit Thermo Fisher 23235).

5.2.9 Quantitative PCR

cDNA was generated using the Bioline Tetro cDNA kit, with the following adjustments to the standard kit protocol. 20 µl cDNA reactions were prepared using 5000 ng of RNA per reaction, random hexamer primers and oligo dTs were used in a 1:1 ratio, the reaction was incubated at 25 °C for 10 minutes followed by a 45 °C incubation for 60 minutes. qPCR reactions were completed in 384 well plates using Genius 2x SYBR Green Fast qPCR Mix (ABclonal RK21204), and primers at 500 nM, in 10 µl final volume reactions. The amount of template used for qPCR was target specific and is presented along with the primer details in SI Table 5-1. Primers were designed using NCBI Primer-BLAST,⁴⁶ unless otherwise stated. Standard curves were generated using RNA generated from wildtype HMC3 cells (see Chapter 4: Assessment of presenilin expression in human brain and CNS related cell lines) to determine primer efficiency and template RNA µg/µl required for all targets. Each biological replicate was run in technical triplicate using the Applied Biosystems Viiia7 real-time PCR system, and average Ct values determined for each gene, *HRPT1* and *RPLP0* reference genes were used for normalisation. Gene expression levels were calculated using the Pfaffl method,⁴⁷ and expression relative to HMC3-EV cells determined.

5.2.10 Immunoblotting

For the detection of all proteins except APP, whole cell lysates samples were prepared in 25% v/v LDS Sample Buffer (Invitrogen NP0008), 50 mM dithiothreitol, and 25 µg total protein, and electrophoresed in 12% v/v bis-tris poly acrylamide gels, prepared using the Invitrogen

SureCast system, at 100 V for approximately 1 hr 45 min, in 5% v/v MES SDS Running Buffer (Invitrogen NP0002). For detection of APP, whole cell lysates were prepared with the following changes, sample buffer used was tris tricine sample buffer to a final concentration of 4% w/v SDS, 50 mM tris, 12% v/v glycerol, 0.125% w/v Coomassie G-250. Samples were electrophoresed with 12% v/v tris-tricine poly acrylamide gels, in tris-tricine cathode buffer (100 mM tris, 100 mM tricine, pH8.3) and tris anode buffer (200 mM tris, pH8.8). Prior to samples being electrophoresed they were incubated for 10 min at temperatures as indicated in

SI Table 5-2.

Protein was transferred from PAGE to 0.2 μm nitrocellulose membrane (BioRad 1620112) via wet transfer in 19.2 mM tris, 2.5 mM glycine, 20 % v/v methanol buffer, at 150 mAmps overnight at 4 °C. Membranes were incubated for 5 min in ponceau (1% w/v Ponceau S, 5% v/v acetic acid), rinsed in deionised water and visualised to confirm transfer quality, after which the ponceau was removed by incubation in boiled TBS with agitation. Membranes were blocked with 5% w/v non-fat dried milk powder (NFDM) in TBS for 1 hr at room temperature with agitation. Membranes were incubated in antibodies prepared in 0.5% w/v NFDM in TBST overnight at 4 °C with agitation. Antibody details and concentrations are available in. Membranes were washed 3-times for 10 min with agitation in TBST, then incubated for 1 hr at room temperature in 0.005% v/v α -mouse or α -rabbit IgG HRP conjugated secondary antibody as appropriate (Thermo Fisher 31430, 31460). Membranes were washed 3-times in TBST as previous, followed by a 5 min wash in TBS with agitation. Membranes were incubated in Clarity ECL (BioRad 1705061) or Prime ECL (Cytiva GERPN2232) as indicated in

SI Table 5-2. Membranes were imaged on BioRad ChemiDoc MP system and band densitometry quantitated using ImageLab (BioRad, version 6.1.0 build 7).

5.2.11 Bulk RNA Sequencing Analysis

RNA was extracted from PS1+PS2+, PS1+, and PS2+ cells as outlined above. Five biological replicates for each cell line were prepared and sent to Azenta Life Sciences (www.azenta.com) for next generation sequencing (NGS) of bulk RNA. Initial quality control of transcript reads was completed by Azenta, the trimmed and filtered data provided at completion of service was subsequently used as raw reads and analysed as follows. Transcript reads were mapped and counted using the Bioconductor package Rsubread⁴⁸ (version 1.1.1) in RStudio (version 2022.12.0 Build 353). Reads were mapped to the inbuilt Rsubread hg38 annotation file⁴⁹ using the ‘subjunc’ function⁵⁰ and read counts generated using the ‘feature counts’ function.⁵¹ Read counts were then uploaded to iDEP1.1 (<http://149.165.154.220/idep11/>)⁵² for differential expression and pathway analysis. Clustering and principal component analysis (PCA) used EdgeR: log₂(CPM+c) where pseudo count c=4 option, missing value imputation was treated as gene median, K-mean clustering used 8 clusters as determined by K-means elbow plot. Differential gene expression analysis combinations completed were ‘PS2+ - PS1+PS2+’, ‘PS1+ - PS1+PS2+’, and ‘PS1+ - PS2+’ using DESeq2, with FDR cutoff = 0.1, Minimum fold-change = 2, and independent filtering of lower counts. Pathway analysis was completed using parametric analysis of gene set enrichment with all samples “PGSEA w/all samples” for KEGG pathways in iDEP1.1, using a pathway significance cutoff (FDR) of 0.05. Genes associated with specific pathways were retrieved from the KEGG^{53, 54} database for further analysis.

5.2.12 Statistical Analysis

Statistical analysis was completed using GraphPad Prism 9.5.0, with the exception of RNA sequencing statistical analysis which was completed within iDEP1.1. Shapiro-Wilk normality test was completed to determine if data was normally distributed. Where only two groups were examined normally distributed data was analysed via unpaired T-test. Where more than two groups are examined one-way ANOVA or two-way ANOVA analysis with Holm-Šidák’s multiple comparison tests are used as appropriate. For multiple group analysis where data was not normally distributed Kruskal-Wallis test and Dunn’s multiple comparison test was applied.

5.3 RESULTS

5.3.1 HMC3 cell response dampened in comparison with BV2

All studies to date investigating PS function in microglia have been undertaken using murine models.^{29, 30} Considering the considerable differences between human and murine microglia, validation in a human cell line is required. Thus, the human immortalised microglia cell line HMC3 was used in this study. This cell line, established in 1995, is not as widely used as the murine BV2 cell line. Consequently, prior to investigating the function of PS1 and PS2 in the HMC3 cells a comparison of the functional responses of wild type BV2 and HMC3 cell lines was performed to assist in interpreting data generated in this study.

The response of both BV2 and HMC3 cells to DAPT treatment is similar with APP-CTF accumulation evident with 10 μ M treatment (Figure 5-1A). The effect of LPS treatment on mRNA expression for both cell lines is similar for *TMEM119* and *TNF* expression (Figure 5-1B,C), however, the response of *IL1B* and *P2RY12* differs. While *IL1B* expression is increased in both cell lines, the amplitude of the response is considerably different with expression being 615-fold higher than vehicle in BV2 cells, compared to only a 2.7-fold increase in HMC3 cells. With LPS treatment, there is a significant decrease in *P2RY12* expression in BV2 cells, while no change was observed in HMC3 cells. Additionally, phagocytic capacity of BV2 and HMC3 wild type cells was also compared. Bead phagocytosis by the BV2 cells is significantly higher than the HMC3 cells at all time points, except at 6 hours likely due to variability in the HMC3 replicate data (Figure 5-1D). Bead phagocytosis is on average 69% higher in BV2 cells than HMC3 cells across all time points. Overall, the data shows that although there are differences in the extent of activity, the HMC3 cell line is a relevant cell line for the functional assays that were used in this study.

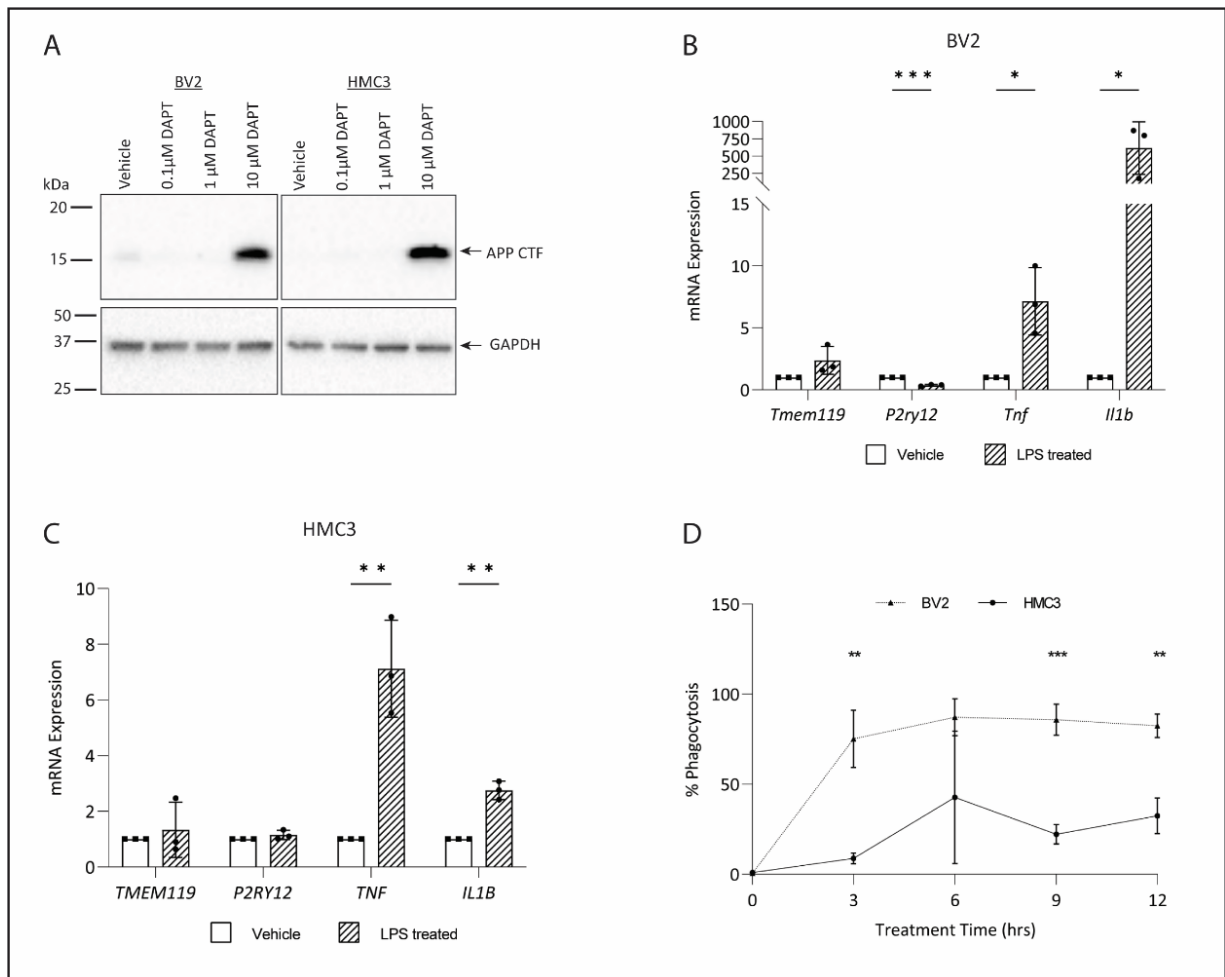


Figure 5-1 Functional comparison of BV2 and HMC3 cells

BV2 and HMC3 wild type cells were assessed to determine response characteristics to DAPT treatment (A) mRNA expression in response to LPS treatment in BV2 cells (B) and HMC3 cells (C) and bead phagocytosis (D). Values shown are mean \pm SD of $n=3$ biological replicates. Statistical tests applied were Multiple Unpaired T-test with FDR correction (B, C), two-way ANOVA with Holm-Šidák's multiple comparison (D), where * = $P < 0.05$, ** = $P < 0.01$, *** = $P < 0.001$, **** = $P < 0.0001$.

5.3.2 HMC3 PS2+ cells show altered morphology

HMC3 cells demonstrate morphological heterogeneity,⁵⁵ which observationally appears altered by the loss of PS. Morphological quantitation of the HMC3 CRISPR cell lines (generated in Chapter 4), assessing cell width, length and roundness revealed significant morphological changes associated with the loss of PS1 or PS2 (Figure 5-2). While there was no significant effect observed on cell width (Figure 5-2D), the PS2+ cells are significantly longer than either the PS1+PS2+ or PS1+ cells (Figure 5-2E). Cell roundness is significantly reduced in both the PS1+ and PS2+ cells compared to PS1+PS2+ cells, and the PS2+ cell roundness is significantly lower than the PS1+ cells (Figure 5-2F). Morphological changes are also indicators of

inflammatory state alteration in microglia. Although the HMC3 cells do not visibly compare to *in vivo* microglia, the increased length and decreased roundness of the PS2+ cells may indicate that they are more ramified and therefore in a ‘quiescent’ state. In contrast, the PS1+PS2+ and PS1+ cells appear more amoeboid, reflecting a more ‘activated’ state.^{8,56,57} As the state of microglia can reflect phagocytic and inflammatory functional responses, these parameters were further investigated.

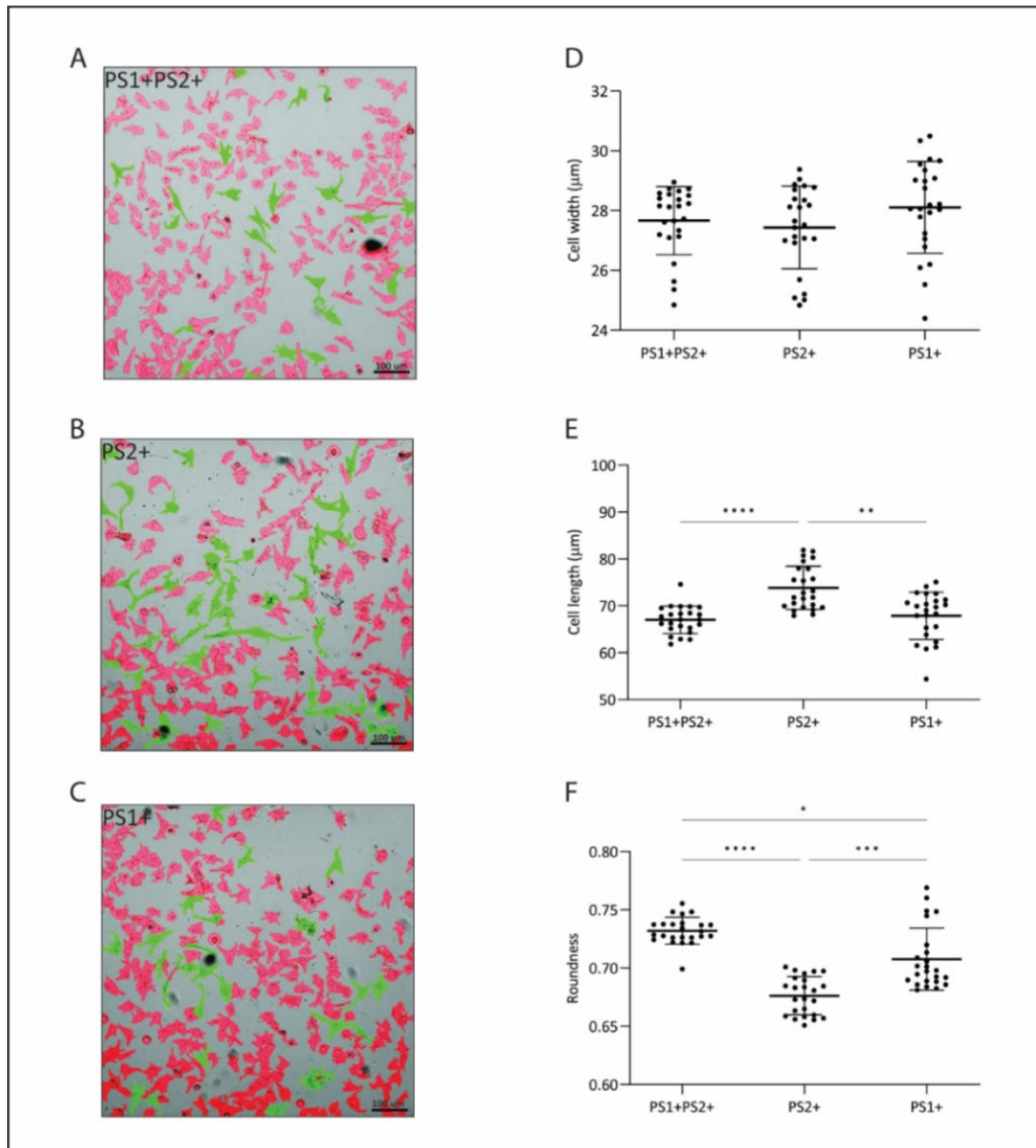


Figure 5-2 Morphological assessment of HMC3 cells with altered PS genotypes

HMC3 PS1+PS2+, PS1+ and PS2+ cells were live cell imaged cells highlighted green have roundness factor < 0.5, cells highlighted red have roundness factor > 0.5 (A-C) to determine cell width (D), cell length (E) and cell roundness (F). Values shown are mean ± SD of n = 24

fields of view (6 fields of view per well, 4 wells per cell line). Statistical tests applied were Kruskal-Wallis test with Dunn's multiple comparison test (D-F), where * = $P < 0.05$, ** = $P < 0.01$, *** = $P < 0.001$, **** = $P < 0.0001$.

5.3.3 HMC3 PS2+ cells show increased phagocytic capacity

Phagocytosis is a primary mechanism by which microglia remove A β . Inhibition of γ -secretase, and PS1 and PS2 deficiency, individually, have been shown to reduce A β phagocytosis in murine models.²⁹ Furthermore, the A β recognition and phagocytosis receptors TREM2, AXL and MER are themselves γ -secretase substrates.^{14, 15, 21, 58-61} Phagocytic capacity of PS1+PS2+, PS1+ and PS2+ cells, as well as PS1+PS2+ treated with 10 μ M DAPT (to inhibit γ -secretase) for fluorescent beads or oA β was assessed (Figure 5-3). The PS2+ cells phagocytose more beads compared to all other cell lines, with approximately 50% greater phagocytosis compared to PS1+PS2+ cells (Figure 5-3A). oA β phagocytosis was assessed by live cell imaging over 24 hours and no significant difference in oA β phagocytosis was evident at 2 and 7 hours. However, at 13, 19 and 24 hours, PS2+ cells phagocytosed significantly more than the PS1+PS2+ cells. Additionally, PS2+ cells phagocytose more oA β than PS1+ cells at 19 and 24 hours, and at 24 hours more than PS1+PS2+ +DAPT cells (Figure 5-3B,C). The phagocytic performance of the different cell lines was also analysed across the complete 24-hour period using linear regression analysis. The results (Figure 5-3B,C) showed that PS2+ cells have significantly higher rate of oA β phagocytosis compared to all other cell lines. Furthermore, PS1+PS2+ +DAPT cell line have increased oA β phagocytic capacity compared to PS1+PS2+ and PS1+ cells, while the PS1+ cell line is not significantly different to PS1+PS2+.

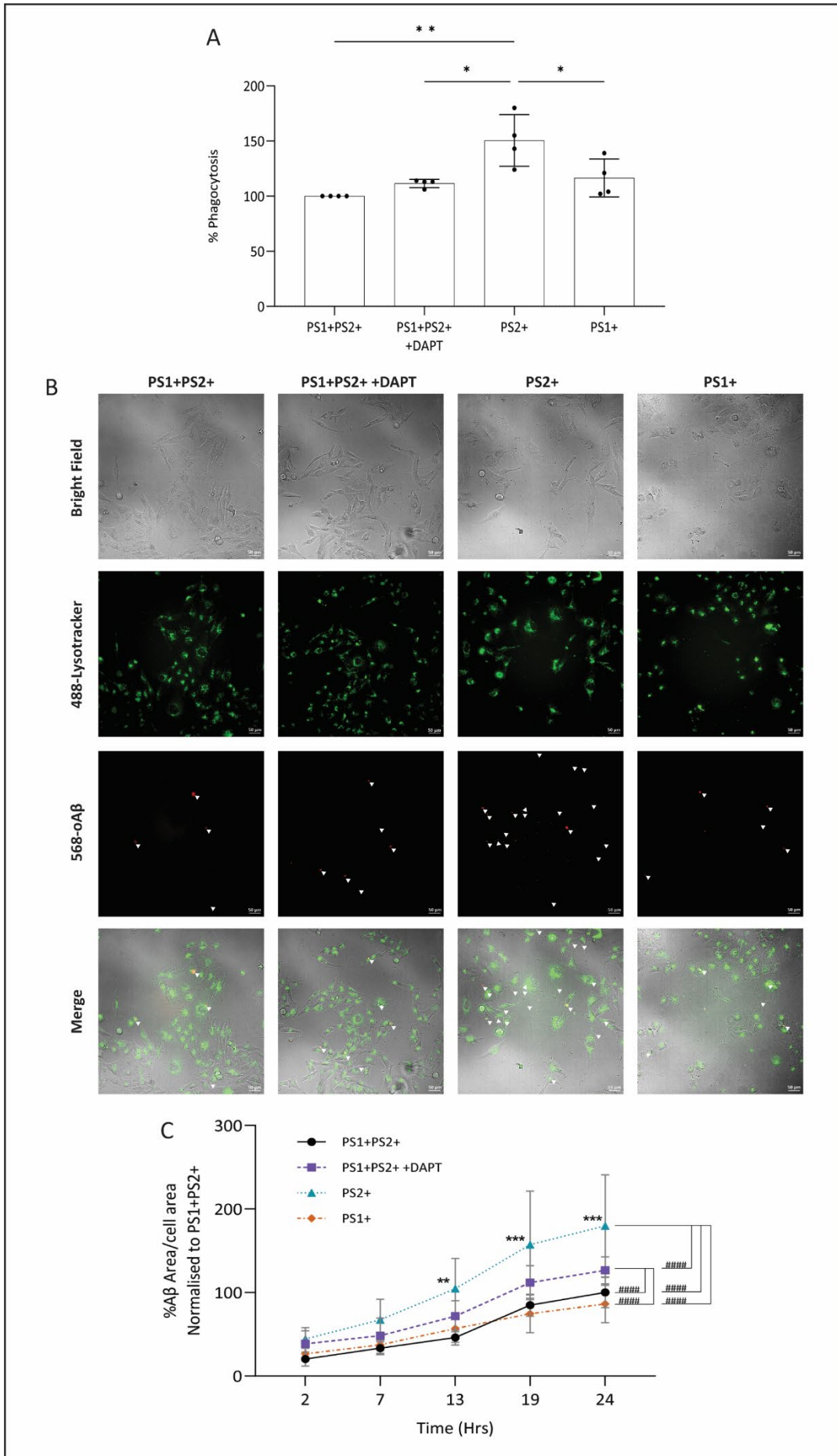


Figure 5-3 Bead and oA β phagocytosis in HMC3 cells with altered PS genotypes

Phagocytosis by HMC3 PS1+PS2+, PS1+PS2+ +DAPT, PS1+ and PS2+ cell lines was assessed using fluorescent beads (A) and fluorescent oA β (B,C). Representative images for each cell line at 24 hours for bright field, lysotracker in 488 channel, oA β in 568 channel, and merged image where scale bar is 50 μ m, engulfed oA β highlighted by white \blacktriangle . Values shown are mean \pm SD of n=4 biological replicates. Statistical tests applied were one-way ANOVA (A), two-way ANOVA results represented by * (C), one-way ANOVA of linear regression results represented by # (C), all with Holm-Šidák's multiple comparison test, where * or # = P < 0.05, ** or ### = P < 0.01, *** or #### = P < 0.001, **** or ##### = P < 0.0001.

5.3.4 PS1 and PS2 differentially regulate pro-inflammatory response to LPS and oA β

PS2 expression has been reported to be critical for maintaining the microglial inflammatory responses to LPS stimulation,^{29, 30} and the inflammatory status of microglia is critical to their success in surveillance and phagocytosis of potential insults in the brain parenchyma, including A β .^{8, 57, 62, 63} Consequently, the inflammatory secretome profile of the PS knockout cells using three inflammatory cytokine bead array panels were assessed to determine the role of PS1 and PS2 on inflammatory responses to LPS and oA β . While the majority of the 37 cytokines and chemokines assessed were not detected, results for 8 pro-inflammatory molecules are presented here. Arginase was detected, but was secreted at levels above the highest standard and hence is not presented here.

Analysis of the effect of either LPS or oA β treatment across all cell lines revealed that PS2+ cells have increased pro-inflammatory cytokine secretion in response to LPS treatment compared with the other cell lines. PS1+ cells, however, have increased cytokine response to oA β treatment (Figure 5-4), compared to all other cell lines. Specifically, PS2+ cells have increased TNF α , IL-6, IL-8, IP-10, GRO α , eotaxin, and ENA-78 secretion with LPS treatment (Figure 5-4A-G). PS1+ cells have increased TNF α , IL-6 and GRO α secretion (Figure 5-4A,B,E) in response to oA β treatment. No significant effect on any cytokine was observed with DAPT treatment.

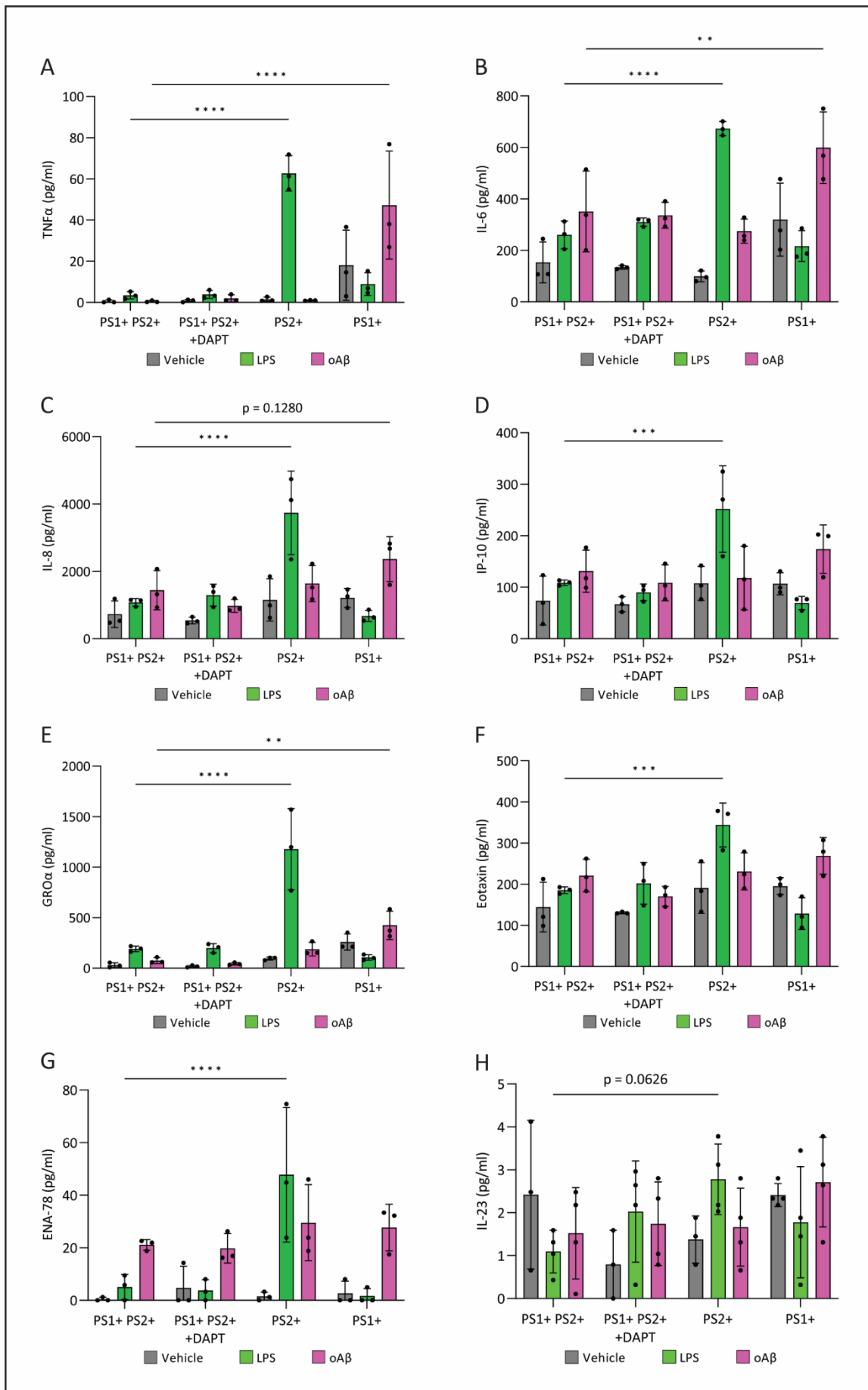


Figure 5-4 Differential cytokine secretion by HMC3 cells with altered PS genotype in response to LPS and oA β treatment

Cytokine bead array analysis detected secretion of TNF α (A), IL-6 (B), IL-8 (C), IP-10 (D), GRO α (E), eotaxin (F), ENA-78 (G), IL-23 (H) in conditioned media from cells treated with LPS or oA β . Values shown are mean \pm SD. Statistical tests applied were two-way ANOVA with Holm-Šidák's multiple comparison (D), where * = P < 0.05, ** = P < 0.01, *** = P < 0.001, **** = P < 0.0001.

5.3.5 Presenilin modulates A β degrading enzyme expression

MME (encodes for neprilysin protein), *MMP2*, and *MMP9* transcript expression was significantly upregulated in the PS2+ and PS1+ cells, compared to both PS1+PS2+ and PS1+PS2+ +DAPT treated cells (Figure 5-5A-C). Furthermore, both *MME* and *MMP9* were further upregulated in PS1+ cells compared to PS2+ cells. *BACE1* transcript, however, was only upregulated in PS2+ cells (Figure 5-5F). In contrast, *IDE* was downregulated in both PS2+ and PS1+ cells, compared to PS2+PS1+ cells (Figure 5-5D), while no changes in *ECE1* expression were evident (Figure 5-5E). The upregulation of *MME* expression observed is incongruent with previous studies.^{40, 41} As such, we investigated the level of the gene product, neprilysin protein, by immunoblotting (Figure 5-5G). This analysis revealed that the observed transcript upregulation did not result in a concomitant increase in protein expression. In both PS2+ and PS1+ cells, neprilysin is significantly reduced compared to PS1+PS2+ and PS1+PS2+ +DAPT cells (Figure 5-5H). These results suggest that in human microglia neprilysin, expression may be regulated via a different mechanism to that previously reported for murine microglia²⁹ and non-microglial human derived cells.^{40, 41}

PS1 deficiency has previously been shown to decrease mature BACE1 expression⁶⁴ and so the expression of this enzyme was also assessed. A similar total protein expression profile to that of neprilysin was observed, where mBACE1 was significantly decreased in the PS2+ and PS1+ cells compared to the PS1+PS2+ cells (Figure 5-5I-J). We also assessed the ratio of mature BACE1 (mBACE1) to the precursor proBACE1 and observed that the level of maturation is significantly decreased in all cell lines compared to the PS1+PS2+ cells. This reduction in BACE1 maturation is particularly evident in the PS2+ and PS1+ cells, which are both significantly reduced compared to the PS1+PS2+ +DAPT cells (Figure 5-5K).

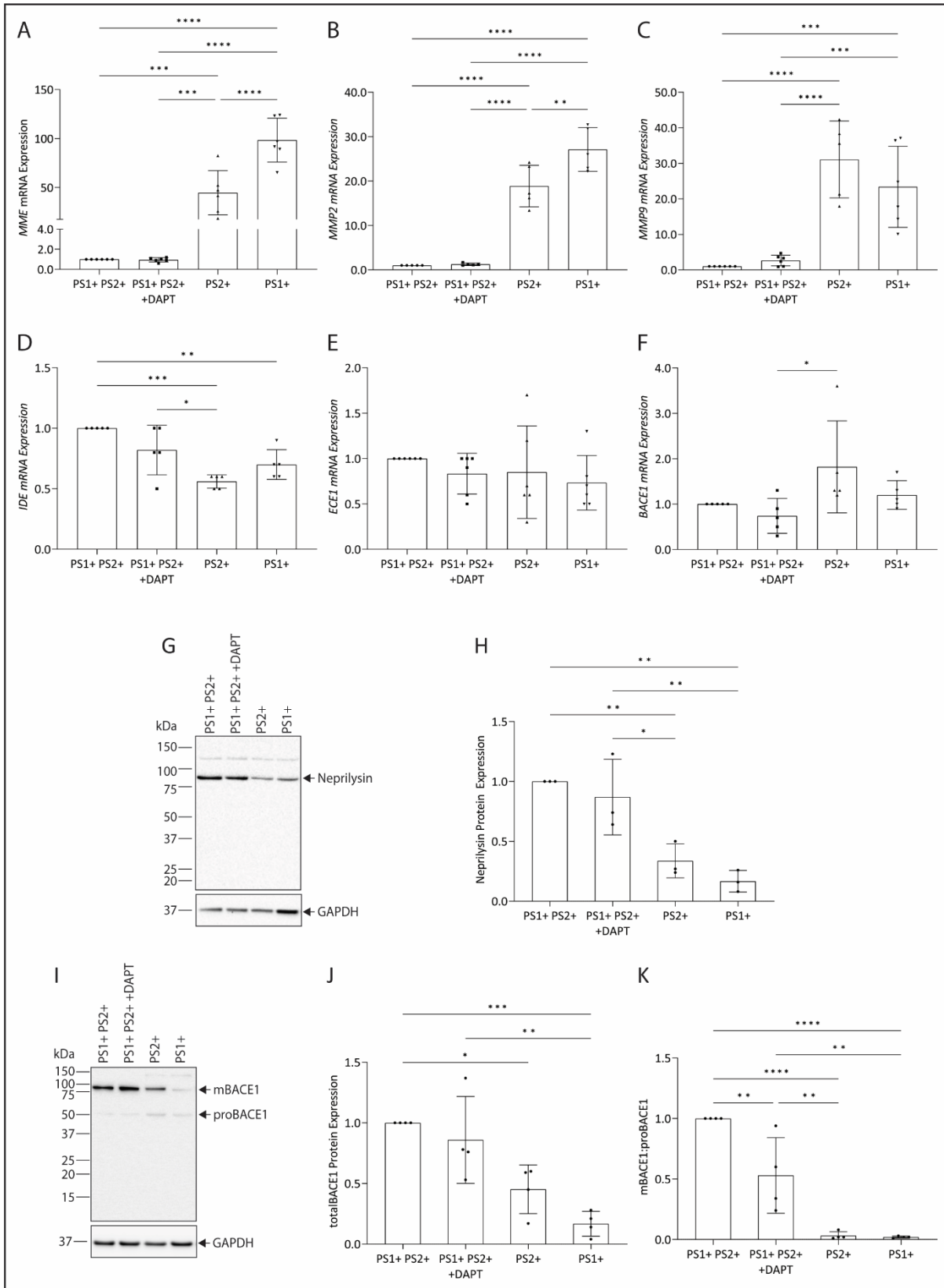


Figure 5-5 Expression of A β degrading enzymes in HMC3 cells with altered PS genotype

A β degrading enzyme transcript expression determined by qPCR for MME (A), MMP2 (B), MMP9 (C), IDE (D), ECE-1 (E), and BACE1 (F). Protein expression was confirmed via immunoblotting and quantitated for neprilysin (G-H) and BACE1 (I-K). Values shown are mean \pm SD, n=5-6 biological replicates for qPCR experiments and n=3-4 biological replicates

for immunoblot experiments. Statistical tests applied were one-way ANOVA with Holm-Šidák's multiple comparison test, where * = $P < 0.05$, ** = $P < 0.01$, *** = $P < 0.001$, **** = $P < 0.0001$.

5.3.6 γ -Secretase substrates associated with AD related microglial function are regulated by presenilin

Several substrates of γ -secretase are involved in microglial functions associated with A β clearance, including TREM2,^{14, 15, 32} CD44,^{22, 23} and VLDLR,⁶⁵⁻⁶⁷ or associated with specific microglial phenotypes linked to AD, including CD44^{68, 69} and APP.⁷⁰ Therefore, to investigate potential regulation of expression due to the loss of either presenilin homologue, both transcript and protein expression were investigated, via qPCR and immunoblotting respectively. *APP* and *VLDLR* transcript expression profiles are concomitant with the protein expression profiles. *APP* expression is significantly increased in the PS2+ cells (Figure 5-6A-C), while *VLDLR* expression is significantly decreased in both PS2+ and PS1+ cells (Figure 5-6D-F). While no significant alteration to *CD44* transcript expression was observed (Figure 5-6G), protein expression is significantly increased in the PS2+ cells and significantly decreased in the PS1+ cells (Figure 5-6H,I).

TREM2 mRNA expression was increased in PS2+ cells compared with PS1+PS2+ and PS1+PS2+ +DAPT cells (Figure 5-6J). Subsequent assessment of TREM2 protein via immunoblotting detected two primary bands: one at 26 kDa, congruent with the theoretical mass of 25.4 kDa, and an additional band at 50 kDa (Figure 5-6K). Other studies that use the same TREM2 antibody (Abclonal A10482) have not reported two bands,⁷¹⁻⁷⁵ only the approximately 25 kDa band, although the product sheet does identify the two bands⁷⁶ and other studies identify larger TREM2 proteins in the range of 40-62 kDa that are likely representative of glycosylated TREM2.⁷⁷⁻⁷⁹ Consequently, both bands were quantitated, while no significant differences were observed in the expression of the 50 kDa band (Figure 5-6L), the level of the 25 kDa band was significantly reduced in PS2+ cells compared to both PS1+PS2+ and PS1+ cells (Figure 5-6M).

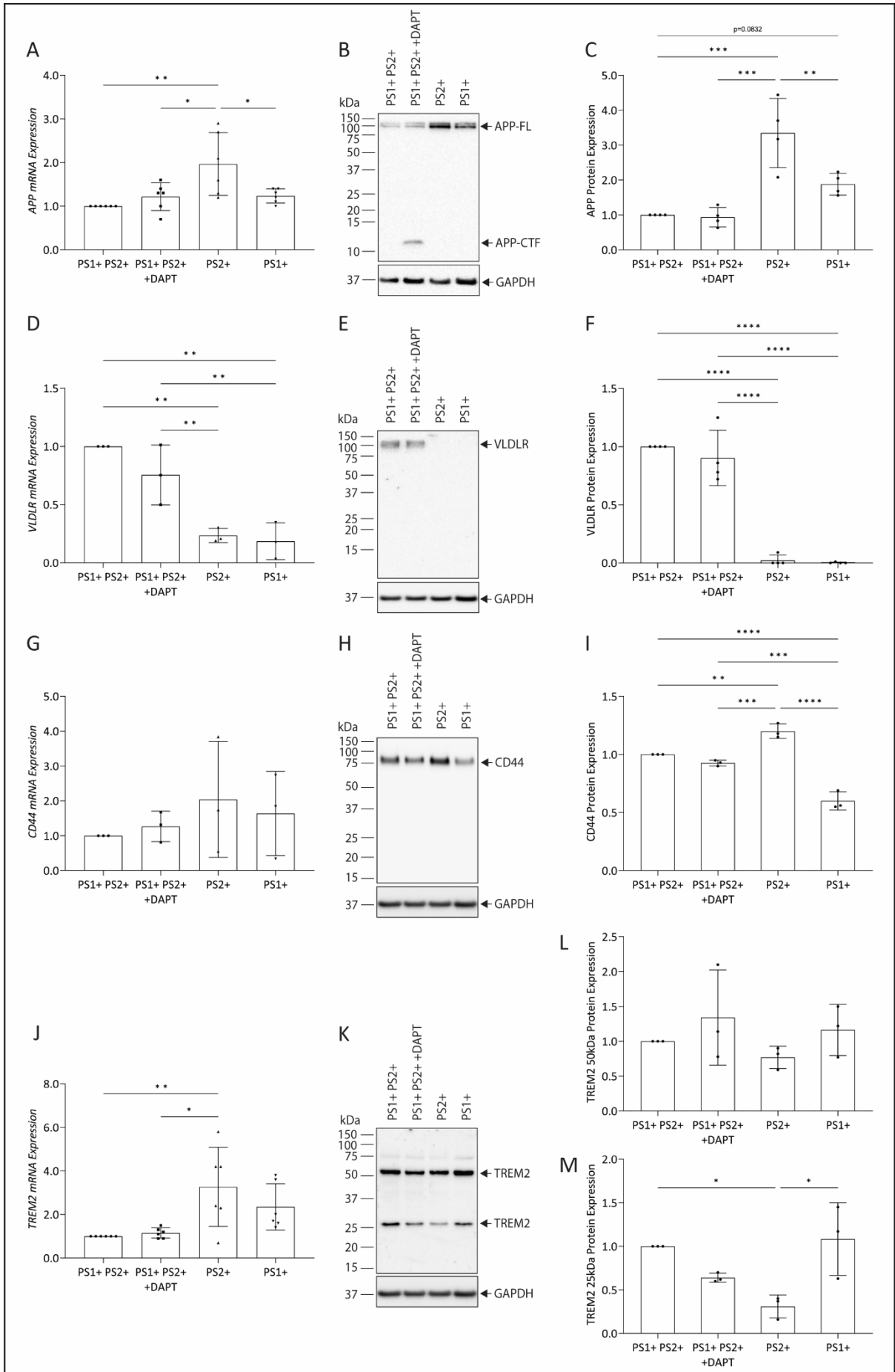


Figure 5-6 Expression of γ -secretase substrates associated with A β removal and microglial phenotypes associated with AD.

Transcript expression determined by qPCR (A, D, G, J) and immunoblotting for protein quantitation (B, C, E, F, H, I, K-M) for APP (A-C), VLDLR (D-F), CD44 (G-I), and TREM2 (J-M). Values shown are mean \pm SD, n=6 biological replicates for APP and TREM2, n=3 biological replicates for VLDLR and CD44 qPCR experiments, and n=3-4 biological replicates for immunoblot experiments. Statistical tests applied were one-way ANOVA with Holm-Šidák's multiple comparison test, where * = P < 0.05, ** = P < 0.01, *** = P < 0.001, **** = P < 0.0001.

5.3.7 Transcriptomic analysis identifies gene groups of interest in differential functional responses of PS1+ and PS2+ microglial cells.

There are some clear morphological and functional differences due to loss of PS1 or PS2. To explore these differences further, bulk RNA sequencing of the PS1+PS2+, PS1+ and PS2+ cells was performed. This experiment aims to investigate the alterations in transcriptional regulation so that potential cellular mechanisms/pathways through which PS1 and PS2 influences microglial A β removal and other response functions can be identified. Initial assessment of the data quality determined that the raw reads for each sample replicate were similar, with an average raw read count of approximately 15 million (SI Figure 5-1A). In addition, no differences between the transformed expression data were observed (SI Figure 5-1B,C). Principal component analysis identified that 66.74% of variation can be explained by principal components 1 and 2, and revealed three highly distinct clusters (Figure 5-7A). Each cluster is populated by all five biological replicates from each cell line, indicating that the loss of PS1 or PS2 results in transcriptionally-distinct cell lines.

K-means clustering was subsequently performed on the top 1000 genes (Figure 5-7B), yielding eight gene groups. In three of these (groups 1, 7, 8) PS2+ and PS1+ cells have similar expression profiles to each other. The remaining five gene groups had different expression profiles between the PS2+ and PS1+ cells. Pathway analysis of these gene groups for Gene Ontology (GO) Biological Processes identified pathways that were subsequently network mapped to reveal related interacting pathways. The gene groups commonly affected in PS2+ and PS1+ cells are involved in neuronal development functions, and immune responses (SI Figure 5-2A-C). Those that differ between PS2+ and PS1+ cells include gene groups involved in cellular and nervous system development (PS2+ > PS1+ Figure 5-7C), circulatory and vascular development (PS2+ > PS1+ Figure 5-7D), and synapse assembly, exocytosis and secretion (PS2+ < PS1+ Figure 5-7F).

Particularly interesting in the context of the differential cytokine response and phagocytosis response reported for the PS2+ and PS1+ cells are group 4 and group 6. The group 4 gene set (Figure 5-7E), where PS2+ gene expression is higher, is primarily engaged with defence responses (GO:0006952) and several other GO Biological Processes involved with response to external, biotic, and cytokine stimuli (GO:0009605, GO:0009607, GO:0071345). Of particular note is the upregulation of multiple C-X-C motif chemokine ligands (*CXCL5*, *CXCL9*, *CXCL10*, *CXCL12*), interferon inducible genes (*IFI6*, *IFI44L*, *IFIT1*, *IFIT3*, *IFITM1*), Wnt family member 5A (*WNT5A*), and complement factor H (CFH). The group 6 gene set (Figure 5-7G) expression is higher in the PS1+ cells. In this group there are three functionally associated clusters of GO biological processes that are transcriptionally regulated, the largest being a cluster of pathways including neuroinflammatory response, inflammatory response, and cytokine production and regulation. Upregulated genes in this group include *APOE*, *C3*, *CD200*, *IL18*, *MMP9*, *TLR2*, *TLR3*, and *TNFRSF1B*.

Differential gene expression analysis revealed that expression of only one presenilin homologue causes 2.09- (PS1+) and 2.30 (PS2+) times more upregulation than downregulation of genes compared with the PS1+PS2+ cells (Figure 5-8A). There are substantially more genes that are commonly upregulated between PS2+ cells and PS1+ cells compared to PS1+PS2+ cells than are down regulated, with 49.9% of upregulated genes being common, while only 32.6% of down regulated genes are common (Figure 5-8B,C). This is reflected in the considerably lower number of genes that are differentially regulated between PS1+ cells and PS2+ cells (Figure 5-8A-C). Volcano plots presented for PS2+ and PS1+ compared to PS1+PS2+ identify the most significantly regulated genes and the genes with the largest amplitude of up and down regulation (Figure 5-8D,E, gene details are available in and SI Table 5-4)

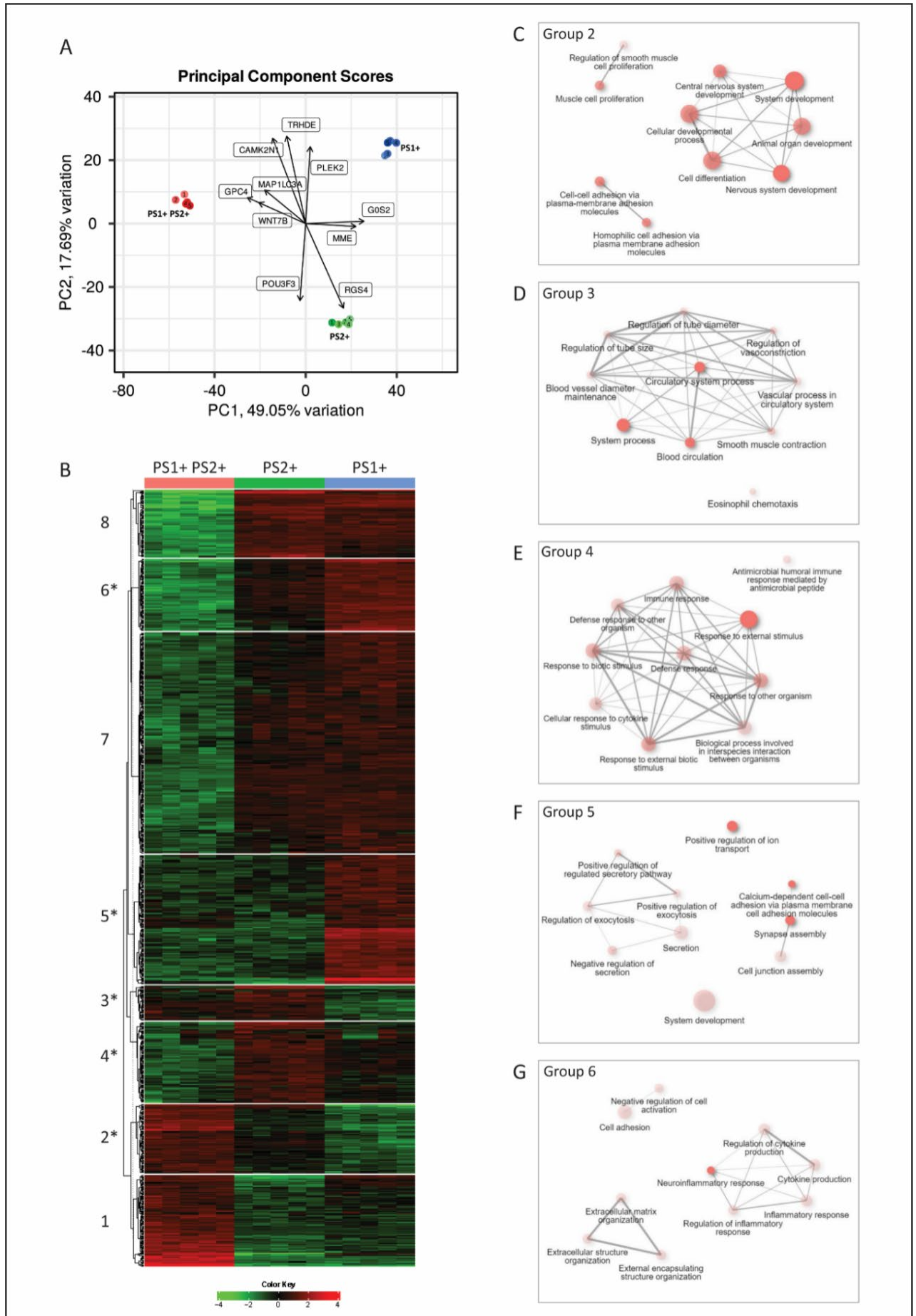


Figure 5-7 Transcript expression cluster analysis of HMC3 cells with altered PS genotype

Principal component analysis (A) and K-means clustered heatmap (B) for RNAseq transformed transcriptional expression data. Heatmap groups labelled with asterisk (*) identifies groups where PS2+ and PS1+ cells gene expression is not approximately equal. Network maps of GO biological processes pathway analysis for these groups are shown here (B-G). Network maps for group 1, 7, and 8 are available in SI Figure 5-2.

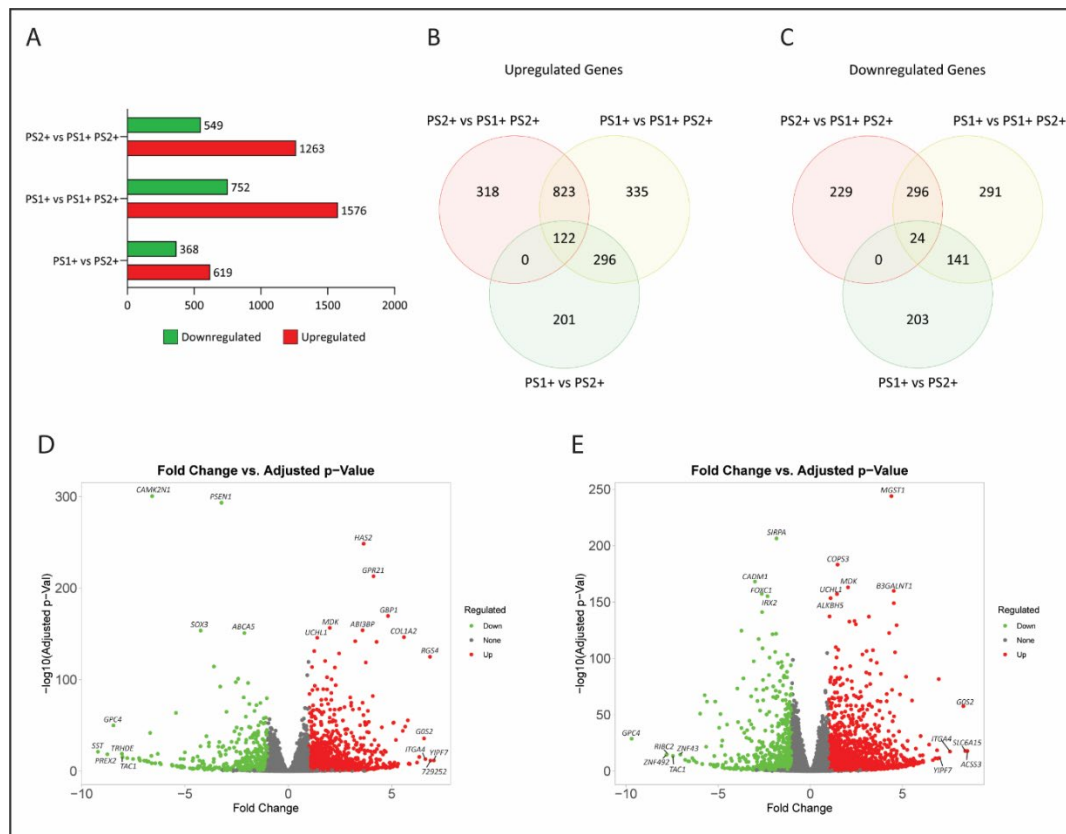


Figure 5-8 Differential gene expression analysis of HMC3 cells with altered PS genotypes

Up and downregulated gene identified in PS2+ and PS1+ cells compared to PS1+PS2+ cells and in PS1+ cells compared with PS2+ cells (A). Venn diagrams identify number of genes either exclusively or commonly upregulated (B) or downregulated (C) between differentially expressed genes. Volcano plot for PS2+ vs PS1+PS2+ (D) and PS1+ vs PS1+PS2+ (E) identify most significant differentially expressed genes, and genes with largest regulation amplitude.

Given that the genes differentially expressed between the PS2+ and PS1+ cells are of particular interest, RNAseq expression differences between PS2+ and PS1+ cells were analysed to identify likely candidates for the differential functions that were observed within these cells. The top ten most significantly regulated genes, and the five most upregulated and downregulated genes were identified (Figure 5-9A). These genes were investigated for microglial-related function and is presented in Table 5-1 and Table 5-2.

Parametric gene set enrichment analysis was performed with all samples to identify enriched KEGG pathways (Figure 5-9B). The top 50 KEGG pathways, with a pathway significance of <0.05 were identified. These pathways were reviewed to identify those where differential activation or suppression between PS2+ and PS1+ cells was evident, and were candidates for influencing the functional differences observed between the two cell lines. Eight KEGG pathways of interest were identified. Three pathways are activated in PS2+ cells; other types of *O*-glycan biosynthesis [has00514], axon guidance [hsa04360], and MAPK signaling pathway [hsa04010]. The remaining five KEGG pathways enriched in PS1+ cells are endocytosis [hsa04144], mTOR signaling pathway [hsa04150], cellular senescence [hsa04218], and bacterial invasion of epithelial cells [hsa05100], which are suppressed, and glycosphingolipid biosynthesis-lacto and neolacto series [hsa00601], which is activated. The complete list of differentially expressed genes from each pathway is available in *SI Table 5-5*.

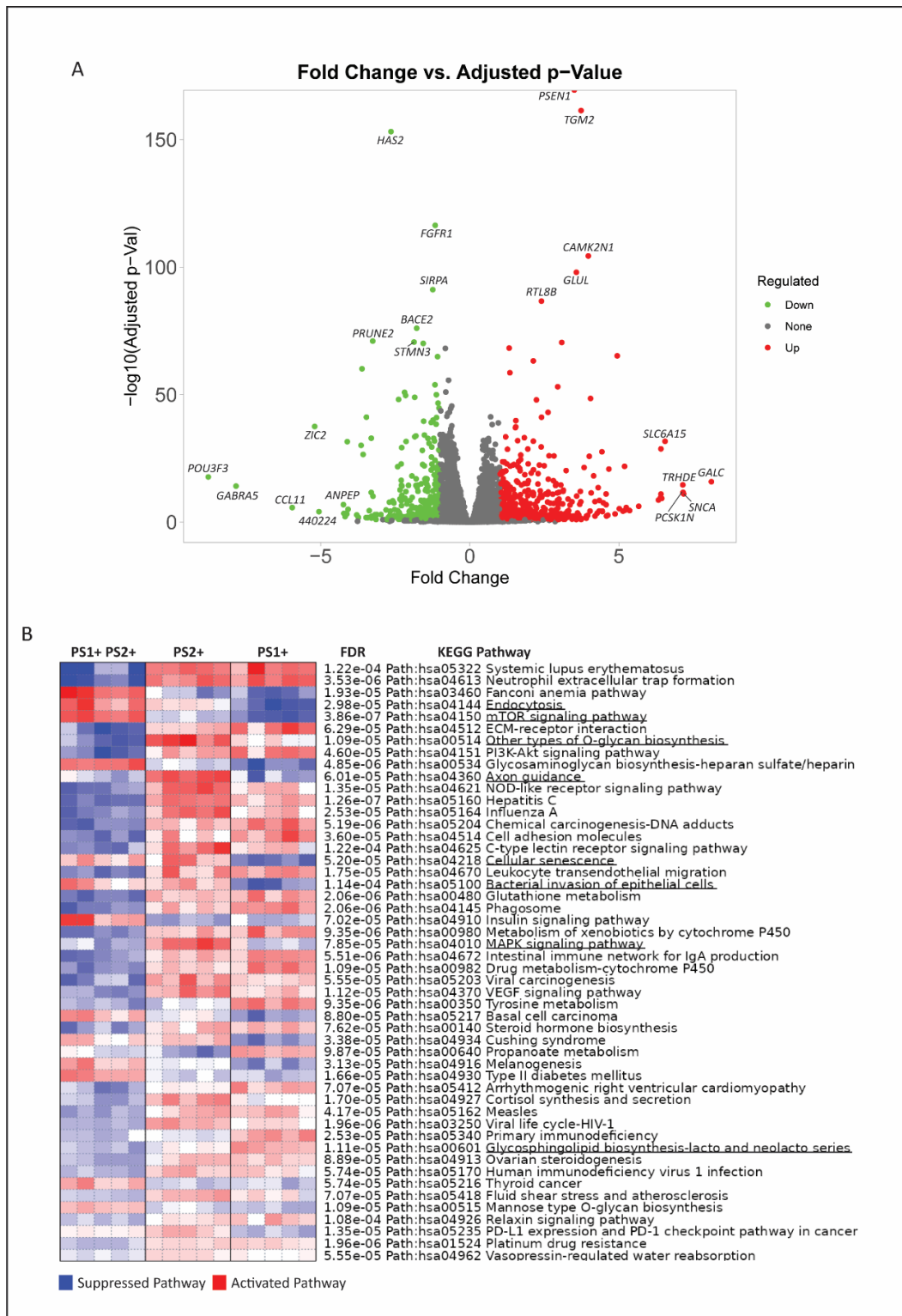


Figure 5-9 Differential gene expression and pathway analysis of PS1+ and PS2+ HMC3 cells

PS1+ vs PS2+ differential genes and pathway analysis. Volcano plot of PS1+ vs PS2+ with top 10 significantly regulated genes and top 5 upregulated and downregulated genes labelled (A). Note PSEN1 is excluded from top 10 most significant gene list (Table 4), and 440224 is excluded from top 5 downregulated gene list as is a pseudogene (Table 5). KEGG pathway enrichment, top 50 pathways (B), pathways of interest are underlined

Table 5-1 Top 10 most significant genes for PS1+ vs PS2+ differential gene comparison

Gene	PS1+ PS2+ Log ₂ [FC] [¶]	q-value	NCBI ID	Protein	CNS related function	Reference
TGM2	3.73	3.99 ⁻¹⁶²	7052	Protein-glutamine gamma-glutamyltransferase 2	Calcium dependent transglutaminase. Regulates nitric oxide generation, microglial inflammation, and synaptic remodelling.	80-83
HAS2	-2.64	6.97 ⁻¹⁵⁴	3037	Hyaluronan synthase 2	Synthesis of hyaluronan. Increased HAS2 associated with increased hyaluronan accumulation in microvasculature of brain with aging	84, 85
FGFR1	-1.16	4.52 ⁻¹¹⁷	2260	Fibroblast growth factor receptor 1	Fibroblast growth factor signalling. Regulates synapse formation, neuronal survival, and long-term potentiation	86, 87
CAMK2N1	3.97	4.13 ⁻¹⁰⁵	55450	Calcium/calmodulin-dependent protein kinase II inhibitor 1	CaMKII modulation during long term potentiation and neuronal plasticity	88, 89
GLUL	3.57	1.11 ⁻⁹⁸	2752	Glutamine synthetase	ATP-dependent catalysis of glutamine. Inhibition of glutamine synthetase upregulates inflammatory response in microglia	90
SIRPA	-1.24	8.13 ⁻⁹²	140885	Tyrosine-protein phosphatase non-receptor type substrate 1	CD47 ligand, modulates microglial activation, migration, and phagocytosis	91, 92
RTL8B	2.40	2.25 ⁻⁸⁷	441518	Retrotransposon Gag-like protein 8B	Retrotransposon, promotes nuclear translocation of UBQLN2	93
BACE2	-1.78	9.55 ⁻⁷⁷	25825	Beta-secretase 2	A β degrading enzyme, cleaves FGFR1 to release ectodomain	94-96
PRUNE2	-3.25	9.88 ⁻⁷²	158471	Protein prune homolog 2	CNS maintenance, particularly mature nervous system	97
STMN3	-1.87	2.37 ⁻⁷¹	50861	Stathmin-3	Microtubule destabilising protein, regulates microtubule dynamics, associated with neuronal differentiation, morphogenesis, and plasticity	98

¶ Where (PS1+ - PS2+ Log₂[FC]) result is +ve then PS1+ > PS2+, where result is -ve then PS2+ > PS1+

Table 5-2 Top 5 up and down regulated genes for PS1+ vs PS2+ differential gene comparison

Gene	PS1+ PS2+ Log2[FC] [¶]	q-value	NCBI ID	Protein	CNS related function	Reference
GALC	8.10	1.43 ⁻¹⁶	2581	Galactocerebrosidase	Hydrolyses galactosylceramide for myelin turnover, regulates myelin phagocytosis in microglia	99-101
SNCA	7.17	8.48 ⁻¹²	6622	α -Synuclein	Regulation of synaptic vesicle trafficking and neurotransmitter release. In microglia regulates haematopoiesis/ differentiation, vesicle formation and inflammatory responses.	102
PCSK1N	7.15	2.10 ⁻¹²	27344	ProSAAS	Regulates neuroendocrine secretion. Blocks fibrilisation of A β and α -synuclein	103-105
TRHDE	7.14	2.51 ⁻¹⁵	29953	Thyrotropin-releasing hormone-degrading ectoenzyme	Terminates neurotropic TRH-signals, hypothalamus–pituitary–thyroid axis regulation	106
SLC6A15	6.55	2.07 ⁻³²	55117	Sodium-dependent neutral amino acid transporter B(0)AT2	Regulates glutamate transmission. Associated with white matter integrity and cortisol secretion	107, 108
POU3F3	-8.77	1.95 ⁻¹⁸	5455	POU domain, class 3, transcription factor 3	Transcription factor, regulates CNS development, neuronal migration, and neurogenesis	109-111
GABRA5	-7.84	7.41 ⁻¹⁵	2558	Gamma-aminobutyric acid receptor subunit alpha-5	GABA inhibitory neurotransmitter receptor. Microglial receptor activation initiates migration and volume sampling	8, 112
CCL11	-5.95	1.99 ⁻⁰⁶	6356	Eotaxin	Eosinophil chemotaxis. Induces ROS in microglia, leading to neurotoxicity. Contrastingly can activate NPC proliferation and migration.	113, 114
ZIC2	-5.20	3.10 ⁻³⁸	7546	Zinc finger protein ZIC 2	Transcription factor critical for forebrain development. Negative regulator of Wnt signalling	115, 116
ANPEP	-4.24	1.39 ⁻⁰⁷	290	Aminopeptidase N	Neuropeptide degradation, regulates neuronal cAMP	117

¶ Where (PS1+ - PS2+ Log2[FC]) result is +ve then PS1+ > PS2+, where result is -ve then PS2+ > PS1+

5.4 DISCUSSION

There is no doubt that PS1 and PS2 play important roles in the pathogenesis of AD, given their role as the catalytic component of γ -secretase, and generation of A β , an association that is further confirmed by inherited mutations in PS1 and PS2 that cause ADAD.²⁵ While there has understandably been significant focus on elucidating the role of mechanisms by which PS1- γ -secretase and PS2- γ -secretase generate A β , there is evidence that identifies potentially important roles for PS1 and PS2 in microglial functions associated with the response to A β and its removal, including cytokine responses, microglial activation, A β phagocytosis, and expression of A β degrading enzymes.^{29, 30} This study investigated the functional role of PS1 and PS2 in the human HMC3 microglial cell line to determine if findings from murine models are recapitulated in a human model. It is particularly prudent to confirm these findings given the increasing recognition that there is significant divergence between murine and human microglial gene expression, particularly evident in relation to AD phenotypes.^{31, 118-120} In light of this, the study also delved deeper into the potential PS1 and PS2 pathways in human microglia by examining alterations in gene expression.

An important finding of this study is the observation of differential PS homologue-specific cellular responses to LPS and oA β treatment, and a specific upregulation of phagocytosis in PS2+ cells. These observations are discordant with those previously reported in murine models. However, there are only a limited number of studies that have investigated the role of PS1 and/or PS2 on microglial function.^{29, 30, 121} The ability to interpret the results in the context of these previous studies is further confounded by their opposing findings. For example, treatment of microglia with γ -secretase inhibitors resulted in reduced A β 42 phagocytosis, pro-inflammatory cytokine expression and secretion in immortalised N9 cells,²⁹ but similar treatment caused an increase in pro-inflammatory cytokine secretion in primary neo-natal microglia.³⁰ Furthermore, Farfara et al. report an overall decrease in microglial function, including gene expression of activation markers, pro-inflammatory cytokines, and A β degrading enzymes, as well as reduced A β phagocytosis, with loss/reduced PS1 or PS2 expression, and pharmacological γ -secretase inhibition.²⁹ Jayadev et al., however, report a PS2-specific response to LPS treatment, where the pro-inflammatory cytokine secretion was elevated in response to the loss of PS2 expression (i.e. PS1+ cells), and a concurrent decrease in secretion, of IL-6, in PS2+ cells (i.e. PS1KO/PS1KD) occurred.

The data presented in this chapter show significant functional effects of ablation of PS1 or PS2, most notably the PS homologue specific increases in pro-inflammatory cytokine responses to LPS and oA β . More specifically, cells that exclusively expressed PS2 responded solely to LPS treatment, whereas cells expressing only PS1 responded to oAb treatment (Figure 5-4). The enhanced pro-inflammatory response of PS2+ cells to LPS may explain why we observed increased bead phagocytic activity in these cells. Surprisingly, a similar increase in oA β phagocytosis by the PS1+ cells was not observed, associated with the increased pro-inflammatory response. Indeed, an unexpected increase in oA β phagocytosis in the PS2+ cells was observed (Figure 5-3).

One explanation for these discordant observations between inflammatory and phagocytic profiles, is that PS1+ cells may be chronically activated, which causes decreased phagocytosis.^{63, 122-124} While the proinflammatory cytokine GRO α is upregulated in vehicle treated PS1+ cells, indicating basal level activation, no other cytokines were significantly upregulated (SI Figure 5-3). While upregulation of TNF α and IL-6 are hallmarks of pro-inflammatory activation, considerable variation is present between the samples, as such the perceived 'increases' do not reach statistical significance. HMC3 cells expressing exclusively PS1 showed increased cell roundness compared to those expressing only PS2 (Figure 5-2). The morphology observed in the PS1-only cells may be indicative of a more amoeboid morphology, which is associated with an activated state.¹²⁵ If these cells are activated it would be a chronic event, as it reflects the untreated 'basal' state of the cells, and may affect phagocytic function. Furthermore, transcriptomic analysis indicates that these PS1+ cells have upregulated expression of genes involved in several inflammatory responses, in particular, neuroinflammatory and cytokine production responses (Figure 5-7G), suggestive of a chronically activated state. The PS2+ cells, however, have upregulated gene expression associated with defence responses, and responses to biotic, external and cytokine stimuli (Figure 5-7E), suggestive of a readiness to respond to stimuli that may be manifesting by increased uptake of beads and oA β .

Further analysis of the transcriptomic data reveals KEGG pathways differentially affected in PS1+ or PS2+ cells that likely influence the observed specific functional responses. Of particular interest is the activation of MAPK signalling pathway in PS2+ cells (Figure 5-9B; SI Figure 5-4). Activation of MAPK signalling is known to increase phagocytosis,¹²⁶ and likely contributes to the enhanced phagocytosis observed in PS2+ cells (Figure 5-3). The conical

adaptor for initiating TLR signalling, MYD88¹²⁷, was down regulated in PS1+ cells compared to PS2+ cells. Macrophages deficient in MYD88 have been shown to have reduced cytokine responses to LPS¹²⁸ and altered killing of external pathogens,^{129, 130} despite normal microbial phagocytosis.^{129, 130} Given this, the reduced MYD88 observed in PS1+ cells may explain reduced cytokine response to LPS exhibited by these cells despite unaltered ability to phagocytose. Future investigation via MYD88 knockdown or overexpression studies in these cell lines is required to confirm this hypothesis.

Other significantly regulated, and the most highly up- and down-regulated genes identified in the PS1+ and PS2+ cells may also provide additional gene candidates of interest for further study. *SCNA*, encoding for α -synuclein, the primary gene causative for familial Parkinson's disease,¹³¹ is highly upregulated in PS1+ cells, compared to both PS2+ and PS1+PS2+ cells (Table 5-2). Involved in regulation of synaptic vesicle trafficking,¹⁰² the aggregation and deposition of α -synuclein in the form of inclusion bodies known as Lewy bodies, has been found deposited in the brains of individuals with ADAD mutations in PS1, PS2 and APP.¹³²⁻¹³⁴ Excess α -synuclein has been shown to impede phagocytosis in both human iPSC macrophage¹³⁵ and murine microglia.¹³⁶ Phagocytosis of fluorescent labelled α -synuclein in our cell lines, similar to what was done for oA β , would provide support for a role of PS in this process and whether there is a predominate role for specific PSs (as observed for PS2 in phagocytosis of oA β). In contrast, *SIRPA*, a negative regulator of phagocytosis,^{137, 138} is downregulated in PS1+ cells, compared to PS2+ cells. In isolation, this may lead to increased oA β phagocytosis, but in combination with other altered pathways and gene expressions identified, may act as a compensatory mechanism to maintain phagocytic levels similar to that observed for the PS1+PS2+ cells.

Microglial phagocytosis of A β can occur via direct or indirect engagement with receptors. TREM2, AXL, and MER are known phagocytic receptors that can bind A β directly.^{14, 21, 59} The consequences of γ -secretase processing of these receptors and the resulting ICD fragments remain to be determined; however, they are likely stable protein products, with a leucine N-terminus (Chapter 3:SI Fig1) consistent with the N-end rule,^{139, 140} and may have self-regulatory mechanisms to control expression levels.¹⁴¹ Alternatively A β can bind apolipoproteins, for example apolipoprotein E (APOE) and clusterin (CLU or APOJ), which mediate indirect internalisation of A β via TREM2, and lipoprotein receptors including VLDLR.^{65, 142-145} Analysis of VLDLR transcript and protein in the cell lines, revealed a

downregulation of gene expression and complete loss of protein expression in both PS2+ and PS1+ cells (Figure 5-6D-F). VLDLR/APOE binding is suggested to down regulate JNK signalling, subsequently increasing APOE expression.¹⁴² Thus, the loss of VLDLR expression would consequently be expected to result in decreased APOE expression. Transcriptomic analysis of the PS cell lines revealed *APOE* transcript expression is upregulated in both the PS2+ and PS1+ cells, incongruent with the notion above. Although there may be species differences (the study above was in a murine model),¹⁴² it must be noted, however, that the conditions used in the current study did not mimic the effect of exogenous/extracellular APOE binding to VLDLR to initiate downstream signalling. It remains unclear why there is a complete absence of VLDLR in both cell lines and indicates that potentially both PSs are required for the transcriptional regulation of VLDLR; creation and analysis of double knockout PS microglia may address this. However, there are additional factors involved in the transcriptional regulation of *APOE* expression,¹⁴⁶ including *PPAR γ* and *SREBF1*, both of which are upregulated in the PS1+ and PS2+ cell transcript. Although these factors are not substrates of γ -secretase, further investigation to understand the role of PS1 and PS2 in their regulation is warranted.

Gene expression of the other key receptor, TREM2 was upregulated in PS2+ cells, while the 25kDa TREM2 protein band was reduced in the PS2+ cells. A larger 50kDa protein band was detected that was not altered in either cell line (Figure 5-6J-M). TREM2 N-glycosylation at two sites on its ectodomain (N20 and N79) occurs as it traffics through the golgi to its functional plasma membrane location and is critical for TREM2/DAP12 mediated signal transduction.¹⁴⁷ Glycosylated TREM2 typically migrates as a smear between 33-50 kDa,^{77, 147, 148} while un-glycosylated TREM2 migrated at 25 kDa after endo-H or PNGase-F treatment.¹⁴⁸ The discrepant band patterning observed in this study requires verification using alternative antibodies and de-glycosylation treatments to confirm the post-translation modification status and expression levels of TREM2, relative to altered PS genotypes in the HMC3 cells.

PS1 has been shown to interact with TREM2, independent of γ -secretase, to regulate intracellular trafficking, although the mechanism of action is unknown. PS1 overexpression reduces surface TREM2 levels, while PS1 knockdown increases surface TREM2.¹⁴⁹ Additionally the authors showed that PS1 overexpression decreased A β phagocytosis (in murine microglia BV2 cells), while PS1 knockdown had no effect, they speculate that the loss of PS1 leads to increased TREM-CTF accumulation that competes with full length TREM2,

subsequently inhibiting DAP12 signalling. However as no consideration of PS2 was made in that study, the possibility that the observations are a function of altered PS2 expression cannot be discounted.¹⁴⁹ In contrast, DAPT treatment, again in BV2 cells, was demonstrated to cause decreased TREM2-dependent phagocytosis, by disrupting TREM2-dependent Ca^{2+} signalling.¹⁵⁰ In another study, TREM2 knockdown in mice, by use of transient antisense oligonucleotides and not long term genetic alterations, increased A β phagocytosis,¹⁵¹ this may be a similar response mechanism to that observed here in the PS2+ cells. However, the conflicting results of these studies, and here where increased phagocytosis in the absence of PS1 expression was observed (Figure 5-3), highlight the need for further studies to clarify the role of PS1 and PS2 in TREM2 related microglial function, and determine what contributions are γ -secretase dependent and independent.

PS expression has previously been shown to affect A β -degrading enzyme expression and activity of IDE^{29, 152}, MMP9,²⁹ and neprilysin^{40, 41} in a variety of human and murine cells of different origin but has not been investigated in human microglia. Consequently, the effect of PS genotype alterations in HMC3 cells on A β degrading enzymes expression was investigated. While expression of *IDE* was downregulated in both PS2+ and PS1+ cells, similar to observations in previous studies,^{29, 152} *MMP2*, *MMP9* and *MME* (encodes for neprilysin) expression was highly upregulated, with a minimum 20-fold increase, in both the PS2+ and PS1+ cells. The upregulation observed by qPCR was recapitulated with RNAseq. Indeed the gene expression regulation of both the A β degrading enzymes and A β removal related substrates investigated are consistent in both the qPCR and RNAseq results (Figure 5-5, Figure 5-6, SI Table 5-7). Such high upregulation of *MME* was unexpected given findings from previous studies. However, further strengthening the findings from qPCR, significant *MME* upregulation was confirmed by RNA sequencing. Expression levels were so highly upregulated in PS2+ and PS1+ cells compared to PS1+PS2+ cells, that *MME* is a major contributor to principal component 1 (Figure 5-7A). *MME* is transcriptionally regulated by the APP intracellular domain (AICD), specifically derived from γ -secretase cleaved β -APP-CTF.^{40, 41} Interestingly we observed increased APP-FL protein expression in PS2+ and PS1+ cells, which may explain the observed increased *MME* expression. Although there is evidence of increased neprilysin expression in PS1KO mouse embryonic fibroblasts,¹⁵³ this has not been consistently reported.^{40, 41, 153-155} As such we investigated the protein levels and interestingly found that neprilysin was significantly decreased (Figure 5-5A,G-H).

The disparate expression between transcript and protein observed for neprilysin was similarly observed for BACE1 and TREM2. Consequently, it was considered whether post-translational degradation pathways may be dysregulated in the PS2+ and PS1+ cells. Some evidence of this is provided by a previous report showing that PS deficiency led to γ -secretase independent upregulation of the Fbw7 E3 ligase, subsequently regulating ubiquitination and proteasomal degradation of epidermal growth factor receptor.¹⁵⁶ Further assessment of the RNA sequencing data identified several E3 ligase, and E3 ligase adaptor proteins that were substantially upregulated ($\text{Log}_2[\text{FC}] > 1.5$) in both PS2+ and PS1+ cells (

Gene	PS2+ - PS1+PS2+		PS1+ - PS1+PS2+		PS1+ - PS2+	
	$\text{Log}_2[\text{FC}]^{\ddagger}$	q-value	$\text{Log}_2[\text{FC}]^{\ddagger}$	q-value	$\text{Log}_2[\text{FC}]^{\ddagger}$	q-value
MME	5.78	3.60E-56	6.97	2.64E-82	1.19	7.74
MMP2	2.56	1.65E-14	3.30	4.28E-24	0.74	6.79
MMP9	2.86	4.34E-08	3.54	2.25E-12	-	-
IDE	-	-	-	-	-	-
ECE1	-	-	-	-	-	-
BACE1	0.61	3.44E-06	0.61	3.47E-06	-	-
APP	0.76	2.58E-48	0.48	6.73E-20	-0.28	13.47
VLDLR	-1.45	8.90E-43	-2.00	8.60E-76	-0.55	7.93
CD44	0.56	4.78E-08	-	-	-0.53	13.84
TREM2	1.48	3.09E-02	1.33	4.81E-02	-	-

\ddagger Where $\text{Log}_2[\text{FC}]$ result is +ve then $\text{PS2+} > \text{PS1+PS2+}$, $\text{PS1+} > \text{PS1+PS2+}$, $\text{PS1+} > \text{PS2+}$, where result is -ve then $\text{PS2+} < \text{PS1+PS2+}$, $\text{PS1+} < \text{PS1+PS2+}$, $\text{PS1+} < \text{PS2+}$

SI Table 5-8). Validation of this regulation is required to confirm presenilin involvement, but these initial findings may reveal novel functions of presenilin.

While the current study offers valuable insights into the functional roles of PS1 and PS2 in microglia, its limitations must be considered. Although this is the first study, to our knowledge, that has developed human microglial cells with altered PS genotypes, we did not generate a PSnull cell line, nor undertake any PS rescue. This is a future goal to further tease apart the role of PSs in microglial function, including that discussed below. Unlike Jayadev et al.³⁰ who observed upregulated functional responses with the loss of PS2 and commensurate down regulation or no effect in cells lacking PS1, a variety of functional responses in PS1+ and PS2+ cells were observed in the current study. While this indicates diverse functional roles for PS1 and PS2 in microglia, the results acquired with the current experimental model do not enable definitive assignment of function to either PS1 or PS2. Given that we observed compensatory increases in the retained PS homologue in response to the loss of both PS1 and PS2, whether the specific responses observed in this study are the result of the loss of the ablated PS or the compensatory increase in expression of the retained PS should be considered.

The results observed in this study do not align with previous studies completed in murine models and identify some potentially novel and highly specific PS1 and PS2 functions, warranting further validation. Furthermore, although DAPT treatment to simulate γ -secretase inhibition was employed, with the intent to assign functions as PS- γ -secretase dependent or independent, only an increased rate of $\alpha\text{A}\beta$ phagocytosis (Figure 5-3C) and accumulation of APP-CTF (Figure 5-6B) was observed. Given the comparatively muted response of the HMC3 cells presented here and commented on by others,⁵⁵ it is possible that the treatment time and concentrations used in this study were inadequate to cause effective γ -secretase inhibition to induce a functional response. This may be particularly important for functions associated with transcriptional regulation. Consequently, assertions as to whether the findings can be attributed to γ -secretase dependence or are independent of enzyme activity are difficult to make.

It would be prudent to develop and/or use human iPSC cell lines with both single and double knockout of PS1 and PS2 differentiated to a microglial cell lineage, a suitable model might be that developed by Watanabe and colleagues.¹⁵⁷ However, the exogenous reintroduction of PS for rescue studies should be approached with caution, as we have shown these ectopic systems do not fully recapitulate the endogenous system¹⁵⁸ and often cause PS holoprotein retention.^{158,}

¹⁵⁹ To overcome this the development of a human iPSC auxin-inducible degron system¹⁶⁰ adapted to enable controlled degradation of either individual PS or both PS simultaneously, should be pursued. This will provide the further advantage of enabling endogenous protein expression to effectively be switched off and on again, allowing for rescue of PS1 or PS2 to assist in improved assignment of specific functions with confidence. Such a system would also enable understanding of the temporality of PS1 and PS2 function, important information for the development of improved therapeutic targeting strategies for γ -secretase.

Understanding the roles of PS1 and PS2 in neuroglia is important if we are to understand the implications of therapeutically targeting γ -secretase on functions other than A β generation. This study has provided significant insight into these roles in novel, PS1+ and PS2+ human microglial cell lines developed in chapter 4. In particular, specific and differential pro-inflammatory responses to different stimuli in PS2+ and PS1+ microglia and increased phagocytic function in PS2+ cells are demonstrated, functions that are incongruent with murine studies. While further validation in improved human models is required, potential novel functions of PS1 and PS2 in microglia have been identified.

5.5 REFERENCES

1. Kettenmann, H., Hanisch, U.-K., Noda, M., and Verkhratsky, A. (2011) Physiology of Microglia. *Physiological Reviews* **91**, 461-553
2. McNamara, N. B., Munro, D. A. D., Bestard-Cuche, N., Uyeda, A., Bogie, J. F. J., et al. (2023) Microglia regulate central nervous system myelin growth and integrity. *Nature* **613**, 120-129
3. Santos, E. N., and Fields, R. D. (2021) Regulation of myelination by microglia. *Science Advances* **7**, eabk1131
4. Holloway, R. K., Zhang, L., Molina-Gonzalez, I., Ton, K., Nicoll, J. A. R., et al. (2023) Localized microglia dysregulation impairs central nervous system myelination in development. *Acta Neuropathologica Communications* **11**, 49
5. Traiffort, E., Kassoussi, A., Zahaf, A., and Laouarem, Y. (2020) Astrocytes and Microglia as Major Players of Myelin Production in Normal and Pathological Conditions. *Frontiers in Cellular Neuroscience* **14**
6. Pérez-Rodríguez, D. R., Blanco-Luquin, I., and Mendoroz, M. (2021) The Participation of Microglia in Neurogenesis: A Review. *Brain Sciences* **11**
7. Sato, K. (2015) Effects of Microglia on Neurogenesis. *Glia* **63**, 1394-1405
8. Nimmerjahn, A., Kirchhoff, F., and Helmchen, F. (2005) Resting microglial cells are highly dynamic surveillants of brain parenchyma in vivo. *Science* **308**, 1314-1318
9. Boche, D., and Gordon, M. N. (2022) Diversity of transcriptomic microglial phenotypes in aging and Alzheimer's disease. *Alzheimer's & Dementia* **18**, 360-376
10. Long, J. M., and Holtzman, D. M. (2019) Alzheimer Disease: An Update on Pathobiology and Treatment Strategies. *Cell* **179**, 312-339

11. Efthymiou, A. G., and Goate, A. M. (2017) Late onset Alzheimer's disease genetics implicates microglial pathways in disease risk. *Molecular Neurodegeneration* **12**, 43
12. Lewcock, J. W., Schlepckow, K., Di Paolo, G., Tahirovic, S., Monroe, K. M., et al. (2020) Emerging Microglia Biology Defines Novel Therapeutic Approaches for Alzheimer's Disease. *Neuron* **108**, 801-821
13. McQuade, A., and Blurton-Jones, M. (2019) Microglia in Alzheimer's Disease: Exploring How Genetics and Phenotype Influence Risk. *Journal of Molecular Biology* **431**, 1805-1817
14. Zhao, Y., Wu, X., Li, X., Jiang, L.-L., Gui, X., et al. (2018) TREM2 Is a Receptor for β -Amyloid that Mediates Microglial Function. *Neuron* **97**, 1023-1031.e1027
15. Akhter, R., Shao, Y., Formica, S., Khrestian, M., and Bekris, L. M. (2021) TREM2 alters the phagocytic, apoptotic and inflammatory response to A β 42 in HMC3 cells. *Molecular Immunology* **131**, 171-179
16. Barthelson, K., Newman, M., and Lardelli, M. (2020) Sorting Out the Role of the Sortilin-Related Receptor 1 in Alzheimer's Disease. *Journal of Alzheimer's Disease Reports* **4**, 123-140
17. Carlo, A. S., Gustafsen, C., Mastrobuoni, G., Nielsen, M. S., Burgert, T., et al. (2013) The pro-neurotrophin receptor sortilin is a major neuronal apolipoprotein E receptor for catabolism of amyloid- β peptide in the brain. *The Journal of Neuroscience* **33**, 358-370
18. Güner, G., and Lichtenthaler, S. F. (2020) The substrate repertoire of γ -secretase/presenilin. *Seminars in Cell & Developmental Biology* **105**, 27-42
19. Galichet, A., Weibel, M., and Heizmann, C. W. (2008) Calcium-regulated intramembrane proteolysis of the RAGE receptor. *Biochemical and Biophysical Research Communications* **370**, 1-5
20. Zhao, W., Fan, J., Kulic, I., Koh, C., Clark, A., et al. (2020) Axl receptor tyrosine kinase is a regulator of apolipoprotein E. *Molecular Brain* **13**, 66
21. Huang, Y., Happonen, K. E., Burrola, P. G., O'Connor, C., Hah, N., et al. (2021) Microglia use TAM receptors to detect and engulf amyloid β plaques. *Nature Immunology* **22**, 586-594
22. Takahashi, K., Eto, H., and Tanabe, K. K. (1999) Involvement of CD44 in matrix metalloproteinase-2 regulation in human melanoma cells. *International Journal of Cancer* **80**, 387-395
23. Dorandish, S., Williams, A., Atali, S., Sendo, S., Price, D., et al. (2021) Regulation of amyloid- β levels by matrix metalloproteinase-2/9 (MMP2/9) in the media of lung cancer cells. *Scientific Reports* **11**, 9708
24. N'Songo, A., Kanekiyo, T., and Bu, G. (2013) LRP1 plays a major role in the amyloid- β clearance in microglia. *Molecular Neurodegeneration* **8**, P33
25. Hoogmartens, J., Cacace, R., and Van Broeckhoven, C. (2021) Insight into the genetic etiology of Alzheimer's disease: A comprehensive review of the role of rare variants. *Alzheimer's & Dementia: Diagnosis, Assessment & Disease Monitoring* **13**, e12155
26. Lee, J., Chan, S. L., and Mattson, M. P. (2002) Adverse effect of a presenilin-1 mutation in microglia results in enhanced nitric oxide and inflammatory cytokine responses to immune challenge in the brain. *Neuromolecular Medicine* **2**, 29-45
27. Fung, S., Smith, C. L., Prater, K. E., Case, A., Green, K., et al. (2020) Early-Onset Familial Alzheimer Disease Variant PSEN2 N141I Heterozygosity is Associated with Altered Microglia Phenotype. *Journal of Alzheimer's Disease* **77**, 675-688
28. Nam, H., Lee, Y., Kim, B., Lee, J.-W., Hwang, S., et al. (2022) Presenilin 2 N141I mutation induces hyperactive immune response through the epigenetic repression of REV-ERBa. *Nature Communications* **13**, 1972

29. Farfara, D., Trudler, D., Segev-Amzaleg, N., Galron, R., Stein, R., et al. (2011) γ -Secretase component presenilin is important for microglia β -amyloid clearance. *Annals of Neurology* **69**, 170-180
30. Jayadev, S., Case, A., Eastman, A. J., Nguyen, H., Pollak, J., et al. (2010) Presenilin 2 Is the Predominant γ -Secretase in Microglia and Modulates Cytokine Release. *PLoS One* **5**
31. Miller, J. A., Horvath, S., and Geschwind, D. H. (2010) Divergence of human and mouse brain transcriptome highlights Alzheimer disease pathways. *Proceedings of the National Academy of Sciences of the United States of America* **107**, 12698-12703
32. Zhou, Y., Song, W. M., Andhey, P. S., Swain, A., Levy, T., et al. (2020) Human and mouse single-nucleus transcriptomics reveal TREM2-dependent and TREM2-independent cellular responses in Alzheimer's disease. *Nature Medicine* **26**, 131-142
33. Ries, M., and Sastre, M. (2016) Mechanisms of A β Clearance and Degradation by Glial Cells. *Frontiers in Aging Neuroscience* **8**
34. Zuroff, L., Daley, D., Black, K. L., and Koronyo-Hamaoui, M. (2017) Clearance of cerebral A β in Alzheimer's disease: reassessing the role of microglia and monocytes. *Cellular and Molecular Life Sciences* **74**, 2167-2201
35. Fluhner, R., Multhaup, G., Schlicksupp, A., Okochi, M., Takeda, M., et al. (2003) Identification of a β -Secretase Activity, Which Truncates Amyloid β -Peptide after Its Presenilin-dependent Generation. *The Journal of Biological Chemistry* **278**, 5531-5538
36. Shi, X.-P., Tugusheva, K., Bruce, J. E., Lucka, A., Wu, G.-X., et al. (2003) β -Secretase Cleavage at Amino Acid Residue 34 in the Amyloid- β Peptide Is Dependent upon γ -Secretase Activity. *The Journal of Biological Chemistry* **278**, 21286-21294
37. Ulku, I., Liebsch, F., Akerman, S. C., Schulz, J. F., Kulic, L., et al. (2023) Mechanisms of amyloid- β 34 generation indicate a pivotal role for BACE1 in amyloid homeostasis. *Scientific Reports* **13**, 2216
38. Hickman, S. E., Allison, E. K., and Khoury, J. E. (2008) Microglial Dysfunction and Defective β -Amyloid Clearance Pathways in Aging Alzheimer's Disease Mice. *The Journal of Neuroscience* **28**, 8354-8360
39. Jang, S. K., Yu, J. M., Kim, S. T., Kim, G. H., Park, D. W., et al. (2015) An A β 42 uptake and degradation via Rg3 requires an activation of caveolin, clathrin and A β -degrading enzymes in microglia. *European Journal of Pharmacology* **758**, 1-10
40. Pardossi-Piquard, R., Petit, A., Kawarai, T., Sunyach, C., Da Costa, C. A., et al. (2005) Presenilin-dependent transcriptional control of the A β -degrading enzyme neprilysin by intracellular domains of β APP and APLP. *Neuron* **46**, 541-554
41. Grimm, M. O. W., Mett, J., Stahlmann, C. P., Grösgen, S., Hauptenthal, V. J., et al. (2015) APP intracellular domain derived from amyloidogenic β - and γ -secretase cleavage regulates neprilysin expression. *Frontiers in Aging Neuroscience* **7**, 77-77
42. Blasi, E., Barluzzi, R., Bocchini, V., Mazzolla, R., and Bistoni, F. (1990) immortalization of murine microglial cells by a v-raf / v-myc carrying retrovirus. *Journal of Neuroimmunology* **27**, 229-237
43. Janabi, N., Peudenier, S., Héron, B., Ng, K. H., and Tardieu, M. (1995) Establishment of human microglial cell lines after transfection of primary cultures of embryonic microglial cells with the SV40 large T antigen. *Neuroscience Letters* **195**, 105-108
44. Stine, W. B., Jungbauer, L., Yu, C., and LaDu, M. J. (2011) Preparing synthetic A β in different aggregation states. *Methods in Molecular Biology* **670**, 13-32
45. Stirling, D. R., Swain-Bowden, M. J., Lucas, A. M., Carpenter, A. E., Cimini, B. A., et al. (2021) CellProfiler 4: improvements in speed, utility and usability. *BMC Bioinformatics* **22**, 433

46. Ye, J., Coulouris, G., Zaretskaya, I., Cutcutache, I., Rozen, S., et al. (2012) Primer-BLAST: a tool to design target-specific primers for polymerase chain reaction. *BMC Bioinformatics* **13**, 134
47. Pfaffl, M. W. (2001) A new mathematical model for relative quantification in real-time RT-PCR. *Nucleic Acids Research* **29**, e45-e45
48. Liao, Y., Smyth, G. K., and Shi, W. (2019) The R package Rsubread is easier, faster, cheaper and better for alignment and quantification of RNA sequencing reads. *Nucleic Acids Research* **47**, e47
49. Chisanga, D., Liao, Y., and Shi, W. (2022) Impact of gene annotation choice on the quantification of RNA-seq data. *BMC Bioinformatics* **23**, 107
50. Liao, Y., Smyth, G. K., and Shi, W. (2013) The Subread aligner: fast, accurate and scalable read mapping by seed-and-vote. *Nucleic Acids Research* **41**, e108
51. Liao, Y., Smyth, G. K., and Shi, W. (2014) featureCounts: an efficient general purpose program for assigning sequence reads to genomic features. *Bioinformatics* **30**, 923-930
52. Ge, S. X., Son, E. W., and Yao, R. (2018) iDEP: an integrated web application for differential expression and pathway analysis of RNA-Seq data. *BMC Bioinformatics* **19**, 534
53. Kanehisa, M., and Goto, S. (2000) KEGG: kyoto encyclopedia of genes and genomes. *Nucleic Acids Research* **28**, 27-30
54. Kanehisa, M. (2019) Toward understanding the origin and evolution of cellular organisms. *Protein Science* **28**, 1947-1951
55. Dello Russo, C., Cappoli, N., Coletta, I., Mezzogori, D., Paciello, F., et al. (2018) The human microglial HMC3 cell line: where do we stand? A systematic literature review. *Journal of Neuroinflammation* **15**, 259
56. Clarke, D., Crombag, H. S., and Hall, C. N. (2021) An open-source pipeline for analysing changes in microglial morphology. *Open Biology* **11**, 210045
57. Tremblay, M., Stevens, B., Sierra, A., Wake, H., Bessis, A., et al. (2011) The role of microglia in the healthy brain. *The Journal of Neuroscience* **31**, 16064-16069
58. Wunderlich, P., Glebov, K., Kemmerling, N., Tien, N. T., Neumann, H., et al. (2013) Sequential proteolytic processing of the triggering receptor expressed on myeloid cells-2 (TREM2) protein by ectodomain shedding and γ -secretase-dependent intramembranous cleavage. *The Journal of Biological Chemistry* **288**, 33027-33036
59. Lessard, C. B., Malnik, S. L., Zhou, Y., Ladd, T. B., Cruz, P. E., et al. (2018) High-affinity interactions and signal transduction between A β oligomers and TREM2. *EMBO Molecular Medicine* **10**, e9027
60. Joshi, P., Riffel, F., Satoh, K., Enomoto, M., Qamar, S., et al. (2021) Differential interaction with TREM2 modulates microglial uptake of modified A β species. *Glia* **69**, 2917-2932
61. Merilahti, J. A. M., Ojala, V. K., Knittle, A. M., Pulliainen, A. T., and Elenius, K. (2017) Genome-wide screen of gamma-secretase-mediated intramembrane cleavage of receptor tyrosine kinases. *Molecular Biology of the Cell* **28**, 3123-3131
62. Lively, S., and Schlichter, L. C. (2018) Microglia Responses to Pro-inflammatory Stimuli (LPS, IFN γ +TNF α) and Reprogramming by Resolving Cytokines (IL-4, IL-10). *Frontiers in Cellular Neuroscience* **12**, 215
63. Milligan Armstrong, A., Porter, T., Quek, H., White, A., Haynes, J., et al. (2021) Chronic stress and Alzheimer's disease: the interplay between the hypothalamic-pituitary-adrenal axis, genetics and microglia. *Biological Reviews* **96**, 2209-2228
64. Kuzuya, A., Uemura, K., Kitagawa, N., Aoyagi, N., Kihara, T., et al. (2007) Presenilin 1 is involved in the maturation of beta-site amyloid precursor protein-cleaving enzyme 1 (BACE1). *Journal of Neuroscience Research* **85**, 153-165

65. Deane, R., Sagare, A., Hamm, K., Parisi, M., Lane, S., et al. (2008) apoE isoform-specific disruption of amyloid beta peptide clearance from mouse brain. *The Journal of Clinical Investigation* **118**, 4002-4013
66. Takahashi, S., Oida, K., Ookubo, M., Suzuki, J., Kohno, M., et al. (1996) Very low density lipoprotein receptor binds apolipoprotein E2/2 as well as apolipoprotein E3/3. *FEBS Letters* **386**, 197-200
67. Ruiz, J., Kouivaskaia, D., Migliorini, M., Robinson, S., Saenko, E. L., et al. (2005) The apoE isoform binding properties of the VLDL receptor reveal marked differences from LRP and the LDL receptor. *Journal of Lipid Research* **46**, 1721-1731
68. Keren-Shaul, H., Spinrad, A., Weiner, A., Matcovitch-Natan, O., Dvir-Szternfeld, R., et al. (2017) A Unique Microglia Type Associated with Restricting Development of Alzheimer's Disease. *Cell* **169**, 1276-1290.e1217
69. Rangaraju, S., Dammer, E. B., Raza, S. A., Rathakrishnan, P., Xiao, H., et al. (2018) Identification and therapeutic modulation of a pro-inflammatory subset of disease-associated-microglia in Alzheimer's disease. *Molecular Neurodegeneration* **13**, 24
70. Manocha, G. D., Floden, A. M., Rausch, K., Kulas, J. A., McGregor, B. A., et al. (2016) APP Regulates Microglial Phenotype in a Mouse Model of Alzheimer's Disease. *The Journal of Neuroscience* **36**, 8471-8486
71. Wang, Q., Yang, W., Zhang, J., Zhao, Y., and Xu, Y. (2020) TREM2 Overexpression Attenuates Cognitive Deficits in Experimental Models of Vascular Dementia. *Neural Plasticity* **2020**, 8834275
72. Yu, T., Fu, H., Sun, J. J., Ding, D. R., and Wang, H. (2021) miR-106b-5p upregulation is associated with microglial activation and inflammation in the mouse hippocampus following status epilepticus. *Experimental Brain Research* **239**, 3315-3325
73. Shi, K., Chen, L., Chen, L., Tan, A., Xie, G., et al. (2022) Epimedii Folium and Curculiginis Rhizoma ameliorate lipopolysaccharides-induced cognitive impairment by regulating the TREM2 signaling pathway. *Journal of Ethnopharmacology* **284**, 114766
74. Shi, D., Xu, Z., Cheng, Y., Lin, Q., Si, Z., et al. (2023) 124I-Labeled Immuno-PET Targeting hTREM2 for the Diagnosis of Gastric Carcinoma. *Molecular Pharmaceutics* **20**, 2235-2244
75. Huang, W., Lv, Q., Xiao, Y., Zhong, Z., Hu, B., et al. (2021) Triggering Receptor Expressed on Myeloid Cells 2 Protects Dopaminergic Neurons by Promoting Autophagy in the Inflammatory Pathogenesis of Parkinson's Disease. *Frontiers in Neuroscience* **15**, 745815
76. ABclonal. (2023) TREM2 Rabbit pAb Catalog No.: A10482. Woburn, MA, USA
77. Park, J.-S., Ji, I. J., Kim, D.-H., An, H. J., and Yoon, S.-Y. (2017) The Alzheimer's Disease-Associated R47H Variant of TREM2 Has an Altered Glycosylation Pattern and Protein Stability. *Frontiers in Neuroscience* **10**
78. Lue, L. F., Schmitz, C. T., Serrano, G., Sue, L. I., Beach, T. G., et al. (2015) TREM2 Protein Expression Changes Correlate with Alzheimer's Disease Neurodegenerative Pathologies in Post-Mortem Temporal Cortices. *Brain Pathology* **25**, 469-480
79. Kober, D. L., Alexander-Brett, J. M., Karch, C. M., Cruchaga, C., Colonna, M., et al. (2016) Neurodegenerative disease mutations in TREM2 reveal a functional surface and distinct loss-of-function mechanisms. *eLife* **5**, e20391
80. Rudlong, J., Cheng, A., and Johnson, G. V. W. (2020) The role of transglutaminase 2 in mediating glial cell function and pathophysiology in the central nervous system. *Analytical Biochemistry* **591**, 113556
81. Hou, Y., Xiao, X., Yu, W., and Qi, S. (2021) Propofol Suppresses Microglia Inflammation by Targeting TGM2/NFκB Signaling. *Journal of Immunology Research* **2021**, 4754454

82. Liu, C., Gao, X., Shi, R.-X., Wang, Y.-Y., He, X.-C., et al. (2023) Microglial transglutaminase 2 deficiency causes impaired synaptic remodelling and cognitive deficits in mice. *Cell Proliferation* **n/a**, e13439
83. Park, K. C., Chung, K. C., Kim, Y.-S., Lee, J., Joh, T. H., et al. (2004) Transglutaminase 2 induces nitric oxide synthesis in BV-2 microglia. *Biochemical and Biophysical Research Communications* **323**, 1055-1062
84. Jacobson, A., Brinck, J., Briskin, M. J., Spicer, A. P., and Heldin, P. (2000) Expression of human hyaluronan synthases in response to external stimuli. *Biochemical Journal* **348 Pt 1**, 29-35
85. Reed, M. J., Vernon, R. B., Damodarasamy, M., Chan, C. K., Wight, T. N., et al. (2017) Microvasculature of the Mouse Cerebral Cortex Exhibits Increased Accumulation and Synthesis of Hyaluronan With Aging. *Journals of Gerontology: Biological Sciences* **72**, 740-746
86. Woodbury, M. E., and Ikezu, T. (2014) Fibroblast growth factor-2 signaling in neurogenesis and neurodegeneration. *Journal of Neuroimmune Pharmacology* **9**, 92-101
87. Klimaschewski, L., and Claus, P. (2021) Fibroblast Growth Factor Signalling in the Diseased Nervous System. *Molecular Neurobiology* **58**, 3884-3902
88. Astudillo, D., Karmelic, D., Casas, B. S., Otmakhov, N., Palma, V., et al. (2020) CaMKII inhibitor 1 (CaMK2N1) mRNA is upregulated following LTP induction in hippocampal slices. *Synapse* **74**, e22158
89. Ling, K. H., Hewitt, C. A., Beissbarth, T., Hyde, L., Cheah, P. S., et al. (2011) Spatiotemporal regulation of multiple overlapping sense and novel natural antisense transcripts at the *Nrgn* and *Camk2n1* gene loci during mouse cerebral corticogenesis. *Cerebral Cortex* **21**, 683-697
90. Palmieri, E. M., Menga, A., Lebrun, A., Hooper, D. C., Butterfield, D. A., et al. (2017) Blockade of Glutamine Synthetase Enhances Inflammatory Response in Microglial Cells. *Antioxidants & Redox Signaling* **26**, 351-363
91. Gheibihayat, S. M., Cabezas, R., Nikiforov, N. G., Jamialahmadi, T., Johnston, T. P., et al. (2021) CD47 in the Brain and Neurodegeneration: An Update on the Role in Neuroinflammatory Pathways. *Molecules* **26**
92. Zhang, H., Li, F., Yang, Y., Chen, J., and Hu, X. (2015) SIRP/CD47 signaling in neurological disorders. *Brain Research* **1623**, 74-80
93. Mohan, H. M., Trzeciakiewicz, H., Pithadia, A., Crowley, E. V., Pacitto, R., et al. (2022) RTL8 promotes nuclear localization of UBQLN2 to subnuclear compartments associated with protein quality control. *Cellular and Molecular Life Sciences* **79**, 176
94. Voytyuk, I., Mueller, S. A., Herber, J., Snellinx, A., Moechars, D., et al. (2018) BACE2 distribution in major brain cell types and identification of novel substrates. *Life Science Alliance* **1**, e201800026
95. Abdul-Hay, S. O., Sahara, T., McBride, M., Kang, D., and Leissring, M. A. (2012) Identification of BACE2 as an avid β -amyloid-degrading protease. *Molecular Neurodegeneration* **7**
96. Sun, X., Wang, Y., Qing, H., Christensen, M. A., Liu, Y., et al. (2005) Distinct transcriptional regulation and function of the human BACE2 and BACE1 genes. *FASEB Journal* **19**, 739-749
97. Iwama, E., Tsuchimoto, D., Iyama, T., Sakumi, K., Nakagawara, A., et al. (2011) Cancer-related PRUNE2 protein is associated with nucleotides and is highly expressed in mature nerve tissues. *Journal of Molecular Neuroscience* **44**, 103-114
98. Chauvin, S., and Sobel, A. (2015) Neuronal stathmins: A family of phosphoproteins cooperating for neuronal development, plasticity and regeneration. *Progress in Neurobiology* **126**, 1-18

99. Scott-Hewitt, N. J., Folts, C. J., and Noble, M. D. (2018) Heterozygous carriers of galactocerebrosidase mutations that cause Krabbe disease have impaired microglial function and defective repair of myelin damage. *Neural Regeneration Research* **13**, 393-401
100. Scott-Hewitt, N. J., Folts, C. J., Hogestyn, J. M., Piester, G., Mayer-Pröschel, M., et al. (2017) Heterozygote galactocerebrosidase (GALC) mutants have reduced remyelination and impaired myelin debris clearance following demyelinating injury. *Human Molecular Genetics* **26**, 2825-2837
101. Weinstock, N. I., Kreher, C., Favret, J., Nguyen, D., Bongarzone, E. R., et al. (2020) Brainstem development requires galactosylceramidase and is critical for pathogenesis in a model of Krabbe disease. *Nature Communications* **11**, 5356
102. Booms, A., and Coetzee, G. A. (2021) Functions of Intracellular Alpha-Synuclein in Microglia: Implications for Parkinson's Disease Risk. *Frontiers in Cellular Neuroscience* **15**
103. Fortenberry, Y., Hwang, J.-R., Apletalina, E. V., and Lindberg, I. (2002) Functional Characterization of ProSAAS: Similarities and differences with 7B2 *The Journal of Biological Chemistry* **277**, 5175-5186
104. Jarvela, T. S., Lam, H. A., Helwig, M., Lorenzen, N., Otzen, D. E., et al. (2016) The neural chaperone proSAAS blocks α -synuclein fibrillation and neurotoxicity. *Proceedings of the National Academy of Sciences of the United States of America* **113**, E4708-4715
105. Hoshino, A., Helwig, M., Rezaei, S., Berridge, C., Eriksen, J. L., et al. (2014) A novel function for proSAAS as an amyloid anti-aggregant in Alzheimer's disease. *Journal of Neurochemistry* **128**, 419-430
106. Charli, J. L., Rodríguez-Rodríguez, A., Hernández-Ortega, K., Cote-Vélez, A., Uribe, R. M., et al. (2020) The Thyrotropin-Releasing Hormone-Degrading Ectoenzyme, a Therapeutic Target? *Frontiers in Pharmacology* **11**, 640
107. Choi, S., Han, K. M., Kang, J., Won, E., Chang, H. S., et al. (2016) Effects of a Polymorphism of the Neuronal Amino Acid Transporter SLC6A15 Gene on Structural Integrity of White Matter Tracts in Major Depressive Disorder. *PLoS One* **11**, e0164301
108. Schuhmacher, A., Lennertz, L., Wagner, M., Höfels, S., Pfeiffer, U., et al. (2013) A variant of the neuronal amino acid transporter SLC6A15 is associated with ACTH and cortisol responses and cognitive performance in unipolar depression. *International Journal of Neuropsychopharmacology* **16**, 83-90
109. Snijders Blok, L., Kleefstra, T., Venselaar, H., Maas, S., Kroes, H. Y., et al. (2019) De Novo Variants Disturbing the Transactivation Capacity of POU3F3 Cause a Characteristic Neurodevelopmental Disorder. *American Journal of Human Genetics* **105**, 403-412
110. McEvelly, R. J., de Diaz, M. O., Schonemann, M. D., Hooshmand, F., and Rosenfeld, M. G. (2002) Transcriptional regulation of cortical neuron migration by POU domain factors. *Science* **295**, 1528-1532
111. Dominguez, M. H., Ayoub, A. E., and Rakic, P. (2013) POU-III transcription factors (Brn1, Brn2, and Oct6) influence neurogenesis, molecular identity, and migratory destination of upper-layer cells of the cerebral cortex. *Cerebral Cortex* **23**, 2632-2643
112. Andoh, M., and Koyama, R. (2023) Microglia and GABA: Diverse functions of microglia beyond GABA-receiving cells. *Neuroscience Research* **187**, 52-57
113. Parajuli, B., Horiuchi, H., Mizuno, T., Takeuchi, H., and Suzumura, A. (2015) CCL11 enhances excitotoxic neuronal death by producing reactive oxygen species in microglia. *Glia* **63**, 2274-2284
114. Wang, F., Baba, N., Shen, Y., Yamashita, T., Tsuru, E., et al. (2017) CCL11 promotes migration and proliferation of mouse neural progenitor cells. *Stem Cell Research & Therapy* **8**, 26

115. Ali, R. G., Bellchambers, H. M., and Arkell, R. M. (2012) Zinc fingers of the cerebellum (Zic): transcription factors and co-factors. *The International Journal of Biochemistry & Cell Biology* **44**, 2065-2068
116. Pourebrahim, R., Houtmeyers, R., Ghogomu, S., Janssens, S., Thelie, A., et al. (2011) Transcription factor Zic2 inhibits Wnt/ β -catenin protein signaling. *The Journal of Biological Chemistry* **286**, 37732-37740
117. Potolicchio, I., Carven, G. J., Xu, X., Stipp, C., Riese, R. J., et al. (2005) Proteomic analysis of microglia-derived exosomes: metabolic role of the aminopeptidase CD13 in neuropeptide catabolism. *The Journal of Immunology* **175**, 2237-2243
118. Friedman, B. A., Srinivasan, K., Ayalon, G., Meilandt, W. J., Lin, H., et al. (2018) Diverse Brain Myeloid Expression Profiles Reveal Distinct Microglial Activation States and Aspects of Alzheimer's Disease Not Evident in Mouse Models. *Cell Reports* **22**, 832-847
119. Miller, J. A., Oldham, M. C., and Geschwind, D. H. (2008) A systems level analysis of transcriptional changes in Alzheimer's disease and normal aging. *The Journal of Neuroscience* **28**, 1410-1420
120. Pembroke, W. G., Hartl, C. L., and Geschwind, D. H. (2021) Evolutionary conservation and divergence of the human brain transcriptome. *Genome Biology* **22**, 52
121. Jayadev, S., Case, A., Alajajian, B., Eastman, A. J., Möller, T., et al. (2013) Presenilin 2 influences miR146 level and activity in microglia. *Journal of Neurochemistry* **127**, 592-599
122. Streit, W. J., Braak, H., Del Tredici, K., Leyh, J., Lier, J., et al. (2018) Microglial activation occurs late during preclinical Alzheimer's disease. *Glia* **66**, 2550-2562
123. Streit, W. J., Sammons, N. W., Kuhns, A. J., and Sparks, D. L. (2004) Dystrophic microglia in the aging human brain. *Glia* **45**, 208-212
124. Streit, W. J., Xue, Q. S., Tischer, J., and Bechmann, I. (2014) Microglial pathology. *Acta Neuropathologica Communications* **2**, 142
125. Stence, N., Waite, M., and Dailey, M. E. (2001) Dynamics of microglial activation: A confocal time-lapse analysis in hippocampal slices. *Glia* **33**, 256-266
126. Xin, C., Quan, H., Kim, J.-M., Hur, Y.-H., Shin, J.-Y., et al. (2019) Ginsenoside Rb1 increases macrophage phagocytosis through p38 mitogen-activated protein kinase/Akt pathway. *Journal of Ginseng Research* **43**, 394-401
127. Blander, J. M., and Medzhitov, R. (2004) Regulation of Phagosome Maturation by Signals from Toll-like Receptors. *Science* **304**, 1014-1018
128. Kawai, T., Adachi, O., Ogawa, T., Takeda, K., and Akira, S. (1999) Unresponsiveness of MyD88-Deficient Mice to Endotoxin. *Immunity* **11**, 115-122
129. Marr, K. A., Balajee, S. A., Hawn, T. R., Ozinsky, A., Pham, U., et al. (2003) Differential role of MyD88 in macrophage-mediated responses to opportunistic fungal pathogens. *Infection and Immunity* **71**, 5280-5286
130. Laroux, F. S., Romero, X., Wetzler, L., Engel, P., and Terhorst, C. (2005) Cutting Edge: MyD88 Controls Phagocyte NADPH Oxidase Function and Killing of Gram-Negative Bacteria. *The Journal of Immunology* **175**, 5596-5600
131. Siddiqui, I. J., Pervaiz, N., and Abbasi, A. A. (2016) The Parkinson Disease gene SNCA: Evolutionary and structural insights with pathological implication. *Scientific Reports* **6**, 24475
132. Kaneko, H., Kakita, A., Kasuga, K., Nozaki, H., Ishikawa, A., et al. (2007) Enhanced accumulation of phosphorylated alpha-synuclein and elevated beta-amyloid 42/40 ratio caused by expression of the presenilin-1 deltaT440 mutant associated with familial Lewy body disease and variant Alzheimer's disease. *The Journal of Neuroscience* **27**, 13092-13097
133. Winslow, A. R., Moussaud, S., Zhu, L., Post, K. L., Dickson, D. W., et al. (2014) Convergence of pathology in dementia with Lewy bodies and Alzheimer's disease: a role for the novel interaction of alpha-synuclein and presenilin 1 in disease. *Brain* **137**, 1958-1970

134. Lippa, C. F., Fujiwara, H., Mann, D. M. A., Giasson, B., Baba, M., et al. (1998) Lewy Bodies Contain Altered α -Synuclein in Brains of Many Familial Alzheimer's Disease Patients with Mutations in Presenilin and Amyloid Precursor Protein Genes. *The American Journal of Pathology* **153**, 1365-1370
135. Haenseler, W., Zambon, F., Lee, H., Vowles, J., Rinaldi, F., et al. (2017) Excess α -synuclein compromises phagocytosis in iPSC-derived macrophages. *Scientific Reports* **7**, 9003
136. Bido, S., Muggeo, S., Massimino, L., Marzi, M. J., Giannelli, S. G., et al. (2021) Microglia-specific overexpression of α -synuclein leads to severe dopaminergic neurodegeneration by phagocytic exhaustion and oxidative toxicity. *Nature Communications* **12**, 6237
137. Andrejeva, G., Capoccia, B. J., Hiebsch, R. R., Donio, M. J., Darwech, I. M., et al. (2021) Novel SIRP α Antibodies That Induce Single-Agent Phagocytosis of Tumor Cells while Preserving T Cells. *The Journal of Immunology* **206**, 712-721
138. Métayer, L. E., Vilalta, A., Burke, G. A. A., and Brown, G. C. (2017) Anti-CD47 antibodies induce phagocytosis of live, malignant B cells by macrophages via the Fc domain, resulting in cell death by phagoptosis. *Oncotarget* **8**, 60892-60903
139. Bachmair, A., Finley, D., and Varshavsky, A. (1986) In Vivo Half-Life of a Protein is a Function of its Amino-Terminal Residue. *Science* **234**, 179-186
140. Gonda, D. K., Bachmair, A., Wüning, I., Tobias, J. W., Lane, W. S., et al. (1989) Universality and structure of the N-end rule. *The Journal of Biological Chemistry* **264**, 16700-16712
141. Dumanis, S. B., Chamberlain, K. A., Jin Sohn, Y., Jin Lee, Y., Guénette, S. Y., et al. (2012) FE65 as a link between VLDLR and APP to regulate their trafficking and processing. *Molecular Neurodegeneration* **7**, 9
142. Pocivavsek, A., Burns, M. P., and Rebeck, G. W. (2009) Low-density lipoprotein receptors regulate microglial inflammation through c-Jun N-terminal kinase. *Glia* **57**, 444-453
143. Garai, K., Verghese, P. B., Baban, B., Holtzman, D. M., and Frieden, C. (2014) The Binding of Apolipoprotein E to Oligomers and Fibrils of Amyloid- β Alters the Kinetics of Amyloid Aggregation. *Biochemistry* **53**, 6323-6331
144. Ghosh, S., Sil, T. B., Dolai, S., and Garai, K. (2019) High-affinity multivalent interactions between apolipoprotein E and the oligomers of amyloid- β . *FEBS Journal* **286**, 4737-4753
145. Yeh, F. L., Wang, Y., Tom, I., Gonzalez, L. C., and Sheng, M. (2016) TREM2 Binds to Apolipoproteins, Including APOE and CLU/APOJ, and Thereby Facilitates Uptake of Amyloid-Beta by Microglia. *Neuron* **91**, 328-340
146. Zannis, V. I., Kan, H. Y., Kritis, A., Zanni, E., and Kardassis, D. (2001) Transcriptional regulation of the human apolipoprotein genes. *Frontiers in Bioscience* **6**, D456-504
147. Shirovani, K., Hatta, D., Wakita, N., Watanabe, K., and Iwata, N. (2022) The role of TREM2 N-glycans in trafficking to the cell surface and signal transduction of TREM2. *Journal of Biochemistry* **172**, 347-353
148. Park, J.-S., Ji, I. J., An, H. J., Kang, M.-J., Kang, S.-W., et al. (2015) Disease-Associated Mutations of TREM2 Alter the Processing of N-Linked Oligosaccharides in the Golgi Apparatus. *Traffic* **16**, 510-518
149. Zhao, Y., Li, X., Huang, T., Jiang, L.-l., Tan, Z., et al. (2017) Intracellular trafficking of TREM2 is regulated by presenilin 1. *Experimental & Molecular Medicine* **49**, e405
150. Glebov, K., Wunderlich, P., Karaca, I., and Walter, J. (2016) Functional involvement of γ -secretase in signaling of the triggering receptor expressed on myeloid cells-2 (TREM2). *Journal of Neuroinflammation* **13**, 17-17
151. Schoch, K. M., Ezerskiy, L. A., Morhaus, M. M., Bannon, R. N., Sauerbeck, A. D., et al. (2021) Acute Trem2 reduction triggers increased microglial phagocytosis, slowing amyloid

deposition in mice. *Proceedings of the National Academy of Sciences of the United States of America* **118**

152. Lauer, A. A., Mett, J., Janitschke, D., Thiel, A., Stahlmann, C. P., et al. (2020) Regulatory feedback cycle of the insulin-degrading enzyme and the amyloid precursor protein intracellular domain: Implications for Alzheimer's disease. *Aging Cell* **19**, e13264

153. Chen, A. C., and Selkoe, D. J. (2007) Response to: Pardossi-Piquard et al., "Presenilin-Dependent Transcriptional Control of the Abeta-Degrading Enzyme Neprilysin by Intracellular Domains of betaAPP and APLP." *Neuron* **46**, 541-554. *Neuron* **53**, 479-483

154. Pardossi-Piquard, R., Dunys, J., Kawarai, T., Sunyach, C., Alves da Costa, C., et al. (2007) Response to Correspondence: Pardossi-Piquard et al., "Presenilin-Dependent Transcriptional Control of the A β -Degrading Enzyme Neprilysin by Intracellular Domains of β APP and APLP." *Neuron* **46**, 541-554. *Neuron* **53**, 483-486

155. Hébert, S. S., Serneels, L., Tolia, A., Craessaerts, K., Derks, C., et al. (2006) Regulated intramembrane proteolysis of amyloid precursor protein and regulation of expression of putative target genes. *EMBO reports* **7**, 739-745

156. Rocher-Ros, V., Marco, S., Mao, J. H., Gines, S., Metzger, D., et al. (2010) Presenilin modulates EGFR signaling and cell transformation by regulating the ubiquitin ligase Fbw7. *Oncogene* **29**, 2950-2961

157. Watanabe, H., Imaizumi, K., Cai, T., Zhou, Z., Tomita, T., et al. (2021) Flexible and accurate substrate processing with distinct presenilin/ γ -secretases in human cortical neurons. *eNeuro* **8**, ENEURO.0500-0520.2021

158. Eccles, M. K., Main, N., Sabale, M., Roberts-Mok, B., Agostino, M., et al. (2023) Quantitative Comparison of Presenilin Protein Expression Reveals Greater Activity of PS2- γ -Secretase. *bioRxiv*, 2023.2005.2009.540102

159. Yonemura, Y., Futai, E., Yagishita, S., Suo, S., Tomita, T., et al. (2011) Comparison of presenilin 1 and presenilin 2 γ -secretase activities using a yeast reconstitution system. *The Journal of Biological Chemistry* **286**, 44569-44575

160. Yesbolatova, A., Saito, Y., Kitamoto, N., Makino-Itou, H., Ajima, R., et al. (2020) The auxin-inducible degron 2 technology provides sharp degradation control in yeast, mammalian cells, and mice. *Nature Communications* **11**, 5701

161. Spandidos, A., Wang, X., Wang, H., Dragnev, S., Thurber, T., et al. (2008) A comprehensive collection of experimentally validated primers for Polymerase Chain Reaction quantitation of murine transcript abundance. *BMC Genomics* **9**, 633

162. Spandidos, A., Wang, X., Wang, H., and Seed, B. (2010) PrimerBank: a resource of human and mouse PCR primer pairs for gene expression detection and quantification. *Nucleic Acids Research* **38**, D792-D799

163. Wang, X., and Seed, B. (2003) A PCR primer bank for quantitative gene expression analysis. *Nucleic Acids Research* **31**, e154

164. Bennett, M. L., Bennett, F. C., Liddelow, S. A., Ajami, B., Zamanian, J. L., et al. (2016) New tools for studying microglia in the mouse and human CNS. *Proceedings of the National Academy of Sciences of the United States of America* **113**, E1738-E1746

165. Witek, E., Hickman, D., Lahiri, D. K., and Srinivasan, M. (2019) Glucocorticoid Induced Leucine Zipper in Lipopolysaccharide Induced Neuroinflammation. *Frontiers in Aging Neuroscience* **10**

5.6 SUPPLEMENTARY TABLES

SI Table 5-1 qPCR primer sequences

Gene Target	Forward Primer	Reverse Primer	RNA (ng/ul)
Gapdh	5'CTCAGGAGAGTGTTTCCTCGTC ^{3'}	5'TTGAGGTCAATGAAGGGGTCG ^{3'}	0.625
Sdha	5'AACTACAAGGGACAGGTGCTG ^{3'}	5'AGAATTTGCTCCAAGCCGGT ^{3'}	0.625
Tmem119	5'CACCCAGAGCTGGTTCATA ^{3'}	5'GAGTGACACAGAGTAGGCCA ^{3'}	1.875
P2ry12	5'TACCTGCTTGGCAACTCACC ^{3'}	5'AGGCAGCCTTGAGTGTTTCTG ^{3'}	1.875
Tnf	5'TTCTCATTCTGCTTGTGGCA ^{3'}	5'CTTCTCATCCCTTTGGGGACC ^{3'}	0.625
Il1b [†]	GCAACTGTTCTGAAGTCAACT ^{3'}	5'ATCTTTTGGGGTCCGTCAACT ^{3'}	0.625
HRPT1	5'CCTGGCGTCGTGATTAGTGAT ^{3'}	5'TCGAGCAAGACGTTTCAGTCC ^{3'}	1.875
RPLP0 [¶]	5'GAAACTCTGCATTCTCGCTTCC ^{3'}	5'GATGCAACAGTTGGGTAGCCA ^{3'}	1.875
TMEM119 [¶]	5'CTTCTGGATGGGATAGTGGAC ^{3'}	5'GCACAGACGATGAACATCAGC ^{3'}	3.750
P2RY12	5'CCACTCTGCAGGTTGCAATAAC ^{3'}	5'TTGCATTTCTTGTTGGTTACCTGA ^{3'}	1.875
TNF	5'GCCCATGTTGTAGCAAACCC ^{3'}	5'TATCTCTCAGCTCCACGCCA ^{3'}	1.875
IL1B [§]	5'AGCTGATGGCCCTAAACAGA	5'GGTCGGAGATTTCGTAGCTGG ^{3'}	3.750
MME	5'TGGTCAAGCATAACAGAGCCT ^{3'}	5'TAGGTTCCACACCACACCTG ^{3'}	3.750
ECE-1	5'TCAAGCACCTCCTCGAAAATC ^{3'}	5'ATTAGAGGTTTGGCCCTGAGC ^{3'}	1.875
IDE	5'ACCCTGCTCTTATTAAGGATACAGC ^{3'}	5'TTACAGTGCAAGGGGTCCAC ^{3'}	3.750
BACE1	5'TCATTGGAGGTATCGACCACT ^{3'}	5'TCTTGTCATAGTTGTACTCCTTGC ^{3'}	1.875
MMP9	5'CGCAGTGACGGAAAGATGTG ^{3'}	5'AACAGGCTGTACCCTTGGTC ^{3'}	3.750
MMP9	5'GGCCACTACTGTGCCTTTGA ^{3'}	5'AATCGCCAGTACTTCCCATCC ^{3'}	3.750
TREM2	5'CCTCTCCGGCTGCTCATCTT ^{3'}	5'CCTGGAACACTGTGGTGTGTG ^{3'}	3.750
APP695	5'TGACCACTCGACCAGGTTC ^{3'}	5'TGTCGGAATTCTGCATCCATC ^{3'}	1.875

[†]Il1b primer retrieved from PrimerBank (ID: 6680415a1).¹⁶¹⁻¹⁶³

[¶]RPLP0 and TMEM119 primers are from Bennett et al. (2016).¹⁶⁴

[§]IL1B Witek et al. (2019)¹⁶⁵

SI Table 5-2 Antibody and sample treatment details for immunoblotting

Protein Target	Reducing Agent	Treatment Temperature	Antibody	Blocking/ Antibody	Antibody Dilution	ECL
APP-FL APP-CTF	DTT	75°C	APP C1/6.1 - 802801 - Biologend	5%NFDM/ 0.5%NFDM	1/2000	Clarity
Neprilysin	DTT	55°C	CD10/MME - A5664 - Abclonal	5%NFDM/ 0.5%NFDM	1/1000	Clarity
BACE1	DTT	55°C	BACE1 - A5266 - Abclonal	5%NFDM/ 0.5%NFDM	1/1000	Clarity
VLDLR	DTT	55°C	VLDLR - A7345 - Abclonal	5%NFDM/ 0.5%NFDM	1/1000	Prime
CD44	DTT	55°C	CD44 - A12410 - Abclonal	5%NFDM/ 0.5%NFDM	1/2000	Clarity
TREM2	DTT	55°C	TREM2 - A10482 - Abclonal	5%NFDM/ 0.5%NFDM	1/1000	Clarity
GAPDH	As per initial sample, as blots stripped and reprobed		GAPDH - A19056 - Abclonal	5%NFDM/ 0.5%NFDM	1/10000	Clarity

Note: DTT = Dithiothreitol [50 mM], NFDM = non-fat dried milk powder.

SI Table 5-3 Top 10 most significant genes for PS2+ vs PS1+PS2+ and PS1+ vs PS1+PS2+ differential gene comparison

PS2+ vs PS1+PS2+				
Gene	Log2[FC] [¶]	q-value	NCBI ID	Protein
CAMK2N1	-6.59	3.09 ⁻³⁰¹	55450	Calcium/calmodulin-dependent protein kinase II inhibitor 1
HAS2	3.65	3.36 ⁻²⁴⁹	3037	Hyaluronan synthase 2
MGST1	4.12	1.51 ⁻²¹³	4257	Microsomal glutathione S-transferase 1
GBP1	4.82	3.28 ⁻¹⁷⁰	2633	Guanylate-binding protein 1
MDK	2.01	3.76 ⁻¹⁵⁷	4192	Midkine (Neurite outgrowth-promoting factor 2)
ABI3BP	3.59	1.46 ⁻¹⁵⁴	25890	Target of Nesh-SH3
SOX3	-4.24	2.70 ⁻¹⁵⁴	6658	Transcription factor SOX-3
ABCA5	-2.12	1.75 ⁻¹⁵¹	23461	Cholesterol transporter ABCA5
COL1A2	5.59	6.13 ⁻¹⁴⁷	1278	Collagen alpha-2(I) chain
UCHL1	1.40	2.40 ⁻¹⁴⁶	7345	Ubiquitin carboxyl-terminal hydrolase isozyme L1
PS1+ vs PS1+PS2+				
Gene	Log2[FC] [¶]	q-value	NCBI ID	Protein
MGST1	4.40	1.42 ⁻²⁴⁴	4257	Microsomal glutathione S-transferase 1
SIRPA	-1.83	6.32 ⁻²⁰⁷	140885	Tyrosine-protein phosphatase non-receptor type substrate 1
COPS3	1.48	7.18 ⁻¹⁸⁴	8533	COP9 signalosome complex subunit 3
CADM1	-3.00	8.74 ⁻¹⁶⁹	23705	Cell adhesion molecule 1
MDK	2.05	1.17 ⁻¹⁶³	4192	Midkine (Neurite outgrowth-promoting factor 2)
B3GALNT1	4.53	1.59 ⁻¹⁶⁰	8706	UDP-GalNAc:beta-1,3-N-acetylgalactosaminyltransferase 1
FOXC1	-2.63	5.93 ⁻¹⁵⁸	2296	Forkhead box protein C1
UCHL1	1.45	8.96 ⁻¹⁵⁸	7345	Ubiquitin carboxyl-terminal hydrolase isozyme L1
IRX2	-2.32	7.48 ⁻¹⁵⁶	153572	Iroquois-class homeodomain protein IRX-2
ALKBH5	1.10	6.80 ⁻¹⁵⁴	54890	RNA demethylase ALKBH5

¶ Where Log2[FC] result is +ve then PS2+ or PS1+ > PS1+PS2+, where result is -ve then PS2+ or PS1+ < PS1+PS2+

SI Table 5-4 Top 5 up and down regulated genes for for PS2+ vs PS1+PS2+ and PS1+ vs PS1+PS2+ differential gene comparison

PS2+ vs PS1+PS2+				
Gene	Log2[FC] [¶]	q-value	NCBI ID	Protein
YIPF7	7.04	2.91 ⁻¹²	285525	Protein YIPF7
729252	6.87	3.62 ⁻¹²	729252	keratin 16 pseudogene 1
RGS4	6.86	1.28 ⁻¹²⁵	5999	Regulator of G-protein signaling 4
ITGA4	6.63	8.79 ⁻¹⁴	3676	Integrin alpha-4
G0S2	6.56	2.33 ⁻³⁶	50486	G0/G1 switch protein 2
SST	-9.21	8.69 ⁻²²	6750	Somatostatin
PREX2	-8.75	4.41 ⁻¹⁹	80243	Phosphatidylinositol 3,4,5-trisphosphate-dependent Rac exchanger 2 protein
GPC4	-8.46	1.38 ⁻⁵⁰	2239	Glypican-4
TRHDE	-8.05	1.19 ⁻¹⁹	29953	Thyrotropin-releasing hormone-degrading ectoenzyme
TAC1	-8.02	5.97 ⁻¹⁶	6863	Protachykinin-1
PS1+ vs PS1+PS2+				
Gene	Log2[FC] [¶]	q-value	NCBI ID	Protein
ACSS3	8.53	1.55 ⁻¹⁸	79611	Acyl-CoA synthetase short-chain family member 3
SLC6A15	8.41	1.43 ⁻¹⁸	55117	Sodium-dependent neutral amino acid transporter B(0)AT2
G0S2	8.30	2.95 ⁻⁵⁸	50486	G0/G1 switch protein 2
ITGA4	7.58	5.41 ⁻¹⁸	3676	Integrin alpha-4
YIPF7	7.00	2.65 ⁻¹²	285525	Protein YIPF7
GPC4	-9.69	1.97 ⁻²⁹	2239	Glypican-4
ZNF492	-7.80	4.16 ⁻¹⁵	57615	Zinc finger protein 492
RIBC2	-7.78	1.71 ⁻¹⁵	26150	RIB43A-like with coiled-coils protein 2
TAC1	-7.45	4.32 ⁻¹⁴	6863	Protachykinin-1
ZNF43	-7.05	2.76 ⁻¹⁵	7594	Zinc finger protein 43

¶ Where Log2[FC] result is +ve then PS2+ or PS1+ > PS1+PS2+, where result is -ve then PS2+ or PS1+ < PS1+PS2+

SI Table 5-5 KEGG pathway genes specifically activated in PS2+ HMC3 cells

Other types O-glycan biosynthesis [hsa00514]		Axon Guidance con't [hsa04360]		MAPK Signalling con't [hsa04360]		MAPK Signalling con't [hsa04360]	
Gene	PS1+ vs PS2+	Gene	PS1+ vs PS2+	Gene	PS1+ vs PS2+	Gene	PS1+ vs PS2+
GXYLT1	0.65	ABL1	-0.47	EPHA2	0.28	MECOM	-0.49
POMT2	0.44	PIK3R2	-0.47	IL1RAP	0.27	KITLG	-0.49
LFNG	0.38	RHOA	-0.47	LAMTOR3	0.25	RPS6KA2	-0.52
GALNT2	-0.17	PLXNA3	-0.47	FGF5	0.25	CACNA2D1	-0.55
GALNT10	-0.23	ENAH	-0.48	NF1	0.24	PPP3CC	-0.55
GALNT11	-0.25	SMO	-0.49	DUSP3	0.24	CACNA1H	-0.56
POMT1	-0.26	MYL9	-0.50	ATF4	0.22	FLNB	-0.56
B4GALT1	-0.28	SSH3	-0.53	MAPK8	0.22	DUSP9	-0.57
B4GALT2	-0.29	PPP3CC	-0.55	MAPK7	0.22	PAK1	-0.59
GALNT14	-0.35	EFNB3	-0.59	MAX	0.22	TGFBR2	-0.59
COLGALT1	-0.45	PAK1	-0.59	IKBKG	0.21	DUSP4	-0.65
GALNT6	-0.49	GNAI2	-0.60	MAP3K7	0.20	TGFBR1	-0.71
PLOD3	-0.60	EFNB2	-0.61	PPP3CA	0.20	VEGFC	-0.72
EOGT	-0.89	EPHB4	-0.74	MAP2K4	0.19	GDNF	-0.79
COLGALT2	-0.95	DPYSL2	-0.74	NRAS	0.19	RELB	-0.86
GALNT12	-1.77	ROBO1	-0.78	RPS6KA1	0.16	NGF	-0.86
Axon Guidance [hsa04360]		SEMA3F	-0.80	STMN1	0.16	BDNF	-0.90
		PARD6A	-0.81	RAP1B	0.13	DUSP2	-0.92
Gene	PS1+ vs PS2+	CAMK2D	-0.85	ELK1	-0.13	FGFR1	-1.16
TRPC3	3.91	SLIT2	-1.01	IRAK1	-0.18	EFNA2	-1.32
SEMA6D	2.00	PLXNB1	-1.04	CASP3	-0.18	RASGRP3	-1.43
NTNG1	0.98	SEMA3D	-1.08	JUN	-0.19	RASGRP1	-1.49
LRRC4C	0.97	SLIT3	-1.08	MAPKAPK2	-0.19	NTF3	-1.74
PARD6B	0.73	SEMA5A	-1.12	MAPK12	-0.22	CACNG7	-1.78
RAC2	0.60	EPHA6	-1.20	MET	-0.22	IGF1R	-1.85
TRPC1	0.58	WNT5A	-1.23	RPS6KA4	-0.22	MYD88	-2.30
KRAS	0.48	EFNA2	-1.32	MAP3K3	-0.23	CACNA1A	-3.64
SEMA3B	0.38	LRRC4	-1.38	MAP3K11	-0.23		
PRKCZ	0.33	BOC	-1.95	JUND	-0.23		
NEO1	0.31	CXCL12	-2.03	RASA1	-0.23		
SSH1	0.28	TRPC4	-2.19	VEGFB	-0.24		
EPHA2	0.28	EPHA5	-2.34	ERBB2	-0.25		
PTPN11	0.27	MAPK Signalling [hsa04360]		MAPKAPK3	-0.26		
PIK3CB	0.25			AKT2	-0.26		
LIMK2	0.23	Gene	PS1+ vs PS2+	MYC	-0.26		
NCK2	0.22	MEF2C	2.99	MAP2K5	-0.27		
PIK3CD	0.21	TGFA	1.52	KIT	-0.27		
PPP3CA	0.20	PGF	1.21	RELA	-0.27		
NRAS	0.19	DUSP6	0.96	RASA2	-0.28		
CFL2	0.15	RASGRF1	0.77	RRAS2	-0.28		
GSK3B	0.15	RPS6KA5	0.76	SRF	-0.28		
MYL12B	-0.15	FAS	0.73	MAP2K7	-0.30		
RYK	-0.15	MAP3K9	0.65	MAP2K2	-0.30		
ITGB1	-0.20	NFATC1	0.65	BRAF	-0.30		
MET	-0.22	DDIT3	0.61	CACNB1	-0.30		
ARHGEF12	-0.23	RAC2	0.60	ECSIT	-0.33		
PTK2	-0.23	CD14	0.58	GADD45A	-0.34		
RASA1	-0.23	RPS6KA6	0.57	HSPB1	-0.34		
BMPR2	-0.27	ERBB3	0.57	PRKACA	-0.35		
SEMA4C	-0.28	DUSP16	0.56	GADD45B	-0.35		
PAK4	-0.30	MAPK8IP2	0.54	RRAS	-0.36		
CFL1	-0.33	KRAS	0.48	MAP2K1	-0.37		
RRAS	-0.36	HSPA1L	0.39	STK3	-0.37		
SEMA6B	-0.37	TNFRSF1A	0.35	MAP3K5	-0.37		
CDK5	-0.37	MAPKAPK5	0.34	RAC3	-0.41		
WNT5B	-0.38	PPM1A	0.34	DUSP1	-0.42		
PLCG2	-0.39	MAP3K4	0.33	FGF1	-0.43		
RAC3	-0.41	FLT4	0.33	RAF1	-0.43		
RGS3	-0.42	MAP3K21	0.32	DUSP7	-0.44		
RAF1	-0.43	VEGFA	0.32	IKKB	-0.46		
MYL12A	-0.44	AKT1	0.31	MAPK11	-0.47		
FES	-0.46	TRADD	0.29	MAPK8IP1	-0.47		

¶ Where (PS1+ - PS2+ Log2[FC]) result is +ve then PS1+ > PS2+, where result is -ve then PS2+ > PS1+

SI Table 5-6 KEGG pathway genes specifically activated/suppressed in PS1+ HMC3 cells

Endocytosis [hsa04144]		Endocytosis con't [hsa04144]		mTOR signalling [hsa04150]	
Gene	PS1+ vs PS2+	Gene	PS1+ vs PS2+	Gene	PS1+ vs PS2+
SH3GL2	4.59	RAB11B	-0.25	WNT10B	1.22
FOLR1	2.34	ARFGEF1	-0.25	DDIT4	0.80
IL2RB	1.31	PLD2	-0.25	ULK2	0.71
PARD6B	0.73	RUFY2	-0.25	PRKAA2	0.63
DNAJC6	0.65	ARPC2	-0.26	RPS6KA6	0.57
AGAP9	0.59	AGAP3	-0.26	NPRL3	0.57
WASHC3	0.56	ZFYVE9	-0.26	KRAS	0.48
GRK3	0.55	EHD1	-0.27	LRP6	0.48
ASAP3	0.51	ACTR3	-0.27	SLC7A5	0.46
HLA-B	0.49	VPS26B	-0.28	TBC1D7	0.40
MDM2	0.48	SNX1	-0.29	ULK1	0.39
VPS25	0.45	WASL	-0.30	PRR5	0.39
ARPC3	0.43	DNM1	-0.31	TNFRSF1A	0.35
HSPA1L	0.39	RBSN	-0.31	WNT3	0.35
RAB5B	0.39	RAB8A	-0.32	ATP6V1A	0.34
ARF6	0.38	ARPC5L	-0.33	LPIN2	0.33
LDLRAP1	0.36	AP2A1	-0.33	AKT1	0.31
CBLB	0.36	CBL	-0.34	WDR24	0.30
ARAP3	0.36	CAPZA2	-0.35	LPIN3	0.30
STAMBP	0.35	RAB5A	-0.35	EIF4B	0.29
GIT2	0.35	RAB11FIP5	-0.35	ATP6V1D	0.28
RAB11FIP2	0.33	VPS37C	-0.38	CLIP1	0.27
PRKCZ	0.33	WASHC5	-0.38	LAMTOR5	0.26
ARAP2	0.33	EPN1	-0.40	LAMTOR3	0.25
EEA1	0.32	DNM2	-0.41	PIK3CB	0.25
ARF3	0.31	USP8	-0.42	PIK3CD	0.21
EPN2	0.31	CHMP7	-0.43	FLCN	0.20
WASHC4	0.29	SMURF1	-0.44	NRAS	0.19
RNF41	0.27	EPS15L1	-0.44	ATP6V1E1	0.19
IGF2R	0.26	ASAP2	-0.44	RRAGA	0.18
PIP5K1A	0.25	MVB12B	-0.44	SEH1L	0.18
SMAP1	0.24	ASAP1	-0.44	RPS6KA1	0.16
WASHC2A	0.24	SH3GL1	-0.45	GSK3B	0.15
SPART	0.24	SPG21	-0.46	RPS6KB2	-0.18
BIN1	0.24	PML	-0.47	STK11	-0.19
SMAP2	0.23	NEDD4	-0.47	PRKAA1	-0.21
SMAD2	0.23	RHOA	-0.47	RICTOR	-0.23
VPS29	0.23	VPS37A	-0.50	ATP6V1G1	-0.23
RAB4A	0.23	DAB2	-0.51	STRADB	-0.24
TFRC	0.22	PIP5K1C	-0.51	AKT1S1	-0.25
VPS45	0.22	IQSEC1	-0.51	AKT2	-0.26
GBF1	0.21	VPS28	-0.53	MAP2K2	-0.30
SNX2	0.20	PDCD6IP	-0.54	BRAF	-0.30
WASHC2C	0.20	EHD2	-0.54	FZD6	-0.34
CHMP1B	0.19	EHD4	-0.55	TSC1	-0.36
RAB35	0.19	PSD3	-0.56	MAP2K1	-0.37
SNX6	0.14	ARPC1B	-0.58	ATP6V1B2	-0.37
RABEP1	0.12	TGFBR2	-0.59	NPRL2	-0.37
CLTC	0.10	RAB11A	-0.60	MAPKAP1	-0.38
VPS4A	-0.13	ARPC4	-0.64	WNT5B	-0.38
RAB10	-0.17	ARF4	-0.64	ATP6V1F	-0.39
GRK2	-0.17	SH3GLB2	-0.66	EIF4EBP1	-0.41
SNX12	-0.18	SMAD3	-0.69	SEC13	-0.42
ACAP2	-0.20	TGFBR1	-0.71	RAF1	-0.43
RAB11FIP3	-0.20	CAV2	-0.73	RHEB	-0.45
WWP1	-0.21	PARD6A	-0.81	IKKB	-0.46
ACTR2	-0.21	CAV1	-1.08	PIK3R2	-0.47
ARF5	-0.21	AMPH	-1.47	RHOA	-0.47
ARPC5	-0.21	IGF1R	-1.85	SGK1	-0.50
AP2S1	-0.23			RPS6KA2	-0.52
CYTH2	-0.24			GRB10	-0.55
ARPC1A	-0.25			FZD9	-0.57

SI Table 5-6 continued KEGG pathway genes specifically activated/suppressed in PS1+ HMC3 cells

mTOR signalling con't [hsa04150]		Cellular senescence con't [hsa04218]		Bacterial invasion of epithelial cells con't [hsa05100]	
Gene	PS1+ vs PS2+	Gene	PS1+ vs PS2+	Gene	PS1+ vs PS2+
LRP5	-0.68	CHEK1	-0.27	SEPTIN9	0.15
RNF152	-1.01	RELA	-0.27	CLTC	0.10
FZD7	-1.03	CAPN2	-0.28	SEPTIN2	-0.12
FZD4	-1.04	RRAS2	-0.28	ACTB	-0.14
WNT9A	-1.06	MAP2K2	-0.30	ITGB1	-0.20
WNT5A	-1.23	CDC25A	-0.33	ACTR2	-0.21
IGF1R	-1.85	LIN37	-0.33	ITGA5	-0.21
RRAGD	-2.12	GADD45A	-0.34	ARPC5	-0.21
Cellular senescence [hsa04218]		GADD45B	-0.35	MET	-0.22
		RRAS	-0.36	PTK2	-0.23
		Gene	PS1+ vs PS2+	Gene	PS1+ vs PS2+
NFATC1	0.65	CALM3	-0.36	ARHGAP10	-0.24
CDK2	0.53	TSC1	-0.36	ARPC1A	-0.25
LIN52	0.50	MAP2K1	-0.37	ARPC2	-0.26
HLA-B	0.49	ATM	-0.37	ACTR3	-0.27
KRAS	0.48	CDKN2A	-0.37	WASL	-0.30
MDM2	0.48	VDAC3	-0.38	SEPTIN6	-0.30
PPP1CC	0.39	EIF4EBP1	-0.41	DNM1	-0.31
CCND3	0.35	RAF1	-0.43	ACTG1	-0.31
CDK4	0.33	CCNB2	-0.44	VCL	-0.32
AKT1	0.31	RHEB	-0.45	ARPC5L	-0.33
BTRC	0.27	MAPK11	-0.47	CTNNB1	-0.33
PIK3CB	0.25	PIK3R2	-0.47	CBL	-0.34
CALM1	0.25	CCND1	-0.51	DNM2	-0.41
SMAD2	0.23	CAPN1	-0.51	PIK3R2	-0.47
PPID	0.23	SERPINE1	-0.52	RHOA	-0.47
VDAC2	0.22	FOXO1	-0.54	CTTN	-0.50
PIK3CD	0.21	PPP3CC	-0.55	ARPC1B	-0.58
PPP3CA	0.20	TGFBR2	-0.59	ARPC4	-0.64
NRAS	0.19	TRPM7	-0.63	CAV2	-0.73
RBBP4	0.19	CDKN2B	-0.67	FN1	-0.90
SLC25A5	0.15	ITPR2	-0.69	CAV1	-1.08
PPP1CB	0.14	SMAD3	-0.69	SEPTIN3	-1.98
E2F1	-0.14	TGFBR1	-0.71	Glycosphingolipid biosynthesis [hsa00601]	
PPP1CA	-0.14	CDK6	-0.74	Gene	PS1+ vs PS2+
RBL1	-0.18	ITPR1	-1.04	B3GNT3	2.94
MAPKAPK2	-0.19	IGFBP3	-1.55	GCNT2	1.92
CCNE2	-0.19	Bacterial invasion of epithelial cells [hsa05100]		A4GALT	1.37
RBL2	-0.20	Gene	PS1+ vs PS2+	FUT4	0.73
MAPK12	-0.22	ARHGFE26	0.51	B3GALNT1	0.26
LIN9	-0.22	PXN	0.49	B4GALT1	-0.28
ETS1	-0.23	ARPC3	0.43	B4GALT2	-0.29
NBN	-0.24	CD2AP	0.28	B3GNT2	-0.41
SLC25A4	-0.26	PIK3CB	0.25	FUT2	-1.35
AKT2	-0.26	CTNNA1	0.24		
MYC	-0.26	PIK3CD	0.21		

¶ Where (PS1+ - PS2+ Log2[FC]) result is +ve then PS1+ > PS2+, where result is -ve then PS2+ > PS1+

SI Table 5-7 RNASeq differential gene expression for A β degrading enzymes and A β removal related substrates investigated in Figure 5-5 and Figure 5-6

Gene	PS2+ - PS1+PS2+		PS1+ - PS1+PS2+		PS1+ - PS2+	
	Log2[FC] [¶]	q-value	Log2[FC] [¶]	q-value	Log2[FC] [¶]	q-value
MME	5.78	3.60E-56	6.97	2.64E-82	1.19	7.74
MMP2	2.56	1.65E-14	3.30	4.28E-24	0.74	6.79
MMP9	2.86	4.34E-08	3.54	2.25E-12	-	-
IDE	-	-	-	-	-	-
ECE1	-	-	-	-	-	-
BACE1	0.61	3.44E-06	0.61	3.47E-06	-	-
APP	0.76	2.58E-48	0.48	6.73E-20	-0.28	13.47
VLDLR	-1.45	8.90E-43	-2.00	8.60E-76	-0.55	7.93
CD44	0.56	4.78E-08	-	-	-0.53	13.84
TREM2	1.48	3.09E-02	1.33	4.81E-02	-	-

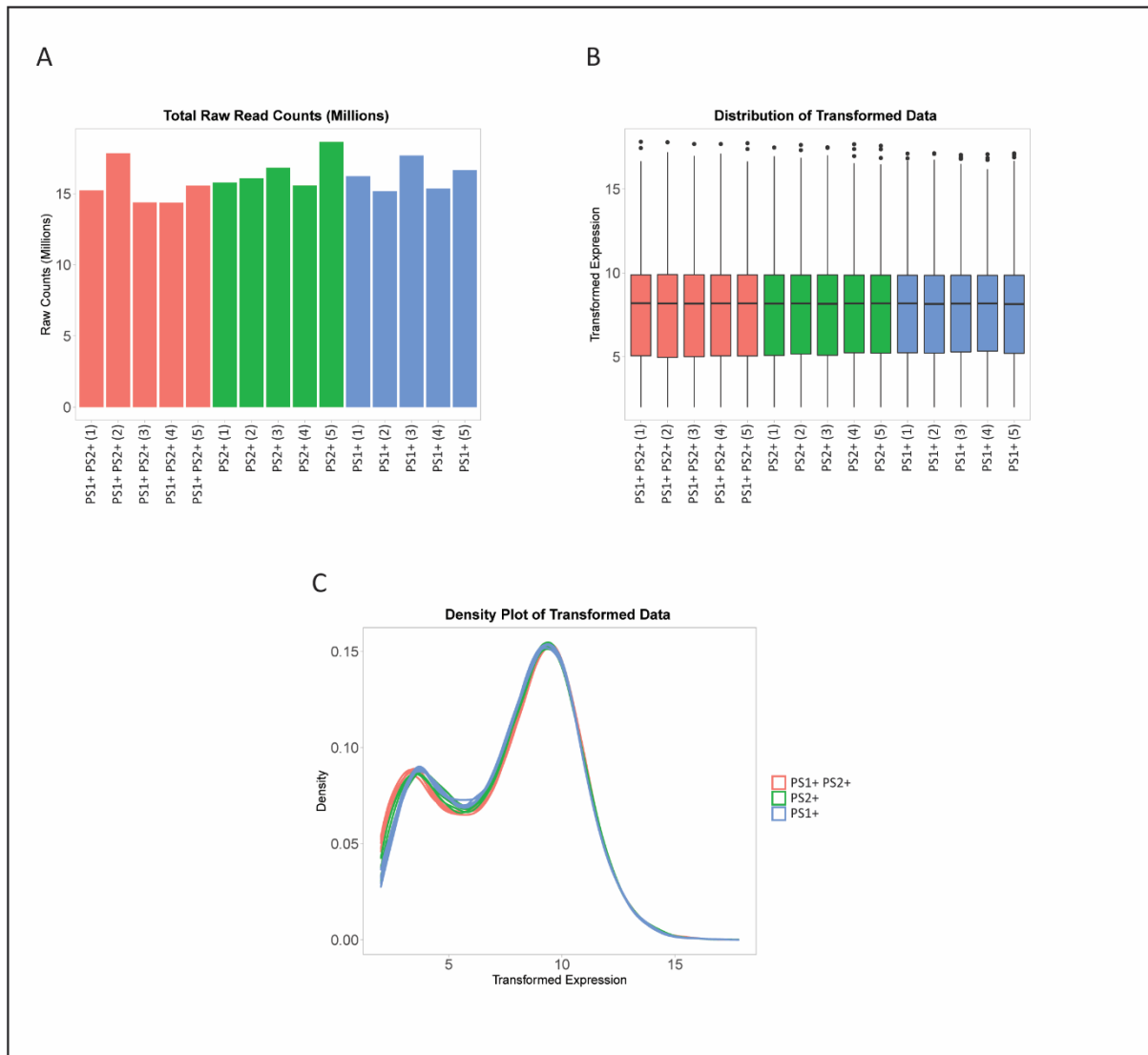
¶ Where Log2[FC] result is +ve then PS2+ > PS1+PS2+, PS1+ > PS1+PS2+, PS1+ > PS2+, where result is -ve then PS2+ < PS1+PS2+, PS1+ < PS1+PS2+, PS1+ < PS2+

SI Table 5-8 E3 ligase and E3 ligase adaptor proteins with $\pm 1.5 \text{ Log}_2[\text{FC}]$

E3 LIGASE			
GENE	Log ₂ [FC] [¶]		
	PS2+ - PS1+PS2+	PS1+ - PS1+PS2+	PS1+ - PS2+
TRIM55	2.55	3.35	0.79
LONRF2	3.12	3.21	-
HERC5	3.04	3.05	-
HERC6	3.63	2.90	-0.74
CHFR	1.55	2.66	1.11
RNF112	2.12	2.40	-
TRIML2	-	2.35	1.82
DTX3L	2.30	1.95	-0.35
TRIM6	1.07	1.91	0.85
PLAG1	0.95	1.68	0.73
RNF144A	1.59	1.58	-
TRIM38	0.92	1.57	0.64
NEURL1B	1.53	1.45	-
RFPL4A	3.08	1.27	-1.80
PLAGL1	0.43	1.18	0.75
BMI1	-	1.06	-
PDZRN3	2.13	1.04	-1.09
SIAH3	-5.22	-5.22	-
DCST1	-1.89	-1.90	-
E3 LIGASE ADAPTOR PROTEIN			
GENE	Log ₂ [FC]		
	PS2+ - PS1+PS2+	PS1+ - PS1+PS2+	PS1+ - PS2+
KCTD12	3.31	3.74	-
KLHL4	2.86	3.72	0.85
FBXL7	2.04	2.86	0.82
ASB9	1.79	2.54	0.75
KLHL13	-	2.37	2.13
KCTD4	1.90	2.33	-
BACH2	1.74	2.28	-
KCND1	1.55	2.15	0.60
BTBD11	-	1.75	-
FBXL16	-1.35	-3.73	-2.39
SPSB4	-4.39	-2.52	-
NACC2	-0.78	-1.56	-0.78
KLHL32	-1.98	-	-

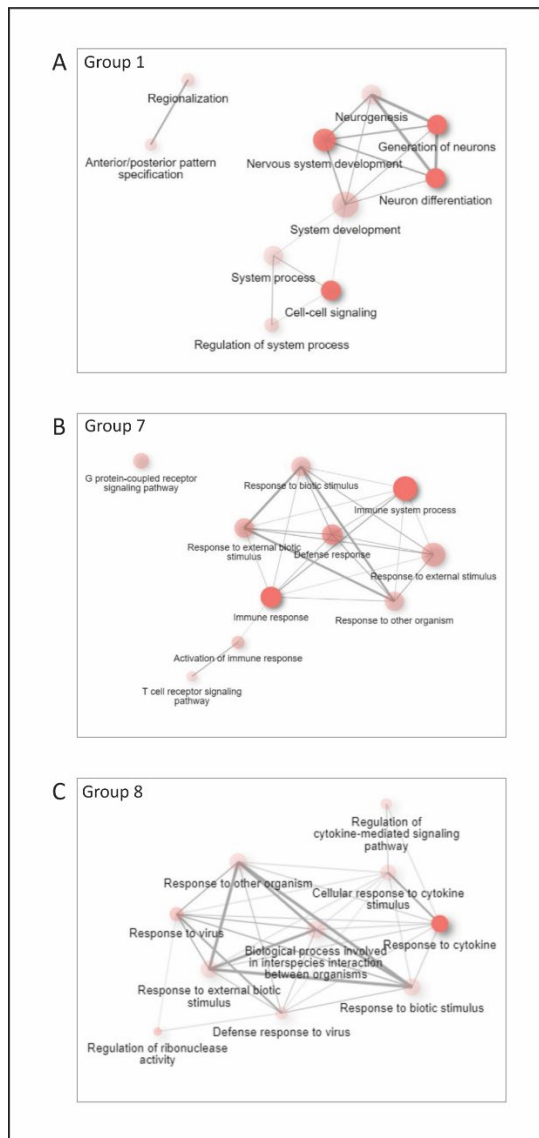
¶ Where Log₂[FC] result is +ve then PS2+ > PS1+PS2+, PS1+ > PS1+PS2+, PS1+ > PS2+, where result is -ve then PS2+ < PS1+PS2+, PS1+ < PS1+PS2+, PS1+ < PS2+

5.7 SUPPLEMENTARY FIGURES



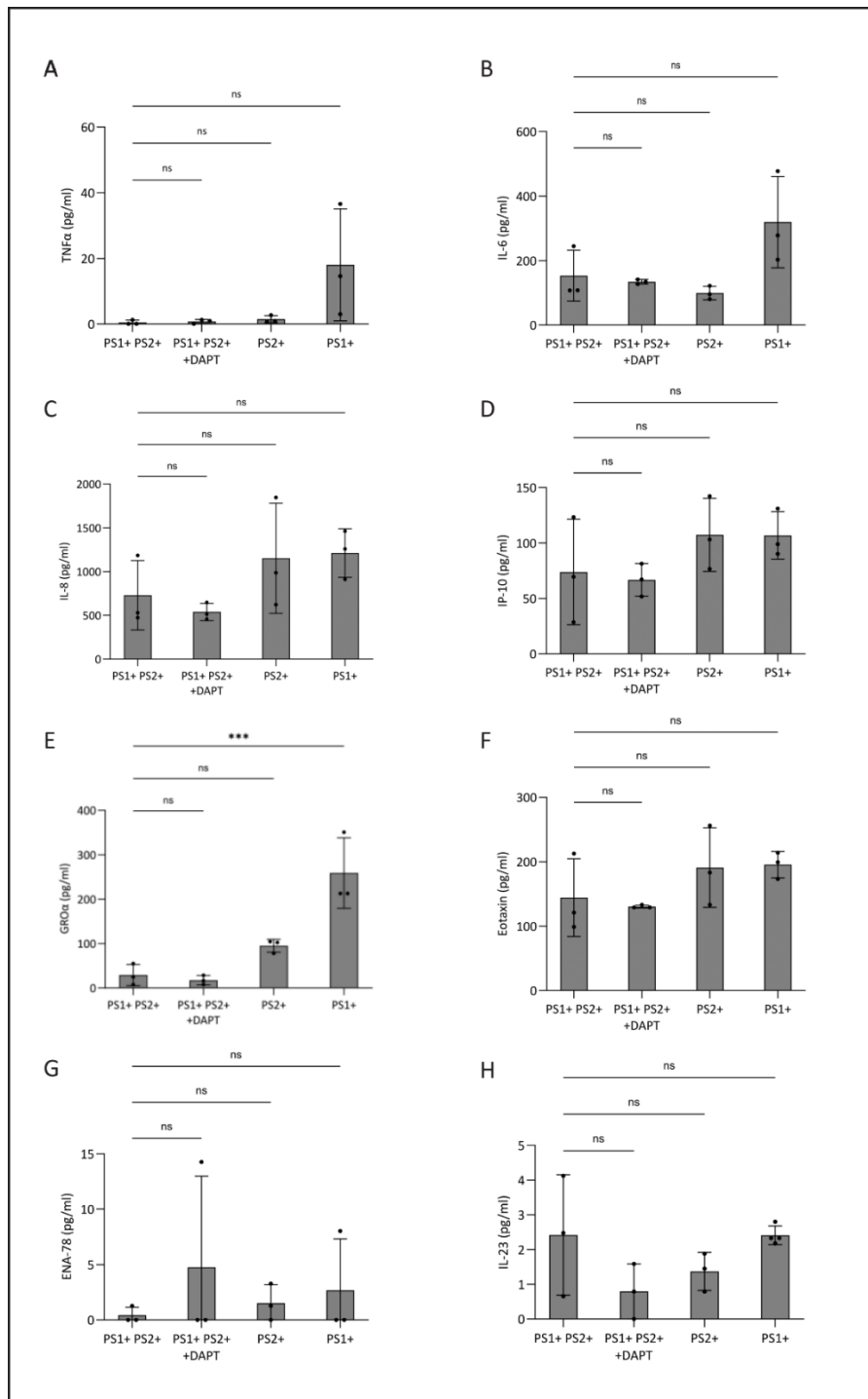
SI Figure 5-1 RNA sequencing read count and data transformation assessment

Quality control metrics after pre-processing in iDEP1.1 plot of total read counts per sample after filtering (A), box plot of transformed data distribution per sample (B), and density plot of transformed data (C) do not identify any bias in sample sets associated with sequencing depth or distribution of transformed data.



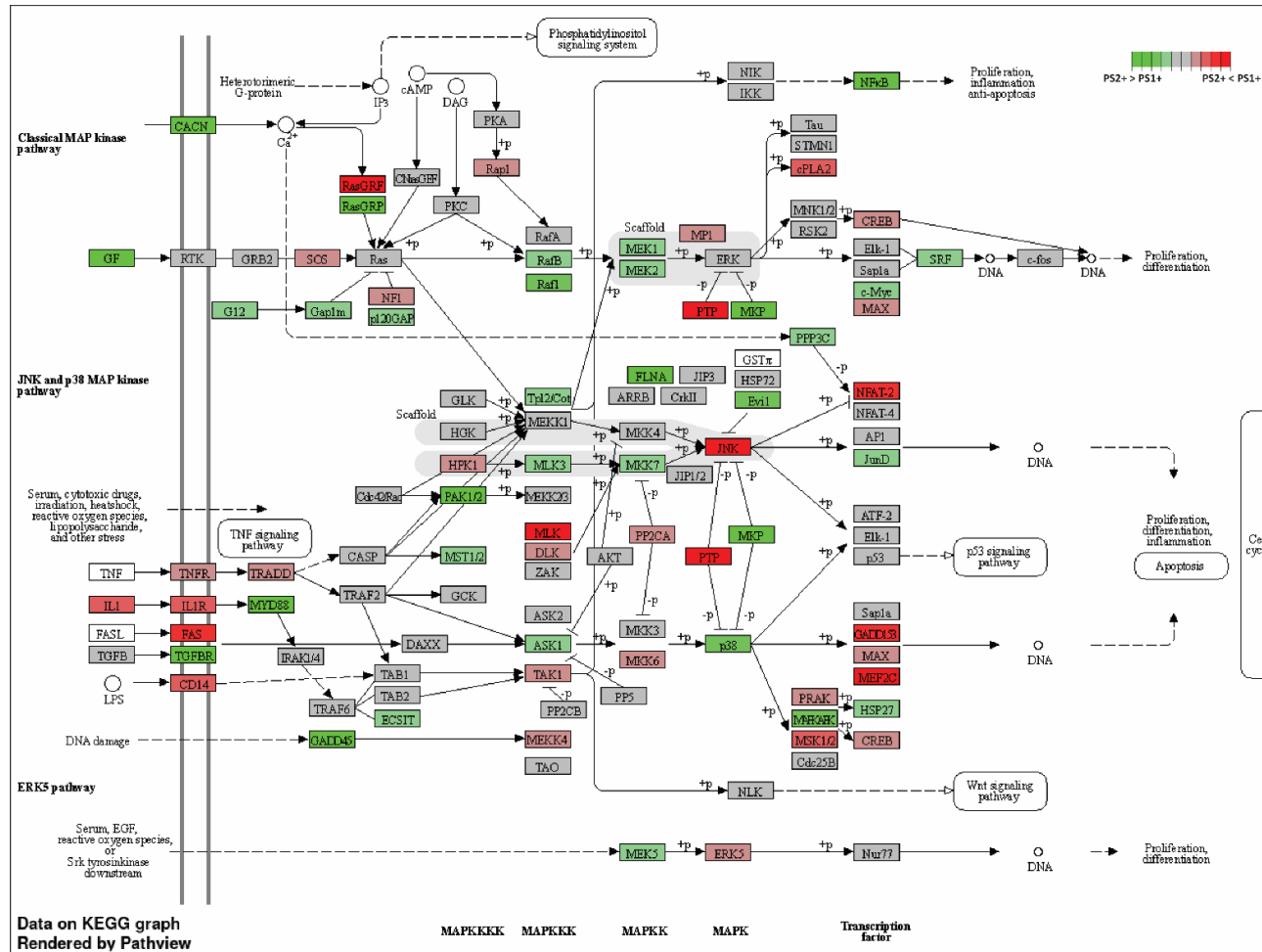
SI Figure 5-2 GO biological process network maps for clusters where PS2+ and PS1+ HMC3 cells have similar gene expression

Network maps for groups 1 (A), 7 (B), and 8 (C) identified by K-mean clustering where PS2+ and PS21+ cell lines have comparable gene expression (relates to Figure 5-7).



SI Figure 5-3 Basal cytokine secretion by HMC3 cells with altered PS genotype

Vehicle control samples from Figure 5-4 analysed to assess basal level cytokine secretion of TNF α (A), IL-6 (B), IL-8 (C), IP-10 (D), GRO α (E), eotaxin (F), ENA-78 (G), IL-23 (H), MCP-1 (I), and IGFBP-4 (J) from cells with different genotypes. Values shown are mean \pm SD. Statistical tests applied were one-way ANOVA with Holm-Šidák's multiple comparison (D), where ns = not statistically significant and *** = $P < 0.001$.



SI Figure 5-4 KEGG MAPK signalling pathway

Differentially expressed genes in KEGG MAPK signalling pathway [hsa04010] for PS2+ and PS1+ cells where green indicates PS2+ expression greater than PS1+ expression, and red indicates PS1+ expression greater than PS2+ expression. Grey indicates no difference between PS1+ and PS2+ cell expression. Generated in iDEP1.1.

6 BIOPHYSICAL CHARACTERISATION OF WILDTYPE AND MUTANT γ -SECRETASE BINDING TO SUBSTRATES ASSOCIATED WITH β -AMYLOID REMOVAL

6.1 INTRODUCTION

Alzheimer's disease (AD) has a complex pathogenesis, typified by a 10–20-year prodromal phase, during which protein accumulation and neuroinflammation commence. The accumulation of β -amyloid ($A\beta$) is a pathological hallmark that commences early in disease progression.^{1,2} As the generation and removal of $A\beta$ involves multifactorial processes, there are numerous opportunities for dysregulation.³⁻⁶ The sporadic form of AD is typically considered to be due to impaired $A\beta$ clearance, while autosomal dominant AD (ADAD), caused by mutations in the *APP*, *PSEN1* and *PSEN2* genes, results from aberrant $A\beta$ generation.¹

$A\beta$ generation is a multistep catabolic process that occurs as a result of regulated intramembrane proteolysis of the type I transmembrane protein amyloid precursor protein (APP) via the amyloidogenic pathway.^{7,8} This pathway is initiated by ectodomain shedding by β -APP-cleaving-enzyme-1 (BACE1)^{9, 10} and followed by γ -secretase processing of the remaining APP-CTF protein, which occurs within the membrane to produce the APP intracellular domain (AICD) and $A\beta$ peptides of multiple lengths.¹¹⁻¹⁵ The most common $A\beta$ products are $A\beta_{40}$ and $A\beta_{42}$, however longer and shorter $A\beta$ products are also generated.^{16, 17} However, alternative processing results in generation of non-amyloidogenic peptide species. The non-amyloidogenic pathway is initiated by a disintegrin and metalloproteinase 10 (ADAM10)¹⁸ family protein cleavage of the ectodomain within the $A\beta$ sequence, subsequent γ -secretase cleavage generates the P3 peptide.¹⁹⁻²³ Mutations in *APP* cause dysregulated $A\beta$ generation by altering the preference for both the initial ectodomain cleavage (i.e., either ADAM or BACE cleavage), or by altering γ -secretase processing of APP, ultimately leading to aberrant $A\beta$ production, and often an increase in the $A\beta_{42}$: $A\beta_{40}$ ratio. Increased $A\beta$ accumulation occurs with increased $A\beta_{42}$ generation due its greater hydrophobicity, and ability to act as a deposition seed for shorter forms of $A\beta$, particularly $A\beta_{40}$.²⁴

Since the identification of γ -secretase and its role in processing APP, over 150 type I transmembrane proteins having been identified as being substrates of this enzyme. γ -Secretase substrate cleavage is not specific for a particular sequence motif, but is influenced by the

structural characteristics of its substrates including, the requirement of a short ectodomain for substrate binding,²⁵ a positive charge cluster at the intracellular membrane border,²⁶ and structural compatibility between substrate residue size and binding pockets in PS active site.²⁷ Hence, type I transmembrane proteins with large ectodomains are not processed by γ -secretase until the ectodomains are shed. While γ -secretase is intimately linked to the generation of A β by virtue of its processing of APP, several other substrates of γ -secretase are involved in many aspects of A β metabolism. This includes regulation of APP trafficking and subcellular localisation,²⁸ A β degradation,²⁹ A β flux across the blood brain barrier,³⁰ and A β phagocytosis.³¹ In this capacity, γ -secretase and the presenilin proteins are a potential link between the sporadic and autosomal dominant forms of AD, given that the drivers of A β accumulation are aberrant clearance and generation in the respective forms of AD. Furthermore, several substrates of γ -secretase that have functional roles in A β metabolism also have variants that are known genetic risk factors for sporadic AD, including sortilin (SORT1), sortilin-related receptor (SORL1), and triggering receptor expressed on myeloid cells 2 (TREM2).³²

γ -Secretase consists of multiple protein components, of which presenilin functions as the catalytic component. Presenilin exists in two homologues: presenilin-1 (PS1) and presenilin-2 (PS2). While the two presenilin homologues both function as catalytic components of γ -secretase and were initially thought to be functionally redundant,¹⁵ a growing body of evidence has identified significant functional differences alongside some shared functionality. PS1 and PS2 form discrete γ -secretase enzyme complexes (herein termed PS1 γ and PS2 γ) that localise differently within cells, with PS2 γ localising specifically to late endosomes and lysosomal compartments, while PS1 γ localises more ubiquitously but predominantly in the plasma membrane.^{33, 34} Although PS1 γ and PS2 γ are both known to process APP and Notch1,^{16, 33-42} PS-specific substrate processing has also been demonstrated. For example N-cadherin is specifically cleaved by PS1 γ ,⁴⁰ while PMEL and TYRP1 are specifically cleaved by PS2 γ .³⁴ However, the specificity of PS1 γ and PS2 γ for substrates more broadly is poorly understood. A key role is suggested for PS2 in immune related functions, in particular because the LPS induced cytokine response is regulated specifically by PS2,^{43, 44} and microglial A β phagocytosis reduces in the absence of PS2.⁴⁵

Pathogenic mutations in the *PSEN1* and *PSEN2* genes cause ADAD, typically causing dysregulated A β generation that leads to increased A β 42:A β 40 and accelerated A β deposition,

similar to *APP* mutations. However, individuals with *PSEN1* or *PSEN2* mutations exhibit significant disease heterogeneity. Individuals with mutations in *PSEN1* have, on average, a significantly earlier age at onset (AAO) of approximately 45 years, compared with individuals with *PSEN2* mutations, which have an average AAO of approximately 55 years.⁴⁶ However, the range of AAO for *PSEN1* mutations is broader than that reported for *PSEN2* mutations (<20-75 years compared with 39-75 years).⁴⁶ Furthermore, both *PSEN1* and *PSEN2* mutations demonstrate variable effects on A β 42:A β 40 ratios and γ -secretase processing of multiple substrates including APP and Notch,^{34, 36, 47-51} associations with other neurodegenerative diseases^{47, 52} and dilated cardiomyopathy^{53, 54}, while *PSEN2* mutations are also associated with breast cancer.⁵⁵ Much of the field's understanding of aberrant A β generation has been determined by investigating the effect of pathogenic APP and presenilin mutations, as well as protective APP mutations, that lead to altered amounts of A β and varied A β 42:A β 40 ratios peptides. However, mutations in PS1 and PS2 have been shown to cause microglial activation,^{56, 57} induce inflammatory responses,⁵⁶⁻⁵⁸ alter microglial phagocytosis,^{56, 59} and dysfunction in lysosomal systems,^{59, 60} all of which can dysregulate A β metabolism. The effect of mutations in PS1 and PS2 on substrate processing beyond APP and Notch, in particular substrates involved in A β removal and the potential influence on ADAD heterogeneity, have not been well studied.

While the processing and turnover of substrates by γ -secretase has been widely studied,^{34, 36, 61, 62} detailed biochemical evaluation of γ -secretase substrate affinity and the effects of mutations *in vitro* is limited.^{36, 63, 64} Assessing the binding energetics and kinetics of γ -secretase with its substrates, and the subsequent effect of mutations, is required to provide significant insight into substrate preference and turnover, as well as the mechanistic effect of mutations. However, whilst achieving this *in vitro* is challenging, investigations *in silico* using structural models can provide further insight for further exploration. Recently, several structures of γ -Secretase bound to small molecules⁶⁵⁻⁶⁸ and APP and Notch1 substrates^{69, 70} have been determined via cryogenic electron microscopy (cryoEM), providing the opportunity to improve our understanding of substrate binding, complex dynamics and the effect of mutations through molecular modelling techniques. Indeed, these structures have been used to initiate well-tempered metadynamics simulations to explore the conformational dynamics of γ -secretase, as presented in Chapter 3. Several molecular modelling studies exploring ADAD mutations in PS have been undertaken, however the majority of these have focussed on PS1 mutations,⁷¹⁻⁸² with only one investigating PS2 mutations.⁸³ Several studies used employed prediction tools for

stability and affinity, examining all pathogenic PS mutations, utilising static molecular dynamics (MD) equilibrated structures, with varying results. PS1 and PS2 mutations were predicted to destabilise the γ -secretase complex,^{72, 75, 77, 83} to have no effect on APP binding affinity,⁷⁷ and additionally failed to predict any significant effect.⁷⁸ However, using coarse grained,⁷⁶ all atom,^{79, 80} and Gaussian accelerated⁸² MD PS mutations have been shown to alter complex configuration^{76, 79, 80, 82} and demonstrate ‘looser’ substrate binding.⁸⁰ These studies however have only considered a limited number of PS1 mutations, thirteen by coarse grain MD⁷⁶ and 3 to 6 by all atom and Gaussian accelerated MD.^{79, 80, 82}

In the current study, well-tempered metadynamics coupled with binding energy calculations was used to investigate if A β metabolism-related substrates exhibit a preference for binding PS1 γ or PS2 γ . Additionally, alchemical perturbation was used to explore the relationship between pathogenicity of PS1 and PS2 mutations and their effect on binding multiple substrates, including, but not limited to, APP. These methods were used to assess the differential effects of PS1 γ and PS2 γ and clinical mutations on A β clearance related substrate binding. It was identified that the majority of substrates investigated demonstrate a preference for being bound in a PS1 γ complex, while TREM2 and LRP8 have a significant preference for being bound in complex with PS2 γ . Furthermore, the severity of ADAD, as measured by AAO, is linked to the effect of PS1 mutations on the binding of APP-CTF(A β 49) (which is positioned to initiate the A β 40 pathway) and RAGE. Interestingly, these relationships contrast one another: the influence of PS1 mutations on APP-CTF(A β 49) exhibits a negative correlation with AAO, whereas the effect on RAGE demonstrates a positive correlation with AAO.

6.2 MATERIALS AND METHODS

6.2.1 Substrate selection

A comprehensive list of γ -secretase substrates was sourced from the literature^{61, 84, 85} and examined to identify proteins that are known to perform functions associated with A β metabolism. For use in this study, thirteen substrates of γ -secretase were selected because of their function in APP trafficking, A β degradation, flux and phagocytosis and are described in Table 6-1. A further three known substrates, in which PS1 γ and PS2 γ preferences have been experimentally reported, were used to validate the computational methods used. Sequences of substrates selected for analysis were downloaded from UniProt.⁸⁶ The sequences used (SI Fig.

1) began at the C-terminal residue of the ectodomain cleavage site (where identified in the literature) and finished approximately 3 residues C-terminal of the putative transmembrane domain (TM), incorporating the charged residues that are typical of γ -secretase substrates and believed to be involved in membrane anchoring.²⁶ Thus, the sequence incorporated the N-terminus luminal sequence, the TM sequence, and approximately 3 residues of the C-terminal cytoplasmic domain.

Where the ectodomain cleavage site was not available in the literature, it was predicted using PROSPEROUS.⁸⁷ The sequence used for ectodomain cleavage site prediction commenced 50 amino acids N-terminal of the TM and concluded 50 amino acids C-terminal of the TM. Three ranked predictions for cleavage by both ADAM10 and ADAM17 were generated. The highest-ranking cleavage site in the 50 amino acid sequence N-terminal of the TM was used as the ectodomain cleavage position.

Table 6-1 A β metabolism substrate function

Substrate	UniProt accession	A β clearance related function	Expressed in¶			
			N	A	M	O
APLP2 – amyloid beta precursor like protein 2	Q06481	Cis-heterodimerisation with APP to reduce A β generation ^{88, 89} APLP2-ICD regulates A β degrading enzyme expression (NEP) ²⁹	✓	✓	✓	✓
AXL – tyrosine-protein kinase receptor UFO	P30530	A β phagocytosis receptor - microglia ⁹⁰ APOE regulation - astrocytes ⁹¹	-	✓	✓	-
CD44 – CD44 antigen	P16070	regulates A β degrading enzymes (MMP2 & MMP9) expression ^{92, 93}	-	✓	✓	✓
INSR – insulin receptor	P06213	Regulates expression of A β degrading enzyme (IDE) ⁹⁴	✓	✓	✓	✓
LDLR – low-density lipoprotein receptor	P01130	A β efflux from brain to periphery ⁹⁵⁻⁹⁷	✓	✓	✓	✓
LRP1 – low-density lipoprotein receptor-related protein 1	Q07954	A β efflux from brain to periphery ³⁰	✓	✓	✓	✓
LRP8 – low-density lipoprotein receptor-related protein 8	Q14114	Regulates APP cell surface retention to promote ADAM cleavage or endocytosis which promotes BACE cleavage ^{98, 99}	✓	✓	✓	✓
MER – tyrosine-protein kinase Mer	Q12866	A β phagocytosis receptor ⁹⁰	✓	✓	✓	-
RAGE – advanced glycosylation end product-specific receptor	Q15109	A β influx from periphery into brain ¹⁰⁰	-	✓	✓	✓
SORL1 – sortilin-related receptor	Q92673	Regulates APP trafficking and spatial association with ADAM/ γ -secretase or BACE/ γ -secretase complex; Binds A β and traffics to lysosome for degradation ²⁸	✓	✓	✓	✓
SORT1 – sortilin	Q99523	Regulates APP trafficking and increases ADAM cleavage ¹⁰¹ Facilitates endocytic uptake of APOE bound A β ¹⁰²	✓	✓	✓	✓
TREM2 – triggering receptor expressed on myeloid cells 2	Q9NZC2	A β phagocytosis receptor ^{31, 103}	-	-	✓	-
VLDLR – very low-density lipoprotein receptor	P98155	A β efflux from brain to periphery ¹⁰⁴ VLDLR interacts with APP and increase APP expression at surface ¹⁰⁵	✓	-	✓	✓

¶ Expression in cells as indicated by single cell RNA Expression (nTPM) data retrieved from Human Protein Atlas¹⁰⁶ at proteintlas.org retrieved on 20/08/23, where N = neurons (both excitatory and inhibitory), A = astrocytes, M= microglia, O = oligodendrocytes.

6.2.2 WTMetaD simulation of γ -secretase complexes

Substrate alignments and homology model generation were performed using the Advanced Homology Modelling tool within Schrodinger Biologics Suite 2018-3. Substrate sequences were aligned to both APP and Notch1 sequences and assessed for similarity. Where the γ -secretase cleavage site was known, this was aligned to the cleavage site of the substrate in the respective structure (SI Figure 6-1). The γ -secretase:substrate complex was modelled against the PDB structure with the highest sequence similarity (SI Figure 6-1). Both PS1 and PS2 γ -secretase complex homology models were generated using Advanced Homology Modelling and prepared within Schrodinger 2018-3 as per Chapter 3, section 3.2.1. For LRP1 and VLDLR substrates, which have long N-terminal loop sequences, additional refinement in this region using the Prime Refine Loops function was performed. Ten structures were reported for each loop refinement, with the model used for further simulations selected from these as the one with the fewest disallowed backbone conformations and smallest solvent-accessible hydrophobic patch (revealed by AggScore analysis¹⁰⁷) within the loop.

Simulation boxes were prepared using CHARMM-GUI,¹⁰⁸ AmberTools,¹⁰⁹ *acpype*,¹¹⁰ and GROMACS 2018.3¹¹¹ and simulated using GROMACS 2018.3¹¹¹ patched with PLUMED 2.5¹¹² as described in Chapter 3. Model convergence was confirmed by assessing the root mean squared deviation between FESs at 1 ns intervals, the Gaussian hill height and the sampling of the collective variable space over the duration of the simulation (SI Figure 6-2, SI Figure 6-3). Where convergence had not been achieved by 500 ns, the simulation was continued for an additional 500 ns, i.e. 1 μ s in total. Identification of low energy states and binding free energy calculations (MM-GB/SA) were similarly performed as per Chapter 3, with the exception that structural ensembles for each minimum in the FES within 5.0 kJ/mol of the global minimum were extracted from the WTMetaD simulations and clustered. The PS1 γ vs PS2 γ substrate binding preference was calculated as:

$$\Delta\Delta G_{PS Pref} = \Delta G_{PS2} - \Delta G_{PS1}$$

Where $\Delta\Delta G_{PS Pref} < 0$ indicates preferential binding of PS2 γ , and $\Delta\Delta G_{PS Pref} > 0$ indicates preferential binding of PS1 γ .

6.2.3 Mutation selection

PS1 mutations were selected for analysis ensuring that there was spatial representation throughout the protein and broad AAO distribution. Preference was given to mutations that had been investigated by Sun et al.⁵⁰ to enable analysis with *in vitro* A β 40 and A β 42 data. Additionally, as there are multiple residues that are mutated to two or more types of residues, a site at which multiple mutations have been identified was selected. AAO data was retrieved in a priority order¹¹³ from 1) curated data set from Ryman (2014)⁴⁶, 2) curated data set from Cruts (2012)¹¹⁴, and 3) reported in Alzforum¹¹⁵ dependent on availability. As PS2 mutations are limited, all mutations that were in positions that could be modelled (i.e. residue is present in the cryoEM structures) where an AAO has been reported for three or more individuals were selected.⁴⁹ An additional recently identified mutation, PS2:A379D, was also selected.¹¹⁶ Mutations assigned as being of uncertain significance with respect to pathogenicity were excluded. AAO for PS2 mutations were retrieved from multiple literature sources.^{49, 116, 117}

In addition to pathogenic mutations identified for investigation, benign and likely benign variants in PS1 and PS2 for use in determining a suitable threshold for subsequent identification of deleterious effects were identified. Eleven such variants (four in PS1 and seven in PS2), that were able to be modelled given the residue positions were retrieved from Gnomad.¹¹⁸

Details of mutation AAO and clinical classification of variants used in this study are available in Table 6-4, and the location of investigated mutations/variants are visualised in Figure 6-1.

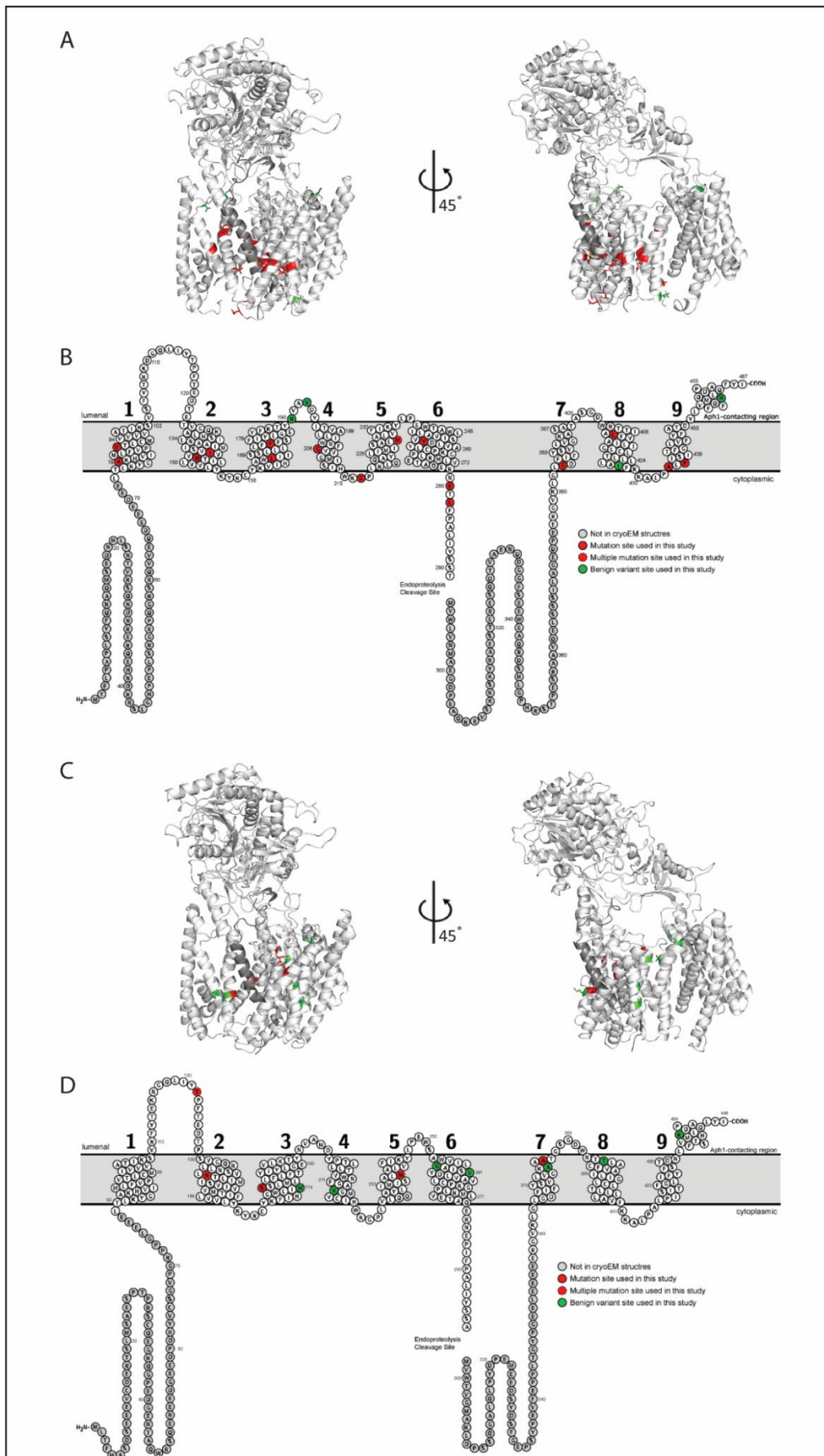


Figure 6-1 Benign and pathogenic variant positions in PS1 and PS2

Benign and pathogenic variant positions shown in PS1 γ (A) and PS2 γ (C) structures where likely pathogenic mutations are in red and likely benign variants are in green. Two dimensional schematics with TM and loop structures accurate as per cryoEM structures and homology models showing positions of variants investigated in this study for PS1 (B) and PS2 (D). Figures prepared using PyMol¹¹⁹ (A, C) and Protter¹²⁰ (B,D)

6.2.4 Thermodynamic integration

Previously described protocols were adapted to facilitate the calculation of relative substrate binding free energy upon mutation.¹²¹ Equilibrated PS1 γ and PS2 γ complexes bound to substrate, as well as unbound PS1 γ and PS2 γ , underwent molecular dynamics simulations using GROMACS 2018.3 for 50ns. Models used for molecular dynamic simulations were those prepared for substrates LRP1, LRP8, RAGE, SORL1, TREM2, and VLDLR, as described in this study, and APP-CTF(A β 49) and APP-CTF(A β 48) substrates as described in Chapter 3.

From these simulations, frames were extracted every 0.5 ns at evenly spaced intervals along the simulation trajectory, giving 100 frames from which alchemical perturbation simulations were initiated. For the alchemical perturbation, proteins were parameterised using the *pmx* variant of the AMBER *ff14SB* forcefield (*ff14SBmut*),^{122, 123} based on the AMBER *ff14SB* force field, while other components were parameterised as per all other simulations (lipids – Lipid14; water – TIP3P; counterions – 150 mM NaCl). In the alchemical perturbation simulations, a given residue in the structure was gradually mutated over the course of the simulation, represented by the coupling parameter λ ; for this work, the wildtype residue is represented by $\lambda = 0$, and its corresponding mutation by $\lambda = 1$. Free energy simulations, 0.5 ns each, were carried out in both the “forward” direction (i.e., initiated at $\lambda = 0$ and finishing at $\lambda = 1$) and the “reverse” direction (i.e., initiated at $\lambda = 1$ and finishing at $\lambda = 0$). The derivative of free energy with respect to λ was calculated over the course of the simulation, and processed via the Bennett acceptance ratio¹²⁴ method within *pmx* to give the free energy associated with introducing the mutation in both bound and unbound enzyme states (ΔG_{bound} , $\Delta G_{\text{unbound}}$). The relative binding free energy upon mutation ($\Delta\Delta G_{\text{mut}}$) was calculated:

$$\Delta\Delta G_{\text{mut}} = \Delta G_{\text{bound}} - \Delta G_{\text{unbound}}$$

A positive $\Delta\Delta G_{\text{mut}}$ indicates decreased (weaker) binding affinity, while a negative $\Delta\Delta G_{\text{mut}}$ indicates increased (stronger) binding affinity.

6.2.5 Assessment of variant classification

Assessment of variant classification was undertaken as previously described.¹²¹ The magnitude of the $\Delta\Delta G$ values calculated for each variant γ -secretase complex bound to either APP-CTF(A β 49) or APP-CTF(A β 48) was ranked from largest to smallest. The frequencies of identifying variants linked to diseases and likely benign variants within the general population were computed at each stage of the ranked list and graphed against each other. The detection rate of disease-associated variants was used as the true positive rate (y-axis), while the detection rate of general population variants served as the false positive rate (x-axis). The primary measure of performance was the area under the curve (AUC) on the graphs, calculated using the trapezoid rule. Performance was evaluated against random discovery, represented by the case where the true positive rate equals the false positive rate (TPR = FPR) and the AUC equals 0.5.

The Matthews correlation coefficient (MCC) was calculated using the absolute $\Delta\Delta G$ value for each variant bound to either APP-CTF(A β 49) or APP-CTF(A β 48). Each variant was classified as either pathogenic or benign as per the clinical classification. The MCC was determined at $\Delta\Delta G$ cut-offs just larger than the each obtained absolute $\Delta\Delta G$ value, except the largest. MCC was calculated on the classification of the number of true positives (TP), false positives (FP), true negatives (TN), false negatives (FN) as determined by use of the specific $\Delta\Delta G$ cut-off:

$$MCC = \frac{TP \times TN - FP \times FN}{\sqrt{(TP + FP)(TP + FN)(TN + FP)(TN + FN)}}$$

6.2.6 Statistical analysis

Normality tests and correlation analyses were performed in GraphPad Prism 9.5.0. All $\Delta\Delta G_{mut}$, AAO, and A β clinical data was tested for normality. Multiple $\Delta\Delta G_{mut}$ data sets were non-parametric. Consequently, all correlation analyses were calculated using Spearman correlation.

6.3 RESULTS

6.3.1 WTMetaD and MM-GB/SA assessment of validation substrates

Prior to analysis of A β metabolism related substrates of γ -secretase, three substrates for which there is experimental support of PS-specific preference were assessed to validate that

WTMetaD and MM/GB-SA assessment can be used to inform substrate preferences. Specifically N-cadherin (CDH2) which has demonstrated preference for PS1 γ processing,⁴⁰ and premelanosome protein (PMEL) and tyrosinase-related protein 1 (TYRP1)) which are preferentially processed by PS2 γ ³⁴ were assessed. WTMetaD was performed within the collective variable space of the position along the path (denoted as s , where $s = 1$ is 6IYC-like and $s = 20$ is 6IDF-like) and deviation from the path (denoted as z , with $z = 0$ being along the path and $z > 0$ being deviation from the path). Derivation of the path is presented in Chapter 3.

The free energy surfaces obtained following WTMetaD of PS1 γ with CDH2, PMEL and TYRP1 revealed only one energetic minimum within 5kJ/mol of the global minimum per complex. While additional local minima are apparent in the PS1 γ :TYRP1 complex, these are higher in energy than the 5 kJ/mol cut-off used for frame extraction. PS2 γ complexes, however, reveal multiple energetic minima within 5kJ/mol of the global minimum when bound to CDH2 and PMEL, and a single energetic minimum when bound to TYRP1 (Figure 6-2, Table 6-2). Notably, both PS1 γ :CDH2 and PS1 γ :PMEL complex minima occur at lower values of s , indicating PS1 γ adopting a conformation similar to APP binding, while the minimum for PS2 γ :TYRP1 occurs at higher s , indicating PS2 γ adopting a conformation similar to Notch1 binding. PS2 γ :CDH2, PS2 γ :PMEL and PS1 γ :TYRP1 conformational minima, however, suggest PS γ conformations distinct from those used to bind either APP or Notch1. Furthermore the PS1 γ :CDH2 and PS1 γ :PMEL complexes appear to be conformationally restricted, as represented by the tight contouring evident in the FES plots, while PS1 γ :TYRP1 and all PS2 γ complexes are likely to have relatively greater conformational flexibility given the broader contouring patterns observed.

MM-GB/SA calculations revealed a clear preference for PS2 γ binding of the PMEL substrate ($\Delta\Delta G_{\text{PS Pref}} = -17.0 \pm 3.6$ kcal/mol). For CDH2 ($\Delta\Delta G_{\text{PS Pref}} = -1.5 \pm 1.7$ kcal/mol) and TYRP1 ($\Delta\Delta G_{\text{PS Pref}} = +2.3 \pm 2.5$ kcal/mol) substrates, no substantial PS specific preference is evident (Table 6-2). WTMetaD and MM-GB/SA analysis of these substrates supports previous *in vitro* experimental results indicating a PS2 γ specific preference for processing of PMEL,³⁴ while the results for CDH2 and TYRP1 suggest there is a similar preference for PS1 γ and PS2 γ processing.

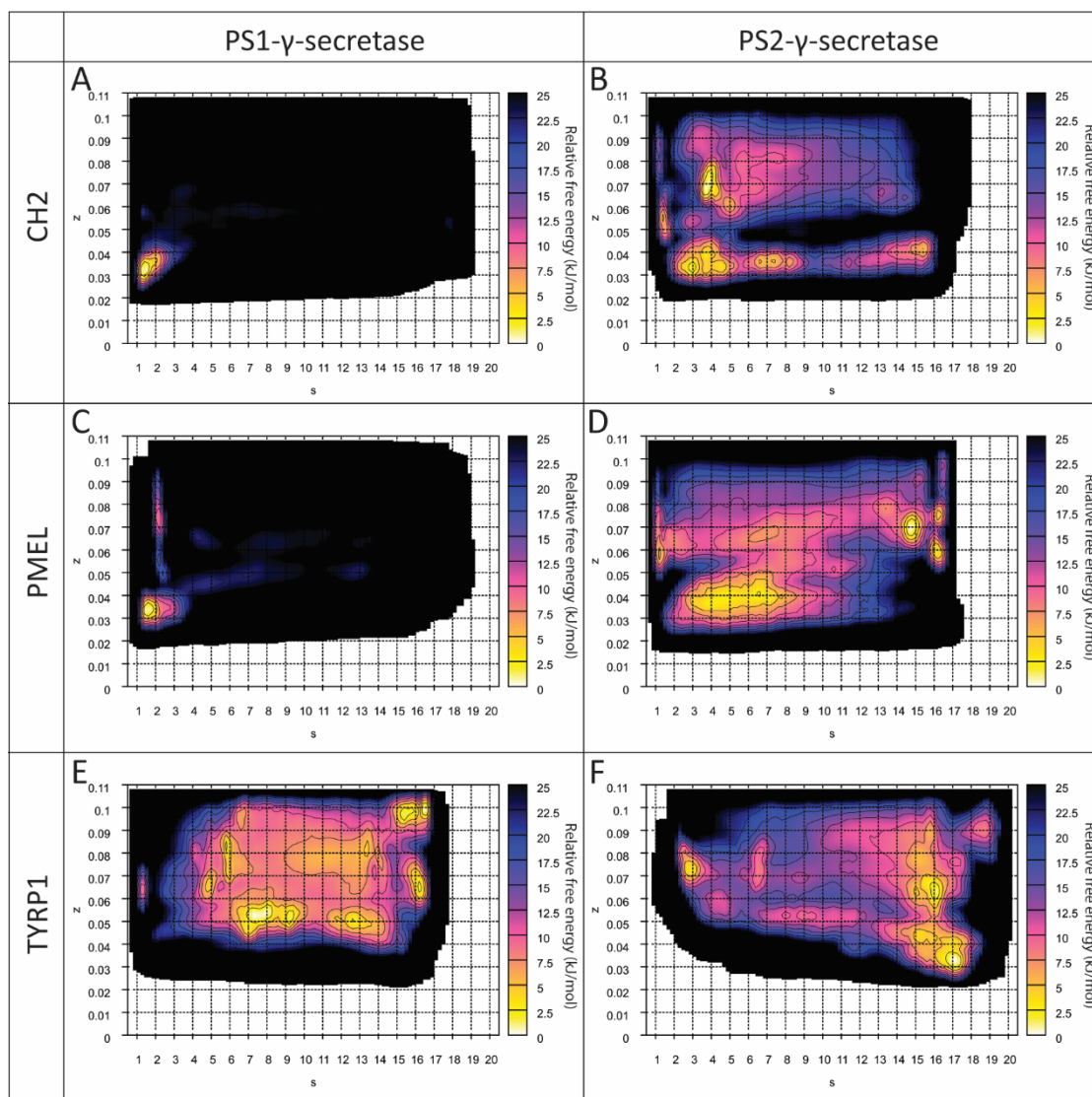


Figure 6-2 Validation substrate conformations

Free energy surfaces derived from well-tempered metadynamics simulations of CDH2 (A,B), PMEL (C,D), and TYRP1 (E,F) in complex with PS1 γ (A,C,E) and PS2 γ (B,D,F).

6.3.2 PS1 γ and PS2 γ form conformationally distinct complexes with A β metabolism related substrates

Having validated the approach with substrates that have known PS γ preference, WTMetaD simulations of the PS1 γ and PS2 γ enzymes complexed with the A β metabolism related substrates were subsequently performed. Assessment of the resulting FES plots identified a single energetic minimum in the majority of complexes, with the exception of PS1 γ :LRP1, PS1 γ :TREM2 and PS2 γ :TREM2 complexes, in which three minima were observed, and PS2 γ :VLDLR, where two minima were identified (Table 6-3). Comparison between the PS1 γ and PS2 γ complexes for each substrate identifies four types of conformational relationships:

1. PS1 γ and PS2 γ complexes are 6IYC-like, which is typified by APLP2 (Figure 6-3A,B), and includes LDLR, RAGE, and SORT1 (SI Figure 6-4).
2. PS1 γ and PS2 γ complexes are 6IDF-like, the only example of which is CD44 (Figure 6-3C,D).
3. PS1 γ and PS2 γ complexes are similar but not 6IDF- or 6IYC-like, the only example of which is LRP8 (Figure 6-3E,F)
4. PS1 γ and PS2 γ are not conformationally similar, this is typified by TREM2 (Figure 6-3G,H), and includes AXL, INSR, LRP1, MER, SORL1, and VLDLR (SI Figure 6-5).

A further assessment of FES contour breadth provides insight into conformational flexibility. Broad contours, indicative of wide energy wells, include large conformational ensembles, suggesting high conformational flexibility. Narrow contours, however, generally have fewer distinct conformations, indicating a more restricted conformational ensemble. While there is a range of FES contour breadth evident, PS1 γ :APLP2 (Figure 6-3A), PS2 γ :INSR (SI Figure 6-5D), and PS1 γ :LDLR (SI Figure 6-4A) complexes are conformational restricted given the very tight contours. The complexes with the highest conformational flexibility, are PS1 γ :AXL (SI Figure 6-5A), PS1 γ :LRP1 (SI Figure 6-5E), and PS1 γ :TREM2 (Figure 6-3G)..

MM-GB/SA calculations were determined using the extracted frames corresponding to the energetic minima identified in the FES plots for the A β metabolism related substrates and the preference for PS1 γ or PS2 γ assessed (Table 6-3). 70% of the substrates (9 of 13) show strong preferences for binding to either PS1 γ or PS2 γ . APLP2, CD44, INSR, LDLR, MER, RAGE, and SORL1 preferentially bind to PS1 γ with a $\Delta\Delta G_{PS Pref}$ range of $+11.7 \pm 2.0$ kcal/mol (APLP2) to $+33.3 \pm 1.1$ kcal/mol (RAGE). Substrates that have a strong preference for binding PS2 γ are LRP8 (-19.4 ± 2.4 kcal/mol) and TREM2 (-32.4 ± 1.3 kcal/mol). Only moderate preferences are evident for SORT1 towards PS1 γ , and LRP1 and VLDLR towards PS2 γ , while AXL demonstrates no substantial preference for PS1 γ or PS2 γ .

Table 6-2 Energy minima parameters for validation substrates

Substrate	PS1					PS2					$\Delta\Delta G_{PS Pref}^{\S}$ $\pm S.E.^{\dagger}$
	s Range		z Range		$\Delta G_{bind} \pm S.E.^{\dagger}$	s Range		z Range		$\Delta G_{bind} \pm S.E.^{\dagger}$	
CDH2	0	2	0.025	0.04	-202.9 \pm 1.4	3	5	0.06	0.08	-204.4 \pm 0.9	-1.5 \pm 1.7
						2	4	0.025	0.045	-194.3 \pm 2.2	
PMEL	1	2.5	0.025	0.045	-217.1 \pm 2.9	14	15.5	0.06	0.08	-234.2 \pm 2.2	-17.0 \pm 3.6
						3	8	0.03	0.05	-226.2 \pm 1.2	
						15.5	17	0.05	0.07	-219.1 \pm 5.6	
TYRP1	6	9	0.045	0.065	-214.4 \pm 0.5	16	18	0.025	0.045	-212.1 \pm 2.4	+2.3 \pm 2.5

\dagger ΔG_{bind} determined by MM-GB/SA; units are kcal/mol. \S $\Delta\Delta G_{PS Pref} < 0$ indicates preferential binding of PS2 γ , and $\Delta\Delta G_{PS Pref} > 0$ indicates preferential binding of PS1 γ .

Table 6-3 Energy minima parameters for A β metabolism related substrates in kcal/mol

Substrate	PS1					PS2					$\Delta\Delta G_{PS Pref}^{\S}$ $\pm S.E.^{\dagger}$
	s Range		z Range		$\Delta G_{bind} \pm S.E.^{\dagger}$	s Range		z Range		$\Delta G_{bind} \pm S.E.^{\dagger}$	
APLP2	0	2	0.02	0.05	-205.1 \pm 1.3	1	4	0.02	0.05	-193.4 \pm 1.5	+11.7 \pm 2.0
AXL	2	3	0.055	0.08	-207.7 \pm 0.7	1	3	0.025	0.045	-206.7 \pm 1.4	+0.9 \pm 1.5
CD44	14	17	0.045	0.065	-182.8 \pm 2.2	15	17	0.04	0.06	-157.9 \pm 1.5	+24.9 \pm 2.7
INSR	2	4	0.045	0.065	-192.0 \pm 1.0	0	2	0.02	0.04	-174.8 \pm 1.7	+17.1 \pm 1.9
LDLR	1	2	0.02	0.04	-197.4 \pm 1.5	1	3.5	0.02	0.04	-174.4 \pm 3.4	+23.0 \pm 3.7
LRP1	11	13.5	0.045	0.06	-187.9 \pm 0.8	15	17.5	0.035	0.05	-192.1 \pm 1.3	-4.3 \pm 1.5
	13	14.5	0.07	0.085	-187.0 \pm 0.8						
	13	15	0.04	0.05	-179.7 \pm 1.2						
LRP8	13	15	0.03	0.05	-187.9 \pm 2.0	12	14	0.03	0.05	-207.3 \pm 1.3	-19.4 \pm 2.4
MER	2	4	0.06	0.08	-213.5 \pm 1.2	3	6	0.035	0.05	-191.0 \pm 0.7	+22.5 \pm 1.4
RAGE	1	4	0.03	0.05	-200.5 \pm 0.8	2	5	0.035	0.06	-167.3 \pm 0.7	+33.3 \pm 1.1
SORL1	13	15	0.05	0.07	-197.9 \pm 1.0	15	18	0.04	0.06	-181.5 \pm 1.5	+16.4 \pm 1.8
SORT1	1	2.5	0.02	0.04	-171.9 \pm 1.4	1	2	0.035	0.05	-164.9 \pm 1.5	+6.9 \pm 2.1
TREM2	2	5	0.065	0.085	-161.3 \pm 1.1	7	9	0.06	0.08	-193.7 \pm 0.8	-32.4 \pm 1.3
	14	17	0.05	0.07	-160.8 \pm 0.7	6	8	0.04	0.06	-192.6 \pm 1.0	
	1	7	0.045	0.065	-159.3 \pm 0.5	1	2	0.055	0.07	-192.8 \pm 4.1	
VLDLR	14.5	17	0.04	0.055	-196.9 \pm 1.2	15	16	0.055	0.075	-206.4 \pm 1.5	-9.5 \pm 1.9
						14	16	0.04	0.055	-194.0 \pm 1.1	

\dagger ΔG_{bind} determined by MM-GB/SA; units are kcal/mol. \S $\Delta\Delta G_{PS Pref} < 0$ indicates preferential binding of PS2 γ , and $\Delta\Delta G_{PS Pref} > 0$ indicates preferential binding of PS1 γ .

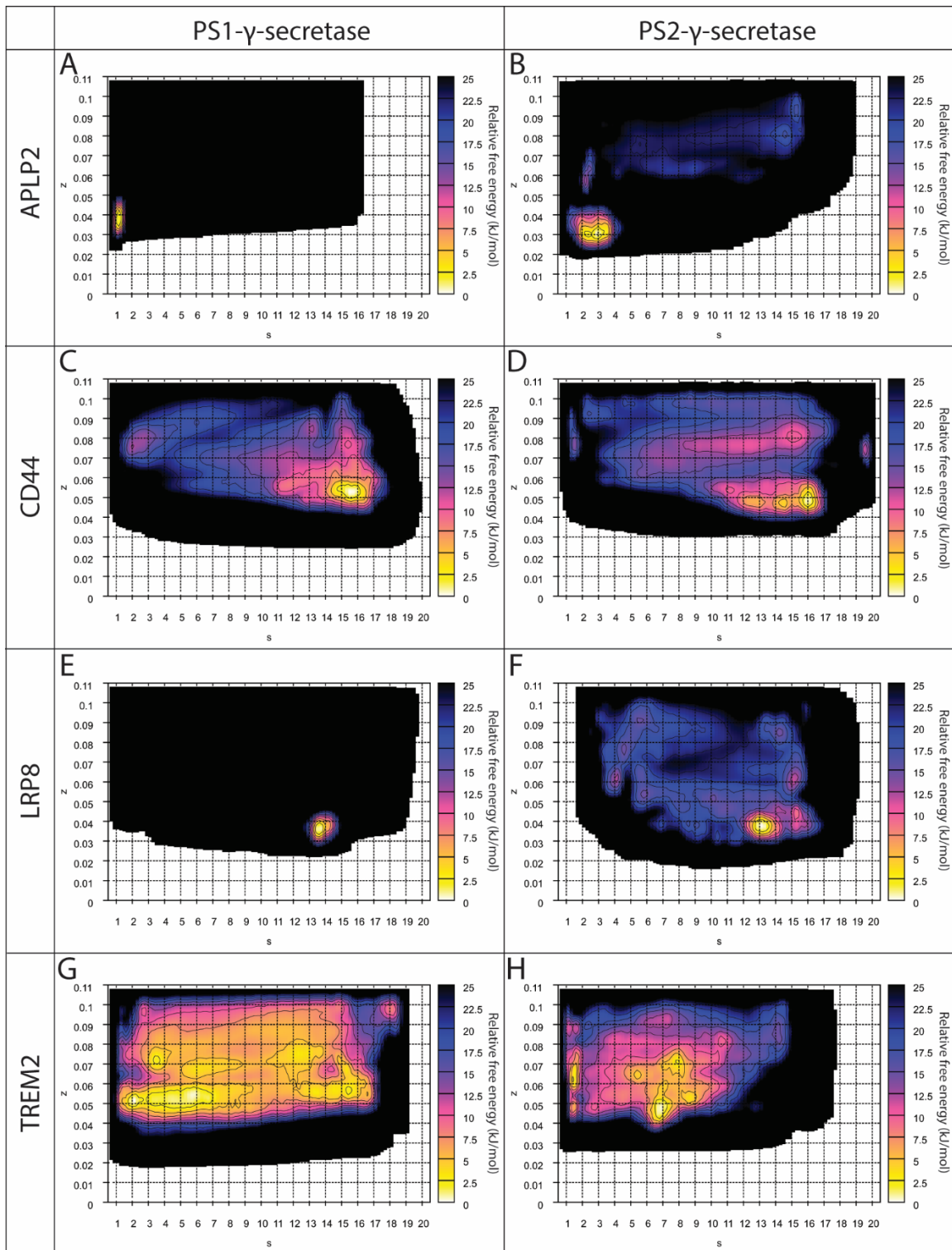


Figure 6-3 Representative complexes for conformational categories

Free energy surfaces derived from well-tempered metadynamics simulations of APLP2 (A,B), CD44 (C,D), LRP8 (E,F), and TREM2 (G,H) in complex with PS1 γ (A,C,E,G) and PS2 γ (B,D,F,H). Where APLP2 is representative of PS1 γ and PS2 γ complex both being 6IYC-like, CD44 is representative of PS1 γ and PS2 γ complex both being 6IDF-like, LRP8 is representative of the PS1 γ and PS2 γ complexes being conformationally similar but not 6IYC-like or 6IDF-like, and TREM2 is representative of PS1 γ and PS2 γ having different conformations.

6.3.3 Evaluation of alchemical perturbation for classifying the disease association of variants in γ -secretase

Having identified that there were PS γ -specific preferences for the majority of analysed substrates and having evidence of PS γ -specific differences in conformation, the effect of known pathogenic PS mutations on the binding of specific substrates was investigated. As mutations in *PSEN1* and *PSEN2* are causal for ADAD, the classification of benign or pathogenic variants is typically determined by the effect of the mutation on the generation of A β peptides and associated A β 42:A β 40 ratio and the presence of disease,¹¹⁵ particularly where the population variant frequency is too low for segregation analysis. To determine the likely pathogenic effect of mutations on substrate binding, alchemical perturbation was performed to determine the difference in binding free energy of PS1 and PS2 variants, as this has previously been shown to perform superiorly to other methods.¹²¹ As alterations in processing of APP-CTF(A β 49) and APP-CTF(A β 48) substrates by PS mutations are known to cause altered A β 42:A β 40 generation,^{36, 50} the relative effect of variants on the $\Delta\Delta G_{\text{mut}}$ for PS γ complexes bound to these substrates was determined (Table 6-4). These substrates were previously examined by WTMetad bound to either PS1 γ or PS2 γ complexes in Chapter 3.

ROC curves were generated to evaluate the classification of PS variants in the context of the APP-CTF(A β 49) and APP-CTF(A β 48) substrate complexes (Figure 6-4A,B). The area under the curve (AUC) analysis demonstrated that both substrate complexes outperform random chance when classifying pathogenic and benign variants in the context of substrate binding. To find the best threshold for $\Delta\Delta G_{\text{mut}}$ values in both the APP-CTF(A β 49) and APP-CTF(A β 48) substrate complexes, the Matthews correlation coefficient (MCC) was calculated across the range of $\Delta\Delta G_{\text{mut}}$ values. The maximum values for the MCC identified the optimal cut-off for the data (Figure 6-4C,D). The MCC for APP-CTF(A β 49) exhibits a biphasic pattern across the range of $\Delta\Delta G_{\text{mut}}$ values. Specifically, MCC peaks at 0.45 for $\Delta\Delta G_{\text{mut}}$ values of both 0.21 kcal/mol and 1.34 kcal/mol. On the other hand, for APP-CTF(A β 48), there's a single MCC peak at 0.42, occurring at a $\Delta\Delta G_{\text{mut}}$ value of 0.15 kcal/mol. However, considering that the average standard error for both APP-CTF(A β 49) and APP-CTF(A β 48) is 0.26 kcal/mol, neither the 0.21 kcal/mol nor the 0.15 kcal/mol $\Delta\Delta G_{\text{mut}}$ thresholds are suitable. Consequently, we opted for a $\Delta\Delta G_{\text{mut}}$ cut-off of 1.34 kcal/mol as the pathogenicity threshold ($\Delta\Delta G_{\text{path}}$).

Table 6-4 Effect of PS mutations on relative binding free energy (kcal/mol) for γ -secretase bound to APP-CTF

Gene	Protein Mutation	Database Classification†		AAO¶	Sun 2016 Data§			APP-CTF(A β 49)	APP-CTF(A β 48)
		ClinVar	AlzForum		A β 42: A β 40	Amount A β 40	Amount A β 42	$\Delta\Delta G_{mut} \pm S.E.$	$\Delta\Delta G_{mut} \pm S.E.$
PSEN1	A79V	P	LP	62.5 ^a	ND	0.01	0.06	-1.90 \pm 0.24	+0.24 \pm 0.23
PSEN1	V89L	NP	P	48.67 ^a	2.53	0.16	0.42	-0.22 \pm 0.17	-0.84 \pm 0.16
PSEN1	I143T	P	P	30 ^a	19.38	0.01	0.26	+2.91 \pm 0.26	+0.73 \pm 0.11
PSEN1	M146V	P	P	39 ^a	-	-	-	+1.66 \pm 0.15	+1.10 \pm 0.14
PSEN1	L166P	P	P	24 ^b	2.71	0.10	0.27	+4.48 \pm 0.48	+1.29 \pm 0.50
PSEN1	F176L	NR	NC	51 ^c	ND	0.01	0.13	+1.00 \pm 0.10	+1.12 \pm 0.09
PSEN1	G206A	P	P	53.53 ^a	3.27	0.17	0.55	-0.30 \pm 0.12	-0.66 \pm 0.10
PSEN1	G217R	NR	LP	44.42 ^a	1.48	0.13	0.19	-8.95 \pm 2.26	-4.28 \pm 1.93
PSEN1	M233L	NP	P	33.5 ^a	1.86	0.70	1.38	+0.56 \pm 0.10	+0.87 \pm 0.12
PSEN1	M233T	P/LP	P	33.67 ^a	9.74	0.30	3.05	+4.48 \pm 0.61	-0.04 \pm 1.24
PSEN1	M233V	P/LP	P	32 ^b	-	-	-	+2.23 \pm 0.13	-0.17 \pm 0.17
PSEN1	Y256S	NP	NC	27.5 ^a	7.86	0.03	0.29	+3.81 \pm 0.16	+7.82 \pm 0.16
PSEN1	E280A	P	P	38.45 ^a	2.00	0.51	0.81	-0.42 \pm 0.18	+3.29 \pm 0.31
PSEN1	L282V	NP	P	46.5 ^a	0.96	1.17	1.05	-1.39 \pm 0.15	-0.19 \pm 0.15
PSEN1	G384A	P	P	36 ^c	171.02	0.01	1.87	+4.60 \pm 0.17	+1.26 \pm 0.05
PSEN1	C410Y	P	P	49.25 ^a	0.95	0.04	0.04	-0.70 \pm 0.94	+4.16 \pm 0.90
PSEN1	A434C	P	P	30.33 ^a	13.45	0.11	1.46	+1.55 \pm 0.13	+2.52 \pm 0.71
PSEN1	P436Q	P	P	28.3 ^b	-	-	-	-0.45 \pm 0.45	+0.92 \pm 0.43
PSEN2	T122P	P/LP	LP	47.9 ^d	No Data Available			-0.50 \pm 0.30	+5.78 \pm 0.46
PSEN2	T122R	P	AtD	57.3 ^d				-1.64 \pm 0.45	+0.53 \pm 0.48
PSEN2	N141I	P	P	53.7 ^d				+0.61 \pm 0.56	-4.34 \pm 0.41
PSEN2	N141Y	NR	LP	46.0 ^e				+1.61 \pm 0.46	-3.11 \pm 0.33
PSEN2	S175C	NR	NC	60.0 ^d				+1.49 \pm 0.07	+0.99 \pm 0.08
PSEN2	M239I	P	P	50.7 ^d				-0.92 \pm 0.13	+0.30 \pm 0.15
PSEN2	M239V	P	P	60.1 ^d				-0.47 \pm 0.12	+0.01 \pm 0.13
PSEN2	A379D	NR	NC	55.0 ^f				-3.05 \pm 0.57	-1.23 \pm 0.55
PSEN1	N190D	NR	NR	No Data Available			+0.53 \pm 0.38	-3.54 \pm 0.34	
PSEN1	V193G	NR	NR				-1.12 \pm 0.12	-0.09 \pm 0.12	
PSEN1	I427V	LB	NR				-0.60 \pm 0.06	-0.14 \pm 0.06	
PSEN1	H463R	NR	NR				-1.23 \pm 0.64	-1.12 \pm 0.59	
PSEN2	M174V	B/LB	B				-0.13 \pm 0.13	+0.22 \pm 0.13	
PSEN2	V214L	B	B				+1.06 \pm 0.21	+2.18 \pm 0.19	
PSEN2	G257S	NR	NR				-0.20 \pm 0.19	-0.09 \pm 0.21	
PSEN2	V261L	NR	NR				-0.16 \pm 0.20	-0.10 \pm 0.24	
PSEN2	A377V	NR	B				+1.34 \pm 0.29	+0.07 \pm 0.40	
PSEN2	T388M	LB	NC				+0.92 \pm 0.40	+1.23 \pm 0.39	
PSEN2	R435W	LB	NR				+2.14 \pm 0.58	-1.51 \pm 0.42	

† AtD = Atypical dementia, B = Benign, B/LB = Benign/Likely benign, LB = Likely benign, LP = Likely pathogenic, NC = Not classified, NP = Not provided, NR = No record, P = Pathogenic.

AAO data retrieved from: a. Ryman (2014)⁴⁶ b. Cruts (2012)¹¹⁴ c. Alzforum mutation database¹¹⁵ d. Jayadev (2010)⁴⁹ e. PS2:N141Y¹¹⁷ f. PS2:A379D¹¹⁶

§ Data retrieved from Sun (2016)⁵⁰ [Table S1. Summary of biochemical characterization of 138 γ -secretase variants with PS1 mutations]

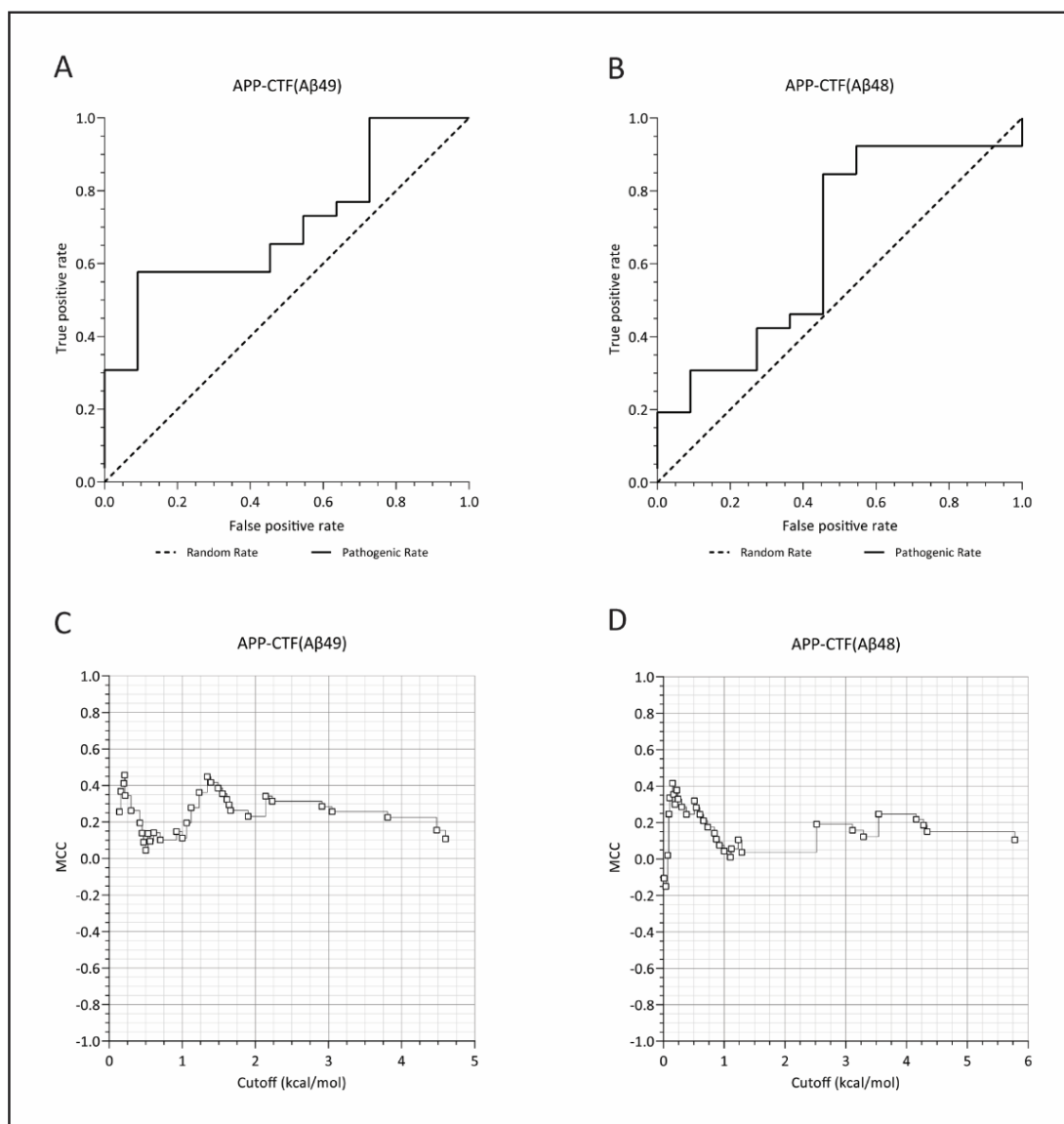


Figure 6-4 Determination of pathogenic $\Delta\Delta G_{\text{path}}$ cut-off

Receiver operating characteristic (ROC) curves evaluating variant classification for $\Delta\Delta G_{\text{mut}}$ determined for APP-CTF(A β 49) (A) and APP-CTF(A β 48) (B) and Matthew correlation coefficient (MCC) calculated at different $\Delta\Delta G_{\text{path}}$ cut-offs for APP-CTF(A β 49) (C) and APP-CTF(A β 48) (D).

6.3.4 Determination of pathogenicity by alchemical perturbation of PS variants on A β metabolism related substrates.

The effect of PS mutations on binding of γ -secretase substrates with functions related to A β removal was assessed to determine potential pathogenic effects. Of the thirteen substrates examined by WTMetaD, LRP1, LRP8, RAGE, SORL1, TREM, and VLDLR were selected to assess via thermodynamic integration to determine what if any effect PS1 and PS2 mutations had on the $\Delta\Delta G_{\text{mut}}$ for binding these substrates. These substrates were selected as they represent the broad range of $\Delta\Delta G_{\text{PS Pref}}$, with representation of PS1 (RAGE, SORL1) and PS2 (LRP1,

LRP8, TREM2, CLDLR) substrate preference. Alchemical perturbation was completed for six PS2 mutations and thirteen PS1 mutations bound to the selected substrates (SI Table 6-1). The $\Delta\Delta G_{\text{path}}$ was then applied to the thermodynamic integration results to classify the likely effect of the variant on pathogenicity and disease presentation (Figure 6-5A).

With the exception of PS2:M239I, all of the examined mutations are likely to be pathogenic, although exert their pathogenicity through differential effects on substrate binding. The most consistently affected substrates are RAGE and VLDLR, with 63% and 58% of mutations respectively resulting in a $\Delta\Delta G_{\text{mut}}$ above the pathogenicity cut-off. Mutations that result in $\Delta\Delta G_{\text{mut}}$ values beyond the pathogenicity cut-off for 6 or more of the 8 substrates examined include PS1:M233T, PS1:G384A, PS1:C410Y, and PS2:T122R. Conversely, the effects of PS1:V89L, PS2:M239V and PS2:I143T appear restricted to specific substrates.

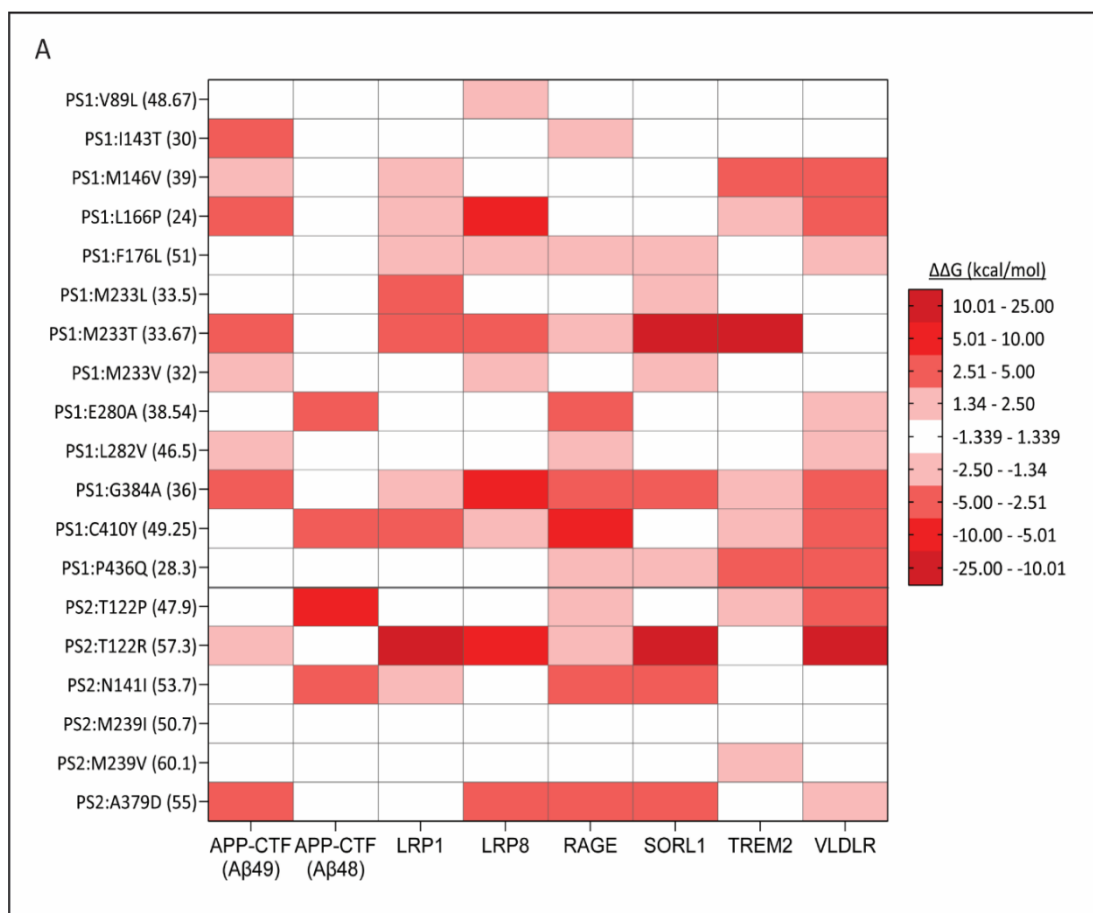


Figure 6-5 Application of $\Delta\Delta G_{\text{path}}$ to assign pathogenicity related to substrate binding

Pathogenic cut-off $\Delta\Delta G_{\text{path}}$ of 1.34 kcal/mol determined and applied to other substrate $\Delta\Delta G_{\text{mut}}$ results to identify variants that have potentially pathogenic effect on substrate processing for LRP1, LRP8, RAGE, SORL1, TREM2, and VLDLR substrates (A). Data used to generate heatmap available in SI Table 6-1.

6.3.5 PS1 mutation $\Delta\Delta G_{mut}$ for APP-CTF(A β 49) correlates with AAO

Next relationships between the calculated $\Delta\Delta G_{mut}$ for mutations classified as pathogenic in ClinVar or AlzForum relative to clinical measures were assessed. Initially the effect of the $\Delta\Delta G_{mut}$ determined for APP-CTF(A β 49) and APP-CTF(A β 48) substrates with AAO was examined (Figure 6-6). Correlation analysis was completed using the combined PS1 and PS2 results (Figure 6-6A,B). $\Delta\Delta G_{mut}$ APP-CTF(A β 49) has a significant ($p=0.0010$) moderate to strong negative correlation with AAO, while $\Delta\Delta G_{mut}$ APP-CTF(A β 48) has moderate negative correlation with AAO that trends towards significance ($p=0.0606$). Given that PS1 and PS2 mutations present with significantly different average AAO, the correlations for PS1 and PS2 mutations were assessed separately (Figure 6-6C-F) to determine if the combined results were influenced by either PS1 or PS2 mutations or were common to both. Interestingly, this segregated assessment revealed that only the $\Delta\Delta G_{mut}$ data for PS1 γ :APP-CTF(A β 49) complexes significantly correlate with AAO (Figure 6-6C), in a moderate to strong negative relationship. This correlation suggests that mutations with higher positive $\Delta\Delta G_{mut}$, indicating reduced substrate binding affinity, are associated with earlier AAO.

Previously published experimental data from Sun et al., analysing 138 pathogenic mutations in PS1 via the same experimental method, which reported data for the amount of A β 40, the amount of A β 42 and A β 42:A β 40 ratio,⁵⁰ was also evaluated. Correlation analyses for each experimental output with both $\Delta\Delta G_{mut}$ APP-CTF(A β 49) and $\Delta\Delta G_{mut}$ APP-CTF(A β 48) was completed, for all PS1 pathogenic mutations where data was available (Figure 6-6G,H, SI Figure 6-6). A significant ($p=0.0166$) strong positive correlative relationship between A β 42:A β 40 ratio and $\Delta\Delta G_{mut}$ APP-CTF(A β 49) was observed, irrespective of the removal or inclusion of the PS1:G384A data point as an outlier (Figure 6-6G, SI Figure 6-6A). No significant relationships were identified between amount of A β 40 or A β 42 and $\Delta\Delta G_{mut}$ for either APP-CTF(A β 49) or APP-CTF(A β 48) (SI Figure 6-6).

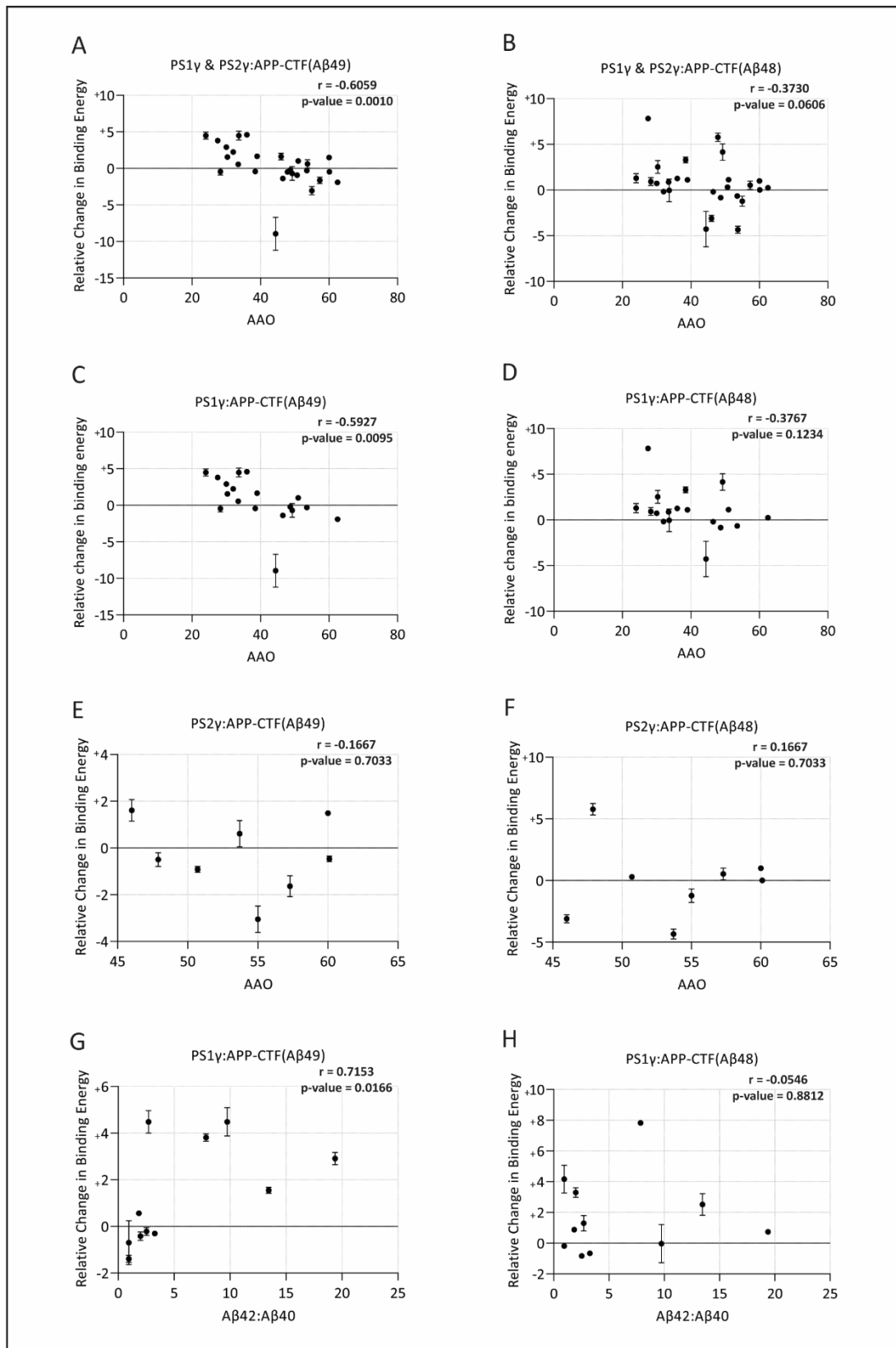


Figure 6-6 $\Delta\Delta G_{mut}$ for PS1 γ and PS2 γ mutation complexes bound to APP-CTF substrates correlation with AAO and A β 42:A β 40

Correlation between AAO and relative change in binding energy ($\Delta\Delta G_{mut}$) for mutations bound to APP-CTF(A β 49) (A, C, E) and APP-CTF(A β 48) (B, D, F) for PS1 γ and PS2 γ mutations combined (A, B), PS1 γ mutations only (C, D), PS2 γ mutations only (E, F). Correlation between

A β 42:A β 40 (Sun et al. data)⁵⁰ and relative change in binding energy ($\Delta\Delta G_{mut}$) for PS1 γ mutations bound to APP-CTF(A β 49) (G) and APP-CTF(A β 48) (H). PS1:G384A data point excluded from A β 42:A β 40 correlations (G, H), correlation including PS1:G384A presented in SI Figure 6-6A,B.

Correlation analyses were similarly performed with the $\Delta\Delta G_{mut}$ results of the other A β metabolism-related substrates for the PS1 and PS2 mutations separately with AAO, to investigate if there were any additional substrates where the binding effect of these mutations correlate (Figure 6-7, Figure 6-8). The only significant correlation that was observed is a moderately strong positive correlation between the PS1 $\Delta\Delta G_{mut}$ effect on RAGE and AAO ($p=0.0402$) (Figure 6-7B). This correlation suggests that mutations with higher positive $\Delta\Delta G_{mut}$, indicating reduced substrate binding affinity, are associated with later AAO. No significant correlations were identified between $\Delta\Delta G_{mut}$ for the remaining substrates investigated and AAO for either PS1 or PS2 mutations.

It was observed that PS1:L166P, and PS1:G384A mutations (associated with aggressive phenotypes, early AAO and rapid disease progression^{36, 125}) resulted in reduced relative binding affinity (positive $\Delta\Delta G_{mut}$) for all substrates (Table 6-4, SI Table 6-1). To determine if mutation severity corresponded to an effect on substrate binding of multiple substrates, the cumulative effects of $\Delta\Delta G_{mut}$ for PS1 and PS2 mutations that had been analysed with all eight substrates were assessed (SI Figure 6-7). As both increased and decreased binding affinity can impact deleteriously on substrate turnover depending on the amplitude of the change in relative binding affinity, both the sum and the sum of the absolute $\Delta\Delta G_{mut}$ values were calculated. No significant correlations were found between the cumulative $\Delta\Delta G_{mut}$ for either PS1 or PS2 mutations and AAO. These results indicate that while some mutations may have a significant deleterious effect on binding affinity of several substrates this is not consistently observed and subsequently does not correlate with disease AAO.

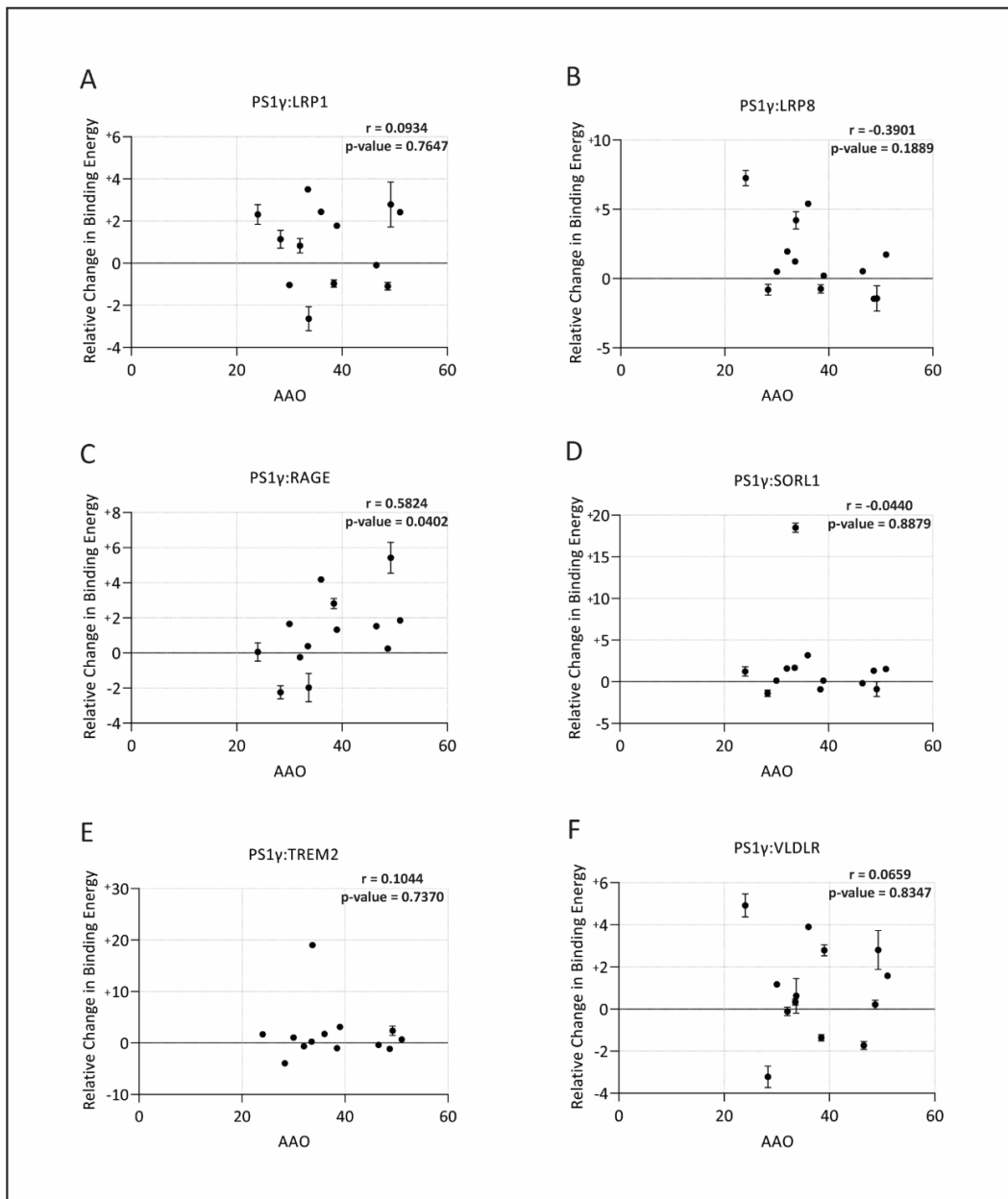


Figure 6-7 AAO correlation with $\Delta\Delta G_{mut}$ for PS1y mutation complexes bound to $A\beta$ metabolism related substrates

Correlation between AAO and PS1 mutation $\Delta\Delta G_{mut}$ effect on binding LRP1 (A), LRP8 (B), RAGE (C), SORL1 (D), TREM2 (E) and VLDLR (F).

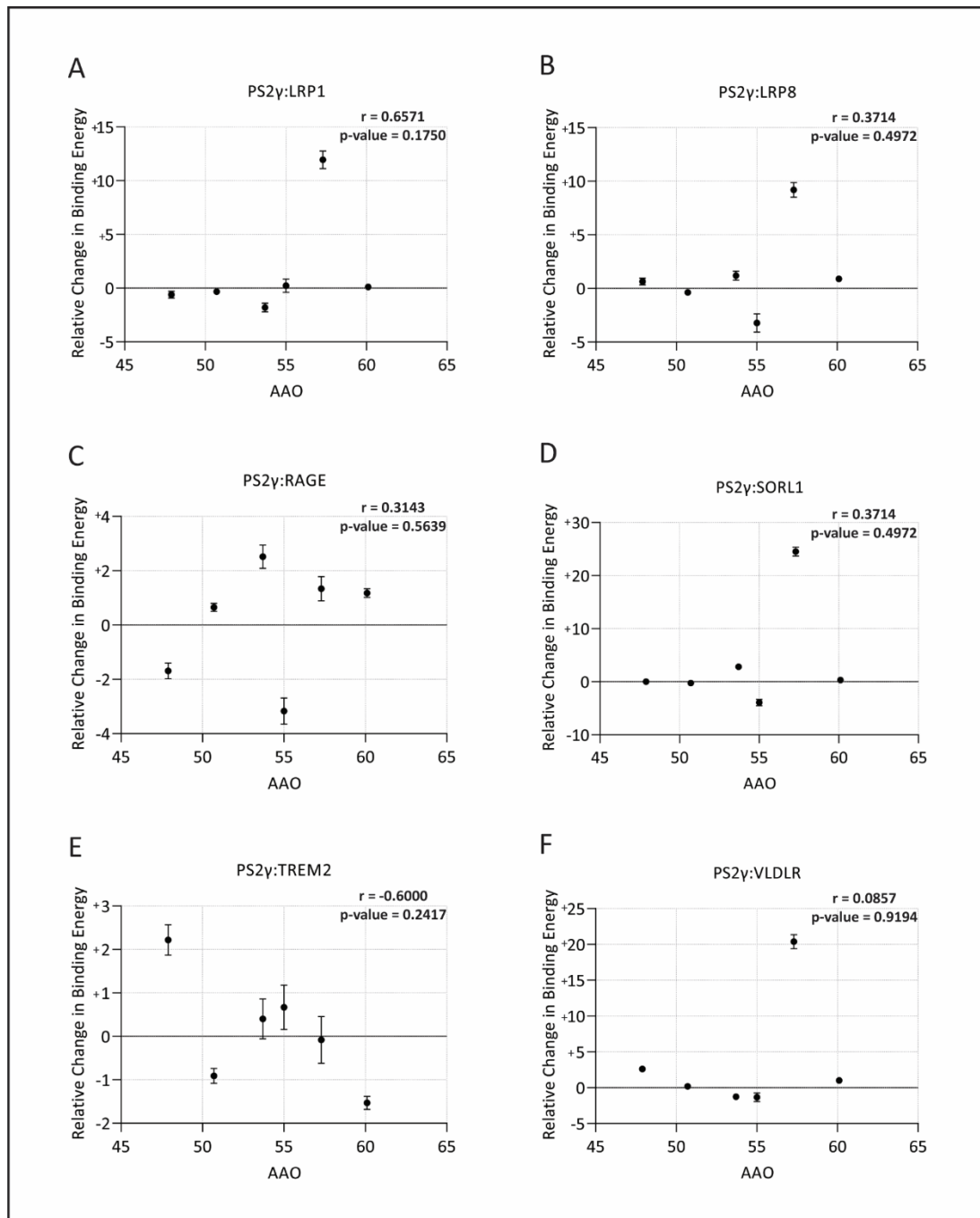


Figure 6-8 AAO correlation with $\Delta\Delta G_{mut}$ for PS2 γ mutation complexes bound to $A\beta$ metabolism related substrates

Correlation between AAO and PS2 mutation $\Delta\Delta G_{mut}$ effect on binding LRP1 (A), LRP8 (B), RAGE (C), SORL1 (D), TREM2 (E) and VLDLR (F).

6.4 DISCUSSION

In this study, well-tempered metadynamics and binding free energy calculations were used to investigate the potentially different affinity of PS1 γ and PS2 γ for substrates related to A β metabolism. The results revealed distinct substrate preferences binding to PS1 γ and PS2 γ complexes. Additionally, alchemical perturbation was utilised to explore how mutations in PS1 and PS2 may affect substrate binding of not only APP, but other A β metabolism related substrates. In doing so, a method for classification of disease associated pathogenicity in APP substrates was devised and applied to other A β metabolism related substrates. Finally, this study explored the potential for relationships between the effect of mutations on substrate binding ($\Delta\Delta G_{mut}$) and disease severity measured by age at onset (AAO).

The availability of experimental data supporting substrate preferences for processing by PS1 γ or PS2 γ is somewhat limited, with the majority focussed on defining the processing preferences for APP and Notch1 substrates.^{33, 34, 41, 42, 126-128} Accurate interpretation of the PS1 γ vs. PS2 γ activity, however, is hampered by the lack of quantitative methods for comparison of endogenous PS expression, and assumptions regarding equi-expression in exogenous PS systems which are extensively discussed and experimental solutions presented in Chapter 2. Simulation approaches have the potential to provide important information regarding substrate binding preferences that can inform the functional understanding of the roles of PS1 γ and PS2 γ , and hence inform structure-based drug design. Consequently, initial validation involved confirming the suitability of WTMetaD and MM/GB-SA methods to inform substrate binding preferences, using substrates that *in vitro* have demonstrated specific PS1 γ (CDH2)⁴⁰ or PS2 γ (PMEL and TYRP1).³⁴ PMEL demonstrated a strong preference for binding to PS2 γ in agreement with its specific processing by PS2 γ observed *in vitro*.³⁴ The MM/GB-SA results for CDH2 and TYRP1 however, exhibit a crossing of the 0 value, when the standard error is considered, indicating no discernible preference for binding to either PS1 γ or PS2 γ (Figure 6-1, Table 6-1). These findings for TYRP1 and CDH2 are discordant with those found *in vitro*.^{34, 40} As these previous studies were performed in whole cell models, it is likely that there is a strong influence of the spatiotemporal relationship between substrate and PS γ ^{129, 130} the effects the apparent substrate processing specificity for either PS1 γ or PS2 γ . PS1 γ has been shown to localize predominantly to the plasma membrane,^{33, 34} where CDH2 similarly localizes in particular in mature neurons^{131, 132} and fibroblasts.¹³³ PS2 γ , however, localizes to late endosomal/lysosomal compartments,^{33, 34, 40} co-localizing with PMEL and TYRP1.³⁴ Consequently, it is possible, given that the current findings show no PS binding preference for CDH2 or TYRP1, that in the absence of spatial barriers, PS1 γ may process TYRP1, and PS2 γ

may process CDH2. This has been shown for CDH2, where when PS2 is genetically altered to mimic PS1 localisation the resultant PS2 γ does process CDH2.³⁴ PMEL processing, however, clearly exhibits PS2 γ processing selectivity *in vitro*³⁴ and a clear MM-GB/SA preference for PS2 γ . Based on these results, WTMetaD combined with MM-GB/SA may be utilized to yield insights into substrate binding preferences for PS1 γ and PS2 γ .

These techniques were applied to a selection of A β metabolism related substrates, other than APP (which has already been extensively investigated in the same manner in Chapter 3). It was observed that substrates typically demonstrate a preference for either PS1 γ or PS2 γ , with only AXL showing no preference for binding either PS γ complex (Table 6-2). Although there is an absence of substantial data identifying processing specificity of substrates *in vitro*, subcellular co-localization may indicate that stronger protein-protein interactions are likely.¹³⁴ Indeed, RAGE¹³⁵, CD44,¹³⁶ APLP2,¹³⁷ and LDLR¹³⁸ all localise with Rab11 in recycling compartments, as does PS1, and all demonstrate a distinct binding preference for PS1 γ .³⁴ PS2 however has been shown to interact specifically with endocytic adaptor protein-1 (AP-1), and not AP-2 or AP-3, in early endosomes to late endosomes/lysosomes.³⁴ Interestingly, LRP1 which demonstrates a preference for PS2 γ binding also binds AP-1 indicating co-localisation in the same endocytic compartments,¹³⁹ whereas LDLR, which demonstrates a preference for binding PS1 γ , binds and localizes with AP-2.¹⁴⁰ *In vitro* processing of these substrates by either PS1 γ or PS2 γ will be particularly interesting to explore given the observed specific binding preferences.

Having established that there were substrate binding preferences for either PS1 γ or PS2 γ , it was next asked if the clinical heterogeneity observed between PS1 and PS2 ADAD mutations⁴⁶ might be related to the effect of these mutations on A β metabolism substrates more broadly, and not just APP. The effect of PS1 and PS2 mutations on the binding of multiple substrates was explored using alchemical perturbation. This method offers a theoretically more robust treatment of relative binding free energy compared to other commonly used approaches and has been shown to outperform these methods that are theoretically less rigorous.¹²¹ In the context of ADAD, PS mutation pathogenicity is typically assessed based on the impact on A β 42:A β 40, which has been demonstrated to correlate with the onset of the disease.¹¹³ Consequently, this study evaluated the influence of both pathogenic and benign variants in PS1 and PS2 on the binding energy of APP-CTF(A β 49) and APP-CTF(A β 48), which initiate the A β 40 and A β 42 pathways, respectively. This data was used to determine an optimal cut-off for

relative binding free energy that can be used to classify pathogenicity. Subsequently, this pathogenic cut-off value was used to analyse the alchemical perturbation results for $\Delta\Delta G_{mut}$. This analysis aimed to identify mutations associated with ADAD that might also have a pathogenic impact on the binding of substrates related to both A β generation and metabolism (Figure 6-5A). No substrates investigated here were consistently affected by all mutations examined. Similarly, no mutation had a consistent effect on all substrates. This is unsurprising given that mutations are broadly distributed throughout the PS1 and PS2 proteins, positioned at APH1 and PEN2 interfaces, within the substrate binding pore, and within the hydrophilic loop regions.^{36, 64, 75-77, 80, 82, 83} PS mutations have been shown to affect affinity and turnover,³⁶ γ -secretase subunit binding,¹⁴¹ enzyme conformation,^{82, 142} stability,⁶⁴ and subcellular localization,^{34, 141} and several mutations have multiple effects. For example, one mutation investigated here, PS1:G384A, is adjacent to the catalytic aspartate on the PS1-CTF, which directly engages with the substrate, and is part of the GXGD motif that is critical for γ -secretase activity,¹⁴³⁻¹⁴⁵ and as such decreases the reaction rate of both APP and Notch1 cleavage.^{36, 146} Consequently it is not surprising that the PS1:G384A mutation has a potentially pathogenic effect on substrate binding on all substrates, except the APP-CTF(48) substrate (Figure 6-5A). This result may also mechanistically explain why PS1:G384A is associated with an increase A β 42:A β 40 ratio,⁵⁰ as substrate binding of APP-CTF(48) – initiating A β 42 pathway – is not affected, while APP-CTF(49) – initiating A β 40 pathway – substrate binding affinity is reduced.

Pathogenic classifications of $\Delta\Delta G_{mut}$ occurred most frequently for ADAD mutations in complex with the RAGE and VLDLR substrates. Notably the effect of mutations on RAGE and VLDLR typically results in reduced (weaker) binding affinity (i.e. positive $\Delta\Delta G_{mut}$) (SI Table 6-1). In the context of AD and A β , RAGE is an influx A β receptor involved in transporting A β across the blood brain barrier (BBB), from the periphery to the brain parenchyma.¹⁰⁰ Ligand activation of RAGE initiates a positive feedback loop increasing cell surface expression, and A β influx from periphery.¹⁴⁷ RAGE ectodomain shedding, by ADAM10 or MMP9,¹⁴⁸ acts as a negative feedback mechanism, resulting in reduced cell surface expression of RAGE.¹⁴⁹ Ectodomain shedding of RAGE allows subsequent γ -secretase cleavage of the remaining C-terminal fragment and release of the RAGE intracellular domain (RICD).¹⁴⁸ Although the function of the RICD remains unknown, it is suggested to translocate to the nucleus, where it may facilitate transcription of genes, including RAGE.¹⁵⁰ Thus, one might speculate that PS mutations that affect the binding affinity of γ -secretase for RAGE may

dysregulate this negative feedback mechanism leading to an increase in RAGE expression, promoting increased A β influx.

VLDLR on the other hand facilitates chaperone (i.e. APOE, APOJ, and α 2M)¹⁵¹ mediated clearance of A β across the BBB from parenchyma to periphery,¹⁰⁴ regulates APOE expression¹⁵², and regulates APP cell surface expression and trafficking.¹⁰⁵ Interestingly, the regulation of APP is associated with FE65 interactions, which bind to the VLDLR intracellular domain to not only increase APP, but also VLDLR, cell surface expression, thus demonstrating autoregulation mechanisms.¹⁰⁵ By increasing APP cell surface expression and retention,¹⁰⁵ VLDLR may increase non-amyloidogenic processing of APP.^{153, 154} Furthermore, an increase in VLDLR at the cell surface increases the efflux of A β into the periphery.¹⁰⁴ The reduced binding affinity associated with PS1 mutations demonstrated here may therefore result in reduced VLDLR-ICD generation, leading to decreased expression and retention of APP on the cell surface, resulting in increased internalization of APP, favouring amyloidogenic processing.^{155, 156} A simultaneous decrease in VLDLR surface expression would likely diminish the A β clearance functions associated with this receptor.

Although only accounting for approximately 1% of AD cases,¹⁵⁷ the study of ADAD associated mutations in APP, PS1 and PS2 provides valuable insight into the pathogenic development of the disease, particularly in relation to A β . Consequently, several efforts have been made to identify relationships between the effect of PS mutations on A β 42:A β 40, and available clinical data, namely (AAO) and disease duration.^{17, 158} These studies, however investigate a limited number of mutations, and the opportunity for a meta-analysis is hampered by the use of different experimental systems. Recently, Sun et al. presented A β generation data for 138 PS1 mutations, in the same experimental system; however, their analysis of A β 42:A β 40 and mean AAO revealed no significant relationship.⁵⁰ Re-examination of the Sun data⁵⁰ with improved, curated AAO data sets, however, revealed a significant correlation between the A β 42:A β 40 and AAO.¹¹³ In the current study both the curated AAO data⁴⁶ and the experimental data from Sun et al.⁵⁰ were used to investigate whether any relationships between $\Delta\Delta G_{mut}$ results were evident. Correlation analyses were conducted to examine the relationship between ADAD associated PS1 and PS2 mutations $\Delta\Delta G_{mut}$ results for each substrate and AAO as a clinical marker of severity. Additionally, where data was available, correlations were explored between $\Delta\Delta G_{mut}$ results of PS1 mutations and the A β 42:A β 40 ratio, as well as the amount of A β 40 or A β 42, to identify potential relationships.

This analysis identified a significant negative correlation between $\Delta\Delta G_{mut}[APP-CTF(A\beta 49)]$ and AAO, for mutations in PS1 γ and PS2 γ , combined, indicating that mutations with an earlier age at onset have reduced (weaker) binding affinity (i.e. positive $\Delta\Delta G_{mut}$). After further interrogation the data was segregated and PS1 γ and PS2 γ $\Delta\Delta G_{mut}$ results analysed separately, where a significant relationship was only retained for PS1 γ mutations (Figure 6-6A-C). In contrast, a trend towards a significant relationship between $\Delta\Delta G_{mut}[APP-CTF(A\beta 48)]$ and AAO was only observed with the combined PS1 γ and PS2 γ mutations (Figure 6-6D-F). These results suggest that PS1 mutations have a specific effect on binding APP-CTF(A β 49), while the effect on binding APP-CTF(A β 48) is common to PS1 and PS2 mutations. It could be speculated that these PS1 mutations have a greater A β 42:A β 40 ratio by reducing A β 40 production, as APP-CTF(A β 49) initiates the A β 40 pathway, as opposed to increasing A β 42 generation, initiated by APP-CTF(A β 48) binding. These results support recent experimental evidence that PS1 mutations consistently reduced AICD(50-99) product component via cleavage at the APP-CTF(A β 49) site, compared to the AICD(49-99) produced by cleavage at the APP-CTF(A β 48) site.⁸² Further support for this notion can be taken from the significant positive correlation between A β 42:A β 40 and $\Delta\Delta G_{mut}[APP-CTF(A\beta 49)]$, where an increase in the relative binding energy, which reduces binding affinity, correlates with increased A β 42:A β 40 ratio (Figure 6-6G).

Analyses between the effect of mutations on the binding of other substrates with AAO, revealed a significant positive correlation with RAGE substrate for PS1 mutations (Figure 6-7C). This positive correlation indicates that PS1 mutations with earlier AAO are associated with increased binding affinity, while later AAO mutations have reduced binding affinity. The positive correlation observed suggests that PS1 mutations with a later AAO may lead to dysregulation of the negative feedback loop associated with proteolysis of RAGE.^{148, 149} This dysregulation, may lead to increased surface expression of RAGE, and subsequently an increase in the influx of A β from the periphery to the brain. When taken together with the observed negative correlation with APP-CTF(A β 49), it is tempting to speculate that the more aggressive PS1 mutations (associated with earlier AAO) have a more pronounced effect on A β generation. In contrast, the less aggressive PS1 mutations (associated with later AAO) may primarily impact A β clearance mechanisms. It must be noted that these conclusions cannot be extended to PS2 mutations as no significant correlations were observed between PS2 $\Delta\Delta G_{mut}$ results, for any substrate, and AAO. It should be acknowledged that the limited number of

ADAD-associated PS2 mutations identified, and investigated in this study, may account for the lack of any associations.

This study provides insight into the preferential binding of multiple A β metabolism related substrates for either PS1 γ or PS2 γ and the effect of PS mutations on the binding of these substrates. However, the limitations of this work must be acknowledged. As only two substrate bound γ -secretase structures have been solved,^{69, 70} there are limited homology modelling templates. Furthermore, collective variable space available for sampling by WTMetaD is limited, by the limited number of substrate bound structures and the lack of a complete high resolution unbound structure.⁶⁵⁻⁶⁸ This will improve as more substrate bound structures are solved, and along with it confidence in simulation results. Further to this, only a selection of mutations were examined; the addition of more mutations will improve confidence for, and interpretation of, results for the substrates examined thus far. However, it must also be acknowledged that the limited population frequency of PS mutations¹¹⁸ impacts on the quality of clinical data available for the majority of mutations. Additionally, only a selection of substrates have been examined, it is possible that mutations are affecting other substrates of γ -secretase, also involved in A β metabolism that have not been explored here, or those implicated in other aspects of neurodegeneration, including cell proliferation, immune response, synapse regulation and axonal outgrowth.⁸⁴ Future studies aimed at validating the substrate preferences and binding affinities of both wildtype and PS mutant γ -secretase employing biochemical and biophysical assays are required. This data, in turn, can enhance computational models, particularly in instances where new structural information is not forthcoming.

In conclusion, this study employs WTMetaD and MM-GB/SA, along with alchemical perturbation, to explore substrate binding preferences of PS1 γ and PS2 γ complexes for A β metabolism related substrates, and the subsequent effect of PS mutations. The findings presented here have shed light on the interactions underlying AD pathogenesis. The investigation reveals distinct substrate preferences, and identifies significant effects of, particularly PS1 mutations on binding on APP-CTF(A β 49), potentially affecting A β 40 generation in a loss of function manner. Despite limitations in available clinical data and computational approaches, this research contributes to the understanding of how PS mutations might influence substrate binding and, consequently, explain the observed disease heterogeneity of ADAD. Future studies incorporating a broader spectrum of mutations, substrates, and experimental techniques will be crucial for a more comprehensive

understanding of the complex mechanisms underlying AD and related mutations, ultimately advancing therapeutic strategies and drug design.

6.5 REFERENCES

1. Selkoe, D. J., and Hardy, J. (2016) The amyloid hypothesis of Alzheimer's disease at 25 years. *EMBO Molecular Medicine* **8**, 595-608
2. Ismail, R., Parbo, P., Madsen, L. S., Hansen, A. K., Hansen, K. V., et al. (2020) The relationships between neuroinflammation, beta-amyloid and tau deposition in Alzheimer's disease: a longitudinal PET study. *Journal of Neuroinflammation* **17**, 151
3. Tan, J. Z. A., and Gleeson, P. A. (2019) The role of membrane trafficking in the processing of amyloid precursor protein and production of amyloid peptides in Alzheimer's disease. *Biochimica et Biophysica Acta (BBA) - Biomembranes* **1861**, 697-712
4. Hur, J.-Y. (2022) γ -Secretase in Alzheimer's disease. *Experimental & Molecular Medicine* **54**, 433-446
5. Ries, M., and Sastre, M. (2016) Mechanisms of A β Clearance and Degradation by Glial Cells. *Frontiers in Aging Neuroscience* **8**
6. Zuroff, L., Daley, D., Black, K. L., and Koronyo-Hamaoui, M. (2017) Clearance of cerebral A β in Alzheimer's disease: reassessing the role of microglia and monocytes. *Cellular and Molecular Life Sciences* **74**, 2167-2201
7. Golde, T. E., Estus, S., Younkin, L. H., Selkoe, D. J., and Younkin, S. G. (1992) Processing of the amyloid protein precursor to potentially amyloidogenic derivatives. *Science* **255**, 728-730
8. Haass, C., Hung, A. Y., Schlossmacher, M. G., Teplow, D. B., and Selkoe, D. J. (1993) beta-Amyloid peptide and a 3-kDa fragment are derived by distinct cellular mechanisms. *The Journal of Biological Chemistry* **268**, 3021-3024
9. Haass, C., Lemere, C. A., Capell, A., Citron, M., Seubert, P., et al. (1995) The Swedish mutation causes early-onset Alzheimer's disease by β -secretase cleavage within the secretory pathway. *Nature Medicine* **1**, 1291-1296
10. Vassar, R., Bennett, B. D., Babu-Khan, S., Kahn, S., Mendiaz, E. A., et al. (1999) β -Secretase Cleavage of Alzheimer's Amyloid Precursor Protein by the Transmembrane Aspartic Protease BACE. *Science* **286**, 735-741
11. Simons, M., de Strooper, B., Multhaup, G., Tienari, P., Dotti, C., et al. (1996) Amyloidogenic processing of the human amyloid precursor protein in primary cultures of rat hippocampal neurons. *The Journal of Neuroscience* **16**, 899-908
12. Hartmann, T., Bieger, S. C., Brühl, B., Tienari, P. J., Ida, N., et al. (1997) Distinct sites of intracellular production for Alzheimer's disease A β 40/42 amyloid peptides. *Nature Medicine* **3**, 1016-1020
13. Annaert, W. G., Levesque, L., Craessaerts, K., Dierinck, I., Snellings, G., et al. (1999) Presenilin 1 Controls γ -Secretase Processing of Amyloid Precursor Protein in Pre-Golgi Compartments of Hippocampal Neurons. *The Journal of Cell Biology* **147**, 277-294
14. Herreman, A., Serneels, L., Annaert, W., Desiré, C., Schoonjans, L., et al. (2000) Total inactivation of γ -secretase activity in presenilin-deficient embryonic stem cells. *Nature Cell Biology* **2**, 461-462
15. Kimberly, W. T., Xia, W., Rahmati, T., Wolfe, M. S., and Selkoe, D. J. (2000) The transmembrane aspartates in presenilin 1 and 2 are obligatory for γ -secretase activity and amyloid β -protein generation. *The Journal of Biological Chemistry* **275**, 3173-3178

16. Acx, H., Chávez-Gutiérrez, L., Serneels, L., Lismont, S., Benurwar, M., et al. (2014) Signature amyloid β profiles are produced by different γ -secretase complexes. *The Journal of Biological Chemistry* **289**, 4346-4355
17. Petit, D., Fernández, S. G., Zoltowska, K. M., Enzlein, T., Ryan, N. S., et al. (2022) A β profiles generated by Alzheimer's disease causing PSEN1 variants determine the pathogenicity of the mutation and predict age at disease onset. *Molecular Psychiatry* **27**, 2821-2832
18. Kuhn, P.-H., Wang, H., Dislich, B., Colombo, A., Zeitschel, U., et al. (2010) ADAM10 is the physiologically relevant, constitutive α -secretase of the amyloid precursor protein in primary neurons. *The EMBO Journal* **29**, 3020-3032
19. Esch, F. S., Keim, P. S., Beattie, E. C., Blacher, R. W., Culwell, A. R., et al. (1990) Cleavage of amyloid beta peptide during constitutive processing of its precursor. *Science* **248**, 1122-1124
20. Haass, C., Koo, E. H., Capell, A., Teplow, D. B., and Selkoe, D. J. (1995) Polarized sorting of beta-amyloid precursor protein and its proteolytic products in MDCK cells is regulated by two independent signals. *The Journal of Cell Biology* **128**, 537-547
21. Kuentzel, S. L., Ali, S. M., Altman, R. A., Greenberg, B. D., and Raub, T. J. (1993) The Alzheimer beta-amyloid protein precursor/protease nexin-II is cleaved by secretase in a trans-Golgi secretory compartment in human neuroglioma cells. *Biochemical Journal* **295** (Pt 2), 367-378
22. Buxbaum, J. D., Liu, K. N., Luo, Y., Slack, J. L., Stocking, K. L., et al. (1998) Evidence that tumor necrosis factor alpha converting enzyme is involved in regulated alpha-secretase cleavage of the Alzheimer amyloid protein precursor. *The Journal of Biological Chemistry* **273**, 27765-27767
23. Lammich, S., Kojro, E., Postina, R., Gilbert, S., Pfeiffer, R., et al. (1999) Constitutive and regulated alpha-secretase cleavage of Alzheimer's amyloid precursor protein by a disintegrin metalloprotease. *Proceedings of the National Academy of Sciences of the United States of America* **96**, 3922-3927
24. Veugelen, S., Saito, T., Saido, T. C., Chávez-Gutiérrez, L., and De Strooper, B. (2016) Familial Alzheimer's Disease Mutations in Presenilin Generate Amyloidogenic A[beta] Peptide Seeds. *Neuron* **90**, 410-416
25. Bolduc, D. M., Montagna, D. R., Gu, Y., Selkoe, D. J., and Wolfe, M. S. (2016) Nicastrin functions to sterically hinder γ -secretase-substrate interactions driven by substrate transmembrane domain. *Proceedings of the National Academy of Sciences of the United States of America* **113**, E509-E518
26. Yan, Y., Xu, T.-H., Melcher, K., and Xu, H. E. (2017) Defining the minimum substrate and charge recognition model of gamma-secretase. *Acta Pharmacologica Sinica*
27. Bolduc, D. M., Montagna, D. R., Seghers, M. C., Wolfe, M. S., and Selkoe, D. J. (2016) The amyloid-beta forming tripeptide cleavage mechanism of γ -secretase. *eLife* **5**, e17578
28. Barthelson, K., Newman, M., and Lardelli, M. (2020) Sorting Out the Role of the Sortilin-Related Receptor 1 in Alzheimer's Disease. *Journal of Alzheimer's Disease Reports* **4**, 123-140
29. Pardossi-Piquard, R., Petit, A., Kawarai, T., Sunyach, C., Da Costa, C. A., et al. (2005) Presenilin-dependent transcriptional control of the A β -degrading enzyme neprilysin by intracellular domains of β APP and APLP. *Neuron* **46**, 541-554
30. Deane, R., Wu, Z., Sagare, A., Davis, J., Du Yan, S., et al. (2004) LRP/Amyloid β -Peptide Interaction Mediates Differential Brain Efflux of A β Isoforms. *Neuron* **43**, 333-344
31. Zhao, Y., Wu, X., Li, X., Jiang, L.-L., Gui, X., et al. (2018) TREM2 Is a Receptor for β -Amyloid that Mediates Microglial Function. *Neuron* **97**, 1023-1031.e1027

32. Bellenguez, C., Küçükali, F., Jansen, I. E., Kleineidam, L., Moreno-Grau, S., et al. (2022) New insights into the genetic etiology of Alzheimer's disease and related dementias. *Nature Genetics* **54**, 412-436
33. Meckler, X., and Checler, F. (2016) Presenilin 1 and presenilin 2 target γ -secretase complexes to distinct cellular compartments. *The Journal of Biological Chemistry* **291**, 12821-12837
34. Sannerud, R., Esselens, C., Ejsmont, P., Mattera, R., Rochin, L., et al. (2016) Restricted location of PSEN2/ γ -secretase determines substrate specificity and generates an intracellular A β pool. *Cell* **166**, 193-208
35. Eccles, M. K., Main, N., Sabale, M., Roberts-Mok, B., Agostino, M., et al. (2023) Quantitative Comparison of Presenilin Protein Expression Reveals Greater Activity of PS2- γ -Secretase. *bioRxiv*, 2023.2005.2009.540102
36. Chávez-Gutiérrez, L., Bammens, L., Benilova, I., Vandersteen, A., Benurwar, M., et al. (2012) The mechanism of γ -Secretase dysfunction in familial Alzheimer disease. *The EMBO Journal* **31**, 2261-2274
37. Lessard, C. B., Rodriguez, E., Ladd, T. B., Minter, L. M., Osborne, B. A., et al. (2019) Individual and combined presenilin 1 and 2 knockouts reveal that both have highly overlapping functions in HEK293T cells. *Journal of Biological Chemistry* **294**, 11276-11285
38. Pimenova, A. A., and Goate, A. M. (2020) Novel presenilin 1 and 2 double knock-out cell line for in vitro validation of PSEN1 and PSEN2 mutations. *Neurobiology of Disease*, 104785
39. Placanica, L., Tarassishin, L., Yang, G., Peethumnongsin, E., Kim, S.-H., et al. (2009) Pen2 and presenilin-1 modulate the dynamic equilibrium of presenilin-1 and presenilin-2 γ -secretase complexes. *The Journal of Biological Chemistry* **284**, 2967-2977
40. Watanabe, H., Imaizumi, K., Cai, T., Zhou, Z., Tomita, T., et al. (2021) Flexible and accurate substrate processing with distinct presenilin/ γ -secretases in human cortical neurons. *eNeuro* **8**, ENEURO.0500-0520.2021
41. Yonemura, Y., Futai, E., Yagishita, S., Kaether, C., and Ishiura, S. (2016) Specific combinations of presenilins and Aph1s affect the substrate specificity and activity of γ -secretase. *Biochemical and Biophysical Research Communications* **478**, 1751-1757
42. Yonemura, Y., Futai, E., Yagishita, S., Suo, S., Tomita, T., et al. (2011) Comparison of presenilin 1 and presenilin 2 γ -secretase activities using a yeast reconstitution system. *The Journal of Biological Chemistry* **286**, 44569-44575
43. Jayadev, S., Case, A., Eastman, A. J., Nguyen, H., Pollak, J., et al. (2010) Presenilin 2 Is the Predominant γ -Secretase in Microglia and Modulates Cytokine Release. *PLoS One* **5**
44. Agrawal, V., Sawhney, N., Hickey, E., and McCarthy, J. V. (2016) Loss of Presenilin 2 Function Is Associated with Defective LPS-Mediated Innate Immune Responsiveness. *Molecular Neurobiology* **53**, 3428-3438
45. Farfara, D., Trudler, D., Segev-Amzaleg, N., Galron, R., Stein, R., et al. (2011) γ -Secretase component presenilin is important for microglia β -amyloid clearance. *Annals of Neurology* **69**, 170-180
46. Ryman, D. C., Acosta-Baena, N., Aisen, P. S., Bird, T., Danek, A., et al. (2014) Symptom onset in autosomal dominant Alzheimer disease: A systematic review and meta-analysis. *Neurology* **83**, 253-260
47. Cai, Y., An, S. S. A., and Kim, S. (2015) Mutations in presenilin 2 and its implications in Alzheimer's disease and other dementia-associated disorders. *Clinical interventions in aging* **10**, 1163-1172
48. Dong, L., Liu, C., Sha, L., Mao, C., Li, J., et al. (2022) PSEN2 Mutation Spectrum and Novel Functionally Validated Mutations in Alzheimer's Disease: Data from PUMCH Dementia Cohort. *Journal of Alzheimer's Disease* **87**, 1549-1556

49. Jayadev, S., Leverenz, J. B., Steinbart, E., Stahl, J., Klunk, W., et al. (2010) Alzheimer's disease phenotypes and genotypes associated with mutations in presenilin 2. *Brain* **133**, 1143-1154
50. Sun, L., Zhou, R., Yang, G., and Shi, Y. (2017) Analysis of 138 pathogenic mutations in presenilin-1 on the in vitro production of A β 42 and A β 40 peptides by γ -secretase. *Proceedings of the National Academy of Sciences of the United States of America* **114**, E476-E485
51. Heilig, E. A., Gutti, U., Tai, T., Shen, J., and Kelleher, R. J. (2013) Trans-Dominant Negative Effects of Pathogenic PSEN1 Mutations on γ -Secretase Activity and A β Production. *The Journal of Neuroscience* **33**, 11606-11617
52. Yang, Y., Bagyinszky, E., and An, S. S. A. (2023) Presenilin-1 (PSEN1) Mutations: Clinical Phenotypes beyond Alzheimer's Disease. *International Journal of Molecular Sciences* **24**, 8417
53. Gianni, D., Li, A., Tesco, G., McKay, K. M., Moore, J., et al. (2010) Protein Aggregates and Novel Presenilin Gene Variants in Idiopathic Dilated Cardiomyopathy. *Circulation* **121**, 1216-1226
54. Li, D., Parks, S. B., Kushner, J. D., Nauman, D., Burgess, D., et al. (2006) Mutations of presenilin genes in dilated cardiomyopathy and heart failure. *The American Journal of Human Genetics* **79**, 1030-1039
55. To, M. D., Gokgoz, N., Doyle, T. G., Donoviel, D. B., Knight, J. A., et al. (2006) Functional characterization of novel presenilin-2 variants identified in human breast cancers. *Oncogene* **25**, 3557-3564
56. Fung, S., Smith, C. L., Prater, K. E., Case, A., Green, K., et al. (2020) Early-Onset Familial Alzheimer Disease Variant PSEN2 N141I Heterozygosity is Associated with Altered Microglia Phenotype. *Journal of Alzheimer's Disease* **77**, 675-688
57. Lee, J., Chan, S. L., and Mattson, M. P. (2002) Adverse effect of a presenilin-1 mutation in microglia results in enhanced nitric oxide and inflammatory cytokine responses to immune challenge in the brain. *Neuromolecular Medicine* **2**, 29-45
58. Nam, H., Lee, Y., Kim, B., Lee, J.-W., Hwang, S., et al. (2022) Presenilin 2 N141I mutation induces hyperactive immune response through the epigenetic repression of REV-ERB α . *Nature Communications* **13**, 1972
59. Ledo, J. H., Liebmann, T., Zhang, R., Chang, J. C., Azevedo, E. P., et al. (2021) Presenilin 1 phosphorylation regulates amyloid- β degradation by microglia. *Molecular Psychiatry* **26**, 5620-5635
60. Cataldo, A. M., Peterhoff, C. M., Schmidt, S. D., Terio, N. B., Duff, K., et al. (2004) Presenilin Mutations in Familial Alzheimer Disease and Transgenic Mouse Models Accelerate Neuronal Lysosomal Pathology. *Journal of Neuropathology & Experimental Neurology* **63**, 821-830
61. Merilahti, J. A. M., Ojala, V. K., Knittle, A. M., Pulliainen, A. T., and Elenius, K. (2017) Genome-wide screen of gamma-secretase-mediated intramembrane cleavage of receptor tyrosine kinases. *Molecular Biology of the Cell* **28**, 3123-3131
62. Wunderlich, P., Glebov, K., Kemmerling, N., Tien, N. T., Neumann, H., et al. (2013) Sequential proteolytic processing of the triggering receptor expressed on myeloid cells-2 (TREM2) protein by ectodomain shedding and γ -secretase-dependent intramembraneous cleavage. *The Journal of Biological Chemistry* **288**, 33027-33036
63. Kamp, F., Winkler, E., Trambauer, J., Ebke, A., Fluhner, R., et al. (2015) Intramembrane Proteolysis of β -Amyloid Precursor Protein by γ -Secretase Is an Unusually Slow Process. *Biophysical Journal* **108**, 1229-1237

64. Szaruga, M., Munteanu, B., Lismont, S., Veugelen, S., Horr , K., et al. (2017) Alzheimer's-Causing Mutations Shift A β Length by Destabilizing γ -Secretase-A β n Interactions. *Cell* **170**, 443-456.e414
65. Bai, X.-c., Rajendra, E., Yang, G., Shi, Y., and Scheres, S. H. W. (2015) Sampling the conformational space of the catalytic subunit of human γ -secretase. *eLife* **4**, e11182
66. Guo, X., Wang, Y., Zhou, J., Jin, C., Wang, J., et al. (2022) Molecular basis for isoform-selective inhibition of presenilin-1 by MRK-560. *Nature Communications* **13**, 6299
67. Sun, L., Zhao, L., Yang, G., Yan, C., Zhou, R., et al. (2015) Structural basis of human γ -secretase assembly. *Proceedings of the National Academy of Sciences of the United States of America* **112**, 6003-6008
68. Yang, G., Zhou, R., Guo, X., Yan, C., Lei, J., et al. (2021) Structural basis of γ -secretase inhibition and modulation by small molecule drugs. *Cell* **184**, 521-533.e514
69. Yang, G., Zhou, R., Zhou, Q., Guo, X., Yan, C., et al. (2018) Structural basis of Notch recognition by human γ -secretase. *Nature*
70. Zhou, R., Yang, G., Guo, X., Zhou, Q., Lei, J., et al. (2019) Recognition of the amyloid precursor protein by human γ -secretase. *Science*, eaaw0930
71. Bhattarai, A., Devkota, S., Bhattarai, S., Wolfe, M. S., and Miao, Y. (2020) Mechanisms of γ -Secretase Activation and Substrate Processing. *ACS Central Science* **6**, 969-983
72. Dehury, B., Tang, N., Mehra, R., Blundell, T. L., and Kepp, K. P. (2020) Side-by-side comparison of Notch- and C83 binding to γ -secretase in a complete membrane model at physiological temperature. *RSC Advances* **10**, 31215-31232
73. Bhattarai, A., Devkota, S., Do, H. N., Wang, J., Bhattarai, S., et al. (2022) Mechanism of Tripeptide Trimming of Amyloid β -Peptide 49 by γ -Secretase. *Journal of the American Chemical Society* **144**, 6215-6226
74. Chen, S. Y., and Zacharias, M. (2022) An internal docking site stabilizes substrate binding to γ -secretase: Analysis by molecular dynamics simulations. *Biophysical Journal* **121**, 2330-2344
75. Somavarapu, A. K., and Kepp, K. P. (2016) Loss of stability and hydrophobicity of presenilin 1 mutations causing Alzheimer's disease. *Journal of Neurochemistry* **137**, 101-111
76. Ch vez-Garc a, C., Aguayo-Ortiz, R., and Dominguez, L. (2019) Quantifying correlations between mutational sites in the catalytic subunit of γ -secretase. *Journal of Molecular Graphics and Modelling* **88**, 221-227
77. Mehra, R., and Kepp, K. P. (2019) Computational analysis of Alzheimer-causing mutations in amyloid precursor protein and presenilin 1. *Archives of Biochemistry and Biophysics* **678**, 108168
78. Tang, N., Dehury, B., and Kepp, K. P. (2019) Computing the Pathogenicity of Alzheimer's Disease Presenilin 1 Mutations. *Journal of Chemical Information and Modeling* **59**, 858-870
79. Chen, S.-Y., and Zacharias, M. (2020) How Mutations Perturb γ -Secretase Active Site Studied by Free Energy Simulations. *ACS Chemical Neuroscience* **11**, 3321-3332
80. Dehury, B., Somavarapu, A. K., and Kepp, K. P. (2020) A computer-simulated mechanism of familial Alzheimer's disease: Mutations enhance thermal dynamics and favor looser substrate-binding to γ -secretase. *Journal of Structural Biology* **212**, 107648
81. Soto-Ospina, A., Araque Mar n, P., Bedoya, G., Sepulveda-Falla, D., and Villegas Lanau, A. (2021) Protein Predictive Modeling and Simulation of Mutations of Presenilin-1 Familial Alzheimer's Disease on the Orthosteric Site. *Frontiers in Molecular Biosciences* **8**, 649990

82. Do, H. N., Devkota, S., Bhattarai, A., Wolfe, M. S., and Miao, Y. (2023) Effects of presenilin-1 familial Alzheimer's disease mutations on γ -secretase activation for cleavage of amyloid precursor protein. *Communications Biology* **6**, 174
83. Dehury, B., Tang, N., and Kepp, K. P. (2020) Insights into membrane-bound presenilin 2 from all-atom molecular dynamics simulations. *Journal of Biomolecular Structure and Dynamics* **38**, 3196-3210
84. Güner, G., and Lichtenthaler, S. F. (2020) The substrate repertoire of γ -secretase/presenilin. *Seminars in Cell & Developmental Biology* **105**, 27-42
85. Haapasalo, A., and Kovacs, D. M. (2011) The Many Substrates of Presenilin/ γ -Secretase. *Journal of Alzheimer's Disease* **25**, 3-28
86. (2017) UniProt: the universal protein knowledgebase. *Nucleic Acids Research* **45**, D158-D169
87. Song, J., Li, F., Leier, A., Marquez-Lago, T. T., Akutsu, T., et al. (2017) PROSPEROus: high-throughput prediction of substrate cleavage sites for 90 proteases with improved accuracy. *Bioinformatics* **34**, 684-687
88. Kaden, D., Voigt, P., Munter, L.-M., Bobowski, K. D., Schaefer, M., et al. (2009) Subcellular localization and dimerization of APLP1 are strikingly different from APP and APLP2. *Journal of Cell Science* **122**, 368-377
89. Eggert, S., Midthune, B., Cottrell, B., and Koo, E. H. (2009) Induced Dimerization of the Amyloid Precursor Protein Leads to Decreased Amyloid- β Protein Production *The Journal of Biological Chemistry* **284**, 28943-28952
90. Huang, Y., Happonen, K. E., Burrola, P. G., O'Connor, C., Hah, N., et al. (2021) Microglia use TAM receptors to detect and engulf amyloid β plaques. *Nature Immunology* **22**, 586-594
91. Zhao, W., Fan, J., Kulic, I., Koh, C., Clark, A., et al. (2020) Axl receptor tyrosine kinase is a regulator of apolipoprotein E. *Molecular Brain* **13**, 66
92. Takahashi, K., Eto, H., and Tanabe, K. K. (1999) Involvement of CD44 in matrix metalloproteinase-2 regulation in human melanoma cells. *International Journal of Cancer* **80**, 387-395
93. Dorandish, S., Williams, A., Atali, S., Sendo, S., Price, D., et al. (2021) Regulation of amyloid- β levels by matrix metalloproteinase-2/9 (MMP2/9) in the media of lung cancer cells. *Scientific Reports* **11**, 9708
94. Zhao, L., Teter, B., Morihara, T., Lim, G. P., Ambegaokar, S. S., et al. (2004) Insulin-degrading enzyme as a downstream target of insulin receptor signaling cascade: implications for Alzheimer's disease intervention. *The Journal of Neuroscience* **24**, 11120-11126
95. Castellano, J. M., Deane, R., Gottesdiener, A. J., Verghese, P. B., Stewart, F. R., et al. (2012) Low-density lipoprotein receptor overexpression enhances the rate of brain-to-blood A β clearance in a mouse model of β -amyloidosis. *Proceedings of the National Academy of Sciences of the United States of America* **109**, 15502-15507
96. Castellano, J. M., Kim, J., Stewart, F. R., Jiang, H., DeMattos, R. B., et al. (2011) Human apoE isoforms differentially regulate brain amyloid- β peptide clearance. *Science Translational Medicine* **3**, 89ra57
97. Kim, J., Castellano, J. M., Jiang, H., Basak, J. M., Parsadanian, M., et al. (2009) Overexpression of low-density lipoprotein receptor in the brain markedly inhibits amyloid deposition and increases extracellular A beta clearance. *Neuron* **64**, 632-644
98. Hoe, H. S., Wessner, D., Beffert, U., Becker, A. G., Matsuoka, Y., et al. (2005) F-spondin interaction with the apolipoprotein E receptor ApoEr2 affects processing of amyloid precursor protein. *Molecular and Cellular Biology* **25**, 9259-9268
99. He, X., Cooley, K., Chung, C. H., Dashti, N., and Tang, J. (2007) Apolipoprotein receptor 2 and X11 alpha/beta mediate apolipoprotein E-induced endocytosis of amyloid-beta

- precursor protein and beta-secretase, leading to amyloid-beta production. *The Journal of Neuroscience* **27**, 4052-4060
100. Deane, R., Du Yan, S., Subramanian, R. K., LaRue, B., Jovanovic, S., et al. (2003) RAGE mediates amyloid- β peptide transport across the blood-brain barrier and accumulation in brain. *Nature Medicine* **9**, 907-913
101. Gustafsen, C., Glerup, S., Pallesen, L. T., Olsen, D., Andersen, O. M., et al. (2013) Sortilin and SorLA display distinct roles in processing and trafficking of amyloid precursor protein. *The Journal of Neuroscience* **33**, 64-71
102. Carlo, A. S., Gustafsen, C., Mastrobuoni, G., Nielsen, M. S., Burgert, T., et al. (2013) The pro-neurotrophin receptor sortilin is a major neuronal apolipoprotein E receptor for catabolism of amyloid- β peptide in the brain. *The Journal of Neuroscience* **33**, 358-370
103. Lessard, C. B., Malnik, S. L., Zhou, Y., Ladd, T. B., Cruz, P. E., et al. (2018) High-affinity interactions and signal transduction between A β oligomers and TREM2. *EMBO Molecular Medicine* **10**, e9027
104. Deane, R., Sagare, A., Hamm, K., Parisi, M., Lane, S., et al. (2008) apoE isoform-specific disruption of amyloid beta peptide clearance from mouse brain. *The Journal of Clinical Investigation* **118**, 4002-4013
105. Dumanis, S. B., Chamberlain, K. A., Jin Sohn, Y., Jin Lee, Y., Guénette, S. Y., et al. (2012) FE65 as a link between VLDLR and APP to regulate their trafficking and processing. *Molecular Neurodegeneration* **7**, 9
106. Karlsson, M., Zhang, C., Méar, L., Zhong, W., Digre, A., et al. (2021) A single-cell type transcriptomics map of human tissues. *Science Advances* **7**, eabh2169
107. Sankar, K., Krystek Jr, S. R., Carl, S. M., Day, T., and Maier, J. K. X. (2018) AggScore: Prediction of aggregation-prone regions in proteins based on the distribution of surface patches. *Proteins: Structure, Function, and Bioinformatics* **86**, 1147-1156
108. Jo, S., Cheng, X., Lee, J., Kim, S., Park, S.-J., et al. (2017) CHARMM-GUI 10 Years for Biomolecular Modeling and Simulation. *Journal of Computational Chemistry* **38**, 1114-1124
109. Salomon-Ferrer, R., Case, D. A., and Walker, R. C. (2013) An overview of the Amber biomolecular simulation package. *Wiley Interdisciplinary Reviews: Computational Molecular Science* **3**, 198-210
110. Sousa da Silva, A. W., and Vranken, W. F. (2012) ACPYPE - AnteChamber PYthon Parser interface. *BMC Research Notes* **5**, 367
111. Abraham, M. J., Murtola, T., Schulz, R., Páll, S., Smith, J. C., et al. (2015) GROMACS: High performance molecular simulations through multi-level parallelism from laptops to supercomputers. *SoftwareX* **1-2**, 19-25
112. Tribello, G. A., Bonomi, M., Branduardi, D., Camilloni, C., and Bussi, G. (2014) PLUMED 2: New feathers for an old bird. *Computer Physics Communications* **185**, 604-613
113. Tang, N., and Kepp, K. P. (2018) A β 42/A β 40 Ratios of Presenilin 1 Mutations Correlate with Clinical Onset of Alzheimer's Disease. *Journal of Alzheimer's Disease* **66**, 939-945
114. Cruts, M., Theuns, J., and Van Broeckhoven, C. (2012) Locus-specific mutation databases for neurodegenerative brain diseases. *Human Mutation* **33**, 1340-1344
115. Alzforum. Mutation Database. In *Alzforum* Vol. 2018, Alzforum, Cambridge (USA)
116. Wang, G., Zhang, D.-F., Jiang, H.-Y., Fan, Y., Ma, L., et al. (2019) Mutation and association analyses of dementia-causal genes in Han Chinese patients with early-onset and familial Alzheimer's disease. *Journal of Psychiatric Research* **113**, 141-147
117. Niu, F., Yu, S., Zhang, Z., Yi, X., Ye, L., et al. (2014) A novel mutation in the PSEN2 gene (N141Y) associated with early-onset autosomal dominant Alzheimer's disease in a Chinese Han family. *Neurobiology of Aging* **35**, 2420.e2421-2420.e2425

118. Karczewski, K. J., Francioli, L. C., Tiao, G., Cummings, B. B., Alföldi, J., et al. (2020) The mutational constraint spectrum quantified from variation in 141,456 humans. *Nature* **581**, 434-443
119. Schrodinger, LLC. The PyMOL Molecular Graphics System, Version 2.1.0.
120. Omasits, U., Ahrens, C. H., Müller, S., and Wollscheid, B. (2013) Protter: interactive protein feature visualization and integration with experimental proteomic data. *Bioinformatics* **30**, 884-886
121. Blake, S., Hemming, I., Heng, J. I.-T., and Agostino, M. (2021) Structure-Based Approaches to Classify the Functional Impact of ZBTB18 Missense Variants in Health and Disease. *ACS Chemical Neuroscience* **12**, 979-989
122. Gapsys, V., Michielssens, S., Seeliger, D., and de Groot, B. L. (2015) pmx: Automated protein structure and topology generation for alchemical perturbations. *Journal of Computational Chemistry* **36**, 348-354
123. Aldeghi, M., Gapsys, V., and de Groot, B. L. (2018) Accurate Estimation of Ligand Binding Affinity Changes upon Protein Mutation. *ACS Central Science* **4**, 1708-1718
124. Bennett, C. H. (1976) Efficient estimation of free energy differences from Monte Carlo data. *Journal of Computational Physics* **22**, 245-268
125. Czirr, E., Leuchtenberger, S., Dorner-Ciossek, C., Schneider, A., Jucker, M., et al. (2007) Insensitivity to A β 42-lowering Nonsteroidal Anti-inflammatory Drugs and γ -Secretase Inhibitors Is Common among Aggressive Presenilin-1 Mutations. *The Journal of Biological Chemistry* **282**, 24504-24513
126. Lai, M.-T., Chen, E., Crouthamel, M.-C., DiMuzio-Mower, J., Xu, M., et al. (2003) Presenilin-1 and presenilin-2 exhibit distinct yet overlapping γ -secretase activities. *The Journal of Biological Chemistry* **278**, 22475-22481
127. Pintchovski, S. A., Schenk, D. B., and Basi, G. S. (2013) Evidence that enzyme processivity mediates differential A β production by PS1 and PS2. *Current Alzheimer Research* **10**, 4-10
128. Shirovani, K., Tomioka, M., Kremmer, E., Haass, C., and Steiner, H. (2007) Pathological activity of familial Alzheimer's disease-associated mutant presenilin can be executed by six different γ -secretase complexes. *Neurobiology of Disease* **27**, 102-107
129. Tarassishin, L., Yin, Y. I., Bassit, B., and Li, Y. M. (2004) Processing of Notch and amyloid precursor protein by γ -secretase is spatially distinct. *Proceedings of the National Academy of Sciences of the United States of America* **101**, 17050-17055
130. Vetrivel, K. S., Cheng, H., Kim, S.-H., Chen, Y., Barnes, N. Y., et al. (2005) Spatial Segregation of γ -Secretase and Substrates in Distinct Membrane Domains. *The Journal of Biological Chemistry* **280**, 25892-25900
131. Yam, P. T., Pincus, Z., Gupta, G. D., Bashkurov, M., Charron, F., et al. (2013) N-Cadherin Relocalizes from the Periphery to the Center of the Synapse after Transient Synaptic Stimulation in Hippocampal Neurons. *PLOS ONE* **8**, e79679
132. Horn, Z., Behesti, H., and Hatten, M. E. (2018) N-cadherin provides a cis and trans ligand for astrotactin that functions in glial-guided neuronal migration. *Proceedings of the National Academy of Sciences of the United States of America* **115**, 10556-10563
133. Mary, S., Charrasse, S., Meriane, M., Comunale, F., Travo, P., et al. (2002) Biogenesis of N-cadherin-dependent cell-cell contacts in living fibroblasts is a microtubule-dependent kinesin-driven mechanism. *Molecular Biology of the Cell* **13**, 285-301
134. Peng, J., Svetec, N., and Zhao, L. (2022) Intermolecular Interactions Drive Protein Adaptive and Coadaptive Evolution at Both Species and Population Levels. *Molecular Biology and Evolution* **39**

135. Perrone, L., Peluso, G., and Melone, M. A. (2008) RAGE recycles at the plasma membrane in S100B secretory vesicles and promotes Schwann cells morphological changes. *Journal of Cellular Physiology* **217**, 60-71
136. López-Ortega, O., and Santos-Argumedo, L. (2017) Myosin 1g Contributes to CD44 Adhesion Protein and Lipid Rafts Recycling and Controls CD44 Capping and Cell Migration in B Lymphocytes. *Frontiers in Immunology* **8**, 1731
137. Tuli, A., Sharma, M., Wang, X., Simone, L. C., Capek, H. L., et al. (2009) Amyloid precursor-like protein 2 association with HLA class I molecules. *Cancer Immunology, Immunotherapy* **58**, 1419-1431
138. Hu, J., Zhu, Z., Chen, Z., Yang, Q., Liang, W., et al. (2022) Alteration in Rab11-mediated endocytic trafficking of LDL receptor contributes to angiotensin II-induced cholesterol accumulation and injury in podocytes. *Cell Proliferation* **55**, e13229
139. Guttman, M., Betts, G. N., Barnes, H., Ghassemian, M., van der Geer, P., et al. (2009) Interactions of the NPXY microdomains of the low density lipoprotein receptor-related protein 1. *Proteomics* **9**, 5016-5028
140. Boll, W., Rapoport, I., Brunner, C., Modis, Y., Prehn, S., et al. (2002) The μ 2 Subunit of the Clathrin Adaptor AP-2 Binds to FDNPVY and YppØ Sorting Signals at Distinct Sites. *Traffic* **3**, 590-600
141. Chen, W.-t., Hsieh, Y.-f., Huang, Y.-j., Lin, C.-c., Lin, Y.-t., et al. (2015) G206D Mutation of Presenilin-1 Reduces Pen2 Interaction, Increases A β 42/A β 40 Ratio and Elevates ER Ca²⁺ Accumulation. *Molecular Neurobiology* **52**, 1835-1849
142. Berezovska, O., Lleo, A., Herl, L. D., Frosch, M. P., Stern, E. A., et al. (2005) Familial Alzheimer's Disease Presenilin 1 Mutations Cause Alterations in the Conformation of Presenilin and Interactions with Amyloid Precursor Protein. *The Journal of Neuroscience* **25**, 3009-3017
143. Yamasaki, A., Eimer, S., Okochi, M., Smialowska, A., Kaether, C., et al. (2006) The GxGD Motif of Presenilin Contributes to Catalytic Function and Substrate Identification of γ -Secretase. *The Journal of Neuroscience* **26**, 3821-3828
144. Pérez-Revuelta, B. I., Fukumori, A., Lammich, S., Yamasaki, A., Haass, C., et al. (2010) Requirement for small side chain residues within the GxGD-motif of presenilin for γ -secretase substrate cleavage. *Journal of Neurochemistry* **112**, 940-950
145. Kretner, B., Fukumori, A., Kuhn, P.-H., Pérez-Revuelta, B. I., Lichtenthaler, S. F., et al. (2013) Important functional role of residue x of the presenilin GxGD protease active site motif for APP substrate cleavage specificity and substrate selectivity of γ -secretase. *Journal of Neurochemistry* **125**, 144-156
146. Futai, E., Osawa, S., Cai, T., Fujisawa, T., Ishiura, S., et al. (2016) Suppressor Mutations for Presenilin 1 Familial Alzheimer Disease Mutants Modulate γ -Secretase Activities. *The Journal of Biological Chemistry* **291**, 435-446
147. Han, S. H., Kim, Y. H., and Mook-Jung, I. (2011) RAGE: the beneficial and deleterious effects by diverse mechanisms of actions. *Molecules and Cells* **31**, 91-97
148. Zhang, L., Bukulin, M., Kojro, E., Roth, A., Metz, V. V., et al. (2008) Receptor for advanced glycation end products is subjected to protein ectodomain shedding by metalloproteinases. *The Journal of Biological Chemistry* **283**, 35507-35516
149. Kierdorf, K., and Fritz, G. (2013) RAGE regulation and signaling in inflammation and beyond. *Journal of Leukocyte Biology* **94**, 55-68
150. Galichet, A., Weibel, M., and Heizmann, C. W. (2008) Calcium-regulated intramembrane proteolysis of the RAGE receptor. *Biochemical and Biophysical Research Communications* **370**, 1-5

151. Deane, R., Bell, R. D., Sagare, A., and Zlokovic, B. V. (2009) Clearance of amyloid-beta peptide across the blood-brain barrier: implication for therapies in Alzheimer's disease. *CNS & Neurological Disorders - Drug Targets* **8**, 16-30
152. Pocivavsek, A., Burns, M. P., and Rebeck, G. W. (2009) Low-density lipoprotein receptors regulate microglial inflammation through c-Jun N-terminal kinase. *Glia* **57**, 444-453
153. Sisodia, S. S. (1992) Beta-amyloid precursor protein cleavage by a membrane-bound protease. *Proceedings of the National Academy of Sciences of the United States of America* **89**, 6075-6079
154. Carey, R. M., Balcz, B. A., Lopez-Coviella, I., and Slack, B. E. (2005) Inhibition of dynamin-dependent endocytosis increases shedding of the amyloid precursor protein ectodomain and reduces generation of amyloid β protein. *BMC Cell Biology* **6**, 30
155. Goodger, Z. V., Rajendran, L., Trutzel, A., Kohli, B. M., Nitsch, R. M., et al. (2009) Nuclear signaling by the APP intracellular domain occurs predominantly through the amyloidogenic processing pathway. *Journal of Cell Science* **122**, 3703-3714
156. Rajendran, L., Honsho, M., Zahn, T. R., Keller, P., Geiger, K. D., et al. (2006) Alzheimer's disease beta-amyloid peptides are released in association with exosomes. *Proceedings of the National Academy of Sciences of the United States of America* **103**, 11172-11177
157. Bateman, R. J., Aisen, P. S., De Strooper, B., Fox, N. C., Lemere, C. A., et al. (2011) Autosomal-dominant Alzheimer's disease: a review and proposal for the prevention of Alzheimer's disease. *Alzheimers Res Ther* **3**, 1
158. Kumar-Singh, S., Theuns, J., Bianca Van, B., Pirici, D., Krist'l, V., et al. (2006) Mean age-of-onset of familial alzheimer disease caused by presenilin mutations correlates with both increased A[β]42 and decreased A[β]40. *Human Mutation* **27**, 686

6.6 SUPPLEMENTAL TABLES

SI Table 6-1 Effect of pathogenic mutations on change in relative binding free energy (kcal/mol) for γ -secretase bound to A β metabolism related substrates.

Gene	Residue Mutation	LRP1 $\Delta\Delta G_{mut} \pm S.E.$	LRP8 $\Delta\Delta G_{mut} \pm S.E.$	RAGE $\Delta\Delta G_{mut} \pm S.E.$	SORL1 $\Delta\Delta G_{mut} \pm S.E.$	TREM2 $\Delta\Delta G_{mut} \pm S.E.$	VLDLR $\Delta\Delta G_{mut} \pm S.E.$
PSEN1	V89L	-1.10 \pm 0.19	-1.45 \pm 0.22	+0.24 \pm 0.15	+1.32 \pm 0.15	-1.14 \pm 0.16	+0.21 \pm 0.21
PSEN1	I143T	-1.04 \pm 0.12	+0.50 \pm 0.11	+1.65 \pm 0.14	+0.14 \pm 0.11	+1.04 \pm 0.10	+1.17 \pm 0.11
PSEN1	M146V	+1.78 \pm 0.13	+0.20 \pm 0.16	+1.32 \pm 0.15	+0.14 \pm 0.15	+3.11 \pm 0.16	+2.79 \pm 0.26
PSEN1	L166P	+2.31 \pm 0.47	+7.25 \pm 0.56	+0.05 \pm 0.52	+1.23 \pm 0.57	+1.67 \pm 0.47	+4.92 \pm 0.54
PSEN1	F176L	+2.42 \pm 0.11	+1.73 \pm 0.08	+1.85 \pm 0.08	+1.53 \pm 0.10	+0.67 \pm 0.08	+1.58 \pm 0.09
PSEN1	M233L	+3.50 \pm 0.12	+1.23 \pm 0.12	+0.39 \pm 0.11	+1.67 \pm 0.13	+0.26 \pm 0.15	+0.34 \pm 0.15
PSEN1	M233T	-2.64 \pm 0.58	+4.21 \pm 0.63	-1.98 \pm 0.81	+18.49 \pm 0.54	+19.02 \pm 0.53	+0.63 \pm 0.83
PSEN1	M233V	+0.83 \pm 0.34	+1.96 \pm 0.13	-0.25 \pm 0.13	+1.59 \pm 0.15	-0.65 \pm 0.15	-0.11 \pm 0.20
PSEN1	E280A	-0.97 \pm 0.17	-0.75 \pm 0.31	+2.81 \pm 0.29	-0.90 \pm 0.22	-1.03 \pm 0.18	-1.36 \pm 0.15
PSEN1	L282V	-0.10 \pm 0.13	+0.53 \pm 0.13	+1.52 \pm 0.11	-0.17 \pm 0.16	-0.39 \pm 0.12	-1.73 \pm 0.18
PSEN1	G384A	+2.44 \pm 0.08	+5.41 \pm 0.09	+4.18 \pm 0.08	+3.17 \pm 0.08	+1.75 \pm 0.08	+3.90 \pm 0.08
PSEN1	C410Y	+2.79 \pm 1.07	-1.43 \pm 0.91	+5.42 \pm 0.88	-0.89 \pm 0.88	+2.37 \pm 0.90	+2.80 \pm 0.93
PSEN1	P436Q	+1.14 \pm 0.43	-0.81 \pm 0.39	-2.25 \pm 0.38	-1.38 \pm 0.38	-3.94 \pm 0.44	-3.22 \pm 0.51
PSEN2	T122P	-0.61 \pm 0.32	+0.64 \pm 0.31	-1.69 \pm 0.29	+0.03 \pm 0.30	+2.22 \pm 0.35	+2.61 \pm 0.33
PSEN2	T122R	+11.94 \pm 0.82	+9.19 \pm 0.68	+1.34 \pm 0.45	+24.52 \pm 0.85	-0.08 \pm 0.54	+20.40 \pm 0.98
PSEN2	N141I	-1.81 \pm 0.40	+1.19 \pm 0.42	+2.52 \pm 0.43	+2.82 \pm 0.42	+0.40 \pm 0.46	-1.19 \pm 0.47
PSEN2	M239I	-0.33 \pm 0.17	-0.37 \pm 0.12	+0.65 \pm 0.15	-0.25 \pm 0.16	-0.91 \pm 0.17	+0.19 \pm 0.18
PSEN2	M239V	+0.10 \pm 0.26	+0.89 \pm 0.13	+1.18 \pm 0.16	+0.32 \pm 0.17	-1.53 \pm 0.15	+1.02 \pm 0.18
PSEN2	A379D	+0.23 \pm 0.62	-3.23 \pm 0.85	-3.17 \pm 0.48	-3.93 \pm 0.62	+0.67 \pm 0.51	-1.34 \pm 0.61

6.7 SUPPLEMENTAL FIGURES

A		Cleavage site reference	
		Ecto [¶]	ICD [§]
6IYC APLP2	LVFFAED-----VGSNKGAIIGLMVGGVVIATVIVIT <u>LV</u> M [¶] LKKK VGGLEERESVGPLREDFSLSSALIGLLVAVAIATVIVIS <u>LV</u> M [¶] LKRK	1	1
6IYC AXL	LVFFAEDV--GSNKGAIIGLMVGGVVIATVIVIT <u>LV</u> M [¶] LKKK HQLVKEPSTPAFSPWPWYVLLGAVVAAACVLILA <u>LV</u> FLVHRR	PROS	Align
6IYC CDH2	LVFFAEDVGSNKGAIIGLMVGGVVIATVIVIT <u>LV</u> M [¶] LKKK IVGAG---LGTGAIIAILLCIILLILVLMF <u>VV</u> WMKRK	2	2
6IYC INSR	LVFFAEDVGS--NKGAIIGLMVGGVVIATVIVIT <u>LV</u> M [¶] LKKK YVDYLDVPSNIAKIIIGPLIFVFLFSVIGSIY <u>LV</u> FLRKRQ	3	Align
6IYC LDLR	LVF-FAEDVGSNKG----AIIGLMVGGVVIATVIVIT <u>LV</u> M [¶] LKKK QALGDVAGRGNEKKPSSVRALSIVLPIVLLVFLCLGV <u>FL</u> LWKNW	PROS	Align
6IYC LRP8	LVF-FAED---VGSN-KGAIIGLMVGGVVIATVIVIT <u>LV</u> M [¶] LKK-K HSQHYANEDSKMGSTVTAAVIGIIVPIVIALLCMSG <u>YL</u> IWRNWK	PROS	Align
6IYC MER	LVFFAEDVGSNKGAIIGLMVGGVVIATVIVIT <u>LV</u> M [¶] LKKK TPAPGN---ADPVLIIFGCFGFIILIGLILYI <u>SL</u> AIRKR	PROS	Align
6IYC PMEL	LVFFAEDVGSNKGAIIGLMVGGVVIATVIVIT <u>LV</u> M [¶] LKKK LIMPGQEAGLQQ---VPLIVGILLVLMAVVLA <u>SL</u> IYRRR	4	Align
6IYC RAGE	LVFFAEDVGSNKGAIIGLMVGGVVIATVIVIT <u>LV</u> M [¶] LKKK SVGGS-GLGT--LALALGILGGLTAALLIGV <u>IL</u> WQRRQ	5	Align
6IYC SORT1	LVFFAEDVGSNKGAIIGLMVGGVVIATVIVIT <u>LV</u> M [¶] LKKK NFLSPEKQNSKNSVPIILAIIVGLMLVTVAG <u>VL</u> IVKKY	PROS	Align
6IYC TREM2	LVFFA--EDVGSNKGAIIGLMVGGVVIATVIVIT <u>LV</u> M [¶] LKKK SISRSLLEGEIPFPPTSILLLLACIFLIKILAAS <u>AL</u> WAAAW	6	7
6IDF CD44	VQSETVEP----PPPAQLHFMYVAAAAFVLLFFVGC <u>VL</u> LSRKRR QEGGANTTSGPIRTPQIPEWLIILASLLALILAVC <u>IA</u> VNSRRR	8	9
6IDF LRP1	VQSETVEPPP-----PPAQLHFMYVAAAAFVLLFFVGC <u>VL</u> LSRKRR KMMPEQCQPPHMTGPRCEEHVFSQQPGHIASILIPLLLLLLLVLAG <u>VV</u> FWYKRR	PROS	Align
6IDF SORL1	VQSETVEPP-----PPAQLHFMYVAAAAFVLLFFVGC <u>VL</u> LSRKRR LYDELGSGADASATQAARSTDVAAVVPILFLLLSLVGVGFA <u>IL</u> YTKHRR	10	Align
6IDF TYRP1	VQSETVEPPPAQLHFMYVAAAAFVLLFFVGC <u>VL</u> LSRKRR IQWPSREFSV-PEIIAIAVVGALLLVALIFGTAS <u>SY</u> LIRARR	PROS	Align
6IDF VLDLR	VQSET-VEPP-----PPAQLHFMYVAAAAFVLLFFVGC <u>VL</u> LSR-KRR EISATSGLVPGGINVTTAVSEVSVPPKGTSAAWAILPLLLLVMAAVGG <u>YL</u> MWRNQH	PROS	Align

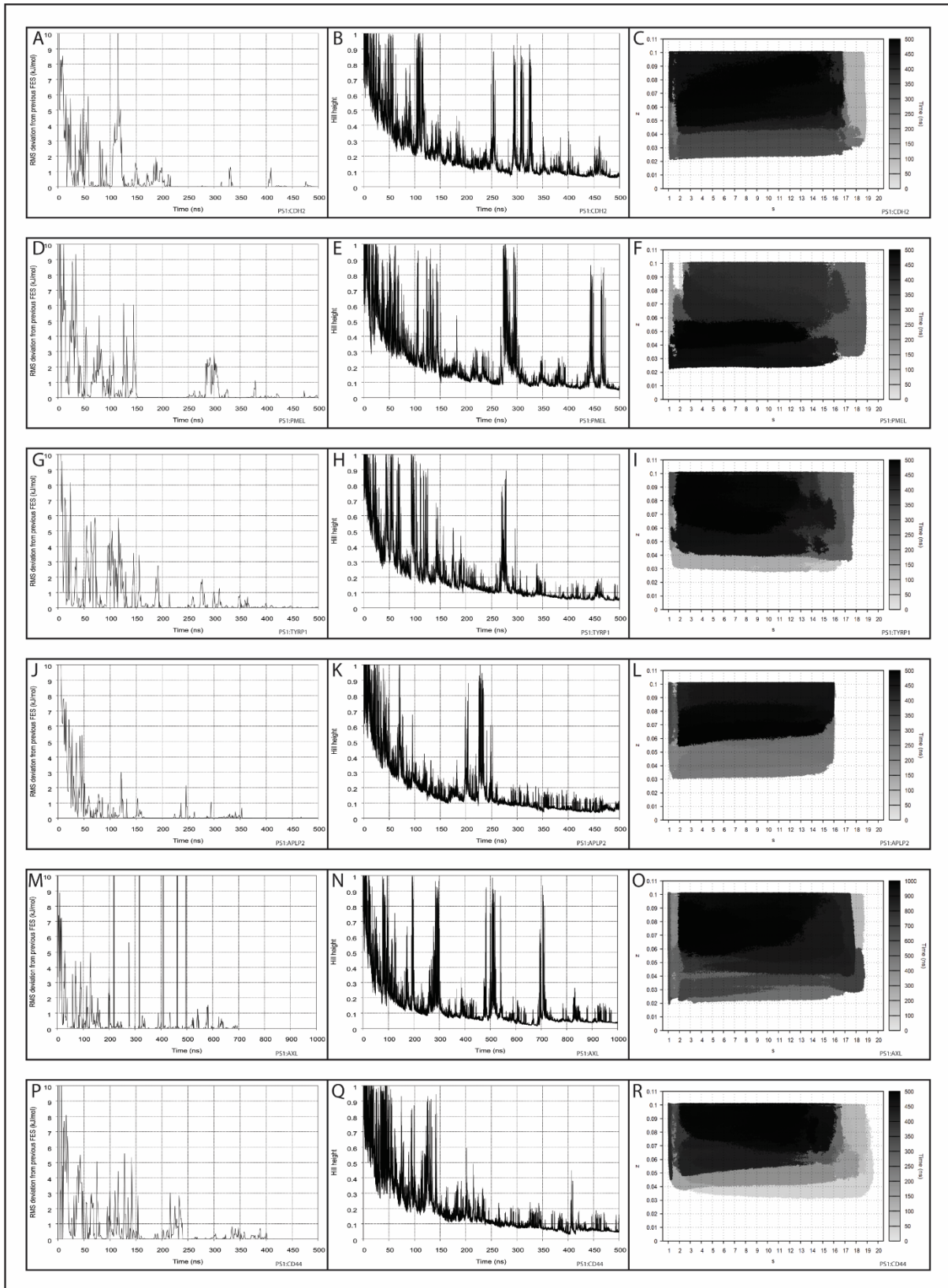
SI Figure 6-1 Substrate alignments for homology modelling

Substrates were aligned and homology modelled to either APP using 6IYC structure (A) or Notch1 using 6IDF structure (B), based on highest similarity between substrates, γ -secretase cleavage site position is underlined.

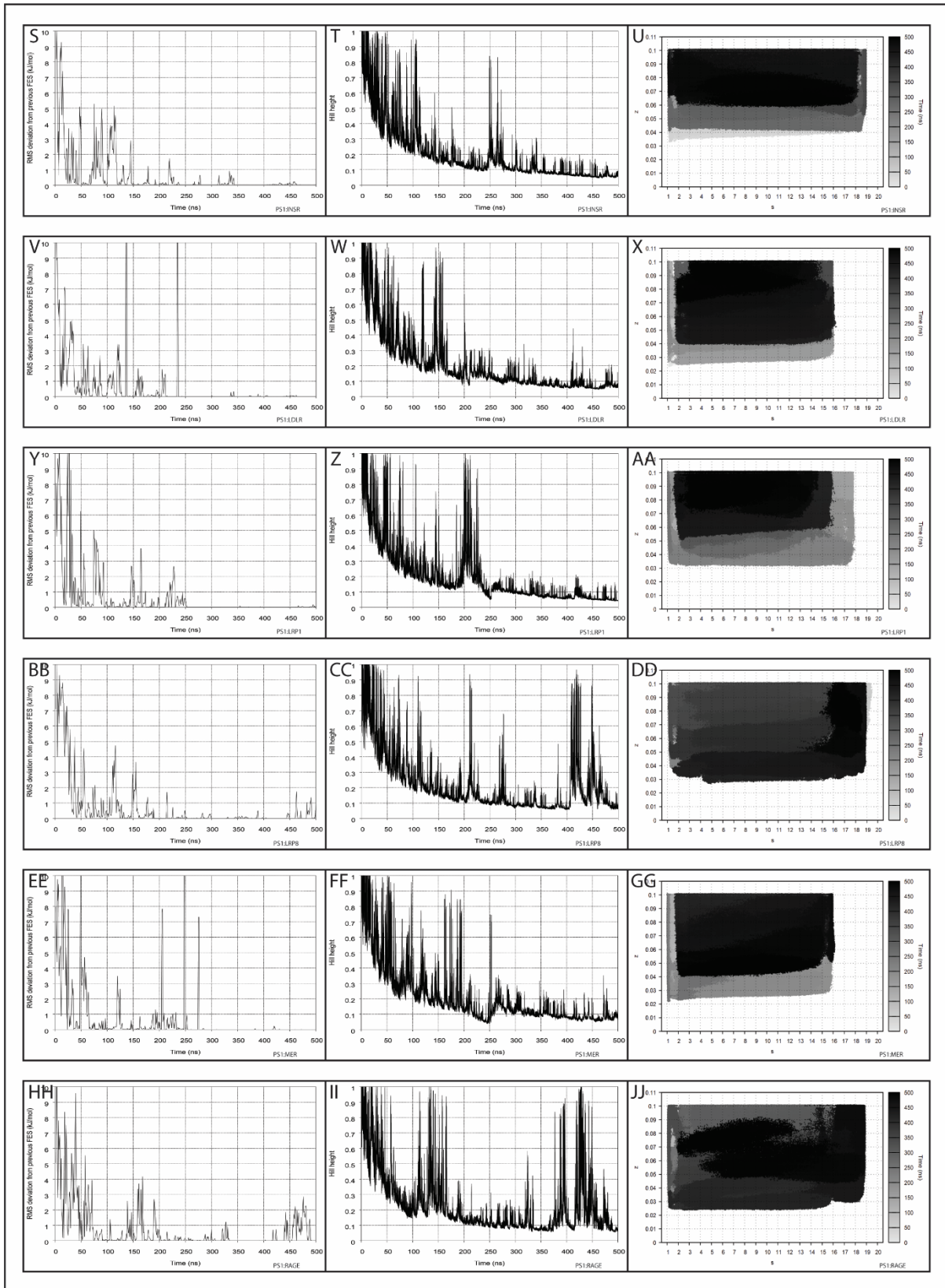
¶ Ectodomain shed site identified from literature, where not available the site was predicted using PROSPEROUS.¹¹

§ γ -secretase ICD cleavage site identified from literature, where not available the site was predicted using alignment function in Advanced Homology Modelling in Schrodinger 2018-3.

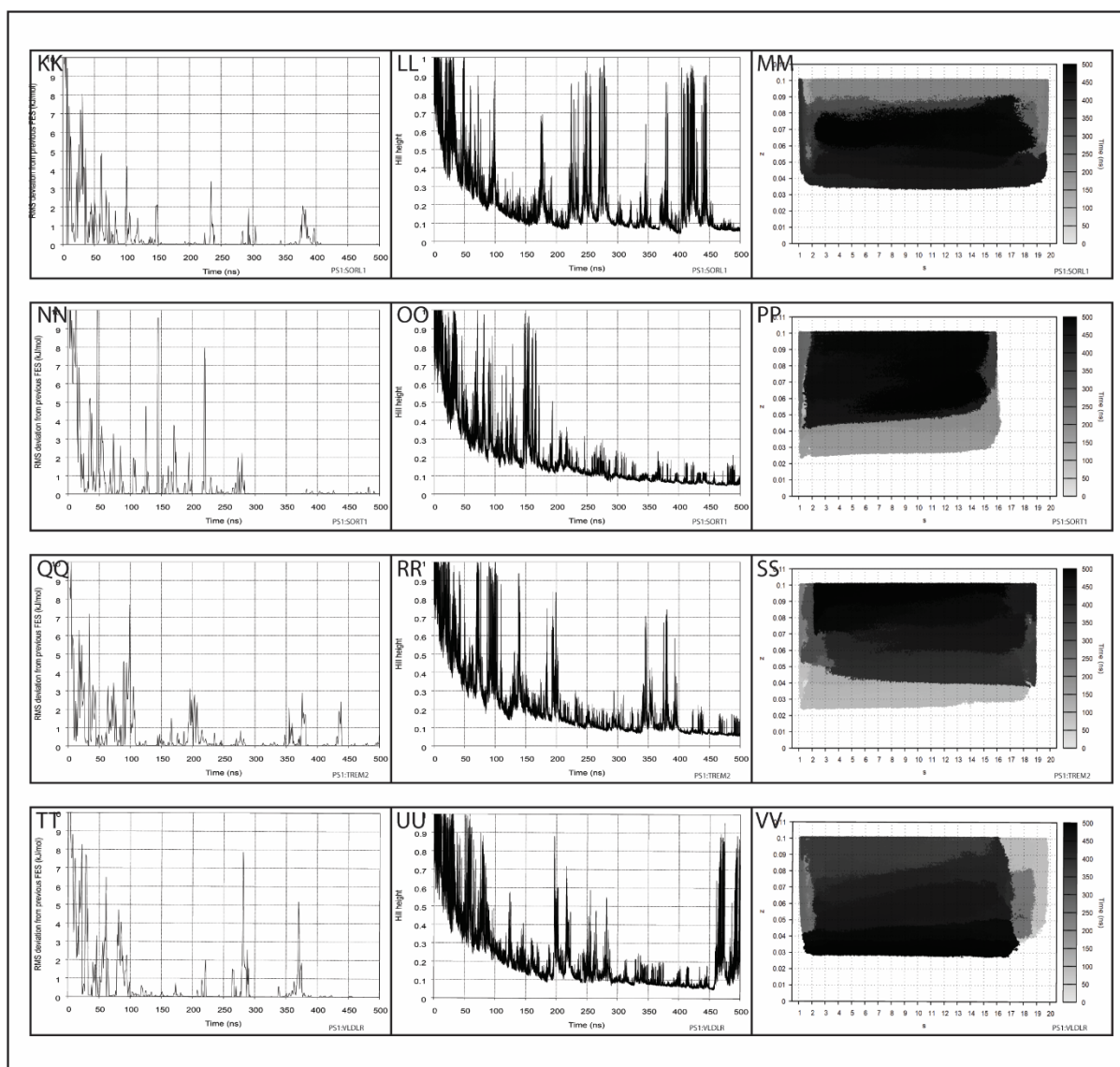
1. Høgl, S., Kuhn, P.-H., Colombo, A., and Lichtenthaler, S. F. (2011) Determination of the Proteolytic Cleavage Sites of the Amyloid Precursor-Like Protein 2 by the Proteases ADAM10, BACE1 and γ -Secretase. *PLoS ONE* **6**, e21337
2. Uemura, K., Kihara, T., Kuzuya, A., Okawa, K., Nishimoto, T., et al. (2006) Characterization of sequential N-cadherin cleavage by ADAM10 and PS1. *Neurosci Lett* **402**, 278-283
3. Meakin, P. J., Mezzapesa, A., Benabou, E., Haas, M. E., Bonardo, B., et al. (2018) The beta secretase BACE1 regulates the expression of insulin receptor in the liver. *Nature Communications* **9**, 1306
4. Kummer, M. P., Maruyama, H., Huelsmann, C., Baches, S., Weggen, S., et al. (2009) Formation of Pmel17 Amyloid Is Regulated by Juxtamembrane Metalloproteinase Cleavage, and the Resulting C-terminal Fragment Is a Substrate for γ -Secretase. *Journal of Biological Chemistry* **284**, 2296-2306
5. Braley, A., Kwak, T., Jules, J., Harja, E., Landgraf, R., et al. (2016) Regulation of Receptor for Advanced Glycation End Products (RAGE) Ectodomain Shedding and Its Role in Cell Function. *J Biol Chem* **291**, 12057-12073
6. Thornton, P., Sevalle, J., Deery, M. J., Fraser, G., Zhou, Y., et al. (2017) TREM2 shedding by cleavage at the H157-S158 bond is accelerated for the Alzheimer's disease-associated H157Y variant. *EMBO Molecular Medicine* **9**, 1366-1378
7. Steiner, A., Schlepckow, K., Brunner, B., Steiner, H., Haass, C., et al. (2020) γ -Secretase cleavage of the Alzheimer risk factor TREM2 is determined by its intrinsic structural dynamics. *The EMBO Journal* **39**, e104247
8. Nakamura, H., Suenaga, N., Taniwaki, K., Matsuki, H., Yonezawa, K., et al. (2004) Constitutive and induced CD44 shedding by ADAM-like proteases and membrane-type 1 matrix metalloproteinase. *Cancer Res* **64**, 876-882
9. Okamoto, I., Kawano, Y., Murakami, D., Sasayama, T., Araki, N., et al. (2001) Proteolytic release of CD44 intracellular domain and its role in the CD44 signaling pathway. *J Cell Biol* **155**, 755-762
10. Christensen, S. K., Narimatsu, Y., Simoes, S., Goth, C. K., Vægter, C. B., et al. (2020) Endosomal trafficking is required for glycosylation and normal maturation of the Alzheimer's-associated protein sorLA. *bioRxiv*, 2020.2007.2012.199885
11. Song, J., Li, F., Leier, A., Marquez-Lago, T. T., Akutsu, T., et al. (2017) PROSPEROus: high-throughput prediction of substrate cleavage sites for 90 proteases with improved accuracy. *Bioinformatics* **34**, 684-687



SI Figure 6-2 PS1 γ complex simulation convergence

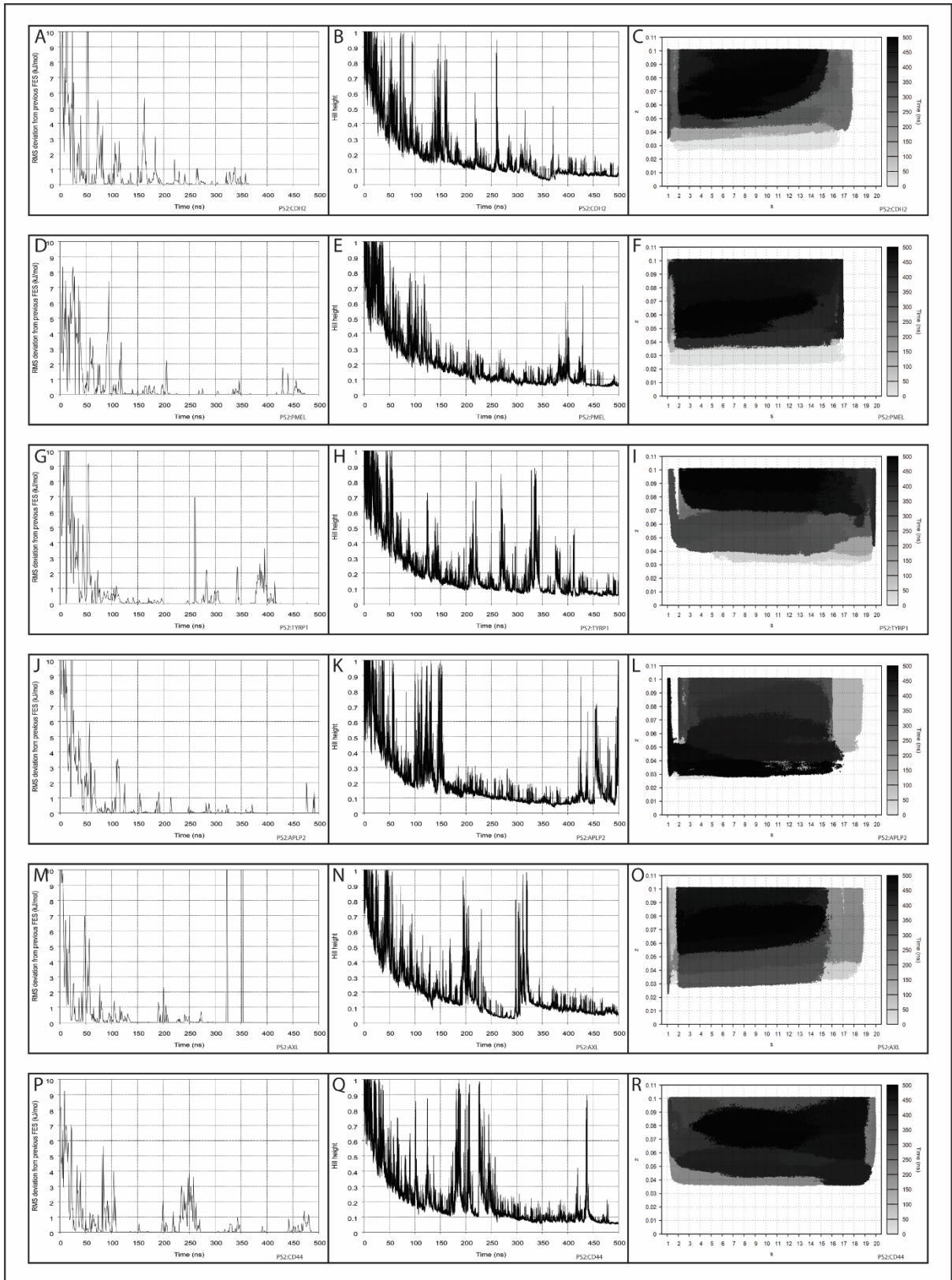


SI Figure 6-2 con't PS1y complex simulation convergence

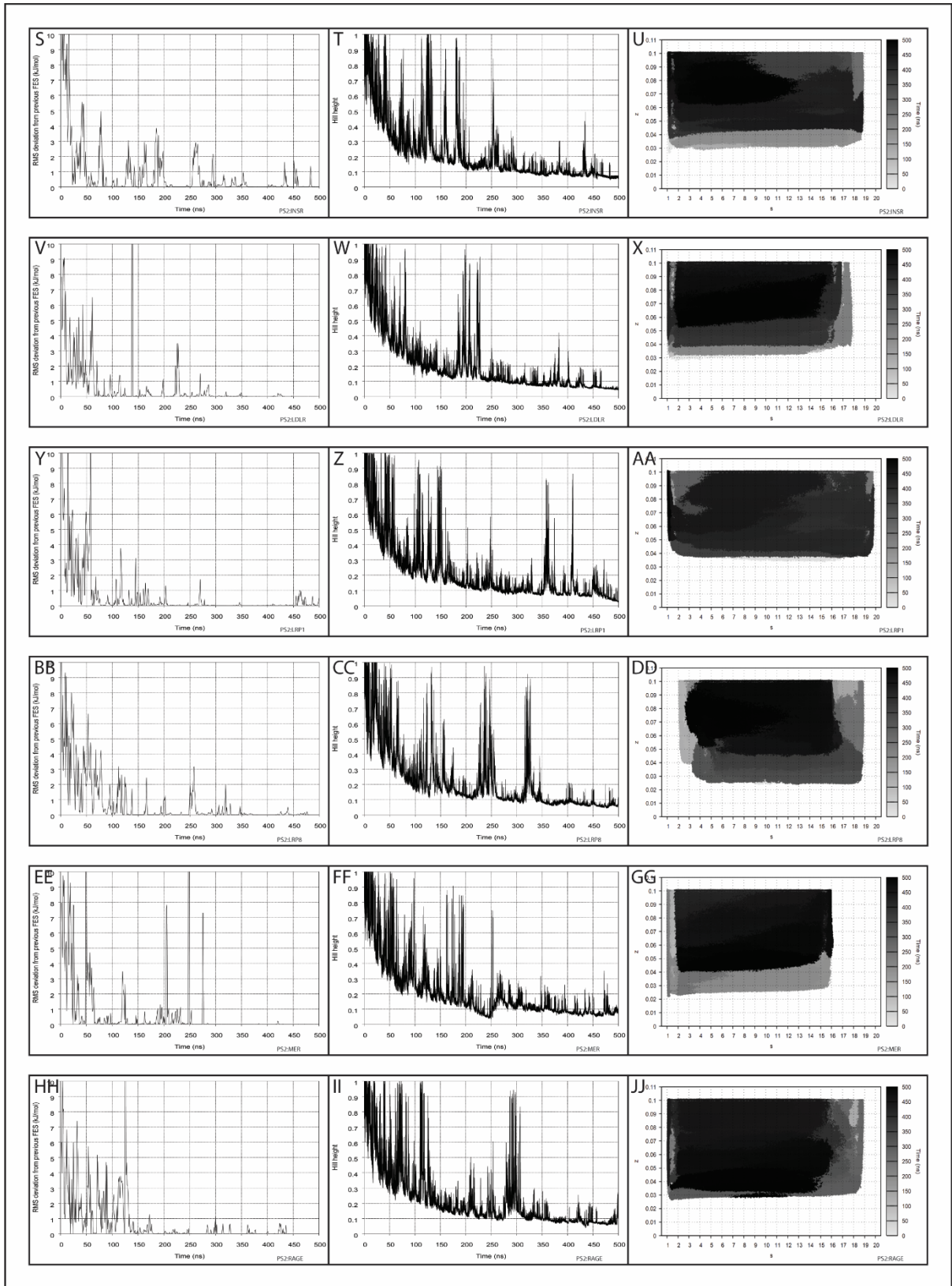


SI Figure 6-2 con't PS1 γ complex simulation convergence

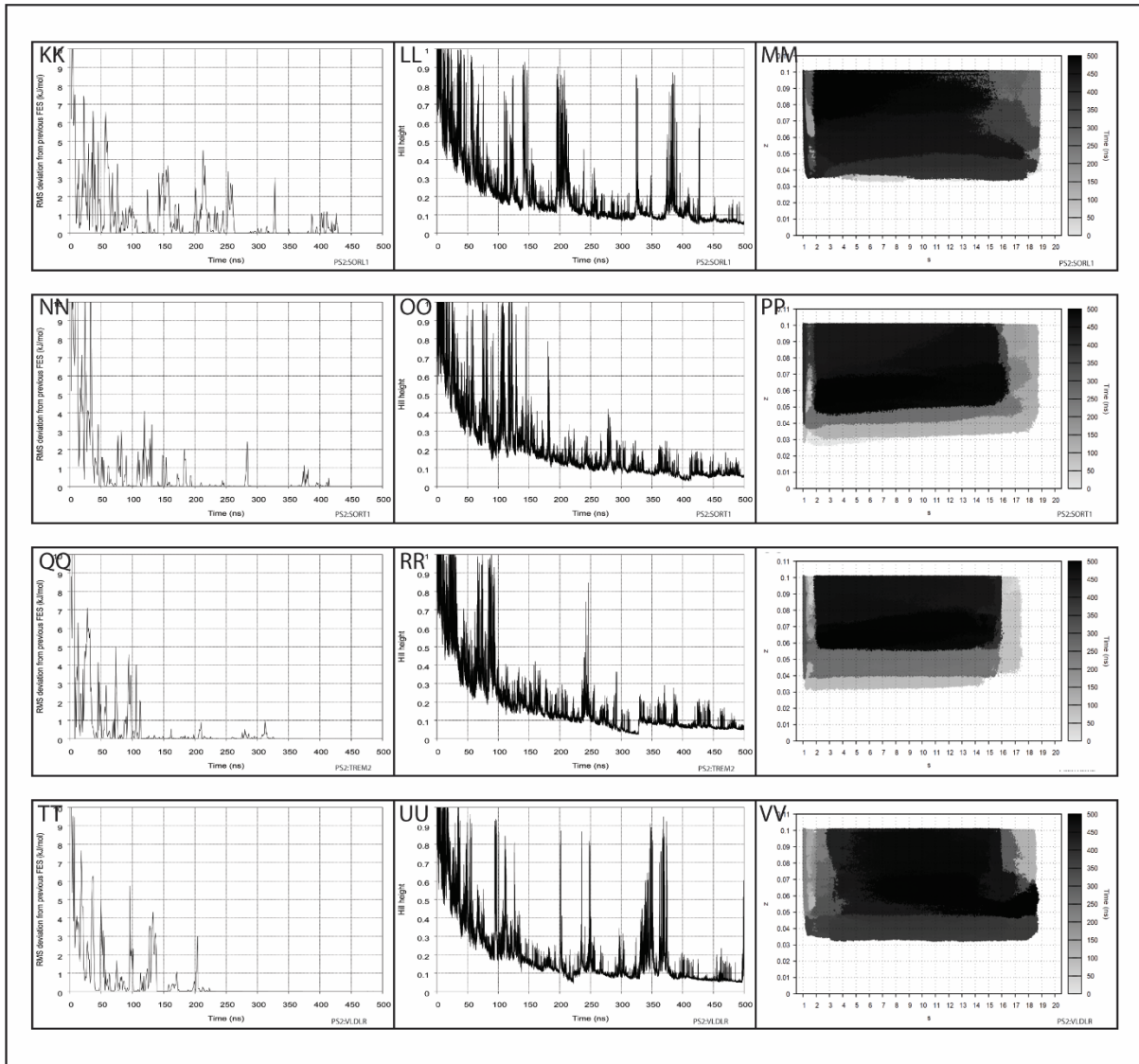
Simulation convergence for PS1 γ models assessed via monitoring RMSD from previous FES at 1ns intervals (A, D, G, J, M, P, S, V, Y, BB, EE, HH, KK, NN, QQ, TT), Gaussian hill height (B, E, H, K, N, Q, T, W, Z, CC, FF, II, LL, OO, RR, UU), and the collective variable space over duration of simulation (C, F, I, L, O, R, U, X, AA, DD, GG, JJ, MM, PP, SS, VV).



SI Figure 6-3 PS2 γ complex simulation convergence

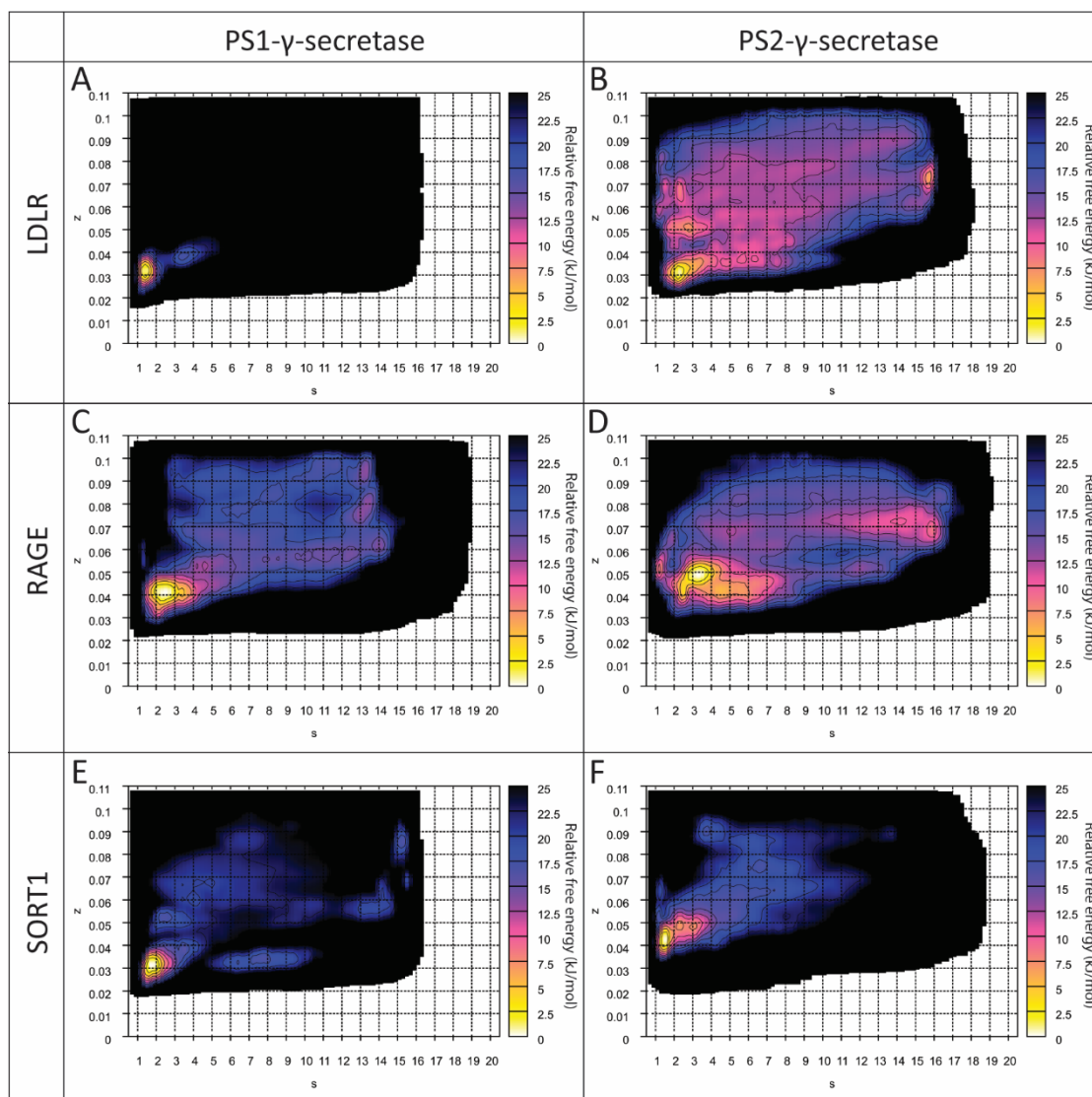


SI Figure 6-3 con't PS2 γ complex simulation convergence



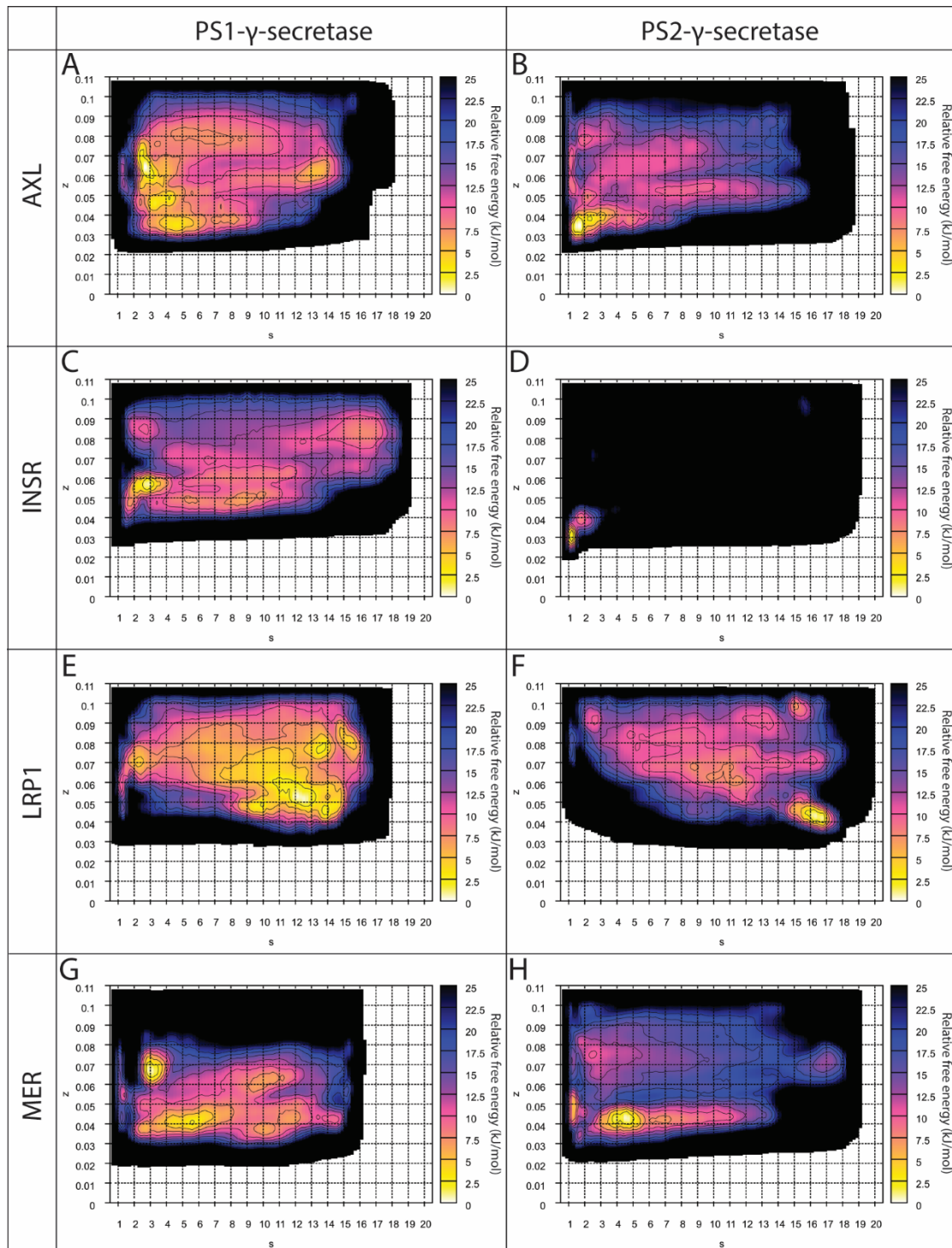
SI Figure 6-3 con't PS2 γ complex simulation convergence

Simulation convergence for PS2 γ models assessed via monitoring RMSD from previous FES at 1ns intervals (A, D, G, J, M, P, S, V, Y, BB, EE, HH, KK, NN, QQ, TT), Gaussian hill height (B, E, H, K, N, Q, T, W, Z, CC, FF, II, LL, OO, RR, UU), and the collective variable space over duration of simulation (C, F, I, L, O, R, U, X, AA, DD, GG, JJ, MM, PP, SS, VV).

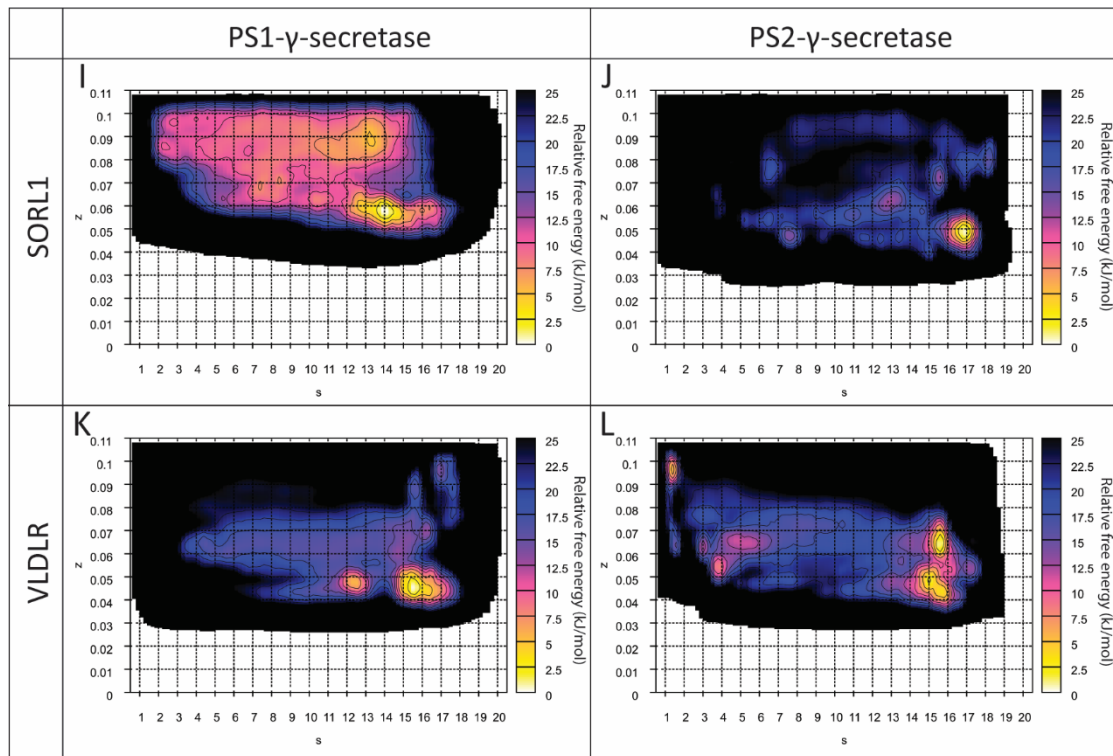


SI Figure 6-4 PS1 γ and PS2 γ complexes are both conformationally 6IYC-like

Free energy surfaces derived from well-tempered metadynamics simulations of LDLR (A,B), RAGE (C,D), SORT1 (E,F), both the PS1 γ and PS2 γ complex have conformational ensembles that are 6IDF-like.

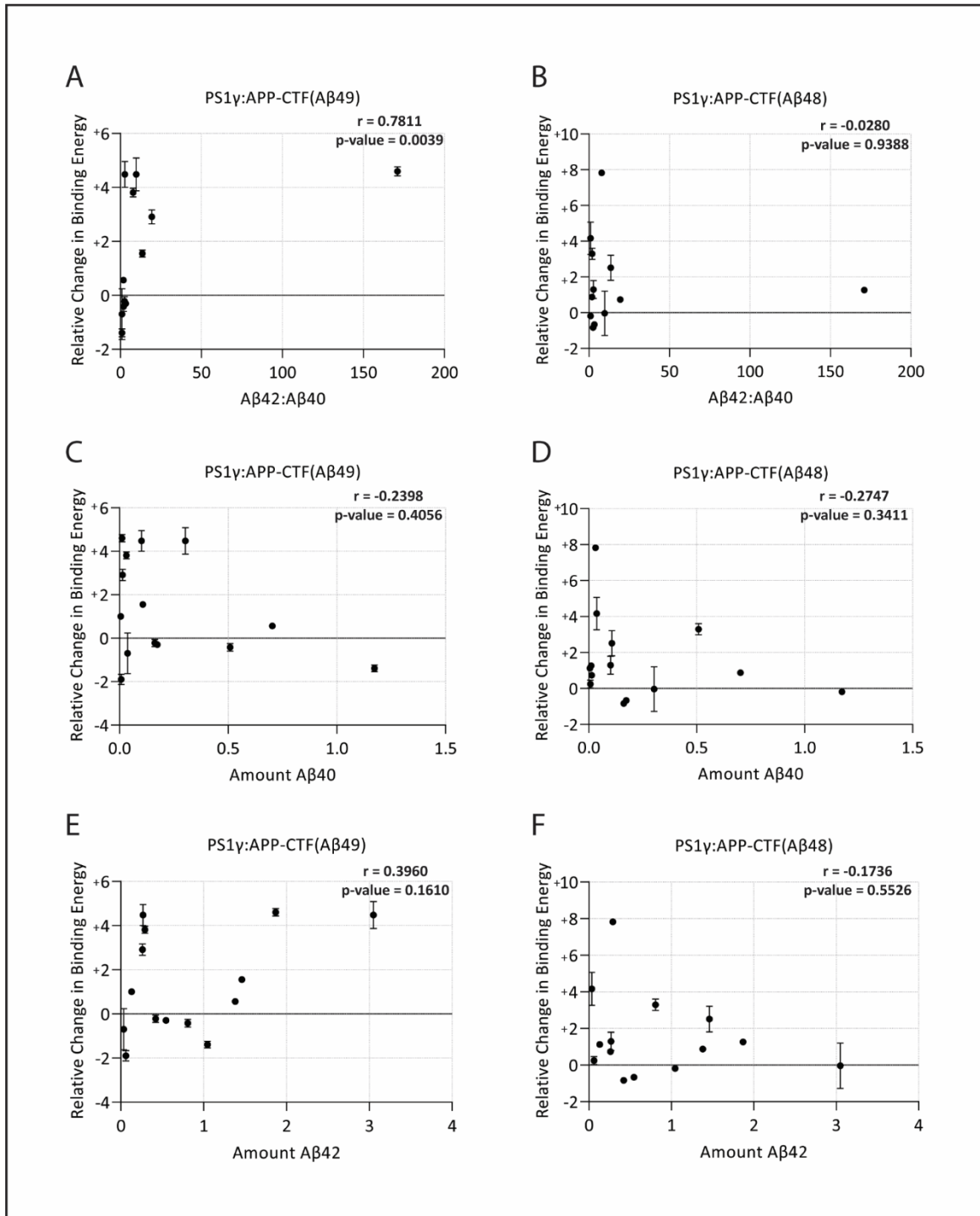


SI Figure 6-5 PS1 γ and PS2 γ complexes are conformationally distinct



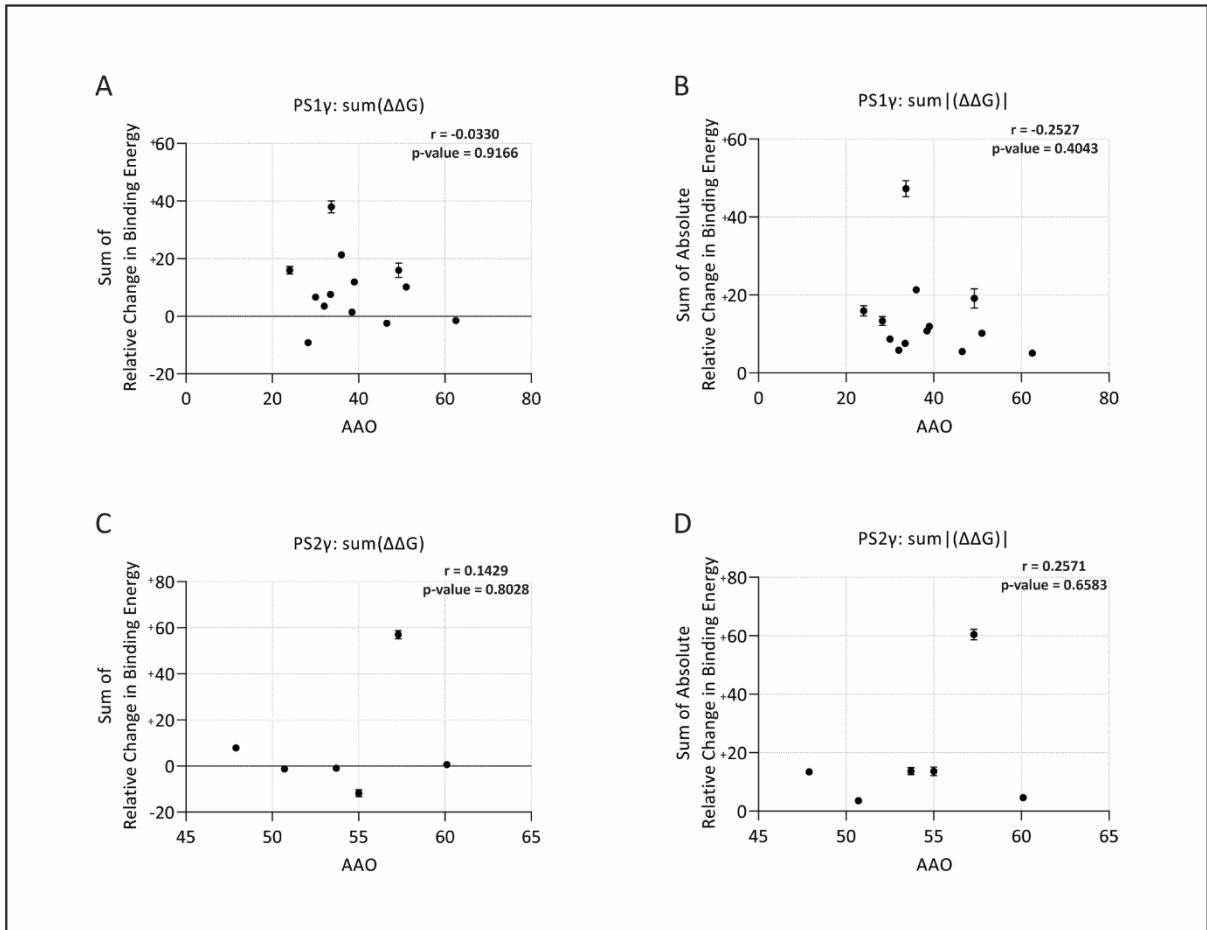
SI Figure 6-5 con't PS1 γ and PS2 γ complexes are conformationally distinct

Free energy surfaces derived from well-tempered metadynamics simulations of AXL (A,B), INSR (C,D), LRP1 (E,F), MER (G,H), SORL1 (I,J), and VLDLR (K,L), where the PS1 γ and PS2 γ complex are conformationally distinct.



SI Figure 6-6 $\Delta\Delta G$ for PS1 γ and PS2 γ mutation complexes bound to APP-CTF substrates correlation with amount of A β 40 and A β 42

Correlation between Sun data⁵⁰ A β 42:A β 40 with PS1:G384A data point included (A-B), amount of A β 40 (C-D) and amount of A β 42 (E-F) with APP-CTF(A β 49) (A, C, E) and APP-CTF(A β 48) (B, D, F) relative change in binding energy ($\Delta\Delta G$) for PS1 γ mutations.



SI Figure 6-7 AAO correlations with the sum and absolute sum of $\Delta\Delta G$ for PS1 γ and PS2 γ mutation complexes

Correlation between AAO and sum of $\Delta\Delta G_{mut}$ (A, C) or sum of absolute $\Delta\Delta G_{mut}$ (B, D) for PS1 mutations (A-B) and PS2 mutations (C-D).

7 GENERAL DISCUSSION

The presenilins are key proteins implicated in AD pathogenesis given they are the catalytic components of γ -secretase that generate A β and *PSEN1* and *PSEN2* mutations lead to ADAD.¹ Yet, there still remains an incomplete understanding of the function, activity and the role for these intriguing proteins in the disease process. With more than 149 known substrates of γ -secretase,²⁻⁵ coupled with the non-proteolytic functions of PS1 and PS2⁶⁻¹¹ and their widespread expression,¹² PS1 and PS2 could be considered pleiotropically prodigious. However, the differences and similarities in structure, expression, and function between these presenilin homologues has been largely understudied in the field. Much of our understanding of PS1 γ and PS2 γ functionality is in association with their A β generative role.¹³⁻¹⁵ It is largely PS1 that has been attributed to the majority of dysregulated A β generation, given the larger number of ADAD related mutations in *PSEN1*,¹⁶ and the reportedly higher processing activity PS1 γ .¹⁷⁻¹⁹ More recently, PS2 γ has been demonstrated to predominantly generate intracellular A β and generate a higher A β 42:A β 40 ratio than PS1 γ ,²⁰⁻²² suggesting that PS2 γ may be more critical in intraneuronal A β toxicity. Furthermore, there is evidence that PS2 expression increases in later developmental stages, with age, and during neuronal maturation.^{12, 22-29} In addition, many substrates of γ -secretase are associated with A β clearance functions,³⁰⁻⁵¹ suggesting that both PS1 γ and PS2 γ may play important roles in A β removal. Indeed, PS1 and PS2 are associated with microglial A β response mechanisms,^{52, 53} with one study highlighting the specific roles for PS2 in inflammatory responses.⁵³ However, the functions of PS1 and PS2 in microglia have not been widely studied.

Significant knowledge gaps regarding the specific contributions to and mechanisms of A β generation by PS1 γ and PS2 γ , and even more so their roles in A β clearance, are evident. This thesis in part closes these gaps, identifying differential functions and mechanisms of PS1 and PS2 related A β generation and A β clearance. The findings of this thesis do not in any way diminish the importance of PS1 γ in A β generation, but elevate the importance of PS2 γ in A β generation. Additionally, this thesis identifies important roles for both PS1 and PS2 in microglial function and A β clearance responses. While further work is required to validate these findings, this thesis demonstrates that ***PS1 and PS2 exhibit distinct roles in A β metabolism.*** A summary of the key findings, and tools developed in, this thesis is presented in Figure 7-1.

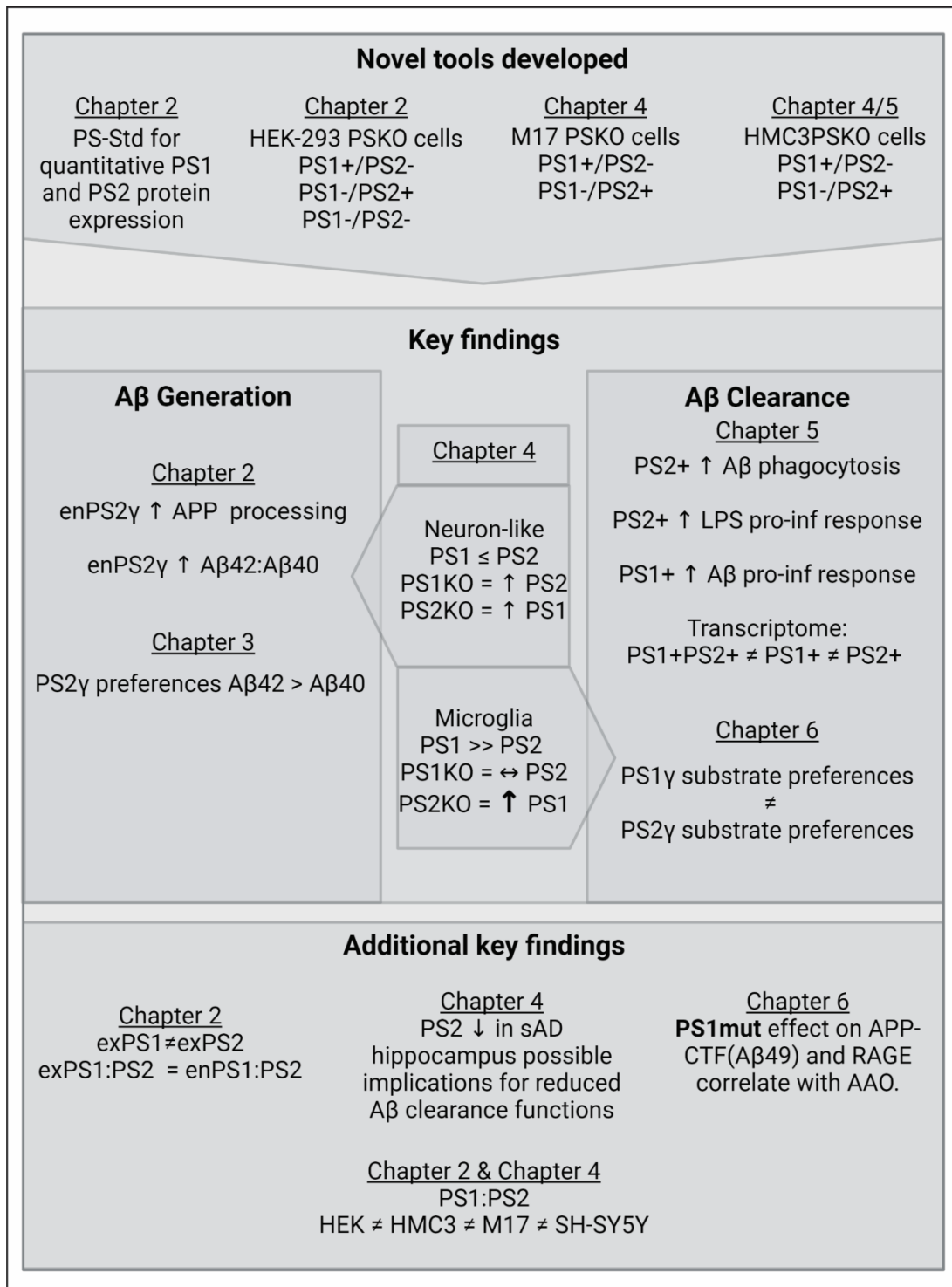


Figure 7-1 Summary of thesis key findings and outputs

Chapter 2 and **Chapter 3** of this thesis focussed on A β generation. The primary objective of these two chapters was to determine the individual enzymatic activities of PS1 γ and PS2 γ in processing APP and to explore the structural mechanisms that underlie the variation in A β 42:A β 40 ratios produced by PS1 γ and PS2 γ . While it has been previously reported that PS1 γ is more active at processing APP, generating both more AICD and A β , these experiments typically use exogenously expressed PS1 or PS2 on a PS1/2 null background.¹⁷⁻¹⁹ These

experimental methods have two flaws. Firstly, there is an assumption that exogenous PS1 or PS2 will be equally expressed, and secondly, the overexpression of PS1 or PS2 often leads to artefactual accumulation of full-length PS protein. A key goal of **Chapter 2** was to develop a method for direct quantitation of endogenous PS1 and PS2, enabling the field to move to more physiologically relevant models. The successful development and validation of the PS-Std enabled direct PS1 versus PS2 protein quantitation, and the opportunity to determine endogenous PS1 γ and PS2 γ substrate processing capacity at an enzymatic level. In doing so, PS2 γ was observed to process more APP than PS1 γ , accumulating less APP-CTF and generating more A β 40 and A β 42. Endogenous PS2 γ was also shown to generate a higher secreted A β 42:A β 40 ratio. The key conclusion from **Chapter 2** is that PS2 γ is more active as an individual enzyme compared with PS1 γ at processing APP, and it generates higher A β 42:A β 40.

Chapter 3 used enhanced sampling approaches for molecular simulation, coupled with binding free energy calculations, to explore APP-CTF and A β intermediate substrate binding by PS1 γ and PS2 γ . The conformational ensembles and binding free energy of γ -secretase in complex with APP/A β substrates, support the propensity for PS2 γ to generate higher A β 42:A β 40. Firstly, PS2 γ binding of APP-CTF(A β 49) [initiating the A β 40 pathway] is conformationally constrained compared to binding APP-CTF(A β 48) [initiating the A β 42 pathway]. Secondly, binding free energy calculations reveal a distinct binding preference of PS2 γ for APP-CTF(A β 48), over APP-CTF(A β 49). Thirdly, subsequent substrates in the A β 42 pathway exhibit comparably unfavourable binding free energies for PS2 γ . Lastly, PS2 γ in complex with A β 42(A β 38) is conformationally restricted. Taken together, these data suggest that PS2 γ preferentially binds APP-CTF(A β 48) to initiate the A β 42 pathway, and the subsequent complexes, with the A β intermediates, in this pathway are less favourable. This suggests a higher likelihood that PS2 γ will release the A β 42 product following A β 45(A β 42) processing, leading to an increased A β 42:A β 40 ration. Thus, **Chapter 3** presents a mechanistic explanation of why PS2 γ generates higher A β 42:A β 40 as observed here in **Chapter 2**, and by other studies.²⁰⁻²²

The conclusions from **Chapter 2** and **Chapter 3** may not be clinically relevant depending on the PS expression levels in the brain. To assess whether PS2 γ has clinically relevant implications in the brain, PS1 and PS2 expression levels in human brain tissue and neural cell lines were quantitatively characterised in **Chapter 4**. PS1 expression was consistently higher

than PS2 in all brain regions and all clinical classifications (PS1 was at a minimum 8.4-times higher than PS2). While these results suggest that PS2 γ may not be clinically relevant, the samples were bulk tissue homogenates, and so contain a combination of all neural cell types. It is possible that the majority of PS1 expression in brain tissue is from oligodendrocytes, as this glial cell accounts for approximately 40% of all neural cells in the neocortex,⁵⁴ and express 8-times more *PSEN1* than any other neural cell ([www.proteinatlas.org/ ENSG00000080815-PSEN1/single+cell+type](http://www.proteinatlas.org/ENSG00000080815-PSEN1/single+cell+type)).⁵⁵ PS2 expression, however, has been shown to increase in neuronal cell lines with differentiation, while PS1 expression levels remain unaffected.^{22, 29} Similar findings were observed in **Chapter 4** where PS2 expression was higher than PS1 upon differentiation of neuroblastoma cells into more ‘neuronal-like’ cells. This observation is reinforced by the genetic ablation of either PS1 or PS2 in M17 neuroblastoma cells, resulting in increased expression of the alternate PS homologue, such that there was no significant difference in total PS expression between either the wildtype, PS1KO, or PS2KO cells. This suggests that in these neuronally derived cells, PS1 and PS2 are capable of complete compensation for the absence of the alternate homologue. Together these findings highlight the importance of neuronal expression of PS2.

Taken together, the results from **Chapter 2**, **Chapter 3**, and **Chapter 4**, suggest that is more efficient at binding and processing APP and that PS2 neuronal expression levels may be similar to or possibly even higher than PS1, and consequently PS2 γ may be the primary generator of A β 42. While further validation of these findings in other models is required, it does highlight that due consideration of PS2 γ is required when designing γ -secretase targeting therapeutics. The use of enhanced sampling methods, such as WTMetaD, applied to γ -secretase for the first time in this thesis, provide the opportunity to develop improved therapeutics using structure-based drug design, to identify compounds that target specific conformations of PS1 γ and PS2 γ , ideally improving therapeutic outcomes.

In **Chapter 4**, the expression levels of PS1 and PS2 were investigated in human microglial (HMC3) cells. PS2 has previously been shown to be the primary PS involved in regulating murine microglia cytokine function.⁵³ In contrast, similar roles for both PS1 and PS2 have also been observed in murine microglia.⁵² These studies highlighted important roles for PS1 and PS2 in A β clearance by microglia. Although A β clearance functions are also performed by other neural cells, this thesis focused on confirming the A β clearance related roles of PS1 and PS2 in human microglia. Using the PS-Std (developed in **Chapter 2**) to quantitate PS1 and

PS2 expression levels in the HMC3 cells, it was observed that PS2 expression levels were very low (PS1:PS2 = 21.72). Indeed, the HMC3 cells had the lowest PS2 expression compared to any other cell lines measured, while PS1 levels were relatively comparable between cell lines. However, subsequent ablation of PS1 or PS2 was very revealing. The loss of PS1 expression did not lead to significant upregulation of PS2 – indeed, there was an overall reduction in the expression of total PS protein. However, the loss of PS2 caused a significant upregulation in PS1 expression, with PS1 expression more than doubled with the loss of a comparatively small amount of PS2 protein expression. This result suggests that PS2 is possibly the functionally important PS in human microglia and as such this notion was consequently explored in **Chapter 5**.

Murine and human microglia have been shown to have considerably different transcriptomes, in particular with respect to the expression of AD related genes.^{56, 57} Consequently, investigating the functional differences between PS1 and PS2 in human microglia has potential implications in the understanding of the roles of PS1 and PS2 in microglial function. In **Chapter 5** HMC3 PS1+ and PS2+ cells (i.e., retaining PS1 or PS2 expression respectively) were comparatively assessed by a variety of functional assays and transcriptomic analysis. Interestingly, PS-specific pro-inflammatory cytokine responses were observed; PS1+ cells specifically responded to A β , while PS2+ cells specifically responded to LPS. HMC3 PS2+ cells were also shown to have increased phagocytic capacity. The response of HMC3 PS2+ cells to LPS and the increase in phagocytosis contrasts with murine microglial responses.^{52, 53} Transcriptomic analysis of the PS1+ and PS2+ cells compared with the wildtype revealed three distinct transcriptional profiles, highlighting that PS1 and PS2 likely have distinct functions in microglial cells.

The expression of three A β clearance related substrates of γ -secretase was assessed in **Chapter 5**. Compared to wild type HMC3 cells, VLDLR expression was almost completely lost in both the PS1+ and PS2+ cells, CD44 expression was downregulated in PS1+ cells and upregulated in PS2+ cells, while TREM2 expression was unchanged in PS1+ cells and decreased in PS2+ cells. These three A β clearance related substrates, along with several others, were also investigated in **Chapter 6** using the computational methods established in **Chapter 3**, to determine if there were specific preferences of either PS1 γ or PS2 γ to bind A β clearance related substrates. Moderate to strong substrate preferences were evident for all substrates assessed, except AXL. With respect to the specific substrates examined in **Chapter 5**, PS1 γ

demonstrated a strong preference for binding CD44, while PS2 γ demonstrated strong and moderate preferences for TREM2 and VLDLR, respectively. While the ICDs of VLDLR³⁸ and CD44⁵⁸ are suggested to have positive autoregulatory functions, it is difficult to draw any direct conclusions from the results of both **Chapter 5** and **Chapter 6** with respect to these substrates without further experiments. In particular the lack of HMC3 PSnull cells, and therefore the ability to rescue PS1 or PS2 expression, makes it difficult to determine if the observed outcome is the result of the upregulated expression of the retained PS or the result of lost expression of the ablated PS. This is acknowledged particularly for **Chapter 5**, and further studies are required to address this limitation and validate the findings. However, it can be concluded from **Chapter 5** that PS1 and PS2 likely have distinct roles in microglial A β clearance, and microglial functions more broadly that warrant further investigation. Furthermore, the substrate binding preferences suggested by binding free energy calculations, and the different conformational ensembles observed for binding of substrates revealed by enhanced sampling simulations in **Chapter 3** and **Chapter 6** again highlights the importance of considering both PS1 γ and PS2 γ in future drug design. Specifically, the observation that different substrates elicit different conformations of PS1 γ and/or PS2 γ suggests the possibility of designing molecules that selectively block specific substrate-binding conformations of PS1 γ and PS2 γ , which may result in safer therapeutics targeting γ -secretase.

Additional findings in **Chapter 4** and **Chapter 6** have potential implications for understanding the role of PS in both sAD and ADAD. Notably in **Chapter 4**, PS2 expression was shown to be decreased in sAD hippocampal tissue compared with control, supporting previous observations.⁵⁹ If the observations of **Chapter 5** are validated in future studies, and PS2 is critical for A β clearance, reduced PS2 expression in the hippocampus may contribute to increased A β related pathology in sAD. In **Chapter 6**, PS1 and PS2 ADAD-related mutations were investigated using alchemical perturbation to determine what effects they may have on binding both APP-CTF and A β clearance related substrates. Interestingly, correlative relationships were observed between AAO and the effect of PS1 mutations on the binding energies of APP-CTF(A β 49) (i.e., in position to initiate the A β 40 pathway) and RAGE (a receptor that mediates A β influx into the brain from the periphery, and thus has implications for clearance). The negative correlation with APP-CTF(A β 49) suggests that mutations with an earlier AAO have a more deleterious effect on the relative binding energy ($\Delta\Delta G_{\text{mut}} > 0$). In contrast, the correlation with RAGE is positive, suggesting mutations with a later AAO have a more deleterious effect on the relative binding energy ($\Delta\Delta G_{\text{mut}} > 0$). This may indicate that

mutations with earlier AAO are associated with changes in A β generation, while later AAO mutations may disrupt A β clearance. This is an interesting finding and implicates mutations in a mechanism underlying A β accumulation in sAD. Further support for this notion is provided by studies that have shown that PS1 mutations prior to residue Leu200, typically have greater pathological similarities to sAD, while those C-terminal of Leu200 have a more severe and distinct pathology.⁶⁰⁻⁶² It will be interesting to re-evaluate the correlations between ADAD associate mutations AAO and the relative binding energies of APP-CTF(A β 49) and RAGE with consideration for the mutation position using multiple regression analysis. However, additional mutations will likely need to be evaluated to ensure adequate statistical power.

Lastly, two additional findings of this thesis are important to reiterate as they have implications for future studies of PS1 and PS2 activity. In **Chapter 2**, exogenous expression of PS1 and PS2 was also compared quantitatively by tagging the exogenous PS. It is commonly assumed that if two homologous genes are expressed exogenously using the same vector, their expression levels will be similar. However, this assumption does not hold true for exogenously expressed PS1 and PS2 in HEK 293 cells, as demonstrated in this thesis, and previously in yeast.⁶³ Indeed, it was shown that the exogenously expressed PS1:PS2 profile closely recapitulated the endogenous PS1:PS2 profile. This is likely the result of tight regulation of the other γ -secretase components and localisation effects of PS1 γ and PS2 γ .^{18, 21, 64, 65} Nonetheless, this finding highlights the importance of considering the quantitative difference in PS1 and PS2 expression levels when making determinations about their individual functions. Additionally, the quantitation of endogenous PS1:PS2 expression profiles of multiple cell lines in **Chapter 2** and **Chapter 4**, namely HEK 293, HMC3, M17 and SH-SY5Y cells, revealed considerable variability between PS1:PS2 profiles. This indicates that caution should be exercised when extending the applicability of findings in one cell model more generally. The PS-Std developed within this thesis, designed for quantitatively assessing the expression levels of endogenous PS1 and PS2, offers a solution to address this issue.

7.1 GENERAL LIMITATIONS

While this thesis has mitigated the limitations associated with quantitative PS1 and PS2 protein expression by developing novel tools in **Chapter 2**, and subsequently demonstrating their utility in **Chapter 4**, there are nonetheless several limitations that must be acknowledged. Firstly, the assessments of PS expression levels, particularly those in **Chapter 2** were in whole

cell lysates. It has been previously suggested that not all γ -secretase complexes are active, and ‘inhibitor-capture tools’ have been developed to pull down ‘active’ γ -secretase.⁶⁶⁻⁶⁸ It may be possible that the individual enzymatic activity attributed to PS1 γ or PS2 γ in **Chapter 2** is overstated as a result. Secondly, the availability of only APP and Notch1 bound PS1 γ structures limits the available templates for homology modelling and the collective variable space used for WTMetaD in **Chapter 3** and **Chapter 6**. The availability of PS2 γ substrate bound structures, and PS1 γ or PS2 γ bound to substrate other than APP and Notch1, as well as high resolution structures of apo PS1 γ and PS2 γ in the future will improve this. Thirdly, in **Chapter 4** compared to the AD brain tissue samples, the number of available samples for control, FTD, and LBD are low (three to five samples). The confidence levels in the results would be improved if additional samples were available, in particular control samples. Lastly, as mentioned above, the lack of HMC3 PSnull cells, and therefore the inability to perform PS rescue, makes it difficult to ascribe the observed results in **Chapter 5** definitively to either PS. Some results may be attributable to either the presence of the retained PS or the loss of expression of the ablated PS. Additionally, the HMC3 cells are not as responsive as other murine models, primary cells, or iPSCs, potentially impacting on the magnitude of the effects seen in this study. Nonetheless, this is the first evidence of PS1 and PS2 specific functions in the absence of the alternate homologue in a human microglial model. Further validation is required in relevant human cell lines such as differentiated iPSC cells, or induced microglia-like cells (iMGs).

7.2 FUTURE STUDIES

In recognition of these limitations, several future studies should be pursued to both resolve these limitations and validate the findings, as well as confirm their clinical relevance. The conclusions of experiments completed in **Chapter 2** would be improved if they were repeated using active- γ -secretase capture. Care should be taken to use an appropriate ‘capture’ method that has equal affinity for both PS1 γ and PS2 γ .⁶⁹⁻⁷¹ Additionally these experiments, typically completed in cell-free assay systems, should be developed in cell-based assays for an accurate reflection of the available ‘active’ γ -secretase pool. The results from the computational methods in **Chapter 3** and **Chapter 6** should be validated using a complementary approach that couples both traditional cell biology methods and other biophysical methods. The direct assessment of substrate processing for the range of substrates investigated in **Chapter 6** should be examined in the HEK-293 cell models developed in this thesis, similarly to experiments

performed in **Chapter 2**. Additionally, assessment of substrate binding kinetics using microscale thermophoresis should be undertaken to verify the binding preference results presented in this thesis.⁷² PS1 and PS2 expression levels in brain tissues presented in **Chapter 4** should be reassessed using additional control samples and would benefit from further exploration of specific neuronal and glial cell populations. Neurocytometry⁷³ and immunopanning⁷⁴ methods can enrich specific neural cell populations using fresh postmortem tissue. Alternatively, the use of human iPSCs would provide valuable insight into the PS1:PS2 expression profiles in different neural cells. A PS1/PS2 auxin-inducible degron human iPSC system would provide the most suitable system,⁷⁵ and would assist in validating the findings presented in **Chapter 5**. This will enable the endogenous expression of PS1 and PS2 to be effectively switched off, then turned back on again. This feature enables functional PS rescue studies to be undertaken without the artefact associated with exogenous PS expression, and as an iPSC would have the added benefit of been able to be differentiated into multiple cell types.

7.3 GENERAL CONCLUSION

This thesis makes significant contributions to furthering our understanding of the complex roles of PS1 and PS2 in AD, shedding light on their diverse functions beyond the well-established involvement in A β generation. **Chapter 2** and **Chapter 3** have explored the enzymatic and structural aspects of PS1 γ and PS2 γ -mediated A β generation, revealing that PS2 γ may play a more critical role in A β generation and in particular A β toxicity through its ability to generate a higher A β ₄₂:A β ₄₀ ratio. Furthermore, **Chapter 4** provides novel insights into PS1 and PS2 expression levels in human brain tissue and various neural cell types, highlighting the potential clinical relevance of PS2 in both neurons and microglia. Focusing on human microglia **Chapter 5**, suggests distinct roles for PS1 and PS2 in microglial function and A β clearance responses. Finally, **Chapter 6** explores PS1 γ and PS2 γ substrate specificity and the effect of PS mutations on substrate binding. Further studies are required to validate and expand on the results presented here. However, of notable significance, this thesis challenges previous assumptions about PS1 γ predominant role in A β generation and highlights potentially critical roles of PS2 γ not only in A β generation but also A β clearance functions, that warrant further investigation. This has clear implications for future endeavours in selectively targeting presenilins/ γ -secretase in AD.

7.4 REFERENCES

1. Hoogmartens, J., Cacace, R., and Van Broeckhoven, C. (2021) Insight into the genetic etiology of Alzheimer's disease: A comprehensive review of the role of rare variants. *Alzheimer's & Dementia: Diagnosis, Assessment & Disease Monitoring* **13**, e12155
2. Haapasalo, A., and Kovacs, D. M. (2011) The Many Substrates of Presenilin/ γ -Secretase. *Journal of Alzheimer's Disease* **25**, 3-28
3. Güner, G., and Lichtenthaler, S. F. (2020) The substrate repertoire of γ -secretase/presenilin. *Seminars in Cell & Developmental Biology* **105**, 27-42
4. Güner, G., Aßfalg, M., Zhao, K., Dreyer, T., Lahiri, S., et al. (2022) Proteolytically generated soluble Tweak Receptor Fn14 is a blood biomarker for γ -secretase activity. *EMBO Molecular Medicine* **14**, e16084
5. Stalin, J., Harhour, K., Hubert, L., Garrigue, P., Nollet, M., et al. (2016) Soluble CD146 boosts therapeutic effect of endothelial progenitors through proteolytic processing of short CD146 isoform. *Cardiovascular Research* **111**, 240-251
6. Zhang, S., Zhang, M., Cai, F., and Song, W. (2013) Biological function of Presenilin and its role in AD pathogenesis. *Translational Neurodegeneration* **2**, 15-15
7. Oikawa, N., and Walter, J. (2019) Presenilins and γ -Secretase in Membrane Proteostasis. *Cells* **8**, 209
8. Makarov, M., Kushnir, L., Papa, M., and Korkotian, E. (2023) Presenilins and mitochondria-an intriguing link: mini-review. *Frontiers in Neuroscience* **17**, 1249815
9. Kang, D. E., Soriano, S., Xia, X., Eberhart, C. G., De Strooper, B., et al. (2002) Presenilin couples the paired phosphorylation of beta-catenin independent of axin: implications for beta-catenin activation in tumorigenesis. *Cell* **110**, 751-762
10. Rybalchenko, V., Hwang, S. Y., Rybalchenko, N., and Koulen, P. (2008) The cytosolic N-terminus of presenilin-1 potentiates mouse ryanodine receptor single channel activity. *The International Journal of Biochemistry & Cell Biology* **40**, 84-97
11. Hayrapetyan, V., Rybalchenko, V., Rybalchenko, N., and Koulen, P. (2008) The N-terminus of presenilin-2 increases single channel activity of brain ryanodine receptors through direct protein-protein interaction. *Cell Calcium* **44**, 507-518
12. Lee, M. K., Slunt, H. H., Martin, L. J., Thinakaran, G., Kim, G., et al. (1996) Expression of presenilin 1 and 2 (PS1 and PS2) in human and murine tissues. *The Journal of Neuroscience* **16**, 7513-7525
13. De Strooper, B., and Annaert, W. (2000) Role of presenilin 1 and presenilin 2 in APP and Notch processing. *Neurobiology of Aging* **21**, Supplement 1, 76
14. Kimberly, W. T., Xia, W., Rahmati, T., Wolfe, M. S., and Selkoe, D. J. (2000) The transmembrane aspartates in presenilin 1 and 2 are obligatory for γ -secretase activity and amyloid β -protein generation. *The Journal of Biological Chemistry* **275**, 3173-3178
15. Kimberly, W. T., LaVoie, M. J., Ostaszewski, B. L., Ye, W., Wolfe, M. S., et al. (2003) γ -Secretase is a membrane protein complex comprised of presenilin, nicastrin, aph-1, and pen-2. *Proceedings of the National Academy of Sciences of the United States of America* **100**, 6382-6387
16. Ryman, D. C., Acosta-Baena, N., Aisen, P. S., Bird, T., Danek, A., et al. (2014) Symptom onset in autosomal dominant Alzheimer disease: A systematic review and meta-analysis. *Neurology* **83**, 253-260
17. Acx, H., Chávez-Gutiérrez, L., Serneels, L., Lismont, S., Benurwar, M., et al. (2014) Signature amyloid β profiles are produced by different γ -secretase complexes. *The Journal of Biological Chemistry* **289**, 4346-4355

18. Meckler, X., and Checler, F. (2016) Presenilin 1 and presenilin 2 target γ -secretase complexes to distinct cellular compartments. *The Journal of Biological Chemistry* **291**, 12821-12837
19. Yonemura, Y., Futai, E., Yagishita, S., Kaether, C., and Ishiura, S. (2016) Specific combinations of presenilins and Aph1s affect the substrate specificity and activity of γ -secretase. *Biochemical and Biophysical Research Communications* **478**, 1751-1757
20. Lessard, C. B., Rodriguez, E., Ladd, T. B., Minter, L. M., Osborne, B. A., et al. (2019) Individual and combined presenilin 1 and 2 knockouts reveal that both have highly overlapping functions in HEK293T cells. *The Journal of Biological Chemistry* **294**, 11276-11285
21. Sannerud, R., Esselens, C., Ejsmont, P., Mattera, R., Rochin, L., et al. (2016) Restricted location of PSEN2/ γ -secretase determines substrate specificity and generates an intracellular A β pool. *Cell* **166**, 193-208
22. Watanabe, H., Imaizumi, K., Cai, T., Zhou, Z., Tomita, T., et al. (2021) Flexible and accurate substrate processing with distinct presenilin/ γ -secretases in human cortical neurons. *eNeuro* **8**, ENEURO.0500-0520.2021
23. Placanica, L., Zhu, L., and Li, Y.-M. (2009) Gender- and age-dependent gamma-secretase activity in mouse brain and its implication in sporadic Alzheimer disease. *PLoS one* **4**, e5088-e5088
24. Thakur, M. K., and Ghosh, S. (2007) Age and sex dependent alteration in presenilin expression in mouse cerebral cortex. *Cellular and Molecular Neurobiology* **27**, 1059-1067
25. Ghosh, S., and Thakur, M. K. (2008) PS1 Expression is Downregulated by Gonadal Steroids in Adult Mouse Brain. *Neurochemical Research* **33**, 365-369
26. Ghosh, S., and Thakur, M. K. (2008) PS2 protein expression is upregulated by sex steroids in the cerebral cortex of aging mice. *Neurochemistry International* **52**, 363-367
27. Kumar, A., and Thakur, M. K. (2012) Presenilin 1 and 2 are expressed differentially in the cerebral cortex of mice during development. *Neurochemistry International* **61**, 778-782
28. Kaja, S., Sumien, N., Shah, V. V., Puthawala, I., Maynard, A. N., et al. (2015) Loss of spatial memory, learning and motor coordination during normal aging is accompanied by changes in brain presenilin 1 and 2 expression levels. *Molecular Neurobiology* **52**, 545-554
29. Culvenor, J. G., Evin, G., Cooney, M. A., Wardan, H., Sharples, R. A., et al. (2000) Presenilin 2 expression in neuronal cells: induction during differentiation of embryonic carcinoma cells. *Experimental Cell Research* **255**, 192-206
30. Barthelson, K., Newman, M., and Lardelli, M. (2020) Sorting Out the Role of the Sortilin-Related Receptor 1 in Alzheimer's Disease. *Journal of Alzheimer's Disease Reports* **4**, 123-140
31. Carlo, A. S., Gustafsen, C., Mastrobuoni, G., Nielsen, M. S., Burgert, T., et al. (2013) The pro-neurotrophin receptor sortilin is a major neuronal apolipoprotein E receptor for catabolism of amyloid- β peptide in the brain. *The Journal of Neuroscience* **33**, 358-370
32. Castellano, J. M., Deane, R., Gottesdiener, A. J., Verghese, P. B., Stewart, F. R., et al. (2012) Low-density lipoprotein receptor overexpression enhances the rate of brain-to-blood A β clearance in a mouse model of β -amyloidosis. *Proceedings of the National Academy of Sciences of the United States of America* **109**, 15502-15507
33. Castellano, J. M., Kim, J., Stewart, F. R., Jiang, H., DeMattos, R. B., et al. (2011) Human apoE isoforms differentially regulate brain amyloid- β peptide clearance. *Science Translational Medicine* **3**, 89ra57
34. Deane, R., Du Yan, S., Subramanian, R. K., LaRue, B., Jovanovic, S., et al. (2003) RAGE mediates amyloid- β peptide transport across the blood-brain barrier and accumulation in brain. *Nature Medicine* **9**, 907-913

35. Deane, R., Sagare, A., Hamm, K., Parisi, M., Lane, S., et al. (2008) apoE isoform-specific disruption of amyloid beta peptide clearance from mouse brain. *The Journal of Clinical Investigation* **118**, 4002-4013
36. Deane, R., Wu, Z., Sagare, A., Davis, J., Du Yan, S., et al. (2004) LRP/Amyloid β -Peptide Interaction Mediates Differential Brain Efflux of A β Isoforms. *Neuron* **43**, 333-344
37. Dorandish, S., Williams, A., Atali, S., Sendo, S., Price, D., et al. (2021) Regulation of amyloid- β levels by matrix metalloproteinase-2/9 (MMP2/9) in the media of lung cancer cells. *Scientific Reports* **11**, 9708
38. Dumanis, S. B., Chamberlain, K. A., Jin Sohn, Y., Jin Lee, Y., Guénette, S. Y., et al. (2012) FE65 as a link between VLDLR and APP to regulate their trafficking and processing. *Molecular Neurodegeneration* **7**, 9
39. Eggert, S., Midthune, B., Cottrell, B., and Koo, E. H. (2009) Induced Dimerization of the Amyloid Precursor Protein Leads to Decreased Amyloid- β Protein Production *The Journal of Biological Chemistry* **284**, 28943-28952
40. Gustafsen, C., Glerup, S., Pallesen, L. T., Olsen, D., Andersen, O. M., et al. (2013) Sortilin and SorLA display distinct roles in processing and trafficking of amyloid precursor protein. *The Journal of Neuroscience* **33**, 64-71
41. He, X., Cooley, K., Chung, C. H., Dashti, N., and Tang, J. (2007) Apolipoprotein receptor 2 and X11 alpha/beta mediate apolipoprotein E-induced endocytosis of amyloid-beta precursor protein and beta-secretase, leading to amyloid-beta production. *The Journal of Neuroscience* **27**, 4052-4060
42. Hoe, H. S., Wessner, D., Beffert, U., Becker, A. G., Matsuoka, Y., et al. (2005) F-spondin interaction with the apolipoprotein E receptor ApoEr2 affects processing of amyloid precursor protein. *Molecular and Cellular Biology* **25**, 9259-9268
43. Huang, Y., Happonen, K. E., Burrola, P. G., O'Connor, C., Hah, N., et al. (2021) Microglia use TAM receptors to detect and engulf amyloid β plaques. *Nature Immunology* **22**, 586-594
44. Kaden, D., Voigt, P., Munter, L.-M., Bobowski, K. D., Schaefer, M., et al. (2009) Subcellular localization and dimerization of APLP1 are strikingly different from APP and APLP2. *Journal of Cell Science* **122**, 368-377
45. Kim, J., Castellano, J. M., Jiang, H., Basak, J. M., Parsadanian, M., et al. (2009) Overexpression of low-density lipoprotein receptor in the brain markedly inhibits amyloid deposition and increases extracellular A beta clearance. *Neuron* **64**, 632-644
46. Lessard, C. B., Malnik, S. L., Zhou, Y., Ladd, T. B., Cruz, P. E., et al. (2018) High-affinity interactions and signal transduction between A β oligomers and TREM2. *EMBO Molecular Medicine* **10**, e9027
47. Pardossi-Piquard, R., Petit, A., Kawarai, T., Sunyach, C., Da Costa, C. A., et al. (2005) Presenilin-dependent transcriptional control of the A β -degrading enzyme neprilysin by intracellular domains of β APP and APLP. *Neuron* **46**, 541-554
48. Takahashi, K., Eto, H., and Tanabe, K. K. (1999) Involvement of CD44 in matrix metalloproteinase-2 regulation in human melanoma cells. *International Journal of Cancer* **80**, 387-395
49. Zhao, L., Teter, B., Morihara, T., Lim, G. P., Ambegaokar, S. S., et al. (2004) Insulin-degrading enzyme as a downstream target of insulin receptor signaling cascade: implications for Alzheimer's disease intervention. *The Journal of Neuroscience* **24**, 11120-11126
50. Zhao, W., Fan, J., Kulic, I., Koh, C., Clark, A., et al. (2020) Axl receptor tyrosine kinase is a regulator of apolipoprotein E. *Molecular Brain* **13**, 66
51. Zhao, Y., Wu, X., Li, X., Jiang, L.-L., Gui, X., et al. (2018) TREM2 Is a Receptor for β -Amyloid that Mediates Microglial Function. *Neuron* **97**, 1023-1031.e1027

52. Farfara, D., Trudler, D., Segev-Amzaleg, N., Galron, R., Stein, R., et al. (2011) γ -Secretase component presenilin is important for microglia β -amyloid clearance. *Annals of Neurology* **69**, 170-180
53. Jayadev, S., Case, A., Eastman, A. J., Nguyen, H., Pollak, J., et al. (2010) Presenilin 2 Is the Predominant γ -Secretase in Microglia and Modulates Cytokine Release. *PLoS One* **5**
54. Pelvig, D. P., Pakkenberg, H., Stark, A. K., and Pakkenberg, B. (2008) Neocortical glial cell numbers in human brains. *Neurobiol Aging* **29**, 1754-1762
55. Karlsson, M., Zhang, C., Méar, L., Zhong, W., Digre, A., et al. (2021) A single-cell type transcriptomics map of human tissues. *Science Advances* **7**, eabh2169
56. Miller, J. A., Horvath, S., and Geschwind, D. H. (2010) Divergence of human and mouse brain transcriptome highlights Alzheimer disease pathways. *Proceedings of the National Academy of Sciences of the United States of America* **107**, 12698-12703
57. Miller, J. A., Oldham, M. C., and Geschwind, D. H. (2008) A systems level analysis of transcriptional changes in Alzheimer's disease and normal aging. *The Journal of Neuroscience* **28**, 1410-1420
58. Okamoto, I., Kawano, Y., Murakami, D., Sasayama, T., Araki, N., et al. (2001) Proteolytic release of CD44 intracellular domain and its role in the CD44 signaling pathway. *The Journal of Cell Biology* **155**, 755-762
59. McMillan, P. J., Leverenz, J. B., and Dorsa, D. M. (2000) Specific downregulation of presenilin 2 gene expression is prominent during early stages of sporadic late-onset Alzheimer's disease. *Molecular Brain Research* **78**, 138-145
60. Ryan, N. S., and Rossor, M. N. (2010) Correlating familial Alzheimer's disease gene mutations with clinical phenotype. *Biomarkers in medicine* **4**, 99-112
61. Mann, D. M., Pickering-Brown, S. M., Takeuchi, A., and Iwatsubo, T. (2001) Amyloid angiopathy and variability in amyloid beta deposition is determined by mutation position in presenilin-1-linked Alzheimer's disease. *The American Journal of Pathology* **158**, 2165-2175
62. Ringman, J. M., Monsell, S., Ng, D. W., Zhou, Y., Nguyen, A., et al. (2016) Neuropathology of Autosomal Dominant Alzheimer Disease in the National Alzheimer Coordinating Center Database. *Journal of Neuropathology & Experimental Neurology* **75**, 284-290
63. Yonemura, Y., Futai, E., Yagishita, S., Suo, S., Tomita, T., et al. (2011) Comparison of presenilin 1 and presenilin 2 γ -secretase activities using a yeast reconstitution system. *The Journal of Biological Chemistry* **286**, 44569-44575
64. Yousefi, R., Jevdokimenko, K., Kluever, V., Pacheu-Grau, D., and Fornasiero, E. F. (2021) Influence of subcellular localization and functional state on protein turnover. *Cells* **10**
65. Thinakaran, G., Harris, C. L., Ratovitski, T., Davenport, F., Slunt, H. H., et al. (1997) Evidence that levels of presenilins (PS1 and PS2) are coordinately regulated by competition for limiting cellular factors. *The Journal of Biological Chemistry* **272**, 28415-28422
66. Frånberg, J., Svensson, A. I., Winblad, B., Karlström, H., and Frykman, S. (2011) Minor contribution of presenilin 2 for γ -secretase activity in mouse embryonic fibroblasts and adult mouse brain. *Biochemical and Biophysical Research Communications* **404**, 564-568
67. Placanica, L., Tarassishin, L., Yang, G., Peethumnongsin, E., Kim, S.-H., et al. (2009) Pen2 and presenilin-1 modulate the dynamic equilibrium of presenilin-1 and presenilin-2 γ -secretase complexes. *The Journal of Biological Chemistry* **284**, 2967-2977
68. Teranishi, Y., Hur, J.-Y., Welandar, H., Frånberg, J., Aoki, M., et al. (2010) Affinity pulldown of γ -secretase and associated proteins from human and rat brain. *Journal of Cellular and Molecular Medicine* **14**, 2675-2686
69. Borgegård, T., Gustavsson, S., Nilsson, C., Parpal, S., Klintonberg, R., et al. (2012) Alzheimer's disease: Presenilin-2 sparing γ -secretase inhibition is a tolerable A β peptide-lowering strategy. *The Journal of Neuroscience* **32**, 17297-17305

70. Crump, C. J., Murrey, H. E., Ballard, T. E., Am Ende, C. W., Wu, X., et al. (2016) Development of sulfonamide photoaffinity inhibitors for probing cellular γ -secretase. *ACS Chemical Neuroscience* **7**, 1166-1173
71. Gertsik, N., am Ende, C. W., Geoghegan, K. F., Nguyen, C., Mukherjee, P., et al. (2017) Mapping the binding site of BMS-708163 on γ -secretase with cleavable photoprobes. *Cell Chemical Biology* **24**, 3-8
72. Romain, M., Thiroux, B., Tardy, M., Quesnel, B., and Thuru, X. (2020) Measurement of Protein-Protein Interactions through Microscale Thermophoresis (MST). *Bio Protocol* **10**, e3574
73. Martin, D., Xu, J., Porretta, C., and Nichols, C. D. (2017) Neurocytometry: Flow Cytometric Sorting of Specific Neuronal Populations from Human and Rodent Brain. *ACS Chemical Neuroscience* **8**, 356-367
74. Nolle, A., van Dijken, I., Waelti, C. M., Calini, D., Bryois, J., et al. (2021) Enrichment of Glial Cells From Human Post-mortem Tissue for Transcriptome and Proteome Analysis Using Immunopanning. *Frontiers in Cellular Neuroscience* **15**
75. Yesbolatova, A., Saito, Y., Kitamoto, N., Makino-Itou, H., Ajima, R., et al. (2020) The auxin-inducible degron 2 technology provides sharp degradation control in yeast, mammalian cells, and mice. *Nature Communications* **11**, 5701